frontiers | Research Topics

Food webs and stable isotopes, volume II

Edited by
Jason Newton, Gabriele Stowasser and Rona A. R. McGill

Published in
Frontiers in Ecology and Evolution

FRONTIERS EBOOK COPYRIGHT STATEMENT

The copyright in the text of individual articles in this ebook is the property of their respective authors or their respective institutions or funders. The copyright in graphics and images within each article may be subject to copyright of other parties. In both cases this is subject to a license granted to Frontiers.

The compilation of articles constituting this ebook is the property of Frontiers.

Each article within this ebook, and the ebook itself, are published under the most recent version of the Creative Commons CC-BY licence. The version current at the date of publication of this ebook is CC-BY 4.0. If the CC-BY licence is updated, the licence granted by Frontiers is automatically updated to the new version.

When exercising any right under the CC-BY licence, Frontiers must be attributed as the original publisher of the article or ebook, as applicable.

Authors have the responsibility of ensuring that any graphics or other materials which are the property of others may be included in the CC-BY licence, but this should be checked before relying on the CC-BY licence to reproduce those materials. Any copyright notices relating to those materials must be complied with.

Copyright and source acknowledgement notices may not be removed and must be displayed in any copy, derivative work or partial copy which includes the elements in question.

All copyright, and all rights therein, are protected by national and international copyright laws. The above represents a summary only. For further information please read Frontiers' Conditions for Website Use and Copyright Statement, and the applicable CC-BY licence.

ISSN 1664-8714
ISBN 978-2-8325-3392-5
DOI 10.3389/978-2-8325-3392-5

About Frontiers

Frontiers is more than just an open access publisher of scholarly articles: it is a pioneering approach to the world of academia, radically improving the way scholarly research is managed. The grand vision of Frontiers is a world where all people have an equal opportunity to seek, share and generate knowledge. Frontiers provides immediate and permanent online open access to all its publications, but this alone is not enough to realize our grand goals.

Frontiers journal series

The Frontiers journal series is a multi-tier and interdisciplinary set of open-access, online journals, promising a paradigm shift from the current review, selection and dissemination processes in academic publishing. All Frontiers journals are driven by researchers for researchers; therefore, they constitute a service to the scholarly community. At the same time, the *Frontiers journal series* operates on a revolutionary invention, the tiered publishing system, initially addressing specific communities of scholars, and gradually climbing up to broader public understanding, thus serving the interests of the lay society, too.

Dedication to quality

Each Frontiers article is a landmark of the highest quality, thanks to genuinely collaborative interactions between authors and review editors, who include some of the world's best academicians. Research must be certified by peers before entering a stream of knowledge that may eventually reach the public - and shape society; therefore, Frontiers only applies the most rigorous and unbiased reviews. Frontiers revolutionizes research publishing by freely delivering the most outstanding research, evaluated with no bias from both the academic and social point of view. By applying the most advanced information technologies, Frontiers is catapulting scholarly publishing into a new generation.

What are Frontiers Research Topics?

Frontiers Research Topics are very popular trademarks of the *Frontiers journals series*: they are collections of at least ten articles, all centered on a particular subject. With their unique mix of varied contributions from Original Research to Review Articles, Frontiers Research Topics unify the most influential researchers, the latest key findings and historical advances in a hot research area.

Find out more on how to host your own Frontiers Research Topic or contribute to one as an author by contacting the Frontiers editorial office: frontiersin.org/about/contact

Food webs and stable isotopes, volume II

Topic editors

Jason Newton — Scottish Universities Environmental Research Centre; University of Glasgow, United Kingdom

Gabriele Stowasser — British Antarctic Survey (BAS), United Kingdom

Rona A. R. McGill — Scottish Universities Environmental Research Centre; University of Glasgow, United Kingdom

Citation

Newton, J., Stowasser, G., McGill, R. A. R., eds. (2023). *Food webs and stable isotopes, volume II*. Lausanne: Frontiers Media SA.

doi: 10.3389/978-2-8325-3392-5

Table of contents

05 The Potential Impacts of Invasive Quagga and Zebra Mussels on Macroinvertebrate Communities: An Artificial Stone Substrate Based Field Experiment Using Stable Isotopes
Hui Zhang, Elizabeth Yohannes and Karl-Otto Rothhaupt

17 Altered Energy Mobilization Within the Littoral Food Web in New Habitat Created by Climate-Induced Changes in Lake Water Level
Kang Wang, Kangshun Zhao, Xiong Xiong, Huan Zhu, Hongyi Ao, Kaili Ma, Zhicai Xie, Chenxi Wu, Huan Wang, Huan Zhang, Peiyu Zhang and Jun Xu

29 Variation Among Species and Populations, and Carry-Over Effects of Winter Exposure on Mercury Accumulation in Small Petrels
Petra Quillfeldt, Yves Cherel, Joan Navarro, Richard A. Phillips, Juan F. Masello, Cristián G. Suazo, Karine Delord and Paco Bustamante

50 Tracking movements and growth of post-hatchling to adult hawksbill sea turtles using skeleto+iso
Calandra N. Turner Tomaszewicz, Michael J. Liles, Larisa Avens and Jeffrey A. Seminoff

67 Terrigenous subsidies in lakes support zooplankton production mainly *via* a green food chain and not the brown food chain
Fumiya Hirama, Jotaro Urabe, Hideyuki Doi, Takehiro Kazama, Takumi Noguchi, Tyler H. Tappenbeck, Izumi Katano, Masato Yamamichi, Takehito Yoshida and James J. Elser

82 Coexisting with the alien: Evidence for environmental control on trophic interactions between a native (*Atherina boyeri*) and a non-indigenous fish species (*Gambusia holbrooki*) in a Mediterranean coastal ecosystem
Cristina Andolina, Geraldina Signa, Giovanna Cilluffo, Simona Iannucci, Antonio Mazzola and Salvatrice Vizzini

94 Stable isotopes elucidate body-size and seasonal fluctuations in the feeding strategies of planktivorous fishes across a semi-enclosed tropical embayment
Christina Skinner, Yu-De Pei, Naoko Morimoto, Toshihiro Miyajima and Alex S. J. Wyatt

112 Temporal dynamics in zooplankton $\delta^{13}C$ and $\delta^{15}N$ isoscapes for the North Atlantic Ocean: Decadal cycles, seasonality, and implications for predator ecology
Boris Espinasse, Anthony Sturbois, Sünnje L. Basedow, Pierre Hélaouët, David G. Johns, Jason Newton and Clive N. Trueman

133 Compound-specific stable isotope analysis of amino acid nitrogen reveals detrital support of microphytobenthos in the Dutch Wadden Sea benthic food web
Philip M. Riekenberg, Tjisse van der Heide, Sander J. Holthuijsen, Henk W. van der Veer and Marcel T. J. van der Meer

150 Carbon, nitrogen, and oxygen stable isotopes in modern tooth enamel: A case study from Gorongosa National Park, central Mozambique
Tina Lüdecke, Jennifer N. Leichliter, Vera Aldeias, Marion K. Bamford, Dora Biro, David R. Braun, Cristian Capelli, Jonathan D. Cybulski, Nicolas N. Duprey, Maria J. Ferreira da Silva, Alan D. Foreman, Jörg M. Habermann, Gerald H. Haug, Felipe I. Martínez, Jacinto Mathe, Andreas Mulch, Daniel M. Sigman, Hubert Vonhof, René Bobe, Susana Carvalho and Alfredo Martínez-García

176 Patterns of dietary niche breadth and overlap are maintained for two closely related carnivores across broad geographic scales
Jenilee Gobin, Christa M. Szumski, James D. Roth and Dennis L. Murray

185 Freshwater wetland–driven variation in sulfur isotope compositions: Implications for human paleodiet and ecological research
Eric J. Guiry, Trevor J. Orchard, Suzanne Needs-Howarth and Paul Szpak

197 Contrasting energy pathways suggest differing susceptibility of pelagic fishes to an invasive ecosystem engineer in a large lake system
Ariana Chiapella, Bianca Possamai, J. Ellen Marsden, Martin J. Kainz and Jason D. Stockwell

frontiers | Frontiers in Ecology and Evolution

ORIGINAL RESEARCH
published: 03 June 2022
doi: 10.3389/fevo.2022.887191

The Potential Impacts of Invasive Quagga and Zebra Mussels on Macroinvertebrate Communities: An Artificial Stone Substrate Based Field Experiment Using Stable Isotopes

*Hui Zhang, Elizabeth Yohannes and Karl-Otto Rothhaupt**

Limnological Institute, University of Konstanz, Konstanz, Germany

OPEN ACCESS

Edited by:
Gabriele Stowasser, British Antarctic Survey (BAS), United Kingdom

Reviewed by:
Teresa Radziejewska, University of Szczecin, Poland
Jan Vanaverbeke, Royal Belgian Institute of Natural Sciences, Belgium

***Correspondence:**
Karl-Otto Rothhaupt
karl.rothhaupt@uni-konstanz.de

Specialty section:
This article was submitted to Population, Community, and Ecosystem Dynamics, a section of the journal Frontiers in Ecology and Evolution

Received: *01 March 2022*
Accepted: *06 May 2022*
Published: *03 June 2022*

Citation:
Zhang H, Yohannes E and Rothhaupt K-O (2022) The Potential Impacts of Invasive Quagga and Zebra Mussels on Macroinvertebrate Communities: An Artificial Stone Substrate Based Field Experiment Using Stable Isotopes. Front. Ecol. Evol. 10:887191. doi: 10.3389/fevo.2022.887191

Over the past decades, the zebra mussel (*Dreissena polymorpha*) and quagga mussel (*D. rostriformis bugensis*) invaded multiple freshwater systems and posed major threats to the overall ecosystem. In Lake Constance where zebra mussels invaded in the 1960s, the quagga mussel invasion progressed at a very high rate since 2016, providing an opportunity to study the ecological impact of both species at an early stage. We conducted a field experiment in the littoral region of the lake and monitored differences in macroinvertebrate community colonization. We used standardized stone substrates, which were blank, glued with empty shells of mussels, with living adult quagga mussels, and with living adult zebra mussels. Empty shells and the shells of both living adult quagga and zebra mussels created more colonization areas for newly settled macroinvertebrates. The abundance of newly settled quagga mussels was higher than zebra mussels, indicating the outcompeting behavior of quagga mussels. We used stable isotopes ($\delta^{13}C$ and $\delta^{15}N$) of both dreissenids and their potential competitors, which include two snail species (New Zealand mud snail *Potamopyrgus antipodarum* and faucet snail *Bithynia tentaculate*) and additional invasive gammarid species (killer shrimp *Dikerogammarus villosus*), in order to investigate their feeding ecology and to evaluate their potential impacts on macroinvertebrate community. The $\delta^{13}C$ and $\delta^{15}N$ of neither the newly settled quagga mussels nor the well-established zebra mussels differed significantly among various treatments. Newly settled quagga mussels had higher $\delta^{13}C$ values than newly settled zebra mussels and showed similar differences in all four stone setups. During the experimental period (with quagga and zebra mussels still coexisting in some regions), these two dreissenids exhibited clear dietary (isotopic) niche segregation. The rapid expansion of invasive quagga mussels coupled with the higher mortality rate of zebra mussels might have caused a dominance shift from zebra to quagga mussels. The study offers the first overview of the progressive invasion of quagga mussel and the reaction of zebra mussels and

other newly settled macroinvertebrates, and compliments the hypothesis of facilitative associations between invasive dreissenids. Results provide an experimental benchmark by which future changes in trophic ecology and invasion dynamics can be measured across the ecosystem.

Keywords: invasive species, macroinvertebrates, colonization, stable isotopes, Lake Constance

INTRODUCTION

The spread of invasive species in freshwater environments is observed as a global phenomenon (Lodge et al., 1998; Francis and Chadwick, 2012; Jones et al., 2021). While investigators have recorded multiple impacts of invasive species on native or established biological communities (Gherardi and Acquistapace, 2007; Stiers et al., 2011; Boltovskoy and Correa, 2015), the prediction of the impact of a newly established non-native species remains a challenge (Williamson, 1999; Roy et al., 2014). This is mainly due to the fact that impacts of a given species may vary over space and time, and might equally depend on the specificity of the invaded ecosystem (Strayer and Malcom, 2006; Karatayev et al., 2021). Moreover, the impact might be potentially measurable only after a considerable delay following invasion (Crooks, 2005; Ricciardi et al., 2013).

Ecologists have, therefore, exerted efforts to understand the potential impacts of invasive species on freshwater systems by utilizing different approaches that include documented knowledge of the literature (Copp et al., 2009; Roy et al., 2014) coupled with mathematical and statistical modeling (Ricciardi, 2003; Kulhanek et al., 2011). While these studies often depend on existing trends, it is more difficult to predict the impacts of the invasion when establishments occur in a novel location with no prior baseline data (Kulhanek et al., 2011). Moreover, some aquatic systems are invaded by more than one biophysically similar or genetically related taxa, although the important species-specific traits seem to be underestimated (Ricciardi, 2003).

Two highly invasive taxa of particular concern in multiple freshwater lakes and rivers are dreissenids of the Ponto-Caspian origin (Son, 2007; Strayer et al., 2020): quagga mussel (*Dreissena rostriformis bugensis*) and zebra mussel (*D. polymorpha*) (Molloy et al., 2007; Evariste et al., 2018). The establishment of these two dreissenids has been extensively reported with synergistic and antagonistic shifts in the community structure of pre-existing freshwater ecosystems (Mörtl and Rothhaupt, 2003; Sousa et al., 2011). Specific changes following invasion include a measurable increase in benthic macroinvertebrate density (Ricciardi, 2003). As such, the physical structural complexity of the mussel bed provides a safe haven or fine-scale refugia against predators (González and Downing, 1999; Ward and Ricciardi, 2007), providing protection against unintended movement of waves that facilitate macroinvertebrates (Ricciardi et al., 1997; Stewart et al., 1998). Evidently, the biofouling of mussels has deleterious effects on certain macroinvertebrates (Sousa et al., 2011; Strayer and Malcom, 2018), and in many lakes, the native bivalves showed a large decrease in abundance after the invasion of dreissenids (Strayer and Malcom, 2007; Burlakova et al., 2014).

Most interestingly, detritivores and grazing herbivorous species may benefit from nutrient release following pseudofeces excretion and biofilm deposition from dreissenids (Kobak et al., 2013). Following mussel invasion, remarkable increases in macroinvertebrate abundance and biomass of gammarids and snails have been documented (MacIsaac, 1996; Bially and MacIsaac, 2000). Finally, as posited by the invasional meltdown hypothesis, in multiple invaded ecosystems, the positive interactions among invaders initiate positive population-level feedback that intensifies influence and promotes further invasions (Simberloff and von Holle, 1999).

In the past decades, several invasive freshwater mussels have colonized most of the European perialpine lakes. In particular, the zebra and quagga mussels pose continuous challenges in Lake Constance. Adult quagga mussel was first reported in the lake in 2016 (Haltiner et al., 2022), while zebra mussel has colonized the lake since the late 1960s (Walz, 1973). In fact, the quagga mussel recently increased its range and density, and replaced the zebra mussel over most parts of the lake, only 2 years after the first record. These observations, combined with the existing increasing invasion rate and invasive species in Lake Constance, tentatively support the "invasional meltdown" model (Simberloff and von Holle, 1999). It could be argued, at least theoretically, that Lake Constance is experiencing an "easier" invasion as the cumulative number of introduced species increases and as facilitative interactions are expected to exacerbate the effect of these invaders. Indeed, the impacts of zebra mussels on the macroinvertebrate communities of Lake Constance have been well investigated (Mörtl and Rothhaupt, 2003; Gergs and Rothhaupt, 2008, 2015). However, the impacts of the recent invader quagga mussels remain unknown.

Therefore, the first objective of this study was to measure and compare the potential impacts of quagga and zebra mussels on macroinvertebrate communities in Lake Constance. Using an experimental approach, we aimed to observe macroinvertebrate colonization across four series of manipulated stone substrates treated with different specimens: blank stones, dead shell analogs of dreissenids, living adult quagga mussels, or living adult zebra mussels. By simulating these four potential substrate "scenarios" here, we aimed to improve our knowledge regarding these two highly concerning invasive species in the absence of robust baseline data (specifically for quagga mussels) for Lake Constance. Understanding food-web interaction using possible scenarios is critical for accurate prediction of future impacts, which would facilitate undertaking necessary prevention and management approaches (Byers et al., 2002). We expected that substrates with living mussel and shell treatments would cause higher macroinvertebrate abundance compared to the blank treatments.

Unraveling the mechanisms that allow multiple aquatic invasive species to coexist can provide insights into freshwater community ecology. However, dietary information on component species of these assemblages is often difficult to obtain. Therefore, our second objective was to identify potential food sources and estimate the relative trophic position of newly settled macroinvertebrate species (on the stone substrates). Therefore, we measured stable carbon and nitrogen isotopes ($\delta^{13}C$ and $\delta^{15}N$) in soft tissue specimens obtained from five macroinvertebrate species (Gergs et al., 2011; Tran et al., 2015). Using the four manipulated substrate setups, we examined whether trophic niche differentiation and microhabitat segregation explain their co-existence in the lake. Both mussels are able to exploit phytoplankton or suspended detritus as significant energy sources. Yet, it is expected that the species might compete with each other in areas of sympatry. Therefore, we hypothesized that the presence of these mussels will influence not only the community composition but also the food resources of newly settled macroinvertebrates. Specifically, we measured and compared the isotopic niche size of each species and that of the whole community, and assessed isotopic niche overlap among the two invasive mussel species using the $\delta^{13}C$ and $\delta^{15}N$ values.

At present, the vast majority of dreissenids found in the littoral zone of Lake Constance are quagga mussels, while a short time ago, this area was dominated by zebra mussels. Species-specific population size may fluctuate because of the variation in the adult mortality rate, and the survival of adult mussels may be an important component of competitive displacement. Therefore, using this *in situ* setup, we opportunistically examined the survivorship of adult quagga and zebra mussels in the four treatments.

MATERIALS AND METHODS

Study Area

The manipulated stone substrate experiment was conducted at the littoral area in Upper Lake Constance (N: 47°41′31.0″, E: 9°12′07.0″), one of the two major basins in Lake Constance, Germany. The littoral area has predominantly stony gravel and pebble substrate. It is surrounded by a semi-natural habitat, with scarce suburban housing and with hardly any extensive artificial land use (Gergs et al., 2011). The stone substrates were deployed at a depth of 0.80 m.

Field Experimental Design

The experimental design followed the former study by Mörtl and Rothhaupt (2003). The standardized stone substrates (commercially available concrete cobblestones) had an upper surface area of 121 cm^2. The upper surface area of each stone substrate was manipulated to obtain four treatments with eight replicates each. The first control treatment (B treatment) consisted of blank and clean stones with no shells and no mussels on them. Treatment 2 (S treatment) consisted of stones with eviscerated shells of mussels that were glued together to mimic intact dead mussels (Botts et al., 1996). Shells were glued to the substrate at their posterior side and positioned in a similar direction, simulating field observations of adult dead mussels at the lakeshore. Treatment 3 (Q treatment) and treatment 4 (Z treatment) consisted of stones with upper surfaces covered by living adult quagga and zebra mussels, respectively. Living mussels of individual species were glued to the substrate at their posterior side. Care was taken to ensure that individual mussels could open and close their shells as in natural cases to ensure survival. The abundance of shells or living mussels on the upper surfaces of stones was equivalent to 3,719 ± 413 ind./m^2. The substrate appearance resembled that of a natural mussel bed or druse, simulating field observations of living mussels. Caution was taken to ensure that glued individual mussels or shells were approximately equidistant.

To prepare the stone treatments, adult quagga and zebra mussels of ca. 20 mm shell length had been collected by hand at a littoral site of the lake where the two dreissenids coexisted by then (i.e., June 2018). Based on the morphological traits, mussels had been identified and separated as quagga or zebra mussels (Pathy and Mackie, 1993; Kerambrun et al., 2018). To prepare the shell treatments, shells of eviscerated mussels were washed and dried in the laboratory at room temperature for 72 h. Stones were deployed at the study site for the experiment between June and July 2018 (28 days). Elsewhere, artificial substrates have been reported to reach stabilized newly settled macroinvertebrate communities within 20–60 days (Roby et al., 1978; Wise and Molles, 1979). Therefore, through the experimental period of 28 days, we envisioned to capture the invasion processes and evaluate their effects on the density and taxonomic richness of newly settled macroinvertebrates within the first 4 weeks (short time duration).

On the last day of the experiment, all the stones were collected from the lake, thoroughly washed, and carefully inspected for attached (newly settled) macroinvertebrates. The newly settled macroinvertebrates were gently removed with a brush, washed, and collected from each stone after filtering through a 200 μm mesh. We took all the newly settled macroinvertebrates in the entire area of the respective stone into account. Afterward, living adult quagga and zebra mussels that had been glued on the stones were gently removed from their respective stones, and their survival was assessed by observing shell gape and soft tissue. If no soft tissue was present inside the shells, then mortality was recorded. One stone in the Z treatment was upside down at the end of the experiment, and this sample was omitted from further analysis.

Macroinvertebrate Counting

In the laboratory, all newly settled macroinvertebrate samples were sorted and counted under a dissecting microscope (× 10 magnification, Zeiss Stemi 2000-C). Identification was made to species or genus level, except for Diptera, which mainly included Chironomidae. Chironomidae were identified at the subfamily level due to morphological ambiguity at their smallest size ranges. The size of macroinvertebrates was measured using a microscope equipped with an ocular micrometer. Newly settled dreissenids larger than 1 mm in length were separated into quagga or zebra mussels based on

morphological traits. We pooled the small dreissenids (≤ 1 mm in length) into one group.

Stable Isotope Analysis

The five common newly settled macroinvertebrate species recorded from the experiment, which included the two mussel species (quagga mussel *D. rostriformis bugensis* and zebra mussel *D. polymorpha*), two snail species (New Zealand mud snail *Potamopyrgus antipodarum* and faucet snail *Bithynia tentaculata*), and one gammarid species (killer shrimp *Dikerogammarus villosus*), were used for stable isotope measurement. The soft tissues of the two mussel species and two snail species were eviscerated for stable isotope analysis. Individuals of the gammarid species were used for stable isotope analysis.

Lipid content was removed from dried and pulverized samples (Post et al., 2007; Rothhaupt et al., 2014) and weighed (ca. 0.85 mg) in tin cups to the nearest 0.001 mg, using a micro-analytical balance. The $^{13}C/^{12}C$ or $^{15}N/^{14}N$ ratios of samples were determined using two instruments. Half of the samples were measured at the stable isotope lab of the University of Konstanz in Germany. Here, samples were combusted in a vario PYRO cube elemental analyzer (Elementar Analysensysteme, Germany) at 1,120°C. Resulting CO_2 and N_2 were separated by gas chromatography and passed into an IsoPrime isotope ratio mass spectrometer (IRMS; Isoprime Ltd., Manchester, United Kingdom). The rest of the samples were measured at the stable isotope laboratory of the University of Erlangen-Nürnberg, Germany. Here samples were combusted in a Costech Elemental Analyzer (ECS 4010; Costech International, Pioltello, Italy; now NC Technologies, Bussero, Italy). The resulting gases were separated and measured using Thermo Scientific Delta V plus IRMS (Thermo Fisher Scientific, Bremen, Germany). The repeatability and comparability of results obtained from the two laboratories were first ensured by measuring multiple macroinvertebrate samples ("dummy" samples) in both laboratories before proceeding with the samples used for this experiment.

All stable isotope values ($\delta^{13}C$ or $\delta^{15}N$) were reported in the δ notation (per mill) where $\delta = [1{,}000 \times (\text{Rsample}/\text{Rstandard}) - 1]$ ‰, relative to the Pee Dee Belemnite (PDB) for carbon and atmospheric N_2 for nitrogen in parts per thousand deviations (‰).

Data Analysis

Non-parametric Kruskal–Wallis test was used to analyze the differences in the abundances of newly settled macroinvertebrates among four different treatments, as the normality of the whole dataset was not reached (Shapiro–Wilk test). Dunn's test was used for *post hoc* pairwise comparisons. Non-parametric Mann–Whitney Wilcoxon test was used to compare the abundances of quagga and zebra mussels in each treatment.

To identify differences in community composition across all treatments, we examined dissimilarities among macroinvertebrate assemblages by applying non-metric multidimensional scaling (NMDS) using Bray–Curtis dissimilarities. Mean abundance data (ind./m^2 of newly settled macroinvertebrate per taxon) were used in the analysis, and data were standardized by the decostand function using the method "total." We then assessed whether the composition of the macroinvertebrate community differed among treatments using analysis of similarity (ANOSIM). In order to reduce distortion of macroinvertebrate assemblage in the community, taxa accounting for less than 0.5% of the total mean abundance per treatment were excluded from the analysis.

Graphical summaries of the mean abundance of abundant newly settled macroinvertebrates (ind./m^2 + SE) per treatment were made for taxa that can be identified up to the genus or species level, which included *D. rostriformis bugensis*, *D. polymorpha*, *Dreissena* (≤ 1 mm), *P. antipodarum*, *B. tentaculata*, *D. villosus*, *Katamysis warpachowskyi,* and *Caenis* (**Figure 1**). A summation of abundances for all the newly settled macroinvertebrates present in each sample is expressed as the total abundance.

The stable isotope values of newly settled macroinvertebrates were not normally distributed (Shapiro–Wilk test). Kruskal–Wallis test was used to analyze the differences in $\delta^{13}C$ and $\delta^{15}N$ values for the five main newly settled macroinvertebrate species among four treatments, and Dunn's test was used for *post hoc* pairwise comparisons. Mann–Whitney Wilcoxon test was used to compare the $\delta^{13}C$ and $\delta^{15}N$ values of quagga and zebra mussels in each treatment. We used Bayesian standard ellipse area (SEA) and size-corrected standard ellipse area for small samples (SEAc) to describe species and community isotopic niche width of newly settled macroinvertebrates among different treatments. We also calculated and reported the 95% confidence intervals of SEA using 10,000 posterior Markov chain Monte Carlo draws (Jackson et al., 2011; Catry et al., 2016).

All calculations and figures were conducted using R (R Core Team, 2021) with the package readxl, tidyverse, DescTools, ggplot2, ggpubr, vegan, and SIBER, in order to import data, reshape data, conduct Dunn's test, make figures, arranges figures, conduct NMDS analysis, and analyze Bayesian standard ellipse areas, respectively.

RESULTS

The Abundance of Newly Settled Macroinvertebrates

The most abundant taxa in all the four treatments were mussels [*D. rostriformis bugensis*, *D. polymorpha*, and *Dreissena* spp. (≤ 1 mm)], snails (*P. antipodarum* and *B. tentaculata*), gammarids (*D. villosus*), mysids (*K. warpachowskyi*), mayfly nymphs (*Caenis* spp.), and chironomid larvae (Chironominae and Orthocladiinae) (**Figures 1**, **2**). Other taxa, such as Trichoptera, that occur infrequently were used only for total abundance analysis.

Differences in the abundances of newly settled macroinvertebrates among the four treatments are presented in **Table 1**. The abundances of newly settled quagga mussels were not significantly different. The abundances of newly settled zebra mussels were also not significantly different. The abundances of newly settled snail *P. antipodarum* and mayfly nymphs *Caenis*

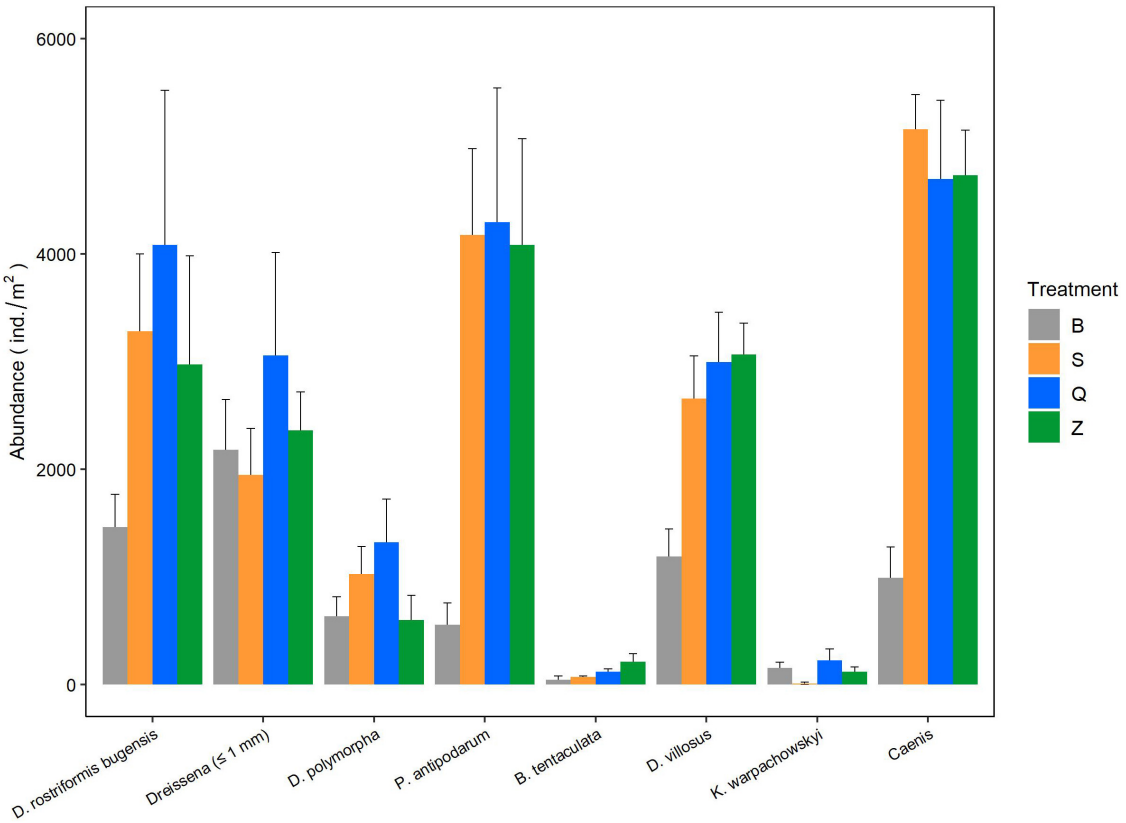

FIGURE 1 | The abundance of abundant newly settled macroinvertebrates in four different treatments. Taxa that can be identified to species or genus level are presented. Error bars indicate standard errors.

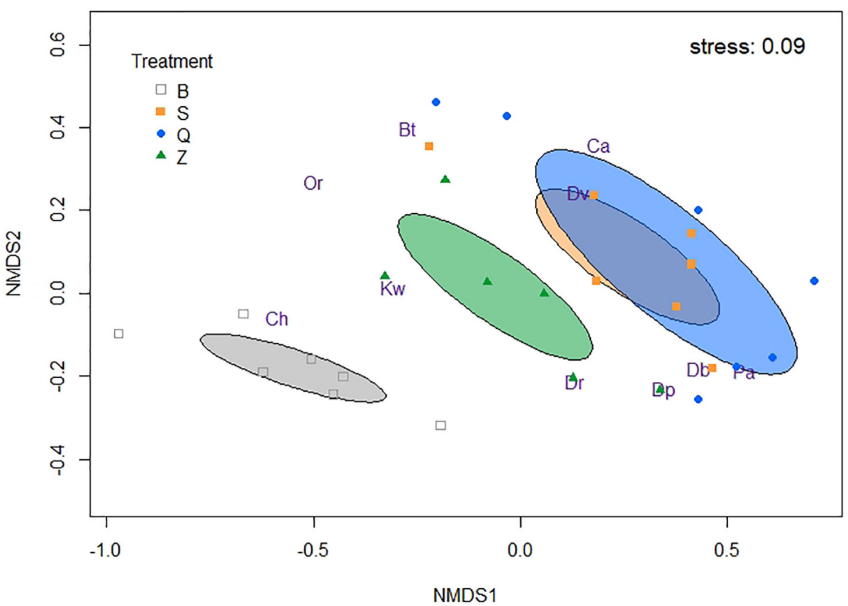

FIGURE 2 | Non-metric multidimensional scaling (NMDS) ordination plot of newly settled macroinvertebrate abundances, representing the community structure in four different treatments. Ellipses draw standard errors of the treatments and show a 95% confidence interval. Db means *D. rostriformis bugensis*, Dp means *D. polymorpha*, Dr means *Dreissena* (≤ 1 mm), Pa means *P. antipodarum*, Bt means *B. tentaculata*, Dv means *D. villosus*, Kw means *K. warpachowskyi*, Ca means *Caenis*, Ch means Chironominae, and Or means Orthocladiinae.

TABLE 1 | The differences in abundances of newly settled macroinvertebrates among four different treatments.

Taxon	Chi-squared	*p*	Rank order
Dreissena rostriformis bugensis	4.12	0.249	n.s.
Dreissena polymorpha	3.11	0.374	n.s.
Dreissena spp. (≤ 1 mm)	0.73	0.867	n.s.
Potamophyrgus antipodarum	12.38	0.006*	S > B, Q > B, Z > B
Bithynia tentaculata	7.20	0.066	n.s.
Dikerogammarus villosus	12.43	0.006*	Z > B, Q > B
Katamysis warpachowskyi	5.84	0.120	n.s.
Caenis spp.	16.00	0.001*	S > B, Z > B, Q > B
Chironominae	19.62	< 0.001*	B > S, B > Q, Z > S, Z > Q
Orthocladiinae	8.09	0.044*	n.s.
Total	13.61	0.004*	Z > B

*Kruskal–Wallis test is used to analyze the differences in abundances among treatments, and significant results of p-values (p ≤ 0.05) are marked with *. Dunn's test is used for post hoc pairwise comparisons, the rank orders are based on the mean values of abundances in each treatment, and only the pairs which are significantly different are shown in the table. n.s. means no significant differences.*

were significantly different ($p < 0.01$), with the B treatment having the lowest numbers. The abundances of newly settled gammarid *D. villosus* were less in B treatments than in Q and Z treatments ($p < 0.05$). The abundances of newly settled chironomid larvae of subfamily Chironominae were higher in Z and B treatments than in S and Q treatments ($p < 0.05$). Total abundances of all newly settled macroinvertebrates were significantly higher in Z treatments than in B treatments ($p = 0.002$).

The total abundance of quagga mussels in the entire experiment area was higher than the total abundance of zebra mussels. In Z treatments, the abundance of newly settled quagga mussels was significantly higher than that of zebra mussels ($p = 0.021$), and additional information is provided in **Supplementary Table 1**.

In the NMDS plot (stress 0.09), the average composition of colonizing macroinvertebrate community across treatments appeared to be most segregated by mussel treatments (ANOSIM global test $R = 0.473$, $p = 0.001$) (**Figure 2**). For this 28-day experiment, Q and S treatments were closely grouped and separated from the Z treatment, while the B treatment was more isolated on the plot.

The mortality rate of glued adult zebra mussels (24.00 ± 2.28%) was significantly higher than that of glued adult quagga mussels (7.33 ± 1.33%) ($p < 0.01$; **Figure 3**). The abundance of newly settled chironomid larvae (subfamily Chironominae) showed a positive correlation with the mortality rate of adult dreissenids (**Figure 3**).

The Stable Isotope Values of Newly Settled Macroinvertebrates

The stable isotope values of five main macroinvertebrate species are shown in the stable isotope ($\delta^{13}C$ and $\delta^{15}N$) bi-plots (**Figure 4**). Confidence intervals of the standard ellipse areas for different treatments and the whole experimental area are shown in the density plot (**Figure 5** and **Supplementary Figure 1**).

Among four treatments, the $\delta^{13}C$ values of newly settled quagga mussels were significantly higher in the B treatment than in the Z treatment ($p = 0.016$; **Table 2**). The $\delta^{13}C$ values of newly settled snail *P. antipodarum* were significantly higher in Z treatment than in S treatment ($p = 0.014$; **Table 2**). The other three species showed no significant differences in $\delta^{13}C$ values among the four treatments. For all five main species, there were no significant differences in $\delta^{15}N$ values among the four treatments.

The SEAc results indicated that the newly settled quagga mussels showed a smaller isotopic niche in Z treatment than in B, S, and Q treatments (**Figure 5** and **Table 3**). The newly settled zebra mussels also exhibited a smaller isotopic niche in Z treatment. The remaining three newly settled (frequent) macroinvertebrate species showed equivalent isotopic niches among the different treatments. Taken together, SEAc for the whole community was higher in B treatment.

For the two dreissenids, the $\delta^{13}C$ values of newly settled quagga mussels were higher than the $\delta^{13}C$ values of newly settled zebra mussels. This pattern was evident in all four treatments ($p \leq 0.01$; **Supplementary Table 2**). In each treatment, the $\delta^{15}N$ values of all newly settled quagga mussels showed no significant differences from zebra mussels. Based on SEAc results, there were no overlaps in the isotopic niches between quagga and zebra mussels in each treatment.

DISCUSSION

The Community Composition of Newly Settled Macroinvertebrates

The reaction of newly settled macroinvertebrates toward the stone substrate treatments complimented the hypothesis of facilitative associations between invasive dreissenids (Ward and Ricciardi, 2007; Ozersky et al., 2011), wherein one species has a positive effect on the establishment of another species. For example, the highest mean density of macroinvertebrates was consistently found in substrate treatments with shells or living mussels. By implication, the presence of mussels or shells was driving significant variation across experiments. Given the uniform *in situ* physicochemical conditions for stone substrate, this variation could be attributed to differences in the presence or absence of zebra and quagga mussels and their respective shells. Indeed, such effects were anticipated, since macroinvertebrates have shown a positive reaction to the physical structure of mussel shells (Ricciardi et al., 1997; Burlakova et al., 2012).

The most frequent newly settled macroinvertebrate taxa in our study, *P. antipodarum*, *D. villosus,* and *Caenis* spp., were mainly present at comparatively higher densities on stone substrate shells (S) and living mussel treatments (Q and Z). The rarity of settling macroinvertebrates on blank stone treatments (B) clearly indicates the feasible benefit of macroinvertebrates from the effects provided. In all three cases, each taxon could indeed benefit from the increased complexity of the

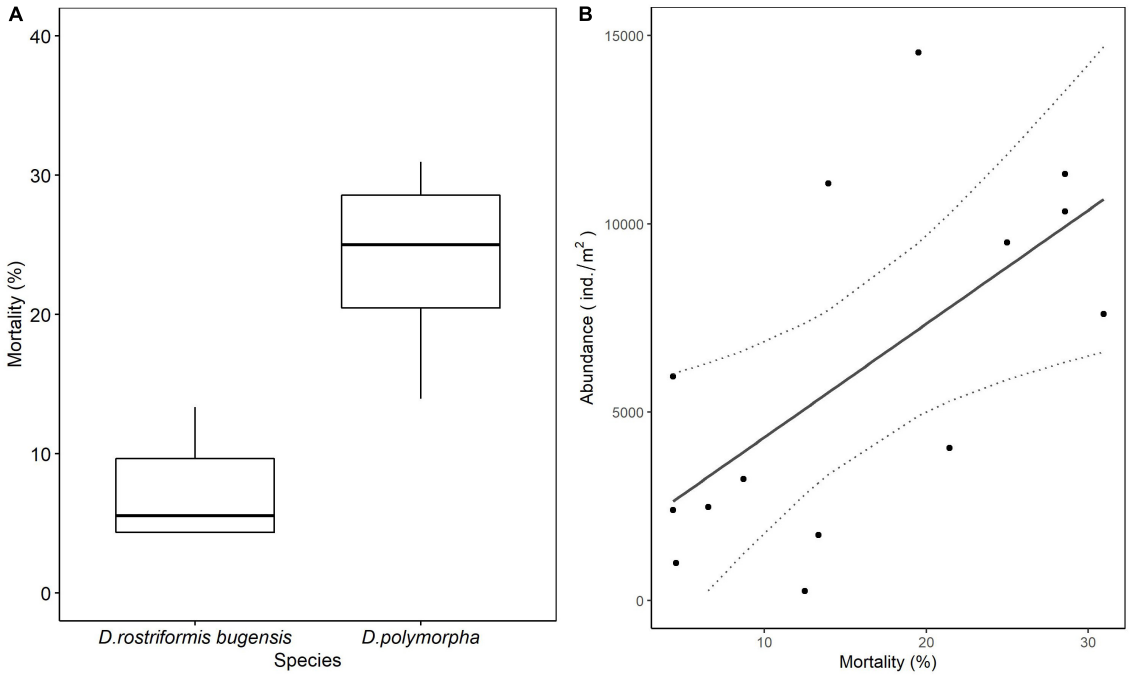

FIGURE 3 | (A) Mortality rates of adult living quagga and zebra mussels glued on the stone substrates. *D.rostriformis bugensis* is the adult mussel used in Q treatments and *D. ploymorpha* is the adult mussel used in Z treatments. **(B)** Linear regression (solid line) and the 95% confidence interval of the regression (dotted line) for abundances of newly settled chironomid larvae (subfamily Chironominae) and mortality rates of adult dreissenids.

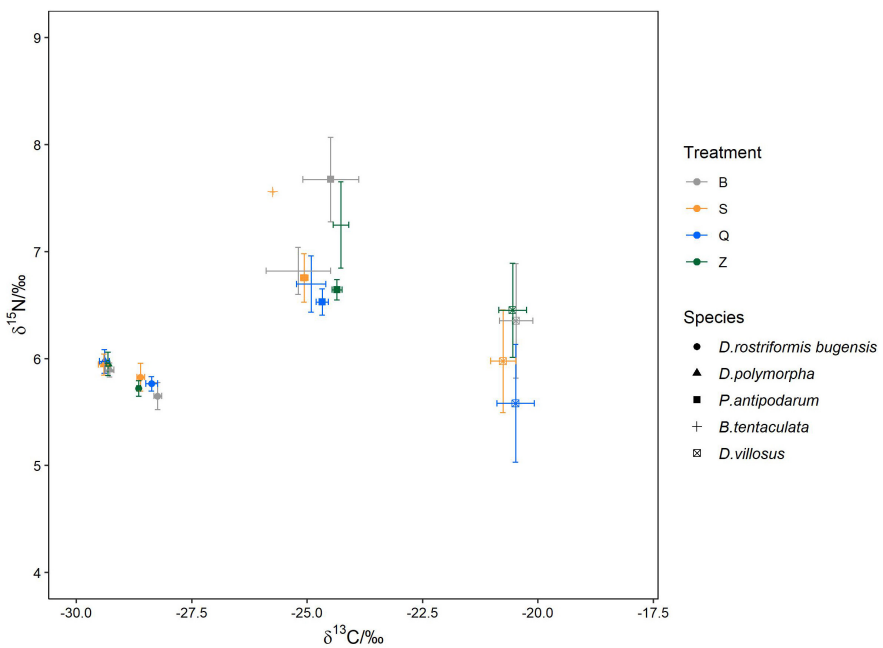

FIGURE 4 | The stable isotope bi-plots ($\delta^{13}C$ and $\delta^{15}N$) of five main newly settled macroinvertebrates in four different treatments. Error bars indicate standard errors.

substratum and surface area associated with natural dreissenid beds (Stewart et al., 1998; Ward and Ricciardi, 2007). Briefly, for *P. antipodarum*, shells may provide a bed substratum on which tubular refuges with protrusion could be constructed for grazing and scraping on detritus and sediments (Broekhuizen et al., 2001). In particular, the zebra mussel has shown mutualistic interactions with killer shrimp *D. villosus* and can benefit them in various ways. As shown during *ex situ* laboratory experiments

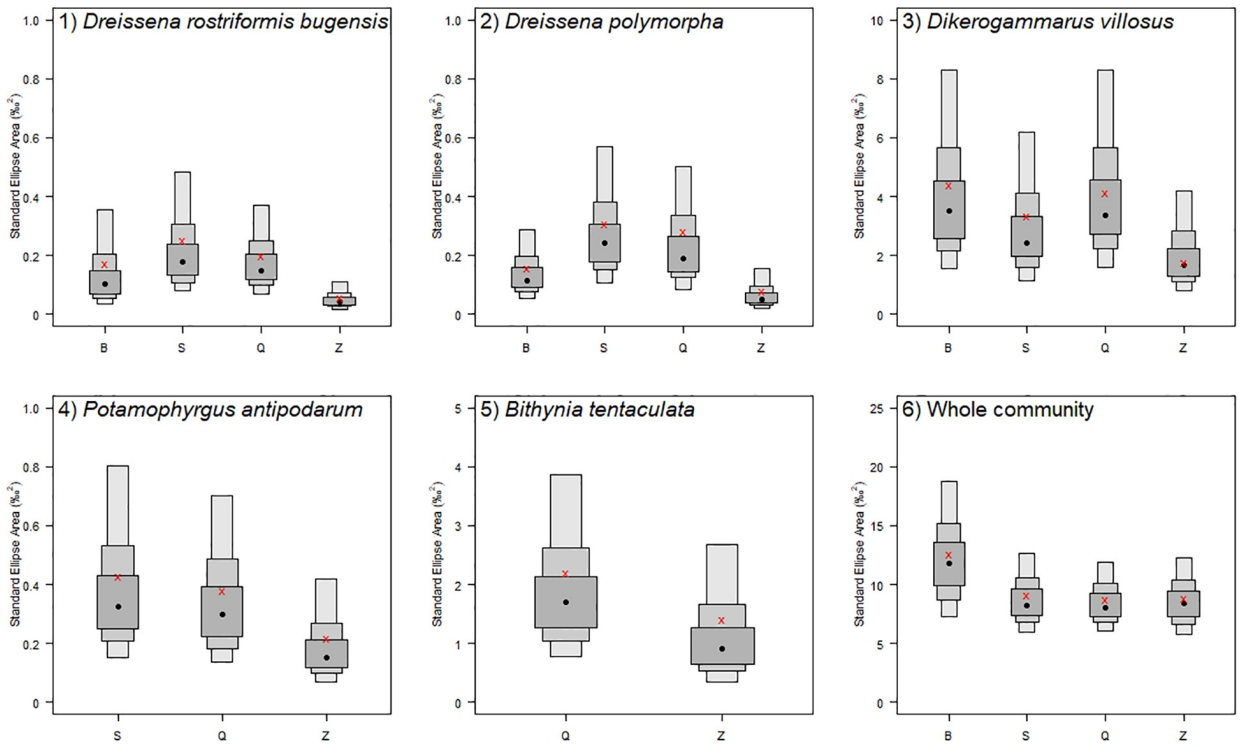

FIGURE 5 | Density plot showing the confidence intervals of the standard ellipse area for five main newly settled macroinvertebrates and the whole community in four different treatments (B, S, Q, and Z). Red crosses correspond to the sample size-corrected standard ellipse areas (SEAc). Boxes shaded from dark to light gray represent the 50, 75, and 95% confidence intervals.

on dreissenids, killer shrimp evidently utilizes mussel beds as protection from fish and allopatric predators more efficiently than other gammarids (Kobak et al., 2014). Similarly, juvenile zebra mussels can attach to the hard cover of the killer shrimp which could facilitate their dispersal (Yohannes et al., 2017), while the production of feces and pseudo-feces by zebra mussels may provide food (Klerks et al., 1996; Gergs and Rothhaupt, 2008). For *Caenis*, the taxon's size might have allowed the use of the physical structure of dreissenids as nearby refuges through the exploitation of small interstices that are typical characteristics of dreissenid beds (Werner and Rothhaupt, 2007).

Like most of the three numerically dominant species, the abundances of newly settled chironomid larvae of subfamily Chironominae were higher in response to the presence of living zebra mussels (Z treatments). However, this species was one of the few species that showed higher density in the absence of mussels (B treatment). Almost all the newly settled chironomid larvae in B treatment were rather small with the average width of head measuring less than 180 μm. The observed pattern is presumably linked to the natural temporal or seasonal life history patterns (in growth, size, and abundance of the species), and perhaps this response was evident due to the 4 weeks of methodological effect. The overall pattern of chironomid larvae abundance and richness from our experimental study reinforces previous findings that zebra mussels facilitate the growth of benthic macroinvertebrate communities. This is in complement with previous studies that showed that the abundance of chironomid larvae increased after the colonization of zebra mussels (Botts et al., 1996;

TABLE 2 | The differences in stable isotope values of newly settled macroinvertebrates among four different treatments.

Item	Taxon	Chi-squared	*p*	Rank order
$\delta^{13}C$				
	Dreissena rostriformis bugensis	10.36	0.016*	B > Z
	Dreissena polymorpha	0.59	0.898	n.s.
	Potamophyrgus antipodarum	10.66	0.014*	Z > S
	Bithynia tentaculata	4.91	0.179	n.s.
	Dikerogammarus villosus	0.61	0.895	n.s.
$\delta^{15}N$				
	Dreissena rostriformis bugensis	2.19	0.533	n.s.
	Dreissena polymorpha	0.47	0.925	n.s.
	Potamophyrgus antipodarum	4.91	0.179	n.s.
	Bithynia tentaculata	3.22	0.360	n.s.
	Dikerogammarus villosus	2.19	0.533	n.s.

*Kruskal–Wallis test is used to analyze the differences in stable isotope values among different treatments, and significant results of p-values ($p \leq 0.05$) are marked with *. Dunn's test is used for post hoc pairwise comparisons, the rank orders are based on the mean values of stable isotope values in each treatment, and only the pairs which are significantly different are shown in the table. n.s. means no significant differences.*

TABLE 3 | Sample size-corrected standard ellipse areas (SEAc) of five newly settled macro-invertebrates and whole community from the four different treatments.

Item	Treatment	SEAc (‰^{2})	Item	Treatment	SEAc (‰^{2})	Item	Treatment	SEAc (‰^{2})
Dreissena rostriformis bugensis	B	0.17	*Dreissena polymorpha*	B	0.16	*Dikerogammarus villosus*	B	4.40
	S	0.25		S	0.31		S	3.34
	Q	0.20		Q	0.28		Q	4.15
	Z	0.06		Z	0.08		Z	1.76
Potamophyrgus antipodarum	S	0.43	*Bitynia tentaculata*	Q	2.20	Whole community	B	12.56
	Q	0.38		Z	1.41		S	9.15
	Z	0.22					Q	8.76
							Z	8.80

Gergs and Rothhaupt, 2008). Nevertheless, the abundance of chironomid larvae in Z treatments was higher than in Q treatments (**Table 1**). The high mortality rate of glued adult zebra mussels than quagga mussels might contribute to the differences, as the animal remains are part of the diet for chironomid larvae (Johnson, 1987).

The results of our analysis using analog shell and live quagga mussels should well be noted again, wherein no significant difference in the abundance of all taxa between S treatments and Q treatments was observed. This finding suggests that macroinvertebrates might primarily respond to the physical structure of quagga mussel shells, as discussed in previous investigations (Botts et al., 1996; Burlakova et al., 2012).

Although zebra mussels invaded the lake first, the rapid expansion in the range of the invasive quagga mussel in Lake Constance has caused a dominance shift from zebra to quagga mussels. However, specific effects of live mussels could offer additive benefits for multiple taxa, including newly settled conspecific zebra and quagga mussels. In fact, taking the whole experimental setup into consideration, the entire abundance of newly settled quagga mussels was higher than the entire abundance of newly settled zebra mussels. These data coupled with the current field observation in Lake Constance indicate that this and/or other similar facilitative invasions do cause major changes in biodiversity and ecosystem. The higher mortality rate of adult zebra mussels than adult quagga mussels may also contribute to the dominance shift. We also observed, based on a laboratory study (own unpublished data), that the quagga mussel has a faster growth rate than the zebra mussel.

Our experiment was conducted in 2018, only 2 years after the initial record of quagga mussels in the lake. Nevertheless, as shown by prior studies in other invaded systems, such initial reactions of macroinvertebrate communities toward dreissenids might reduce after several years (Strayer and Malcom, 2006; Karatayev et al., 2015). At the current particular population levels (5,708 ind./m^2), we may conclude that quagga mussels would significantly impact the structure of the benthic community in this system. Indeed, this initial establishment of the species at this littoral site could be considered surprising; however, the highest densities of invasive populations have been recorded in higher depths of North American lakes, such as 342,000, 75,000, and 16,000 ind./m^2 in Lakes Erie, Huron, and Michigan, respectively (Nalepa, 1995; Howell et al., 1996; Nalepa et al., 2009).

Food Resources of Newly Settled Macroinvertebrates

We were able to note significant differences in the food resources of newly settled macroinvertebrates using mainly δ^{13}C values (Layman et al., 2012). Among the four treatments applied, the newly settled quagga mussels in B treatments showed higher δ^{13}C values than in Z treatments, which was probably related to the smaller size of newly settled quagga mussels in B treatments ($p < 0.001$). The newly settled snail *P. antipodarum* is known as a grazer and feeds on periphyton (Larson and Ross Black, 2016), and as expected, showed higher δ^{13}C values in Z treatments than in S treatments, thus the higher mortality of the adult zebra mussels in Z treatments may have generated a different nutrient resource. Comparing Q treatments and the other treatments, there were no significant differences in δ^{13}C and δ^{15}N values of newly settled macroinvertebrates. Previous studies by Gergs et al. (2011) found that the stable isotope values of gammarids were significantly and positively related to the biodeposition of zebra mussels. Here, the presence of the adult quagga mussels did not show a strong influence on the isotope values of the newly settled macroinvertebrates, which might be related to the smaller study area (experiment) and shorter study (invasion) period than the previous study.

Nonetheless, the newly settled quagga mussels had significantly higher δ^{13}C values than the newly settled zebra mussels in each treatment. Quagga and zebra mussels attained from shallow depth of Lake Constance in 2018 also showed higher δ^{13}C values of quagga mussels than that of zebra mussels (own unpublished data). The diet of dreissenids can be very flexible, and contains phytoplankton and suspended detritus (Garton et al., 2005). The benthic primary producers normally have a higher δ^{13}C value compared to pelagic primary producers (more negative) (France, 1995; Mitchell et al., 1996). In our study period, the newly settled quagga mussels might consume a higher percentage of benthic food or a lower percentage of pelagic food, in comparison to newly settled zebra mussels. A similar result showed that after the invasion by smallmouth bass and rock bass, lake trout switched to consuming a lower percentage of littoral prey and had a lower δ^{13}C value than the reference lakes (vander Zanden et al., 1999). One study found that the δ^{13}C values of quagga mussels are more negative than those of zebra mussels (Verhofstad et al., 2013), and the explanation was that quagga

mussels consumed more chemoautotrophs which have highly reduced $\delta^{13}C$ values. The difference between our study and the study of Verhofstad et al. (2013) may be due to the differences in the substrates, depth ranges, or measurements. Some other studies did not find any difference in the stable isotope values between quagga and zebra mussels (Garton et al., 2005).

No overlaps in the isotopic niche of quagga and zebra mussels were observed in our field experiment. The lengths of newly settled quagga and zebra mussels in S, Q, and Z treatments did not show significant differences, thus the differences in stable isotope values of quagga and zebra mussels were not caused by the differences in the size of dreissenids. At our study site where quagga and zebra mussels coexisted, the dietary segregation or partition of colonized space may be the mechanism for the co-existence of quagga and zebra mussels (Diggins et al., 2004; Rothhaupt et al., 2014). Our experiment was conducted in 2018 in Lake Constance, only 2 years after the first record of quagga mussels. During the early colonization period, quagga mussels might occupy a different niche from zebra mussels to reduce resource competition with zebra mussels (Jackson and Britton, 2014).

CONCLUSION

In our study, the abundance of gastropods, gammarids, and some insect larvae increased with the presence of dreissenid shells in the littoral region. The macroinvertebrate communities might change after quagga mussels replace zebra mussels and occupy a high percentage in the total biomass of benthic macroinvertebrates, particularly in deep regions where adult quagga mussels can also live (Mills et al., 1993; Nalepa et al., 2020). After the invasion of dreissenids in the Great Lakes, the abundance of dressenids increased in the profundal region; however, the abundance of non-dreissenid profundal macroinvertebrates decreased, which is different from the changes in the littoral region (Burlakova et al., 2018). In our study, there was apparent niche partitioning between newly settled quagga and zebra mussels. The interesting patterns of dietary segregation between quagga and zebra mussels might be a common phenomenon in the early stage of quagga mussel invasions when the two dreissenids coexisted in lakes. These results provide a benchmark by which future changes in trophic ecology and invasion dynamics can be measured across the ecosystem. However, for future experiments, we recommend a longer stone substrate deployment duration encompassing standardized seasonal periods for individual species to achieve stabilized assemblages of wider coverage of macroinvertebrates. Yet, this study offers the first overview of the quagga mussel's progressive invasion and the reaction of the zebra mussels and other newly settled macroinvertebrates, and contributes to the hypothesis of facilitative associations between invasive mussel species.

In summary, following the occurrence of quagga mussels in Lake Constance, significant changes in the benthic macroinvertebrate community are observed. Only about 5 years after the first detection of quagga mussel, it has become the most dominant macroinvertebrate in the littoral area of the lake. A recent study that analyzed the stomach content showed that benthic whitefish (*Coregonus macrophthalmus*), roach (*Rutilus rutilus*), and tench (*Tinca tinca*) showed high levels of consumption of quagga mussels (Baer et al., 2022). Although equivalent and empirical data on the actual impact of the invasive mussels on the accompanying macroinvertebrates are not available, these dietary shifts observed in multiple benthic dwelling fish species imply alternation in the dietary sources following quagga mussel colonization in Lake Constance.

DATA AVAILABILITY STATEMENT

The raw data supporting the conclusions of this article will be made available by the authors, without undue reservation.

AUTHOR CONTRIBUTIONS

K-OR, EY, and HZ designed the field experiment. K-OR secured the funding for the project. HZ conducted the field experiment, counted the macroinvertebrate samples, and prepared the samples for stable isotope analysis. HZ analyzed the data with guidance from EY and K-OR. HZ and EY wrote the draft. All authors revised the draft, read, and approved the submitted version.

FUNDING

This project was supported by funding from the Limnological Institute, University of Konstanz (AFF grant to K-OR). HZ received funding from the Chinese Scholarship Council (grant no. 201704910903) for a living stipend.

ACKNOWLEDGMENTS

We would like to thank Christian Fiek for his great help with conducting the experiment and counting macroinvertebrates. Ioanna Salvarina also provided guidance for counting macroinvertebrates. We would also like to thank Wolfgang Kornberger, Yao Zhiyijun, Christian Hanke, and Robert van Geldern for their assistance in the stable isotope analysis of the macroinvertebrates and the members of SeeWandel: Life in Lake Constance – the past, present and future for valuable discussions about the experiment. Martin Wolf also helped with the preparation of stone substrates for the experiment.

SUPPLEMENTARY MATERIAL

The Supplementary Material for this article can be found online at: https://www.frontiersin.org/articles/10.3389/fevo.2022.887191/full#supplementary-material

REFERENCES

Baer, J., Spiessl, C., Auerswald, K., Geist, J., and Brinker, A. (2022). Signs of the times: isotopic signature changes in several fish species following invasion of Lake Constance by quagga mussels. *J. Great Lakes Res.* 48, 746–755. doi: 10.1016/j.jglr.2022.03.010

Bially, A., and MacIsaac, H. J. (2000). Fouling mussels (*Dreissena spp.*) colonize soft sediments in Lake Erie and facilitate benthic invertebrates. *Freshwater Biol.* 43, 85–97. doi: 10.1046/j.1365-2427.2000.00526.x

Boltovskoy, D., and Correa, N. (2015). Ecosystem impacts of the invasive bivalve *Limnoperna fortunei* (golden mussel) in South America. *Hydrobiologia* 746, 81–95. doi: 10.1007/s10750-014-1882-1889

Botts, P. S., Patterson, B. A., and Schloesser, D. W. (1996). Zebra mussel effects on benthic invertebrates: physical or biotic? *J. North Am. Benthol. Soc.* 15, 179–184. doi: 10.2307/1467947

Broekhuizen, N., Parkyn, S., and Miller, D. (2001). Fine sediment effects on feeding and growth in the invertebrate grazers *Potamopyrgus antipodarum* (Gastropoda, Hydrobiidae) and *Deleatidium sp*. (Ephemeroptera, Leptophlebiidae). *Hydrobiologia* 457, 125–132. doi: 10.1023/A:1012223332472

Burlakova, L. E., Barbiero, R. P., Karatayev, A. Y., Daniel, S. E., Hinchey, E. K., and Warren, G. J. (2018). The benthic community of the Laurentian Great Lakes: analysis of spatial gradients and temporal trends from 1998 to 2014. *J. Great Lakes Res.* 44, 600–617. doi: 10.1016/j.jglr.2018.04.008

Burlakova, L. E., Karatayev, A. Y., and Karatayev, V. A. (2012). Invasive mussels induce community changes by increasing habitat complexity. *Hydrobiologia* 685, 121–134. doi: 10.1007/s10750-011-0791-794

Burlakova, L. E., Tulumello, B. L., Karatayev, A. Y., Krebs, R. A., Schloesser, D. W., Paterson, W. L., et al. (2014). Competitive replacement of invasive congeners may relax impact on native species: interactions among zebra, quagga, and native unionid mussels. *PLoS One* 9:e114926. doi: 10.1371/journal.pone.0114926

Byers, J. E., Reichard, S., Randall, J. M., Parker, I. M., Smith, C. S., Lonsdale, W. M., et al. (2002). Directing research to reduce the impacts of nonindigenous species. *Conservation Biol.* 16, 630–640. doi: 10.1046/j.1523-1739.2002.01057.x

Catry, T., Lourenço, P. M., Lopes, R. J., Carneiro, C., Alves, J. A., Costa, J., et al. (2016). Structure and functioning of intertidal food webs along an avian flyway: a comparative approach using stable isotopes. *Funct. Ecol.* 30, 468–478. doi: 10.1111/1365-2435.12506

Copp, G. H., Vilizzi, L., Mumford, J., Fenwick, G. V., Godard, M. J., and Gozlan, R. E. (2009). Calibration of FISK, an invasiveness screening tool for nonnative freshwater fishes. *Risk Anal.* 29, 457–467. doi: 10.1111/j.1539-6924.2008.01159.x

Crooks, J. A. (2005). Lag times and exotic species: the ecology and management of biological invasions in slow-motion. *Ecoscience* 12, 316–329. doi: 10.2980/i1195-6860-12-3-316.1

Diggins, T. P., Weimer, M., Stewart, K. M., Baier, R. E., Meyer, A. E., Forsberg, R. F., et al. (2004). Epiphytic refugium: are two species of invading freshwater bivalves partitioning spatial resources? *Biol. Invasions* 6, 83–88.

Evariste, L., David, E., Cloutier, P. L., Brousseau, P., Auffret, M., Desrosiers, M., et al. (2018). Field biomonitoring using the zebra mussel *Dreissena polymorpha* and the quagga mussel *Dreissena bugensis* following immunotoxic reponses. is there a need to separate the two species? *Environ. Pollut.* 238, 706–716. doi: 10.1016/j.envpol.2018.03.098

France, R. L. (1995). Differentiation between littoral and pelagic food webs in lakes using stable carbon isotopes. *Limnol. Oceanography* 40, 1310–1313. doi: 10.4319/lo.1995.40.7.1310

Francis, R. A., and Chadwick, M. A. (2012). "Invasive alien species in freshwater ecosystems: a brief overview," in *A Handbook of Global Freshwater Invasive Species*, ed. R. A. Francis (Abingdon: Earthscan), 3–21. doi: 10.1093/icb/icaa023

Garton, D. W., Payne, C. D., and Montoya, J. P. (2005). Flexible diet and trophic position of dreissenid mussels as inferred from stable isotopes of carbon and nitrogen. *Canadian J. Fisheries Aquatic Sci.* 62, 1119–1129. doi: 10.1139/f05-025

Gergs, R., and Rothhaupt, K. O. (2008). Effects of zebra mussels on a native amphipod and the invasive *Dikerogammarus villosus*: the influence of biodeposition and structural complexity. *J. North Am. Benthol. Soc.* 27, 541–548. doi: 10.1899/07-151.1

Gergs, R., and Rothhaupt, K. O. (2015). Invasive species as driving factors for the structure of benthic communities in Lake Constance, Germany. *Hydrobiologia* 746, 245–254. doi: 10.1007/s10750-014-1931-1934

Gergs, R., Grey, J., and Rothhaupt, K. O. (2011). Temporal variation in zebra mussel (*Dreissena polymorpha*) density structure the benthic food web and community composition on hard substrates in Lake Constance, Germany. *Biol. Invasions* 13, 2727–2738. doi: 10.1007/s10530-011-9943-9948

Gherardi, F., and Acquistapace, P. (2007). Invasive crayfish in Europe: the impact of *Procambarus clarkii* on the littoral community of a Mediterranean lake. *Freshwater Biol.* 52, 1249–1259. doi: 10.1111/j.1365-2427.2007.01760.x

González, M. J., and Downing, A. (1999). Mechanisms underlying amphipod responses to zebra mussel (*Dreissena polymorpha*) invasion and implications for fish-amphipod interactions. *Canadian J. Fisheries Aquatic Sci.* 56, 679–685. doi: 10.1139/f98-211

Haltiner, L., Zhang, H., Anneville, O., de Ventura, L., DeWeber, T. J., Hesselschwerdt, J., et al. (2022). The distribution and spread of quagga mussels in perialpine lakes north of the Alps. *Aquatic Invasions* 17, 153–173. doi: 10.3391/ai.2022.17.2.02

Howell, E. T., Marvin, C. H., Bilyea, R. W., Kauss, P. B., and Somers, K. (1996). Changes in environmental conditions during *Dreissena* colonization of a monitoring station in eastern Lake Erie. *J. Great Lakes Res.* 22, 744–756. doi: 10.1016/S0380-1330(96)70993-70990

Jackson, A. L., Inger, R., Parnell, A. C., and Bearhop, S. (2011). Comparing isotopic niche widths among and within communities: SIBER - Stable Isotope Bayesian Ellipses in R. *J. Animal Ecol.* 80, 595–602. doi: 10.1111/j.1365-2656.2011.01806.x

Jackson, M. C., and Britton, J. R. (2014). Divergence in the trophic niche of sympatric freshwater invaders. *Biol. Invasions* 16, 1095–1103. doi: 10.1007/s10530-013-0563-563

Johnson, R. K. (1987). Seasonal variation in diet of *Chironomus plumosus* (L.) and *C.anthracinus* Zett. (Diptera-Chironomidae) in mesotrophic Lake Erken. *Freshwater Biol.* 17, 525–532. doi: 10.1111/j.1365-2427.1987.tb01073.x

Jones, P. E., Tummers, J. S., Galib, S. M., Woodford, D. J., Hume, J. B., Silva, L. G. M., et al. (2021). The use of barriers to limit the spread of aquatic invasive animal species: a global review. *Front. Ecol. Evol.* 9:611631. doi: 10.3389/fevo.2021.611631

Karatayev, A. Y., Burlakova, L. E., and Padilla, D. K. (2015). Zebra versus quagga mussels: a review of their spread, population dynamics, and ecosystem impacts. *Hydrobiologia* 746, 97–112. doi: 10.1007/s10750-014-1901-x

Karatayev, A. Y., Karatayev, V. A., Burlakova, L. E., Mehler, K., Rowe, M. D., Elgin, A. K., et al. (2021). Lake morphometry determines *Dreissena* invasion dynamics. *Biol. Invasions* 23, 2489–2514. doi: 10.1007/s10530-021-02518-2513

Kerambrun, E., Delahaut, L., Geffard, A., and David, E. (2018). Differentiation of sympatric zebra and quagga mussels in ecotoxicological studies: a comparison of morphometric data, gene expression, and body metal concentrations. *Ecotoxicol. Environ. Saf.* 154, 321–328. doi: 10.1016/j.ecoenv.2018.02.051

Klerks, P., Fraleigh, P. C., and Lawniczak, E. (1996). Effects of zebra mussels (*Dreissena polymorpha*) on seston levels and sediment deposition in western Lake Erie. *Canadian J. Fisheries Aquatic Sci.* 53, 2284–2291. doi: 10.1139/f96-190

Kobak, J., Jermacz, Ł, and Płąchocki, D. (2014). Effectiveness of zebra mussels to act as shelters from fish predators differs between native and invasive amphipod prey. *Aquatic Ecol.* 48, 397–408. doi: 10.1007/s10452-014-9492-9491

Kobak, J., Kakareko, T., Jermacz, Ł, and Poznańska, M. (2013). The impact of zebra mussel (*Dreissena polymorpha*) periostracum and biofilm cues on habitat selection by a Ponto-Caspian amphipod *Dikerogammarus haemobaphes*. *Hydrobiologia* 702, 215–226. doi: 10.1007/s10750-012-1322-1327

Kulhanek, S. A., Leung, B., and Ricciardi, A. (2011). Using ecological niche models to predict the abundance and impact of invasive species: application to the common carp. *Ecol. Appl.* 21, 203–213. doi: 10.1890/09-1639.1

Larson, M. D., and Ross Black, A. (2016). Assessing interactions among native snails and the invasive New Zealand mud snail, *Potamopyrgus antipodarum*, using grazing experiments and stable isotope analysis. *Hydrobiologia* 763, 147–159. doi: 10.1007/s10750-015-2369-z

Layman, C. A., Araujo, M. S., Boucek, R., Hammerschlag-Peyer, C. M., Harrison, E., Jud, Z. R., et al. (2012). Applying stable isotopes to examine food-web structure: an overview of analytical tools. *Biol. Rev.* 87, 545–562. doi: 10.1111/j.1469-185X.2011.00208.x

Lodge, D. M., Stein, R. A., Brown, K. M., Covich, A. R., Christer, B., Garvey, J. E., et al. (1998). Predicting impact of freshwater exotic species on native biodiversity: challenges in spatial scaling. *Australian J. Ecol.* 23, 53–67. doi: 10.1111/j.1442-9993.1998.tb00705.x

MacIsaac, H. J. (1996). Potential abiotic and biotic impacts of zebra mussels on the inland waters of North America. *Am. Zool.* 36, 287–299. doi: 10.1093/icb/36.3.287

Mills, E. L., Dermott, R. M., Roseman, E. F., Dustin, D., Mellina, E., Conn, D. B., et al. (1993). Colonization, ecology, and population structure of the "quagga" mussel (Bivalvia: Dreissenidae) in the Lower Great Lakes. *Canadian J. Fisheries Aquatic Sci.* 50, 2305–2314. doi: 10.1139/f93-255

Mitchell, M. J., Mills, E. L., Idrisi, N., and Michener, R. (1996). Stable isotopes of nitrogen and carbon in an aquatic food web recently invaded by *Dreissena polymorpha* (Pallas). *Canadian J. Fisheries Aquatic Sci.* 53, 1445–1450. doi: 10.1139/f96-053

Molloy, D. P., Bij, De Vaate, A., Wilke, T., and Giamberini, L. (2007). Discovery of *Dreissena rostriformis* bugensis (Andrusov 1897) in Western Europe. *Biol. Invasions* 9, 871–874. doi: 10.1007/s10530-006-9078-9075

Mörtl, M., and Rothhaupt, K. O. (2003). Effects of adult *Dreissena polymorpha* on settling juveniles and associated macroinvertebrates. *Int. Rev. Hydrobiol.* 88, 561–569. doi: 10.1002/iroh.200310640

Nalepa, T. F. (1995). Initial colonization of the zebra mussel (*Dreissena polymorpha*) in Sagniaw Bay, Lake Huron: population recruitment, density, and size structure. *J. Great Lakes Res.* 21, 417–434.

Nalepa, T. F., Burlakova, L. E., Elgin, A. K., and Karatayev, A. Y. (2020). Abundance and biomass of benthic macroinvertebrates in Lake Michigan in 2015, with a summary of temporal trends. *NOAA Techn. Memorandum GLERL* 175, 1–41. doi: 10.25923/g0d3-3v41

Nalepa, T. F., Fanslow, D. L., and Lang, G. A. (2009). Transformation of the offshore benthic community in Lake Michigan: recent shift from the native amphipod *Diporeia spp*. to the invasive mussel *Dreissena rostriformis* bugensis. *Freshwater Biol.* 54, 466–479. doi: 10.1111/j.1365-2427.2008.02123.x

Ozersky, T., Barton, D. R., and Evans, D. O. (2011). Fourteen years of dreissenid presence in the rocky littoral zone of a large lake: effects on macroinvertebrate abundance and diversity. *J. North Am. Benthol. Soc.* 30, 913–922. doi: 10.1899/10-122.1

Pathy, D. A., and Mackie, G. L. (1993). Comparative shell morphology of *Dreissena polymorpha*, *Mytilopsis leucophaeata*, and the "quagga" mussel (Bivalvia: Dreissenidae) in North America. *Canadian J. Zool.* 71, 1012–1023. doi: 10.1139/z93-135

Post, D. M., Layman, C. A., Arrington, D. A., Takimoto, G., Quattrochi, J., and Montaña, C. G. (2007). Getting to the fat of the matter: models, methods and assumptions for dealing with lipids in stable isotope analyses. *Oecologia* 152, 179–189. doi: 10.1007/s00442-006-0630-x

R Core Team (2021). *R: A Language and Environmental for Statistical Computing*. Vienna: R Foundation for Statistical Computing.

Ricciardi, A. (2003). Predicting the impacts of an introduced species from its invasion history: an empirical approach applied to zebra mussel invasions. *Freshwater Biol.* 48, 972–981. doi: 10.1046/j.1365-2427.2003.01071.x

Ricciardi, A., Hoopes, M. F., Marchetti, M. P., and Lockwood, J. L. (2013). Progress toward understanding the ecological impacts of nonnative species. *Ecol. Monographs* 83, 263–282. doi: 10.1890/13-0183.1

Ricciardi, A., Whoriskey, F. G., and Rasmussen, J. B. (1997). The role of the zebra mussel (*Dreissena polymorpha*) in structuring macroinvertebrate communities on hard substrata. *Canadian J. Fisheries Aquatic Sci.* 54, 2596–2608. doi: 10.1139/f97-174

Roby, K. B., Newbold, J. D., and Erman, D. C. (1978). Effectiveness of an artificial substrate for sampling macroinvertebrates in small streams. *Freshwater Biol.* 8, 1–8. doi: 10.1111/j.1365-2427.1978.tb01420.x

Rothhaupt, K. O., Hanselmann, A. J., and Yohannes, E. (2014). Niche differentiation between sympatric alien aquatic crustaceans: an isotopic evidence. *Basic Appl. Ecol.* 15, 453–463. doi: 10.1016/j.baae.2014.07.002

Roy, H. E., Peyton, J., Aldridge, D. C., Bantock, T., Blackburn, T. M., Britton, R., et al. (2014). Horizon scanning for invasive alien species with the potential to threaten biodiversity in Great Britain. *Global Change Biol.* 20, 3859–3871. doi: 10.1111/gcb.12603

Simberloff, D., and von Holle, B. (1999). Positive interactions of nonindigenous species: invasional meltdown? *Biol. Invasions* 1, 21–32. doi: 10.1023/A:1010086329619

Son, M. O. (2007). Native range of the zebra mussel and quagga mussel and new data on their invasions within the Ponto-Caspian Region. *Aquatic Invasions* 2, 174–184. doi: 10.3391/ai.2007.2.3.4

Sousa, R., Pilotto, F., and Aldridge, D. C. (2011). Fouling of European freshwater bivalves (Unionidae) by the invasive zebra mussel (*Dreissena polymorpha*). *Freshwater Biol.* 56, 867–876. doi: 10.1111/j.1365-2427.2010.02532.x

Stewart, T. W., Miner, J. G., and Lowe, R. L. (1998). Quantifying mechanisms for zebra mussel effects on benthic macroinvertebrates: organic matter production and shell-generated habitat. *J. North Am. Benthol Soc.* 17, 81–94. doi: 10.2307/1468053

Stiers, I., Crohain, N., Josens, G., and Triest, L. (2011). Impact of three aquatic invasive species on native plants and macroinvertebrates in temperate ponds. *Biol. Invasions* 13, 2715–2726. doi: 10.1007/s10530-011-9942-9949

Strayer, D. L., and Malcom, H. M. (2006). Long-term demography of a zebra mussel (*Dreissena polymorpha*) population. *Freshwater Biol.* 51, 117–130. doi: 10.1111/j.1365-2427.2005.01482.x

Strayer, D. L., and Malcom, H. M. (2007). Effects of zebra mussels (*Dreissena polymorpha*) on native bivalves: the beginning of the end or the end of the beginning? *J. North Am. Benthol Soc.* 26, 111–122.

Strayer, D. L., and Malcom, H. M. (2018). Long-term responses of native bivalves (Unionidae and Sphaeriidae) to a *Dreissena* invasion. *Freshwater Sci.* 37, 697–711. doi: 10.1086/700571

Strayer, D. L., Fischer, D. T., Hamilton, S. H., Malcom, H. M., Pace, M. L., and Solomon, C. T. (2020). Long-term variability and density dependence in Hudson River Dreissena populations. *Freshwater Biol.* 65, 474–489. doi: 10.1111/fwb.13444

Tran, T. N. Q., Jackson, M. C., Sheath, D., Verreycken, H., and Britton, J. R. (2015). Patterns of trophic niche divergence between invasive and native fishes in wild communities are predictable from mesocosm studies. *J. Animal Ecol.* 84, 1071–1080. doi: 10.1111/1365-2656.12360

vander Zanden, M. J., Casselman, J. M., and Rasmussen, J. B. (1999). Stable isotope evidence for the food web consequences of species invasions in lakes. *Nature* 401, 464–467. doi: 10.1038/46762

Verhofstad, M. J., Grutters, B. M. C., van der Velde, G., and Leuven, R. S. E. W. (2013). Effects of water depth on survival, condition and stable isotope values of three invasive dreissenid species in a deep freshwater lake. *Aquatic Invasions* 8, 157–169. doi: 10.3391/ai.2013.8.2.04

Walz, N. (1973). Studies on the biology of *Dreissena polymorpha* in Lake Constance. *Arch. Hydrobiol. Suppl.* 42, 452–482.

Ward, J. M., and Ricciardi, A. (2007). Impacts of *Dreissena* invasions on benthic macroinvertebrate communities: a meta-analysis. *Diversity Distrib.* 13, 155–165. doi: 10.1111/j.1472-4642.2007.00336.x

Werner, S., and Rothhaupt, K.-O. (2007). Effects of the invasive bivalve *Corbicula fluminea* on settling juveniles and other benthic taxa. *J. North Am. Benthol Soc.* 26, 673–680. doi: 10.1899/07-017R.1

Williamson, M. (1999). Invasions. *Ecography* 22, 5–12. doi: 10.1111/j.1600-0587.1999.tb00449.x

Wise, D. H., and Molles, M. C. (1979). Colonization of artificial substrates by stream insects: influence of substrate size and diversity. *Hydrobiologia* 65, 69–74. doi: 10.1007/BF00032721

Yohannes, E., Ragg, R. B., Armbruster, J. P., and Rothhaupt, K. O. (2017). Physical attachment of the invasive zebra mussel *Dreissena polymorpha* to the invasive gammarid *Dikerogammarus villosus*: supplementary path for invasion and expansion? *Fundamental Appl. Limnol.* 191, 79–85. doi: 10.1127/fal/2017/1063

Conflict of Interest: The authors declare that the research was conducted in the absence of any commercial or financial relationships that could be construed as a potential conflict of interest.

Publisher's Note: All claims expressed in this article are solely those of the authors and do not necessarily represent those of their affiliated organizations, or those of the publisher, the editors and the reviewers. Any product that may be evaluated in this article, or claim that may be made by its manufacturer, is not guaranteed or endorsed by the publisher.

Copyright © 2022 Zhang, Yohannes and Rothhaupt. This is an open-access article distributed under the terms of the Creative Commons Attribution License (CC BY). The use, distribution or reproduction in other forums is permitted, provided the original author(s) and the copyright owner(s) are credited and that the original publication in this journal is cited, in accordance with accepted academic practice. No use, distribution or reproduction is permitted which does not comply with these terms.

frontiers | Frontiers in Ecology and Evolution

ORIGINAL RESEARCH
published: 13 June 2022
doi: 10.3389/fevo.2022.886372

Altered Energy Mobilization Within the Littoral Food Web in New Habitat Created by Climate-Induced Changes in Lake Water Level

Kang Wang[1,2], Kangshun Zhao[1], Xiong Xiong[1], Huan Zhu[1], Hongyi Ao[1], Kaili Ma[3], Zhicai Xie[1], Chenxi Wu[1], Huan Wang[1], Huan Zhang[1]*, Peiyu Zhang[1]* and Jun Xu[1]**

[1] State Key Laboratory of Freshwater Ecology and Biotechnology of China, Institute of Hydrobiology, Chinese Academy of Sciences, Wuhan, China, [2] College of Advanced Agricultural Sciences, University of Chinese Academy of Sciences, Beijing, China, [3] Research Monitoring and Evaluation Center of Qinghai National Park, Xining, China

OPEN ACCESS

Edited by:
Gabriele Stowasser,
British Antarctic Survey (BAS),
United Kingdom

Reviewed by:
Herwig Stibor,
Ludwig Maximilian University of Munich, Germany
Christian Henri Nozais,
Université du Québec à Rimouski, Canada

***Correspondence:**
Huan Wang
wanghuan@ihb.ac.cn
Huan Zhang
zhanghuan@ihb.ac.cn
Peiyu Zhang
zhangpeiyu@ihb.ac.cn
Jun Xu
xujun@ihb.ac.cn

Specialty section:
This article was submitted to Population, Community, and Ecosystem Dynamics, a section of the journal Frontiers in Ecology and Evolution

Received: 28 February 2022
Accepted: 24 May 2022
Published: 13 June 2022

Citation:
Wang K, Zhao K, Xiong X, Zhu H, Ao H, Ma K, Xie Z, Wu C, Wang H, Zhang H, Zhang P and Xu J (2022) Altered Energy Mobilization Within the Littoral Food Web in New Habitat Created by Climate-Induced Changes in Lake Water Level. Front. Ecol. Evol. 10:886372. doi: 10.3389/fevo.2022.886372

Littoral zones in oligotrophic lakes play an essential role in supporting animal consumers and in the exchange of matter between the water body and the terrestrial sources, but are easily altered by changes in water level. We studied Qinghai Lake, a deep oligotrophic lake in northwest China, where lake water level has increased rapidly in recent years, altering the character of the littoral zones. We sampled common organisms and used stable carbon and nitrogen isotope analyses to compare how contributions of different sources (allochthonous and autochthonous) to the diets of consumers differed between sand (original habitat, OH) and submerged grassland (new habitat, NH) substrate habitat conditions. Our results showed that allochthonous resources (i.e., terrestrial detritus) constituted the largest diet proportion of consumers in OH due to poor nutrient conditions, while consumers in NH utilized more autochthonous resources (i.e., *Cladophora* and phytoplankton). We also found that terrestrial nutrient subsidies from soil and decomposed grass led to increased biomasses of *Cladophora*, phytoplankton, zooplankton and zoobenthos in NH compared to those in OH, accounting for autochthonous replacement of part of the allochthonous resources in NH. Therefore, hydrological conditions may alter the trophic interactions within littoral food webs, contributing to a more complex and interconnected food web. Overall, our results suggest that the littoral food webs of Qinghai Lake are vulnerable to changes in hydrological conditions, which may be enhanced by climate change.

Keywords: climate change, food webs, stable isotopes, terrestrial subsidies, *Cladophora*, Qinghai Lake

INTRODUCTION

Lakes provide a range of services for human beings, and are also a key component of global biogeochemical, ecological and hydrological processes (Fan et al., 2021). Lakes are also sensitive to changes in climate (Tao et al., 2020; Woolway et al., 2020), which can lead to significant changes in the water level, water storage and inundation area of lakes (Tao et al., 2020). For instance, the amount of water storage on the Tibetan Plateau has increased, and most lakes in the region are increasing in size in response to these changes (Huang et al., 2011; Zhang et al., 2017). Such

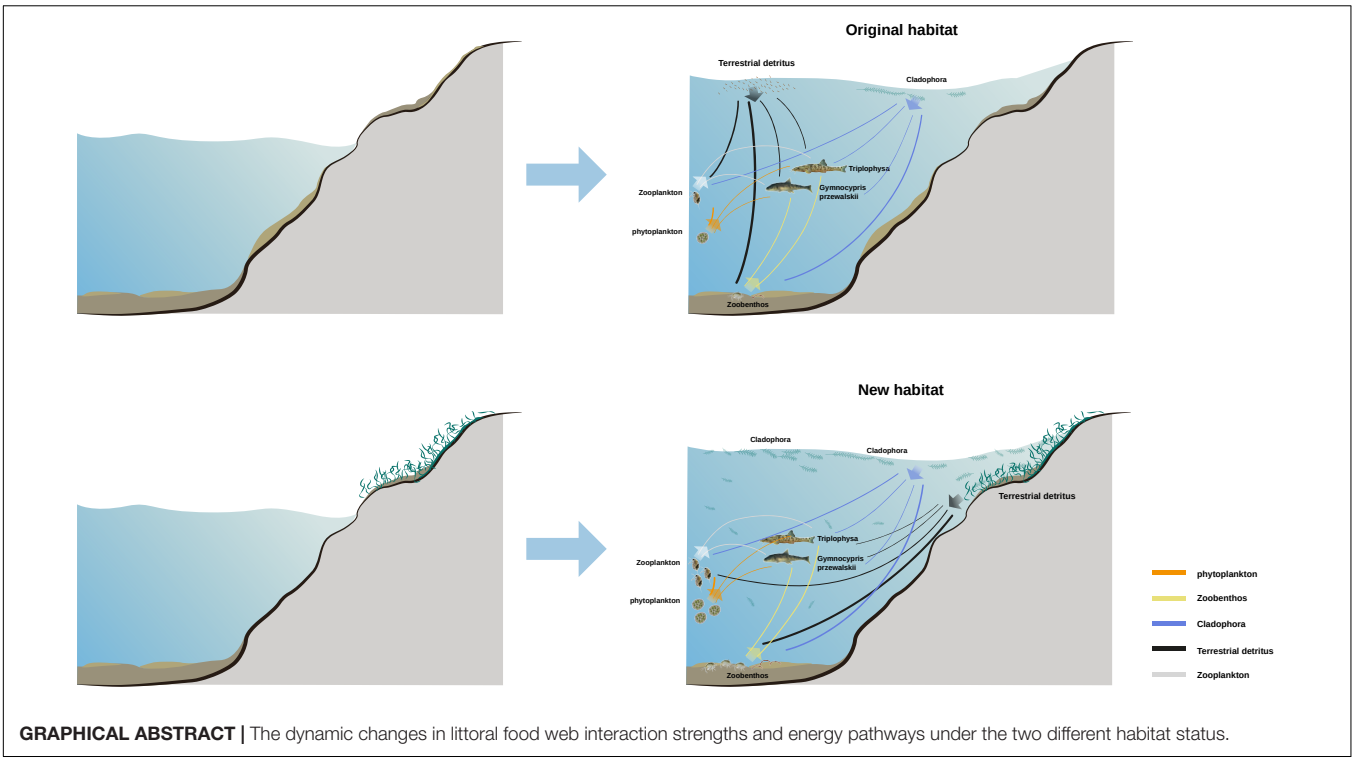

GRAPHICAL ABSTRACT | The dynamic changes in littoral food web interaction strengths and energy pathways under the two different habitat status.

changes in water level may be expected to create new habitats in the littoral zones and to modify existing habitats, and hence may trigger responses in littoral food webs by affecting the growth of littoral phytoplankton and the quantity and quality of terrestrial sources exported to lakes (Wiegner et al., 2009).

Changes in hydrology and climate collectively contribute to transformations of the landscape, which lead to alterations in the catchment vegetation. Delivery of nutrients and organic materials across distinct habitat boundaries constitute ecosystem subsidy, and cross-ecosystem nutrient subsidies can have strong effects on lake systems by changing nutrient limitation and increasing autochthonous resources (Brahney et al., 2015; Slemmons et al., 2015). Therefore, cross-ecosystem nutrient subsidies caused by factors such as climate change may have far-reaching consequences on freshwater ecosystems. Indeed, there is evidence that allochthonous terrestrial subsidies increase secondary production in lakes (Pace et al., 2007), especially in lakes with lower productivity, where most of the food resources used by consumers can be underpinned by terrestrial subsidies (Karlsson et al., 2012). The water flow from the inundation area brings a large amount of dissolved and particulate organic matter of terrestrial origin, stimulates primary productivity, and the quality and quantity of food can increase in nutrient-limited systems ultimately supporting higher trophic levels (Klug, 2002; Finstad et al., 2014).

Food webs are fundamental to ecosystem functioning because their structure controls fluxes of energy and supports key processes such as productivity (Albouy et al., 2014). Any change in energy flow can affect the wider lake ecosystem function. For example, changes in primary production associated with variation in energy flows have a large bottom-up effect from primary consumers to the fish community, which may lead to large-scale re-structuring of the whole food web (Xu et al., 2014). Nakano et al. (1999) suggested that the predation pressure of fish shifted rapidly from terrestrial to aquatic arthropods when terrestrial arthropod inputs to the stream, which can provide energy subsidies, were reduced and the resulting impact may cascade eventually affect primary producers through the food web.

The extent to which littoral communities can be subsidized by increased energy flows, and the impact of such allochthonous inputs on the food webs through cascading trophic interaction are still poorly understood. Indeed, the dynamic features of the food web, such as the trophic interactions and energy flux, are still one of the least understood subjects in aquatic ecosystems (Xu et al., 2014; Mao et al., 2021). Qinghai Lake, in the northeast of the Tibetan Plateau, provides a good site for empirical studies to address this gap in understanding. The water level of Qinghai Lake has experienced substantial changes over the past 50 years with the water level having risen by nearly 3 m between 2004 and 2018 (Zhang et al., 2014; Dong et al., 2019), so there is a considerable flux of energy and nutrients from the surrounding terrestrial landscape to the lake's littoral habitats. However, some littoral zones in the lake are not fundamentally affected by the rise of water level where the area that has been inundated has basically the same substrata as the original littoral. Hence, because the terrestrial subsidies vary spatially due to the spatial heterogeneity of physical and geographical elements, this lake is an ideal ecosystem for examining alterations in energy mobilization within littoral food webs.

We measured stable C and N isotopes of food web components to identify which kind of resources were the main contributors to the diets of local consumers. We hypothesized that: (i) the lack of the availability of autochthonous resources in original habitat and the increase in the availability of allochthonous resources have resulted in a greater demand for terrestrial subsidies by consumers than in new habitat; and (ii) compared with original habitat, the biomass of phytoplankton and zooplankton in new habitat will be larger because of the existence of more terrestrial nutrient subsidies, which will ultimately support fishes. To test these hypotheses, we established the food web structures for old and new habitats, characterized the contributions of allochthonous and autochthonous resources to consumers respectively, and focused on the dynamic changes in littoral food web interaction strengths and energy pathways under the two different habitat states.

MATERIALS AND METHODS

Study Site and Sample Collection

Qinghai Lake (36°32′-37°15′N, 99°36′-100°16′E) is located in the northeast part of the Tibet Plateau. with the water level at 3,196 m asl. It is the largest saline lake in China with a surface area of approximately 4,472 km^2 (measured in 2018) (Fan et al., 2021), and is surrounded by alpine meadows. Due to the rapid increase of water level, a large inundation area has appeared around the lake and two types of habitats have formed. One habitat substratum is sand, which is similar to that in the main lake body and hence can be regarded as an outward expansion of the original littoral habitat of Qinghai Lake (original habitat, OH); the other habitat substratum is submerged grassland (new habitat, NH). The bottom topography of both habitats is flat (depth range 1.0–1.2 m).

Cladophora filaments were sparsely scattered in OH, whereas NH with submerged grassland supports large amounts of *Cladophora*. No growth of macrophytes was observed in either habitat. We collected food web samples for this study from the two different habitats in July 2020 by dividing each habitat into 10 equal sites and sampling them so as to ensure that the collected samples accurately represent the ecological characteristics of the habitat (**Supplementary Figure 1**). In addition, fishes, benthic invertebrates, plankton, *Cladophora* and terrestrial detritus were sampled for stable isotope analyses to determine changes in consumer diets and food web structure in the different habitats. Water samples were collected by mixing the surface (0.6 m below the surface), middle and bottom water column (0.6 m above the bottom) in 2 L pre-cleaned polyethylene bottles, and total phosphorus (TP) and nitrogen (TN) concentrations were measured using methods developed by Kotlash and Chessman (1998). *Cladophora* samples were collected by plant grab (0.5 m × 0.4 m) at each site and we measured their fresh biomass after removing sediment and water.

Zooplankton and phytoplankton samples for biomass calculation were collected by sieving 20 L surface water through a 112-μm mesh size plankton net and sieving 1 L surface water through a 64-μm mesh size plankton net respectively, and all the material were preserved with 4% Lugol's iodine solution. The Lugol samples were placed under laboratory conditions, and after more than 48 h of standing and precipitation, concentrated into 30 ml for identification and counting under the microscope, and assume that 1 mm^3 of volume is equivalent to 1 mg of wet weights biomass. Wet weights of the zooplankton were calculated from the length-weight regressions of Huang et al. (1999); and wet weights of the phytoplankton were calculated from the cell numbers and size measurements (Huang et al., 1999).

Shed leaves from the most abundant grassland species including *Achnatherum splendens* and *Orinus kokonorica* surrounding the shoreline in OH were collected as potential terrestrial detritus, as these are more easily carried by the wind or washed into the lake than fresh leaves. Owing to the emergence of inundation areas there was a deep layer of terrestrial detritus on the bottom of NH, so decomposing grass leaves were also collected, and impurities and zoobenthos were removed. *Cladophora* was collected by hand and washed with distilled water and a soft toothbrush to remove silt and other impurities.

Zooplankton samples for stable isotope analysis a were collected using a 112-μm mesh size plankton net and then particulate contaminants were removed through visual inspection (Mack et al., 2012). The filtered water through a 64-μm mesh size plankton net again to collects phytoplankton samples for stable isotope analysis and then predatory zooplankton and particulate contaminants with large individuals were removed through visual inspection (Li et al., 2020).

Benthic invertebrates were obtained from both habitats using an Ekman grab (1/16 m^2) and washed with a hand net (mesh size 1 mm), including *Chironomus salinarius* and *Gammarus suifunensis* which were dominant in these areas (Wang et al., 2021), and these were the only species chosen for subsequent stable isotope analysis. For all invertebrate species, the masses of single sample were not sufficient for analyses, so it was necessary to prepare homogenous samples of pooled individuals.

Zooplankton and benthic invertebrates were washed and kept in distilled water for 12 h to enable gut evacuation (Wang et al., 2021), in order to remove any bias caused by the gut contents themselves. Using distilled water for gut evacuation experiments might cause osmotic stress and thus changes in respiration for both zooplankton and benthic invertebrates. However, the exposure time (12 h) is likely not long enough to cause any significant changes in isotopic signatures. Zooplankton samples processed by gut evacuation and phytoplankton samples for stable isotope analysis were then filtered onto a pre-combusted (450°C, 4 h) Whatman GF/F filter. The GF/F filter of phytoplankton samples used for stable isotope analysis were examined under microscopic to remove protozoa and rotifers to reduce the impact of mixed samples.

Fish, including *Gymnocypris przewalskii* and *Triplophysa*, were captured using gill nets and traps from two random transects from littoral zones in each habitat, nets and traps were in place for approximately 24 h. The weight of fish caught of *G. przewalskii* and *Triplophysa* in OH were 4.44 and 0.31 kg respectively, and 4.79 and 0.6 kg in NH. We collected white dorsal muscle samples from the larger fish individuals (>100 mm) and homogenized separately for stable isotope analysis. This reduces

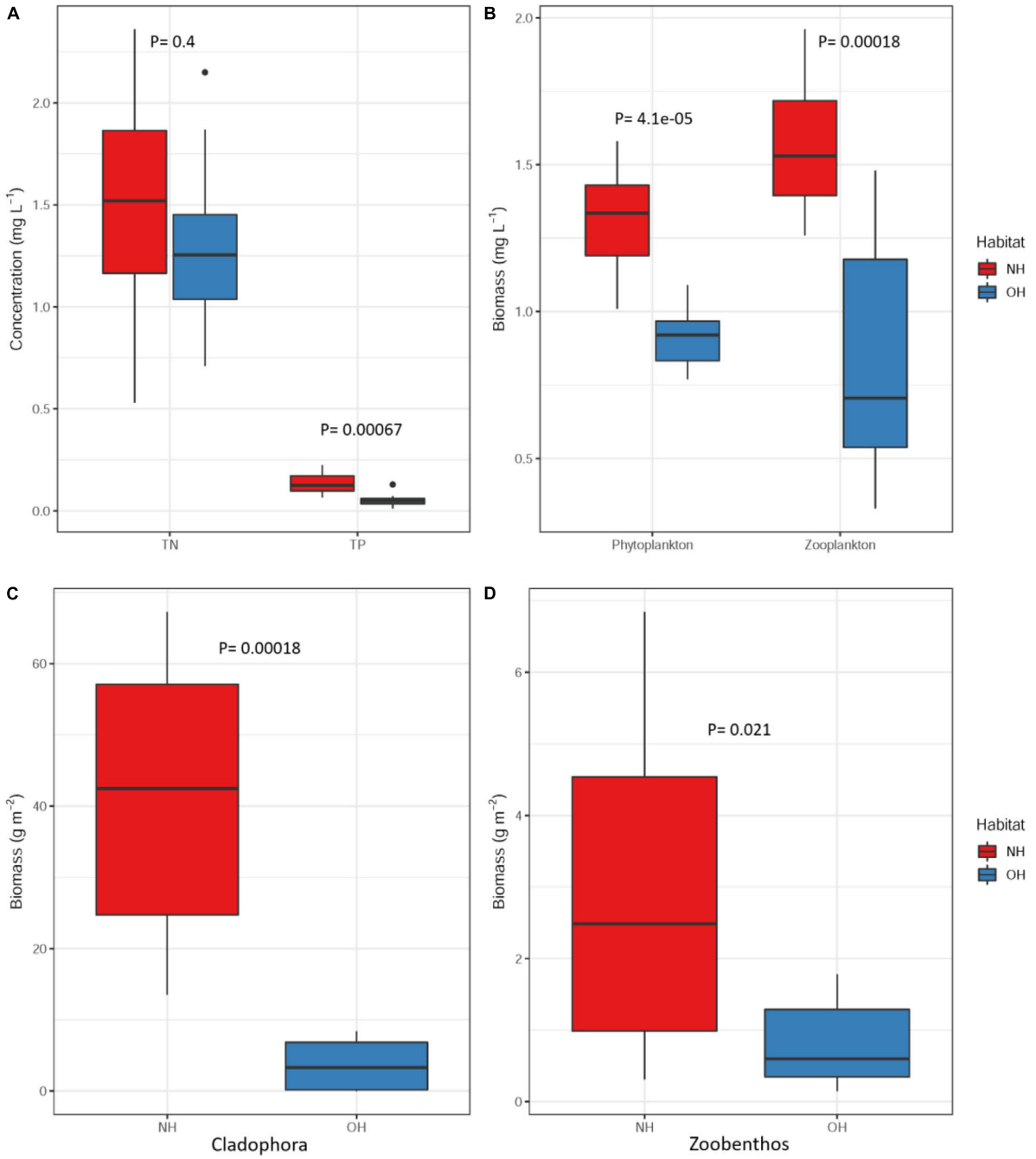

FIGURE 1 | Changes in total phosphorus and total nitrogen **(A)**, phytoplankton and zooplankton biomass **(B)**, *Cladophora* biomass **(C)**, and zoobenthos biomass **(D)** in Qinghai Lake between original (blue) and new (red) habitats. *P*-values are marked above the box plots.

possible bias caused by foraging shifts by fish individuals in their early life cycles (Xu et al., 2014).

We also determine water turbidity in two habitats by Hach 2100Q portable turbidimetry.

Stable Isotope Analysis and Modeling

All samples for stable isotope analysis were stored frozen until analysis. Terrestrial detritus was treated with 1 M hydrochloric acid to eliminate possible carbonate contamination and then rinsed in distilled water (Wang et al., 2021). All samples were dried to constant weight at 60°C, then ground into a homogeneous fine powder with a mortar and pestle and finally packed separately in tin capsules. The stable C and N isotope ratio values were generated after analysis of samples at the Institute of Hydrobiology, Chinese Academy of Sciences, using a Delta Plus (Finnigan, Bremen, Germany) continuous-flow isotope ratio

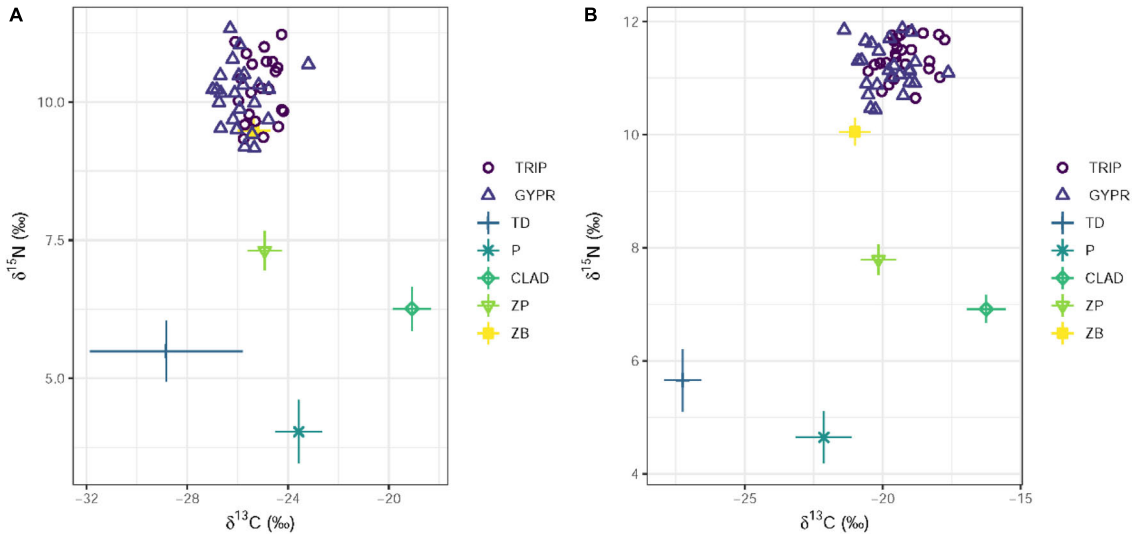

FIGURE 2 | Raw (not including trophic discrimination factors) stable carbon and nitrogen isotope values (mean ± SD) of basal food sources and consumers in original **(A)** and new **(B)** habitats. TRIP, *Triplophysa*; GYPR, *Gymnocypris przewalskii*; ZP, zooplankton; ZB, zoobenthos; P, phytoplankton; CLAD, *Cladophora*; TD, terrestrial detritus.

mass spectrometer coupled to a Carlo Erba NA2500 elemental analyzer (Carlo Erba Reagenti, Milan, Italy). Stable isotope ratios were expressed in δ notation as parts per thousand (‰) deviation from the international standards according to the equation: $\delta X = [(R_{sample}/R_{standard}) - 1] \times 1{,}000$, where X is ^{15}N or ^{13}C and R is the corresponding ratio $^{15}N/^{14}N$ or $^{13}C/^{12}C$. δ is the measure of heavy to light isotope in the sample, whereby higher δ values denote a greater proportion of the heavy isotope. The standard reference material for carbon was Vienna Pee Dee Belemnite and for nitrogen was atmospheric nitrogen (N_2). The reference material for $\delta^{13}C$ was carbonate (IAEA–USGS24) and for $\delta^{15}N$ was ammonium sulfate (IAEA-USGS26), supplied by the US Geological Survey (Denver, Colombia) and certified by the International aAomic Energy Agency (Vienna, Austria). Urea ($\delta^{15}N$ = -1.53‰, $\delta^{13}C$ = -49.44‰) was used as the daily internal working standard. Twenty percent of the samples were run as replicates, and the average standard errors of replicate measurements for $\delta^{13}C$ and $\delta^{15}N$ were both less than 0.2‰.

The trophic enrichment factors (TEF), caused by isotope fractionation during the process of digestion and metabolism, of $\Delta\delta^{13}C = 1.70 \pm 0.40$‰ and $\Delta\delta^{15}N = 2.80 \pm 0.30$‰ as proposed by Arcagni et al. (2013) were used to correct stable isotope values of food sources. Potential food sources for consumers were chosen based on published diet information (Drenner et al., 1996; Jacobsen et al., 2017). We chose terrestrial detritus, phytoplankton and *Cladophora* as food sources for zooplankton, zoobenthos, *Triplophysa* and *G. przewalskii*; zooplankton and zoobenthos were also included as food sources for *Triplophysa* and *G. przewalskii*.

Statistics

The trophic relationships among the species were compared visually through stable isotope biplots of consumers and potential food sources. Before analysis, the normality and heteroscedasticity of relevant data were evaluated by Shapiro–Wilk test and Bartlett test (Mao et al., 2021). Student's *t*-tests were also used to test the differences in the biomass of phytoplankton, zooplankton, zoobenthos, and *Cladophora*, the concentration of total nitrogen, total phosphorus, stable isotope values of species and turbidity between the two habitats. All statistical analyses were set at $\alpha = 0.05$ statistical significance levels.

We used an expanded Bayesian isotope mixing model (BIMM) to estimate dietary proportions of every consumers in the food web to obtain a quantitative food web implemented in the "IsoWeb" package (Kadoya et al., 2012). This model required information for stable isotope values of all consumers and resources, and a topological web to generate hypothetical dietary proportions for the food web of each habitat. This approach takes into account variation in trophic enrichment factors among different consumer-resource links to achieve more accurate estimates (Kadoya et al., 2012). BIMM fitting was implemented using the "R2WinBugs" package in R version 4.0.3 for Windows (Team, 2020); the accuracy of the model was determined by comparing the difference between the isotopic values of samples and the predicted values of the model. In order to ensure the convergence of the three chains, the parameters in the Markov Chain Monte Carlo were specified as chain length 10,000 burn-in 5,000 and thin by 10. Through the output of posterior distributions, we could then calculate the mean, standard deviation, and Bayesian credible intervals for the contribution of potential prey sources to consumers.

We estimated the mean contribution of sources to the diet of each consumer, and then we compared the distributions of values for the different habitats to examine differences in source utilization and energy mobilization. When calculating

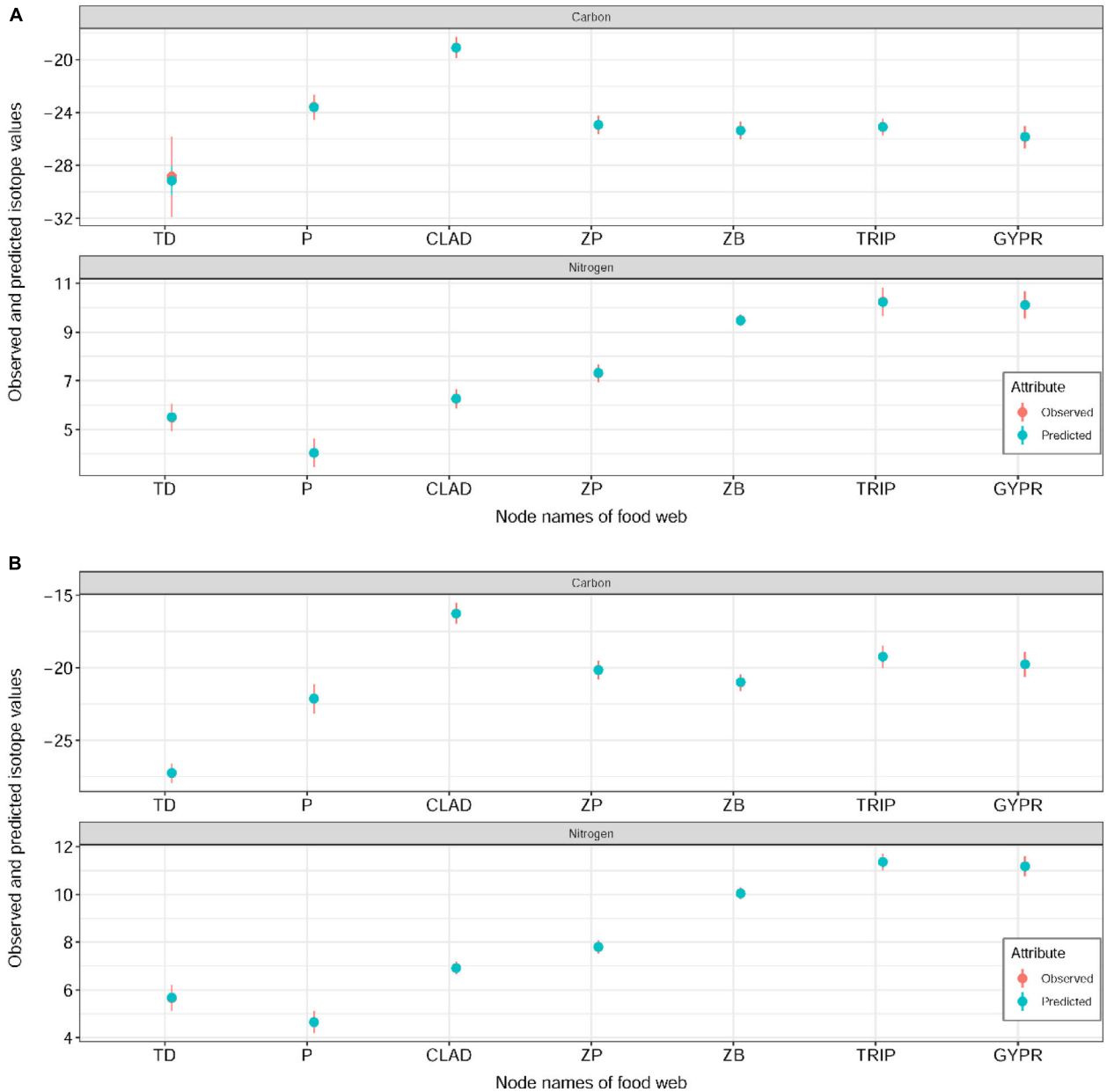

FIGURE 3 | Comparison of model predictions (blue) and observations (red) in original **(A)** and new **(B)** habitats. The solid points show the medians of observed and predicted values, whereas error bars represent 95% confidence intervals for each source.

the difference between two states, effect sizes based on standardized differences between the means are typically used (Fritz et al., 2012). Cohen (2013) introduced a measure parameter *D*, which was calculated according to the following equation:

$$D = \frac{M1 - M2}{\sqrt{\frac{S1^2 + S2^2}{2}}}$$

where *D* is effect sizes, *M*1, *M*2 and *S*1, *S*2 are the means and the standard deviation for the two groups respectively (Fritz et al., 2012). Three levels of size of effect to be detected were set: small (0–0.2), medium (0.21–0.5), and large (0.51 and above); a larger effect size indicates a greater difference, and a bigger impact of the variable causing a difference (Cohen, 1962).

RESULTS

There was no significant difference in water depth between OH and NH (**Supplementary Table 1**) and both habitats were crystal clear, with no difference in transparency evident

TABLE 1 | Bayesian isotope mixing model estimates of diet proportions for consumers in original (OH) and new (NH) habitats.

Habitat	Edge name	Diet proportion	Standard deviation	Confidence interval
OH	TD|ZP	0.42	0.18	0.43–0.41
	TD|ZB	0.65	0.12	0.66–0.64
	TD|TRIP	0.22	0.11	0.23–0.21
	TD|GYPR	0.26	0.12	0.27–0.25
	P|ZP	0.37	0.14	0.38–0.36
	P|TRIP	0.15	0.12	0.15–0.14
	P|GYPR	0.14	0.05	0.14–0.13
	CLAD|ZP	0.21	0.11	0.22–0.2
	CLAD|ZB	0.35	0.14	0.36–0.34
	CLAD|TRIP	0.15	0.13	0.15–0.14
	CLAD|GYPR	0.14	0.13	0.15–0.13
	ZP|TRIP	0.23	0.18	0.24–0.22
	ZP|GYPR	0.22	0.09	0.23–0.21
	ZB|TRIP	0.25	0.13	0.26–0.25
	ZB|GYPR	0.25	0.13	0.25–0.24
NH	TD|ZP	0.27	0.18	0.28–0.26
	TD|ZB	0.58	0.12	0.59–0.58
	TD|TRIP	0.14	0.07	0.14–0.13
	TD|GYPR	0.16	0.08	0.17–0.16
	P|ZP	0.47	0.15	0.49–0.46
	P|TRIP	0.16	0.13	0.16–0.15
	P|GYPR	0.16	0.06	0.17–0.16
	CLAD|ZP	0.26	0.08	0.27–0.25
	CLAD|ZB	0.42	0.13	0.42–0.41
	CLAD|TRIP	0.17	0.12	0.18–0.16
	CLAD|GYPR	0.16	0.12	0.16–0.15
	ZP|TRIP	0.23	0.18	0.24–0.22
	ZP|GYPR	0.24	0.11	0.24–0.23
	ZB|TRIP	0.31	0.1	0.32–0.3
	ZB|GYPR	0.28	0.1	0.29–0.27

"A|B" represents a trophic link in the food web with resource and consumer denoted by "A" and "B," respectively.

to the naked eye. However, both the water chemistry and biomasses of major resources in NH differed significantly from those in OH. TP in NH was 0.14 mg L^{-1} higher than in OH (*t*-test, $p < 0.01$), but TN differed little (**Figure 1A** and **Supplementary Table 1**). The rise of water level resulted in the appearance of submerged grassland e in large areas in NH, with an accompanying higher phytoplankton biomass (*t*-test, $p < 0.01$), zooplankton biomass (*t*-test, $p = 0.021$), zoobenthos biomass and *Cladophora* biomass (*t*-test, $p < 0.01$), with *Cladophora* especially increasing from 3.62 g m^{-2} in OH to 41.33 g m^{-2} in NH (**Figures 1B–D** and **Supplementary Table 1**).

Supplementary Tables 2, **3** summarize the isotope values of all samples collected from OH and NH. Comparison of the isotope space biplots of each habitat (**Figure 2**) indicates that almost all taxa from NH tend to have higher $\delta^{15}N$ and $\delta^{13}C$ values than their counterparts in OH. Within the basal sources, phytoplankton and *Cladophora* from NH had significantly higher $\delta^{15}N$ and $\delta^{13}C$ values than in OH (*t*-test $p < 0.05$), but no differences were observed in $\delta^{15}N$ and $\delta^{13}C$ values of terrestrial detritus between the two habitats (**Supplementary Table 4**). In both habitats, invertebrates and fishes in NH showed significantly higher $\delta^{15}N$ and $\delta^{13}C$ values than in OH (**Supplementary Table 4**). *Triplophysa* and *G. przewalskii* from within the same habitat had similar $\delta^{15}N$ values (11.37 ± 0.34‰ in *Triplophysa* and 11.18 ± 0.42‰ in *G. przewalskii*), suggesting closely similar feeding habits.

BIMM was used to estimate the relative contribution of the various resources to consumers. The isotope values from OH and NH food webs were treated as observed values and compared with predicted values from the BIMM estimates and the observed points broadly lie in the predicted value intervals, showing that the model can make reasonably accurate estimates (**Figure 3**). According to the results of the BIMM, trophic interactions of food web components in the two habitats are different. In the OH, terrestrial detritus showed the highest contribution to the diet of zooplankton (42%), zoobenthos (65%) and *G. przewalskii* (26%), and the contribution to *Triplophysa* (22%) also accounts for a considerable part compared with other resources, whereas *Cladophora* and phytoplankton contributed the least to *G. przewalskii* (14%, 14%) and *Triplophysa* (15%, 15%) (**Table 1**). Interestingly, in the NH, the dependence of all consumers on terrestrial detritus decreased in varying degrees, replaced by an increase in *Cladophora* and phytoplankton assimilation, which was most obvious in zooplankton and zoobenthos. Zooplankton in NH heavily reduced dependence on terrestrial detritus (down from 42 to 27%), and increased their dependence on *Cladophora* (up from 21 to 26%) and phytoplankton (up from 37 to 47%) at the same time (**Table 1**). Zoobenthos in NH also reduced dependence on terrestrial detritus (down from 65 to 58%), and increased their dependence on *Cladophora* (up from 35 to 42%). Zooplankton and zoobenthos were important to fishes; however, the support by zooplankton for *Triplophysa* tended to be similar between habitats, whereas zoobenthos contributed more to *G. przewalskii* (up from 25 to 28%) and *Triplophysa* (up from 25 to 31%) in NH (**Table 1**).

Using effect sizes to measure the changes in the interaction strength of trophic links between the two habitats, a conceptualized diagram was constructed for visualization (**Figures 4**, **5**). It can be seen that, except for the trophic links related to terrestrial detritus, the interaction strength of the other links was strong in NH, especially the links between *Cladophora* and zooplankton (0.53, medium effect), *Cladophora* and zoobenthos (0.51, medium effect), phytoplankton and zooplankton (0.69, medium effect), and zoobenthos and *Triplophysa* (0.52, medium effect). However, the difference in interaction strength of trophic links related to terrestrial detritus between two habitats were almost the largest, as seen from the links between terrestrial detritus and zooplankton (-0.83, large effect), zoobenthos (-0.58, medium effect), *Triplophysa* (-0.87, large effect) and *G. przewalskii* (-0.98, large effect) (**Figures 4**, **5**). This indicates that the interaction strength of food webs with similar trophic structures shows different intensity in the two

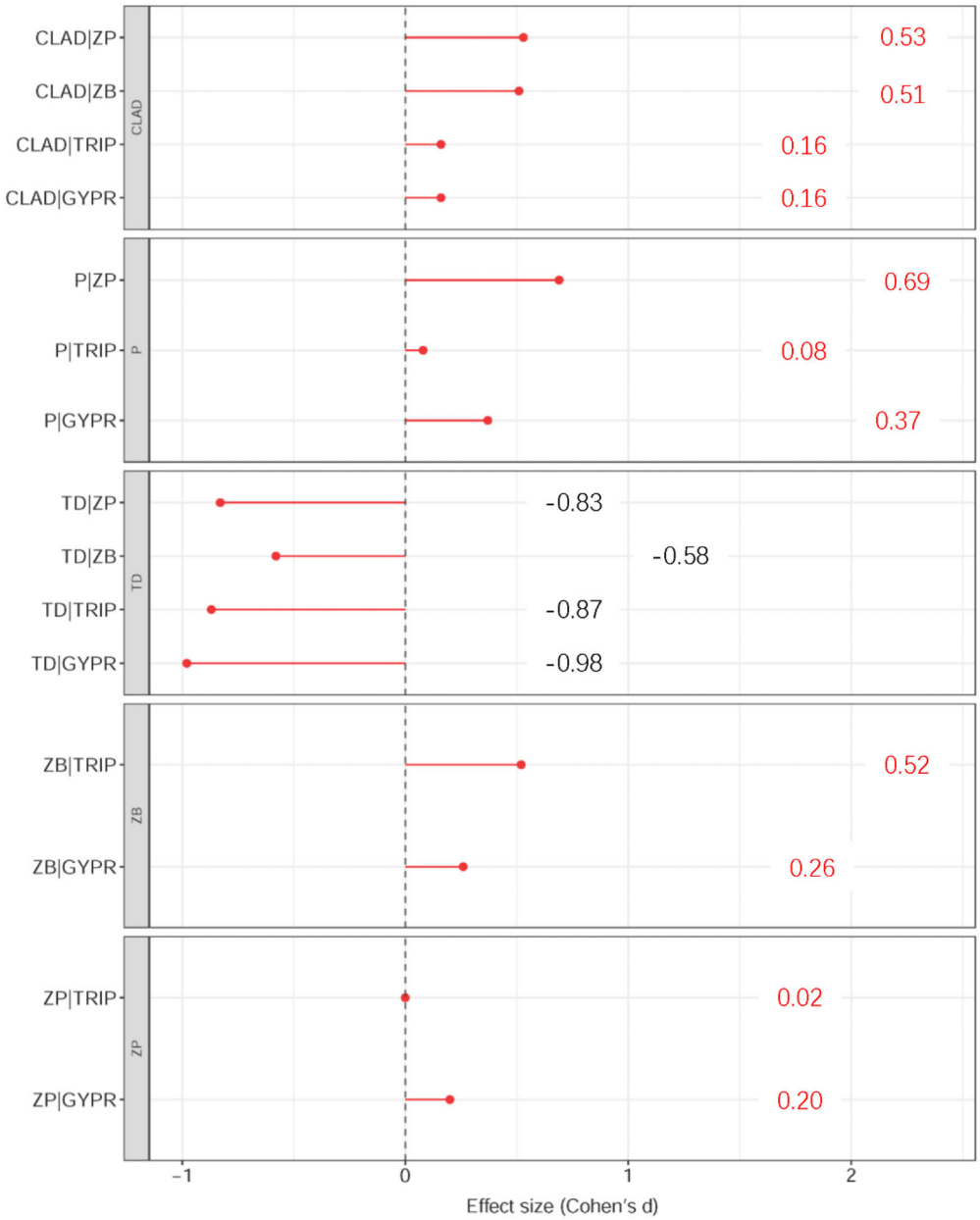

FIGURE 4 | Mean effect sizes of the difference in interaction strength of the same trophic links between the two habitats. Positive effects sizes indicate that the link is stronger in the new habitat whereas negative effect sizes indicate that the link is stronger in the original habitat.

habitats. For most consumers in OH, autochthonous resources were the most important carbon source, while allochthonous resources contributed most to consumers in NH (**Table 1**).

DISCUSSION

Changes in Habitats

Ongoing climate change can affect lake water level fluctuations through increasing abnormally wet years, glacier meltwater and other factors (Tao et al., 2020; Fan et al., 2021), which in turn affects the ecological processes and patterns of lake littoral zones. However, our understanding of the mechanisms underlying these affects is still limited. The resulting inundation areas will form new aquatic habitats and feeding grounds, and the nutrient load released from soil particles and organic matter will also increase (Steinman et al., 2012), providing nutrients directly or indirectly for the local habitat. Indeed, due to nutrient inputs, the concentrations of total phosphorus, phytoplankton and *Cladophora* biomass in NH were significantly increased compare with OH, whereas total nitrogen did not change (**Figures 1A–C**). Even so, like many other alpine lakes,

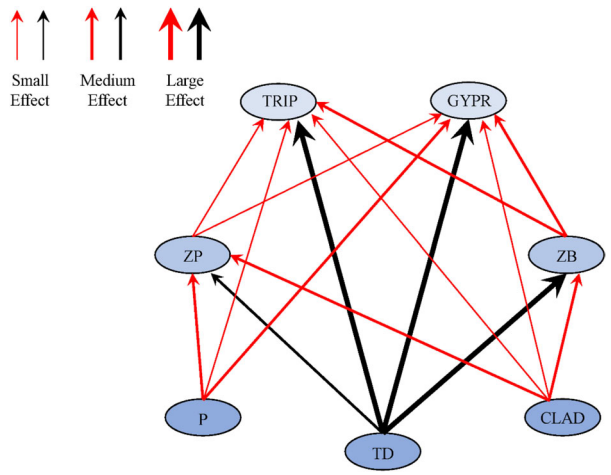

FIGURE 5 | Schematic diagram of the strengths of trophic links investigated in this study. The width of the arrows between resources and consumers reflects estimated effect sizes: small (0–0.2), medium (0.21–0.5), and large (0.51 and above). Positive effects sizes and negative effects sizes are represented in red and black, respectively.

these two littoral habitats still belong to the low nutrient category (**Supplementary Table 1**), and we did not find any sign of regime shift from clear to turbid water caused by nutrient released to water columns (Jeppesen et al., 1998), Hence, even though the biomass of phytoplankton did increase, t *Cladophora* in NH probably quickly incorporates most additional nutrients near shoreline development. The unnatural *Cladophora* blooms in this clear lake can be explained by the availability of nutrients and substrata. Increased algal biomass at NH strongly suggests that these sites receive increased nutrients. Compared with the sand substratum in OH, we conclude that submerged grassland in NH, which has higher phosphorus content, provided enough nutrients for growth of *Cladophora* (**Figure 1A**). Moreover, the relatively high transparency and the low water depth (<1.3 m) of the two habitats allows enough light penetration to the lake bottom to support growth of *Cladophora*. Previous studies have shown that phosphate is the limiting factor for the growth of *Cladophora* (Ren et al., 2019), and the *Cladophora* biomass of Qinghai Lake was positively correlated with total phosphate concentrations, whereas no obvious correlation was observed with total nitrogen (Zhu et al., 2020), which is also consistent with our findings.

In addition to nutrients, submerged grassland substratum in NH provided additional attachment points for the growth of *Cladophora* enabling them to expand into areas that were previously difficult to colonize (Francoeur et al., 2017).

Carbon Sources for Consumers

Inundation areas may increase the exchange of matter and energy between the terrestrial and aquatic environments in the littoral zones of lakes and thus change the basal food sources supporting the food web (Leira and Cantonati, 2008). In Qinghai Lake the contributions of allochthonous and autochthonous carbon to consumers were different in different habitats. BIMM estimates revealed that the most important carbon source for zooplankton, zoobenthos and fishes in OH was terrestrial detritus, i.e., allochthonous carbon, whereas in NH, it was autochthonous carbon and especially *Cladophora* (**Table 1**). In fact, we also found that $\delta^{13}C$ values of zoobenthos and fishes showed an obvious trend away from values of terrestrial detritus toward values of *Cladophora* (**Supplementary Table 1**), which means that compared with OH, consumers in NH potentially had assimilated considerable amount of carbon derived from *Cladophora*. This change in the contributions of allochthonous and autochthonous carbon sources to consumers can be explained by resource availability. Food webs in oligotrophic lakes commonly rely strongly on terrestrially produced organic matter because of their poor nutritional condition (Jonsson et al., 2001). In OH the low production of autochthonous carbon sources such as phytoplankton and *Cladophora* (**Figures 1B,C**) is insufficient to maintain the biomass of consumer species; instead, we believe that the large inputs of terrestrial detritus from nearshore grassland provides a sufficient food source to subsidize the growth of consumers in OH. With the increase of submerged grassland area and amount in NH, these subsidies have not become more important, which we consider may be caused by two reasons. Firstly, as mentioned above, nutrient input from soil particles and decomposed grass supports the growth of autochthonous carbon sources in NH, which replace a considerable part of allochthonous carbon sources in the food web. Secondly, algae are considered higher-quality food for consumers than terrestrial detritus, because of their higher content of polyunsaturated fatty acids required to meet physiological requirements (Lau et al., 2009; Guo et al., 2016). More *Cladophora* and phytoplankton in NH increased availability of high-quality food sources, which consumers preferred. Thus, autochthonous carbon resources were ingested more than allochthonous carbon resources in NH. In addition, we emphasize that allochthonous resources subsidize rather than entirely replacing autochthonous resources, and habitat characteristics also partly determine the strength of this subsidy, which has proven to be closely related to climate change (Bartley et al., 2019).

Shift in Energetic Mobilization of Food Webs

Cross-ecosystem nutrient subsidies tend to bring nutrients from areas with higher productivity into areas with lower productivity, and these inputs can alter habitat stability, which causes corresponding changes in interaction strength and food web structure (Huxel and McCann, 1998; Atwood et al., 2012). For example, omnivorous fish in the Pantanal wetland have been observed to respond to flooding-induced changes in energy pathways and nutrients by ingesting more plant food (Wantzen et al., 2002), which indicates that omnivorous fish can reduce this effect through establishing direct or indirect links with a

variety of energy subsidies (Polis and Strong, 1996). Therefore, we believe that the increased contribution of autochthonous resources to higher consumers in NH after the allochthonous nutrient inputs will help stabilize the food web. Following the increased availability of autochthonous resources in NH, the need for consumers to use terrestrial subsidies to maintain secondary production will be alleviated (Brett et al., 2017).

Zooplankton and zoobenthos are recognized as critical links between primary production and higher consumers, and are considered high-quality aquatic prey which can change the food base of fishes by delivering more carbon sources from primary producers to higher consumers (Vander Zanden and Vadeboncoeur, 2002; Mao et al., 2021). The diet proportions of fish may depend on the availability of food resources in the littoral zone, and the increase in allochthonous nutrients in the lake basin may have a positive effect. Supporting this view is the fact that support by phytoplankton, *Cladophora*, zooplankton, and zoobenthos resources for *G. przewalskii* and *Triplophysa* all showed positive effects, although to varying degrees (**Figure 5**). With the increased biomass of phytoplankton and *Cladophora*, more autochthonous resources were consumed by the zooplankton and zoobenthos subsequently preyed on by fishes (**Figures 1B,C**). Accordingly, the contribution of phytoplankton and *Cladophora* to zooplankton and zoobenthos also showed a positive effect (**Figure 5**). These shifts in trophic interactions and energy flux were reflected by the variation in $\delta^{15}N$ values of related species; for instance, significantly higher $\delta^{15}N$ values were observed for the fishes in NH (**Supplementary Table 4**). Consumers could gain more effective energy subsidies from zooplankton and zoobenthos, which were animal items and had a higher $\delta^{15}N$ value than other resources, which may influence fish prey selection (Mao et al., 2021). Therefore, increased allochthonous nutrient support for autochthonous resources, and then transfer along the food chain could be an important part of the reason for maintaining the stability of the food web in NH.

At the same time, we also found that the contribution of terrestrial detritus decreased when the contribution of autochthonous resource increased, suggesting that the use of terrestrial subsidies by aquatic consumers depends in part on the stock biomass of aquatic prey (Kraus et al., 2016). Unlike the situation in OH where species consumed more terrestrial detritus to cope with a low resource availability, the availability of autochthonous resource in NH was much higher, and could replace part of the terrestrial subsidies. Nutritional asymmetry between aquatic and terrestrial resources in consumers is also an important factor (Twining et al., 2019).

CONCLUSION

In this study, we demonstrated that the water level fluctuations in Qinghai Lake caused by climate change have a far-reaching impact on its littoral habitat. Allochthonous inputs supported consumers in OH directly due to poor nutrient conditions and supported consumers in NH indirectly by improving the relative availability of autochthonous resources. Our results emphasize that lake and littoral ecosystems should be regarded as an integrated management unit, because the integrity of one is strongly associated with the other (Larsen et al., 2016). Moreover, terrestrial subsidies should attract greater concern when formulating lake ecosystem management strategy.

DATA AVAILABILITY STATEMENT

The original contributions presented in this study are included in the article/**Supplementary Material**, further inquiries can be directed to the corresponding author/s.

ETHICS STATEMENT

This animal study was reviewed and approved by the Research Monitoring and Evaluation Center of Qinghai National Park.

AUTHOR CONTRIBUTIONS

JX and KW conceived the study. KW, KZ, XX, HZu, HA, and KM conducted field and laboratory measurements. JX and KW analyzed the data. All authors drafted and revised the manuscript, contributed to the article, and approved the submitted version.

FUNDING

This research was supported by the National Key R&D Program of China (Grant No. 2018YFD0900904) and the Water Pollution Control and Management Project of China (Grant No. 2018ZX07208005). JX acknowledges the support received from the International Cooperation Project of the Chinese Academy of Sciences (Grant No. 152342KYSB20190025) and the National Natural Science Foundations of China (Grant No. 31872687).

ACKNOWLEDGMENTS

KW acknowledges designer Jin Wang from Bauhaus University for her efforts in graphical abstract.

SUPPLEMENTARY MATERIAL

The Supplementary Material for this article can be found online at: https://www.frontiersin.org/articles/10.3389/fevo.2022.886372/full#supplementary-material

REFERENCES

Albouy, C., Velez, L., Coll, M., Colloca, F., Le Loc'h, F., Mouillot, D., et al. (2014). From projected species distribution to food-web structure under climate change. *Glob. Chang. Biol.* 20, 730–741. doi: 10.1111/gcb.12467

Arcagni, M., Campbell, L. M., Arribere, M. A., Kyser, K., Klassen, K., Casaux, R., et al. (2013). Food web structure in a double-basin ultra-oligotrophic lake in Northwest Patagonia, Argentina, using carbon and nitrogen stable isotopes. *Limnologica* 43, 131–142. doi: 10.1016/j.limno.2012.08.009

Atwood, T. B., Wiegner, T. N., and MacKenzie, R. A. (2012). Effects of hydrological forcing on the structure of a tropical estuarine food web. *Oikos* 121, 277–289. doi: 10.1111/j.1600-0706.2011.19132.x

Bartley, T. J., McCann, K. S., Bieg, C., Cazelles, K., Granados, M., Guzzo, M. M., et al. (2019). Food web rewiring in a changing world. *Nat. Ecol. Evol.* 3, 345–354. doi: 10.1038/s41559-018-0772-3

Brahney, J., Mahowald, N., Ward, D. S., Ballantyne, A. P., and Neff, J. C. (2015). Is atmospheric phosphorus pollution altering global alpine Lake stoichiometry? *Glob. Biogeochem. Cycles* 29, 1369–1383. doi: 10.1002/2015GB005137

Brett, M. T., Bunn, S. E., Chandra, S., Galloway, A. W. E., Guo, F., Kainz, M. J., et al. (2017). How important are terrestrial organic carbon inputs for secondary production in freshwater ecosystems? *Freshw. Biol.* 62, 833–853. doi: 10.1111/fwb.12909

Cohen, J. (1962). The statistical power of abnormal-social psychological research: a review. *J. Abnorm. Soc. Psychol.* 65, 145–153. doi: 10.1037/h0045186

Cohen, J. (2013). *Statistical Power analysis for the Behavioral Sciences*. Cambridge, MA: Academic Press. doi: 10.4324/9780203771587

Dong, H., Song, Y., and Zhang, M. (2019). Hydrological trend of Qinghai Lake over the last 60 years: driven by climate variations or human activities? *J. Water Clim. Change* 10, 524–534. doi: 10.2166/wcc.2018.033

Drenner, R. W., Smith, J. D., and Threlkeld, S. T. (1996). Lake trophic state and the limnological effects of omnivorous fish. *Hydrobiologia* 319, 213–223. doi: 10.1007/BF00013734

Fan, C., Song, C., Li, W., Liu, K., Cheng, J., Fu, C., et al. (2021). What drives the rapid water-level recovery of the largest lake (Qinghai Lake) of China over the past half century? *J. Hydrol.* 593:125921. doi: 10.1016/j.jhydrol.2020.125921

Finstad, A. G., Helland, I. P., Ugedal, O., Hesthagen, T., and Hessen, D. O. (2014). Unimodal response of fish yield to dissolved organic carbon. *Ecol. Lett.* 17, 36–43. doi: 10.1111/ele.12201

Francoeur, S. N., Winslow, K. A. P., Miller, D., and Peacor, S. D. (2017). Mussel-derived stimulation of benthic filamentous algae: the importance of nutrients and spatial scale. *J. Great Lakes Res.* 43, 69–79. doi: 10.1016/j.jglr.2016.10.013

Fritz, C. O., Morris, P. E., and Richler, J. (2012). Effect size estimates: current use, calculations, and interpretation. *J. Exp. Psychol. Gen.* 141, 2–18. doi: 10.1037/a0024338

Guo, F., Kainz, M. J., Sheldon, F., and Bunn, S. E. (2016). The importance of high-quality algal food sources in stream food webs - current status and future perspectives. *Freshw. Biol.* 61, 815–831. doi: 10.1111/fwb.12755

Huang, L., Liu, J., Shao, Q., and Liu, R. (2011). Changing inland lakes responding to climate warming in Northeastern Tibetan Plateau. *Clim. Change* 109, 479–502. doi: 10.1007/s10584-011-0032-x

Huang, X., Chen, W., and Cai, Q. (1999). Survey, observation and analysis of lake ecology. Standard methods for observation analysis in Chinese Ecosystem Research Network, Series V.

Huxel, G. R., and McCann, K. (1998). Food web stability: the influence of trophic flows across habitats. *Am. Nat.* 152, 460–469. doi: 10.1086/286182

Jacobsen, D., Laursen, S. K., Hamerlik, L., Moltesen, K., Michelsen, A., and Christoffersen, K. S. (2017). Fish on the roof of the world: densities, habitats and trophic position of stone loaches (*Triplophysa*) in Tibetan streams. *Mar. Freshw. Res.* 68, 53–64. doi: 10.1071/MF15225

Jeppesen, E., Sondergaard, M., Jensen, J. P., Mortensen, E., Hansen, A. M., and Jorgensen, T. (1998). Cascading trophic interactions from fish to bacteria and nutrients after reduced sewage loading: an 18-year study of a shallow hypertrophic lake. *Ecosystems* 1, 250–267. doi: 10.1007/s100219900020

Jonsson, A., Meili, M., Bergstrom, A. K., and Jansson, M. (2001). Whole-lake mineralization of allochthonous and autochthonous organic carbon in a large Humic lake (Ortrasket, N. Sweden). *Limnol. Oceanogr.* 46, 1691–1700. doi: 10.4319/lo.2001.46.7.1691

Kadoya, T., Osada, Y., and Takimoto, G. (2012). IsoWeb: a Bayesian isotope mixing model for diet analysis of the whole food web. *PLoS One* 7:e41057. doi: 10.1371/journal.pone.0041057

Karlsson, J., Berggren, M., Ask, J., Bystrom, P., Jonsson, A., Laudon, H., et al. (2012). Terrestrial organic matter support of lake food webs: evidence from lake metabolism and stable hydrogen isotopes of consumers. *Limnol. Oceanogr.* 57, 1042–1048. doi: 10.4319/lo.2012.57.4.1042

Klug, J. L. (2002). Positive and negative effects of allochthonous dissolved organic matter and inorganic nutrients on phytoplankton growth. *Can. J. Fish. Aquat. Sci.* 59, 85–95. doi: 10.1139/f01-194

Kotlash, A. R., and Chessman, B. C. (1998). Effects of water sample preservation and storage on nitrogen and phosphorus determinations: implications for the use of automated sampling equipment. *Water Res.* 32, 3731–3737. doi: 10.1016/S0043-1354(98)00145-6

Kraus, J. M., Pomeranz, J. F., Todd, A. S., Walters, D. M., Schmidt, T. S., and Wanty, R. B. (2016). Aquatic pollution increases use of terrestrial prey subsidies by stream fish. *J. Appl. Ecol.* 53, 44–53. doi: 10.1111/1365-2664.12543

Larsen, S., Muehlbauer, J. D., and Marti, E. (2016). Resource subsidies between stream and terrestrial ecosystems under global change. *Glob. Change Biol.* 22, 2489–2504. doi: 10.1111/gcb.13182

Lau, D. C. P., Leung, K. M. Y., and Dudgeon, D. (2009). Are autochthonous foods more important than allochthonous resources to benthic consumers in tropical headwater streams? *J. N. Am. Benthol. Soc.* 28, 426–439. doi: 10.1899/07-079.1

Leira, M., and Cantonati, M. (2008). Effects of water-level fluctuations on lakes: an annotated bibliography. *Hydrobiologia* 613, 171–184. doi: 10.1007/s10750-008-9465-2

Li, Y. R., Meng, J., Zhang, C., Ji, S. P., Kong, Q., Wang, R. Q., et al. (2020). Bottom-up and top-down effects on phytoplankton communities in two freshwater lakes. *PLoS One* 15:e0231357. doi: 10.1371/journal.pone.0231357

Mack, H. R., Conroy, J. D., Blocksom, K. A., Stein, R. A., and Ludsin, S. A. (2012). A comparative analysis of zooplankton field collection and sample enumeration methods. *Limnol. Oceanogr. Methods* 10, 41–53. doi: 10.4319/lom.2012.10.41

Mao, Z., Gu, X., Cao, Y., Luo, J., Zeng, Q., Chen, H., et al. (2021). Pelagic energy flow supports the food web of a shallow lake following a dramatic regime shift driven by water level changes. *Sci. Total Environ.* 756:143642. doi: 10.1016/j.scitotenv.2020.143642

Nakano, S., Miyasaka, H., and Kuhara, N. (1999). Terrestrial-aquatic linkages: riparian arthropod inputs alter trophic cascades in a stream food web. *Ecology* 80, 2435–2441. doi: 10.1890/0012-9658(1999)080[2435:TALRAI]2.0.CO;2

Pace, M. L., Carpenter, S. R., Cole, J. J., Coloso, J. J., Kitchell, J. F., Hodgson, J. R., et al. (2007). Does terrestrial organic carbon subsidize the planktonic food web in a clear-water lake? *Limnol. Oceanogr.* 52, 2177–2189. doi: 10.4319/lo.2007.52.5.2177

Polis, G. A., and Strong, D. R. (1996). Food web complexity and community dynamics. *Am. Nat.* 147, 813–846. doi: 10.1086/285880

Ren, Z., Niu, D. C., Ma, P. P., Wang, Y., Fu, H., and Elser, J. J. (2019). Cascading influences of grassland degradation on nutrient limitation in a high mountain lake and its inflow streams. *Ecology* 100:e02755. doi: 10.1002/ecy.2755

Slemmons, K. E. H., Saros, J. E., Stone, J. R., McGowan, S., Hess, C. T., and Cahl, D. (2015). Effects of glacier meltwater on the algal sedimentary record of an alpine lake in the central US Rocky Mountains throughout the late Holocene. *J. Paleolimnol.* 53, 385–399. doi: 10.1007/s10933-015-9829-3

Steinman, A. D., Ogdahl, M. E., Weinert, M., Thompson, K., Cooper, M. J., and Uzarski, D. G. (2012). Water level fluctuation and sediment-water nutrient exchange in Great Lakes coastal wetlands. *J. Great Lakes Res.* 38, 766–775. doi: 10.1016/j.jglr.2012.09.020

Tao, S., Fang, J., Ma, S., Cai, Q., Xiong, X., Tian, D., et al. (2020). Changes in China's lakes: climate and human impacts. *Natl. Sci. Rev.* 7, 132–140. doi: 10.1093/nsr/nwz103

Team, R. D. C. (2020). *R: A Language and Environment for Statistical Computing*. Vienna, Austria: R Foundation for Statistical Computing.

Twining, C. W., Brenna, J. T., Lawrence, P., Winkler, D. W., Flecker, A. S., and Hairston, N. G. Jr. (2019). Aquatic and terrestrial resources are not nutritionally reciprocal for consumers. *Funct. Ecol.* 33, 2042–2052. doi: 10.1111/1365-2435.13401

Vander Zanden, M. J., and Vadeboncoeur, Y. (2002). Fishes as integrators of benthic and pelagic food webs in lakes. *Ecology* 83, 2152–2161. doi: 10.2307/3072047

Wang, K., Sha, Y. C., Xu, J., Zhang, T. L., Hu, W., and Zhu, Z. Y. (2021). Do sympatric transgenic and non-transgenic common carps partition the trophic niche? A whole-lake manipulation study. *Sci. Total Environ.* 787:147516. doi: 10.1016/j.scitotenv.2021.147516

Wantzen, K. M., Machado, F. D., Voss, M., Boriss, H., and Junk, W. J. (2002). Seasonal isotopic shifts in fish of the Pantanal wetland, Brazil. *Aquat. Sci.* 64, 239–251. doi: 10.1007/PL00013196

Wiegner, T. N., Tubal, R. L., and MacKenzie, R. A. (2009). Bioavailability and export of dissolved organic matter from a tropical river during base- and stormflow conditions. *Limnol. Oceanogr.* 54, 1233–1242. doi: 10.4319/lo.2009.54.4.1233

Woolway, R. I., Kraemer, B. M., Lenters, J. D., Merchant, C. J., O'Reilly, C. M., and Sharma, S. (2020). Global lake responses to climate change. *Nat. Rev. Earth Environ.* 1, 388–403. doi: 10.1038/s43017-020-0067-5

Xu, J., Wen, Z., Ke, Z., Zhang, M., Zhang, M., Guo, N., et al. (2014). Contrasting energy pathways at the community level as a consequence of regime shifts. *Oecologia* 175, 231–241. doi: 10.1007/s00442-013-2878-2

Zhang, G., Xie, H., Yao, T., Li, H., and Duan, S. (2014). Quantitative water resources assessment of Qinghai Lake basin using Snowmelt Runoff Model (SRM). *J. Hydrol.* 519, 976–987. doi: 10.1016/j.jhydrol.2014.08.022

Zhang, G., Yao, T., Shum, C., Yi, S., Yang, K., Xie, H., et al. (2017). Lake volume and groundwater storage variations in Tibetan Plateau's endorheic basin. *Geophys. Res. Lett.* 44, 5550–5560. doi: 10.1002/2017GL073773

Zhu, H., Xiong, X., Ao, H., Wu, C., He, Y., Hu, Z., et al. (2020). *Cladophora* reblooming after half a century: effect of climate change-induced increases in the water level of the largest lake in Tibetan Plateau. *Environ. Sci. Pollut. Res. Int.* 27, 42175–42181. doi: 10.1007/s11356-020-10386-y

Conflict of Interest: The authors declare that the research was conducted in the absence of any commercial or financial relationships that could be construed as a potential conflict of interest.

Publisher's Note: All claims expressed in this article are solely those of the authors and do not necessarily represent those of their affiliated organizations, or those of the publisher, the editors and the reviewers. Any product that may be evaluated in this article, or claim that may be made by its manufacturer, is not guaranteed or endorsed by the publisher.

Copyright © 2022 Wang, Zhao, Xiong, Zhu, Ao, Ma, Xie, Wu, Wang, Zhang, Zhang and Xu. This is an open-access article distributed under the terms of the Creative Commons Attribution License (CC BY). The use, distribution or reproduction in other forums is permitted, provided the original author(s) and the copyright owner(s) are credited and that the original publication in this journal is cited, in accordance with accepted academic practice. No use, distribution or reproduction is permitted which does not comply with these terms.

frontiers | Frontiers in Ecology and Evolution

ORIGINAL RESEARCH
published: 30 June 2022
doi: 10.3389/fevo.2022.915199

Variation Among Species and Populations, and Carry-Over Effects of Winter Exposure on Mercury Accumulation in Small Petrels

Petra Quillfeldt[1], Yves Cherel[2], Joan Navarro[3], Richard A. Phillips[4], Juan F. Masello[1], Cristián G. Suazo[1], Karine Delord[2] and Paco Bustamante[5,6]*

[1] Department of Animal Ecology and Systematics, Justus Liebig University Giessen, Giessen, Germany, [2] Centre d'Etudes Biologiques de Chizé, UMR 7372 CNRS - La Rochelle Université, Villiers-en-Bois, France, [3] Institut de Ciències del Mar, Consejo Superior de Investigaciones Científicas, Barcelona, Spain, [4] British Antarctic Survey, Natural Environment Research Council, Cambridge, United Kingdom, [5] Littoral Environnement et Sociétés, UMR 7266 CNRS - La Rochelle Université, La Rochelle, France, [6] Institut Universitaire de France, Paris, France

OPEN ACCESS

Edited by:
Jason Newton,
University of Glasgow,
United Kingdom

Reviewed by:
Nathan Wolf,
Alaska Pacific University,
United States
Yang Wang,
Hebei Normal University, China
Shaun Lancaster,
Montanuniversitaet Leoben, Austria

***Correspondence:**
Petra Quillfeldt
petra.quillfeldt@bio.uni-giessen.de

Specialty section:
This article was submitted to Population, Community, and Ecosystem Dynamics, a section of the journal Frontiers in Ecology and Evolution

Received: 07 April 2022
Accepted: 06 June 2022
Published: 30 June 2022

Citation:
Quillfeldt P, Cherel Y, Navarro J, Phillips RA, Masello JF, Suazo CG, Delord K and Bustamante P (2022) Variation Among Species and Populations, and Carry-Over Effects of Winter Exposure on Mercury Accumulation in Small Petrels. Front. Ecol. Evol. 10:915199. doi: 10.3389/fevo.2022.915199

Even in areas as remote as the Southern Ocean, marine organisms are exposed to contaminants that arrive through long-range atmospheric transport, such as mercury (Hg), a highly toxic metal. In previous studies in the Southern Ocean, inter-specific differences in Hg contamination in seabirds was generally related to their distribution and trophic position. However, the Blue Petrel (*Halobaena caerulea*) was a notable exception among small seabirds, with higher Hg levels than expected. In this study, we compared the Hg contamination of Blue Petrels and Thin-billed Prions (*Pachyptila belcheri*), which both spend the non-breeding season in polar waters, with that of Antarctic Prions (*Pachyptila desolata*), which spend the winter in subtropical waters. We collected body feathers and blood samples, representing exposure during different time-frames. Hg concentrations in feathers, which reflect contamination throughout the annual cycle, were related to $\delta^{13}C$ values, and varied with ocean basin and species. Blue Petrels from breeding colonies in the southeast Pacific Ocean had much higher feather Hg concentrations than expected after accounting for latitude and their low trophic positions. Both Hg concentrations and $\delta^{15}N$ in blood samples of Blue Petrels were much lower at the end than at the start of the breeding period, indicating a marked decline in Hg contamination and trophic positions, and the carry-over of Hg burdens between the wintering and breeding periods. Elevated Hg levels may reflect greater reliance on myctophids or foraging in sea-ice environments. Our study underlines that carry-over of Hg concentrations in prey consumed in winter may determine body Hg burdens well into the breeding season.

Keywords: distribution, mercury, petrels, stable isotopes, trophic position

INTRODUCTION

Seabirds are often used as bioindicators of marine pollution (Van den Steen et al., 2011; Becker et al., 2016; Thébault et al., 2021). They are long-lived animals, feed at high trophic levels, and thus integrate and bioaccumulate contaminants from the food webs on which they rely (Albert et al., 2019). Often, seabirds nest in accessible breeding colonies, but roam over vast areas of ocean that

can thus be monitored. Our knowledge of their diets and at-sea distribution has greatly increased in the last years with the advances in biologging methods that are now suitable for the smallest seabird species (Quillfeldt et al., 2015), trophic tracers such as compound-specific stable isotope analyses (Lorrain et al., 2009; Quillfeldt and Masello, 2020), and metabarcoding from faecal samples (Kleinschmidt et al., 2019).

Among the contaminants that increase in the marine environment due to human activities, mercury (Hg) is a highly toxic non-essential metal that has deleterious effects on the behaviour, neurology, endocrinology and development of wildlife (Scheuhammer et al., 2007; Tan et al., 2009). Released from both natural and anthropogenic sources, Hg reaches remote polar and sub-polar regions through long-range atmospheric transport (Fitzgerald et al., 1998). In seabirds, Hg is incorporated from the food and accumulates in soft tissues such as liver and muscle (Bearhop et al., 2000a; Carravieri et al., 2014a). Birds can excrete up to 90% of the Hg accumulated since the previous moult in the new growing feathers and thus, feathers – which can be sampled non-destructively – are an archive of year-round Hg contamination (Thompson et al., 1998; Albert et al., 2019). Birds may also show a substantial carry-over of Hg among seasons, and slow changes in Hg over time. For example, Double-Crested Cormorants (*Phalacrocorax auritus*) and Caspian Terns (*Hydroprogne caspia*) with high Hg exposure in winter still had elevated blood Hg values in summer (Lavoie et al., 2014).

Among seabirds, species with high trophic position in marine food webs have elevated Hg concentrations due to the biomagnification of methylmercury (MeHg), the most bioavailable form of Hg in marine ecosystems (Seco et al., 2021). This pattern has been shown in the seabird community of the subantarctic Kerguelen Islands (Blévin et al., 2013; Carravieri et al., 2014a). In particular, species feeding in colder waters to the south had lower Hg concentrations than species feeding in northern, warmer waters. At the scale of the Southern Hemisphere, such a pattern (higher Hg concentrations in birds feeding in subtropical and subantarctic waters) has been confirmed for diverse species, including penguins, skuas, and albatrosses (Carravieri et al., 2014b, 2016, 2017, 2020; Cherel et al., 2018). However, the Blue Petrel (*Halobaena caerulea*) seems to be a marked exception to this general pattern, as Hg concentrations in tissues are one order of magnitude higher than in other species of small petrels (Bocher et al., 2003).

Blue Petrels and Prions, *Pachyptila* spp. are a similar size (∼200 g). The largest breeding populations of Blue Petrels are at Diego Ramírez Islands, Chile in the southeast Pacific Ocean (>2 million individuals or ∼1.35 million pairs; Schlatter and Riveros, 1997; Lawton et al., 2006), Kerguelen Islands in the southern Indian Ocean (100,000–200,000 pairs; Weimerskirch et al., 1989) and Marion Island in the Indian Ocean (110,000–180,000 pairs; Dilley et al., 2017). Muscle tissue sampled from Blue Petrels breeding at Kerguelen Islands contains far higher Hg concentrations than expected, given the relatively low Hg levels in epipelagic fish and crustaceans in the same region (Bocher et al., 2003). Proposed explanations include the relative longevity of Blue Petrels (up to 20 years) and thus, Hg bioaccumulation over the long term, and from their consumption of mesopelagic fish (Cherel et al., 2002b), which contain high Hg concentrations (Bustamante et al., 2003; Cipro et al., 2018; Seco et al., 2020). Blue Petrels at Marion Island in the southern Indian Ocean showed the highest feather Hg concentrations reported for the species so far (Becker et al., 2016). At South Georgia, studies reported either relatively high Hg concentrations in feathers of Blue Petrels (Becker et al., 2002) or Hg levels in a similar range to Antarctic Prions (*Pachyptila desolata*) and Diving Petrels, *Pelecanoides* spp. (Anderson et al., 2009).

Although Hg in Southern Ocean seabirds has received considerable attention (Anderson et al., 2009; Blévin et al., 2013; Becker et al., 2016; Carravieri et al., 2020), the influence of sea ice on Hg dynamics has not yet been explored. Recent studies identified bacteria of the genus *Nitrospina* as a potential Hg methylator within sea ice and brine, and proposed that Antarctic waters associated with sea ice can harbour a microbial source of MeHg in the Southern Ocean (Gionfriddo et al., 2016). Thus, total Hg (i.e., inorganic Hg and MeHg) and methylated Hg (MeHg) concentrations are elevated in these zones, related to high atmospheric Hg deposition and subsequent *in situ* methylation (Gionfriddo et al., 2016). A study of the Hg species distribution suggested that the Southern Ocean Hg cycle is characterized by a net atmospheric Hg deposition on surface waters near the ice edge, and Hg enrichment in brine during sea-ice formation (Cossa et al., 2011). Studies in coastal Antarctica have shown greatly enhanced total Hg concentrations in surface snow at the sea-ice edge adjacent to the freezing ocean surface (McMurdo/Ross Sea region: Brooks et al., 2008; Casey station/East Antarctica: Cossa et al., 2011). The Hg concentrations found in fast ice near Casey station were three orders of magnitude above the concentrations in surface water in the Southern Ocean (Cossa et al., 2011). A seasonal study of elemental and total Hg concentrations in the Antarctic sea-ice environment (Nerentorp Mastromonaco et al., 2016) found that the concentration of total Hg in sea ice halved from winter to spring (average 9.7 ng/l to 4.7 ng/l). A recent analysis has related high winter Hg concentrations to the frequency of katabatic winds, bringing Hg from the Antarctic ice sheet to coastal waters (Yu et al., 2021).

In the present study, we compared Hg concentrations in blood and feathers of Blue Petrels, Antarctic Prions, and Thin-billed Prions (*P. belcheri*), each at their largest colonies in widely separated oceans. Of the three species, Blue Petrels spend the non-breeding season at the most southerly latitudes (Quillfeldt et al., 2013, 2015; Navarro et al., 2015), and have disproportionately high Hg values (Bocher et al., 2003). We therefore used tracking data to examine if exposure to sea ice may play a part in explaining variability in Hg concentrations. We used stable isotope analyses to determine trophic positions and distributions (water mass) used by each species. In the Southern Ocean, $\delta^{13}C$ values in seabird tissues correspond to the location of their foraging habitats (Phillips et al., 2009; Jaeger et al., 2010; Quillfeldt et al., 2010b) and $\delta^{15}N$ values increase with trophic position (Cherel et al., 2010). As novel questions, we aimed to test (1) if foraging close to sea-ice-covered polar waters results in higher exposure to Hg, and (2) if there is carry-over of Hg between wintering and breeding grounds.

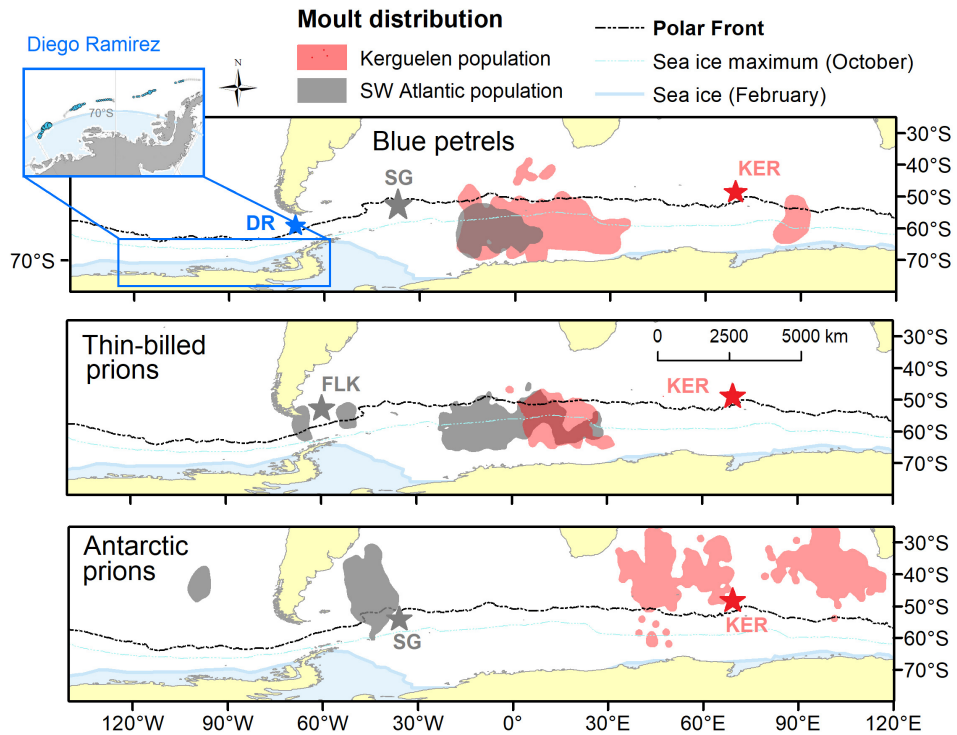

FIGURE 1 | Distribution of Blue Petrels, Thin-billed Prions, and Antarctic Prions during primary moult (i.e., the core moult area). Colony sites: Diego Ramirez (DR), South Georgia (SG), Falkland Islands (Malvinas) (FLK), and Kerguelen (KER). Blue Petrels moulting in February between 71°S, 119°W and 67°S, 78°W are most likely birds from the large Diego Ramirez colony (Ryan et al., 2020). Moult takes place around the time of the minimum sea-ice extent (February–April) in Blue Petrels and Thin-billed Prions, and during August–October in Antarctic Prions.

MATERIALS AND METHODS

Study Species

Blue Petrels, Thin-billed Prions, and Antarctic Prions have wide distributions in the Southern Ocean. We sampled breeding populations in the south-west Atlantic Ocean (Falkland Islands for Thin-billed Prions; South Georgia for Blue Petrels and Antarctic Prions) and in the Indian Ocean (Kerguelen Islands, all three species) (**Figure 1**). In addition, a population of Blue Petrels was sampled on Diego Ramírez Islands, Chile, southeast Pacific Ocean. In total, we sampled seven populations (**Figure 1**). Thin-billed Prions breed mainly on the Falkland and Kerguelen Islands. New Island, in the Falkland Islands, is the most important known breeding site for Thin-billed Prions with an estimated two million breeding pairs. South Georgia and Kerguelen are the most important breeding sites (with populations > 1 million) of Antarctic Prions.

These three petrel species migrate away from their breeding grounds during the non-breeding season, where they segregate latitudinally (Navarro et al., 2015; Quillfeldt et al., 2015). Antarctic Prions migrate to subtropical waters, and Thin-billed Prions and Blue Petrels moult in polar waters (Quillfeldt et al., 2013, 2015; Navarro et al., 2015). The species also show breeding allochrony, with Blue Petrels arriving at colonies in September, Thin-billed Prions in October and Antarctic Prions in November to early December (Quillfeldt et al., 2020). After several days of pair formation, the birds leave on a pre-laying exodus, and return ready for egg-laying and incubation, with the mean start of the first trip by the female in incubation at Kerguelen of 28 October (Blue Petrel), 19 November (Thin-billed Prion) and 26 December (Antarctic Prion) (Quillfeldt et al., 2020).

Differences in habitat use in the breeding season are less pronounced than in winter, and diets largely overlap. The three species are zooplanktivorous, with a preference for crustaceans (Prince, 1980; Cherel et al., 2002a,b; Quillfeldt et al., 2010a), and forage on the surface or up to depths of 5–7 m (Chastel and Bried, 1996; Cherel et al., 2002a; Navarro et al., 2013).

Study Sites and Seasons

Adult Blue Petrels and the two species of Prions were trapped either at the burrow or by mist net. Fieldwork at Kerguelen was carried out in colonies of Thin-billed Prions and Blue Petrels at Île Mayès (49°28′S, 69°57′E) during incubation, late chick-rearing or post-moult periods (when Blue Petrels return to clean out their burrows) of five breeding seasons (**Tables 1**, **2**). Sampling in 2010/11 was carried out as part of the POLARTOP project (Carravieri et al., 2014a,b) and in 2011/12, blood and feather samples were collected during the deployment and retrieval of geolocator-immersion loggers (Quillfeldt et al., 2015). Antarctic Prions were sampled at Île Verte (49°30′S, 70°02′E; n = 10) in 2011/12. Mist netting of Blue Petrels was carried

TABLE 1 | Summary of stable isotope and mercury data of Blue Petrels (mean ± standard deviation), as well as trophic position (TP) estimates based on linear models (TP_{LM}) or compound-specific isotope analyses of amino acids (TP_{CSIA}).

	POLARTOP ***Kerguelen 2010/11***	**GLS deployments** ***Kerguelen 2011/12***	**GLS recoveries** ***Kerguelen 2012/13***	***Kerguelen 2018/19***	***Diego Ramirez 2010/11***	***South Georgia 2010/11***	**GLS recoveries** ***South Georgia 2011/12***
Body feathers							
N	10	Not sampled	17	20	30 (16 for Hg)	20	8
$\delta^{13}C$ (‰)	−24.4 ± 0.7		−24.9 ± 0.5	−25.7 ± 1.1	−23.6 ± 1.3	−25.0 ± 1.3	−24.8 ± 0.8
$\delta^{15}N$ (‰)	9.0 ± 0.4		8.6 ± 0.5	8.3 ± 0.5	10.3 ± 0.9	8.8 ± 0.9	9.1 ± 0.7
TP_{CSIA}	–		–	3.21 ± 0.04	3.79 ± 0.11	–	–
TP_{LM}	3.34 ± 0.04		3.30 ± 0.03	3.27 ± 0.05	3.43 ± 0.07	3.31 ± 0.08	3.33 ± 0.04
Hg (μg/g dw)	1.44 ± 0.42		2.09 ± 1.65	1.68 ± 0.96	4.42 ± 2.72	1.69 ± 1.51	1.09 ± 0.72
Blood (early breeding season)							
N (sample time)	10 (September)	Not sampled	17 (November)	20 (November)	Not sampled	16 (20 November–4 December)	Not sampled
$\delta^{13}C$ (‰)	−22.4 ± 1.2		−24.0 ± 0.9	−24.1 ± 0.9		−23.4 ± 0.6	
$\delta^{15}N$ (‰)	10.3 ± 0.8		9.3 ± 0.5	9.2 ± 0.6		9.7 ± 0.4	
TP_{CSIA}	–		–	3.55 ± 0.24		–	
Hg (μg/g dw)	6.00 ± 2.78		4.58 ± 1.83	4.01 ± 1.63		2.76 ± 1.81	
Blood (late breeding season)							
N	11 (February)	20 (29 December–6 January)	Not sampled	20 (April)	24 (6 December–26 January)	Not sampled	Not sampled
$\delta^{13}C$ (‰)	−24.3 ± 0.5	−23.9 ± 1.1		−27.0 ± 0.3	−24.6 ± 0.2		
$\delta^{15}N$ (‰)	8.0 ± 0.3	9.1 ± 0.3		7.9 ± 0.4	8.8 ± 0.5		
TP_{CSIA}	–	–		–	3.43 ± 0.06		
Hg (μg/g dw)	2.06 ± 0.74	2.43 ± 1.05		0.49 ± 0.15	2.92 ± 0.74		

Early breeding season: arrival (September) to incubation (November), late breeding season: chick-feeding (December–February) to post-moult return (April).

out at Isla Gonzalo, Diego Ramírez Islands (56°29′S, 68°44′W) in December 2010 to January 2011. Thin-billed Prions were sampled at New Island, Falkland/Malvinas Islands (51°43′S, 61°18′W) in 2006/07 and 2017/18. Blue Petrels and Antarctic Prions were sampled at Bird Island, South Georgia (54°00′S, 38°03′W) in burrows during the austral summer 2010/11, when the incubation period overlaps between the two species, and feathers were also collected from Blue Petrels when geolocators were retrieved in austral summer 2011/12.

Sample Collection

We sampled two different tissue types, body feathers and blood. Body feathers, moulted annually, represent Hg accumulated over the annual cycle (Albert et al., 2019). To assess seasonal changes in Hg exposure, we sampled blood at different stages in the breeding season as blood reflects the contamination for the 1−2 previous months (half-life of 30 days in Great Skuas *Stercorarius skua*: Bearhop et al., 2000a; 40–65 days in Cory's Shearwaters *Calonectris borealis*: Monteiro and Furness, 2001). For sample times and sizes see **Tables 1**–**3**.

Feather samples (body feathers) were stored in individual Ziploc bags. Antarctic Prions moult their primaries towards the end of the non-breeding season, and Blue Petrels and Thin-billed Prions directly after the breeding season (Cherel et al., 2016). Less is known about body feather moult, but this is thought to occur over a longer period. Blue Petrels collected in January (i.e., likely non-breeders or failed breeders) had extensive body moult coinciding with primary and secondary feather moult (Bierman and Voous, 1950), but very few Blue Petrels moult body feathers in winter (Brown et al., 1986). Blue Petrels return to the colony after their moult, mostly in May (Brooke, 2004; own observations from tracking data).

Feathers were cleaned in a chloroform:methanol solution (2:1, v/v) in an ultrasonic bath and rinsed two times in methanol. After 48 h drying at 45°C in an oven, they were cut into tiny fragments with stainless steel scissors. Blood (0.2–0.4 ml) was sampled by puncture of the wing vein and collected using heparinized capillaries, or syringes. Blood was stored in ethanol (Diego Ramírez, Kerguelen 2012/13), or separated by centrifugation, and the pellet of red blood cells was frozen (Kerguelen 2010/11 and 2018/19, Falkland Islands, and South Georgia). Both whole blood and blood cells were freeze-dried and ground to powder for Hg and stable isotope analyses. As Hg from whole blood is mainly found in red blood cells (>95%), it is equivalent to analyse one or the other, when referring to dry mass.

The half-life of isotope turnover for avian red blood cells was 29.8 days in American Crows (*Corvus brachyrhynchos*) (Hobson and Clark, 1993). For this, blood samples collected from petrels therefore likely represented the diet ingested ca. 2–4 weeks before sampling. After return from the wintering areas, stable isotope ratios in blood quite quickly reach values characteristic of the summer habitat and diet (Cherel et al., 2014; Lavoie et al., 2014). In contrast, there can be substantial carry-over of Hg among

TABLE 2 | Summary of stable isotope and mercury data of Thin-billed Prions (mean ± standard deviation), as well as trophic position (TP) estimates based on linear models (TP_{LM}) or compound-specific isotope analyses of amino acids (TP_{CSIA}).

	New Island ***Falkland/Malvinas*** ***2006/07***	***Falkland/Malvinas*** ***2017/18***	**POLARTOP** ***Kerguelen*** ***2010/11***	**GLS recoveries** ***Kerguelen*** ***2012/13***	***Kerguelen*** ***2018/19***
Feathers (moult)					
N	20	20	12	23	14
$\delta^{13}C$ (‰)	−22.1 ± 2.8	−21.6 ± 1.8	−24.0 ± 1.0	−23.5 ± 1.0	−25.3 ± 0.9
$\delta^{15}N$ (‰)	10.5 ± 3.4	10.7 ± 1.94	9.1 ± 0.3	8.7 ± 0.3	8.2 ± 0.4
TP_{CSIA}	3.53 ± 0.06	3.39 ± 0.10	–	–	3.34 ± 0.07
TP_{LM}	3.51 ± 0.27	3.50 ± 0.14	3.35 ± 0.04	3.35 ± 0.03	3.27 ± 0.03
Hg (μg/g dw)	0.76 ± 0.61	1.13 ± 0.74	0.90 ± 0.29	1.62 ± 0.67	1.04 ± 0.52
Blood (early breeding season)					
N (month)	12	20	10 (October)	23 (26 November–3 December 2012)	14 (November)
$\delta^{13}C$ (‰)	−18.8 ± 0.8	−19.8 ± 0.5	−23.4 ± 1.5	−23.3 ± 1.2	−23.8 ± 0.5
$\delta^{15}N$ (‰)	12.4 ± 1.2	11.2 ± 1.1	9.3 ± 0.6	8.9 ± 0.3	8.2 ± 0.3
TP_{CSIA}	–	3.60 ± 0.07	–	–	3.56 ± 0.08
Hg (μg/g dw)	0.80 ± 0.25	0.99 ± 0.25	1.46 ± 0.39	1.29 ± 0.39	1.31 ± 0.31
Blood (late breeding season)					
N	6	20	12 (February)	Not sampled	3 (April)
$\delta^{13}C$ (‰)	−19.5 ± 1.9	−17.9 ± 1.1	−24.0 ± 0.6		−25.1 ± 0.2
$\delta^{15}N$ (‰)	12.1 ± 1.3	11.9 ± 0.9	8.0 ± 0.2		7.5 ± 0.2
TP_{CSIA}	–	3.47 ± 0.05	–		–
Hg (μg/g dw)	0.61 ± 0.24	0.63 ± 0.15	0.73 ± 0.20		0.72 ± 0.12

Early breeding season: arrival (October) to incubation (December), late breeding season: chick-feeding (January–April).

TABLE 3 | Summary of stable isotope and mercury data of Antarctic Prions (mean ± standard deviation), as well as trophic position (TP) estimates based on linear models (TP_{LM}).

	Antarctic Prion - GLS recoveries ***Kerguelen*** ***2012/13***	**Antarctic Prion** ***South Georgia*** ***2010/11***	**Antarctic Prion - GLS recoveries** ***South Georgia*** ***2011/12***
Feathers (moult)			
N	10	20	6
$\delta^{13}C$ (‰)	−18.8 ± 0.9	−18.7 ± 1.1	−20.9 ± 1.0
$\delta^{15}N$ (‰)	9.9 ± 0.8	10.5 ± 1.8	10.1 ± 1.0
TP_{LM}	3.53 ± 0.05	3.56 ± 0.12	3.49 ± 0.07
Hg (μg/g dw)	2.39 ± 0.58	1.68 ± 0.75	1.49 ± 0.44
Blood (early breeding season)			
N (month)	10 (January)	15 (December–January)	Not sampled
$\delta^{13}C$ (‰)	−23.8 ± 0.8	−21.8 ± 0.7	
$\delta^{15}N$ (‰)	8.2 ± 02	8.2 ± 0.4	
Hg (μg/g dw)	0.71 ± 0.18	0.39 ± 0.13	
Blood (late breeding season)			
N	Not sampled	2 (February)	Not sampled
$\delta^{13}C$ (‰)		−21.6 ± 1.8	
$\delta^{15}N$ (‰)		8.9 ± 0.3	
Hg (μg/g dw)		0.34 ± 0.20	

Early breeding season: incubation (December–January), late breeding season: chick-feeding (February).

seasons and slow changes in the body pool of Hg over time, especially for individuals with high Hg exposure in winter (Lavoie et al., 2014). This suggests a slow depuration rate and storage in internal tissues, such that levels in the blood reflect both recent and past exposure. Renal excretion of MeHg is low and bile excretion is followed by intestinal reabsorption, thus retaining Hg in the organism. Hence, Hg values in blood at a given time may be influenced by previous exposure at distant locations.

Mercury Analyses

Mercury concentrations were determined on aliquots with an Advanced Mercury Analyser spectrophotometer Altec AMA-254 [aliquots: blood ∼2 mg dry weight (dw), feathers ∼1 mg dw] as described in Bustamante et al. (2006). AMA measures total Hg but bird blood and feathers contain virtually 100% methylmercury (Thompson and Furness, 1989; Renedo et al., 2017; Manceau et al., 2021). Measurements were repeated two to three times for each sample, until the relative standard deviation (RSD) was <10%. For each set of samples, accuracy and reproducibility of the results were tested by preparing analytical blanks and performing replicate measurements of certified reference materials (TORT-2: lobster hepatopancreas, certified concentration: 0.27 ± 0.06 μg/g dw; DOLT-5: dogfish liver, certified concentration: 0.44 ± 0.18 μg/g dw; National Research Council of Canada). Measured Hg concentrations for the certified reference materials were: 0.26 ± 0.02 μg/g dw ($n = 18$) and 0.42 ± 0.01 μg/g dw ($n = 15$) for TORT-2 and DOLT-5, respectively, corresponding to a recovery rate of 96 ± 2% for TORT-2 and 96 ± 1% for DOLT-5. The limit of detection (LOD) was 0.005 μg/g dw. Hg concentrations are expressed in μg/g dw.

Bulk Stable Isotope Analyses

To perform bulk stable isotope analyses, 0.2–0.4 mg of sample was weighed into tin cups. $\delta^{13}C$ and $\delta^{15}N$ values were determined with a continuous-flow mass spectrometer (Thermo Scientific Delta V Advantage) coupled to an elemental analyser (Thermo Scientific Flash EA 1112). Results are expressed in parts per thousand (‰) in the usual δ notation, relative to Vienna Pee Dee Belemnite for $\delta^{13}C$ and atmospheric N_2 for $\delta^{15}N$, following the formula:

$$\delta^{13}C \text{ or } \delta^{15}N = \left(\frac{R_{sample}}{R_{standard}} - 1\right) \times 10^3$$

where R is $^{13}C/^{12}C$ or $^{15}N/^{14}N$, respectively. Measurements of internal laboratory standards were conducted using acetanilide and peptone and indicated an experimental precision of ±0.15 ‰ for both elements.

Compound-Specific Isotope Analyses of Amino Acids

Compound-specific isotope analyses of amino acids (CSIA-AA) data can provide a good estimate of the trophic position of marine organisms even from temporally and spatially variable environments. CSIA-AA were performed at the UC Davis Stable Isotope facility (United States), as described previously (Quillfeldt and Masello, 2020). Trophic positions (TP) were calculated from the $\delta^{15}N$ values of glutamic acid (Glx) and phenylalanine (Phe), using a stepwise trophic discrimination factor (multi-$TDF_{Glx-Phe}$, for detailed discussion, see Quillfeldt and Masello, 2020), with the following equations:

$$\text{TP[feathers]} = 2 + \frac{Glx - Phe - 3.5\ ‰ - 3.4\ ‰}{6.2\ ‰}$$

$$\text{TP[blood cells]} = 2 + \frac{Glx - Phe - 4.0\ ‰ - 3.4\ ‰}{6.2\ ‰}$$

Due to high analytical costs, only small sample sizes were analysed with CSIA-AA. For Blue Petrels (**Table 1**), we analysed 10 blood samples and 10 feathers (five from Kerguelen and five from Diego Ramírez, respectively). For Thin-billed Prions (**Table 2**), we included 20 blood samples (5 from Kerguelen and 15 from New Island: 5 each in 2 years and 2 parts of the season), and 21 feathers (5 from Kerguelen and 16 from New Island: 5 from 2017 to 2018, and 11 from 2006 to 2007).

Calculation of Trophic Positions

Trophic positions were calculated as described in Thébault et al. (2021). In the Southern Hemisphere, a latitudinal enrichment in $\delta^{15}N$ baseline values occurs from Antarctic to subtropical waters (Jaeger et al., 2010; Quillfeldt et al., 2010b). To correct for this latitudinal effect, we calculated the trophic positions of the birds by applying linear regression models to the relationship between TP_{CSIA} and bulk stable isotope values ($\delta^{13}C$ and $\delta^{15}N$). Trophic positions calculated with linear models are referred as TP_{LM}.

Linear regression models were used to test relationships between TP_{CSIA} and bulk stable isotope values ($\delta^{13}C$ and $\delta^{15}N$). Models were applied separately for blood samples, both reflecting short-term food intake and with similar TDF – 4.0 ‰ (Quillfeldt and Masello, 2020) and 4.1 ‰ (Hebert et al., 2016), respectively, and feather samples (which reflect trophic ecology at the time of moult). For feathers, the linear regression model was statistically significant ($R^2 = 0.58$, $F_{28,2} = 19.1$, $p < 0.001$), and the following equation was used to calculate trophic positions from bulk stable isotope values:

$$TP_{LM}\left[\text{feathers, N} = 31\right] = 3.476 + 0.026 \times \delta^{13}C + 0.055 \times \delta^{15}N$$

However, the linear regression model was not statistically significant for blood TP_{CSIA} values ($R^2 = 0.05$, $F_{22,2} = 0.5$, $p = 0.596$). Thus, we did not calculate trophic positions from bulk stable isotope values for blood.

Distribution, Moult and Sea Ice Concentrations

Moulting times and distributions were determined using three steps, as described previously in Cherel et al. (2016): using the information recorded by the geolocator-immersion loggers (i) extraction of daily data on activity using the ACTAVE tool (Mattern et al., 2015), (ii) fitting a Generalized Additive Model (GAM) to the variable 'on-water' (i.e., the total time spent on water) separately for each individual, and (iii) calculating the dates when the fitted 'on-water' value exceeded 75% of the

maximum (which indicates the core moult area; Cherel et al., 2016).

We defined habitat zones following Cherel et al. (2018), based on feather $\delta^{13}C$ isoscapes (Jaeger et al., 2010), as Subtropical Zone (STZ): $\delta^{13}C > -18.3$ ‰, Subantarctic Zone (SAZ): $\delta^{13}C$ values of -21.2 to -18.3 ‰, and Antarctic Zone (AZ): $\delta^{13}C < -21.2$ ‰. Likewise, in blood, habitat was derived from $\delta^{13}C$ as Subtropical Zone (STZ): $\delta^{13}C > -20.1$ ‰, Subantarctic Zone (SAZ): $\delta^{13}C$ values of -22.9 to -20.1 ‰, and Antarctic Zone (AZ): $\delta^{13}C < -22.9$ ‰ (Jaeger et al., 2010).

The populations were assigned to the ocean basin where they spend most of their annual cycle. Thus, although Blue Petrels from Kerguelen moult in the Atlantic, and Blue Petrels from South Georgia spend 2 months in winter in the Pacific, they were assigned to the ocean basin of their breeding colony, i.e., Indian and Atlantic Ocean, respectively.

Using geolocator data, we calculated an index of sea-ice concentrations used by tracked birds, obtained through the Environmental Data Automated Track Annotation System (Env-DATA) on Movebank[1]. Sea-ice values (ECMWF Interim Full Daily SFC Sea Ice Cover, scale 0–1) for each location were summarized by individual and month. From these, we calculated the maximum value and mean annual sea-ice concentration. The maximum values were reached in the weeks before the breeding season, and we tested for a relationship with Hg values in blood collected in the early breeding season. An exception was the Thin-billed Prions from New Island, where the sea-ice maximum was reached earlier in the winter; however, this population was excluded from analyses as Hg was not measured in feathers and blood of tracked animals. As body feathers integrate the Hg contamination over the year, we tested for a relationship with the mean annual sea-ice values of tracked birds during the breeding and non-breeding season.

Data Analyses

Data were analysed in R4.1.0., and visualized in R and in ArcGIS 10.2.2. Normality was tested using Shapiro tests and QQ plots. Stable isotopes and Hg values were not normally distributed, and univariate statistics were carried out using non-parametric tests, while the data were successfully transformed using transform Tukey in the R package "rcompanion" before carrying out multivariate statistics such as linear models. A comparison of the model outputs did not show any large differences between models using transformed and untransformed data. Thus, effect plots are given from models of untransformed data to enhance readability, i.e., showing the actual scale of the data.

As Hg concentrations differed among the species and did not show a linear relationship with stable isotope values, we ran GAMs in the R package "mgcv", separately for the species. As proxies for the trophic position, we included either $\delta^{15}N$ or the estimated trophic position based on the linear regression of feather $\delta^{15}N$ and $\delta^{13}C$ values (TP_{LM}). As proxies for distribution, we included either $\delta^{13}C$ or the distribution zone. We checked all GAMs for model convergence and random distribution of residuals, and reported statistics (effective degrees of freedom and *p*-values) for the GAMs run separately for each parameter.

We further ran a model selection separately for each species with the dredge function in the R package MuMIn on the full models for feathers: gam(THg.feathers $\sim$ s(TP_est) + s(δ^{13}C.feathers) + s(δ^{15}N.feathers) + habitat + ocean), and for blood: gam(THg.blood $\sim$ s(δ^{13}C.blood) + s(δ^{15}N.blood) + season + habitat + ocean). For the selected best models, we report the coefficients and, as a measure of effect size, calculated eta squared values (η^2) obtained with the EtaSq function in the R package "DescTools". Unless indicated otherwise, mean values are given ± SD.

RESULTS

Year-Round Distribution and Moulting Sites

The three species and their different populations had distinct moulting sites and winter distributions (**Figures 1**, **2**). Blue Petrels and Thin-billed Prions moulted south of the Antarctic Polar Front, and Antarctic Prions to its north. In all three species, birds from Kerguelen started the core period of moult later than birds from the south-west Atlantic colonies (mean 12 days, 11 days, and 28 days later in Blue Petrels, Thin-billed Prions, and Antarctic Prions, respectively: **Supplementary Figure 1** and **Supplementary Table 1**). Blue Petrels from South Georgia and Kerguelen moulted in the Southern Ocean between 20°W and 30°E, overlapping between 20°W and 10°E (**Figure 1**). Based on the immersion data, the core moult phase took place on average between early February and late March in Blue Petrels from South Georgia, and between mid-February and early April in Blue Petrels from Kerguelen (**Supplementary Figure 1** and **Supplementary Table 1**). The latitudes during the breeding and moulting period differed only slightly for Blue Petrels from Kerguelen and South Georgia (**Supplementary Figure 2**), whereas ship-based observations indicate that Blue Petrels from Diego Ramírez moult at higher latitudes (c. 70°S; Ryan et al., 2020). Blue Petrels from Kerguelen and South Georgia spent the mid-winter mostly south of 55°S (**Figure 2** and **Supplementary Figure 2**). Although both populations moulted in the Atlantic Ocean, subsequent longitudinal movements were in opposite directions; birds from Kerguelen returned to the Indian Ocean, whereas those from South Georgia entered the Pacific Ocean in mid-winter (July–August) (**Supplementary Figure 2**).

The moulting areas of Thin-billed Prions were southeast and southwest of the Falkland Islands, and most birds from the Falklands and Kerguelen moulted in waters between 25°W and 30°E, overlapping between 0° and 30°E (**Figure 1**). The core moult period was between late February and early April in Thin-billed Prions from the Falkland Islands, and between early March and late April in Thin-billed Prions from Kerguelen (**Supplementary Figure 1** and **Supplementary Table 1**). The year-round latitudinal distribution was very similar for Thin-billed Prions from both colonies (**Supplementary Figure 3**), whereas longitudinal movements were in opposite directions

[1] movebank.org

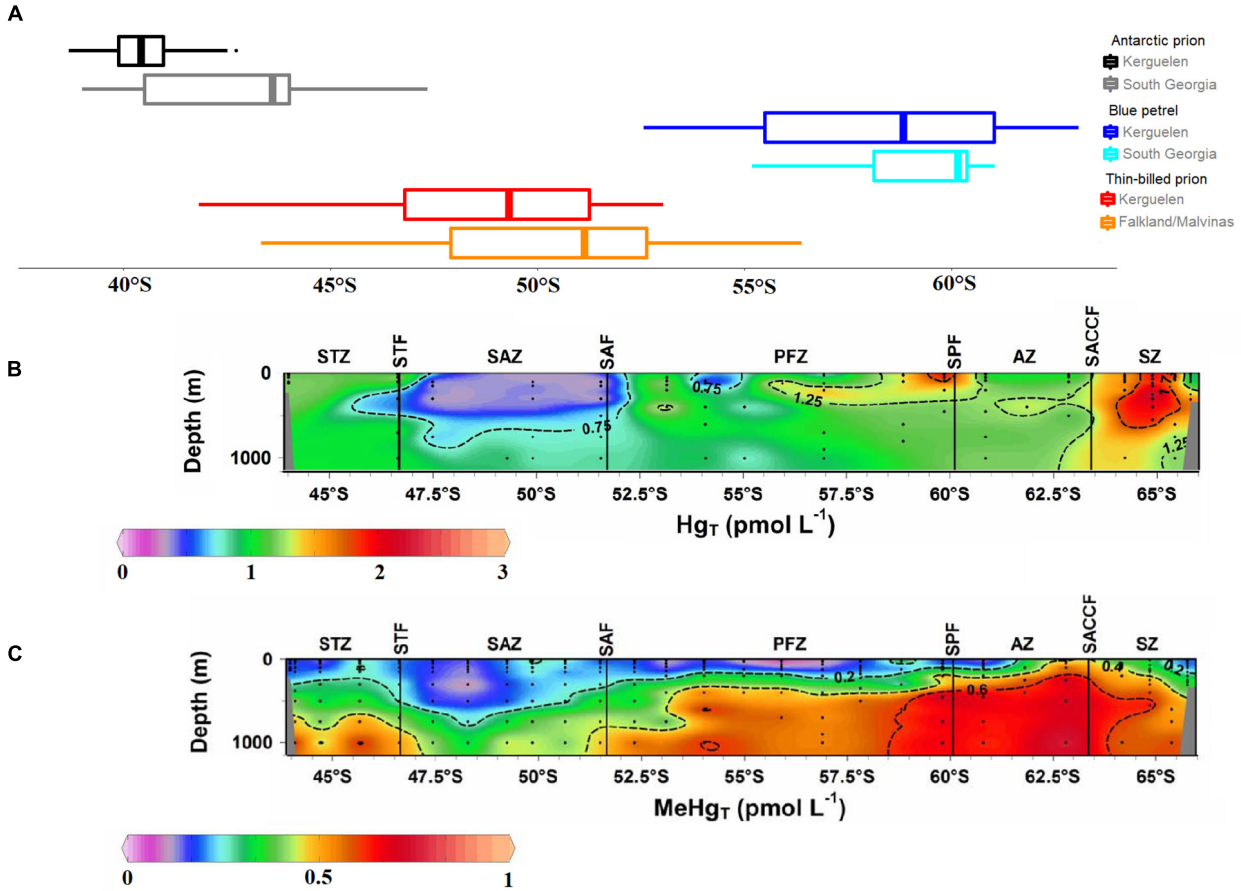

FIGURE 2 | (A) Latitudinal distribution of geolocator tracked Blue Petrels, Thin-billed Prions, and Antarctic Prions during the mid-winter months (June to August), and a mercury transect shown for comparison: **(B)** total mercury and **(C)** methyl mercury concentrations along a transect from Hobart to the Antarctic (adapted from Figures 3 and 6 in Cossa et al., 2011). STZ, Subtropical Zone; STF, Subtropical Front; SAZ, Subantarctic Zone; SAF, Subantarctic Front; PFZ, Polar Frontal Zone; SPF, Polar Front; AZ, Antarctic Zone; SACCF, Southern Antarctic Circumpolar Current Front; SZ, Southern Zone. Note that the position of the fronts changes longitudinally (e.g., see Polar Front in **Figure 1**).

(**Supplementary Figure 3**). Thin-billed Prions spent the mid-winter mostly between 45°S and 55°S, intermediate between the other two species (**Figure 2** and **Supplementary Figure 3**).

Antarctic Prions generally moulted north of the Antarctic Polar Front, and the moult areas of the birds from South Georgia and Kerguelen did not overlap (**Figure 1**). The core moult took place in the pre-breeding period, between late July and mid-October in Antarctic Prions from South Georgia, and between early August and late October in Antarctic Prions from Kerguelen (**Supplementary Figure 1** and **Supplementary Table 1**). The latitudes during the breeding period were slightly lower, and those in the winter and moult periods slightly higher, for Antarctic Prions from Kerguelen (**Figure 2** and **Supplementary Figure 4**), and longitudinal movements were relatively short in this species (**Supplementary Figure 4**). Antarctic Prions spent the mid-winter mostly north of 45°S (**Figure 2** and **Supplementary Figure 4**), and moulted during this time. Antarctic Prions had longer core-moult periods (71 and 88 days) than the other two species (43–53 days, **Supplementary Table 1**).

Feather Stable Isotope Values

Stable isotope values of feathers differed among species (**Tables 1–3** and **Supplementary Figure 5**), with the $\delta^{13}C$ and $\delta^{15}N$ values increasing from Blue Petrels to Thin-billed Prions to Antarctic Prions (Kruskal–Wallis tests; for $\delta^{13}C$: $\chi^2 = 100.2$, *d.f.* = 2, $p < 0.001$, *post-hoc* Dunn-tests: all $p < 0.001$, for $\delta^{15}N$: $\chi^2 = 27.6$, *d.f.* = 2, $p < 0.001$, *post-hoc* Dunn-tests: Blue Petrels vs. Thin-billed Prions $p = 0.292$, all other $p < 0.001$). Trophic positions based on the subset of feathers analysed for CSIA from Thin-billed Prions and Blue Petrels ranged from 3.0 to 4.3. A linear model detected no significant difference in trophic positions between the species (ANOVA tests; $F_{1,26} = 1.04$, $p = 0.316$, $\eta^2 = 0.045$), whereas differences among the oceans were significant ($F_{2,26} = 3.82$, $p = 0.035$, $\eta^2 = 0.227$), as were differences among feathers from AZ and SAZ distributions ($F = 46.9$, $p < 0.001$, $\eta^2 = 0.511$; **Supplementary Figure 6**). Trophic positions were higher in the Pacific population, and birds with more northerly distributions (**Figure 3** and **Supplementary Figure 6**).

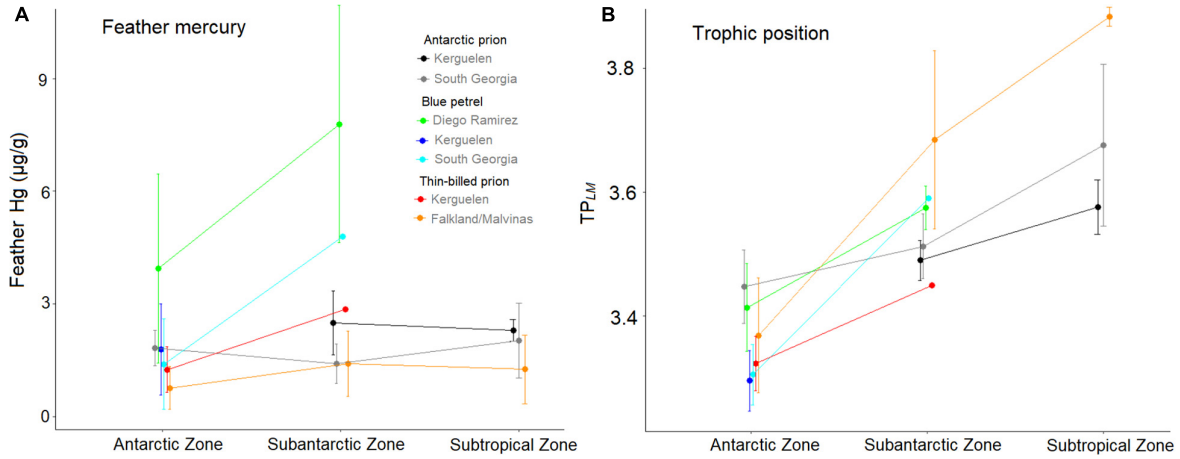

FIGURE 3 | Mercury and trophic position in feathers of Blue Petrels, Thin-billed Prions, and Antarctic Prions (BP, TBP, and AP, respectively). The mercury **(A)** and trophic position **(B)** values are shown for the seven populations, separately for habitat zones. Habitat was derived from $\delta^{13}C$ following Cherel et al. (2018), as Subtropical Zone (STZ): $\delta^{13}C > -18.3$ ‰, Subantarctic Zone (SAZ): $\delta^{13}C$ values of –21.2 to –18.3 ‰, and Antarctic Zone (AZ): $\delta^{13}C < -21.2$ ‰.

Across species, the trophic positions determined from feathers using linear models (TP_{LM}), ranged from 3.2 to 3.9. Using this larger data set, we detected moderate differences in TP_{LM} among species ($F_{2,206} = 109.4$, $p < 0.001$, $\eta^2 = 0.148$) and oceans ($F_{2,206} = 23.2$, $p < 0.001$, $\eta^2 = 0.184$), and strong differences among distributions ($F_{2,206} = 263.0$, $p < 0.001$, $\eta^2 = 0.574$). Trophic positions were elevated and highly variable in the Pacific population, and birds with more northerly distributions (**Figure 4**).

Mercury concentrations in feathers differed among species (Kruskal–Wallis ANOVA: $\chi^2 = 85.5$, *d.f.* = 2, $p < 0.001$, *post-hoc* Dunn-tests: Blue Petrels vs. Antarctic Prions $p = 0.265$, all other $p < 0.001$). The highest mean Hg concentrations were in Blue Petrels (2.17 ± 1.94 µg/g), followed by Antarctic Prions (1.85 ± 0.75 µg/g), and Thin-billed Prions (1.14 ± 0.69 µg/g). Of the seven populations, Blue Petrels from Diego Ramírez (Pacific Ocean) had much higher Hg concentrations than predicted by their latitudinal distribution and trophic positions (**Figure 4** and **Supplementary Figures 7–9**).

Generalized Additive Models (**Figure 4** and **Table 4**) showed a significant effect of ocean basin in all three species, with the most elevated Hg values in the Pacific Ocean and the lowest in the Atlantic Ocean (**Figure 5**). In Blue Petrels and Thin-billed Prions, distribution ($\delta^{13}C$, habitat zone) as well as trophic position ($\delta^{15}N$, TP_{LM}) influenced Hg values (**Figure 4** and **Table 4**). Model selection retained only ocean basin for Antarctic Prions (**Figure 6**), but all parameters except habitat zone for Blue Petrels and Thin-billed Prions. Coefficients for the effect of trophic position ($\delta^{15}N$, TP_{LM}) on feather Hg indicated a strong positive relationship for Blue Petrels, a weaker, negative relationship for Thin-billed Prions, and no influence for Antarctic Prions (**Figure 6**).

Blood Stable Isotope Values

Mean blood $\delta^{13}C$ values were lowest in Blue Petrels (−24.4 ± 1.4 ‰), and higher in Thin-billed Prions (−21.4 ± 2.6 ‰) and Antarctic Prions (−22.5 ± 1.3 ‰, Kruskal–Wallis ANOVA: $\chi^2 = 90.3$, *d.f.* = 2, $p < 0.001$), with no significant difference between the last two species (*post-hoc* Dunn-tests: Thin-billed vs. Antarctic Prions $p = 0.474$, all other $p < 0.001$). Blood $\delta^{15}N$ values differed among species, and were lowest in Antarctic Prions (8.3 ± 0.3 ‰), intermediate in Blue Petrels (9.0 ± 0.8 ‰), and highest in Thin-billed Prions (10.1 ± 1.9 ‰, Kruskal–Wallis ANOVA: $\chi^2 = 38.5$, *d.f.* = 2, $p < 0.001$, *post-hoc* Dunn-tests: all $p < 0.001$).

The trophic positions based on the subset of blood samples analysed for CSIA ranged from 3.3 to 4.0 in Thin-billed Prions (3.5 ± 0.1) and Blue Petrels (3.5 ± 0.2). According to TP_{CSIA} values, the trophic positions of the two species did not differ significantly (*t*-test, $t = -0.7$, *d.f.* = 11.6, $p = 0.480$).

Mean Hg concentrations in blood differed among species (Kruskal–Wallis ANOVA: $\chi^2 = 124.0$, *d.f.* = 2, $p < 0.001$, *post-hoc* Dunn-tests: all $p < 0.001$), with the highest concentrations in Blue Petrels (2.99 ± 1.97 µg/g), then Thin-billed Prions (0.99 ± 0.41 µg/g), and Antarctic Prions (0.51 ± 0.22 µg/g).

Species-specific GAMs showed a significant effect of latitudinal distribution ($\delta^{13}C$, habitat zone) in all three species (**Table 5** and **Figures 7**, **8**). However, this was only clearly positive in Blue Petrels (**Figures 7**, **8** and **Supplementary Figure 10**). The trophic position ($\delta^{15}N$) influenced Hg values in Blue Petrels and Thin-billed Prions (**Table 5**), with a clear increase only in Blue Petrels (**Figure 8**). There was a significant effect of ocean basin for Antarctic and Thin-billed Prions (**Table 5**). Changes in Hg and stable isotope values over the season were apparent in blood of Blue Petrels and, to a lesser extent, of Thin-billed Prions (**Table 5** and **Figure 7**). There was a decrease of an order of magnitude in Hg concentrations in blood of Blue Petrels, which were sampled from arrival in September to the post-moult visit to the colony in April (**Figure 9**).

For blood Hg, all parameters except $\delta^{15}N$ and habitat were retained in the best models for Antarctic Prions (**Figure 6D**). Habitat was also excluded for Blue Petrels (**Figure 6E**), and in

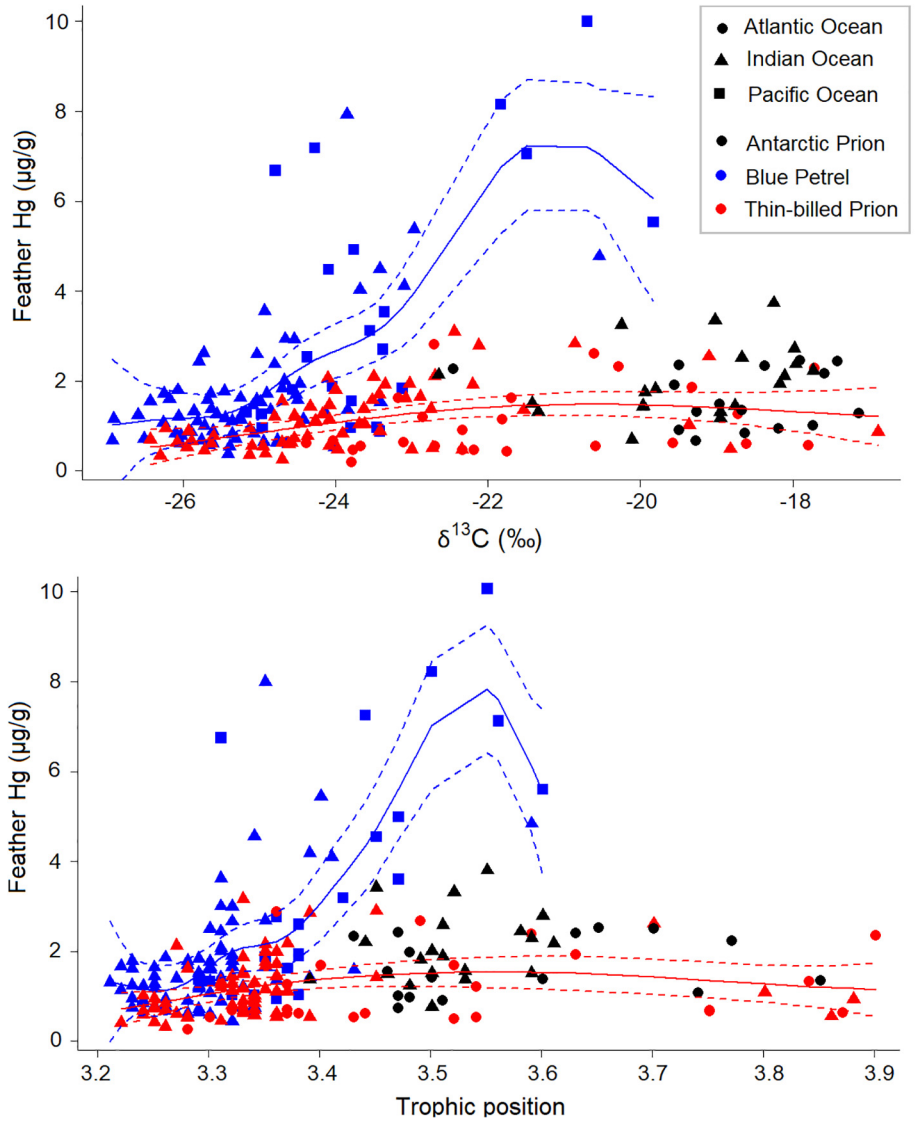

FIGURE 4 | Species-specific Generalized Additive Model (GAM) model fits for mercury values in feathers of Antarctic Prions, Blue Petrels, and Thin-billed Prions. Estimated smoothing curves for mercury values in feathers in relation to $\delta^{13}C$ and trophic position (derived from $\delta^{15}N$ and $\delta^{13}C$ values, with 95% confidence intervals) are given where statistically significant. For GAM statistics, see **Table 4**.

three of four best models for Thin-billed Prions (**Figure 6F**). Coefficients for the effect of trophic position ($\delta^{15}N$) on the feather Hg indicated a strong positive relationship for Blue Petrels, but values close to zero for Thin-billed Prions and Antarctic Prions (**Figure 6**).

Sea-Ice Concentration

The year-round sea-ice concentration in areas used by tracked Blue Petrels, Thin-billed Prions and Antarctic Prions (**Figure 10**) from the Atlantic and Indian Ocean showed two annual peaks: in April for Blue Petrels and Thin-billed Prions from Atlantic colonies, and again in August–September for Blue Petrels. Blue Petrels from the Indian Ocean had higher sea-ice overlap than birds from the Atlantic in April to August (**Figure 10**). Blue Petrels from Diego Ramírez have not yet been tracked (but see distribution in **Figure 1**). The highest exposure to sea ice was in September for all populations except Thin-billed Prions from New Island (Falklands) (**Figure 10**).

During the period of wing moult (**Supplementary Figure 1** and **Supplementary Table 1**), sea-ice exposure was low (<0.01) for all populations.

Data From Individually Tracked Birds

Matching data on blood Hg and sea-ice exposure were available for tracked individuals from four populations (**Figure 11A**), and on feather Hg and sea-ice exposure for five populations (**Figure 11B**). Model selection suggested that species differences were sufficient to explain differences in blood Hg values,

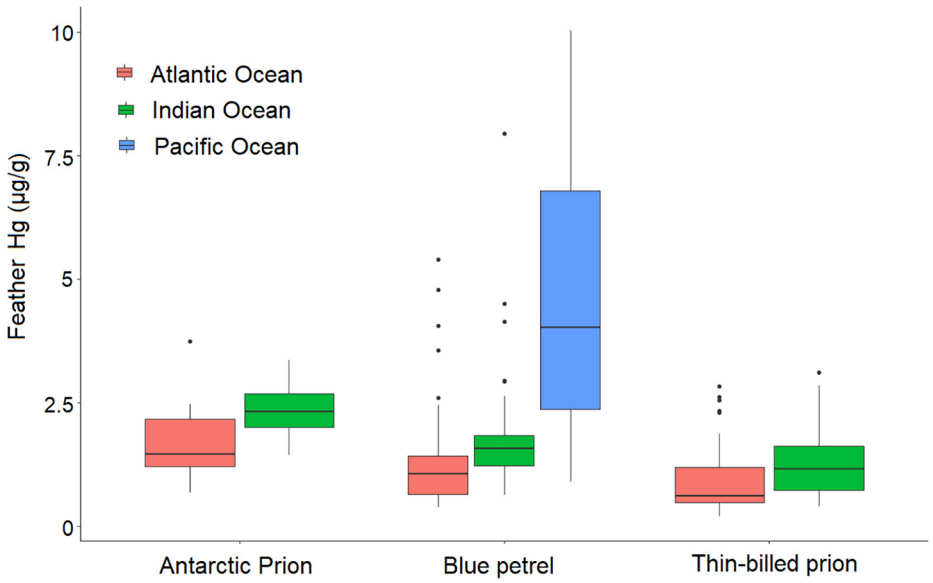

FIGURE 5 | Mercury values in feathers of Antarctic Prions, Blue Petrels, and Thin-billed Prions from different ocean basins. Boxplots showing medians, interquartile ranges, and outliers.

TABLE 4 | Generalized Additive Model (GAM) results for feather mercury values, separately for the species, as a function of distribution ($\delta^{13}C$, habitat), trophic position ($\delta^{15}N$, TP_{LM}), and ocean basin (Atlantic, Indian, or Pacific).

Species	Variable	Smoother edf (*P*)	Effect size	Estimate (SE) *P*
Blue Petrel	**$\delta^{13}C$**	**5.29 (*P* < 0.001)**	**0.532**	
(*n* = 90)	**$\delta^{15}N$**	**5.58 (*P* < 0.001)**	**0.536**	
	TP_{LM}	**6.09 (*P* < 0.001)**	**0.592**	
	Habitat		**0.198**	**4.78 (1.02) *P* < 0.001**
	Ocean		**0.299**	**2.90 (0.51) *P* < 0.001**
Thin-billed Prion	**$\delta^{13}C$**	**2.23 (*P* = 0.002)**	**0.176**	
(*n* = 87)	$\delta^{15}N$	1.57 (*P* = 0.523)	0.023	
	TP_{LM}	**2.35 (*P* = 0.029)**	**0.120**	
	Habitat		**0.049**	**0.46 (0.22) *P* = 0.043**
	Ocean		**0.050**	**0.31 (0.15) *P* = 0.037**
Antarctic Prion	$\delta^{13}C$	1.30 (*P* = 0.699)	0.030	
(*n* = 36)	$\delta^{15}N$	1.70 (*P* = 0.454)	0.073	
	TP_{LM}	1.62 (*P* = 0.562)	0.056	
	Habitat		0.077	0.13 (0.41) *P* = 0.267
	Ocean		**0.205**	**0.75 (0.25) *P* = 0.006**

Habitat was derived from $\delta^{13}C$ following Cherel et al. (2018), as Subtropical Zone (STZ): $\delta^{13}C > -18.3$ ‰, Subantarctic Zone (SAZ): $\delta^{13}C$ values of -21.2 to -18.3 ‰, and Antarctic Zone (AZ): $\delta^{13}C < -21.2$ ‰. GAM results are reported for separate models for each parameter. Parameters with a statistically significant effect on feather mercury values are marked bold.

but when analysing the dataset across species, a GAM suggested that blood Hg values increased with maximum sea-ice exposure (**Figure 11A** and **Table 6**). In contrast, feather Hg concentrations were not related to mean annual sea-ice exposure (**Figure 11B** and **Table 6**).

DISCUSSION

In the present study, we examined temporal and spatial effects on stable isotope values and Hg concentrations in seven populations of three species of small petrels in widely separated oceans. We found evidence that higher trophic level and the distribution may result in higher exposure to Hg. We also found a carry-over effect of Hg exposure between wintering and breeding grounds.

Variation Among Species and Populations in Mercury Concentrations

We found interspecific differences in Hg concentrations in both blood and feathers, with the highest value for both tissues in Blue Petrels. In the literature, differences among

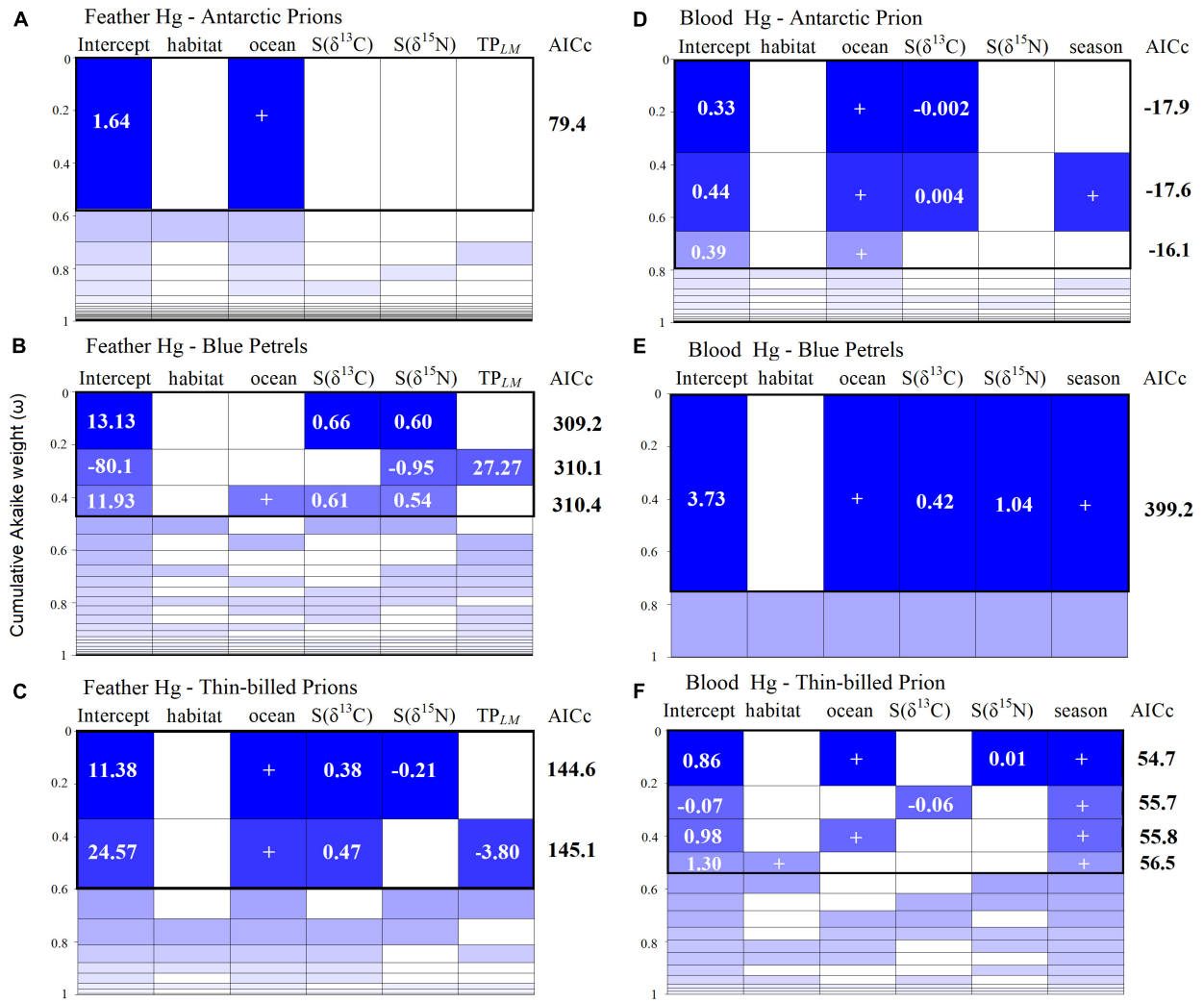

FIGURE 6 | Summary of GAM model selection (dredge function in the R package MuMIn) on the full models for feathers **(A–C)**: gam(THg.feathers ~ s(TP_est) + s(δ^{13}C.feathers) + s(δ^{15}N.feathers) + habitat + ocean), and for blood **(D–F)**: gam(THg.blood ~ s(δ^{13}C.blood) + s(δ^{15}N.blood) + season + habitat + ocean). The selected best models are outlined, and their AICs given on the right. Blue cells note the retained parameter, with coefficients reported in white letters.

species in Hg concentrations are mostly discussed in relation to biomagnification processes and thus, trophic position (e.g., Becker et al., 2002; Anderson et al., 2009; Blévin et al., 2013; Gatt et al., 2020). However, we here compared three small-bodied petrel species of similar trophic positions, according to δ^{15}N values in feathers and blood samples. We found that similar trophic position in different water masses did not lead to the same degree of Hg biomagnification. For example, Thin-billed Prions had the highest trophic positions relative to their distribution, but lower Hg concentrations than Blue Petrels. This result does not agree with the suggestion that the trophic position is the most important factor explaining variation in Hg concentrations in Southern Ocean seabirds (Becker et al., 2002). Likewise, in tunas trophic effects (i.e., geographical changes in foraging ecology) had a limited influence on the spatial variability of tissue Hg concentrations (Médieu et al., 2022).

Despite generally low trophic positions, dietary differences exist among the species, especially in the relative importance of fish. At South Georgia, crustaceans, and particularly Antarctic krill (*Euphausia superba*), predominated in Antarctic Prion and Blue Petrel diets, but fish was considerably more important for the Blue Petrels (Prince, 1980). In Blue Petrels at Marion Island (Steele and Klages, 1986), the diet consisted of 60% crustaceans, 21% myctophid fish and 16% squid by mass. In Blue Petrels at Kerguelen, however, the contribution of fish was higher (57%, Cherel et al., 2002b). Compared to King Penguins (*Aptenodytes patagonicus*) at Kerguelen which have a diet consisting of primarily (>90%) myctophids, Blue Petrels at the same island group have only slightly lower feather Hg values (**Table 1**, King Penguins = 2.2 ± 0.5 μg/g; Carravieri et al., 2013). In comparison, the proportion of fish taken by Thin-billed Prions and Antarctic Prions is very low both in Kerguelen (Cherel

TABLE 5 | Generalized Additive Model (GAM) results for blood mercury values, separately for the species, as a function of distribution ($\delta^{13}C$, habitat), trophic position ($\delta^{15}N$), period (early = arrival to incubation vs. late = chick-rearing), and ocean basin (Atlantic, Indian, or Pacific).

Species	Variable	Smoother edf (*P*)	Effect size	Estimate (SE) *P*
Blue Petrel	**$\delta^{13}C$**	**2.99 (*P* < 0.001)**	**0.498**	
(*n* = 135)	**$\delta^{15}N$**	**1.76 (*P* < 0.001)**	**0.546**	
	Period		**0.373**	**−2.54 (0.28) *P* < 0.001**
	Ocean		0.002	0.28 (0.53) *P* = 0.602
	Habitat		**0.196**	**2.76 (0.48) *P* < 0.001**
Thin-billed Prion	**$\delta^{13}C$**	**2.85 (*P* < 0.001)**	**0.321**	
(*n* = 120)	**$\delta^{15}N$**	**4.70 (*P* < 0.001)**	**0.356**	
	Period		**0.339**	**−0.50 (0.06) *P* < 0.001**
	Ocean		**0.238**	**0.40 (0.07) *P* < 0.001**
	Habitat		**0.238**	**−0.42 (0.07) *P* < 0.001**
Antarctic Prion	**$\delta^{13}C$**	**1.00 (*P* = 0.002)**	**0.344**	
(*n* = 26)	$\delta^{15}N$	1.33 (*P* = 0.353)	0.087	
	Period		0.050	−0.19 (0.16) *P* = 0.271
	Ocean		**0.503**	**0.32 (0.06) *P* < 0.001**
	Habitat		**0.311**	**−0.20 (0.08) *P* = 0.014**

Habitat was derived from $\delta^{13}C$ following Jaeger et al. (2010), as Subtropical Zone (STZ): $\delta^{13}C$ > −20.1 ‰, Subantarctic Zone (SAZ): $\delta^{13}C$ values of −22.9 to −20.1 ‰, and Antarctic Zone (AZ): $\delta^{13}C$ < 22.9 ‰. GAM results are reported for separate models for each parameter, and parameters with a statistically significant effect on blood mercury values are marked bold.

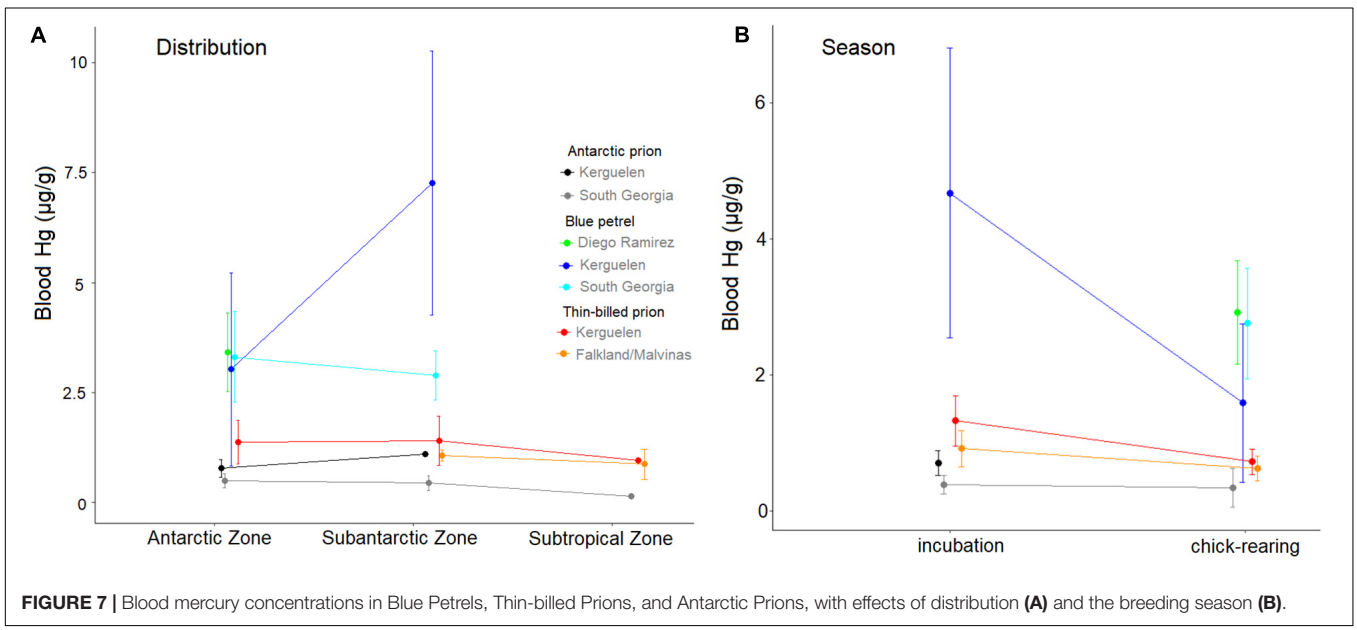

FIGURE 7 | Blood mercury concentrations in Blue Petrels, Thin-billed Prions, and Antarctic Prions, with effects of distribution **(A)** and the breeding season **(B)**.

et al., 2002a) and the Falkland Islands (Quillfeldt et al., 2010a). The hyperiid amphipod *Themisto gaudichaudii* was consistently the dominant prey item for Thin-billed Prions. These predatory pelagic crustaceans may be responsible for the relatively high trophic position of Thin-billed Prions (**Figure 3**), but result in little Hg take-up. At Kerguelen, Hg concentrations were higher in myctophid fish (up to 0.424 µg/g dw) and, to a lesser extent, squid (up to 0.270 µg/g dw) compared to crustaceans (up to 0.034 in amphipods, 0.074 in copepods and 0.125 in euphasiids) (Cipro et al., 2018), and fish in the diet was suggested to be the most important driver of elevated Hg values in seabirds (Bocher et al., 2003).

While Blue Petrels are the most piscivorous of the species in the present study, they also use the most southerly habitats over the non-breeding season (Quillfeldt et al., 2015; **Figure 2**). Blue Petrels from Kerguelen spent the winter in waters with >10% sea-ice (**Figure 10**), and all Blue Petrels spent time in waters with 30–40% sea-ice before the start of the breeding season in August–September (**Figure 10**). Observations off west Antarctica suggested that Blue Petrels avoided areas with dense pack ice, but were found just outside the marginal ice zone, at sea surface temperatures of −0.7 to 0.9°C (Ryan et al., 2020). Mercury measurements along a transect from Hobart to the Antarctic (Cossa et al., 2011; see **Figure 2**) identified two zones of elevated

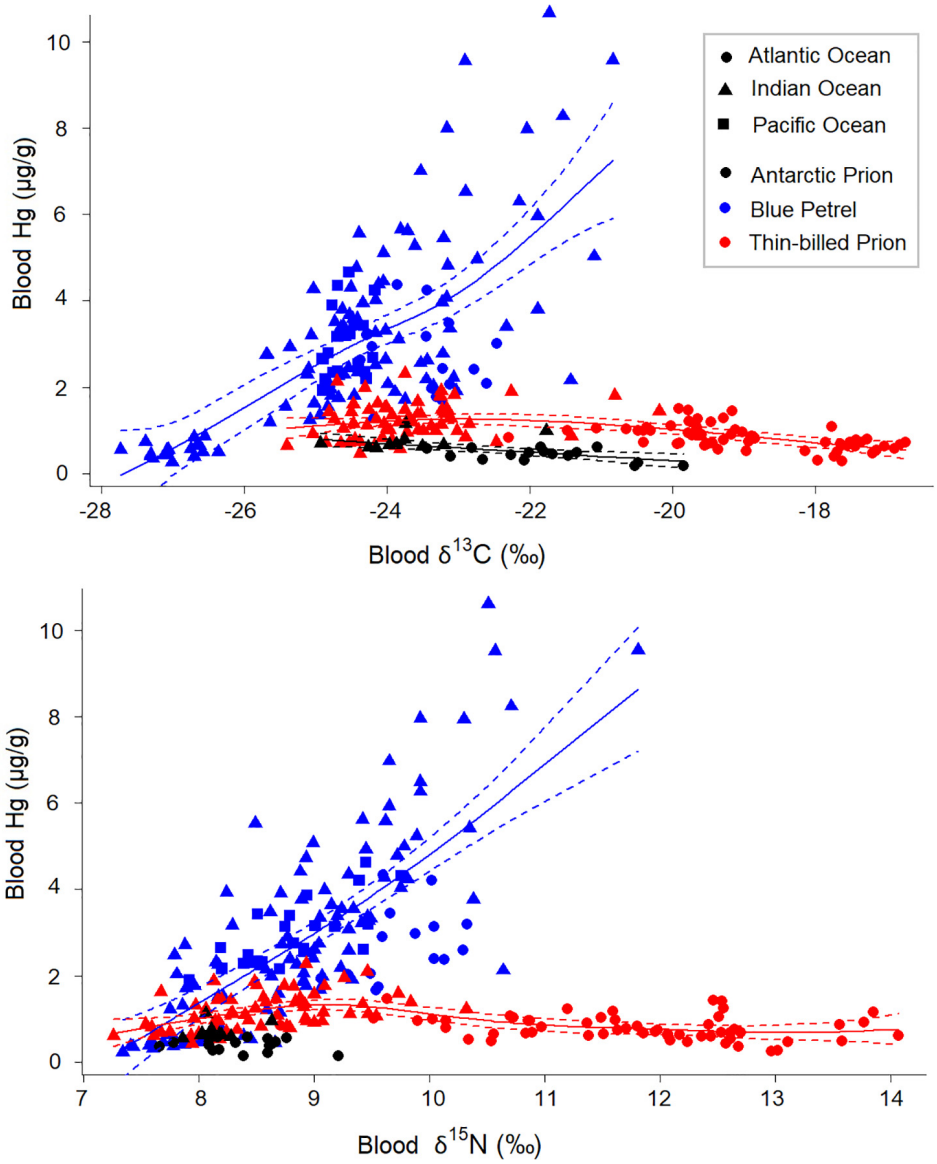

FIGURE 8 | Species-specific Generalized Additive Model (GAM) model fits for mercury values in blood of Antarctic Prions, Blue Petrels, and Thin-billed Prions. Estimated smoothing curves for mercury values in blood in relation to $\delta^{13}C$ and $\delta^{15}N$ are given with 95% confidence intervals where statistically significant. For GAM statistics, see **Table 5**.

dissolved Hg concentrations: in the Southern Zone where it is caused by processes in the ice-atmosphere-ocean interface like brine formation, and south of the Antarctic Polar Front (Cossa et al., 2011). In the Southern Zone, there is further a build-up of MeHg-enriched surface waters during winter months, when the sea-ice extent increases and the sea surface is protected from the UV and, thus, from MeHg photo-reduction (Cossa et al., 2011). However, the MeHg concentration was highest close to the Southern Antarctic Circumpolar Current Front, due to upwelling of waters from the minimum oxygen zone (Cossa et al., 2011; see **Figure 2**).

Some Antarctic seabirds have a strong affinity to the sea-ice environment, in particular Snow Petrels (*Pagodroma nivea*), Antarctic Petrels (*Thalassoica antarctica*), Adélie Penguins (*Pygoscelis adeliae*), and Emperor Penguins (*Aptenodytes forsteri*). As Procellariiformes (albatrosses, shearwaters, petrels, and storm-petrels) tend to have higher feather Hg concentrations than other species owing to their protracted moulting periods (Braune and Gaskin, 1987; Stewart et al., 1999), their Hg concentrations are particularly relevant here. However, a comparison with these species shows no particularly elevated Hg concentrations. In Snow Petrels from Adélie Land, the blood Hg concentration averaged 2.7 ± 1.1 (range: 1.0–5.3) µg/g dw in the pre-laying season (Tartu et al., 2014), lower than the values in our study for Blue Petrels in the early breeding season (**Figure 9**). Likewise, Antarctic Petrels had moderate mean Hg

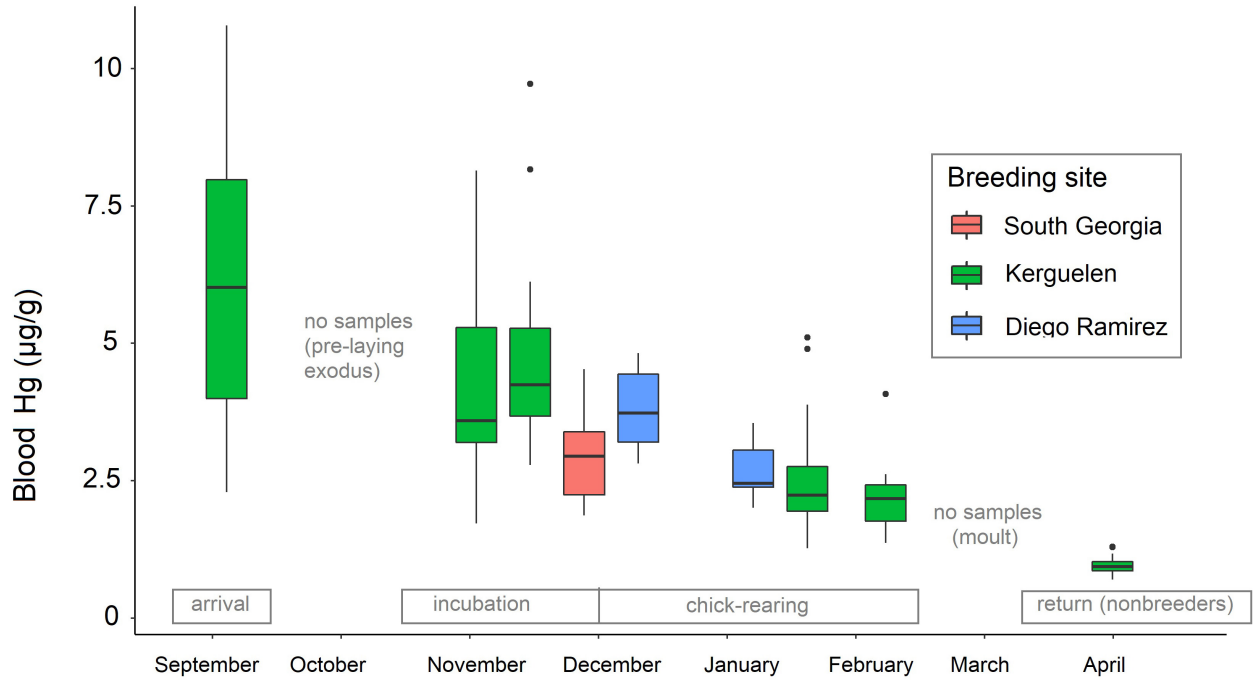

FIGURE 9 | Temporal changes in mercury concentrations in blood of Blue Petrels from different breeding locations over the breeding season.

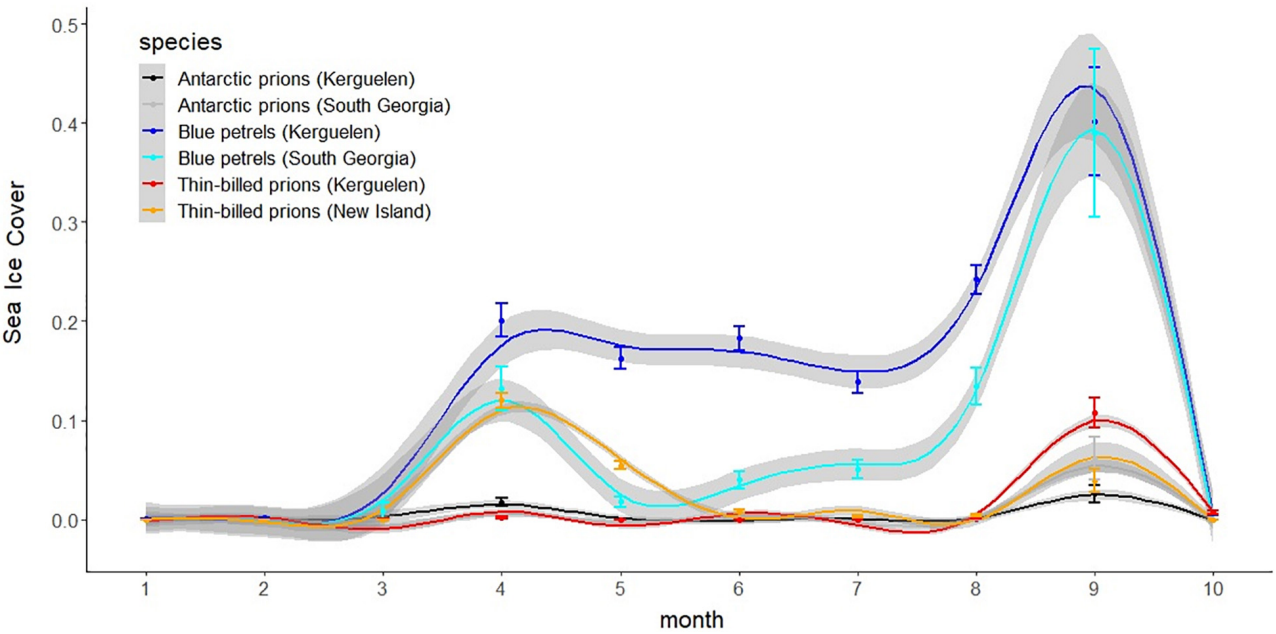

FIGURE 10 | Year-round percentage of sea-ice concentration (mean ± SD, and smooth lines with 95% confidence intervals) of geolocator tracked Blue Petrels, Thin-billed Prions, and Antarctic Prions.

concentrations in feathers (2.41 ± 0.83 µg/g dw) and blood cells (1.38 ± 0.43 µg/g dw; Carravieri et al., 2021). Similarly, Adélie Penguins and Emperor Penguins from the Ross Sea had low feather Hg concentrations (0.592 ± 0.015 µg/g and 1.351 ± 0.058 µg/g, respectively; Pilcher et al., 2020). Therefore, the high values observed for Blue Petrels are unlikely to be explained directly by foraging in southern waters with up to 40% sea-ice concentration, but might have a connection with fish that migrate to the surface from the oxygen minimum layer, and with the elevated MeHg concentration close to the Southern

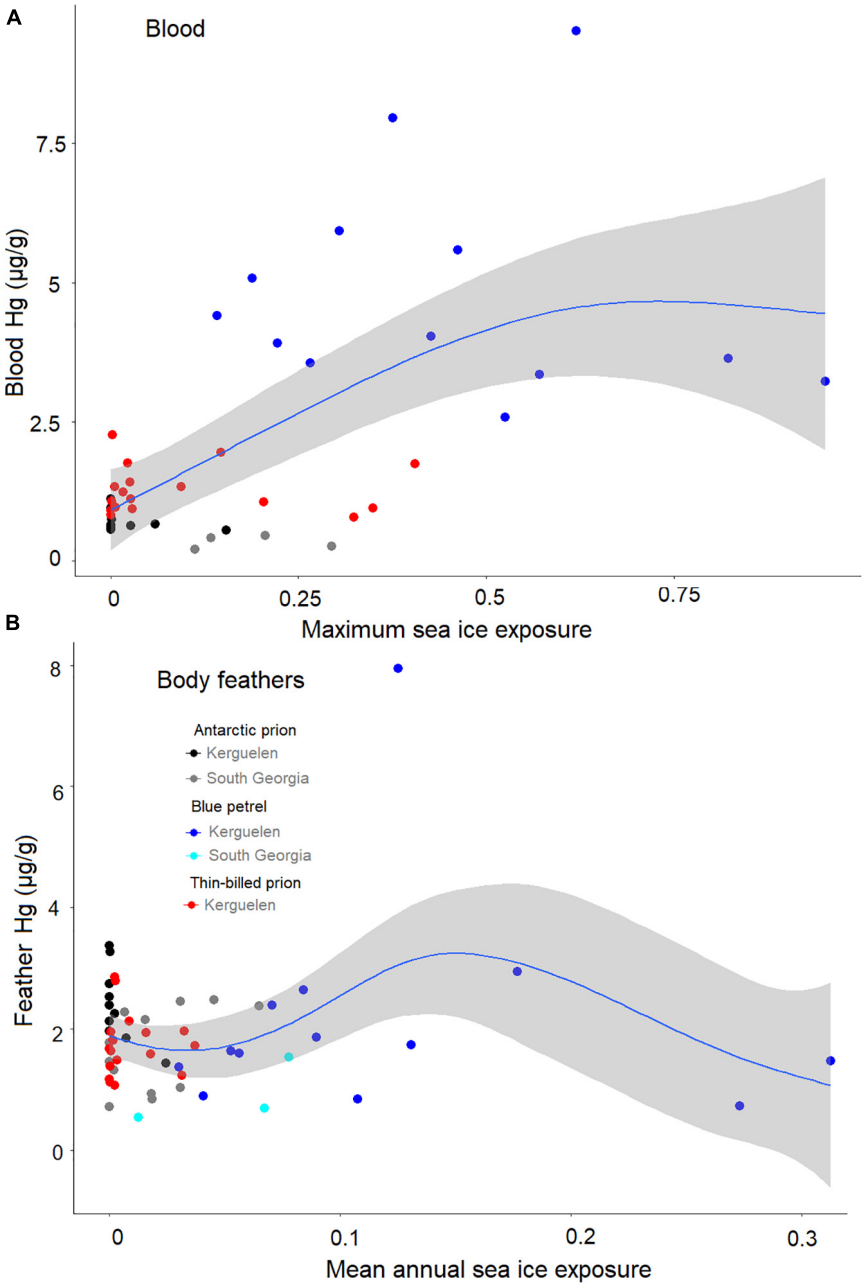

FIGURE 11 | Mercury concentrations in relation to the year-round sea-ice exposure of tracked Blue Petrels, Thin-billed Prions, and Antarctic Prions, shown for blood samples **(A)** and body feathers **(B)**. Grey shaded areas show GAM smoothed 95% confidence intervals, obtained in the R package "ggplot2", across the whole dataset.

Antarctic Circumpolar Current Front and, thus, in waters from the minimum oxygen zone (Cossa et al., 2011; see **Figure 2**). Further research should be dedicated to test this hypothesis.

Ivory Gulls (*Pagophila eburnean*) have the highest Hg concentrations in their eggs of any Arctic bird (Miljeteig et al., 2009; Bond et al., 2015). They consume ice-associated marine fish and scavenge on marine mammal carcasses. While the trophic position remained unchanged between 1877 and 2007 in ivory gulls from Arctic Canada and western Greenland (Bond et al., 2015), their feather Hg concentration increased by a factor of 45 (from 0.09 to 4.11 µg/g). Due to human activities such as coal and oil combustion, cement production, waste incineration, mining, smelting, and other industrial processes, the total and bioavailable amounts of Hg have dramatically increased in the environment since the industrial revolution (Pirrone et al., 2010; Arctic Monitoring and Assessment Programme [AMAP], 2019). The concentration of Hg that causes deleterious effects in birds depends on

TABLE 6 | Generalized Additive Model (GAM) results for tracked individuals, separately for blood and feathers, as a function of species and sea ice cover.

Tissue	Variable	Smoother edf (*P*)	Effect size	Estimate (SE) *P*
Blood	**Species**		**0.729**	**4.22 (0.43) *P* < 0.001**
	Sea-ice cover (max)	**2.24 (*P* < 0.001)**	**0.395**	
Feathers	Species		0.321	−0.25 (0.35) *P* = 0.478
	Sea-ice cover (mean)	3.98 (*P* = 0.072)	0.209	

GAM results are reported for separate models for each parameter, and parameters with a statistically significant effect on mercury values are marked bold.

different factors, including diet composition, moult duration and the ability to demethylate Hg in the liver (Heinz et al., 2009), and has been given as 5–40 μg/g in feathers in general (Burger and Gochfeld, 1997), or 10–15 μg/g in piscivorous divers (Evers et al., 2014). All values observed here were below 10 μg/g, but the highest values in Blue Petrels approached this concentration (**Figure 4**), warranting further monitoring in the future.

Temporal Differences in Mercury Concentrations

We found temporal differences in Hg concentrations in blood samples, which were most pronounced in Blue Petrels. The highest concentrations were noted in September, after arrival from the wintering grounds, indicating that the adults arrived from Hg contaminated water masses or after feeding on prey with high Hg levels, but then switched to less contaminated prey. Hg in blood then decreased continually over the breeding season, and reached very low levels in birds sampled after returning to the colony post-moult. This was paralleled by a decline in trophic position, as indicated by $\delta^{15}N$ values. Results of a previous study showed that mean $\delta^{15}N$ values in adult Blue Petrels at Kerguelen decreased continuously throughout the annual cycle, from 9.5 ± 1.1 ‰ on arrival in the colony in September, to 7.3 ± 0.5 ‰ in the immediate post-breeding period in April to May (Cherel et al., 2014). In the present study, we measured a similar decrease from means of 10.3 ± 0.8 ‰ on arrival in the colony in September to 7.9 ± 0.4 ‰ at the post-nuptial stage in April (**Table 1**). The very low levels in April can be directly related to the Hg reset after Hg depuration in feathers, at a time when $\delta^{15}N$ values are also very low (most likely indicating feeding on Antarctic krill).

Antarctic Prions did not show a pronounced seasonal trend in Hg concentrations, but had low values throughout the breeding season. In both Thin-billed Prion populations and all years, the blood Hg values were somewhat higher early in the breeding season. Diet composition of Thin-billed Prions at the Falkland Islands changes during the breeding season: from 60% squid and 35% amphipods during incubation to more equal proportions of amphipods, krill and squid during chick rearing (Quillfeldt et al., 2010a).

Mercury in blood represents two components: Hg incorporated from the diet during blood formation, and Hg stored in other tissues, such as the liver, kidneys and muscles, since the last feather moult. Residual Hg in other tissues is thought to equilibrate with levels in muscle (especially MeHg; Renedo et al., 2021) and liver, which act as the main storage organs for Hg between moults (Bearhop et al., 2000b). It has been shown that a carry-over of Hg can occur from remote places, such that high exposure in winter may lead to elevated blood Hg values until late in the summer (Lavoie et al., 2014). Especially for individuals with high winter exposure to Hg, slow changes in blood Hg over time were reported, suggesting a fast uptake rate and slow depuration (Lavoie et al., 2014). Carry-over of Hg among seasons would also explain the temporal patterns observed in Blue Petrels in our study.

Spatial Differences in Mercury

In the Blue Petrels, the population of Diego Ramírez most likely moulted off west Antarctica, i.e., in the Pacific Ocean sector of the Southern Ocean, from 67 to 71°S and 78 to 119°W (Ryan et al., 2020). Ryan et al. (2020) observed large numbers of moulting Blue Petrels sitting on the water in dense flocks in mid-February, which is in line with the 10.7 ± 2.5 h per day spent sitting on the water by Blue Petrels from Kerguelen during moult (Cherel et al., 2016). Ryan et al. (2020) suggested that most of the birds observed in west Antarctica probably breed at Diego Ramírez, and this is also suggested by a comparison with distribution data of Blue Petrels from other colonies. Blue Petrels from both Kerguelen and South Georgia were found in the Atlantic sector of the Southern Ocean (20°W to 30°E) in March, during the core moulting period, and thus far away from the moulting aggregations observed off west Antarctica (Ryan et al., 2020).

Latitudinal differences in distribution influence Hg exposure, with lower Hg in Antarctic waters compared to subantarctic waters, a trend reported in previous studies (e.g., Carravieri et al., 2014b, 2016, 2017, 2020; Cherel et al., 2018). We found no further increase towards subtropical waters. The trophic position also increased from polar to subantarctic waters, but continued to increase to subtropical waters. Thus, differences in trophic position would not fully explain the observed patterns. Indeed, a more detailed analysis revealed that not all populations show an increase in blood Hg concentrations associated with $\delta^{13}C$ values. Differences in prey as well as carry-over effects of Hg may mask spatial differences.

Further spatial differences in Hg values were observed when comparing populations from different ocean sectors. Values were lowest in the Atlantic Ocean, intermediate in the Indian Ocean, and highest in the Pacific Ocean, although this was only based on one population. That population, Blue Petrels from Diego Ramírez, had high feather Hg concentrations (4.42 ± 2.72 μg/g dw), comparable with Blue Petrels on Marion Island, Indian Ocean (4.62 ± 4.11 μg/g dw, **Supplementary Table 2**). Tracking and dietary data are still lacking from both populations.

A difference in Hg has also been observed for other organisms such as Marbled Rockcod (*Notothenia rossii*), where mean muscle

Hg concentrations of fish in waters around Kerguelen (0.255 μg/g dw; Bustamante et al., 2003) were three times higher than in the South Shetland Islands in the Atlantic sector of the Southern Ocean (0.077 μg/g dw; Cipro et al., 2017). Such differences may be due to differences in Hg sources and oceanographic features.

CONCLUSION

In line with previous studies, we found high Hg concentrations in Blue Petrels. As a novel result, we further found important population differences. We highlight that Blue Petrels did not have a northerly distribution or high trophic position, which usually account for elevated Hg concentrations in Southern Ocean seabirds. Instead, they have the most southern winter distribution of our three study species, and feed mainly on crustaceans, except on Kerguelen where myctophid fish constitute a substantial proportion of the diet. As other seabirds exposed to high Hg levels in winter, they have a notable temporal carry-over of high blood Hg values into the breeding season.

While the Kerguelen population of Blue Petrels has been tracked recently (e.g., Quillfeldt et al., 2015, 2020; Cherel et al., 2016), there are no diet or tracking data from the major population at Diego Ramírez. Our study suggests that this population has particularly high exposure to Hg (e.g., **Figure 3** and **Supplementary Figure 8**), which can be an additional stressor and impact reproduction and survival in birds (Goutte et al., 2014; Mills et al., 2020). Further study of their movements and foraging ecology are therefore required, in particular to confirm if the high Hg concentrations in feathers are related to differences in diet or sea-ice exposure. Additionally, a comparison of Hg in flight feathers, and of spatial and temporal variation in Hg concentrations of their crustacean and fish prey in relation to biogeography and ecology would help reveal the factors driving differences among seabird species in terms of Hg exposure and contamination. A combination of ship-based and tracking studies could address the question of how the foraging and movement ecology of predators and spatial differences interact to produce the patterns in Hg burdens observed in these and other wildlife in the Southern Ocean.

DATA AVAILABILITY STATEMENT

The raw data supporting the conclusions of this article will be made available by the authors, without undue reservation.

ETHICS STATEMENT

The study involved wild individuals and was carried out under permits from the Falkland Islands Government (Environmental Planning: R21.2012), and the Animal Ethic Committee of the IPEV. All work conducted at Bird Island was approved by the Ethics Committee of the British Antarctic Survey and carried out under permit from the Government of South Georgia and the South Sandwich Islands. Seabird work in Diego Ramírez was approved by Res. N° 959 and N° 6093, Servicio Agrícola y Ganadero (Agriculture and Livestock Service), Chile.

AUTHOR CONTRIBUTIONS

PQ and PB conceived and designed the study. PQ, JM, JN, RP, and CS carried out the fieldwork. YC and PB carried out the lab work. PQ, JN, RP, KD, and YC carried out the data curation. PQ carried out the data analyses. PQ and PB drafted the manuscript. All authors reviewed the final draft of the manuscript.

FUNDING

This study was funded by the Deutsche Forschungsgemeinschaft (DFG) in the framework of the priority programme SPP1154 "Antarctic Research with comparative investigations in Arctic ice areas" (Grant No. Qu148/18). The fieldwork at Kerguelen was supported financially and logistically by the Institut Polaire Français Paul Emile Victor (IPEV, Programme N°109, C. Barbraud) and the Terres Australes et Antarctiques Françaises. We are grateful to the Contrat de Projet Etat-Région (CPER) and the Fonds Européen de Développement Régional (FEDER) for funding the Advanced Mercury Analyzer and the isotope-ratio mass spectrometers of LIENSs laboratory. The Institut Universitaire de France (IUF) is acknowledged for its support to PB as a Senior Member. This study represents a contribution to the Ecosystems component of the British Antarctic Survey Polar Science for Planet Earth Programme, funded by NERC. Logistical support in Bird Island was provided by the Collaborative Gearing Scheme of the Natural Environment Research Council Antarctic Funding Initiative (AFI-NERC).

ACKNOWLEDGMENTS

We thank the New Island Conservation Trust. Justine Thébault collected samples in 2018–19 and prepared samples for analysis. We are grateful to C. Churlaud and M. Brault-Favrou from the "Plateforme Analyses Elémentaires" of LIENSs for their assistance during mercury analysis and to G. Guillou from the "Plateforme analyses isotopiques" of LIENSs for running stable isotope analyses. We thank A. Corbeau, J. Ferrer-Obiol, M. Passerault, and T. Lacombe for fieldwork assistance in Kerguelen. We thank Jaime A. Cursach who assisted with sample collection and the III Naval Zone - Chilean Navy - for all their logistical and personnel support during our fieldwork in the Diego Ramírez Archipelago, Chile.

SUPPLEMENTARY MATERIAL

The Supplementary Material for this article can be found online at: https://www.frontiersin.org/articles/10.3389/fevo.2022.915199/full#supplementary-material

REFERENCES

Albert, C., Renedo, M., Bustamante, P., and Fort, J. (2019). Using blood and feathers to investigate large-scale Hg contamination in Arctic seabirds: a review. *Environ. Res.* 177:108588. doi: 10.1016/j.envres.2019.108588

Anderson, O. R. J., Phillips, R. A., McDonald, R. A., Shore, R. F., McGill, R. A. R., and Bearhop, S. (2009). Influence of trophic position and foraging range on mercury levels within a seabird community. *Mar. Ecol. Prog. Ser.* 375, 277–288.

Arctic Monitoring and Assessment Programme [AMAP] (2019). *Technical Background Report for the Global Mercury Assessment 2018*. Oslo: Arctic Monitoring and Assessment Programme.

Bearhop, S., Phillips, R. A., Thompson, D. R., Waldron, S., and Furness, R. W. (2000a). Variability in mercury concentrations of great skuas *Catharacta skua*: the influence of colony, diet and trophic status inferred from stable isotope signatures. *Mar. Ecol. Prog. Ser.* 195, 261–268.

Bearhop, S., Ruxton, G. D., and Furness, R. W. (2000b). Dynamics of mercury in blood and feathers of great skuas. *Environ. Toxicol. Chem.* 19, 1638–1643.

Becker, P. H., González-Solís, J., Behrends, B., and Croxall, J. (2002). Feather mercury levels in seabirds at South Georgia: influence of trophic position, sex and age. *Mar. Ecol. Prog. Ser.* 243, 261–269.

Becker, P. H., Goutner, V., Ryan, P. G., and González-Solís, J. (2016). Feather mercury concentrations in Southern Ocean seabirds: variation by species, site and time. *Environ. Pollut.* 216, 253–263. doi: 10.1016/j.envpol.2016.05.061

Bierman, W. H., and Voous, K. H. (1950). Birds observed and collected during the whaling expeditions of the 'Willem Barendsz' in the Antarctic, 1946–1947 and 1947–1948. *Ardea* 37, 1–121.

Blévin, P., Carravieri, A., Jaeger, A., Chastel, O., Bustamante, P., and Cherel, Y. (2013). Wide range of mercury contamination in chicks of Southern Ocean seabirds. *PLoS One* 8:e54508. doi: 10.1371/journal.pone.0054508

Bocher, P., Caurant, F., Cherel, Y., Miramand, P., and Bustamante, P. (2003). Influence of the diet on the bioaccumulation of heavy metals in zooplankton-eating petrels at Kerguelen archipelago, Southern Indian Ocean. *Polar Biol.* 26, 759–767.

Bond, A. L., Hobson, K. A., and Branfireun, B. A. (2015). Rapidly increasing methyl mercury in endangered ivory gull (*Pagophila eburnea*) feathers over a 130 year record. *Proc. R. Soc. B* 282:20150032. doi: 10.1098/rspb.2015.0032

Braune, B. M., and Gaskin, D. E. (1987). Mercury levels in Bonaparte's gulls (*Larus philadelphia*) during autumn molt in the Quoddy region, New Brunswick, Canada. *Arch. Environ. Contam. Toxicol.* 16, 539–549.

Brooke, M. (2004). *Albatrosses and Petrels Across the World*. Oxford: Oxford University Press.

Brooks, S., Lindberg, S., Southworth, G., and Arimoto, R. (2008). Springtime atmospheric mercury speciation in the McMurdo, Antarctica coastal region. *Atmos. Environ.* 42, 2885–2893.

Brown, R. S., Norman, F. I., and Eades, D. W. (1986). Notes on Blue and Kerguelen petrels found beach-washed in Victoria, 1984. *Emu* 86, 228–238.

Burger, J., and Gochfeld, M. (1997). Risk, mercury levels, and birds: relating adverse laboratory effects to field biomonitoring. *Environ. Res.* 75, 160–172. doi: 10.1006/enrs.1997.3778

Bustamante, P., Bocher, P., Cherel, Y., Miramand, P., and Caurant, F. (2003). Distribution of trace elements in the tissues of benthic and pelagic fish from the Kerguelen Islands. *Sci. Total Environ.* 313, 25–39. doi: 10.1016/S0048-9697(03)00265-1

Bustamante, P., Lahaye, V., Durnez, C., Churlaud, C., and Caurant, F. (2006). Total and organic Hg concentrations in cephalopods from the North East Atlantic waters: influence of geographical origin and feeding ecology. *Sci. Total Environ.* 368, 585–596.

Carravieri, A., Bustamante, P., Churlaud, C., and Cherel, Y. (2013). Penguins as bioindicators of mercury contamination in the Southern Ocean: birds from the Kerguelen Islands as a case study. *Sci. Total Environ.* 454, 141–148. doi: 10.1016/j.scitotenv.2013.02.060

Carravieri, A., Bustamante, P., Labadie, P., Budzinski, H., Chastel, O., and Cherel, Y. (2020). Trace elements and persistent organic pollutants in chicks of 13 seabird species from Antarctica to the subtropics. *Environ. Int.* 134:105225. doi: 10.1016/j.envint.2019.105225

Carravieri, A., Cherel, Y., Blévin, P., Brault-Favrou, M., Chastel, O., and Bustamante, P. (2014a). Mercury exposure in a large subantarctic avian community. *Environ. Pollut.* 190, 51–57. doi: 10.1016/j.envpol.2014.03.017

Carravieri, A., Bustamante, P., Tartu, S., Meillère, A., Labadie, P., Budzinski, H., et al. (2014b). Wandering albatrosses document latitudinal variations in the transfer of persistent organic pollutants and mercury to southern ocean predators. *Environ. Sci. Technol.* 48, 14746–14755. doi: 10.1021/es504601m

Carravieri, A., Cherel, Y., Brault-Favrou, M., Churlaud, C., Peluhet, L., Labadie, P., et al. (2017). From Antarctica to the subtropics: contrasted geographical concentrations of selenium, mercury, and persistent organic pollutants in skua chicks (*Catharacta spp.*). *Environ. Pollut.* 228, 464–473. doi: 10.1016/j.envpol.2017.05.053

Carravieri, A., Cherel, Y., Jaeger, A., Churlaud, C., and Bustamante, P. (2016). Penguins as bioindicators of mercury contamination in the southern Indian Ocean: geographical and temporal trends. *Environ. Pollut.* 213, 195–205. doi: 10.1016/j.envpol.2016.02.010

Carravieri, A., Warner, N. A., Herzke, D., Brault-Favrou, M., Tarroux, A., Fort, J., et al. (2021). Trophic and fitness correlates of mercury and organochlorine compound residues in egg-laying Antarctic petrels. *Environ. Res.* 193:110518. doi: 10.1016/j.envres.2020.110518

Chastel, O., and Bried, J. (1996). Diving ability of Blue Petrels and Thin-billed Prions. *Condor* 98, 627–629. doi: 10.1242/jeb.00286

Cherel, Y., Barbraud, C., Lahournat, M., Jaeger, A., Jaquemet, S., Wanless, R. M., et al. (2018). Accumulate or eliminate? Seasonal mercury dynamics in albatrosses, the most contaminated family of birds. *Environ. Pollut.* 241, 124–135. doi: 10.1016/j.envpol.2018.05.048

Cherel, Y., Bocher, P., Trouvé, C., and Weimerskirch, H. (2002b). Diet and feeding ecology of Blue Petrels *Halobaena caerulea* at Iles Kerguelen, Southern Indian Ocean. *Mar. Ecol. Prog. Ser.* 228, 283–299.

Cherel, Y., Bocher, P., de Broyer, C., and Hobson, K. A. (2002a). Food and feeding ecology of the sympatric Thin-billed *Pachyptila belcheri* and Antarctic *P. desolata* Prions at Iles Kerguelen, Southern Indian Ocean. *Mar. Ecol. Prog. Ser.* 228, 263–281.

Cherel, Y., Connan, M., Jaeger, A., and Richard, P. (2014). Seabird year-round and historical feeding ecology: blood and feather $\delta^{13}C$ and $\delta^{15}N$ values document foraging plasticity of small sympatric petrels. *Mar. Ecol. Prog. Ser.* 505, 267–280.

Cherel, Y., Fontaine, C., Richard, P., and Labat, J. P. (2010). Isotopic niches and trophic levels of myctophid fishes and their predators in the Southern Ocean. *Limnol. Oceanogr.* 55, 324–332.

Cherel, Y., Quillfeldt, P., Delord, K., and Weimerskirch, H. (2016). Combination of at-sea activity, geolocation and feather stable isotopes documents where and when seabirds molt. *Front. Ecol. Evol.* 4:3. doi: 10.3389/fevo.2016.00003

Cipro, C. V. Z., Cherel, Y., Bocher, P., Caurant, F., Miramand, P., and Bustamante, P. (2018). Trace elements in invertebrates and fish communities off the Kerguelen Islands. *Polar Biol.* 41, 175–191.

Cipro, C. V. Z., Montone, R. C., and Bustamante, P. (2017). Mercury in the ecosystem of Admiralty Bay, King George Island, Antarctica: occurrence and trophic distribution. *Mar. Pollut. Bull.* 114, 564–570. doi: 10.1016/j.marpolbul.2016.09.024

Cossa, D., Heimbürger, L. E., Lannuzel, D., Rintoul, S. R., Butler, E. C., Bowie, A. R., et al. (2011). Mercury in the southern ocean. *Geochim. Cosmochim. Acta* 75, 4037–4052.

Dilley, B. J., Davies, D., Schramm, M., Connan, M., and Ryan, P. G. (2017). The distribution and abundance of Blue Petrels (*Halobaena caerulea*) breeding at subantarctic Marion Island. *Emu* 117, 222–232.

Evers, D. C., Schmutz, J. A., Basu, N., DeSorbo, C. R., Fair, J., Gray, C. E., et al. (2014). Historic and contemporary mercury exposure and potential risk to yellow-billed loons (*Gavia adamsii*) breeding in Alaska and Canada. *Waterbirds* 37, 147–159.

Fitzgerald, W. F., Engstrom, D. R., Mason, R. P., and Nater, E. A. (1998). The case for atmospheric mercury contamination in remote areas. *Environ. Sci. Technol.* 32, 1–7. doi: 10.1007/s10661-005-9180-7

Gatt, M. C., Reis, B., Granadeiro, J. P., Pereira, E., and Catry, P. (2020). Generalist seabirds as biomonitors of ocean mercury: the importance of accurate trophic position assignment. *Sci. Total Environ.* 740:140159. doi: 10.1016/j.scitotenv.2020.140159

Gionfriddo, C. M., Tate, M. T., Wick, R. R., Schultz, M. B., Zemla, A., Thelen, M. P., et al. (2016). Microbial mercury methylation in Antarctic sea ice. *Nat. Microbiol.* 1:16127. doi: 10.1038/nmicrobiol.2016.127

Goutte, A., Bustamante, P., Barbraud, C., Delord, K., Weimeskirch, H., and Chastel, O. (2014). Demographic responses to mercury exposure in two closely-related Antarctic top predators. *Ecology* 95, 1075–1086. doi: 10.1890/13-1229.1

Hebert, C. E., Popp, B. N., Fernie, K. J., Ka'apu-Lyons, C., Rattner, B. A., and Wallsgrove, N. (2016). Amino acid specific stable nitrogen isotope values in avian tissues: insights from captive American kestrels and wild herring gulls. *Environ. Sci. Technol.* 50, 12928–12937. doi: 10.1021/acs.est.6b04407

Heinz, G. H., Hoffman, D. J., Klimstra, J. D., Stebbins, K. R., Kondrad, S. L., and Erwin, C. A. (2009). Species differences in the sensitivity of avian embryos to methylmercury. *Arch. Environ. Contam. Toxicol.* 56, 129–138. doi: 10.1007/s00244-008-9160-3

Hobson, K. A., and Clark, R. G. (1993). Turnover of 13C cellular and plasma reactions of blood: implications for non-destructive sampling in avian dietary studies. *Auk* 110, 638–641.

Jaeger, A., Lecomte, V. J., Weimerskirch, H., Richard, P., and Cherel, Y. (2010). Seabird satellite tracking validates the use of latitudinal isoscapes to depict predators'foraging areas in the Southern Ocean. *Rapid Commun. Mass Spectrom.* 24, 3456–3460. doi: 10.1002/rcm.4792

Kleinschmidt, B., Burger, C., Dorsch, M., Nehls, G., Heinänen, S., Morkûnas, J., et al. (2019). The diet of red-throated divers (Gavia stellata) overwintering in the German Bight (North Sea) analysed using molecular diagnostics. *Mar. Biol.* 166:77.

Lavoie, R. A., Baird, C. J., King, L. E., Kyser, T. K., Friesen, V. L., and Campbell, L. M. (2014). Contamination of mercury during the wintering period influences concentrations at breeding sites in two migratory piscivorous birds. *Environ. Sci. Technol.* 48, 13694–13702. doi: 10.1021/es502746z

Lawton, K., Robertson, G., Kirkwood, R., Valencia, J., Schlatter, R., and Smith, D. (2006). An estimate of population sizes of burrowing seabirds at the Diego Ramirez archipelago, Chile, using distance sampling and burrow-scoping. *Polar Biol.* 29, 229–238.

Lorrain, A., Graham, B., Ménard, F., Popp, B., Bouillon, S., van Breugel, P., et al. (2009). Nitrogen and carbon isotope values of individual amino acids: a tool to study foraging ecology of penguins in the Southern Ocean. *Mar. Ecol. Prog. Ser.* 391, 293–306.

Manceau, A., Gaillot, A. C., Glatzel, P., Cherel, Y., and Bustamante, P. (2021). In vivo formation of HgSe nanoparticles and Hg-tetraselenolate complex from methylmercury in seabird – Implications for the Hg-Se antagonism. *Environ. Sci. Technol.* 55, 1515–1526. doi: 10.1021/acs.est.0c06269

Mattern, T., Masello, J. F., Ellenberg, U., and Quillfeldt, P. (2015). Actave.net - a web-based tool for the analysis of seabird activity patterns from saltwater immersion geolocators. *Methods Ecol. Evol.* 6, 859–864.

Médieu, A., Point, D., Itai, T., Angot, H., Buchanan, P. J., Allain, V., et al. (2022). Evidence that Pacific tuna mercury levels are driven by marine methylmercury production and anthropogenic inputs. *Proc. Nat. Acad. Sci. U.S.A.* 119:e2113032119. doi: 10.1073/pnas.2113032119

Miljeteig, C., Strøm, H., Gavrilo, M. V., Volkov, A., Jennsen, B. M., and Gabrielsen, G. W. (2009). High levels of contaminants in ivory gull *Pagophila eburnea*n eggs from the Russian and Norwegian Arctic. *Environ. Sci. Technol.* 43, 5521–5528. doi: 10.1021/es900490n

Mills, W. F., Bustamante, P., McGill, R. A. R., Anderson, O. R. J., Bearhop, S., Cherel, Y., et al. (2020). Mercury exposure in an endangered seabird: long-term changes and relationships with trophic ecology and breeding success. *Proc. R. Soc. B* 287:20202683. doi: 10.1098/rspb.2020.2683

Monteiro, L. R., and Furness, R. W. (2001). Kinetics, Dose-Response, and excretion of methylmercury in free-living adult Cory's shearwaters. *Environ. Sci. Technol.* 35, 739–746. doi: 10.1021/es000114a

Navarro, J., Cardador, L., Brown, R., and Phillips, R. A. (2015). Spatial distribution and ecological niches of non-breeding planktivorous petrels. *Sci. Rep.* 5:12164.

Navarro, J., Votier, S. C., Aguzzi, J., Chiesa, J. J., Forero, M. G., and Phillips, R. A. (2013). Ecological segregation in space, time and trophic niche of sympatric planktivorous petrels. *PLoS One* 8:e62897. doi: 10.1371/journal.pone.0062897

Nerentorp Mastromonaco, M. G., Gårdfeldt, K., Langer, S., and Dommergue, A. (2016). Seasonal study of mercury species in the Antarctic sea ice environment. *Environ. Sci. Technol.* 50, 12705–12712. doi: 10.1021/acs.est.6b02700

Phillips, R. A., Bearhop, S., McGill, R. A. R., and Dawson, D. A. (2009). Stable isotopes reveal individual variation in migration strategies and habitat preferences in a suite of seabirds during the nonbreeding period. *Oecologia* 160, 795–806. doi: 10.1007/s00442-009-1342-9

Pilcher, N., Gaw, S., Eisert, R., Horton, T. W., Gormley, A. M., Cole, T. L., et al. (2020). Latitudinal, sex and inter-specific differences in mercury and other trace metal concentrations in Adélie and Emperor penguins in the Ross Sea, Antarctica. *Mar. Pollut. Bull.* 154:111047. doi: 10.1016/j.marpolbul.2020.111047

Pirrone, N., Cinnirella, S., Feng, X., Finkelman, R. B., Friedli, H. R., Leaner, J., et al. (2010). Global mercury emissions to the atmosphere from anthropogenic and natural sources. *Atmos. Chem. Phys.* 10, 5951–5964.

Prince, P. A. (1980). The food and feeding ecology of Blue petrel (*Halobaena caerulea*) and dove Prion (*Pachyptila desolata*). *J. Zool.* 190, 59–76.

Quillfeldt, P., and Masello, J. F. (2020). Compound-specific stable isotope analyses in Falkland Islands seabirds reveal seasonal changes in trophic positions. *BMC Ecol.* 20:21. doi: 10.1186/s12898-020-00288-5

Quillfeldt, P., Cherel, Y., Delord, K., and Weimerkirch, H. (2015). Cool, cold or colder? Spatial segregation of Prions and Blue Petrels is explained by differences in preferred sea surface temperatures. *Biol. Lett.* 11:20141090. doi: 10.1098/rsbl.2014.1090

Quillfeldt, P., Masello, J. F., McGill, R. A., Adams, M., and Furness, R. W. (2010b). Moving polewards in winter: a recent change in the migratory strategy of a pelagic seabird? *Front. Zool.* 7:15. doi: 10.1186/1742-9994-7-15

Quillfeldt, P., Michalik, A., Veit-Köhler, G., Strange, I. J., and Masello, J. F. (2010a). Inter-annual changes in diet and foraging trip lengths in a small pelagic seabird, the Thin-billed Prion *Pachyptila belcheri*. *Mar. Biol.* 157, 2043–2050.

Quillfeldt, P., Masello, J. F., Navarro, J., and Phillips, R. A. (2013). Year-round distribution suggests spatial segregation of two small petrel species in the South Atlantic. *J. Biogeogr.* 40, 430–441.

Quillfeldt, P., Weimerskirch, H., Delord, K., and Cherel, Y. (2020). Niche switching and leapfrog foraging: movement ecology of sympatric petrels during the early breeding season. *Mov. Ecol.* 8, 1–14. doi: 10.1186/s40462-020-00212-y

Renedo, M., Bustamante, P., Tessier, E., Pedrero, Z., Cherel, Y., and Amouroux, D. (2017). Assessment of mercury speciation in feathers using species-specific isotope dilution analysis. *Talanta* 174, 100–110. doi: 10.1016/j.talanta.2017.05.081

Renedo, M., Pedrero, Z., Amouroux, D., Cherel, Y., and Bustamante, P. (2021). Mercury isotopes of key tissues document mercury metabolic processes in seabirds. *Chemosphere* 263:127777. doi: 10.1016/j.chemosphere.2020.127777

Ryan, P. G., Lee, J. R., and Le Bouard, F. (2020). Moult intensity in Blue Petrels and a key moult site off West Antarctica. *Antarct. Sci.* 32, 1–9.

Scheuhammer, A. M., Meyer, M. W., Sandheinrich, M. B., and Murray, M. W. (2007). Effects of environmental methylmercury on the health of wild birds, mammals, and fish. *AMBIO* 36, 12–19. doi: 10.1579/0044-7447(2007)36[12:eoemot]2.0.co;2

Schlatter, R. P., and Riveros, G. M. (1997). Historia natural del Archipiélago Diego Ramírez, Chile. *Serie Científica INACH* 47, 87–112

Seco, J., Aparício, S., Brierley, A. S., Bustamante, P., Coelho, J. P., Philips, R., et al. (2021). Mercury biomagnification in a Southern Ocean food web. *Environ. Pollut.* 275:116620. doi: 10.1016/j.envpol.2021.116620

Seco, J., Xavier, J. C., Bustamante, P., Coelho, J. P., Saunders, R. A., Ferreira, N., et al. (2020). Main drivers of mercury levels in Southern Ocean Lantern fish Myctophidae. *Environ. Pollut.* 264:114711. doi: 10.1016/j.envpol.2020.114711

Steele, W. K., and Klages, N. T. (1986). Diet of the Blue petrel at sub-Antarctic Marion Island. *Afr. Zool.* 21, 253–256.

Stewart, F. M., Phillips, R. A., Bartle, J. A., Craig, J., and Shooter, D. (1999). Influence of phylogeny, diet, moult schedule and sex on heavy metal concentrations in New Zealand Procellariiformes. *Mar. Ecol. Prog. Ser.* 178, 295–305.

Tan, S. W., Meiller, J. C., and Mahaffey, K. R. (2009). The endocrine effects of mercury in humans and wildlife. *Crit. Rev. Toxicol.* 39, 228–269. doi: 10.1080/10408440802233259

Tartu, S., Bustamante, P., Goutte, A., Cherel, Y., Weimerskirch, H., and Bustnes, J. O. (2014). Age-Related Mercury Contamination and Relationship with Luteinizing Hormone in a Long-Lived Antarctic Bird. *PLoS One* 9:e103642. doi: 10.1371/journal.pone.0103642

Thébault, J., Bustamante, P., Massaro, M., Taylor, G., and Quillfeldt, P. (2021). Influence of species-specific feeding ecology on mercury concentrations in seabirds breeding on the Chatham Islands, New Zealand. *Environ. Toxicol. Chem.* 40, 454–472. doi: 10.1002/etc.4933

Thompson, D. R., and Furness, R. W. (1989). The chemical form of mercury stored in South Atlantic seabirds. *Environ. Pollut.* 60, 305–317. doi: 10.1016/0269-7491(89)90111-5

Thompson, D. R., Bearhop, S., Speakman, J. R., and Furness, R. W. (1998). Feathers as a means of monitoring mercury in seabirds: insights from stable isotope analysis. *Environ. Pollut.* 101, 193–200. doi: 10.1016/s0269-7491(98)00078-5

Van den Steen, E., Poisbleau, M., Demongin, L., Covaci, A., Dirtu, A. C., Pinxten, R., et al. (2011). Organohalogenated contaminants in eggs of rockhopper penguins (*Eudyptes chrysocome*) and imperial shags (*Phalacrocorax atriceps*) from the Falkland Islands. *Sci. Total Environ.* 409, 2838–2844. doi: 10.1016/j.scitotenv.2011.04.002

Weimerskirch, H., Zotier, R., and Jouventin, P. (1989). The avifauna of the Kerguelen Islands. *Emu* 89, 15–29.

Yu, B., Yang, L., Liu, H., Yang, R., Fu, J., and Wang, P. (2021). Katabatic Wind and Sea–Ice Dynamics Drive Isotopic Variations of Total Gaseous Mercury on the Antarctic Coast. *Environ. Sci. Technol.* 55, 6449–6458. doi: 10.1021/acs.est.0c07474

Conflict of Interest: The authors declare that the research was conducted in the absence of any commercial or financial relationships that could be construed as a potential conflict of interest.

Publisher's Note: All claims expressed in this article are solely those of the authors and do not necessarily represent those of their affiliated organizations, or those of the publisher, the editors and the reviewers. Any product that may be evaluated in this article, or claim that may be made by its manufacturer, is not guaranteed or endorsed by the publisher.

Copyright © 2022 Quillfeldt, Cherel, Navarro, Phillips, Masello, Suazo, Delord and Bustamante. This is an open-access article distributed under the terms of the Creative Commons Attribution License (CC BY). The use, distribution or reproduction in other forums is permitted, provided the original author(s) and the copyright owner(s) are credited and that the original publication in this journal is cited, in accordance with accepted academic practice. No use, distribution or reproduction is permitted which does not comply with these terms.

frontiers | Frontiers in Ecology and Evolution

TYPE Original Research
PUBLISHED 24 August 2022
DOI 10.3389/fevo.2022.983260

Check for updates

OPEN ACCESS

EDITED BY
Jason Newton,
University of Glasgow, United Kingdom

REVIEWED BY
Yik Hei Sung,
Lingnan University, China
André Sucena Afonso,
Center for Marine and Environmental Sciences (MARE), Portugal

*CORRESPONDENCE
Calandra N. Turner Tomaszewicz
cali.turner@noaa.gov

SPECIALTY SECTION
This article was submitted to Population, Community, and Ecosystem Dynamics, a section of the journal Frontiers in Ecology and Evolution

RECEIVED 30 June 2022
ACCEPTED 01 August 2022
PUBLISHED 24 August 2022

CITATION
Turner Tomaszewicz CN, Liles MJ, Avens L and Seminoff JA (2022) Tracking movements and growth of post-hatchling to adult hawksbill sea turtles using skeleto+iso. *Front. Ecol. Evol.* 10:983260. doi: 10.3389/fevo.2022.983260

COPYRIGHT
© 2022 Turner Tomaszewicz, Liles, Avens and Seminoff. This is an open-access article distributed under the terms of the Creative Commons Attribution License (CC BY). The use, distribution or reproduction in other forums is permitted, provided the original author(s) and the copyright owner(s) are credited and that the original publication in this journal is cited, in accordance with accepted academic practice. No use, distribution or reproduction is permitted which does not comply with these terms.

Tracking movements and growth of post-hatchling to adult hawksbill sea turtles using skeleto+iso

Calandra N. Turner Tomaszewicz[1,2,3]*, Michael J. Liles[4], Larisa Avens[5] and Jeffrey A. Seminoff[3]

[1]National Research Council, Washington, DC, United States, [2]The Ocean Foundation, San Diego, CA, United States, [3]NOAA National Marine Fisheries Service, Southwest Fisheries Science Center, La Jolla, CA, United States, [4]Asociación ProCosta, Eastern Pacific Hawksbill Initiative (ICAPO), San Salvador, El Salvador, [5]NOAA National Marine Fisheries Service, Southeast Fisheries Science Center, Beaufort, CA, United States

In the eastern Pacific Ocean, hawksbill sea turtles (*Eretmochelys imbricata*) are adapted to use coastal habitats and ecosystems uncharacteristic of most other sea turtles. Once considered extirpated from this region, hawksbills had sought refuge in estuaries, nesting on muddy banks among the tangles of mangrove roots. This population is at high risk of bycatch during fishing efforts in the estuaries (blast fishing) and adjacent coastal rocky reefs (gillnets), and is further impacted by habitat degradation from coastal development and climate change. The conservation and population recovery of hawksbills in this region is highly dependent on management actions (e.g., nest relocation, habitat protection, bycatch mitigation), and a better understanding of how hawksbills use and move between distinct habitats will help prioritize conservation efforts. To identify multi-year habitat use and movement patterns, we used stable carbon (δ^{13}C) and nitrogen (δ^{15}N) isotope analysis of skin and bone growth layers to recreate movements between two isotopically distinct habitats, a nearshore rocky reef and a mangrove estuary, the latter distinguishable by low δ^{13}C and δ^{15}N values characteristic of a mangrove-based foodweb. We applied skeletochronology with sequential δ^{13}C and δ^{15}N analysis of annual growth layers, "skeleto+iso," to a dataset of 70 hawksbill humeri collected from coastal El Salvador. The results revealed at least two unique habitat-use patterns. All turtles, regardless of stranding location, spent time outside of the mangrove estuaries during their early juvenile years (< 35 cm curved carapace length, CCL, age 0–5), showing that an oceanic juvenile stage is likely for this population. Juveniles *ca.* > 35 cm then began to recruit to nearshore areas, but showed divergent habitat-use as some of turtles occupied the coastal rocky reefs, while others settled into the mangrove estuaries. For turtles recruiting to the estuaries, settlement age and size ranged from 3 to 13 years and 35–65 cm CCL. For the adult turtles, age-at-sexual-maturity ranged from 16 to 26 years, and the

maximum reproductive longevity observed was 33 years. The skeleto+iso also showed that adult hawksbills have long-term habitat fidelity, and the results demonstrate the importance of both mangrove estuary and nearshore rocky reefs to the conservation of hawksbills in the eastern Pacific.

KEYWORDS

sea turtle, stable isotopes, post-hatchlings, habitat use, conservation

Introduction

Hawksbill sea turtles (*Eretmochelys imbricata*) are a globally distributed species, considered critically endangered throughout their range (IUCN, 2018). Their unique keratinized carapace shells have made them the target of harvesting for the now-illegal tortoiseshell or *bekko* trade, and several populations are still recovering from this past historical harvesting (Limpus and Miller, 1990; LaCasella et al., 2021). In the eastern Pacific Ocean, hawksbills were once considered extirpated from the region, but were scientifically "rediscovered" in 2007 (Vásquez and Liles, 2008; Gaos and Yañez, 2012). This unique population of hawksbills in the eastern Pacific (EP) had sought refuge in dense mangrove estuaries, nesting in the sand banks dispersed among mangrove roots, an atypical behavior for sea turtles, in addition to more typical scattered nesting at contiguous, open-coast sandy beach sites (Bolten, 2003; Gaos et al., 2010, 2012a). This population remains at high risk of bycatch during fishing efforts in the estuaries (blast fishing; Liles et al., 2011; Wedemeyer-Strombel et al., 2021) and adjacent coastal rocky reefs (bottom-set gillnets; Liles et al., 2017), and is further impacted by habitat degradation from coastal development and climate change. The conservation and population recovery of hawksbills in the EP is highly dependent on management actions (i.e., nest relocation, habitat protection, bycatch mitigation), and a better understanding of how hawksbills use and move between distinct habitats that will help prioritize conservation efforts (Liles et al., 2015a,b, 2019).

Satellite tags and mark-recapture efforts using flipper or internal (PIT) tags are often the best methods for tracking sea turtle movements within and between habitats, as well as attempting to estimate residency duration in specific habitats (Plotkin, 2003; Godley et al., 2008; Hays and Hawkes, 2018). Yet these methods cannot easily provide sequential multi-year data on sea turtle location and movement because satellite tags rarely remain attached for more than ∼3 years (e.g., Hawkes et al., 2012), and are difficult to place on small and or rapidly-growing juveniles (Mansfield et al., 2021). Moreover, flipper and PIT tags can only provide information after the turtle has been captured once and tagged, after which data generation is limited to moments in time when the turtle is actively re-captured during on-site monitoring or recovered dead. As a result, these traditional methods leave gaps in our knowledge about the movements and life history patterns of these long-lived animals. Alternative methods, however, are emerging to help generate and recreate sequential multi-year habitat use data, including photo-identification (Dunbar et al., 2021), often with the help of community scientists (e.g., Hanna et al., 2021), and the combination of skeletochronology (the study of growth layers) with stable isotope analysis "skeleto+iso" (Snover et al., 2010; Avens et al., 2013, 2021; Ramirez et al., 2015; Turner Tomaszewicz et al., 2016, 2017a).

Skeletochronology analysis produces time-series data on individual turtles that includes estimated age, body size, annual growth, and calendar year for each growth layer identified within a bone (Avens et al., 2015; Turner Tomaszewicz et al., 2015b, 2017a; Goshe et al., 2020). The onset of maturity can also be estimated during the analysis, producing key demographic parameters such as age- and size-at-sexual-maturation (ASM, SSM) and reproductive longevity (Avens et al., 2020; Turner Tomaszewicz et al., 2022). When these data are used to guide precision sampling of individual bone annual growth layers for stable isotope analysis (Turner Tomaszewicz et al., 2016), biogeochemical data are added to the dataset and can inform habitat use and diet for each year as well. The result is a multi-year, sequential record for individual turtles on age- and size-specific habitat location, diet, and growth for specific calendar years. For long-lived and migratory species like sea turtles, this skeleto+iso method can recreate movements of hard-to-study life stages, such as post-hatchlings and young juveniles, or long-term foraging patterns of adults, which are important pieces of information to guide habitat-specific conservation efforts.

The application of stable isotopes to track animal movement is especially useful when there are at least two isotopically distinct habitats being considered (Seminoff et al., 2012; Ramirez et al., 2015; Vander Zanden et al., 2015; Turner Tomaszewicz et al., 2017a). A variety of physical and biological factors affect the stable isotope values in animals. Following the "you are what you eat" analogy, diet is reflective in consumer tissues (Fry, 2006), and differences across landscapes (and oceanscapes) also affect isotope patterns in animals (West et al., 2006; Hobson and Wassenaar, 2018). The isotopic values at the base of the foodweb in a particular location are largely dictated by the dominant nutrient cycling processes in each area (Montoya,

2008; McMahon et al., 2013). For example, in open ocean habitats where primary productivity is relatively low, stable carbon isotope values ($\delta^{13}C$) are typically lower in comparison to other high productivity regions such as coastal neritic zones (DeNiro and Epstein, 1978; Oczkowski et al., 2016; Espinasse et al., 2019). An exception to this low-to-high pattern moving from offshore-to-near shore occurs in some coastal areas where the $\delta^{13}C$ values can be lower due to terrestrial inputs or C_3 plant species, such as mangroves (France, 1995; Bouillon et al., 2008; Seminoff et al., 2021). Similarly, in nutrient-limited open ocean habitats, the stable nitrogen isotope ($\delta^{15}N$) values are typically lower than coastal areas due to nitrogen fixation by cyanobacteria being the dominant cycling regime in oligotrophic areas (Montoya et al., 2004; Deutsch et al., 2011). By contrast, in most neritic areas, denitrification is more present in foodwebs from the input of nutrient-cycling benthic prey (both flora and fauna), as well as the upwelling of cycled nitrogen into the pelagic water column foodweb, producing higher $\delta^{15}N$ values (Deutsch et al., 2011; Seminoff et al., 2012; Fleming et al., 2016; Oczkowski et al., 2016). This pattern has been demonstrated for several sea turtle species such as North Pacific loggerheads (*Caretta caretta*) in the pelagic central North Pacific vs. in the neritic eastern North Pacific (Allen et al., 2013; Turner Tomaszewicz et al., 2017a), pelagic vs. benthic foraging loggerheads (McClellan et al., 2010; Ramirez et al., 2015) and green sea turtles (*Chelonia mydas*; Turner Tomaszewicz et al., 2018; Seminoff et al., 2021), and turtle moving among ocean basins (Wallace et al., 2006; Pajuelo et al., 2010; Seminoff et al., 2012).

In El Salvador, the two high-use habitats for hawksbills, mangrove estuaries and nearshore rocky reefs, are known to be isotopically distinct because of the uniquely low $\delta^{13}C$ values that characterize the mangrove-based foodweb (Seminoff et al., 2021; Wedemeyer-Strombel et al., 2021). Like in other mangrove-based foodwebs, the low $\delta^{13}C$ values are a result of the carbon cycle used by these marine angiosperms, which differ from other marine flora such as macroalgae and seagrasses that have higher $\delta^{13}C$ values (Marshall et al., 2007; Bouillon et al., 2008). As a result, these mangrove habitats are isotopically distinct from open ocean and coastal reef areas (Fry and Ewel, 2003; McMahon et al., 2011; Wedemeyer-Strombel et al., 2021). These habitats in El Salvador—both estuaries and rocky reefs—are under increasing pressure from local fishing efforts, which have resulted in high levels of fishery-related bycatch and, subsequently, offer the opportunity to collect humeri samples from turtles stranded in each of these locations. Here, we applied skeleto+iso to the bones of these dead-stranded hawksbill turtles to characterize key demographic parameters such as age, growth rates, ASM, and SSM, and also establish multi-year habitat use, movement patterns and residency duration of each isotopically distinct habitat. These results will help inform habitat-specific risk assessments of hawksbills, where each type of spatially explicit threat requires a different approach to minimize bycatch and increase hawksbill survival rates.

Materials and methods

Study area

Our study was conducted at two primary nesting and foraging areas for hawksbills in the EP (Gaos et al., 2012a, 2017; Liles et al., 2017): Bahía de Jiquilisco (13°13′N, 88°32′W) and Punta Amapala (13°08′N, 87°55′W) in El Salvador (**Figure 1**). Small-scale, nearshore fisheries provide important livelihood support for coastal residents at both sites. At the same time, these fisheries also constitute the greatest threat to hawksbills through bycatch mortality (Liles et al., 2011, 2017). Bahía de Jiquilisco and Punta Amapala are situated within the migration corridor of post-nesting hawksbills (Gaos et al., 2012b), further increasing the potential for fisheries interactions.

Bahía de Jiquilisco (635 km^2) is a National Conservation Area, RAMSAR wetland, and UNESCO Biosphere Reserve (MARN, 2014). It is the largest mangrove forest in El Salvador and includes numerous estuaries, channels, and islands. Bahía de Jiquilisco hosts ∼40% of known hawksbill nesting in the EP region, which primarily occurs along a series of inshore sand beaches. Blast fishing and bottom-set longlines are serious threats to hawksbills in the estuary, particularly during the nesting season (May–October) when reproductively active adults congregate near nesting beaches. Conversion of mangrove forests to shrimp farms and uncontrolled development of nesting habitat further threaten the species in Bahía de Jiquilisco.

Punta Amapala (26 km^2), approximately 60 km east of Bahía de Jiquilisco, flanks the western border of the Gulf of Fonseca and is comprised primarily of submerged volcanic reef formations at depths ranging from 0 to 30 m. It hosts diverse marine communities, including corals, sponges, and fishes (Domínguez-Miranda, 2010), and constitutes one of the most important open-coast nesting beaches for hawksbills in the eastern Pacific (Liles et al., 2011; Gaos et al., 2017). Lobster gillnet fishing along the rocky reef is a major threat to hawksbills at Punta Amapala and represents the greatest single source of human-induced, in-water mortality of hawksbills in the eastern Pacific (Liles et al., 2017).

Sample collection and processing

During 2015–2019, tissue samples were collected from stranded and bycaught hawksbills from the two main study areas—Bahía de Jiquilisco and Punta Amapala (**Figure 1**). Upon carcass recovery, turtles were searched for flipper and passive integrated PIT tags, body size was measured as curved

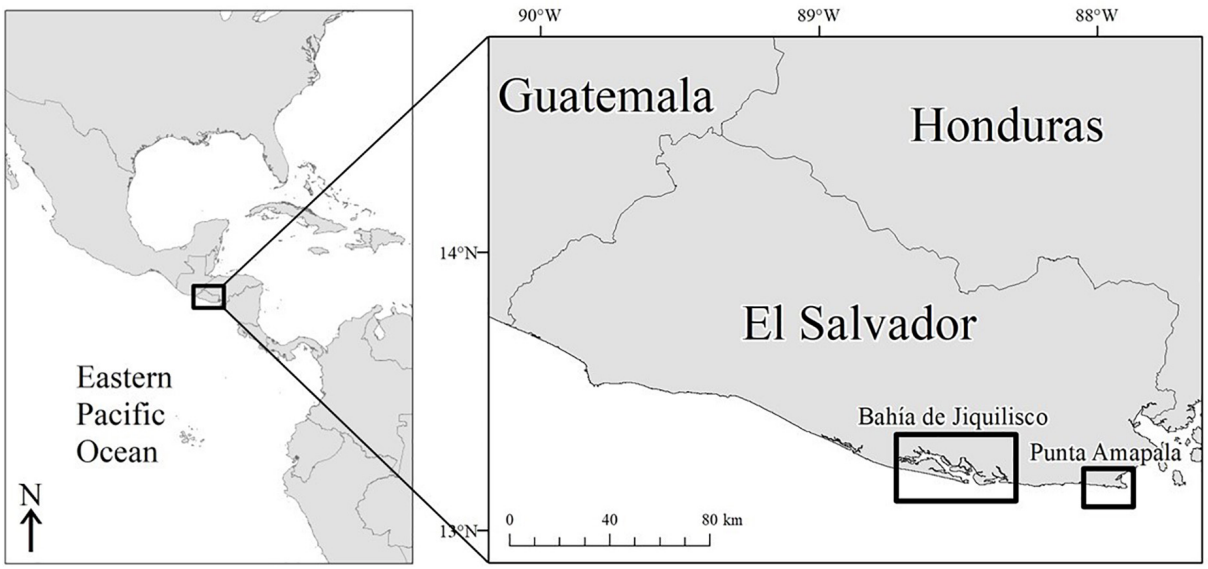

FIGURE 1
Study site in El Salvador where the 70 hawksbill turtles were recovered. A total of 35 turtles were recovered from the mangrove estuary, Bahía de Jiquilisco, and 35 were recovered from the rocky reef area at Punta Amapala.

carapace length (CCL) and sex was assigned if (1) the turtle was tagged from a previous nesting event (F) or (2) a necropsy was conducted and gonads identified. Skin samples were collected using a scalpel and stored in salt until processed. Bone samples were removed, cleaned, and air dried until processed. All samples were sent to San Diego, CA under CITES permits for processing at the NOAA NMFS Southwest Fisheries Science Center. In the lab, skin samples were rinsed, cut, lyophilized, and then weighed to 1.5 mg and packed in tin capsules for SIA processing.

Bone samples were first processed for skeletochronological analysis and then stable isotope analysis as described in Turner Tomaszewicz et al. (2016) and Goshe et al. (2020). Briefly, we first cross-sectioned two 3-mm pieces from each humerus using an Isomet slow speed saw and diamond wafer blade. The proximal section was use for isotope analysis (see below) and the distal section was used for the skeletochronology aging analysis. The aging section was fixed in 10% buffered formalin and decalcified in a commercial "RDO" solution by Apex, before being sliced into 25-μm-thin sections using a freezing-stage sliding microtome by Leica. Thin sections were then stained in a modified Ehrlich's stain, visually inspected for completeness, mounted to a slide, and digitally imaged to produce a high-resolution record of the bone revealing lines of arrested growth (LAGs) that denote the outer edges of individual skeletal growth marks. Imaging was conducted on an Olympus CX43 microscope using cellSens software. In hard-shelled sea turtles, annual LAG formation has been validated in multiple species, including hawksbills, and was therefore also assumed true for this population (hawksbill, Snover et al., 2012; other species: loggerhead, Kemp's ridley, Snover and Hohn, 2004; green, Snover et al., 2011). The digitized images were then visually inspected by two independent readers (CTT, LA), following standard skeletochronology protocol, whereby each person marked the location and total count of LAGs observed in each bone (Avens and Snover, 2013; Turner Tomaszewicz et al., 2015a; Goshe et al., 2016), and the marked reads were compiled, compared, and a final consensus was reached.

Age, size, and growth estimation

For each consensus image, we determined the final LAG location and number for all bones and recorded the LAG diameters as measured along the antero-posterior axis (Zug et al., 1986). We used these data for age, size and growth estimation analyses as described below (Snover et al., 2007). First, any bone containing a distinctive diffuse mark, characteristic of the first-year annulus, marked the first year of a turtle's life (Snover and Hohn, 2004; Goshe et al., 2016; Avens et al., 2021) and was directly aged ($n = 43$). Bones without the first-year annulus mark ($n = 27$) had resorbed some LAGs during bone growth, and required the application of a correction factor to estimate the number of LAGs lost as described in Avens et al. (2012, 2015, 2021). We established and applied correction factors for these bones, all of which had at least one LAG diameter smaller than the largest LAG from the directly aged bones (23.4 mm). The estimated age-at-stranding of each turtle was then calculated by summing together the total number of observed LAGs with the calculated number of LAGs lost.

Once the final age was estimated for each bone, we assigned an estimated age to each subsequent LAG by subtracting one for each LAG moving inward from the outermost LAG.

Once age was estimated, we back-calculated body size (CCL) at each measured LAG using the relationship between body size (CCL) and humerus (and LAG) diameter to produce estimated size and incremental growth, following standard skeletochronology analytical methods (Snover et al., 2007; Avens et al., 2015; Goshe et al., 2016). Here, we applied the body proportional hypothesis (BPH)-corrected (Francis, 1990) allometric equation modified for application to sea turtles to yield a back-calculated CCL for each turtle at each measured LAG as recommended in Snover et al. (2007) and commonly applied in other sea turtle studies (Avens et al., 2012; Avens and Snover, 2013; Turner Tomaszewicz et al., 2018, 2022). First, we characterized the relationship between CCL and humerus section diameter using the following allometric equation (Snover et al., 2007; Goshe et al., 2010):

$$L = L_{op} + b(D - D_{op})^{c} \quad (1)$$

Here, L is the estimated length (CCL), L_{op} is the minimum hatchling carapace length, D is the humerus section diameter, D_{op} is the minimum hatchling humerus diameter, b is the slope of the relationship, and c is the proportional coefficient. To obtain values for east Pacific hawksbill hatchling CCL and humerus diameter we collected and measured these values for 20 hatchlings retrieved during nest exhumations from hatchery-relocated nests at Bahía de Jiquilisco sites, and recorded the minimum humerus diameter (1.7 mm) and minimum carapace length (3.5 cm). Hatchling carapace lengths were measured as straight carapace length (SCL), and here we assumed the SCL and CCL differences were less than 1–4 mm (based on paired SCL:CCL measurements, and comparable to standard measuring error, ProCosta, *unpub.*) and were therefore equivalent measurements for the purposes of this analysis. Parameters b and c were optimized using the non-linear least squares function "nls" in the "stats" package in R version 4.0.1 (R Core Team, 2021). Then, to apply this relationship to LAG diameters, we modified Equation 1 such that LAG diameter was used in place of humerus section diameter, to yield a back-calculated BPH-corrected body size (CCL) at time of LAG formation (Snover et al., 2007):

$$L_{initial} = \left[L_{op} + b\left(D_{initial} - D_{op}\right)^{c}\right] \times \left[L_{final}\right] \times \left[L_{op} + b\left(D_{\mathrm{final}} - D_{op}\right)^{c}\right]^{-1} \quad (2)$$

We used these back-calculated CCL estimates to then calculate the incremental annual growth for sequential growth layers. For year^{-1} growth, we used the difference between the size (CCL) at age 1 and the mean hatchling size (3.8 cm) used in this study.

For any individual turtle where we observed compression of LAG spacing at the lateral edge of the bone (i.e., rapprochement), which is associated with sexual maturity, we determined estimated age and size at maturation (ASM, SSM) (Francillon-Vieillot et al., 1990; Avens et al., 2012, 2015).

To model the size-at-age relationship of these hawksbills, we applied a generalized additive mixed model (GAMM) and a von Bertalanffy growth curve using the paired size, age, and growth data, from each individual turtle bone (Avens et al., 2015, 2017; Turner Tomaszewicz et al., 2018, 2022). The GAMM accounted for individual variation and repeated observations by including individual identity as a random effect (Chaloupka and Musick, 1997; Avens et al., 2013, 2015; Turner Tomaszewicz et al., 2018, 2022). We conducted the analysis using the "mgcv" package and the "gamm" function in R version 4.0.1 (Wood, 2017; R Core Team, 2021). After converting all measurable LAG diameters to back-calculated CCL estimates, we used the size-at-age data to fit a smoothing spline model to characterize size-at-age, and we generated the predicted fit for the same data, with 95% confidence intervals, using the "smooth.spline" function in the "stats" package in R (Hastie and Tibshirani, 1990; R Core Team, 2021). Next, we generated von Bertalanffy growth models using a bootstrapped method, as described in Avens et al. (2015, 2017) and Turner Tomaszewicz et al. (2018, 2022). To do this, we repeatedly sampled the back-calculated somatic growth rate data in the model to extract a single growth-at-length data point for each individual turtle in the sample and then used these non-parametric bootstrap samples to estimate the growth parameter, k, and estimate upper size limit, L_{inf}, for Fabens modification of the von Bertalanffy growth curve. Here we conducted randomized re-sampling of the growth rate data 1,000 times to describe uncertainty in the von Bertalanffy parameters (Avens et al., 2015, 2017). For all analysis, we evaluated significance as $\alpha = 0.05$, and present results as mean ± standard error unless otherwise noted.

Stable isotope analysis

To extract samples from individual growth layers for stable isotope analysis (SIA), the paired digital aging image from skeletochronology processing was used as a guide to target sampling paths on the adjacent proximal bone section (Turner Tomaszewicz et al., 2016, 2017a). Using one of two computer-guided micromill units (CM-2 Carpenter micromill and an Elemental Scientific Lasers MicroMill2), we extracted 1.5 mg of bone powder from individual growth layers and weighed samples into 5 × 9 mm^2 tin capsules for SIA. No additional treatment was necessary for lipid extraction or removal of inorganic carbonate (Turner Tomaszewicz et al., 2015b, 2017b).

All samples were sent to and processed at the University of Florida, Gainesville, FL Stable Isotope Laboratory. Samples already loaded into tin capsules were placed in a 50-position automated Zero Blank sample carousel on a N.C. Technologies ECS 8020 elemental analyzer. After combustion in a quartz

column at 1,000°C in an oxygen-rich atmosphere, the sample gas was transported in a He carrier stream and passed through a hot reduction column (650°C) consisting of elemental copper to remove oxygen. The effluent stream then passed through a chemical (magnesium perchlorate) trap to remove water followed by a 1.5-m gas chromatography (GC) column at 55°C to separate N_2 from CO_2. The sample gas next passed into a ConFlo IV interface and into the inlet of a Thermo Electron Delta V Advantage isotope ratio mass spectrometer running in continuous flow mode where the sample gas was measured relative to laboratory reference N_2 and CO_2 gases. All carbon isotopic results are expressed in standard delta notation relative to Vienna Pee Dee Belemnite (VPDB). All nitrogen isotopic results are expressed in standard delta notation relative to AIR. To account for the trace amount of carbonate in the cortical bone samples, the $\delta^{13}C$ values of all bone samples were then mathematically corrected as recommended in Turner Tomaszewicz et al. (2015b) using the following equation specific for sea turtles in the Pacific:

$$\delta^{13}C_{cor} = (1.2 \times \delta^{13}C_{raw}) + 2.1 \quad (3)$$

To isotopically distinguish two separate habitats, we referenced hawksbill skin stable isotope values previously published and from the current study to help characterize the mangrove estuary (Bahía de Jiquilisco, Wedemeyer-Strombel et al., 2021) and the rocky reef / ocean (Punta Amapala, current study) as two isotopically distinct locations (inside or outside estuary). In Wedemeyer-Strombel et al. (2021), skin from juvenile (<65 cm CCL) hawksbills captured in Bahía de Jiquilisco had stable carbon isotope values that ranged from *ca.* −22 to −16‰ and were correlated with turtle body size; the smaller turtles (*ca.* 40 cm CCL) captured in the estuary had higher $\delta^{13}C$ values (*ca.* −16‰) than the larger turtles (*ca.* 50 cm CCL, *ca.* −22‰) also captured in the estuaries. The same study also sampled prey from mangrove estuaries, with a mean $\delta^{13}C$ value of −24‰ (−20‰ without the 4‰ trophic offset), further supporting lower $\delta^{13}C$ values to characterize a mangrove-based foodweb. We also analyzed skin samples in the current study (see "Results" below) from turtles recovered from the two distinct locations to further support the designation of a $\delta^{13}C$ values to characterize each habitat. Specifically, the skin samples collected from turtles in Punta Amapala had $\delta^{13}C$ values between −14.9 and −17.6‰ (**Table 2**). Based on these new and previously published data, we assigned −18‰ as the threshold $\delta^{13}C$ value for hawksbill skin indicating mangrove estuary habitat use and foraging. To ensure this threshold value from a skin tissue was directly comparable to stable isotope values from bone tissue (the samples used in the rest of the current study), we converted −18‰ skin to a bone-equivalent value using the equation from Turner Tomaszewicz et al. (2017b) and applied in other studies, including Turner Tomaszewicz et al. (2018). The application of this conversion equation yielded a bone threshold $\delta^{13}C$ value of −18.03‰ to indicate use of the mangrove estuary habitat of Bahía de Jiquilisco; this minimal difference between the skin and bone $\delta^{13}C$ value was expected given the findings of Turner Tomaszewicz et al. (2017b) which found a minimal difference between paired bone and skin tissues.

Finally, we combined all the skeleto+iso data and to each growth layer we assigned a corresponding estimated age, body size, annual growth, calendar year, and habitat. The habitat assignment was based on stable isotope values ($\delta^{13}C < -18$‰ = mangrove estuary and $\delta^{13}C > -18$‰ = ocean/rocky reef), the final (outermost) growth layer was assigned to the habitat where the turtle stranded, regardless of SIA values. If the $\delta^{13}C$ value did not match with the habitat in which the turtle was found, it was assumed to be newly recruited to that habitat. We then used these habitat-assignments to identify timing of habitat shifts (age and size), and to subsequently examine if there were any growth advantages associated with a particular habitat for a given size class (Wilcoxon Rank Sum, aka Mann–Whitney comparison, significance level at $p < 0.05$).

Results

Skeletochronology size and age estimates

A total of 70 bones were processed for age and size analysis, 12 of which were from females, four from males, and the remaining 54 of unknown sex. We identified 599 individual LAGs within the 70 bones processed for skeletochronology, and body sizes at stranding ranged from 28.5 to 90.7 cm. The sizes of the turtle recovered in Bahía de Jiquilisco (n = 35) ranged from 35.4 to 90.7 cm CCL [58.3 ± 2.9 cm (mean ± SE)], and the turtles recovered from Punta Amapala (n = 35) ranged in size from 28.5 to 73.6 cm CCL (41.4 ± 2.1 cm). The bones from the 70 turtles analyzed retained between 2 and 48 LAGs (8.3 ± 0.95), for a total of 580 identified and measured LAGs. At the time of carcass recovery, the CCL was recorded for 55 of the 70 turtles, and the following linear relationship between total humerus section diameter (THD) and turtle size (CCL) was used to estimate CCL for the remaining 15 turtles:

$$CCL = 3.02 \times THD - 4.87 \quad (R^2 = 0.91, \textbf{Supplementary Figure 1}) \quad (4)$$

A total of 43 bones retained the year-1 annulus and could therefore be directly aged, where 1 LAG equals 1 year. The final age-at-stranding for these 43 turtles ranged from 2 to 10 (mean ± SE 5.0 ± 0.3). Using the measurable internal LAG diameters (n = 210) from these 43 directly-aged bones, we determined the best-fit correction factor equation (CF1) which was a linear equation:

$$CF1: y = 1.52x + 7.01 (R^2 = 0.83, \textbf{Supplementary Figure 2}) \quad (5)$$

where y is the LAG diameter and x is the LAG number. Using this CF1 equation, we estimated the number of LAGs lost due to resorption, where LAG diameter y was each bone's innermost LAG or resorption core diameter, for the remaining 27 bones (those without an annulus, and with at least one LAG diameter less than 23.4 mm, the max THD of the Group 1 bones). For the 27 bones with CF1 applied, we then summed this resulting LAG-lost number with the number of LAGs retained in each bone to obtain final estimated age at stranding. The number of estimated LAGs lost (resorbed) from these larger bones ranged from one to 10 (mean ± SE 4.7 ± 0.5) LAGs. Final estimated age (LAGs retained + LAGs resorbed, with all ages rounded to the nearest whole number) for all 70 turtles ranged from 2 to 54 years old (mean ± SE 10.1 ± 1.2 years; **Figure 2**). The age at stranding for the turtles recovered in Bahía de Jiquilisco (n = 35) ranged from 3 to 41 years (mean ± SE 12.0 ± 1.6) and the turtles recovered from Punta Amapala (n = 35) ranged from 2 to 54 years (mean ± SE 8.2 ± 1.8; **Figure 2**).

Back-calculated body size estimates corresponding to the measured LAG diameters ranged from 14.8 to 90.7 cm CCL (mean ± SE 60.8 ± 0.33). For all 70 bones, we applied east Pacific hawksbill-specific hatchling parameters (min CL: 3.5 cm, min hatchling THD: 1.7 mm, slope b = 2.526, proportionality coefficient c = 1.038) to the BPH back-calculated CCL equation (Equation 2) at each measurable LAG. This yielded 573 CCL-at-age estimates (**Figures 3**, **4**) and 541 annual somatic growth estimates (**Supplementary Figure 3**).

Growth and maturation timing

Of the 541 incremental growth estimates, annual growth ranged from 0 to 24.4 cm CCL (mean ± SE 3.4 ± 0.07). The annual growth was greatest for age zero to one, as expected (mean 17.4 cm; range = 11.0 to 24.4 cm), and for all other ages (ages 2+), annual growth ranged from 0 to 12.6 cm CCL (mean 2.9 ± 0.04). Growth rates decreased with age and size, and are discussed in more detail below in context of habitat use (**Figure 4**, **Supplementary Figure 3**, and **Supplementary Table 1**). The growth modeled by both the GAMM smoothing spline and the bootstrapped von Bertalanffy models showed close congruence, with turtles increasing in size steadily until age ∼15, when growth then began to slow and approach near-zero annual growth at ∼80 cm CCL between age 20–30, the presumed onset of maturity (**Figure 4**).

A total of ten turtles showed LAG compaction indicating maturity, and the corresponding age and size at those growth layers represent the timing of maturity (**Table 1**). For these ten turtles, the SSM ranged from 61.2 to 89.5 cm CCL (mean ± SE 76.9 ± 2.76, coefficient of variation, CV = 0.11) and ASM ranged from 16 to 26 years (mean ± SE 19.5 ± 1.01, CV = 0.16), with the reproductive longevity (estimated as the number of LAGs or years beyond the onset of maturity) observed at a maximum 33 years (**Table 1**). Mean annual growth post-maturation was 0.24 cm/year (n = 108 growth layers). Seven of the 10 mature turtles were female, and were all recovered from Bahía de Jiquilisco. Two turtles were male and one turtle was unknown sex, and all three of these were recovered from Punta Amapala (**Figure 3**). The turtle with the largest SSM (89.5 cm CCL) was a female from Bahía de Jiquilisco with an estimated ASM of 16 years, and the turtle with the smallest SSM (61.2 cm CCL) was a male from Punta Amapala with ASM of 22 years (**Table 1**).

The GAMM smoothing spline, fit to the length-at-age dataset of the 70 turtles, was significant ($p < 0.0001$, Edf = 7.457, adj. r^2 = 0.887; **Figure 4**). The mean estimated SSM obtained at rapprochement for the 10 mature bones analyzed in the current study (76.9 cm CCL) corresponded to a spline-predicted ASM of 20 years (95% CI: 18 to 23 years). The minimum SSM from rapprochement, 61.2 cm CCL, yielded a spline-predicted ASM of ∼11.5 years (**Figure 4** and **Table 1**), and the mean nesting size for hawksbills in this region (81.6 cm CCL, Liles et al., 2011) yielded a spline-estimated ASM of ∼35 years (the ASM estimated by skeletochronology for a turtle with SSM near this size was 21 years for a 81.7 cm CCL female from Bahía de Jiquilisco; **Table 1**). The bootstrapped von Bertalanffy model, based on growth-at-length, estimated the ASM for the mean SSM (76.9 cm CCL) from rapprochement in this study at 22.5 ± 0.21 years (95% CI: 22.1 to 22.9 years), the estimated upper size limit, L_{inf}, was 80.6 ± 0.19 cm (95% CI: 80.2 to 81.0 cm) and the intrinsic growth rate parameter, k, was 0.142 ± 0.0008 (95% CI: 0.141 to 0.144; **Figure 4**).

Stable isotope analysis and habitat use

We processed a total of 58 skin samples for the current study, 15 from Bahía de Jiquilisco (six of these were hatchlings: CL mean 3.8 cm; and the rest juveniles and adults: n = 9, CCL 39.7 to 84.5, mean 55.5 cm), and 43 from Punta Amapala (all juveniles CCL 32.9 to 53.6, mean 40.0 cm). The stable carbon isotope ($\delta^{13}C$) values of the samples from turtles captured in the mangrove estuary (Bahía de Jiquilisco) were lower in comparison to the $\delta^{13}C$ values of the skin from turtles captured outside the estuary (Punta Amapala), mean ± SE –20.5 ± 5.29‰ vs. –16.2 ± 2.47‰, respectively, while the $\delta^{15}N$ values were similar (**Table 2**). All skin samples collected from turtles in Punta Amapala had $\delta^{13}C$ values greater than the designated threshold value of –18‰, further supporting the use of this value as an indicator of movement into a mangrove estuary.

Of the 70 turtles analyzed for age and size using skeletochronology, a subset of 40 bones were analyzed for sequential stable isotope analysis (20 recovered from Bahía de Jiquilisco and 20 from Punta Amapala). The size of the 20 turtles sampled from Bahía de Jiquilisco ranged from 35.4 to 90.7 cm CCL, with very few (6 out of 20) large turtles > 70 cm CCL (median 59.2 cm CCL), while the turtles from Punta Amapala

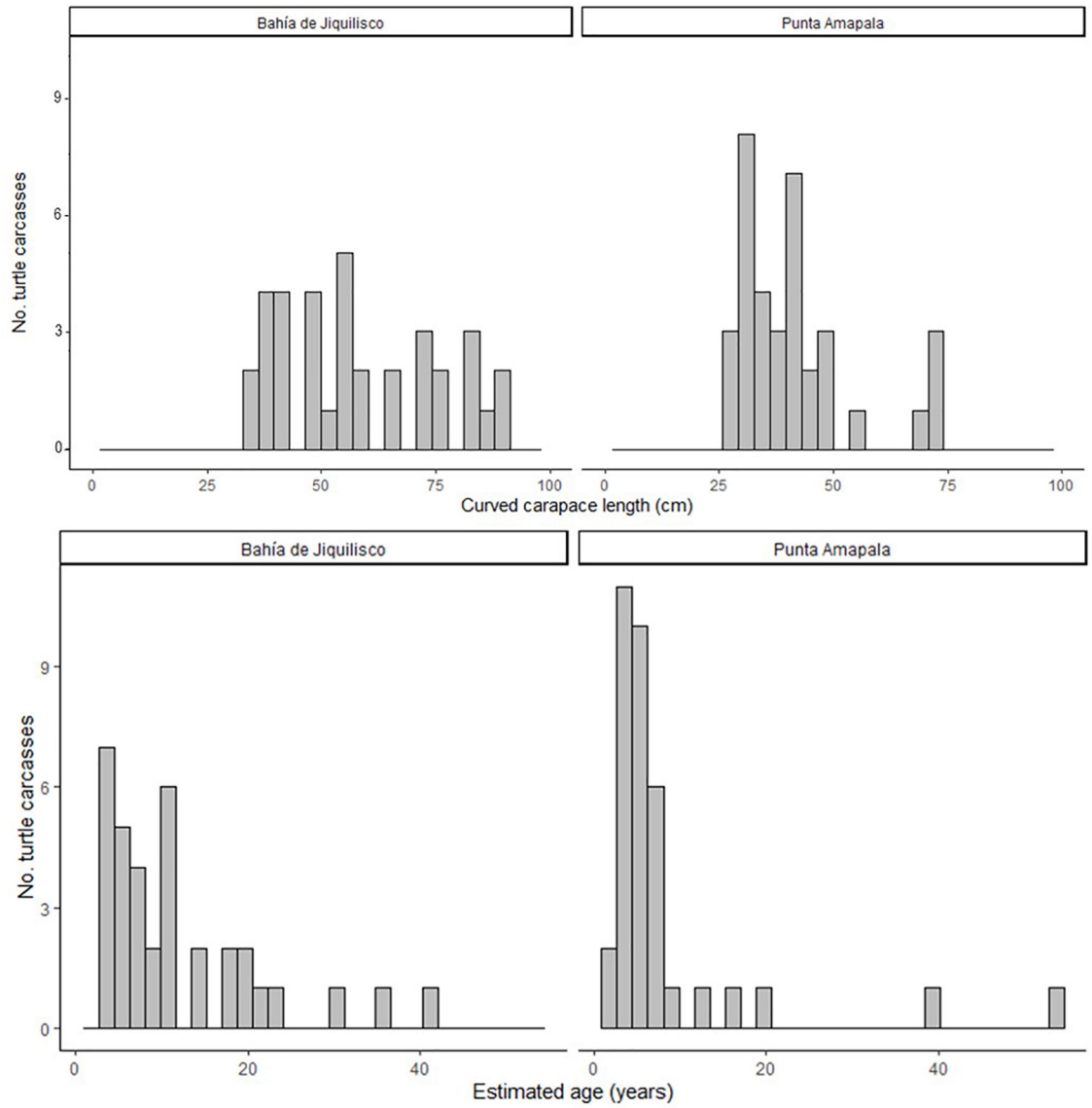

FIGURE 2
The body size (curved carapace length, CCL, cm) and estimated age (years) for the 70 hawksbill turtles analyzed for skeletochronology (35 from Bahía de Jiquilisco, 35 from Punta Amapala).

ranged from 28.5 to 73.6 cm CCL (median 47.0 cm CCL, 3 out of 20 were > 70 cm CCL); from each group, a total of 95 and 89 individual growth layers were subsampled for SIA, respectively. The stable carbon isotope ($\delta^{13}C$) values for all samples (n = 184) ranged from –27.1 to –11.9‰ (mean ± SE –16.9 ± 1.25‰) and the stable nitrogen isotope ($\delta^{15}N$) values ranged from 9.7 to 18.0‰ (mean ± SE 13.6 ± 1.00‰; **Table 2**). When separated by final stranding location, the $\delta^{13}C$ values (n = 95) ranged from –27.1 to –14.4 ‰ (mean ± SE –18.7 ± 1.92‰) and the $\delta^{15}N$ values ranged from 9.7 to 15.6‰ (mean ± SE 13.0 ± 1.33‰) for the 20 turtles recovered in Bahía de Jiquilisco, while the samples from the 20 turtles recovered from Punta Amapala (n = 89) had $\delta^{13}C$ values that ranged from –22.1 to –11.9‰ (mean ± SE –15.0 ± 1.60‰) and $\delta^{15}N$ values that ranged from 11.1 to 18.0‰ (mean ± SE 14.3 ± 1.52‰; **Table 2**).

Using the SIA-assigned habitats and corresponding age and size estimates for each growth layer, multiyear habitat-use patterns were observed. All turtles, regardless of final stranding location, had $\delta^{13}C$ values above the –18‰ threshold during years where body size was less than *ca.* 35 cm CCL (age range *ca.* 0–5 years), representative of spent time outside of the mangrove estuaries during these early juvenile years (mean ± SE $\delta^{13}C$: –15.0 ± 1.8‰ and $\delta^{15}N$: 14.1 ± 1.7‰, n = 30 turtles, 71 growth layers; **Figure 5**). The SIA values of

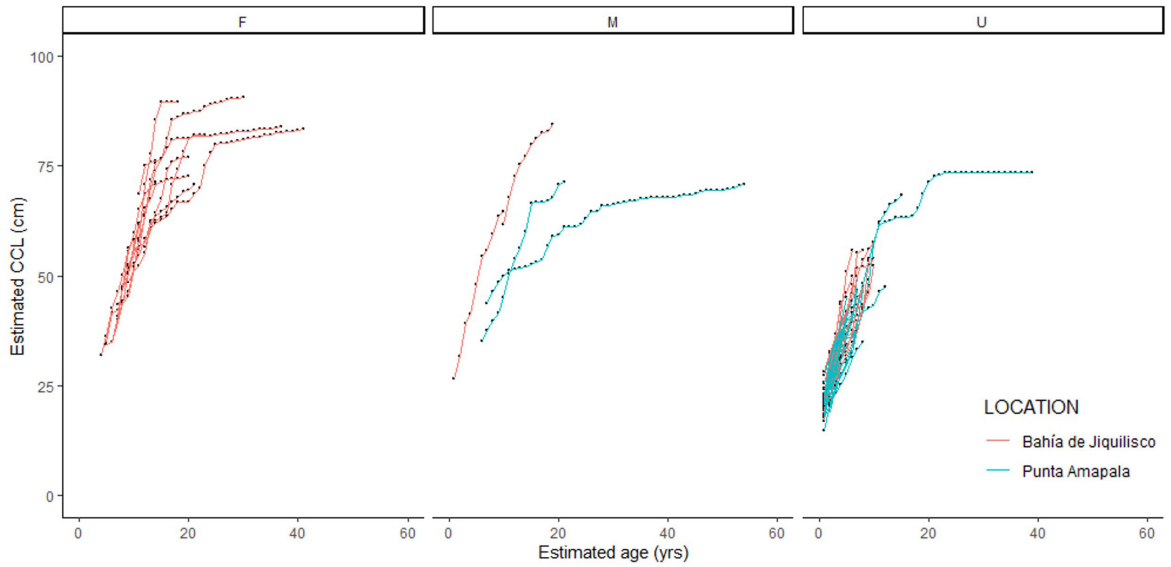

FIGURE 3
Estimated body size (curved carapace length, CCL, cm) and corresponding estimated age (years) for the 70 hawksbill turtles aged using skeletochronology. Individuals with known sex are separated as female (F), male (M) and unknown (U), and colors indicate stranding location, red = mangrove estuary of Bahía de Jiquilisco, blue = rocky reef area of Punta Amapala.

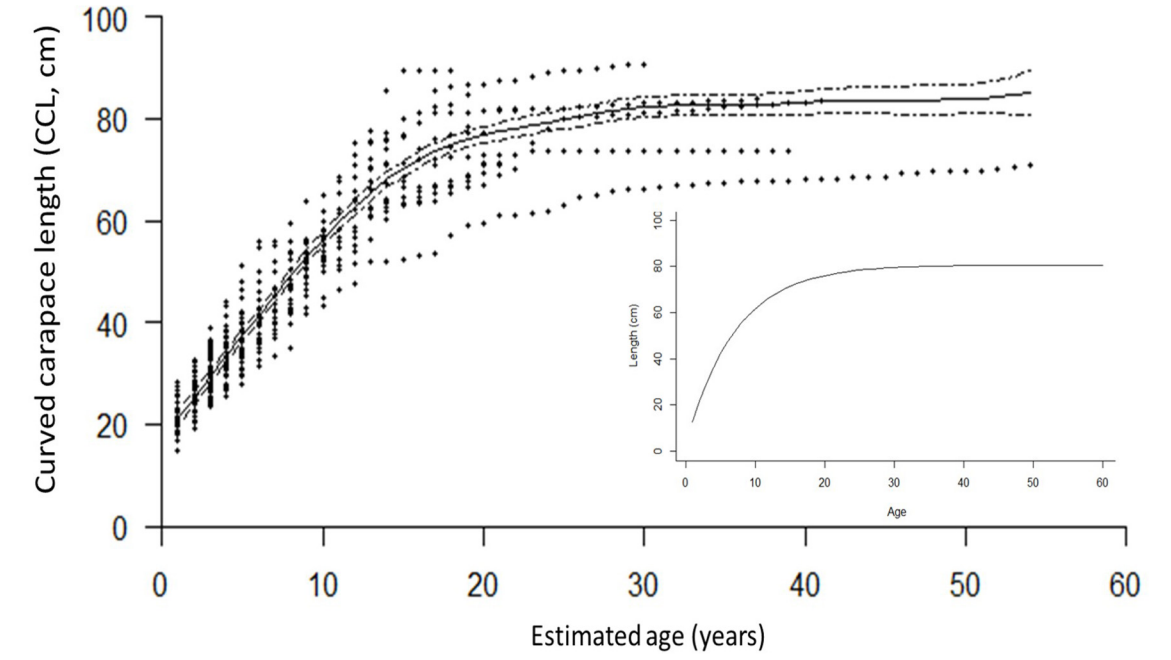

FIGURE 4
The generalized additive mixed model (GAMM) smoothing spline, fit to the length-at-age dataset of the 70 turtles, was significant ($p < 0.0001$, Edf = 7.457, adj. $r^2 = 0.887$), and showed close correspondence with the bootstrapped von Bertalanffy model (inset), based on growth-at-length data. The mean SSM at rapprochement, 76.9 cm CCL, was used to estimate the growth parameters L_{inf}: 80.6 ± 0.19 cm (95% CI: 80.2–81.0 cm) k: 0.142 ± 0.0008 (95% CI: 0.141–0.144).

growth layers with associated body size *ca.* > 35 cm showed divergent patterns, with some turtles' $\delta^{13}C$ values higher than the –18‰ threshold, associated with ocean and coastal rocky reef habitats (mean ± SE –15.3 ± 2.0‰ $n = 22$ turtles, 61 growth layers), while other turtles had $\delta^{13}C$ values lower than –18‰, associated with the mangrove estuaries (mean ± SE –22.0 ± 3.2

TABLE 1 Detailed information for the ten hawksbill turtles determined to reach maturity based on rapprochement observed during skeletochronology.

ID	Location	Sex	Age-at-sexual-maturity (ASM, yrs)	Size-at-sexual-maturity (SSM, cm)	Final CCL (cm)	Final Age (yrs)	Minimum reproductive longevity (yrs)
Ei_8	Bahía de Jiquilisco	F	16	89.5	89.5	18	3
Ei_10	Bahía de Jiquilisco	F	17	72.2	72.8	20	4
Ei_20	Bahía de Jiquilisco	F	18	81.2	82	23	6
Ei_9	Bahía de Jiquilisco	F	18	86.1	90.7	30	13
Ei_19	Bahía de Jiquilisco	F	19	77	77	20	2
Ei_7	Bahía de Jiquilisco	F	21	81.7	84.3	37	17
Ei_21	Bahía de Jiquilisco	F	26	80.3	83.5	41	16
Ei_30	Punta Amapala	M	16	66.7	72	21	6
Ei_29	Punta Amapala	M	22	61.2	71.1	54	33
Ei_38	Punta Amapala	U	22	73	73.6	39	18
	Mean ± SE		19.5 ± 1.01	76.9 ± 2.76			
	Range		16–26	61.2–89.5			
Ei_16	Bahía de Jiquilisco	F	NA	NA	71.4	14	NA
Ei_17	Bahía de Jiquilisco	F	NA	NA	70.9	21	NA
Ei_22	Bahía de Jiquilisco	M	NA	NA	84.5	19	NA
Ei_25	Punta Amapala	U	NA	NA	68.5	15	NA

Stranding location, sex (if known), age-at-sexual-maturity (ASM), size-at-sexual-maturity (SSM), final CCL, final estimated age, and reproductive longevity provided. An additional four turtles with final CCL near maturation size, but not yet showing rapprochement, are also included.

TABLE 2 The range, mean, and standard error (SE) of stable carbon ($\delta^{13}C$) and nitrogen ($\delta^{15}N$) isotope values of the two tissues sampled: bone individual growth layers, and skin.

Tissue	Group	Carbon (‰) range	Mean ± SE (‰)	Nitrogen (‰) range	Mean ± SE (‰)	n
Bone	all	−27.1 to −11.9	−16.9 ± 1.25	9.7–18.0	13.6 ± 1.00	184
	BJ stranded	−27.1 to −14.4	−18.7 ± 1.92	9.7–15.6	13.0 ± 1.33	95
	PA stranded	−22.1 to −11.9	−15.0 ± 1.60	11.1–18.0	14.3 ± 1.52	89
Skin	BJ stranded	−25.4 to −14.2	−20.5 ± 5.29	9.6–14.8	12.3 ± 3.18	15
	PA stranded	−17.6 to −14.9	−16.2 ± 2.47	10.9–14.7	12.8 ± 1.96	43

Groups show the values for all bone growth layer samples together, and the bone and skin samples divided between the two stranding locations, Bahía de Jiquilisco (BJ) and Punta Amapala (PA).

‰, n = 17 turtles, 48 growth layers; Figure 5). These same growth layer groups also had the same pattern for $\delta^{15}N$ values, mean ± SE 14.4 ± 1.9‰ (n = 22 turtles, 61 growth layers) for those with body size *ca.* > 35 cm, and mean ± SE 11.8 ± 1.7‰ for the larger body sizes (n = 17 turtles, 48 growth layers; Figure 5).

By identifying the earliest (innermost) growth layer with $\delta^{13}C$ values lower than the −18‰ threshold value, the timing of this habitat shift into the mangrove estuary was identified for 16 turtles recovered in Bahía de Jiquilisco (Figure 5 and Supplementary Figures 3A,B), which ranged from age 3–13 years old (mean ± SE 7.0 ± 0.69 years) and CCL from 34.8 to 64.8 cm (mean ± SE 45.9 ± 2.51 cm). The other four turtles sampled for SIA and recovered from Bahía de Jiquilisco had only stable isotope values associated with mangrove estuary habitat use, indicative of consistent, long-term habitat use (final ages: 20, 37, 18, 30 years; final CCLs: 72.8, 84.3, 89.5, 90.7 cm). The residency duration in mangrove estuarine habitats (likely in Bahía de Jiquilisco) for these four turtles ranged from 8 to 21 years (Figure 5 and Supplementary Figures 3A,B).

Of the 20 turtles recovered at Punta Amapala and sampled for SIA, 84 out of the 89 growth layer samples had $\delta^{13}C$ values higher than the mangrove threshold value of −18‰, indicating near-exclusive use of habitats outside of mangrove estuaries for these turtles recovered at Punta Amapala's rocky reef (Figure 5 and Supplementary Figures 3C,D). The five growth layer samples below the −18‰ threshold (−22.1 to −18.5‰) were collected from four different turtles, suggesting at least 1 year of previous mangrove estuary habitat use by these turtles during mid-juvenile years (ages: 7, 7, 8, 9, 14 years old; CCLs: 43.6, 50.0, 46.5, 48.6, 60.2 cm). Yet all four turtles showed several years of consistent habitat use and residency/fidelity outside of estuaries during their most recent years prior to stranding (Figure 5 and Supplementary Figures 3C,D).

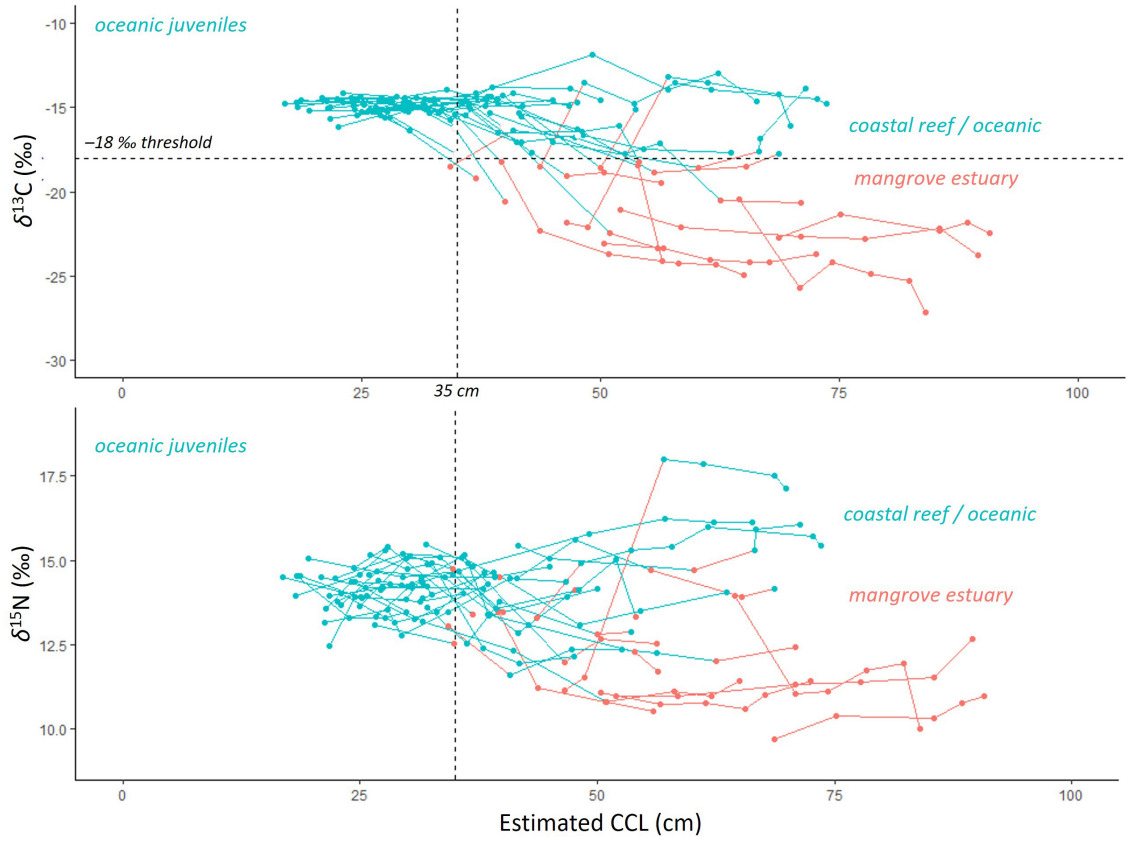

FIGURE 5
All stable isotope data, aligned with body size (curved carapace length, CCL, cm) for the 40 turtles processed by skeletochronology and then sampled for stable carbon ($\delta^{13}C$, *top*) and nitrogen ($\delta^{15}N$, *bottom*) isotope analysis. Lines show data for individual turtles. The threshold value of −18‰ $\delta^{13}C$ is shown as the dashed horizontal line on the top plot, with values above representing the ocean / coastal reef habitat (blue), while the values below indicate mangrove estuary habitat (red). The $\delta^{15}N$ values from the corresponding growth layers are color coded to indicate the $\delta^{13}C$-assigned habitat of "ocean" (> −18‰ $\delta^{13}C$) or "estuary" (< −18‰ $\delta^{13}C$). The 35 cm CCL body size is shown as the vertical dashed line and marks the size at which juveniles begin to recruit to near shore habitats.

Finally, when we compared the incremental growth rate data associated with the same size class groups but assigned to different habitats (mangrove estuary vs. ocean/rocky reef), we found slight growth advantages for turtles in the mangrove estuary of Bahía de Jiquilisco for two size class groups, 60–70 cm and 70–80 cm CCL ($p \leq 0.0001$, Wilcoxon Rank Sum; **Figure 6**).

Discussion

Here we present useful demographic and population ecology parameters for hawksbills in the EP using skeletochronology, in addition to multi-year movement and habitat residency patterns using complementary stable isotope analysis (skeleto+iso). Our empirical estimates on the maturation timing for this population show maturity occurring between 16 and 26 years old, with potential differences between nesting and foraging location (mangrove estuary vs. open coast), dietary preference and between sexes (males vs. females) that are worth future investigations. The non-estuary stable isotope signal that was found consistently in the age 0–3 growth layers strongly suggests that this hawksbill population does not immediately settle into the mangrove estuary, but instead has an offshore, if not oceanic, juvenile stage.

Maturation

The maturation age range of 16–26 years, based on rapprochement, came from only 10 adult individuals, yet was similar to what has been estimated for other hawksbill populations in previous studies. Snover et al. (2012) and Avens et al. (2021) both used skeletochronology and reported ASM between 15 and 25 years and 17–22 for hawksbills in the western North Atlantic and Hawaii, respectively. Various mark-recapture studies have estimated hawksbill ASM ranging from 13 to 20 years (e.g., Yucatan region, Garduño-Andrade et al., 1999; Brazil, Bellini et al., 2019), and 14–24 years based on

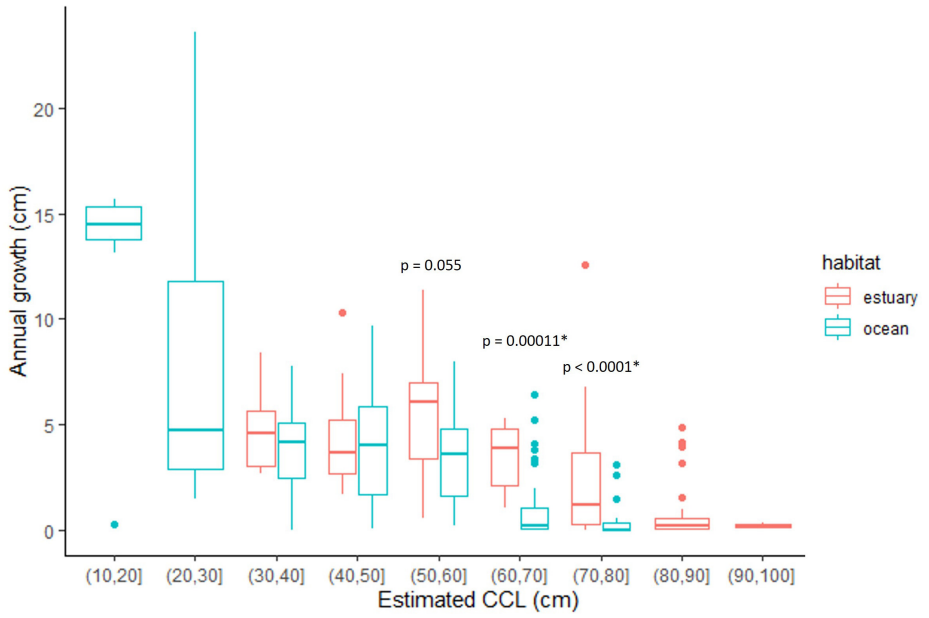

FIGURE 6
Annual growth (cm/yr) for growth layers assigned to a habitat–either mangrove estuary (in red), or rocky reef/ocean (in blue)– based on stable carbon isotope values ($\delta^{13}C$). The *p*-values show the results from the Mann–Whitney comparison tests for the relevant size-class groups. *Indicates *p*-values are significant at $p < 0.05$.

genetic inference for hawksbills nesting in Antigua [Levasseur et al., 2021; and see Avens et al. (2020) for further insight on ASM estimates]. These estimates are also substantially lower than the estimated average ASM reported for hawksbills in the Indo-Pacific region based on somatic growth rates (31–36 years; Limpus and Miller, 2000). The empirical results from the current study provide a baseline for this east Pacific population, and ideally the ASM estimate will be further refined in the future with increased adult samples for skeletochronology and validated using genetic fingerprinting (i.e., when a genetically sampled hatchling returns to nest as a genetically identified neophyte nester). Continued monitoring of both mangrove and open beach nesting sites will also help refine the demographic parameters estimated here, including reproductive longevity.

Based on the number of LAGs observed beyond rapprochement, estimated reproductive longevity ranged from 2 to 33 years (**Table 1**), and this estimated maximum longevity beyond maturation is in the mid-range of what has been found for several other sea turtle species (Avens and Snover, 2013; Kemp's ridleys *Lepidochelys kempii*, 10 years, Avens et al., 2017; flatbacks *Natator depressus*, 31 years, Turner Tomaszewicz et al. *in press*; leatherbacks *Dermochelys coriacea*, 18–22 years, max 31 years, Avens et al., 2020; green turtles, > 40 years, Limpus and Chaloupka, 1997, 27 years, Turner Tomaszewicz et al., 2022; and loggerheads, 46 years, Avens et al., 2015). To date, nesting site monitoring at Bahía de Jiquilisco, which began in 2008, has recorded at least one turtle nesting for 14 years ($n = 177$ turtles tagged), and of the 27 turtles tagged while nesting at Punta Amapala since 2015, seven is the maximum number of years a turtle has been observed returning to nest (M. Liles, ProCosta, *unpub.*).

Given the range of ASM and SSM observed in the current study, future work should also focus on examining potential difference in growth rates and maturation timing between sexes and foraging location (see section below). The seven mature females in the current study were all recovered from the mangrove estuary (Bahía de Jiquilisco) and had estimated ASM ranging from 16 to 26 years (mean ± SE 19.3 ± 1.27 years), and SSM ranging from 72.2 to 89.5 cm CCL (mean ± SE 81.1 ± 2.14 cm). Unfortunately, there were no mature male turtles recovered from Bahía de Jiquilisco, only two males that were 65.1 and 84.5 cm CCL and 10 and 19 years old, respectively. Yet the larger, older male turtle was likely nearing maturity given that its body size and age was within the range observed for mature females from Bahía de Jiquilisco (**Figure 3**). This suggests similar sizes for adult males and females within the estuary (**Figure 3**).

At Punta Amapala, the two mature males recovered (71.1 and 72 cm CCL, and age 21 and 54 years old, respectively) were smaller than most of the mature turtles recovered at Bahía de Jiquilisco, and unfortunately there were no known females recovered at this location. The 54-year-old male was the oldest turtle aged in the current study, and suggests that at least some adult male turtles at Punta Amapala are smaller than those found in the mangrove habitat. This potential pattern is also observed for nesting females at the different

sites. On-site monitoring of turtle body sizes at these nesting sites do show some potential size differences, with nesters at Bahía de Jiquilisco typically being larger (range: 68.2–98 cm, mean 83.5 cm CCL, n = 177) than those nesting at Punta Amapala (62.2–91 cm, mean 76.7 cm CCL, n = 27) and another open coast (non-estuary) site slightly north (Los Cóbanos: 63–97 cm, mean 80.5 cm CCL, n = 67; M. Liles, ProCosta, *unpubl.*). We acknowledge that the skeletochronology sample sizes are small, but together with the nesting size data, there is reason to encourage further research to explore the possibility of size difference by foraging and/or nesting site and to more fully characterize these important sex- and location-specific demographics.

Habitat use and movement patterns

The combination of sequential stable isotope analysis with skeletochronology facilitated the recreation of multi-year movement and habitat use patterns for 40 hawksbills. From this skeleto+iso analysis, three key habitat use patterns were revealed: (1) All post-hatchlings have a non-estuary juvenile stage where they likely occupy oceanic habitats for a minimum 1–3 years; (2) Juvenile turtles (∼35 cm CCL) then recruit to neritic habitats, but in at least two divergent ways—some settling into the nearshore rocky reefs and some settling into the mangrove estuaries; and (3) Turtles appear to have high fidelity to their selected habitat, with very little movement between the two habitats observed.

First, the non-estuary stable isotope signal, characterized by $\delta^{13}C$ values greater than –18‰, was found consistently in all the age 0–3 growth layers, regardless of where the turtle eventually stranded. Previous speculation on post-hatchling movement has questioned if some hatchlings from mangrove nests might have short-dispersal oceanic developmental periods (Gaos et al., 2017) or perhaps even remain within the estuary, growing rapidly and never undertaking an oceanic juvenile stage characteristic of most hard-shelled sea turtle species (Bolten, 2003). However, findings here strongly suggest that this is not the case—that hawksbills in this population do not immediately settle into the mangrove estuary, but instead spend at least a few years in an offshore, if not oceanic, habitat during their post-hatchling juvenile stage. These results are also supported by the SIA of hawksbill scute layers by Wedemeyer-Strombel et al. (2021) which also found higher $\delta^{13}C$ values in the earliest scute layers. This offshore movement pattern is further supported when the growth rates estimated in the current study are related to the length-frequency distribution of turtles found in both the mangrove estuary and the rocky reef habitats. In both Bahía de Jiquilisco and the rocky reefs at Punta Amapala, other than newly emerged hatchlings, no turtles < 14 cm CCL have ever been observed since more regular community-based monitoring in the area around 2007 (Gaos et al., 2010), and very few turtles < 30 cm CCL have been encountered (Liles et al., 2017).

In Bahía de Jiquilisco, the smallest turtle encountered was 35.4 cm CCL; in Punta Amapala, the average size retrieved from gillnets during Liles et al. (2017) was 31.6 cm CCL ± 14.7 S.D. (n = 20), and the smallest turtle used in the current study was 28.5 cm CCL and recovered at Punta Amapala. Using skeletochronology, the back calculated body sizes at age 1 for turtles found across both sites (n = 38) ranged in size from 14.8 to 28.2 cm CCL (mean 21.2 ± 3.4 cm), and at age 2 (n = 44) CCL ranged from 19.0 to 32.7 cm (mean 26.3 ± 4.0 cm). These sizes are similar to the size achieved at 1-year for three captive raised hawksbills collected from relocated nests in Bahía de Jiquilisco (364 days, straight carapace length, SCLs: 18.9, 23.7, 26.0 cm CCL; M. Liles, ProCosta, *unpubl.*). Together, these findings suggest that turtles are at least a year old when they recruit to neritic habitats after having spent time in oceanic regions.

Upon recruitment to a nearshore habitat, the turtles then appear to diverge in their habitat use patterns, with turtles of similar size, *ca.* 35 cm CCL, selecting different habitats in which to settle—in this case, either a mangrove estuary or rocky reef habitat. The mechanisms driving this divergent behavior are not clear and should be explored further. The selection of settlement habitat (estuary or reef) may be influenced by a variety of factors including physical environmental conditions (e.g., currents, water temperature, food availability), biological predisposition (e.g., genetics) or perhaps habitat-type is selected by chance (e.g., Bolten, 2003; Chevis et al., 2017; Griffin et al., 2020). Once turtles do settle into one of these neritic habitats, it is likely that they remain as foragers in that habitat-type through the rest of their lives, given that the adult turtles showed consistent habitat use with long term (10–30 years) residency durations. The four adult turtles from Bahía de Jiquilisco all showed constant low $\delta^{13}C$ and $\delta^{15}N$ values indicating mangrove estuary residency, and the two adult turtles from Punta Amapala that had constant high $\delta^{13}C$ and $\delta^{15}N$ values indicating residency outside of mangrove estuaries, likely at the rocky reefs along the open coast (**Figure 5** and **Supplementary Figure 4**). In addition to the large mangrove estuary at Bahía de Jiquilisco, there are other similar estuaries in the region, also known to have foraging and nesting hawksbills, including Barra de Santiago to the north (Massey and McCord, 2017) and Estero Padre Ramos in Nicaragua to the south (Liles et al., 2011; Gaos et al., 2012b), and it is possible there is movement of foraging turtles between these different estuaries. Turtles inhabiting these nearby mangrove habitats are known to have stable carbon isotope values similar to those in Bahía de Jiquilisco (Wedemeyer-Strombel et al., 2021), so it is possible that some mangrove-foraging turtles do move between different mangrove estuaries. However, currently, there is more evidence that hawksbills have fidelity to just one mangrove estuary, as demonstrated by genetic studies, long-term recapture, and nesting histories showing high levels of natal foraging philopatry (Gaos et al., 2017, 2018).

Yet inspection of the SIA values of individual turtles also reveals more intricate patterns, including the potential for some individuals to undertake movements between the estuary and reef habitats. For instance, one of the Punta Amapala adult turtles that showed long term rocky reef (non-estuary) habitat use from the age of *ca.* 17 to death at 54 years old, had apparently spent time in the mangrove estuaries between the age of *ca.* 10 to *ca.* 17 (*ca.* 45–55 cm CCL; **Figure 5** and **Supplementary Figure 4**). It is therefore likely that some flexibility exists within this population with regard to habitat use. Continuing research employing tagging (e.g., flipper, PIT, satellite) will help to further elucidate these complex movement patterns for east Pacific hawksbills in this region and to begin to identify the drivers and implications of these variable habitat use strategies.

Growth rates among different habitats

Overall, the annual growth rates were highest for the youngest (<5 years) and smallest turtles (<30 cm CCL), then gradually slowed as turtles grew and eventually approached maturity, a growth pattern typical for sea turtles (**Figures 4**, **6**). Sea turtle growth is known to be affected by environmental conditions such as temperature and food availability and quality (Chaloupka and Musick, 1997; Balazs and Chaloupka, 2004; Eguchi et al., 2012), and has also been shown to be density dependent (Bjorndal et al., 2000). Stable isotopes are a useful tool to help better examine the potential effects some of these factors—particularly food and habitat—may have on growth. In the current study, the incremental growth data of the mid-size classes (50–80 cm CCL) suggests that habitat selection may affect growth, with a potential growth-advantage for those turtles settling into mangrove estuaries (**Figure 6**). It is unknown how or if this difference in growth rates may impact the ultimate fecundity of turtles once they become adults, but the pattern should be examined further to determine if there are somatic growth consequences of habitat choice.

Based on other trends documented for sea turtles, increased growth, for example, could result in (1) earlier maturation (lower ASM) and/or (2) larger size of maturation (larger SSM), both of which could translate to higher reproductive output if reproductive longevity is longer (given the lower ASM), or if clutch size is larger (given the larger SSM). These potential age- and size-related life history characteristics should be the focus of future work, as these differences have implications for population growth and ecology of this recovering stock.

Conservation implications

These long-term habitat use patterns and estimated demographic parameters are important in helping to understand the life history of this population and in guiding conservation efforts to prioritize critical habitat. Offshore and coastal rocky reef habitats are likely used by all hawksbills in this population during an early juvenile stage, and fishing and other anthropogenic activities that take place in these waters should be monitored to minimize impact to these turtles. Similarly, the age- and size-specific habitat use patterns showed that mangrove estuaries are very important, not only for providing long term habitats, but also by potentially facilitating rapid growth, which may positively affect the population's recovery rate. Continued community engagement that is focused on monitoring hawksbills in these nearshore habitats while also working to minimize mortality (fishing-related bycatch, entanglement, blast fishing; and egg harvesting) has already made incredible progress in the past 15 years and is essential to the continuing recovery of this population.

Data availability statement

The original contributions presented in the study are included in the article/**Supplementary material**, further inquiries can be directed to the corresponding author/s.

Ethics statement

Ethical review and approval was not required for the animal study because all tissue samples used in this study were collected from already dead (stranded) sea turtles, with all appropriate collection and export/import permits in place.

Author contributions

CTT, JS, and ML conceived of the study. ML coordinated the sample collection in the field. CTT conducted the lab work, data analysis, and wrote the first draft of the manuscript. LA contributed to the skeletochronology data analysis. All authors revised and helped to edit the final manuscript.

Funding

This work was supported by a NOAA—NMFS Sea Turtle Stock Assessment Award 18–19, which supported CTT during a National Research Council Research Associateship.

Acknowledgments

We acknowledge the dedicated members of ProCosta in El Salvador for collecting, cleaning, and drying

the hundreds of samples necessary for this study, especially Sofia Chavarria, Ani Henriquez, Carlos Pacheco, Marivn Pineda, Neftaly Sanchez, and Melissa Valle. At the Southwest Fisheries Science Center, we thank Allison Johnson and Toni Lohroff for assistance in processing the bone and skin samples, and Erin LaCasella for guiding the CITES sample import process.

Conflict of interest

The authors declare that the research was conducted in the absence of any commercial or financial relationships that could be construed as a potential conflict of interest.

Publisher's note

All claims expressed in this article are solely those of the authors and do not necessarily represent those of their affiliated organizations, or those of the publisher, the editors and the reviewers. Any product that may be evaluated in this article, or claim that may be made by its manufacturer, is not guaranteed or endorsed by the publisher.

Supplementary material

The Supplementary Material for this article can be found online at: https://www.frontiersin.org/articles/10.3389/fevo.2022.983260/full#supplementary-material

References

Allen, C. D., Lemons, G. E., Eguchi, T., LeRoux, R. A., Fahy, C. C., Dutton, P. H., et al. (2013). Stable isotope analysis reveals migratory origin of loggerhead turtles in the Southern California Bight. *Mar. Ecol. Prog. Ser.* 472, 275–285. doi: 10.3354/meps10023

Avens, L., Goshe, L. R., Coggins, L., Shaver, D. J., Higgins, B., Landry, A. M., et al. (2017). Variability in age and size at maturation, reproductive longevity, and long-term growth dynamics for Kemp's ridley sea turtles in the Gulf of Mexico. *PLoS One* 12:173999. doi: 10.1371/journal.pone.0173999

Avens, L., Goshe, L. R., Harms, C. A., Anderson, E. T., Hall, A. G., Cluse, W. M., et al. (2012). Population characteristics, age structure, and growth dynamics of neritic juvenile green turtles in the northeastern Gulf of Mexico. *Mar. Ecol. Prog. Ser.* 458, 213–229. doi: 10.3354/meps09720

Avens, L., Goshe, L. R., Pajuelo, M., Bjorndal, K. A., MacDonald, B. D., Lemons, G. E., et al. (2013). Complementary skeletochronology and stable isotope analyses offer new insight into juvenile loggerhead sea turtle oceanic stage duration and growth dynamics. *Mar. Ecol. Prog. Ser.* 491, 235–251. doi: 10.3354/meps10454

Avens, L., Goshe, L. R., Zug, G. R., Balazs, G. H., Benson, S. R., and Harris, H. (2020). Regional comparison of leatherback sea turtle maturation attributes and reproductive longevity. *Mar. Biol.* 167, 1–12. doi: 10.1007/s00227-019-3617-y

Avens, L., Ramirez, M. D., Goshe, L. R., Clark, J. M., Meylan, A. B., Teas, M., et al. (2021). Hawksbill sea turtle life-stage durations, somatic growth patterns, and age at maturation. *Endang Species Res.* 45, 127–145. doi: 10.3354/esr01123

Avens, L., and Snover, M. (2013). "Age and age estimation in sea turtles," in *Biology of Sea Turtles Volume III*, eds J. Wyneken, K. J. Lohmann, and J. A. Musick (Boca Raton, FL: CRC Press), 97–133.

Avens, L. A., Goshe, L. R., Coggins, L., Snover, M. L., Pajuelo, M., Bjorndal, K. A., et al. (2015). Age and size at maturation- and adult-stage duration for loggerhead sea turtles in the western North Atlantic. *Mar. Biol.* 162, 1749–1767. doi: 10.1007/s00227-015-2705-x

Balazs, G. H., and Chaloupka, M. (2004). Spatial and temporal variability in somatic growth of green sea turtles (Chelonia mydas) resident in the Hawaiian Archipelago. *Mar. Biol.* 145, 1043–1059. doi: 10.1007/s00227-004-1387-6

Bellini, C., Santos, A. J. B., Patrício, A. R., Bortolon, L. F. W., Godley, B. J., Marcovaldi, M. A., et al., (2019). Distribution and growth rates of immature hawksbill turtles Eretmochelys imbricata in Fernando de Noronha, Brazil. *Endang. Species Res.* 40, 41–52. doi: 10.3354/esr00979

Bjorndal, K. A., Bolten, A. B., and Chaloupka, M. Y. (2000). Green turtle somatic growth model: evidence for density-dependence. *Ecol. Appl.* 10, 269–282. doi: 10.1890/1051-0761(2000)010[0269:GTSGME]2.0.CO;2

Bolten, A. B. (2003). "Variation in sea turtle life history patterns: neritic vs. oceanic developmental stages," in *The Biology of Sea Turtles*, Vol. II, eds P. L. Lutz, J. Musick, and J. Wyneken (Boca Raton, FL: CRC Press), 243–257. doi: 10.1201/9781420040807.ch9

Bouillon, S., Connolly, R. M., and Lee, S. Y. (2008). Organic matter exchange and cycling in mangrove ecosystems: recent insights from stable isotope studies. *J. Sea Res.* 59, 44–58. doi: 10.1016/j.seares.2007.05.001

Chaloupka, M. Y., and Musick, J. A. (1997). "Age, growth and population dynamics," in *The Biology of Sea Turtles*, Chap. 9, eds P. L. Lutz and J. A. Musick (Boca Raton, FL: CRC Press), 233–276.

Chevis, M. G., Godley, B. J., Lewis, J. P., Lewis, J. J., Scales, K. L., and Graham, R. T. (2017). Movement patterns of juvenile hawksbill turtles Eretmochelys imbricata at a Caribbean coral atoll: long-term tracking using passive acoustic telemetry. *Endang. Species Res.* 32, 309–319. doi: 10.3354/esr00812

DeNiro, M. J., and Epstein, S. (1978). Influence of diet on the distribution of carbon isotopes in animals. *Geochim. Cosmochim. Acta* 42, 495–506. doi: 10.1016/0016-7037(78)90199-0

Deutsch, C. A., Gruber, N. P., Key, R. M., Sarmiento, J. L., and Ganachaud, A. (2011). Denitrification and N2 fixation in the Pacific Ocean. *Global Biogeochem. Cycles* 15, 483–506. doi: 10.1029/2000GB001291

Domínguez-Miranda, J. P. (2010). *Caracterización Biofísca del área marina frente a Playa Las Tunas, Playas Negras, Playas Blancas, Playa Maculís, y las Mueludas, Municipio de Conchagua, Departamento de La Unión, El Salvador*. San Salvador: USAID, 83.

Dunbar, S. G., Anger, E. C., Parham, J. R., Kingen, C., Wright, M. K., Hayes, C. T., et al. (2021). HotSpotter: using a computer-driven photo-id application to identify sea turtles. *J. Exp. Mar. Biol. Ecol.* 535, 151490. doi: 10.1016/j.jembe.2020.151490

Eguchi, T., Seminoff, J. A., Leroux, R. A., Dutton, D. L., and Dutton, P. H. (2012). Morphology and growth rates of the green sea turtle (Chelonia mydas) in a northern-most temperate foraging ground. *Herpetologica* 68, 76–87. doi: 10.1655/HERPETOLOGICA-D-11-00050.1

Espinasse, B., Hunt, B. P. V., Batten, S. D., and Pakhomov, E. A. (2019). Defining isoscapes in the Northeast Pacific as an index of ocean productivity. *Global Ecol. Biogeogr.* 29, 246–261. doi: 10.1111/geb.13022

Fleming, A. H., Clark, C. T., Calambokidis, J., and Barlow, J. (2016). Humpback whale diets respond to variance in ocean climate and ecosystem conditions in the California Current. *Glob. Change Biol.* 22, 1214–1224. doi: 10.1111/gcb.13171

France, R. L. (1995). Carbon-13 enrichment in benthic compared to planktonic algae: foodweb implications. *Mar. Ecol. Prog. Ser.* 124, 307–312. doi: 10.3354/meps124307

Francillon-Vieillot, H., Arntzen, J. W., and Géraudie, J. (1990). Age, growth and longevity of sympatric *Triturus cristatus T. marmoratus* and their hybrids (Amphibia, Urodela): A Skeletochronological Comparison. *J. Herpetol.* 24, 13–22. doi: 10.2307/1564284

Francis, R. I. C. C. (1990). Back-calculation of fish length: A critical review. *J. Fish Biol.* 36, 883–902. doi: 10.1111/j.1095-8649.1990.tb05636.x

Fry, B. (2006). *Stable Isotope Ecology*. New York, NY: Springer New York, 308. doi: 10.1007/0-387-33745-8

Fry, B., and Ewel, K. C. (2003). Using stable isotopes in mangrove fisheries research - a review and outlook. *Isotopes Environ. Health Stud.* 39, 191–196. doi: 10.1080/1025601031000160106 7

Gaos, A. R., Abreu-Grobois, F. A., Alfaro-Shigueto, J., Amorocho, D., Arauz, R., Baquero, A., et al. (2010). Signs of hope in the eastern Pacific: international collaboration reveals encouraging status for a severely depleted population of hawksbill turtles Eretmochelys imbricata. *Oryx* 44, 595–601. doi: 10.1017/S0030605310000773

Gaos, A. R., Lewison, R. L., Jensen, M. P., Liles, M. J., Henriquez, A., Chavarria, S., et al. (2017). Natal foraging philopatry in eastern Pacific hawksbill turtles. *R. Soc. Open Sci.* 4:170153. doi: 10.1098/rsos.170153

Gaos, A. R., Lewison, R. L., Jensen, M. P., Liles, M. J., Henriquez, A., Chavarria, S., et al. (2018). Rookery contributions, movements and conservation needs of hawksbill turtles at foraging grounds in the eastern Pacific Ocean. *Mar. Ecol. Prog. Ser.* 586, 203–2016. doi: 10.3354/meps12391

Gaos, A. R., Lewison, R. L., Yañez, I. L., Wallace, B. P., Liles, M. J., Nichols, W. J., et al. (2012a). Shifting the life-history paradigm: discovery of novel habitat use by hawksbill turtles. *Biol. Lett.* 8, 54–56. doi: 10.1098/rsbl.2011.0603

Gaos, A. R., Lewison, R. L., Wallace, B. P., Yañez, I. L., Liles, M. J., Nichols, W. J., et al. (2012b). Spatial ecology of critically endangered hawksbill turtles *Eretmochelys imbricata*: implications for management and conservation. *Mar. Ecol. Prog. Ser.* 450, 181–194. doi: 10.3354/meps09591

Gaos, A. R., and Yañez, I. L. (2012). "Saving the eastern Pacific hawksbill from extinction: Last chance or chance lost?," in *Sea Turtles of the Eastern Pacific: Advances in Research and Conservation*, eds J. A. Seminoff and B. P. Wallace (Tucson: University of Arizona Press), 244–262. doi: 10.2307/j.ctv21hrddc.14

Garduño-Andrade, M., Guzman, V., Miranda, E., Briseño-Dueñas, R., and Abreu-Grobois, F. A. (1999). Increases in hawksbill turtle (*Eretmochelys imbricata*) nestings in the Yucatan Peninsula, Mexico, 1977-1996: data in support of successful conservation? *Chelonian Conserv. Biol.* 3, 286–295.

Godley, B. J., Blumenthal, J. M., Broderick, A. C., Coyne, M. S., Godfrey, M. H., Hawkes, L. A., et al. (2008). Satellite tracking of sea turtles: where have we been and where do we go next? *Endanger. Species Res.* 4, 3–22. doi: 10.3354/esr00060

Goshe, L. R., Avens, L., Scharf, F. S., and Southwood, A. L. (2010). Estimation of age at maturation and growth of Atlantic green turtles (*Chelonia mydas*) using skeletochronology. *Mar. Biol.* 157, 1725–1740. doi: 10.1007/s00227-010-1446-0

Goshe, L. R., Avens, L., Snover, M. L., and Hohn, A. A. (2020). "Protocol for processing sea turtle bones for age estimation," in *Proceedings of the NOAA Technical Memorandum NMFS-SEFSC*, 43. (Washington, DC: NOAA),

Goshe, L. R., Snover, M. L., Hohn, A. A., and Balazs, G. H. (2016). Validation of back-calculated body lengths and timing of growth mark deposition in Hawaiian green sea turtles. *Ecol. Evol.* 6, 3208–3215. doi: 10.1002/ece3.2108

Griffin, L. P., Smith, B. J., Cherkiss, M. S., Crowder, A. G., Pollock, C. G., Hillis-Starr, Z., et al. (2020). Space use and relative habitat selection for immature green turtles within a Caribbean marine protected area. *Anim. Biotelemetry* 8:22. doi: 10.1186/s40317-020-00209-9

Hanna, M. E., Chandler, E. M., Semmens, B. X., Eguchi, T., Lemons, G. E., and Seminoff, J. A. (2021). Citizen-sourced sightings and underwater photography reveal novel insights about green sea turtle distribution and ecology in Southern California. *Front. Mar. Sci.* 8:671061. doi: 10.3389/fmars.2021.671061

Hastie, T. J., and Tibshirani, R. J. (1990). "Generalized additive models," in *Monographs on Statistics and Applied Probability*, Ed. G. Wetherill (London: Chapman and Hall), 43.

Hawkes, L. A., Tomas, J., Revuelta, O., Leon, Y. M., Blumenthal, J. M., Broderick, A. C., et al. (2012). Migratory patterns in hawksbill turtles described by satellite tracking. *Mar. Ecol. Prog. Ser.* 461, 223–232. doi: 10.3354/meps09778

Hays, G. C., and Hawkes, L. A. (2018). Satellite tracking sea turtles: opportunities and challenges to address key questions. *Front. Mar. Sci.* 5:432. doi: 10.3389/fmars.2018.00432

Hobson, K. A., and Wassenaar, L. I. (eds) (2018). *Tracking Animal Migration with Stable Isotopes*. Cambridge, MA: Academic Press. doi: 10.1016/B978-0-12-814723-8.00001-5

IUCN (2018). *2018 IUCN Red List of Threatened Species*. Gland: IUCN-SSC.

LaCasella, E. L., Jensen, M. P., Madden, H., Bell, I. P., Frey, A., and Dutton, P. H. (2021). Mitochondrial DNA profiling to combat the illegal trade in tortoiseshell products. *Front. Mar. Sci.* 7:595853. doi: 10.3389/fmars.2020.595853

Levasseur, K. E., Stapleton, S. P., and Quattro, J. M. (2021). Precise natal homing and an estimate of age at sexual maturity in hawksbill turtles. *Anim. Conserv.* 24, 523–535. doi: 10.1111/acv.12657

Liles, M. J., Gaos, A. R., Bolanos, A. D., Lopez, W. A., Arauz, R., Gadea, V., et al. (2017). Survival on the rocks: high bycatch in lobster gillnet fisheries threatens hawksbill turtles on rocky reefs along the Eastern Pacific coast of Central America. *Latin Am. J. Aquat. Res.* 45, 521–539. doi: 10.3856/vol45-issue3-fulltext-3

Liles, M. J., Jandres, M. V., Lopez, W. A., Mariona, G. I., Hasbun, C. R., and Seminoff, J. A. (2011). Hawksbill turtles Eretmochelys imbricata in El Salvador: nesting distribution and mortality at the largest remaining nesting aggregation in the eastern Pacific Ocean. *Endanger. Species Res.* 14, 23–30. doi: 10.3354/esr00338

Liles, M. J., Peterson, M. J., Lincoln, Y. S., Seminoff, J. A., Gaos, A. R., and Peterson, T. R. (2015a). Connecting international priorities with human wellbeing in low-income regions: lessons from hawksbill turtle conservation in El Salvador. *Local Environ.* 20, 1383–1404. doi: 10.1080/13549839.2014.905516

Liles, M. J., Peterson, M. J., Seminoff, J. A., Altamirano, E., Henríquez, A. V., Gaos, A. R., et al. (2015b). One size does not fit all: importance of adjusting conservation practices for endangered hawksbill turtles to address local nesting habitat needs in the eastern Pacific Ocean. *Biol. Conservat.* 184, 405–413. doi: 10.1016/j.biocon.2015.02.017

Liles, M. J., Peterson, T. R., Seminoff, J. A., Gaos, A. R., Altamirano, E., Henríquez, A. V., et al. (2019). Potential limitations of behavioral plasticity and the role of egg relocation in climate change mitigation for a thermally sensitive endangered species. *Ecol. Evol.* 9, 1603–1622. doi: 10.1002/ece3.4774

Limpus, C. J., and Chaloupka, M. (1997). Nonparametric regression modeling of green sea turtle growth rates (southern Great Barrier Reef). *Mar. Ecol. Prog. Ser.* 149, 23–34. doi: 10.3354/meps149023

Limpus, C. J., and Miller, J. D. (1990). The use of measured scutes of hawksbill turtles. Eretmochelys imbricata, in the management of the tortoiseshell (bekko) trade. *Aust. Wildl. Res.* 17, 633–639. doi: 10.1071/WR9900633

Limpus, C. J., and Miller, J. D. (2000). *Final Report for Australian Hawksbill Turtle Population Dynamics Project. Unpublished Report to the Japan Bekko Association*. Brisbane: Queensland Parks and Wildlife Services.

Mansfield, K. L., Wyneken, J., and Luo, J. (2021). First Atlantic satellite tracks of 'lost years' green turtles support the importance of the Sargasso Sea as a sea turtle nursery. *Proc. R. Soc. B Biolog. Sci.* 288:20210057. doi: 10.1098/rspb.2021.0057

MARN (2014). *MARN y líderes locales del Bajo Lempa unen esfuerzos para construer Plan Ambiental*. Riyadh: MARN.

Marshall, J. D., Brookes, J. R., and Lajtha, K. (2007). "Sources of variation in the stable isotopic composition of plants," in *Stable Isotopes in Ecology and Environmental Sciences*, eds R. Michener and K. Lajtha (Oxford: Blackwell Publishing), 22–50. doi: 10.1002/9780470691854.ch2

Massey, L., and McCord, P. (2017). *AMBAS in Action: How and all-women's group is leading sea turtle conservation efforts in El Salvador*. Capstone Thesis. San Diego, CA: University of California, San Diego.

McClellan, C. M., Braun-McNeill, J., Avens, L., Wallace, B. P., and Read, A. J. (2010). Stable isotopes confirm a foraging dichotomy in juvenile loggerhead sea turtles. *J. Exp. Mar. Biol. Ecol.* 387, 44–51. doi: 10.1016/j.jembe.2010.02.020

McMahon, K. W., Berumen, M. L., Mateo, I., Elsdon, T. S., and Thorrold, S. R. (2011). Carbon isotopes in otolith amino acids identify residency of juvenile snapper (Family: Lutjanidae) in coastal nurseries. *Coral Reefs* 30, 1135–1145. doi: 10.1007/s00338-011-0816-5

McMahon, K. W., Hamady, L., and Thorrold, S. R. (2013). A review of ecogeochemistry approaches to estimating movements of marine animals. *Limnol. Oceanog.* 58:697. doi: 10.4319/lo.2013.58.2.0697

Montoya, J. (2008). "Nitrogen stable isotopes in marine environments," in *Nitrogen in the Marine Environment*, Chap. 29, eds D. G. Capone, D. A. Bronk, M. R. Mullholland, and E. J. Carpenter (Burlington, MA: Academic Press, Elsevier), 1277–1302. doi: 10.1016/B978-0-12-372522-6.00029-3

Montoya, J., Holl, C., Zehr, J., Hansen, A., Villareal, T., and Capone, D. G. (2004). High rates of N2 fixation by unicellular diazotrophs in the oligotrophic Pacific Ocean. *Nature* 430, 1027–1032. doi: 10.1038/nature02824

Oczkowski, A., Kreakie, B., McKinney, R. A., and Prezioso, J. (2016). Patterns in stable isotope values of nitrogen and carbon in particulate matter from the Northwest Atlantic continental shelf, from the Gulf of Maine to Cape Hatteras. *Front. Mar. Sci.* 3:252.doi: 10.3389/fmars.2016.00252

Pajuelo, M., Bjorndal, K. A., Alfaro-Shigueto, J., Seminoff, J. A., Mangel, J., and Bolten, A. B. (2010). Stable isotope dichotomy in loggerhead turtles reveals Pacific-Atlantic oceanographic differences. *Mar. Ecol. Prog. Ser.* 417, 277–285. doi: 10.3354/meps08804

Plotkin, P. T. (2003). "Adult migrations and habitat use," in *The Biology of Sea Turtles: II*, eds P. Lutz, J. Musick, and J. Wyneken (Boca Raton, FL: CRC Press), 225–241. doi: 10.1201/9781420040807.ch8

R Core Team (2021). *A Language and Environment for Statistical Computing*. Vienna: R Foundation for Statistical Computing.

Ramirez, M. D., Avens, L., Seminoff, J. A., Goshe, L. R., and Heppell, S. S. (2015). Patterns of loggerhead turtle ontogenetic shifts revealed through isotopic analysis of annual skeletal growth increments. *Ecosphere* 6:244. doi: 10.1890/ES15-00255.1

Seminoff, J. A., Benson, S. R., Arthur, K. E., Dutton, P. H., Tapilatu, R., and Popp, B. N. (2012). Stable isotope tracking of endangered sea turtles: validation with satellite telemetry and δ15N analysis of amino acids. *PLoS One* 7:e37403. doi: 10.1371/journal.pone.0037403

Seminoff, J. A., Komoroske, L. M., Amorocho, D., Arauz, R., Chacón-Chaverrí, D., de Paz, N., et al. (2021). Large-scale patterns of green turtle trophic ecology in the eastern Pacific Ocean. *Ecosphere* 12:e03479. doi: 10.1002/ecs2.3479

Snover, M., Avens, L., and Hohn, A. (2007). Back-calculating length from skeletal growth marks in loggerhead sea turtles *Caretta caretta*. *Endanger. Species Res.* 3, 95–104. doi: 10.3354/esr003095

Snover, M. L., Balazs, G. H., Murakawa, S. K. K., Hargrove, S. K., Rice, M. R., and Seitz, W. A. (2012). Age and growth rates of Hawaiian hawksbill turtles (Eretmochelys imbricata) using skeletochronology. *Mar. Biol.* 160, 37–46. doi: 10.1007/s00227-012-2058-7

Snover, M. L., and Hohn, A. A. (2004). Validation and interpretation of annual skeletal marks in loggerhead (*Caretta caretta*) and Kemp's ridley (*Lepidochelys kempii*) sea turtles. *Fish. Bull.* 102, 682–692.

Snover, M. L., Hohn, A. A., Crowder, L. B., and Macko, S. A. (2010). Combining stable isotopes and skeletal growth marks to detect habitat shifts in juvenile loggerhead sea turtles *Caretta caretta*. *Endanger. Species Res.* 13, 25–31. doi: 10.3354/esr00311

Snover, M. L., Hohn, A. A., Goshe, L. R., and Balazs, G. H. (2011). Validation of annual skeletal marks in green sea turtles *Chelonia mydas* using tetracycline labeling. *Aquat. Biol.* 12, 197–204. doi: 10.3354/ab00337

Turner Tomaszewicz, C. N., Avens, L., LaCasella, E. L., Eguchi, T., Dutton, P. H., LeRoux, R. A., et al. (2022). Mixed-stock aging analysis reveals variable sea turtle maturity rates in a recovering population. *J. Wildl. Manag.* 2022:e22217. doi: 10.1002/jwmg.22217

Turner Tomaszewicz, C. N., Seminoff, J. A., Avens, L., and Kurle, C. M. (2016). Methods for sampling sequential annual bone growth layers for stable isotope analysis. *Methods Ecol. Evol.* 7, 556–564. doi: 10.1111/2041-210X.12522

Turner Tomaszewicz, C. N., Seminoff, J. A., Avens, L. A., Goshe, L. R., Rodriguez-Baron, J. M., Peckham, S. H., et al. (2018). Expanding the coastal forager paradigm: Long-term pelagic habitat use by green turtles (*Chelonia mydas*) in the eastern Pacific Ocean. *Mar. Ecol. Prog. Ser.* 587, 217–234. doi: 10.3354/meps12372

Turner Tomaszewicz, C. N., Seminoff, J. A., Ramirez, M. D., and Kurle, C. M. (2015b). Effects of demineralization on the stable isotope analysis of bone samples. *Rapid Commu. Mass Spectrom.* 29, 1879–1888. doi: 10.1002/rcm.7295

Turner Tomaszewicz, C. N., Seminoff, J. A., Peckham, S. H., Avens, L., Goshe, L., Bickerman, K., et al. (2015a). Age and residency duration of loggerhead turtles at a North Pacific bycatch hotspot using skeletochronology. *Biol. Conserv.* 186, 134–142. doi: 10.1016/j.biocon.2015.03.015

Turner Tomaszewicz, C. N., Seminoff, J. A., Peckham, S. H., Avens, L., and Kurle, C. M. (2017a). Intrapopulation variability in the timing of ontogenetic habitat shifts in sea turtles revealed using δ15N values from bone growth rings. *J. Anim. Ecol.* 86, 694–704. doi: 10.1111/1365-2656.12618

Turner Tomaszewicz, C. N., Seminoff, J. A., Price, M., and Kurle, C. M. (2017b). Stable isotope discrimination factors and between-tissue isotope comparisons for bone and skin from captive and wild green sea turtles (*Chelonia mydas*). *Rapid Commun. Mass Spectrom.* 231, 1903–1914. doi: 10.1002/rcm.7974

Vander Zanden, H. B., Tucker, A. D., Hart, K. M., Lamont, M. M., Fujisaki, I., Addison, D. S., et al. (2015). Determining foraging area origin in a migratory marine vertebrate by integrating stable isotope analysis and satellite tracking: a novel approach. *Ecol. Appl.* 25, 320–335. doi: 10.1890/14-0581.1

Vásquez, M., and Liles, M. J. (2008). "Estado actual de las tortugas marinas en El Salvador, con énfasis en la tortuga carey," in *Proceedings of the XII Congreso de la Sociedad Mesoamericana para la Biología y la Conservación*, San Salvador.

Wallace, B. P., Seminoff, J. A., Kilham, S. S., Spotila, J. R., and Dutton, P. H. (2006). Leatherback turtles as oceanographic indicators: Stable isotope analyses reveal a trophic dichotomy between ocean basins. *Mar. Biol.* 149, 953–960. doi: 10.1007/s00227-006-0247-y

Wedemeyer-Strombel, K. R., Seminoff, J. A., Liles, M. J., Sánchez, R. N., Chavarría, S., Valle, M., et al. (2021). Fishers' ecological knowledge and stable isotope analysis reveal mangrove estuaries as key developmental habitats for critically endangered sea turtles. *Front. Conserv. Sci.* 2:796868. doi: 10.3389/fcosc.2021.796868

West, J. B., Bowen, G. J., Cerling, T. E., and Ehleringer, J. R. (2006). Stable isotopes as one of nature's ecological recorders. *Trends Ecol. Evol.* 21, 408–414. doi: 10.1016/j.tree.2006.04.002

Wood, S. N. (2017). *Generalized Additive Models: An Introduction With R, Generalized Additive Models: An Introduction with R*, 2nd Edn. (Boca Raton, FL: CRC Press), doi: 10.1201/9781315370279

Zug, G. R., Wynn, A. H., and Ruckdeschel, C. (1986). Age determination of loggerhead sea turtles, *Caretta caretta*, by incremental growth marks in the Skeleton. *Smithson. Contrib. to Zool.* 427, 1–34. doi: 10.5479/si.00810282.427

frontiers | Frontiers in Ecology and Evolution

TYPE Original Research
PUBLISHED 25 August 2022
DOI 10.3389/fevo.2022.956819

Check for updates

OPEN ACCESS

EDITED BY
Rona A. R. McGill,
University of Glasgow, United Kingdom

REVIEWED BY
Mojmir Vasek,
Biology Centre of the Czech Academy of Sciences, Czechia
Jonathan Cole,
Cary Institute of Ecosystem Studies, United States

*CORRESPONDENCE
Jotaro Urabe
urabe@tohoku.ac.jp

†PRESENT ADDRESSES
Takehiro Kazama,
Graduate School of Human Development and Environment, Kobe University, Kobe, Japan

Masato Yamamichi,
School of Biological Sciences, The University of Queensland, Brisbane, QLD, Australia

SPECIALTY SECTION
This article was submitted to Population, Community, and Ecosystem Dynamics, a section of the journal Frontiers in Ecology and Evolution

RECEIVED 30 May 2022
ACCEPTED 25 July 2022
PUBLISHED 25 August 2022

CITATION
Hirama F, Urabe J, Doi H, Kazama T, Noguchi T, Tappenbeck TH, Katano I, Yamamichi M, Yoshida T and Elser JJ (2022) Terrigenous subsidies in lakes support zooplankton production mainly *via* a green food chain and not the brown food chain.
Front. Ecol. Evol. 10:956819.
doi: 10.3389/fevo.2022.956819

COPYRIGHT
© 2022 Hirama, Urabe, Doi, Kazama, Noguchi, Tappenbeck, Katano, Yamamichi, Yoshida and Elser. This is an open-access article distributed under the terms of the Creative Commons Attribution License (CC BY). The use, distribution or reproduction in other forums is permitted, provided the original author(s) and the copyright owner(s) are credited and that the original publication in this journal is cited, in accordance with accepted academic practice. No use, distribution or reproduction is permitted which does not comply with these terms.

Terrigenous subsidies in lakes support zooplankton production mainly *via* a green food chain and not the brown food chain

Fumiya Hirama[1], Jotaro Urabe[1]*, Hideyuki Doi[2], Takehiro Kazama[1†], Takumi Noguchi[1], Tyler H. Tappenbeck[3], Izumi Katano[4,5], Masato Yamamichi[6†], Takehito Yoshida[6,7] and James J. Elser[3]

[1]Aquatic Ecology Laboratory, Graduate School of Life Sciences, Tohoku University, Sendai, Japan, [2]Graduate School of Simulation Studies, University of Hyogo, Kobe, Japan, [3]Flathead Lake Biological Station, University of Montana, Polson, MT, United States, [4]Graduate School of Humanities and Sciences, Nara Women's University, Nara, Japan, [5]KYOUSEI Science Center for Life and Nature, Nara Women's University, Nara, Japan, [6]Department of General Systems Studies, University of Tokyo, Tokyo, Japan, [7]Research Institute for Humanity and Nature, Kyoto, Japan

Terrestrial organic matter (t-OM) has been recognized as an important cross-boundary subsidy to aquatic ecosystems. However, recent evidence has shown that t-OM contributes little to promote secondary production in lakes because it is a low-quality food for aquatic consumers. To resolve this conflict, we performed a field experiment using leaf litter as t-OM. In the experiment, we monitored zooplankton biomass in enclosures with and without addition of leaf litter under shaded and unshaded conditions and assessed food web changes with stable isotope analyses. We then examined whether or not leaf litter indeed stimulates lake secondary production and, if it does, which food chain, the detritus-originated food chain ("brown" food chain) or the algae-originated food chain ("green" food chain), contributes more to this increase. Analyses with stable isotopes showed the importance of t-OM in supporting secondary production under ambient lake conditions. However, the addition of the leaf litter increased the zooplankton biomass under unshaded conditions but not under shaded conditions. We found that phosphorus was leached from leaf litter at much faster rate than organic carbon and nitrogen despite its low content in the leaf litter. These results showed that leaf litter stimulated the increase in zooplankton biomass mainly through the green food chain rather than the brown food chain because the leaf litter supplied limiting nutrients (i.e., phosphorus) for primary producers.Our results indicate that the functional stoichiometry of the subsidized organic

matter plays a crucial role in determining the relative importance of brown and green food chains in promoting production at higher trophic levels in recipient ecosystems.

KEYWORDS

ecological stoichiometry, lake ecosystems, leaf litter, phosphorus, stable isotope analysis, terrestrial subsidy, secondary production

Introduction

Ecosystems are not necessarily isolated from each other, and the food webs therein are often sustained by subsidies of energy and organic matter transferred from adjacent ecosystems (Lindeman, 1942; Polis et al., 1997; Nakano and Murakami, 2001). An example of such subsidies across an ecosystem boundary is terrestrial organic matter (t-OM) that enters into food webs in rivers and lakes (Gasith and Hosler, 1976; Doucett et al., 2007; Cole et al., 2011; Carpenter et al., 2016; Brett et al., 2017). Several studies reported that t-OM is an important energy source for sustaining production at higher trophic levels in lakes (Doucett et al., 2007; Cole et al., 2011; Cole, 2013; Tanentzap et al., 2017). Although the role of t-OM in supporting the production of higher trophic levels in aquatic ecosystems is well-recognized (Carpenter et al., 2016), some studies have questioned the generality and magnitude of this impact on lake ecosystems (Brett et al., 2009; Kelly et al., 2014; Taipale et al., 2014). For example, recent studies showed that the growth rate of zooplankton decreased with an increasing proportion of t-OM relative to phytoplankton in the diets because t-OM is a poor-quality resource for aquatic consumers (Brett et al., 2009; Taipale et al., 2014). In addition, increased dissolved organic carbon (DOC), the dissolved fraction of t-OM, reduces light penetration into waters and thus reduces algal production (Ask et al., 2009; Karlsson et al., 2015). These studies suggest that a positive impact of t-OM on secondary production in lakes may not be a general phenomenon, since the input of t-OM does not necessarily promote zooplankton production in lakes (Carpenter et al., 2016; Brett et al., 2017).

However, some studies have shown that the input of leaf litter, a major component of t-OM, increased zooplankton production (Cottingham and Narayan, 2013; Fey et al., 2015). As a source of carbon and energy, t-OM is consumed by bacteria that in turn are consumed by protozoans such as heterotrophic nanoflagellates (HNF) that are edible food for most zooplankton (Tranvik, 1992; Jansson et al., 2007). This material pathway is often referred to as the brown food chain (Wolkovich et al., 2014) since the chain transfers organic carbon originating from terrigenous organic carbon to higher trophic levels. During this process, consumption of bacteria by HNF may mineralize nitrogen (N) and phosphorus (P) within t-OM to inorganic forms that are available to algae (Bloem et al., 1989). More importantly, leaching rates of P from the leaf litter are often higher than those of C and N (Baldwin, 1999; Schreeg et al., 2013), suggesting that t-OM directly supplies growth-limiting P for phytoplankton production. If this were the case, t-OM would support production at higher trophic levels through the "green food chain" that originates from organic carbon fixed by primary producers. Thus, the input of t-OM can promote zooplankton production through (1) material transfer along with the food chains originating from the organic carbon in the t-OM (brown food chain) and (2) material transfer along with the food chains originating from phytoplankton whose production is promoted by nutrients released from t-OM (green food chain). However, no study has yet examined the relative importance of brown and green food chains in mediating the impact of t-OM on zooplankton production.

Therefore, in this study, we examined (1) whether or not t-OM indeed stimulates production at higher trophic levels, and, if that were the case, (2) which food chain, brown or green, contributed more in increasing zooplankton production. We focused on zooplankton as secondary producers since they prey not only on phytoplankton but also on bacteria and heterotrophic protozoans (Adrian et al., 2001; Yoshida et al., 2001; Wolkovich et al., 2014) and are consumed by carnivores such as fish (McQueen et al., 1989; Carpenter and Kitchell, 1996), which integrates the brown and green food chains in lake ecosystems. We performed a field experiment using enclosures to manipulate the supply of t-OM and the rate of primary production and analyzed food sources of zooplankton with stable isotopes. We used mechanically ground leaf litter as a t-OM source since leaf litter is a quantitatively important terrestrial subsidy to many aquatic ecosystems (Gasith and Hosler, 1976; Rau, 1976; Hanlon, 1981; Wallace et al., 1997). We manipulated primary production by shading the enclosures to reduce the penetration of sunlight.

Materials and methods

Terrestrial organic matter

Fallen leaves and needles used in this study were composed mainly of Paper Birch (*Betula papyrifera*), Black Cottonwood

(*Populus balsamifera*), and Ponderosa Pine trees (*Pinus ponderosa*) with some of the other taxa, and collected in a forest at the Flathead Lake Biological Station (FLBS), University of Montana, (Montana, United States), in November 2016. These leaves were dried and stored in plastic bags at room temperature for 7 months until the performance of the experiment. To physically promote the decomposition process of t-OM, 3 kg of these leaves were chopped using a large hand immersion blender and mixed in 100 L of distilled water and then stirred for 3 days in a room held at ∼20°C. After 3 days, the mixed leaf water was filtered sequentially through 3-mm mesh to a final 35-μm mesh and stored overnight at room temperature. Hereafter, this t-OM mixture is denoted as leaf homogenate. Before its use in the experiment, the leaf homogenate was subsampled to determine concentrations of total phosphorus (P), total nitrogen (N), and organic carbon (C).

Enclosures

The field experiment was conducted from 12 June 2017 to 14 August 2017 in Lost Lake located within the Flathead Valley of western Montana, United States (47.6729685 N, −114.066614 W). Lost Lake lies just east of the Mission Mountain Range at an elevation of 938 m. The lake's maximum depth is 11 m with a surface area of 3 hectares. Four days before initiating the experiment, we installed 12 enclosures with 1-m diameter and 2-m depth that consisted of clear polyethylene tubes with closed bottoms (**Figure 1A**). We enveloped six out of 12 enclosures with black shade cloth to reduce the penetration of sunlight to 10% of ambient level (D: shaded treatment). The rest of enclosures were left unwrapped (L: unshaded treatment). Each enclosure was fixed to a floating deck anchored at the center of the lake: positions of the enclosures with different treatments at the deck were randomly assigned. Then, the enclosures were filled with 1,000 L of lake water, which was collected from a depth of 1–2 m, and passed through 100-μm plankton net to remove the large zooplankton species. On the following day, we collected zooplankton from Lost Lake by vertically towing a 100-μm mesh plankton net and added live zooplankton equivalent to 1,000 L in abundance to each enclosure. In addition, 200 individuals of *Daphnia pulicaria* collected at a nearby lake were added to each of the enclosures, as large zooplankton typical of small lakes in Montana were not abundant in Lost Lake when the experiment was initiated. Since animals contained in the shallow 2-m enclosures were unable to migrate to a deep depth and thus faced potentially harmful ultraviolet (UV) exposure, each enclosure was then covered by a Plexiglas plate to reduce UV exposure. On 12 June 2017, we initiated the enclosure experiment by adding 10 L of the leaf homogenate to a half of the unshaded and shaded enclosures, resulting in a total of four treatments each with three replicates; LA: unshaded with leaf homogenate, LB: unshaded without leaf homogenate, DA: shaded with leaf homogenate, and DB: shaded without leaf homogenate. During the experimental period, we added an additional 5 L of the leaf homogenate to enclosures with LA and DA treatments on both 3 July and 24 July 2017 using fresh leaf homogenate prepared as above.

Sampling and *in situ* measurements

We sampled water and plankton in each enclosure weekly from 12 June to 14 August. Before the sampling, we measured water temperature (°C), pH, and dissolved oxygen (mg O_2/L) using a multiprobe sonde (Hydrolab® MS5, OTT HydroMet, CO., United States). Then, enclosures were gently mixed by raising and lowering a PVC disk (60 cm in diameter) several times. We then sampled 2 L of the water from the bottom to the surface using an integrated water column sampler to obtain samples for chemistry, chlorophyll *a*, microbes (bacteria and flagellates), and microzooplankton (ciliates, amoebas, rotifers, and small crustaceans such as copepod nauplii) and 13 L of water for examining mesozooplankton (cladocerans and copepods). The mesozooplankton samples were concentrated by passing the 13 L of water through a 100-μm mesh net and were then placed in sample jars. Screened water was returned to the enclosure.

We also routinely measured concentrations of pCO_2 at the surface of the enclosures using a bottle head space method 3 days after the sampling. For measuring pCO_2, we collected the surface water from each of the enclosures with two sets of 1.1-L High-Density Polyethylene (HDPE) Nalgene® bottles. We made a headspace by putting 50 mL of ambient air into each bottle using a syringe and then shook the bottle for at least 3 min by hand to equilibrate the CO_2 between air and water. The air in the headspace was then collected by a syringe and used to measure CO_2 with a portable infrared gas analyzer (EGM-4, PP Systems, MA, United States). After the measurement of pCO_2, we homogenized the enclosures as above.

Chemical analyses

The leaf homogenate was subsampled prior to being used in the experiment and subsamples were concentrated onto GF/F filters. Filters were analyzed for seston particulate phosphorus (P), nitrogen (N), and organic carbon (C) concentrations. Water samples from the enclosures were also filtered onto the GF/F filters for chemical and chlorophyll *a* analyses. The filtrates of the leaf homogenate and the enclosure water samples were used for measuring dissolved P, dissolved N, and dissolved organic C concentrations. When zooplankton became abundant after 3 weeks (3 July 2017), the water samples were passed through a 100-μm mesh net to eliminate mesozooplankton and used for analyses. In addition, we occasionally concentrated water

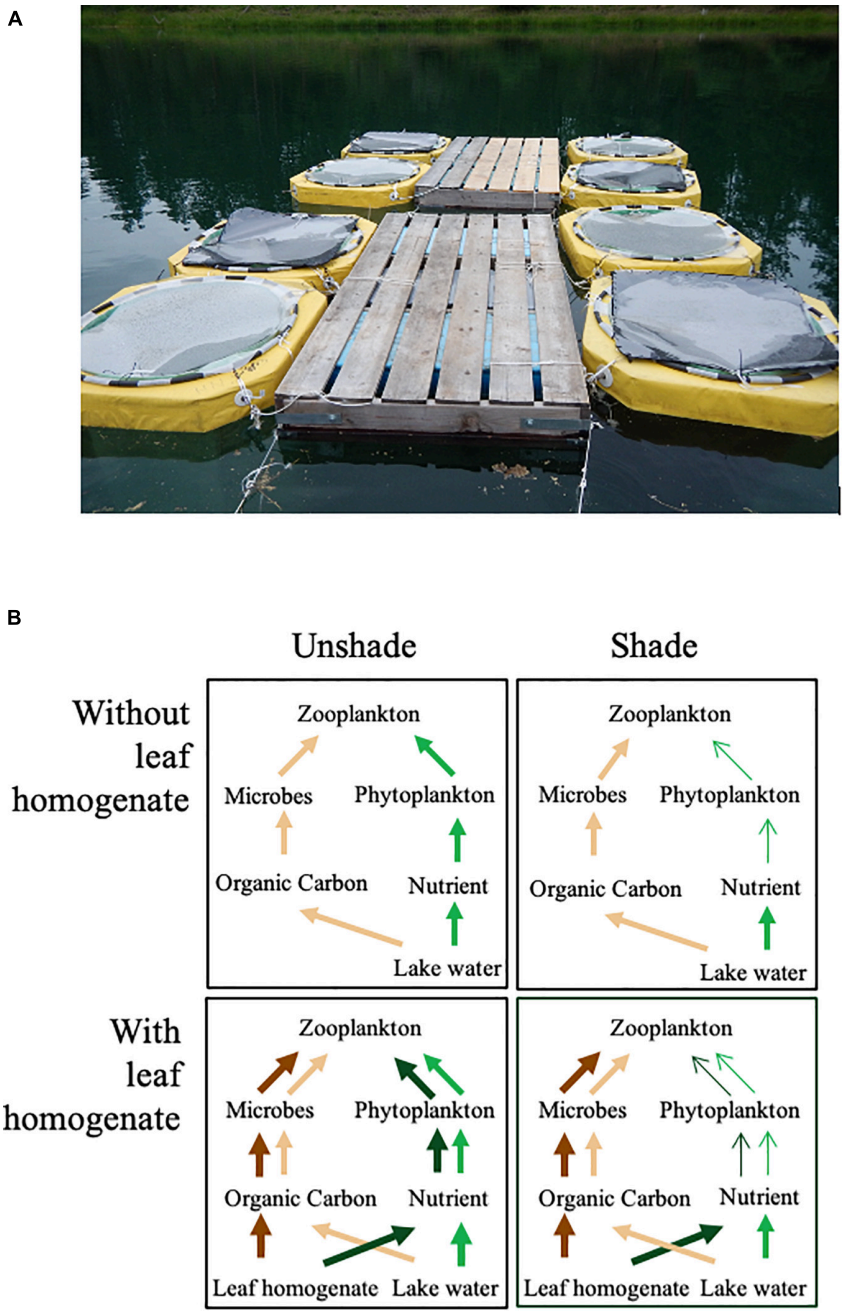

FIGURE 1
(A) Photo showing enclosures used in the experiment. **(B)** Schemes showing the contribution of brown and green food chains for mass transfer to zooplankton under shaded and unshaded conditions with and without leaf homogenate. Light green arrows represent the effect of ambient nutrients on the green food chain (G_{Base}), light brown arrows represent the effect of ambient organic matter on the brown food chain (B_{Base}), dark green arrows represent the effect of leaf homogenate on the green food chain (G_{Add}), and dark brown arrows represent the effects of leaf homogenate on the brown food chain (B_{Add}).

samples passed through a 30-μm mesh net onto the GF/F filters for measuring chlorophyll *a* concentration of small algae. Filters for chlorophyll *a* analysis were stored at −20°C and those for sestonic C, N, and P were dried at 60°C for 48 h and stored in a desiccator. Filtrates for measuring dissolved N, P, and organic C concentrations were stored at −20°C until analysis.

Chlorophyll *a* was measured using a fluorometer. Filters for seston C and N were measured using a carbon, hydrogen, and nitrogen (CHN) analyzer (Perkin Elmer 2400 series II; Perkin Elmer Inc., MA, United States). Seston P was measured using a spectrophotometer according to molybdenum blue method after digesting the filter samples with potassium persulfate at

121°C for 30 min. Dissolved N and dissolved organic C were measured using a total organic carbon and nitrogen analyzer (multi N/C 3100; Analytik Jena AG, Jana, Germany). Dissolved P was measured using the same method as seston P. We also measured organic C, total N, and total P contents of fallen leaves and leaf homogenate as above.

Enumeration of plankton

Samples for mesozooplankton were fixed with ethanol immediately after collection and preserved in 99% ethanol. Samples for bacteria and HNF were fixed with glutaraldehyde (1% final concentration) and stored at 4 °C in the dark. For examining microzooplankton, 500 ml of sample water was fixed with a Lugol's solution (5% final concentration), and all organisms in the sample were concentrated down to 50 ml by gravity. Bacteria and HNF were quantitatively counted under an epifluorescence microscope at 1,000 × magnification. Mesozooplankton (cladocerans and copepods) and microzooplankton (rotifers, ciliates, and amoebas) were enumerated according to genus or finest taxonomic level under microscopes at 25–400 × magnification with the measurements of their body or cell sizes. The biomasses of these plankters were estimated with the appropriate conversion factors based on the body sizes. Details of these methods are described in **Supplementary Methods**.

Stable isotope analyses

In addition to the weekly sampling described, we sampled mesozooplankton for isotopic analysis on 3 and 17 August by vertical tows of 100-μm plankton net from the bottom to the surface of the enclosures. We also sampled water from the bottom to the surface of the enclosures using an integrating water column sampler. Particulate organic matter (POM) in the enclosures was concentrated onto GF/F filters by filtering an aliquot of the water samples. For measuring δ^2H of the water, 100-mL of surface water was collected from the enclosures using a plastic bottle.

We taxonomically sorted the dominant cladocerans and copepods, and then 10–100 individuals of each taxon were placed in tin cups for carbon isotope analysis and in a silver cup for hydrogen isotope analysis. We also collected filamentous algae (mainly Zygnematophyceae) that were found in the mesozooplankton samples and placed these in cups. These were used as green food sources. The tin and silver cups with zooplankton and algae were dried at 60°C for 48 h and stored in desiccators until isotope analysis. Samples of POM were obtained by filtering 500 ml of surface lake water onto Whatman GF/F glass fiber filters (pre-combusted at 530 °C for 2 h). For brown food sources, we analyzed mixed leaves and needles that were used in making the leaf homogenate as well as five leaves from Poaceae plants surrounding the lake. The leaf samples were grounded by a homogenizer. The filters and well-mixed leaf samples were placed both in tin and silver cups.

The C isotope ratios of the samples were measured using a continuous-flow isotope mass spectrometer (Thermo Delta V Advantage, Thermo Fisher, MA, United States) interfaced with an elemental analyzer (NC2500, CE Instruments, Wigan, England) in the Cornell University Stable Isotope Laboratory (COIL). We expressed δ^{13}C values using notation relative to Vienna Pee Dee Belemnite. The precision of δ^{13}C values estimated by several internal organic standards was $< \pm 0.5$ (/‰). We also analyzed samples for δ^2H using a Thermo Delta V isotope mass spectrometer interfaced with a Temperature Conversion Elemental Analyzer (TC/EA, Thermo Fisher). The δ^2H of water samples were analyzed by a GasBench II (Thermo Fisher) connected to a DELTA V (Thermo Fisher), which offered precision comparable to dual-inlet methods for H_2 and CO_2 water equilibration. In this analysis, non-exchangeable δ^2H values were equilibrated for isotope exchange and normalized using the same procedure and standards as those in the previous studies (Wassenaar and Hobson, 2003; Doucett et al., 2007). All δ^2H values are expressed as ordinal notation relative to the international standard, Vienna Standard Mean Ocean Water (VSMOW). All isotope analyses were performed by COIL.

Statistical analyses

We analyzed the initial difference in organic carbon and nutrient levels among enclosures with and without leaf homogenate using *t*-tests. For the main data, we performed a generalized linear mixed model (GLMM) to examine the effects of the leaf homogenate and light manipulation on water chemistry and biomass values of plankton consumers. In this analysis, we excluded data of the first three sampling dates to remove effects of initial conditions commonly among the enclosures and used data obtained from 3 July to 14 August. In the GLMM, the addition of leaf homogenate, light manipulation, and their interactions was set as fixed factors, and sampling date and enclosure were used as random factors. Before the analysis, chlorophyll *a* concentration, cell abundances of HNF and bacteria, and biomasses of zooplankters were log (n+1) transformed. The significance of the fixed effects was determined by type II ANOVA with *F*-tests of Kenward-Roger approximation. The analysis was done using "lmer" function of the "lme4" package and "car" function of the "car" package in R 3.4.0 (R Core Team, 2016).

We estimated the average biomass of zooplankton during the period from 3 July to 14 August for each treatment (ZB_{DB}, ZB_{LB}, ZB_{DA}, and ZB_{LA}). Then, by assuming that mass flow along with the brown food chain was not affected by light

condition, the contributions of the brown and green food chains to zooplankton production were separated as follows:

$$B_{Base} = ZB_{DB} \quad (1a)$$

$$G_{Base} = ZB_{LB} - ZB_{DB} \quad (1b)$$

$$B_{Add} = ZB_{DA} - ZB_{DB} \quad (1c)$$

$$G_{Add} = ZB_{LA} - ZB_{DA} - ZB_{LB} + ZB_{DB} \quad (1d)$$

where B_{Base} and G_{Base} are the fractions of zooplankton biomass produced by ambient organic matter and nutrients through brown and green chains, respectively, and B_{Add} and G_{Add} are the fractions of zooplankton biomass promoted by the addition of leaf homogenate through brown and green food chains, respectively (**Figure 1B**).

The statistical significance of differences among B_{Add}, G_{Add}, B_{Base}, and G_{Base} was assessed by comparing the 95% confidence limits that were estimated with a bootstrap method. In this study, we had four treatments with three replications (a total of 12 enclosures). Therefore, we randomly selected zooplankton biomass data in three enclosures from the 12 enclosers and assigned these for each treatment with repetition. Then, we estimated the average biomass for treatment (ZB_{DB}, ZB_{LB}, ZB_{DA}, and ZB_{LA}) and calculated values in Equations (1a–d). We repeated this procedure 999 times, estimated upper and lower 2.5% values for the 999 resampling values plus the original value and used these as a 95% confidence interval. If the 95% confidence intervals of a given contribution did not overlap with that of another contribution, we concluded that these contributions differed from each other. All analyses were performed in R 3.4.0 (R Core Team, 2016).

We also estimated the contributions of brown and green sources to zooplankton production using a Bayesian stable isotope mixing model, "MixSIAR" ver. 3.1.10 package (Stock et al., 2018) with JAGS ver. 4.3.0 connected with "rjags" package ver. 4–8 in R 3.4.0 (R Core Team, 2016). The "MixSIAR" model is a Bayesian stable isotope mixing model with unifying multiple error structures, including isotopes of consumers and sources, trophic enrichment of consumers. The model equations and details are in Stock et al. (2018). Before developing the mixing model, we bi-plotted the stable isotope values of all the samples (**Supplementary Figure 1**) to check that those consumers fell within the proper mixing polygon considering the trophic discrimination and food resources. Then, we excluded some outlier data (n = 7) from the polygon in the ensuing mixing model analysis. To confirm the validity of the result, we also analyzed with all of the data. In this analysis, we used filamentous algae and the leaf litter that was used for leaf homogenate as the potential food sources of autochthonous (green) and allochthonous origin (brown), respectively. We estimated the contribution of those two sources to the food that zooplankton assimilated. We assumed that the carbon and hydrogen isotope values of filamentous algae were the same for edible and filamentous algae as suggested by the previous studies (France, 1995; Hondula et al., 2014; Grosbois et al., 2017). In this analysis, we did not include POM since its stable isotope values were found between those of the algae and the leaf homogenate that themselves were similar to the values of leaf litter collected around the lake (**Supplementary Figure 1**).

Conventional trophic enrichment factors were used for zooplankton; +0.5 for $\delta^{13}C$ (Post, 1997), and ± 0.0 for $\delta^{2}H$ with 1.3 standard deviation in all the values (Post, 1997). We performed the mixing model of $\delta^{2}H$; $\delta^{2}H_{consumer} = [(1-\omega_{compound}) \times \delta^{2}H \text{ diet}] + (\omega_{compound} \times \delta^{2}H_{water})$ with surface water values ($\delta^{2}H_{water}$ = -119.4 ± 3.6, mean ± *SD*, N = 24). Although the environmental water correction for the consumer ($\omega_{compound}$) is known to vary depending on consumers (Wilkinson et al., 2015), Solomon et al. (2009) showed that it was around 0.20 ± 0.04 (mean ± SD) for zooplankton in freshwater systems. We used this value for $\omega_{compound}$ in our analysis. We did not use $\delta^{15}N$ values in the analysis because the trophic levels of zooplankton taxa feeding on both brown and green foods were uncertain.

We ran the model with Markov chain Monte Carlo (MCMC) parameters that were set for "short" runs as defined in MixSIAR (Chain length = 50,000, Burn-in = 25,000, thin = 25, number of MCMC chains = 3) and evaluated the degree of convergence by the Gelman–Rubin test. We also assessed the correlations of posterior values for each final model to determine its ability to isolate contributions from different food sources–strong negative correlations between diets in close proximity in isotopic space indicate problems. We set the threshold correlation coefficient value, for a "strong" correlation at 0.7. We tested the appropriateness of the mixing model using two fictitious discrimination-corrected consumers with 100% of brown (allochthonous) and green (autochthonous) resource uses (Brett, 2014) and confirmed that the model output could provide reasonable resource contributions with ± SD = 0.103 (100% of allochthonous: allochthonous = 0.814 ± 0.130, 100% of autochthonous: autochthonous = 0.761 ± 0.103).

Results

Elemental contents of leaf homogenate

Total organic carbon content (TOC, as percent of dry mass) of the fallen leaves themselves was 35 and 300 times higher than total nitrogen (TN) and total phosphorus contents (TP), respectively (**Table 1**). Elemental analyses showed that TOC relative to TN and TP in the leaf homogenate was much lower than in the fallen leaves, indicating that leaching rates from the

TABLE 1 Mean and standard deviation (*SD*) of total organic carbon, total nitrogen, and total phosphorus contents of leaf litter (fallen leaves) and leaf homogenate used in the experiment, and concentrations of these elements in enclosures at the beginning of experiment.

	t-OM		Enclosures	
Element	**Leaf litters (mg/g dry leaf)**	**Leaf homogenate (mg/g dry leaf)**	**Without leaf homogenate (mg/L ± *SD*)**	**With leaf homogenate (mg/L ± *SD*)**
Organic carbon	410.08 ± 2.03	34.24 ± 0.19 (19.78 ± 0.53)	3.15 ± 0.10 (2.50 ± 0.04)	12.71 ± 1.391 (8.05 ± 1.20)
Total nitrogen	11.37 ± 1.37	1.37 ± 0.01 (0.46 ± 0.03)	0.24 ± 0.026 (9.13 ± 0.01)	0.66 ± 0.056 (0.22 ± 0.01)
Total phosphorous	1.332 ± 0.125	0.827 ± 0.042 (0.691 ± 0.001)	0.017 ± 0.003 (0.007 ± 0.002)	0.240 ± 0.040 (0.194 ± 0.041)

Concentrations of dissolved form are shown in parenthesis. Concentrations of organic C, total N, and total P in the enclosure without leaf homogenate correspond to those in lake water at the start of experiment.

fallen leaves differed among the three elements. Our calculations indicated that 60% of P in the fallen leaves was leached into the leaf homogenate, but only 10% of N and organic C in the fallen leaves was leached (Table 1). In addition, in the leaf homogenate, 83% of P in the leaf homogenate was in the dissolved fraction, whereas 58 and 30% in C and N were in dissolved form, respectively.

Effect of the manipulations on environmental conditions

Water samples collected just after the addition of the leaf homogenate showed that the concentrations of TOC and TN were significantly increased by three to four times in enclosures with the leaf homogenate compared with those without it (Table 1; $p < 0.001$, Supplementary Table 1 and Supplementary Figures 2A,B). Addition of the leaf homogenate also significantly elevated the concentration of TP by 10-fold (Table 1; $p < 0.001$, Supplementary Table 1 and Supplementary Figure 2C). The concentrations of these elements also tended to increase after the second and third additions of the leaf homogenate in the LA and DA treatments (Supplementary Figure 2).

In enclosures with leaf homogenate (LA and DA), seston C, N, and P concentrations varied temporally and reached high levels during the last half of the experimental period (Supplementary Figures 2D–F). In enclosures without leaf homogenate (LB and DB), however, seston C, N, and P concentrations were stable at low levels. Accordingly, seston C, N, and P concentrations were, on average, significantly different between enclosures with and without leaf homogenate ($p < 0.001$, Supplementary Table 2) but were not affected by light conditions ($p > 0.1$, Supplementary Table 2). Seston C: N ratio tended to increase in all the treatments (Figure 2B), but this trend was not statistically significant among the treatments ($p > 0.05$, Supplementary Table 2). Seston C: P ratio temporally varied depending on treatments (Figure 2A). In both the LA and DA treatments, the C: P ratio gradually decreased and was stabilized at a level < 200 (atomic). Seston C: P ratio was significantly higher in enclosures without leaf homogenate than in enclosure with leaf homogenate ($p < 0.01$, Supplementary Table 2) and was often > 300 especially in the LB treatment (Figure 2A), although no significant difference was detected between the unshaded and shaded treatments ($p > 0.1$, Supplementary Table 2).

During the experiment, water temperature varied from 18°C in mid-June to 22°C in early August (Figure 2C) and was significantly higher in the unshaded enclosures with leaf homogenate ($p < 0.001$, Supplementary Table 1), although the difference was always less than 0.5°C. In enclosures with leaf homogenate, pCO_2 reached levels > 1,500 ppm at the beginning of the experiment (Figure 2D). However, while remaining at high levels throughout the experiment in the shaded treatment (DA), pCO_2 gradually decreased and stabilized at a low level in the unshaded treatment (LA). In enclosures without the leaf homogenate, pCO_2 was consistently and significantly lower than in enclosures with the homogenate ($p < 0.001$, Supplementary Table 2). In enclosures without leaf homogenate, dissolved oxygen (DO) concentration was temporally stable and similar between the unshaded (LB) and shaded enclosures (DB). In enclosures with leaf homogenate, DO concentration was ∼5 mg/L at the beginning of the experiment but gradually increased to a level > 8 mg/L (Supplementary Figure 2G). On average, DO was significantly lower in the shaded treatments than in the unshaded treatments ($p < 0.001$, Supplementary Table 1) but not affected by the addition of the leaf homogenate ($p > 0.05$).

Response of plankton to the manipulations

Chlorophyll *a* concentration varied over time (Figure 3A) and increased toward the end of the experiments, especially in enclosures with leaf homogenate (LA and DA). More than 60%

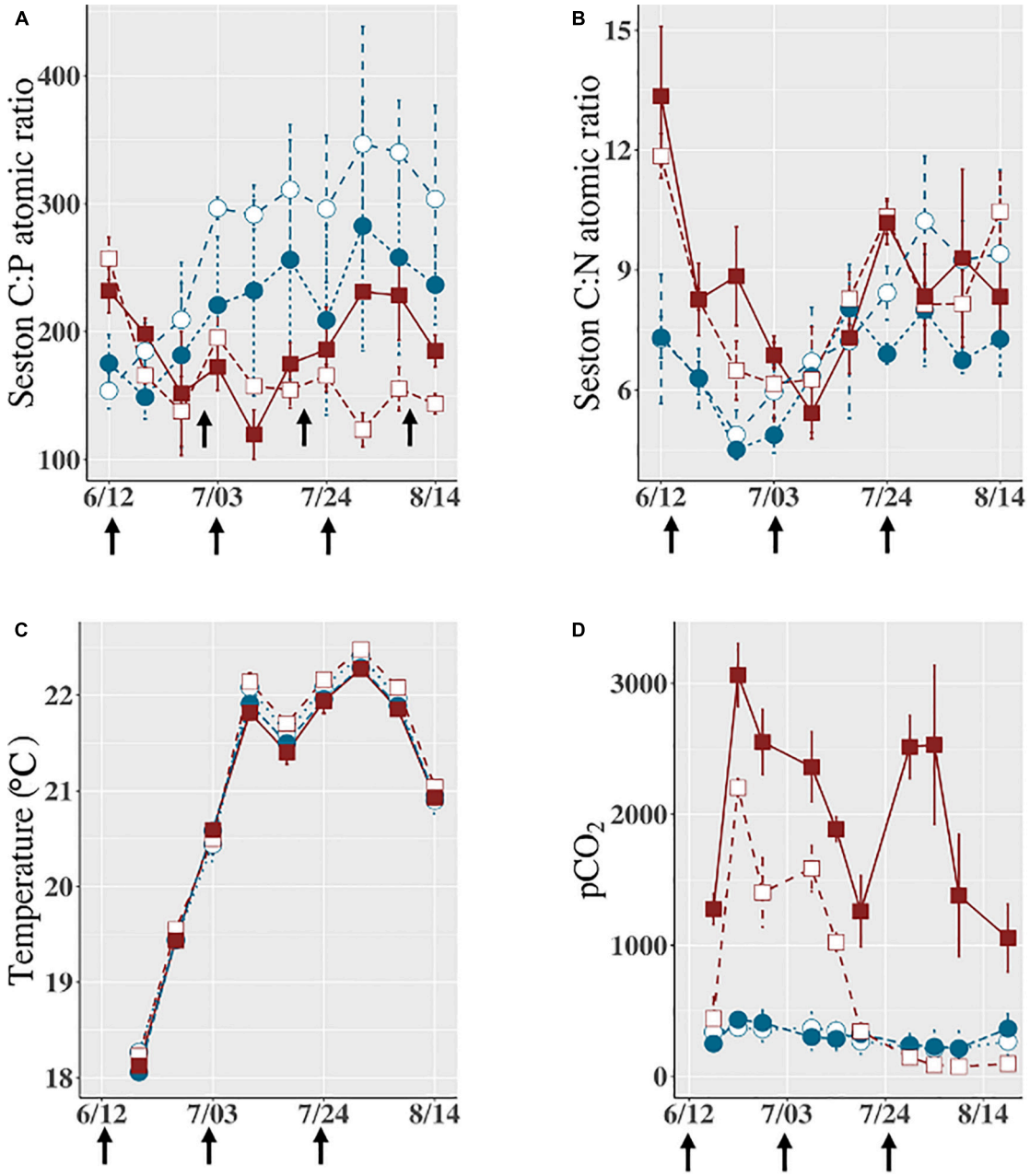

FIGURE 2
Changes in **(A)** Seston C: P atomic ratio, **(B)** seston C: N atomic ratio, **(C)** water temperature during the experiment from 12 June to 14 August 2017, and **(D)** pCO_2 that was measured beginning on 15th June. White squares indicate the LA treatment (unshaded, with leaf homogenate), brown squares indicate the DA treatment (shaded, with leaf homogenate), white circles indicate the LB treatment (unshaded, without leaf homogenate), and blue circles indicate the DB treatment (shaded, without leaf homogenate). Vertical bar on each data point indicates ± *SD* on the mean (3 replicates). The black arrows at the bottom of the graph are the dates when leaf homogenate was added to LA and DA treatments.

of chlorophyll *a* was smaller than 30 μm in all the enclosures except for the last 2 weeks when chlorophyll *a* concentration increased due to an increase in abundance of filamentous algae (**Supplementary Figure 3**). On average, chlorophyll *a* concentration was significantly higher in enclosures with leaf homogenate (LA and DA) than those without (LB and DB). However, chlorophyll *a* concentration was not affected by light conditions (**Supplementary Table 2**). Bacterial abundance increased when leaf homogenate was added but always decreased rapidly to a level similar to the enclosures without the homogenate (**Figure 3B**). On average, bacterial abundance did not differ among experimental treatments

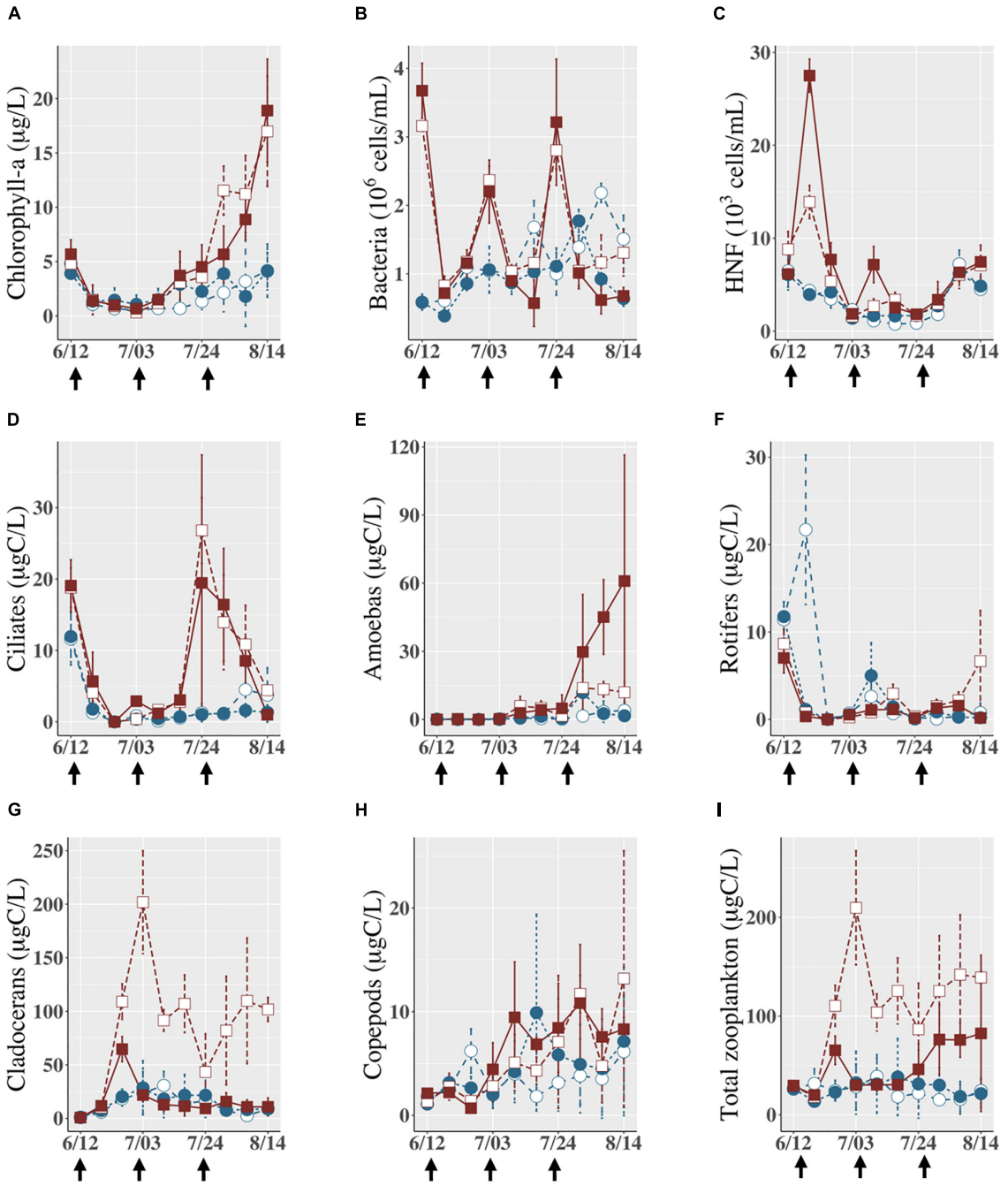

FIGURE 3
Abundances of **(A)** chlorophyll *a* (<100 µm), **(B)** bacteria, **(C)** HNF, and biomasses of **(D)** ciliates, **(E)** amoebas, **(F)** rotifers, **(G)** cladocerans, **(H)** copepods, and **(I)** sum of this zooplankton during the experiment. White squares indicate the LA treatment (unshaded, with leaf homogenate), brown squares indicate the DA treatment (shaded, with leaf homogenate), white circles indicate the LB treatment (unshaded, without leaf homogenate), and blue circles indicate the DB treatment (shaded, without leaf homogenate). Vertical bars on each data point indicate ± SD on the mean (3 replicates). The black arrows at the bottom of the graph are the dates when leaf homogenate was added to LA and DA treatments.

(Supplementary Table 2). The abundance of HNF was also not affected by light conditions but did vary over time and was higher in enclosures with leaf homogenate compared with those without (Figure 3C and Supplementary Table 2).

During the study period, a variety of zooplankton taxa were observed (Supplementary Tables 3–5). Among the enclosures, cladocerans were the most abundant taxa, followed by copepods (Supplementary Figure 4). Except for the

first several weeks, cladocerans were consistently abundant throughout the experiment in the LA treatment compared with other treatments, as evidenced by significant interaction effects of light and leaf homogenate on their abundance (Figure 3G and Supplementary Table 2). Copepod biomass was significantly higher in enclosures with leaf homogenate than in those without, regardless of light condition (Figure 3H and Supplementary Table 2). During the study period, rotifer biomass was low (Figure 3F) and did not differ among treatments (Supplementary Table 2). The biomass of ciliates and amoebas was significantly affected by the addition of leaf homogenate but not by light conditions (Supplementary Table 2). Ciliates increased their biomass from late-July to early-August in both the LA and DA treatments (Figure 3D), while the biomass of amoebas was especially high in late-August in the DA treatment (Figure 3E).

Although responses to the addition of leaf homogenate and light manipulation differed somewhat among taxonomic groups, as shown above, the sum of their biomass was significantly higher in enclosures with leaf homogenate compared with those without but was not consistently affected by light conditions (Supplementary Table 2). Reflecting the predominance of cladocerans in the zooplankton communities (Supplementary Figure 4), total zooplankton biomass (ZB: crustaceans, rotifers, and ciliated and amoeba protozoans) increased in the LA treatment and was consistently higher than those in other treatments (Figure 3I). Total zooplankton biomass in the DA treatment was similar to biomass in the LB and DB treatments in the first half of experimental period but gradually increased to a higher level in the last half of experiment, mainly to increased amoeba biomass. Total zooplankton biomass in the LB and DB treatments was stable at a low level throughout the experimental period.

Responses of brown and green food chains to manipulations

Using Equations (1a)–(1d), we estimated zooplankton biomass produced by brown food and green food chains (Figure 4). In enclosures without leaf homogenate, the contribution of zooplankton biomass produced by ambient nutrients and organic matter through green food chain (G_{Base}) was 0–25 μg C/L and, as evidenced by a large overlap of the 95% cl, did not significantly differ from the contribution generated through brown food chains (B_{Base}). The contribution of zooplankton biomass produced by the addition of leaf homogenate through the brown chain (B_{Add}) was similar to that produced by ambient nutrients and organic matter (G_{Base} and B_{Base}). However, the contribution to zooplankton biomass produced by the leaf homogenate through the green chain (G_{Add}) was as high as 90 μg C/L and its 95% cl did not overlap with other contributions, indicating that the addition of leaf homogenate significantly increased zooplankton production and that the role of the green food chain in supporting zooplankton production was 3–4 times larger than that of the brown food chain.

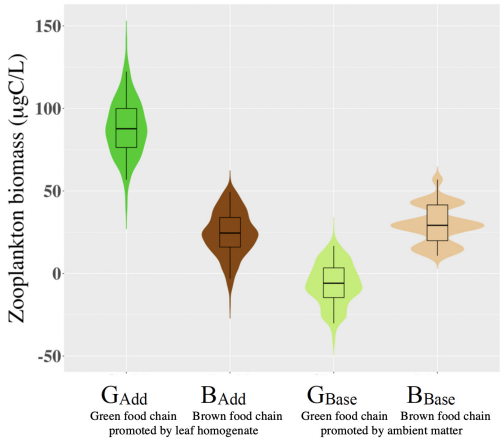

FIGURE 4
Contribution to zooplankton biomass by ambient organic matter and nutrients through the green chain (G_{Base}) and the brown food chain (B_{Base}) and those by leaf homogenate through green food chain (G_{Add}) and brown food chain (B_{Add}). Filled areas indicate the frequency of distributions of bootstrap data, boxplots represent the median and the first and third quantiles, and vertical bars are ± 95% CI on the mean.

Contribution of autochthonous food sources to zooplankton biomass

The relative contribution of autochthonous materials to food sources that zooplankton assimilated (estimated from stable isotope analyses, excluding data that were outside of the range polygon in the ensuing mixing model) varied from 20 to 80% depending on experimental treatment (Figure 5), but was similar in each treatment between 3 and 17 August. The relative contribution was only 20% in shaded enclosures with added t-OM (DA treatment) on average but was higher than 40% in other treatments (Figure 5). Using a GLMM analysis with ANOVA and Tukey post-hoc comparison tests, we confirmed that the relative contribution of the green food chain was significantly lower in the DA treatment and higher in the LA treatment when compared to the rest of treatments. In the LB and DB treatment, the mean autochthonous contribution ranged from 40 to 55%, indicating that half of the zooplankton biomass was produced by food derived from autochthonous materials. Almost the same results were obtained when we made the analysis with minimum (lower 2.5%) and maximum (upper 2.5%) contributions of autochthonous sources to zooplankton using all of the stable isotope data (Supplementary Figures 5, 6). We also assessed if the relative contribution of the green

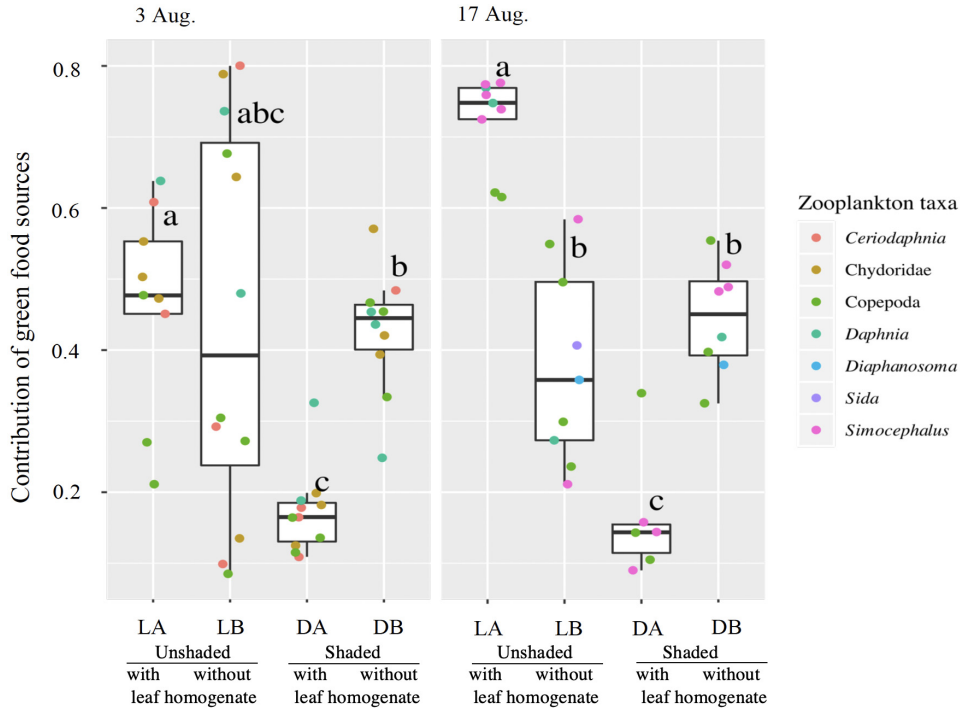

FIGURE 5
Contributions of autochthonous sources to zooplankton production. The bold line in the box indicates the median value. The upper and lower limits of the box, and the whisker plots indicate the first and third quartiles, and ± 1.5 × interquartile range, respectively. Significant differences among treatments are denoted by different letters. Points with different colors represent values for different zooplankton taxa.

food chain was significantly different among zooplankton taxa using GLMM (**Supplementary Table 6**). The result showed the contribution did not differ among the zooplankton taxa (GLMM, $p = 0.108$).

Discussion

Since the pioneering work by Lindeman (1942), a number of studies have examined the importance of t-OM in supporting the production of higher trophic levels in lake ecosystems (Gasith and Hosler, 1976; Tranvik, 1992; Doucett et al., 2007; Ask et al., 2009; Brett et al., 2009; Cole et al., 2011). However, an overall view of the contribution of t-OM to lake food webs has been elusive and even controversial (Doucett et al., 2007; Carpenter et al., 2016; Brett et al., 2017). Carpenter et al. (2016) stated that zooplankton biomass is limited even when allochthony (consumption and assimilation of allochthonous material) is high because allochthonous organic matter is low-quality food, while zooplankton biomass would show wide variations depending on P supply rate when allochthony is low. Our study showed that t-OM can be an important P source, implying that low allochthony does not mean that t-OM contributes less to zooplankton production. Indeed, this study clearly showed that t-OM promoted a 4- to 5-fold increase in zooplankton biomass under ambient light conditions by stimulating mass transfer through the green food chain.

In our experiment, bacterial density increased only during the period immediately after leaf homogenate was added on 12 June, 3 July, and 24 July (**Figure 3B**) and did not show significant differences among enclosures with and without leaf homogenate. However, abundances of HNF were significantly increased in enclosures with the leaf homogenate. This result suggests that, although bacteria likely consumed and respired the leaf homogenate, their biomass did not accumulate due to increased predation by bacterivores. Supporting this inference, pCO_2 at the surface was high in enclosures with leaf homogenate in the shaded treatments, indicating that leaf homogenate was respired and mineralized, and promoted mass transfer along with the brown food chain. However, even in the enclosures with leaf homogenate pCO_2 was much lower under the unshaded conditions relative to the shaded condition. These results indicate that much more CO_2 was consumed for photosynthesis by algae. Nonetheless, the abundance of chlorophyll *a* in these enclosures was similar between shaded and unshaded conditions. The results suggest that primary production in the unshaded enclosures was harvested for secondary production by the zooplankton. Indeed, zooplankton biomass increased in the unshaded enclosures with leaf homogenates.

According to the stable isotope analyses, half of the zooplankton biomass was produced directly or indirectly by allochthonous materials in the enclosures without leaf homogenate. The result indicates the importance of the terrigenous organic matter in sustaining the lake community and that the brown food chain plays a substantial role in supporting secondary production under ambient lake conditions (Doucett et al., 2007; Cole et al., 2011, Cole, 2013, Tanentzap et al., 2017). However, leaf homogenates did not increase the zooplankton biomass in the shaded enclosures, although they assimilated more materials from the brown food chain. These results imply that mass transfer along with the microbial chain extends less into zooplankton production. These findings confirm previous experimental studies that both terrigenously derived organic matter and heterotrophic microbes fueled by these are low-quality food for most herbivorous zooplankton (Brett et al., 2009; Kelly et al., 2014; Taipale et al., 2014). It should be noted that in the shaded enclosures with leaf homogenate, total zooplankton biomass gradually increased toward the end of the experiment. This increase was mainly due to an increase in the abundance of amoebas (**Figure 3E**) that are known to consume diverse organisms including algae, bacteria, and other micro heterotrophs (Mieczan, 2007).

Substantial amounts of leaf litter have been reported to enter into small lakes, such as Lost Lake (Gasith and Hosler, 1976; Rau, 1976; Hanlon, 1981). However, t-OM has often been viewed primarily as an energy or carbon source to aquatic ecosystems (e.g., Polis et al., 1997; Doucett et al., 2007; Cole et al., 2011; Carpenter et al., 2016; Brett et al., 2017) and not as a P source presumably due to its relatively high C to P ratio. Our study showed that P was leached from leaf litter much faster rate than organic carbon and nitrogen, despite its low content in the leaf litter. In freshwater ecosystems, P is often limiting for algal growth (Elser et al., 2007). Thus, the input of leaf litter can be an important P source for stimulating lake primary production. Studies examining leaf litter of various tree species have also shown that, among C, N, and P, P is the most efficiently leached across all litter types (Baldwin, 1999; Schreeg et al., 2013).

Some studies suggest that dissolved t-OM may decrease primary production by reducing light penetration into lakes (Carpenter et al., 1998; Ask et al., 2009; Karlsson et al., 2015). In this study, such a negative effect of t-OM was not detected. Rather, t-OM stimulated primary production by supplying limited nutrients. It should be noted that in this study, we used shallow enclosures where sufficient light was provided throughout the water column. However, in lakes where epilimnion extends into a deep depth, it is likely that dissolved t-OM reduces the light availability for phytoplankton (Carpenter et al., 1998; Karlsson et al., 2015). In such lakes, the positive effects of t-OM found in this study may be undermined by the negative effect. In other words, the relative importance of negative (light limitation) and positive effects (P supply) of t-OM on primary producers may vary depending on the lake depth.

Cottingham and Narayan (2013) and Fey et al. (2015) have shown that the addition of tree leaves to lake water elevated TP relative to organic C and TN and increased zooplankton production. However, it was not clear that which food chains, brown or green, contributed more to increased zooplankton production when t-OM was amended. In this study, therefore, we tried to separate the contributions of brown and green food chains to raising zooplankton production using the Equations (1a)–(1d), which assume that mass flow along with the brown food chains was not affected by light conditions. However, this assumption may not be correct if the majority of the DOC in our t-OM amendment was refractory but was photochemically transformed to labile forms, promoting bacterial production (Tranvik and Bertilsson, 2001). Moreover, increased primary production under the unshaded conditions may have facilitated bacterial production through the supply of autochthonous DOC (Karlsson et al., 2002, Kritzberg et al., 2005). In this case, our calculation of the contribution from the green food chains to zooplankton production may be overestimated. However, some primary production did occur in the shaded treatments since there was 10% irradiance, likely resulting in an overestimate of the flow of the brown food chains in the shaded treatments. To solve these uncertainties, we examined the diets of zooplankton using stable isotopes. The analysis showed that 50–75% of food sources assimilated by zooplankton were autochthonous in the unshaded enclosures even when leaf homogenate was added (the LA treatment). These results suggest that the addition of leaf homogenate promoted zooplankton production mainly through green food chains.

Zooplankton growth is often limited by food quality especially when the C: P ratio of phytoplankton food is > 200 (e.g., Frost et al., 2006; Urabe et al., 2018). In the unshaded enclosures without leaf homogenate, the seston C: P ratio was > 300 for most of the dates, although the seston C: N ratio did not differ substantially among the enclosures with different treatments. Therefore, phytoplankton may have been stoichiometrically low-quality food for zooplankton under ambient lake conditions, suggesting that even if the primary production rate is substantial, the contribution of the green food chain to production at a higher trophic level can be limited relative to that of the brown food chain in P deficient lakes. However, in enclosures with leaf homogenate, seston C: P ratio was lower and close to Redfield ratio in the unshaded condition (LA) than in the shaded condition (DA) especially during the last several weeks of the experiment. This result suggests that the leaf homogenate provided sufficient amounts of P to primary producers and improved the stoichiometric quality of phytoplankton as food for zooplankton.

The effects of C, N, and P in t-OM on aquatic ecosystems may depend on the timescale considered because of differences among these elements in rates of leaching. According to

Schreeg et al. (2013), > 50% of P in the leaf litter was released in inorganic forms within only 4 h when these were soaked in water, but immediate release rates of DOC and TN from the leaf litter were < 10% and varied depending on tree species. Although we artificially processed leaf litters by mechanical shredding, the release rates of these elements from the leaf litter to leaf homogenate (**Table 1**) produced similar results. Thus, P leached from leaf litter can affect the aquatic food web on short time scales in nature. However, since the majority of C and N in t-OM is less efficiently leached over short time scales and decomposes slowly through shredding and crushing processes by benthic organisms, its effects may be more modest but temporally prolonged. Hence, we need to examine the long-term effects of t-OM on the aquatic food web and production (Fey et al., 2015).

Although fallen leaves entering a lake provide POC and DOC every year, the effects of t-OM on aquatic food web may change depending on the timing of input. Although this study was made in summer, the majority of litterfall occurs in the fall in north temperate areas (e.g., Gasith and Hosler, 1976). Since the water temperatures are relatively low in fall, the input of leaf litter into lakes in the fall may have little impact on aquatic food webs. However, nutrients leached from leaf litter in fall may be left unused in winter and be able to support aquatic production in the following spring. More importantly, the seasonality of leaf litter production differs depending on region and vegetation type in watersheds (e.g., evergreen vs. deciduous species: Gasith and Hosler, 1976; Alhamd et al., 2004). For example, although the production of litterfall is generally high in the fall in north temperate areas, summer peaks of the litterfall are often found even in deciduous forests such as that composed of *Alnus* (Kikuzawa et al., 1984). Moreover, the stoichiometry and leaching rates of nutrients will differ among leaf litter from different tree species. Thus, the effects of t-OM on green and brown food chains likely differ depending on the timing of the litter input and the types of vegetation in the watershed.

In this study, amendment of leaf homogenate increased DOC concentrations by 3 times and TP by 10 times when compared with the ambient levels. Although the TP level was lower than those in plankton culture media used for experimental studies (e.g., Lindström, 1983; Kilham et al., 1998), this study may have exaggerated the effects of leaf litters on zooplankton production. In addition, this study removed a large size fraction of leaf litter by screening. This large size fraction may be an important resource for benthic invertebrates (Batt et al., 2015). Shredding and crushing leaf litter by benthic invertebrates can promote brown food chains and nutrient cycling (Covich et al., 1999; Cross et al., 2005). This suggests that, in addition to research examining the contributions of green vs. brown food chains to higher trophic levels, benthic–pelagic coupling also requires further attention to more fully understand how t-OM affects aquatic food webs.

Conclusion

Although t-OM is rich in C, most of C in leaf litter is refractory while P is easily leached. Classically, t-OM has been viewed as a carbon or energy source for aquatic ecosystems. However, it can also be an important P source for primary producers as suggested by Cottingham and Narayan (2013) and thus promote mass transfer to higher trophic levels along with green food chain. As shown in this study, the stoichiometry of materials leached from t-OM is not necessarily the same as that of the t-OM itself. To understand the roles of trophic subsidies to ecosystems, therefore, we need to consider stoichiometric functions of the subsidized materials for green and brown food chains.

Data availability statement

The datasets presented in this study can be found in the online Dryad Repository, Dataset, https://doi.org/10.5061/dryad.8pk0p2nqv.

Author contributions

JU, FH, and JE planned and designed the enclosure experiment. JE and TT arranged access to Lost Lake for the experiment. FH, JU, HD, TK, TN, TT, IK, MY, TY, and JE contributed to the experimental setup and carried out the experiment. FH, TK, TN, and TT performed chemical analyses and enumerated plankton. HD and IK performed stable isotope analysis. JU, FH, and HD performed statistical analyses. JU and FH wrote the draft. All authors contributed to the article and approved the submitted version.

Funding

This study was financially supported by the Japan Society for the Promotion of Science (JSPS) Grant-in-Aid for Scientific Research (KAKENHI) (16H02522 and 20H03315).

Acknowledgments

We appreciate Adam Bauman, Matthew Church, and staff at the FLBS for their help in lab work and Tamaki Doi and Tamon Doi for their assistance with field works during the experiment. We also thank the Crecelius and Sailors families for permission to work on their lake and conduct our enclosure experiment.

Conflict of interest

The authors declare that the research was conducted in the absence of any commercial or financial relationships that could be construed as a potential conflict of interest.

Publisher's note

All claims expressed in this article are solely those of the authors and do not necessarily represent those of their affiliated organizations, or those of the publisher, the editors and the reviewers. Any product that may be evaluated in this article, or claim that may be made by its manufacturer, is not guaranteed or endorsed by the publisher.

Supplementary material

The Supplementary Material for this article can be found online at: https://www.frontiersin.org/articles/10.3389/fevo.2022.956819/full#supplementary-material

References

Alhamd, L., Arakaki, S., and Hagihara, A. (2004). Decomposition of leaf litter of four tree species in a subtropical evergreen broad-leaved forest, Okinawa Island, Japan. *For. Ecol. Manage.* 202, 1–11. doi: 10.1016/j.foreco.2004.02.062

Adrian, R., Wickham, S. A., and Butler, N. M. (2001). Trophic interactions between zooplankton and the microbial community in contrasting food webs: The epilimnion and deep chlorophyll maximum of a mesotrophic lake. *Aquat. Microb. Ecol.* 24, 83–97. doi: 10.3354/ame024083

Ask, J., Karlsson, J., Persson, L., Askm, P., Byström, P., and Jansson, M. (2009). Terrestrial organic matter and light penetration: Effects on bacterial and primary production in lakes. *Limnol. Oceanogr.* 54, 2034–2040. doi: 10.4319/lo.2009.54.6.2034

Baldwin, D. S. (1999). Dissolved organic matter and phosphorus leached from fresh and 'terrestrially' aged river red gum leaves: Implications for assessing river–floodplain interactions. *Freshw. Biol.* 41, 675–685. doi: 10.1046/j.1365-2427.1999.00404.x

Batt, R. D., Carpenter, S. R., Cole, J. J., Pace, M. L., Johnson, R. A., Kurtzweil, J. T., et al. (2015). Altered energy flow in the food web of an experimentally darkened lake. *Ecosphere* 6, 1–23. doi: 10.1890/ES14-00241.1

Bloem, J., Albert, C., Bar-Gillissen, M.-J. B., Berman, T., and Cappenberg, T. E. (1989). Nutrient cycling through phytoplankton, bacteria and protozoa, inselectively filtered Lake Vechten water. *J. Plankton Res.* 11, 119–131. doi: 10.1093/plankt/11.1.119

Brett, M. T. (2014). Resource polygon geometry predicts Bayesian stable isotope mixing model bias. *Mar. Ecol. Prog. Ser.* 514, 1–12. doi: 10.3354/meps11017

Brett, M. T., Kainz, M. J., Taipale, S. J., and Seshan, H. (2009). Phytoplankton not allochthonous carbon, sustains herbivorous zooplankton production. *Proc. Natl. Acad. Sci. U.S.A.* 106, 21197–21201. doi: 10.1073/pnas.0904129106

Brett, M. T., Bunn, S. E., Chandra, S., Galloway, A. W., et al. (2017). How important are terrestrial organic carbon inputs for secondary production in freshwater ecosystems? *Freshw. Biol.* 62, 833–853. doi: 10.1111/fwb.12909

Carpenter, S. R., and Kitchell, J. F. (1996). *The trophic cascade in lakes*. Cambridge: Cambridge University Press.

Carpenter, S. R., Cole, J. J., Pace, M. L., and Wilkinson, G. B. (2016). Response of plankton to nutrients, planktivory and terrestrial organic matter: A model analysis of whole-lake experiments. *Ecol. Lett.* 19, 230–239. doi: 10.1111/ele.12558

Carpenter, S. R., Cole, J. J., Kitchell, J. F., and Pace, M. L. (1998). Impact of dissolved organic carbon, phosphorus, and grazing on phytoplankton biomass and production in experimental lakes. *Limnol. Oceanogr.* 43, 73–80. doi: 10.4319/lo.1998.43.1.0073

Cole, J. J., Carpenter, S. R., Kitchell, J., Pace, M. L., Solomon, C. T., and Weidel, B. (2011). Strong evidence for terrestrial support of zooplankton in small lakes based on stable isotopes of carbon, nitrogen, and hydrogen. *Proc. Natl. Acad. Sci. U.S.A.* 108, 175–1980. doi: 10.1073/pnas.1012807108

Cole, J. J. (2013). "Freshwater ecosystems and the carbon cycle," in *Excellence in ecology*, Vol. 18, ed. O. Kinne (Oldendorf: International Ecology Institute), 146.

Cottingham, K. L., and Narayan, L. (2013). Subsidy quantity and recipient community structure mediate plankton responses to autumn leaf drop. *Ecosphere* 4, 1–18. doi: 10.1890/ES13-00128.1

Covich, A. P., Palmer, M. A., and Crowl, T. A. (1999). The role of benthic invertebrate species in freshwater ecosystems: Zoobenthic species influence energy flows and nutrient cycling. *BioScience* 49, 119–127. doi: 10.2307/1313537

Cross, W. F., Benstead, J. P., Frost, P. C., and Thomas, S. A. (2005). Ecological stoichiometry in freshwater benthic systems: Recent progress and perspectives. *Freshw. Biol.* 50, 1895–1912. doi: 10.1111/j.1365-2427.2005.01458.x

Doucett, R. R., Marks, J. C., Blinn, D. W., Caron, M., and Hungate, B. A. (2007). Measuring terrestrial subsidies to aquatic food webs using stable isotopes of hydrogen. *Ecology* 88, 1587–1592. doi: 10.1890/06-1184

Elser, J. J., Matthew, M. E. S., Cleland, E. E., Gruner, D. S., Harpole, W. S., Hillebtand, H., et al. (2007). Global analysis of nitrogen and phosphorus limitation of primary producers in freshwater, marine and terrestrial ecosystems. *Ecol. Lett.* 10, 1135–1142. doi: 10.1111/j.1461-0248.2007.01113.x

Fey, S. B., Mertens, A. N., and Cottingham, K. L. (2015). Autumn leaf subsidies influence spring dynamics of freshwater plankton communities. *Oecologia* 178, 875–885. doi: 10.1007/s00442-015-3279-5

France, R. L. (1995). Differentiation between littoral and pelagic food webs in lakes using stable carbon isotopes. *Limnol. Oceanogr.* 40, 1310–1313. doi: 10.4319/lo.1995.40.7.1310

Frost, P. C., Benstead, J. P., Cross, W. F., James, H. H., Marguerite, H. L., Xenopoulos, A., et al. (2006). Threshold elemental ratios of carbon and phosphorus in aquatic consumers. *Ecol. Lett.* 9, 774–779. doi: 10.1111/j.1461-0248.2006.00919.x

Gasith, A., and Hosler, A. D. (1976). Airborne litterfall as a source of organic matter in lakes. *Limnol. Oceanogr.* 21, 253–258. doi: 10.4319/lo.1976.21.2.0253

Grosbois, G., Del Giorgio, P. A., and Rautio, M. (2017). Zooplankton allochthony is spatially heterogeneous in a boreal lake. *Freshw. Biol.* 62, 474–490. doi: 10.1111/fwb.12879

Hanlon, R. D. G. (1981). Allochthonous plant litter as a source of organic material in an oligotrophic lake (Llyn Frongoch). *Hydrobiologia* 80, 257–261. doi: 10.1007/BF00018365

Hondula, K. L., Pace, M. L., Cole, J. J., and Batt, R. D. (2014). Hydrogen isotope discrimination in aquatic primary producers: Implications for aquatic food web studies. *Aquat. Sci.* 76, 217–229. doi: 10.1007/s00027-013-0331-6

Jansson, M., Persson, L., De Roos, A. M., Jones, R. I., and Tranvik, L. J. (2007). Terrestrial carbon and intraspecific size-variation shape lake ecosystems. *Trends Ecol. Evol.* 22, 316–322. doi: 10.1016/j.tree.2007.02.015

Karlsson, J., Bergstom, A. K., Bystrom, P., Gudasz, C., Rodriguez, P., and Hein, C. (2015). Terrestrial organic matter input suppresses biomass production in lake ecosystems. *Ecology* 96, 2870–2876. doi: 10.1890/15-0515.1

Karlsson, J., Jansson, M., and Jonsson, A. (2002). Similar relationships between pelagic primary and bacterial production in clearwater and humic lakes. *Ecology* 83, 2902–2910. doi: 10.1890/0012-9658(2002)083[2902:SRBPPA]2.0.CO;2

Kelly, P. T., Solomon, C. T., Weidel, B. C., and Jones, S. E. (2014). Terrestrial carbon is a resource, but not a subsidy, for lake zooplankton. *Ecology* 95, 1236–1242. doi: 10.1890/13-1586.1

Kikuzawa, K., Asai, T., and Fukuchi, M. (1984). Leaf-litter production in a plantation of *Alnus inokumae*. *J. Ecol.* 72, 993–999. doi: 10.2307/2259546

Kilham, S. S., Kreeger, D. A., Lynn, S. G., Goulden, C. E., and Herrera, L. (1998). COMBO: A defined freshwater culture medium for algae and zooplankton. *Hydrobiologia* 377, 147–159. doi: 10.1023/A:1003231628456

Kritzberg, E. S., Cole, J. J., Pace, M. M., and Granéli, W. (2005). Does autochthonous primary production drive variability in bacterial metabolism and growth efficiency in lakes dominated by terrestrial C inputs? *Aquat. Microb. Ecol.* 38, 103–111. doi: 10.3354/ame038103

Lindeman, R. L. (1942). The trophic-dynamic aspect of ecology. *Ecology* 23, 399–417. doi: 10.2307/1930126

Lindström, K. (1983). Selenium as a growth factor for plankton algae in laboratory experiments and in some Swedish lakes. *Hydrobiologia* 101, 35–48. doi: 10.1007/BF00008655

McQueen, D. J., Johannes, M. R. S., Post, J. R., Steward, T. J., and Lean, D. R. S. (1989). Bottom–up and top–down impacts on freshwater pelagic community structure. *Ecol. Monogr.* 59, 289–310. doi: 10.2307/1942603

Mieczan, T. (2007). Seasonal patterns of testate amoebae and ciliates in three peatbogs: Relationship to bacteria and flagellates (Poleski National Park, Eastern Poland). *Ecohydrol. Hydrobiol.* 7, 77–89. doi: 10.1016/S1642-3593(07)70191-X

Nakano, S., and Murakami, M. (2001). Reciprocal subsidies: Dynamic interdependence between terrestrial and aquatic food webs. *Proc. Natl. Acad. Sci. U.S.A.* 98, 166–170. doi: 10.1073/pnas.98.1.166

Polis, G. A., Anderson, W. B., and Holt, R. D. (1997). Toward an integration of landscape and food web ecology: The dynamics of spatially subsidized food webs. *Annu. Rev. Ecol. Syst.* 28, 289–316. doi: 10.1146/annurev.ecolsys.28.1.289

Post, D. M. (2002). Using stable isotopes to estimate trophic position: models, methods, and assumptions. *Ecology*, 83, 703–718. doi: 10.1890/0012-9658(2002)083[0703:USITET]2.0.CO;2

R Core Team (2016). *R: A language and environment for statistical computing*. Vienna: R Foundation for Statistical Computing.

Rau, G. H. (1976). Dispersal of terrestrial plant litter into a subalpine lake. *Oikos* 27, 153–160. doi: 10.2307/3543445

Schreeg, L. A., Mack, M. C., and Turner, B. L. (2013). Nutrient-specific solubility patterns of leaf litter across 41lowland tropical woody species. *Ecology* 94, 94–105. doi: 10.1890/11-1958.1

Solomon, C. T., Cole, J. J., Doucett, R. R., Pace, M. L., Preston, N. D., Smith, L. E., et al. (2009). The influence of environmental water on the hydrogen stable isotope ratio in aquatic consumers. *Oecologia* 161, 313–324. doi: 10.1007/s00442-009-1370-5

Stock, B. C., Jackson, A. L., Ward, E. J., Parnell, A. C., Phillips, D. L., and Semmens, B. X. (2018). Analyzing mixing systems using a new generation of Bayesian tracer mixing models. *PeerJ* 6:e5096. doi: 10.7717/peerj.5096

Taipale, S. T., Brett, M. T., Hahn, M. W., Martin-Creuzburg, D., Yeung, S., Hiltunen, M., et al. (2014). Differing *Daphnia magna* assimilation efficiencies for terrestrial, bacterial, and algal carbon and fatty acids. *Ecology* 95, 563–576. doi: 10.1890/13-0650.1

Tanentzap, A. J., Kielstra, B. W., Wilkinson, G. M., Berggren, M., Craig, N., Del Giorgio, P. A., et al. (2017). Terrestrial support of lake food webs: Synthesis reveals controls over cross-ecosystem resource use. *Sci. Adv.* 3:e1601765. doi: 10.1126/sciadv.1601765

Tranvik, L. J., and Bertilsson, S. (2001). Contrasting effects of solar UV radiation on dissolved organic sources for bacterial growth. *Ecol. Lett.* 4, 458–463. doi: 10.1046/j.1461-0248.2001.00245.x

Tranvik, L. J. (1992). Allochthonous dissolved organic matter as an energy source for pelagic bacteria and the concept of the microbial loop. *Dissolved Org. Matter Lacustrine Ecosyst.* 229, 107–114. doi: 10.1007/BF00006994

Urabe, J., Shimizu, Y., and Yamaguchi, T. (2018). Understanding the stoichiometric limitation of herbivore growth: The importance of feeding and assimilation flexibilities. *Ecol. Lett.* 21, 197–206. doi: 10.1111/ele.12882

Wallace, J. B., Eggert, S. L., Meyer, J. L., and Webster, J. R. (1997). Multiple trophic levels of a forest stream linked to terrestrial litter inputs. *Science* 522, 102–104. doi: 10.1126/science.277.5322.102

Wassenaar, L. I., and Hobson, K. A. (2003). Comparative equilibration and online technique for determination of non-exchangeable hydrogen of keratins for use in animal migration studies. *Isotopes Environ. Health Stud.* 39, 211–217. doi: 10.1080/1025601031000096781

Wilkinson, G. M., Cole, J. J., and Pace, M. L. (2015). Deuterium as a food source tracer: Sensitivity to environmental water, lipid content, and hydrogen exchange. *Limnol. Oceanogr. Methods* 13, 213–223. doi: 10.1002/lom3.10019

Wolkovich, E. M., Allesina, S., Cottingham, K. L., Moore, J. C., Sandin, S. A., and de Mazancourt, C. (2014). Linking the green and brown worlds: The prevalence and effect of multichannel feeding in food webs. *Ecology* 95, 3376–3386. doi: 10.1890/13-1721.1

Yoshida, T., Gurung, T., Kagami, M., and Urabe, J. (2001). Contrasting effects of a cladoceran (*Daphnia galeata*) and a calanoid copepod (*Eodiaptomus japonicus*) on algal and microbial plankton in a Japanese lake, Lake Biwa. *Oecologia* 129, 602–610. doi: 10.1007/s004420100766

frontiers | Frontiers in Ecology and Evolution

TYPE Original Research
PUBLISHED 08 September 2022
DOI 10.3389/fevo.2022.958467

Check for updates

OPEN ACCESS

EDITED BY
Rona A. R. McGill,
University of Glasgow, United Kingdom

REVIEWED BY
Jessica Rettig,
Denison University, United States
Rosilene Luciana Delariva,
Universidade Estadual do Oeste do Paraná, Brazil

*CORRESPONDENCE
Geraldina Signa
geraldina.signa@unipa.it

SPECIALTY SECTION
This article was submitted to Population, Community, and Ecosystem Dynamics, a section of the journal Frontiers in Ecology and Evolution

RECEIVED 31 May 2022
ACCEPTED 12 August 2022
PUBLISHED 08 September 2022

CITATION
Andolina C, Signa G, Cilluffo G, Iannucci S, Mazzola A and Vizzini S (2022) Coexisting with the alien: Evidence for environmental control on trophic interactions between a native (*Atherina boyeri*) and a non-indigenous fish species (*Gambusia holbrooki*) in a Mediterranean coastal ecosystem. *Front. Ecol. Evol.* 10:958467. doi: 10.3389/fevo.2022.958467

COPYRIGHT
© 2022 Andolina, Signa, Cilluffo, Iannucci, Mazzola and Vizzini. This is an open-access article distributed under the terms of the Creative Commons Attribution License (CC BY). The use, distribution or reproduction in other forums is permitted, provided the original author(s) and the copyright owner(s) are credited and that the original publication in this journal is cited, in accordance with accepted academic practice. No use, distribution or reproduction is permitted which does not comply with these terms.

Coexisting with the alien: Evidence for environmental control on trophic interactions between a native (*Atherina boyeri*) and a non-indigenous fish species (*Gambusia holbrooki*) in a Mediterranean coastal ecosystem

Cristina Andolina[1,2], Geraldina Signa[1,2]*, Giovanna Cilluffo[1,2], Simona Iannucci[1,3], Antonio Mazzola[1,2] and Salvatrice Vizzini[1,2]

[1]Department of Earth and Marine Sciences, University of Palermo, Palermo, Italy, [2]Consorzio Nazionale Interuniversitario per le Scienze del Mare (CoNISMa), Rome, Italy, [3]Department of Life Sciences, University of Trieste, Trieste, Italy

Biological invasions are a widespread problem worldwide, as invasive non-indigenous species (NIS) may affect native populations through direct (e.g., predation) or indirect (e.g., competition) trophic interactions, leading to changes in the food web structure. The trophic relationships of the invasive eastern mosquitofish *Gambusia holbrooki* and the native big-scale sand smelt *Atherina boyeri* coexisting in three Mediterranean coastal ponds characterized by different trophic statuses (from oligotrophic to hypereutrophic) were assessed in spring through isotopic niche analysis and Bayesian mixing models. The two fish relied on the distinctive trophic pathways in the different ponds, with the evidence of minimal interspecific niche overlap indicating site-specific niche divergence mechanisms. In more detail, under hypereutrophic and mesotrophic conditions, the two species occupied different trophic positions but relying on a single trophic pathway, whereas, under oligotrophic conditions, both occupied a similar trophic position but belonging to distinct trophic pathways. Furthermore, the invaders showed the widest niche breadth while the native species showed a niche compression and displacement in the ponds at a higher trophic status compared to the oligotrophic pond. We argue that this may be the result of an asymmetric competition arising between the two species because of the higher competitive ability of *G. holbrooki* and may have been further shaped by the trophic status of the ponds, through a conjoint effect of prey availability and habitat complexity. While the high trophic plasticity and adaptability of both species to different environmental

features and resource availability may have favored their coexistence through site-specific mechanisms of niche segregation, we provide also empirical evidence of the importance of environmental control in invaded food webs, calling for greater attention to this aspect in future studies.

KEYWORDS

biological invasion, alien species, stable isotopes, mosquitofish, sand smelt, coastal ponds

Introduction

The invasion of non-indigenous species (NIS) is considered among the major threats for marine ecosystem functioning and services worldwide. The consequences of species invasion and establishment in recipient ecosystems are complex and depend on the interaction between the ecological characteristics of the invader species and the environmental and biological attributes of the recipient ecosystem (Occhipinti-Ambrogi, 2007; Chan and Briski, 2017). In particular, while high dispersal ability and physiological plasticity, fast growth, high feeding rate, and generalist feeding strategies are among the key factors of success for invasive NIS (David et al., 2017 and reference therein), the establishment of self-sustaining NIS populations is further favored in disturbed habitats (Chan and Briski, 2017).

Change in trophic dynamics and structure with severe consequences for native species is one of the most common ecological processes that the establishment of invasive NIS may trigger in recipient ecosystems (Jackson et al., 2012; Britton et al., 2018; Costa-Pereira et al., 2019). Depending on the trophic position of the invader species, direct trophic interactions with native species can exert bottom-up or top-down cascading controls on local food webs (Vander Zanden et al., 1999; Gallardo et al., 2016). On the contrary, interspecific exploitative competition mechanisms may occur when invasive and native species are trophically analogous and may lead to competitive exclusion or coexistence through niche differentiation mechanisms, such as spatial segregation or resource partitioning (David et al., 2017 and references therein). As invasive NIS are known for their high competitive abilities, they may induce changes in habitat or resource use by natives, displacement and/or contraction of their trophic niche, and alteration of trophic interactions and food web structure (Vander Zanden et al., 1999; Carmona-Catot et al., 2013; Tran et al., 2015). Therefore, the study of trophic niche and food web structure in invaded ecosystems can help to reveal the ecological changes driven by the biological invasion, to understand how trophic relationships between invasive and native species promoted their coexistence, and to predict the future evolution of recently invaded ecosystems.

The eastern mosquitofish *Gambusia holbrooki* has been intentionally introduced from the southern USA to European and Australian freshwaters since the early 1900s with the purpose to control mosquito populations and reduce the risk of spreading mosquito-related diseases. In addition to freshwaters, *G. holbrooki* thrives in a wide range of habitats, including estuaries and near-shore marine areas, and has been identified as one of the most widespread invasive fish worldwide (Lowe et al., 2000). It is a voracious predator with high feeding rates (Rehage et al., 2005), also known as an omnivore with opportunistic feeding strategies (Blanco et al., 2004; Kalogianni et al., 2014). A large array of terrestrial and aquatic organisms have been identified as common prey, along with macrophyte detritus (Blanco et al., 2004; Rehage et al., 2005; Remon et al., 2016). Besides high physiological adaptability and trophic plasticity and feeding rates, viviparity, high fecundity, and resistance to pollutants provide mosquitofish with a high competitive ability compared to native fish (Pyke, 2005).

Overall, a strong competitive impact of *G. holbrooki* on native species has been well documented in a variety of ecosystems (Alcaraz et al., 2008; MacDonald et al., 2012; Ruiz-Navarro et al., 2013). In particular, laboratory and field studies demonstrated the influence of abiotic factors in shaping the performance of mosquitofish, including the competitive effects on native species (Rincón et al., 2002; Blanco et al., 2004; Carmona-Catot et al., 2013; Ruiz-Navarro et al., 2013). High frequency of aggressive behaviors and higher feeding rate than native species have been observed at higher water temperature (Rincón et al., 2002; Carmona-Catot et al., 2013) and lower salinity (Alcaraz et al., 2008; Ruiz-Navarro et al., 2013). On the contrary, a limited influence of habitat features (e.g., size and complexity) and water quality (e.g., nutrient concentration and turbidity) on mosquitofish life-history traits and predation has been reported (Blanco et al., 2004; Cano-Rocabayera et al., 2019). Even with the large body of literature existing on the ecological effects of invasive fish, including mosquitofish, in aquatic systems, the trophic aspects have been scantly addressed especially in combination with environmental stressors.

Carbon and nitrogen stable isotope analysis (SIA, $\delta^{13}C$, and $\delta^{15}N$) is a powerful tool to investigate trophic interactions (e.g., Michener and Kaufman, 2008; Mancinelli and Vizzini, 2015; Nielsen et al., 2018) and has been widely used to describe trophic niche features within an isotopic framework (e.g., isotopic niche breadth and overlap) (Chen et al., 2011;

Abrantes et al., 2014), ontogenetic diet shifts (Layman et al., 2011; Andolina et al., 2020), and organic matter pathways (Vizzini et al., 2005; Signa et al., 2013b). Furthermore, SIA has the potential to infer the effects of invasive species on aquatic food webs, including resource shift deriving from intraspecific and interspecific competitions (Jackson et al., 2012; Mancinelli et al., 2017; Britton et al., 2018).

Here, we studied the isotopic niche as a proxy for the trophic niche (*sensu* Bearhop et al., 2004) of the invasive eastern mosquitofish *G. holbrooki* (Girard, 1859) and the native big-scale sand smelt *Atherina boyeri* (Risso, 1810), coexisting in a Mediterranean coastal system (Marinello ponds, Italy) featured by several small, shallow, and brackish ponds with different marine influences, geomorphological features, and trophic conditions (from oligotrophic to hypereutrophic) due to the external subsidies of gull guano (Signa et al., 2012). The big-scale sand smelt is a small euryhaline fish that inhabits the littoral zones of the Eastern Atlantic and the Mediterranean Sea, where it is frequently found in large schools both along the coasts and in lagoons and coastal lakes (Kara and Quignard, 2019). Alongside physiological adaptability, the big-scale sand smelt shows also high trophic plasticity and a generalist trophic behavior (Vizzini and Mazzola, 2002, 2005).

We hypothesize that generalist feeding behavior and trophic plasticity of both *G. holbrooki* and *A. boyeri* represent strategies which promote the coexistence of the two species through resource partitioning, therefore resulting in the separation of the trophic niche and different isotopic niche features (e.g., breadth, overlap). We also hypothesize that the contrasting trophic conditions may modulate this process by shaping the trophic niches according to prey availability and habitat complexity.

Materials and methods

Study area

The study was carried out in the coastal system of Marinello located along the north-eastern coast of Sicily (Italy, Mediterranean Sea) (Figure 1), consisting of five small (1–4 ha), shallow (max depth: 2–4 m), and brackish (mean salinity: 26–34 PSU) ponds (Verde, Fondo Porto, Porto Vecchio, Mergolo, and Marinello), separated from the adjacent sea by littoral bars and lacking direct freshwater input (Mazzola et al., 2010). The present research focused on three of the five ponds (i.e., VE, Verde; ME, Mergolo; and FP, Fondo Porto), on which several studies were conducted and found high inter-pond variability in terms of trophic status and primary production (Signa et al., 2012), contamination level (Signa et al., 2013a,b), macrobenthic communities (Signa et al., 2015), and trophic structure (Vizzini et al., 2016). These differences were attributed to the guano-derived fertilization induced by the colony of the yellow-legged gull *Larus michahellis* (Naumann, 1840) resident in the cliff next to the pond VE alongside the variability in geomorphological features of the ponds. The deeper landward ponds, VE, and ME (max depth, respectively, 3 and 3.5 m, Mazzola et al., 2010), are characterized by seabird-induced hypereutrophication (i.e., guanotrophication) and mesotrophic conditions, respectively (mean Chl-*a*: 44.7 and 8.8 mg m^{-3}; mean TSI_{CHL} (Trophic State Index, *sensu* Acquavita et al., 2015): 65 and 41 mg m^{-3}), resulting in high (although seasonally fluctuating) phytoplanktonic production and high internal variability (littoral vs. deeper area) (Signa et al., 2012, 2015). In contrast, the smaller (1.3 ha) and shallower (1.2 m deep, Mazzola et al., 2010) seaward pond FP is oligotrophic (mean Chl-*a*: 3.3 mg m^{-3}; mean TSI_{CHL}: 35 mg m^{-3}) and features higher water transparency and a macrophyte-covered seabed (Signa et al., 2012, 2015). Accordingly, biotic communities and trophic pathways vary among ponds (Vizzini et al., 2016), with benthic assemblages partially mirroring the strong environmental gradients, namely showing not only decreasing abundances from FP to VE but also the highest structural and functional diversity in ME (Signa et al., 2015). As regards fish, comparable assemblages characterize the three Marinello ponds, with the native *A. boyeri* and the invasive *G. holbrooki* among the most abundant species in the three ponds, where they coexist throughout the year, with the highest abundance in spring (Vizzini et al., 2016).

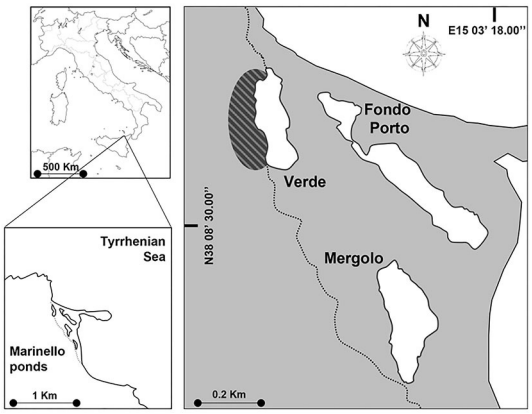

FIGURE 1
Map of the Marinello coastal system. The ponds studied were Verde (VE), Mergolo (ME), and Fondo Porto (FP) at increasing distance from the gull colony indicated by the striped oval. The dotted line indicates the edge of the Tindari promontory.

Sample collection

Atherina boyeri and *Gambusia holbrooki* specimens were collected using a small beach seine (4 m length, 3 mm mesh) in the three ponds Verde (VE), Mergolo (ME), and Fondo

TABLE 1 Sample size (*N*), biometric measures (Mean ± SD), and trophic position (TP) of small and large specimens of *A. boyeri* (ATE) and *G. holbrooki* (GAM) from the three ponds of the Marinello coastal system.

Pond	Species	Size-class	N	Standard length (mm)	Wet weight (mg)	TP
Verde	ATE	Small	10	23.8 ± 1.6	121.8 ± 19.6	3.8 ± 0.2
		Large	10	32.9 ± 1.6	336.4 ± 51.9	3.8 ± 0.2
	GAM	Small	8	22.3 ± 1.3	141.4 ± 35.9	3.3 ± 0.4
		Large	10	38.3 ± 1.4	1,098.7 ± 251.6	3.1 ± 0.2
Mergolo	ATE	Small	10	24.9 ± 1.2	120.9 ± 15.5	3.1 ± 0.2
		Large	9	35.1 ± 6.5	423.7 ± 282.1	3.1 ± 0.1
	GAM	Small	9	21.8 ± 1.1	139.9 ± 36.7	3.7 ± 0.4
		Large	8	35.2 ± 4.6	517.2 ± 314.6	3.3 ± 0.2
Fondo	ATE	Large	9	35.7 ± 1.7	343.6 ± 65.0	2.8 ± 0.4
Porto	GAM	Small	10	21.5 ± 0.8	119.2 ± 36.1	3.2 ± 0.3
		Large	5	31.7 ± 0.3	352.3 ± 84.3	3.2 ± 0.2

Porto (FP) in spring 2012 when the ponds host the highest diversity and abundances of fish, invertebrates, and organic matter sources (Signa et al., 2015). The hauls were performed at each pond in triplicate by dragging the seine on a perpendicular line (10 m) from a depth of about 1.5 m up to the shoreline. In addition, the percent coverage of macrophytes (macroalgae and seagrasses) was estimated by visual census along the shores and the central area of each pond and ranked according to the marine version of the Braun-Blanquet score developed by Kenworthy et al. (1993) as a proxy for habitat complexity.

After collection, fish were kept cool and in the dark upon arrival at the laboratory, where they were identified, subjected to biometric measurements (standard length SL, wet weight WW), and grouped per size class: small (SL $<$ 30 mm) and large (SL $>$ 30 mm), according to previous studies carried out in Mediterranean lagoons (Vizzini and Mazzola, 2002; Blanco et al., 2004). Both size classes of the two species were found in all the ponds, except for small *A. boyeri*, which was not found in FP. Total fish abundance was calculated for both species and size class by pooling data obtained from the three hauls and expressed as individuals per 100 m^2. Moreover, a minimum of five and a maximum of ten specimens per size class were randomly taken for each species from each pond (Table 1) and processed for isotopic analyses, with this sample size being sufficient to ensure reliable isotopic niche determination through the specific statistical package SIBER (Jackson et al., 2011; see Section Data analysis for details). Dorsal muscle was dissected, dried at 60°C to constant weight, and ground to a fine homogeneous powder using a mortar and pestle. Stable isotope analysis was performed through an isotope ratio mass spectrometer (Thermo Delta Plus XP) connected to an elemental analyzer (Thermo Flash EA 1112). Stable isotopes were expressed in standard delta (δ) notation as parts per thousand (‰):

$$\delta^{13}C \text{ or } \delta^{15}N = \left[\left(R_{sample} - R_{standard}\right)/R_{standard}\right] x\ 1000,$$

where R is the ratio ^{13}C:^{12}C or ^{15}N:^{14}N. The results were reported relative to Vienna Pee Dee Belemnite (VPDB) for $\delta^{13}C$ and atmospheric air for $\delta^{15}N$. Analytical precision based on the standard deviation of replicates of internal standards (International Atomic Energy Agency IAEA-CH-6 for $\delta^{13}C$ and IAEA-NO-3 for $\delta^{15}N$) was 0.1‰ for $\delta^{13}C$ and 0.2‰ for $\delta^{15}N$.

Data analysis

To assess isotopic niche breadth and overlap of the populations of the two species (*Atherina boyeri* and *Gambusia holbrooki*) across size classes in the three ponds, $\delta^{13}C$ and $\delta^{15}N$ data were first corrected to avoid any potential bias given by differences in basal resources of the three ponds (Olsson et al., 2009).

The surface-grazing snail *Hydrobia ventrosa* was used as baseline, according to Vizzini et al. (2016), to correct both $\delta^{13}C$ and $\delta^{15}N$. In more detail, the corrected $\delta^{13}C$ was calculated following the equation by Olsson et al. (2009):

$$\delta^{13}C_{corr} = \delta^{13}C_f - \delta^{13}C_{bmean}/CR_b,$$

where $\delta^{13}C_f$ is the carbon isotopic value of the fish, $\delta^{13}C_{bmean}$ is the mean carbon isotopic value of the baseline ($\delta^{13}C$ mean value ± standard deviation: −17.4 ± 0.7‰ in VE, −16.4 ± 0.5‰ in ME, and −17.4 ± 0.2‰ in FP), and CR_b is the carbon range ($\delta^{13}C_{max}$-$\delta^{13}C_{min}$) of the baseline (1.3‰ in VE, 1.0‰ in ME, and 0.3‰ in FP) (data from Vizzini et al., 2016).

The same baseline was used to correct $\delta^{15}N$, i.e., estimating the fish trophic position (TP) following the equation by Post (2002):

$$TP = \left[\left(\delta^{15}N_f - \delta^{15}N_b\right)/\Delta_n\right] + \lambda,$$

with $\delta^{15}N_f$ being the nitrogen isotopic value of the fish, $\delta^{15}N_b$ being the mean nitrogen isotopic value of the baseline ($\delta^{15}N$ mean value ± standard deviation: 13.4 ± 0.4‰ in VE, 6.9 ± 0.7‰ in ME, and 10.9 ± 0.1‰ in FP), Δ_n being the expected enrichment in $\delta^{15}N$ per trophic level (3.4‰ according to Post, 2002), and λ being the trophic level of the species used as a baseline that was set as 2.

Corrected $\delta^{13}C$ and $\delta^{15}N$ data were then used to estimate the standard ellipse area corrected for small sample size (SEAc), the SEAc overlap, and the Bayesian standard ellipse area (SEAb) (Jackson et al., 2011) using the SIBER package v 2.1.5 (Stable Isotope Bayesian Ellipses in R) (Jackson et al., 2011) in R v.

TABLE 2 Macroalgae and seagrass percentage cover of the three ponds of the Marinello coastal system (shores and central area) ranked according to the marine version of the Braun-Blanquet score (Kenworthy et al., 1993).

Pond	Site	Seagrass cover %		Macroalgae cover %		BB score range
		Min	Max	Min	Max	
Verde	Shore	0	25–100	0	75–50	0–5
	Center	0	0	0	0	0
Mergolo	Shore	0	25–50	0	50–75	0–4
	Center	25–50	100	0	25–50	0–5
Fondo Porto	Shore	5–25	50–75	5–25	50–75	2–4
	Center	25–50	25–50	25–50	75–100	3–5

4.0.2 (R Core Team, 2020). The SEAc encompassed 40% of the data and was expressed as single values; the SEAb was derived from 100,000 posterior iterations and was expressed as a range of probable values reported in posterior density plots reflecting estimation uncertainty (Jackson et al., 2011). Differences in TP and SEAb among ponds, fish species, and size classes were tested, respectively, with non-parametric permutational analysis of variance (PERMANOVA, PRIMER-E Ltd., Plymouth, UK; Anderson, 2017) and ANOVA (R v. 4.0.2; R Core Team, 2020) followed by pairwise comparisons.

In addition, to estimate the main trophic pathways sustaining the two species' population in the ponds, Bayesian mixing models were run using MixSIAR v 3.1.11 (Stock et al., 2018) in R (R Core Team, 2020). Carbon and nitrogen stable isotope data (not corrected) of all possible basal sources of organic matter in each pond were taken from Vizzini et al. (2016). Sources included in the models were seagrasses, macroalgae, suspended particulate organic matter (SPOM), and sedimentary organic matter (SOM) (see Supplementary Table S1 for species list and isotopic values). Trophic enrichment factors (TEFs) used in the model were, respectively, 0.4 ± 1.3‰ for $\delta^{13}C$ and 3.4 ± 1.0‰ for $\delta^{15}N$, according to Post (2002), which were doubled as these fish are secondary consumers/omnivores. Whenever more than one species belonged to the seagrass or macroalgae source categories, the mixing model output was reported as the a posteriori sum of the contribution of each species (see Supplementary Table S1).

Results

The three ponds were characterized by different habitat complexity in terms of macrophyte cover and marine Braun-Blanquet score. High internal variability characterized both ponds at a higher trophic status, Verde (VE) andMergolo (ME), in contrast to what was observed in the oligotrophic pond Fondo Porto (FP). In particular, the shores of both VE and ME were covered with patches of seagrasses and macroalgae interspersed with bare bottom ranging from 0 to 50% for seagrasses in both ponds and from 0 to 100% and to 75% for macroalgae in VE and ME, respectively (Table 2). In contrast, the shores of FP were entirely covered by macrophytes with the percentage ranging between 5 and 75% for both seagrasses and macroalgae (Table 2). The greatest variability among the ponds was found in the central areas, with no macrophytes recorded in VE, patchy macrophyte cover in ME (25–100 and 0–50% for seagrasses and macroalgae, respectively), and higher and more homogeneous coverage of both seagrasses (25–50%) and macroalgae (25–100%) in FP. Accordingly, the marine Braun-Blanquet score varied from 0 to 5 in both VE and ME and only from 2 to 5 in FP (Table 2).

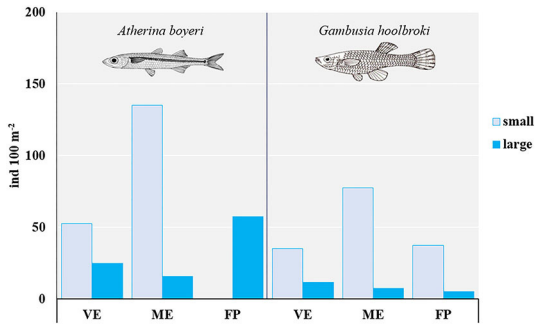

FIGURE 2
Total abundance (ind. 100 m^{-2}) of small and large specimens of *A. boyeri* and *G. holbrooki* from the three ponds of the Marinello coastal system: VE, Verde; ME, Mergolo; FP, Fondo Porto.

Overall, the native big-scale sand smelt *A. boyeri* outnumbered the invasive eastern mosquitofish *G. holbrooki* (Figure 2). Small specimens predominated over large specimens in each pond, except for *A. boyeri* in FP where no small fish were found and were more abundant in ME than in the other ponds.

$\delta^{13}C$ and $\delta^{15}N$ of fish varied among the three ponds according to their trophic status: values were overall more depleted in both carbon and nitrogen in the mesotrophic ME, intermediate in carbon and most enriched in nitrogen in the guanotrophic VE, and most enriched in carbon and intermediate

in nitrogen in the oligotrophic FP (Figure 3A). Similarly, the standard ellipse area (SEAc), representing the "core" isotopic niche of the two fish species, showed a clear grouping by pond within the corrected isotopic space ($\delta^{13}C_{corr}$–TP bi-plot) (Figure 3B). The niche of both species collected in ME showed a more carbon-depleted position, followed by the niches in VE and FP, which showed the most carbon-enriched position. Within each pond, the niches of the two fish across size classes were positioned in different ways: both in VE and ME, the niches of the two species showed a similar positioning along the $\delta^{13}C_{corr}$ axis, while they clustered apart along the TP axis, with *A. boyeri* at higher TP values than *G. holbrooki* in VE and conversely in ME (Figure 3B). In contrast, in FP, the niches of the two species differed mainly in $\delta^{13}C_{corr}$ values, with more $^{13}C_{corr}$-enriched values for *G. holbrooki* than *A. boyeri* (Figure 3B). In line with these patterns, the niche overlap between the two species at all size classes was negligible in all the ponds (range: 0–12%, Table 3). High intraspecific SEAc overlap was observed for *A. boyeri*: 87 and 98% of the niche of large specimens overlapped with that of small specimens in VE and ME, respectively (Figure 3B, Table 3). In contrast, only a partial overlap was observed between the two size classes of *G. holbrooki* in all the ponds (38, 33, and 24%, respectively, in VE, ME, and FP; Figure 3B, Table 3).

The isotopic niche breadth of the two species, expressed as SEAb, showed overall wider niches for small mosquitofish than all the other fish and wider niche in FP than in the other ponds (Figure 4). Moreover, in the three ponds, the niche breadth of both mosquitofish and sand smelt was significantly wider in small than large specimens ($p < 0.001$), but only in VE and ME, the niche breadth of sand smelt was smaller than that of both mosquitofish size classes (Figure 4). At the same time, comparing ponds, both small and large *G. holbrooki* showed significant decreasing niche breadth from FP to ME and VE, while large *A. boyeri* showed larger niche in FP than both ME and VE ($p < 0.001$). Similar to the large specimens, the niche of small *A. boyeri* was rather narrow and comparable between VE and ME (Figure 4).

The trophic position (TP) estimated showed that the two species broadly occupy a trophic level comprised between 3 and 4 while varying among ponds, species, and size classes (Table 1, Supplementary Table S2). Moreover, in the eutrophic pond VE, *A. boyeri* showed a significantly higher TP than *G. holbrooki*, while the opposite trend emerged in the other two ponds, where *G. holbrooki* showed higher TP than *A. boyeri*. Moreover, *A. boyeri* showed significantly increasing TP values from FP to ME and VE and *G. holbrooki* showed higher TP only in ME than in the other ponds. As regards size classes, only mosquitofish showed significant differences with higher values in small than large specimens (Table 1, Supplementary Table S2).

Mixing models revealed that the basal organic matter sources provided a different proportional contribution to the trophic pathways sustaining the two fish species in the different ponds (Figure 5, Supplementary Table S1 for details). In VE, sedimentary organic matter (SOM) was the dominant basal source underlying the diet of all fish, with the exception of large mosquitofish, for which the proportional contribution of SOM decreased in favor of macroalgae. A clear different pattern was found in ME, where the suspended particulate organic matter (SPOM) was the prevailing basal resource in the trophic pathways supporting the diet of all fish (Figure 5, Supplementary Table S1). Lastly, in FP, all the basal resources contributed in similar proportions to the pathways underlying the diet of large sand smelts, while macroalgae and seagrasses prevailed for mosquitofish (Figure 5, Supplementary Table S1).

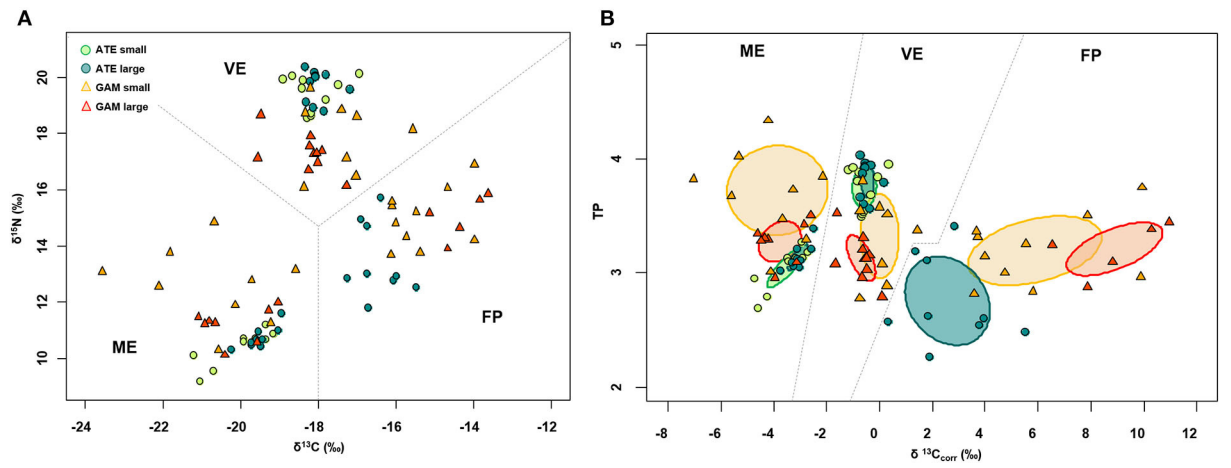

FIGURE 3
Bi-plots showing **(A)** raw and **(B)** baseline corrected $\delta^{13}C$ ($\delta^{13}C_{corr}$) and $\delta^{15}N$ (TP) of small and large specimens of *A. boyeri* (ATE) and *G. holbrooki* (GAM) from the three ponds of the Marinello coastal system: VE, Verde; ME, Mergolo; FP, Fondo Porto. In **(B)** is reported standard ellipse area corrected for small sample size (SEAc ‰^{2}) representing the isotopic niches.

10.3389/fevo.2022.958467

TABLE 3 Pairwise comparisons of SEAc (based on corrected stable isotope data) and overlap values (‰^{2}) estimated between small (S) and large (L) specimens of *A. boyeri* (ATE) and *G. holbrooki* (GAM) from the three ponds of the Marinello coastal system.

Pond	Group 1 vs. group 2	SEAc group 1 (‰^{2})	SEAc group 2 (‰^{2})	Overlap (‰^{2})	% of SEAc 1 overlapped by SEAc 2	% of SEAc 2 overlapped by SEAc 1
Verde	ATE-S–ATE-L	0.3	0.2	0.1	46	87
	ATE-S–GAM-S	0.3	1.0	0.03	12	4
	ATE-S–GAM-L	0.3	0.3	–	–	–
	ATE-L–GAM-S	0.2	1.0	0.003	2	0.3
	ATE-L–GAM-L	0.2	0.3	–	–	–
	GAM-S–GAM-L	1.0	0.3	0.1	12	38
Mergolo	ATE-S–ATE-L	0.3	0.1	0.1	36	98
	ATE-S–GAM-S	0.3	2.1	–	–	–
	ATE-S–GAM-L	0.3	0.5	0.02	10	5
	ATE-L–GAM-S	0.1	2.1	–	–	–
	ATE-L–GAM-L	0.1	0.5	–	–	–
	GAM-S–GAM-L	2.1	0.5	0.2	8	33
Fondo Porto	ATE-L–GAM-S	2.1	2.5	0.05	2	2
	ATE-L–GAM-L	2.1	1.4	–	–	–
	GAM-S–GAM-L	2.5	1.4	0.3	13	24

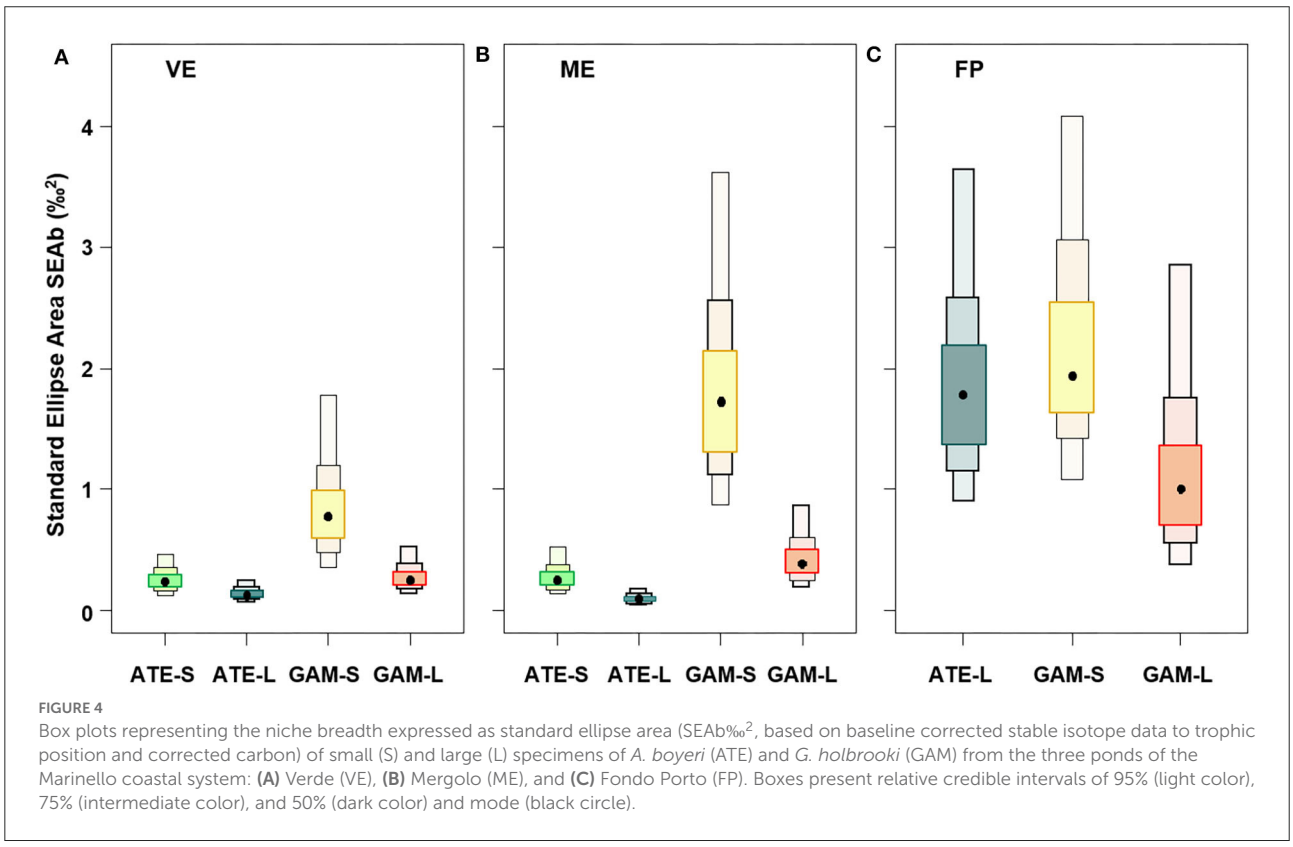

FIGURE 4
Box plots representing the niche breadth expressed as standard ellipse area (SEAb‰^{2}, based on baseline corrected stable isotope data to trophic position and corrected carbon) of small (S) and large (L) specimens of *A. boyeri* (ATE) and *G. holbrooki* (GAM) from the three ponds of the Marinello coastal system: **(A)** Verde (VE), **(B)** Mergolo (ME), and **(C)** Fondo Porto (FP). Boxes present relative credible intervals of 95% (light color), 75% (intermediate color), and 50% (dark color) and mode (black circle).

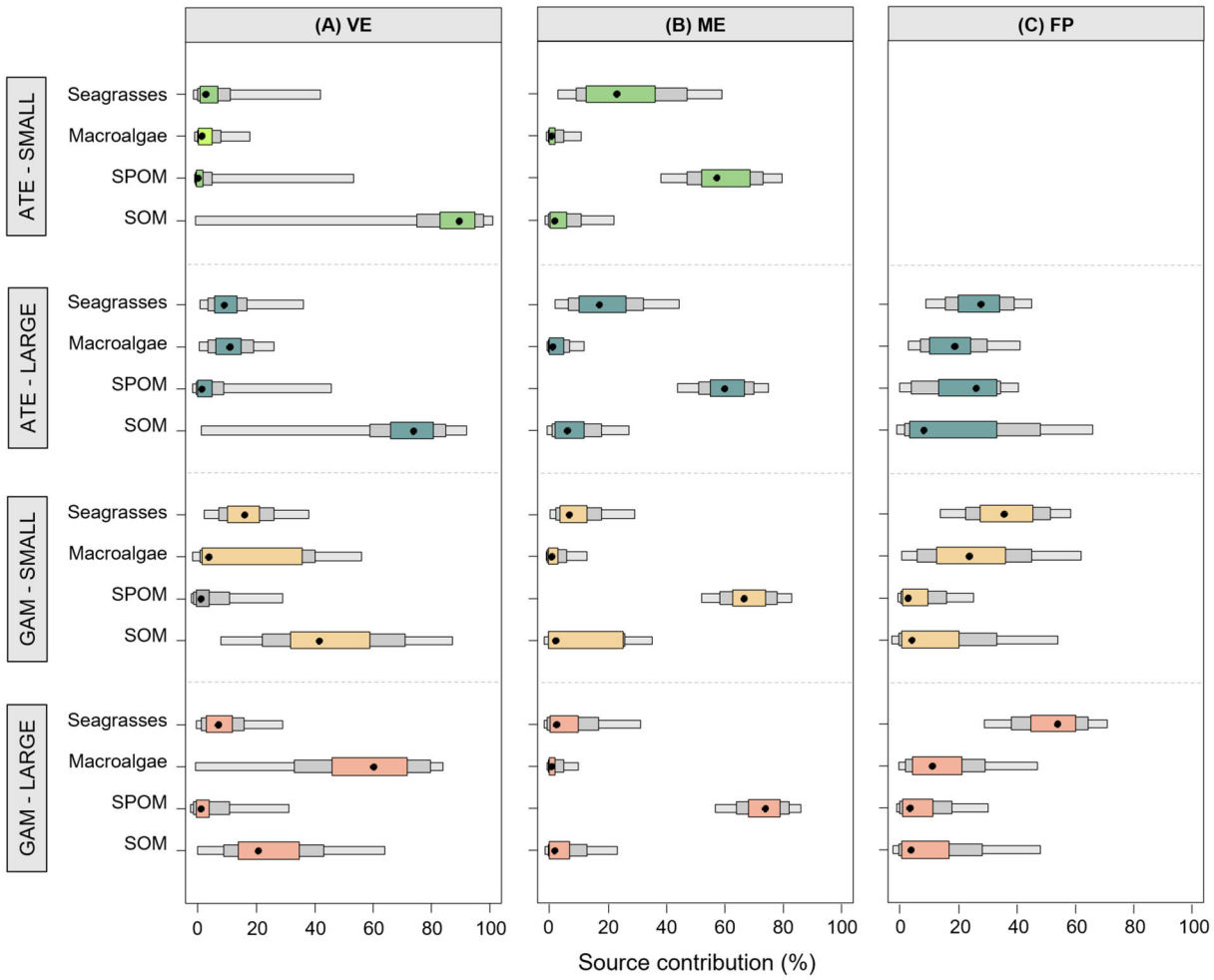

FIGURE 5
Percentage contribution of different basal resource categories to the diet of small (S) and large (L) specimens of *A. boyeri* (ATE) and *G. holbrooki* (GAM) from the three ponds of the Marinello coastal system: **(A)** Verde (VE), **(B)** Mergolo (ME), and **(C)** Fondo Porto (FP). Boxes present relative credible intervals of 95% (light color), 75% (intermediate color), and 50% (dark color) and mode (black circle). Details of the Bayesian isotopic mixing model output are presented in Supplementary Table S1.

Discussion

This study analyses the trophic relationships between the invasive eastern mosquitofish *G. holbrooki* and the native big-scale sand smelt *A. boyeri* co-occurring in the brackish ponds of the Marinello coastal system at the beginning of the productive season (i.e., spring). The results obtained highlighted a clear differentiation in the fish isotopic values and niche position, consistent with the distinct trophic background of the coastal ponds and the reliance of fish on different trophic pathways.

The nutrient subsidies arising from the gull colony (*L. michahellis*) strongly influence the neighboring Verde pond (VE), but only to a limited extent the nearby Fondo Porto pond (FP) and the farthest Mergolo pond (ME) (Signa et al., 2012; Vizzini et al., 2016). $\delta^{15}N$ is acknowledged as a powerful proxy for the ornithogenic input in terrestrial and coastal areas, due to the high values of bird guano (Mizutani and Wada, 1988; Signa et al., 2021 and references therein). Accordingly, the different positioning of the fish populations along the vertical axis of the isotopic bi-plot found in this study mirrors the gradual decrease in the incorporation of guano-derived nutrients into local food webs (Vizzini et al., 2016), with the highest influence in the closest pond VE and the lowest in the farthest ME. On the contrary, we found that the different positioning along the $\delta^{13}C$ axis mirrors the reliance of fish on distinct organic matter pathways. The overlap between the $\delta^{13}C$ values of guano ($\delta^{13}C = -20.2 \pm 2.5$ ‰, Vizzini et al., 2016) and those of both sedimentary organic matter (SOM) (-19.5 ± 1.1‰, Supplementary Table S1) and macroalgae (-20.0 ± 0.8‰, Supplementary Table S1) in VE indicates, in fact, a

clear accumulation of seabird-derived organic matter in the system and its incorporation in basal sources (Vizzini et al., 2016). Moreover, Bayesian mixing models revealed that the avian-subsidized SOM and the opportunistic macroalgae (e.g., *Cladophora* sp.), which are particularly abundant in the littoral zone forming dense patches, were the main basal sources supporting the trophic pathway leading to both fish species in VE. In contrast, we observed a single planktonic pathway based on suspended particulate organic matter (SPOM) dominating in the mesotrophic ME and a mixed benthic pathway characterized by a high contribution of macrophytes dominating in the seaward and oligotrophic FP. This is consistent with previous findings that showed a dominance of benthic pathways in VE in spring (Vizzini et al., 2016) and inter-pond variability in resource availability and habitat complexity that reflects on benthic abundance and diversity (Signa et al., 2015), confirming, therefore, that the observed differences in trophic pathways are driven in part by the differing seabird subsidies. Alongside the reliance on different organic matter pathways in the three ponds, the patterns observed within each pond in terms of isotopic niche positioning and trophic level suggest that the coexistence of the two species may have been promoted by site-specific mechanisms of niche differentiation. First, the negligible niche overlap between the two species throughout the ponds indicates a clear resource partitioning, consistent with previous studies of invasive fish, including mosquitofish. In particular, both in Australian wetlands and Mediterranean lagoons, mosquitofish coexists with other endemic fish, including sand smelt, with limited niche sharing (Gisbert et al., 1996; Stoffels and Humphries, 2003; MacDonald et al., 2012). Niche divergence, rather than convergence, is suggested, indeed, as a general pattern within invaded fish communities, except in cases of high invader abundance (Tran et al., 2015; Britton et al., 2018), a condition not observed in this study. Second, the different niche positioning in the three ponds indicated that the two species have developed different trophic, and maybe behavioral, strategies to coexist, depending on different trophic conditions, presumably mediated by different resource availability (e.g., habitat complexity and prey diversity and abundance). It is not new that resource availability can change significantly over space and time due to the presence of ecological gradients, such as seasonality and productivity, and that, in turn, this can affect species niches and competitive interactions (Abbey-Lee et al., 2013; Costa-Pereira et al., 2019). Here, we found that, in the oligotrophic shallow pond (FP), characterized by mixed macrophyte-covered bottoms and a high abundance of deposit feeders, the two fish species belonged to distinct benthic pathways, with SOM as the main basal carbon source for sand smelts, and macroalgae and seagrasses for mosquitofish. While habitat complexity would provide different niches that are partitioned by the two species (Beisel et al., 2000; MacDonald et al., 2012), the high abundance of food resources throughout the pond may have facilitated the integration of mosquitofish into the native food web by being able to exploit unused resources and thus avoid competitive interactions (Britton et al., 2018).

In contrast, in the ponds characterized by higher trophic state and lower habitat complexity (VE and ME), the Bayesian mixing models revealed that the two coexisting fish tended to rely on the same trophic pathway, rather than exploit distinct pathways, probably as an effect of the limited range of exploitable pathways under mesotrophic and hypereutrophic conditions. At the same time, the change in trophic positions and the reduction of the niche breadth (SEAb) observed for the native big-scale sand smelt from the oligotrophic to both mesotrophic and hypereutrophic ponds helped to recall the classical niche theories and found confirmation in several empirical studies. It has been postulated, indeed, that invasive species tend to out-compete native species through asymmetrical competitive mechanisms, such as by contracting and/or displacing the native's niche to lower or higher trophic positions due to their higher competitive ability (Vander Zanden et al., 1999; Jackson et al., 2012; Britton et al., 2018). Under this framework, the different patterns observed in the two ponds at higher trophic state may find justification in the different levels of biodiversity that characterizes them. While the harsh conditions of the guanotrophic VE support low-diversity communities featured by only benthic deposit feeders (i.e., chironomids, amphipods, and small gastropods) and epifaunal carnivorous palaemonid shrimps, the mesotrophic ME is characterized by high-diversity communities with benthic filter feeders and deposit feeders, as well as carnivorous polychaetes (Signa et al., 2015). Therefore, we suggest that, in the less diverse and harsher pond VE, the mosquitofish included plant materials in their diet to balance the decrease in animal prey abundance (Blanco et al., 2004; Kalogianni et al., 2014) and restricted the access of sand smelts to only a few high-order consumers, such as the juveniles of the palaemonid shrimps that thrive in the pond. In contrast, the higher structural and functional biodiversity of ME favored the invader's niche expansion, particularly evident in small specimens, consistent with the "resource diversity hypothesis" (MacArthur, 1969), and constrained the native species' diet to a few low-order consumers, such as epifaunal filter/deposit feeders.

Looking at the intraspecific level, the narrow niche breadth (SEAb), together with the high niche overlap (>90%) of small- and big-sized sand smelts from ME and VE, indicates a specialist diet across size classes, contrary to what was observed in FP where the wider niche of large specimens may indicate release from intraspecific competition (Britton et al., 2018). This clear spatial pattern of SEAb also indicates lower trophic diversity and variety of both exploited resources and trophic levels for both small and large specimens from VE and ME than FP. *A. boyeri* can shift between small hyperbenthic and epifaunal prey (e.g., isopods, amphipods, mysids, polychaetes, gastropods, and bivalves) in shallow vegetated coastal areas, because of its

high trophic plasticity (Vizzini and Mazzola, 2002, 2005; Chrisafi et al., 2007). Such flexible feeding habits, coupled with the high abundance, may have represented the winning strategy that allowed the sand smelt to accommodate a certain degree of niche contraction rather than its suppression.

In contrast, the mosquitofish *G. holbrooki* exhibited a low intraspecific niche overlap (∼20%) between size classes in all ponds and a clear niche narrowing from small to larger specimens, suggesting ontogenetic dietary specialization. The high niche breadth of the small mosquitofish indicated a clear generalist feeding behavior, as well as high trophic diversity and omnivory degree. Omnivory plays an important stabilizing role in spatially compressed food webs, alleviating the strong destabilizing force of top-down pressures potentially exerted by top predators (McCann et al., 2005). At the same time, the large among-individual variability may also indicate that individual mosquitofish use different foraging tactics feeding on only a subset of the available resources (Abbey-Lee et al., 2013) from different trophic pathways and levels, as a mechanism for reducing intraspecific competition (Matthews and Mazumder, 2004; Abbey-Lee et al., 2013) and ensuring population growth (Blanco et al., 2004). The eastern mosquitofish is acknowledged, indeed, not only as an opportunistic predator with a very wide prey spectrum, including zooplankton, insects, benthic invertebrates, fish, and amphibian larvae and eggs (Specziár, 2004; Pyke, 2005), but also as an omnivore able to ingest large amounts of algae and vegetal detritus in turbid and shallow estuaries and lakes (Blanco et al., 2004; Franco et al., 2008).

Lastly, assuming that the two species occupy a similar fundamental niche (i.e., the multidimensional environmental conditions within which a species can live in the absence of competitors, *sensu* Hutchinson, 1957), we infer that the native sand smelt has been induced to undergo different mechanisms of trophic displacement and/or contraction of its realized niche to coexist with the invasive mosquitofish. While this is consistent with the general adaptative response of native species subject to asymmetric competition with invaders exhibiting superior competitive abilities (Byers, 2000; Carey and Wahl, 2010; Tran et al., 2015), we provided evidence for the occurrence of site-specific environmental control on invaded trophic niches as a result of the combined effect of differing resource availability and habitat complexity.

Conclusion

We used a combination of isotopic niche analysis and Bayesian mixing models to reveal complex site-specific trophic relationships between the invasive eastern mosquitofish *Gambusia holbrooki* and the sympatric big-scale sand smelt *Atherina boyeri* co-occurring in shallow coastal ponds with different environmental features. The interplay of the trophic status and geomorphological features of the ponds influenced the availability of resources, in terms of prey diversity and habitat complexity, leading to site-specific mechanisms of trophic niche divergence. Moreover, under oligotrophic conditions, the high habitat complexity and abundances of benthic prey provided different niches that were partitioned by the two species. In contrast, under higher trophic state and lower habitat complexity, an asymmetric competition between the two species might have arisen due to the competitive superiority of mosquitofish, leading to a clear displacement and contraction of the sand smelt niche. At the same time, the broadening of the invader's niche, especially marked for small specimens, may have been driven by a high prey diversity level, consistent with the "resource diversity hypothesis" (MacArthur, 1969). Although a large body of literature exists on the ecological effects of invasive fish in coastal systems, trophic aspects have been scantly addressed especially in combination with environmental stressors. This research gives new insights into the mechanisms that promote the coexistence of invasive and native species in shallow and highly variable marine coastal systems. However, our study is limited by the short temporal context serving as a snapshot of the trophic relationships between invasive and native species under the trophic gradient that occurs during the productive spring season. Given the highly variable nature of coastal ponds, we did not exclude seasonal changes of the trophic relationships of the two fish species according to resource availability, which ensures the success of their long coexistence. Lastly, while we demonstrated the great potential of isotopic niche analysis for detecting complex ecosystem responses to invasion by NIS, additional studies are advocated to further understand the interaction between environmental stressors and fish resource partitioning on a larger temporal scale.

Data availability statement

The original contributions presented in the study are included in the article/Supplementary material, further inquiries can be directed to the corresponding author.

Ethics statement

Ethical review and approval was not required for the animal study because Samplings were conducted with permits from the Authority of the Laghetti di Marinello Nature Reserve (permit # 28599). No other permits were needed. All applicable international, national, and/or institutional guidelines for the care and use of animals were followed.

Author contributions

GS, SV conceived, designed, and supervised data integration and interpretation. CA performed the mixing models and isotopic niche analysis. CA, GS, and GC performed data analysis and interpretation. AM, SV funded the study. All authors contributed to the manuscript drafting and revision. All authors read and approved the submitted version.

Funding

This study was funded by the University of Palermo and CoNISMa-Marine Strategy.

Acknowledgments

The authors acknowledge the Director and the Staff of the Nature Reserve Laghetti di Marinello for the permission to work and the logistic support to access the study sites. The authors are also grateful to Andrea Savona for assistance during field activities and Elisa A. Aleo for help with laboratory analysis.

Conflict of interest

The authors declare that the research was conducted in the absence of any commercial or financial relationships that could be construed as a potential conflict of interest.

Publisher's note

All claims expressed in this article are solely those of the authors and do not necessarily represent those of their affiliated organizations, or those of the publisher, the editors and the reviewers. Any product that may be evaluated in this article, or claim that may be made by its manufacturer, is not guaranteed or endorsed by the publisher.

Supplementary material

The Supplementary Material for this article can be found online at: https://www.frontiersin.org/articles/10.3389/fevo.2022.958467/full#supplementary-material

References

Abbey-Lee, R. N., Gaiser, E. E., and Trexler, J. C. (2013). Relative roles of dispersal dynamics and competition in determining the isotopic niche breadth of a wetland fish. *Freshw. Biol.* 58, 780–792. doi: 10.1111/fwb.12084

Abrantes, K. G., Barnett, A., and Bouillon, S. (2014). Stable isotope-based community metrics as a tool to identify patterns in food web structure in east African estuaries. *Funct. Ecol.* 28, 270–282. doi: 10.1111/1365-2435.12155

Acquavita, A., Aleffi, I. F., Benci, C., Bettoso, N., Crevatin, E., Milani, L., et al. (2015). Annual characterization of the nutrients and trophic state in a Mediterranean coastal lagoon: the marano and grado lagoon (northern Adriatic Sea). *Reg. Stud. Mar. Sci.* 2, 132–144. doi: 10.1016/j.rsma.2015.08.017

Alcaraz, C., Bisazza, A., and García-Berthou, E. (2008). Salinity mediates the competitive interactions between invasive mosquitofish and an endangered fish. *Oecologia* 155, 205–213. doi: 10.1007/s00442-007-0899-4

Anderson, M. J. (2017). "Permutational multivariate analysis of variance (PERMANOVA)," in **** Wiley StatsRef: Statistics Reference Online* (Hoboken, NJ: Wiley), 1–15. doi: 10.1002/9781118445112.stat07841

Andolina, C., Franzoi, P., Jackson, A. L., Mazzola, A., and Vizzini, S. (2020). Vegetated habitats trophically support early development stages of a Marine migrant fish in a coastal lagoon. *Estuar. Coasts* 43, 424–437. doi: 10.1007/s12237-019-00683-2

Bearhop, S., Adams, C. E., Waldron, S., Fuller, R. A., and Macleod, H. (2004). Determining trophic niche width: a novel approach using stable isotope analysis. *J. Anim. Ecol.* 73, 1007–1012. doi: 10.1111/j.0021-8790.2004.00861.x

Beisel, J. N., Usseglio-Polatera, P., and Moreteau, J. C. (2000). The spatial heterogeneity of a river bottom: a key factor determining macroinvertebrate communities. *Hydrobiologia* 422–423, 163–171. doi: 10.1023/A:1017094606335

Blanco, S., Romo, S., and Villena, M. J. (2004). Experimental study on the diet of mosquitofish (*Gambusia holbrooki*) under different ecological conditions in a shallow lake. *Int. Rev. Hydrobiol.* 89, 250–262. doi: 10.1002/iroh.200310684

Britton, J. R., Ruiz-Navarro, A., Verreycken, H., and Amat-Trigo, F. (2018). Trophic consequences of introduced species: comparative impacts of increased interspecific vs. intraspecific competitive interactions. *Funct. Ecol.* 32, 486–495. doi: 10.1111/1365-2435.12978

Byers, J. E. (2000). Competition between two estuarine snails: implications for invasions of exotic species. *Ecology* 81, 1225–1239. doi: 10.1890/0012-9658(2000)081[1225:CBTESI]2.0.CO;2

Cano-Rocabayera, O., de Sostoa, A., Coll, L., and Maceda-Veiga, A. (2019). Managing small, highly prolific invasive aquatic species: exploring an ecosystem approach for the eastern mosquitofish (*Gambusia holbrooki*). *Sci. Total Environ.* 673, 594–604. doi: 10.1016/j.scitotenv.2019.02.460

Carey, M. P., and Wahl, D. H. (2010). Native fish diversity alters the effects of an invasive species on food webs. *Ecology* 91, 2965–2974. doi: 10.1890/09-1213.1

Carmona-Catot, G., Magellan, K., and García-Berthou, E. (2013). Temperature-specific competition between invasive mosquitofish and an endangered cyprinodontid fish. *PLoS ONE* 8, e54734. doi: 10.1371/journal.pone.0054734

Chan, F. T., and Briski, E. (2017). An overview of recent research in marine biological invasions. *Mar. Biol.* 164, 121. doi: 10.1007/s00227-017-3155-4

Chen, G., Wu, Z., Gu, B., Liu, D., Li, X., and Wang, Y. (2011). Isotopic niche overlap of two planktivorous fish in southern China. *Limnology* 12, 151–155. doi: 10.1007/s10201-010-0332-2

Chrisafi, E., Kaspiris, P., and Katselis, G. (2007). Feeding habits of sand smelt (*Atherina boyeri*, Risso 1810) in Trichonis Lake (Western Greece). *J. Appl. Ichthyol.* 23, 209–214. doi: 10.1111/j.1439-0426.2006.00824.x

Costa-Pereira, R., Araújo, M. S., Souza, F. L., and Ingram, T. (2019). Competition and resource breadth shape niche variation and overlap in multiple trophic dimensions. *Proc. R. Soc. B Biol. Sci.* 286, 1–9. doi: 10.1098/rspb.2019.0369

David, P., Thébault, E., Anneville, O., Duyck, P. F., Chapuis, E., and Loeuille, N. (2017). Impacts of invasive species on food webs: a review of empirical data. *Adv. Ecol. Res.* 56, 1–60. doi: 10.1016/bs.aecr.2016.10.001

Franco, A., Elliott, M., Franzoi, P., and Torricelli, P. (2008). Life strategies of fishes in European estuaries: the functional guild approach. *Mar. Ecol. Prog. Ser.* 354, 219–228. doi: 10.3354/meps07203

Gallardo, B., Clavero, M., Sánchez, M. I., and Vilà, M. (2016). Global ecological impacts of invasive species in aquatic ecosystems. *Glob. Chang. Biol.* 22, 151–163. doi: 10.1111/gcb.13004

Gisbert, E., Cardona, L., and Castelló, F. (1996). Resource partitioning among planktivorous fish larvae and fry in a Mediterranean coastal lagoon. *Estuar. Coast. Shelf Sci.* 43, 723–735. doi: 10.1006/ecss.1996.0099

Hutchinson, G. E. (1957). Concluding remarks, coldspring harbor symposium. *Quant. Biol.* 22, 415–427. doi: 10.1101/SQB.1957.022.01.039

Jackson, A. L., Inger, R., Parnell, A. C., and Bearhop, S. (2011). Comparing isotopic niche widths among and within communities: SIBER—stable isotope bayesian ellipses. *R. J. Anim. Ecol.* 80, 595–602. doi: 10.1111/j.1365-2656.2011.01806.x

Jackson, M. C., Donohue, I., Jackson, A. L., Britton, J. R., Harper, D. M., and Grey, J. (2012). Population-level metrics of trophic structure based on stable isotopes and their application to invasion ecology. *PLoS ONE* 7, 1–12. doi: 10.1371/journal.pone.0031757

Kalogianni, E., Giakoumi, S., Andriopoulou, A., and Chatzinikolaou, Y. (2014). Prey utilisation and trophic overlap between the non native mosquitofish and a native fish in two Mediterranean rivers. *Mediterr. Mar. Sci.* 15, 287–301. doi: 10.12681/mms.609

Kara, M. H., and Quignard, J. P. (2019). *Fishes in Lagoons and Estuaries in the Mediterranean 2: Sedentary Fish*. Hoboken, NJ: John Wiley and Sons, Inc. doi: 10.1002/9781119452768

Kenworthy, W. J., Durako, M. J., Fatemy, S. M. R., Valavi, H., and Thayer, G. W. (1993). Ecology of seagrasses in northeastern Saudi Arabia 1 year after the Gulf War oil spill. *Mar. Pollut. Bull.* 27, 213–222. doi: 10.1016/0025-326X(93)90027-H

Layman, C. A., Hammerschlag-peyer, C. M., Yeager, L. A., and Araújo, M. S. (2011). A hypothesis-testing framework for studies investigating ontogenetic niche shifts using stable isotope ratios. *PLoS ONE* 6, e27104. doi: 10.1371/journal.pone.0027104

Lowe, S., Browne, M., Boudjelas, S., and De Poorter, M. (2000). 100 of the World's worst invasive alien species: a selection from the global invasive species database. *Encycl. Biol. Invas.* 12, 159. doi: 10.1525/9780520948433-159

MacArthur, R. H. (1969). Patterns of communities in the tropics. *Biol. J. Linn. Soc.* 1, 19–30. doi: 10.1111/j.1095-8312.1969.tb01809.x

MacDonald, J. I., Tonkin, Z. D., Ramsey, D. S. L., Kaus, A. K., King, A. K., and Crook, D. A. (2012). Do invasive eastern gambusia (*Gambusia holbrooki*) shape wetland fish assemblage structure in south-eastern Australia? *Mar. Freshw. Res.* 63, 659–671. doi: 10.1071/MF12019

Mancinelli, G., Guerra, M. T., Alujević, K., Raho, D., Zotti, M., and Vizzini, S. (2017). Trophic flexibility of the Atlantic blue crab *Callinectes sapidus* in invaded coastal systems of the Apulia region (SE Italy): a stable isotope analysis. *Estuar. Coast. Shelf Sci.* 198, 421–431. doi: 10.1016/j.ecss.2017.03.013

Mancinelli, G., and Vizzini, S. (2015). Assessing anthropogenic pressures on coastal marine ecosystems using stable CNS isotopes: state of the art, knowledge gaps, and community-scale perspectives. *Estuar. Coast. Shelf Sci.* 156, 195–204. doi: 10.1016/j.ecss.2014.11.030

Matthews, B., and Mazumder, A. (2004). A critical evaluation of intrapopulation variation of $\delta^{13}C$ and isotopic evidence of individual specialization. *Oecologia* 140, 361–371. doi: 10.1007/s00442-004-1579-2

Mazzola, A., Bergamasco, A., Calvo, S., Caruso, G., Chemello, R., Colombo, F., et al. (2010). Sicilian transitional waters: current status and future development. *Chem. Ecol.* 26, 267–283. doi: 10.1080/02757541003627704

McCann, K. S., Rasmussen, J. B., and Umbanhowar, J. (2005). The dynamics of spatially coupled food webs. *Ecol. Lett.* 8, 513–523. doi: 10.1111/j.1461-0248.2005.00742.x

Michener, R. H., and Kaufman, L. (2008). "Stable isotope ratios as tracers in marine food webs: an update," in *Stable Isotopes in Ecology and Environmental Science, 2nd Edn*, eds R. Michener, and K. Lajtha (Hoboken, NJ: Blackwell Publishing Ltd), 238–282. doi: 10.1002/9780470691854.ch9

Mizutani, H., and Wada, E. (1988). Nitrogen and carbon isotope ratios in seabird rookeries and their ecological implications. *Ecology* 69, 340–349. doi: 10.2307/1940432

Nielsen, J. M., Clare, E. L., Hayden, B., Brett, M. T., and Kratina, P. (2018). Diet tracing in ecology: method comparison and selection. *Methods Ecol. Evol.* 9, 278–291. doi: 10.1111/2041-210X.12869

Occhipinti-Ambrogi, A. (2007). Global change and marine communities: alien species and climate change. *Mar. Pollut. Bull.* 55, 342–352. doi: 10.1016/j.marpolbul.2006.11.014

Olsson, K., Stenroth, P., Nyström, P., and Granéli, W. (2009). Invasions and niche width: does niche width of an introduced crayfish differ from a native crayfish? *Freshw. Biol.* 54, 1731–1740. doi: 10.1111/j.1365-2427.2009.02221.x

Post, D. M. (2002). Using stable isotopes to estimate trophic position: models, methods, and assumptions. *Ecology* 83, 703–718. doi: 10.1890/0012-9658(2002)083[0703:USITET]2.0.CO;2

Pyke, G. H. (2005). A review of the biology of *Gambusia affinis* and *G. holbrooki*. *Rev. Fish Biol. Fish.* 15, 339–365. doi: 10.1007/s11160-006-6394-x

R Core Team. (2020). *R: A Language and Environment for Statistical Computing*. Vienna: R Foundation for Statistical Computing. Available online at: https://www.R-project.org/

Rehage, J. S., Barnett, B. K., and Sih, A. (2005). Foraging behaviour and invasiveness: do invasive *Gambusia* exhibit higher feeding rates and broader diets than their noninvasive relatives? *Ecol. Freshw. Fish* 14, 352–360. doi: 10.1111/j.1600-0633.2005.00109.x

Remon, J., Bower, D. S., Gaston, T. F., Clulow, J., and Mahony, M. J. (2016). Stable isotope analyses reveal predation on amphibians by a globally invasive fish (*Gambusia holbrooki*). *Aquat. Conserv. Mar. Freshw. Ecosyst.* 26, 724–735. doi: 10.1002/aqc.2631

Rincón, P. A., Correas, A. M., Morcillo, F., Risueño, P., Lobón-Cerviá, J., Risueno, P., et al. (2002). Interaction between the introduced eastern mosquitofish and two autochthonous Spanish toothcarps. *J. Fish Biol.* 61, 1560–1585. doi: 10.1111/j.1095-8649.2002.tb02498.x

Ruiz-Navarro, A., Torralva, M., and Oliva-Paterna, F. J. (2013). Trophic overlap between cohabiting populations of invasive mosquitofish and an endangered toothcarp at changing salinity conditions. *Aquat. Biol.* 19, 1–11. doi: 10.3354/ab00512

Signa, G., Mazzola, A., Costa, V., and Vizzini, S. (2015). Bottom-up control of macrobenthic communities in a guanotrophic coastal system. *PLoS ONE* 10, e0117544. doi: 10.1371/journal.pone.0117544

Signa, G., Mazzola, A., Tramati, C. D., and Vizzini, S. (2013a). Gull-derived trace elements trigger small-scale contamination in a remote Mediterranean nature reserve. *Mar. Pollut. Bull.* 74, 237–243. doi: 10.1016/j.marpolbul.2013.06.051

Signa, G., Mazzola, A., and Vizzini, S. (2012). Effects of a small seagull colony on trophic status and primary production in a Mediterranean coastal system (Marinello ponds, Italy). *Estuar. Coast. Shelf Sci.* 111, 27–34. doi: 10.1016/j.ecss.2012.06.008

Signa, G., Mazzola, A., and Vizzini, S. (2021). Seabird influence on ecological processes in coastal marine ecosystems: an overlooked role? A critical review. *Estuar. Coast. Shelf Sci.* 250, 107164. doi: 10.1016/j.ecss.2020.107164

Signa, G., Tramati, C. D., and Vizzini, S. (2013b). Contamination by trace metals and their trophic transfer to the biota in a Mediterranean coastal system affected by gull guano. *Mar. Ecol. Prog. Ser.* 479, 13–24. doi: 10.3354/meps10210

Specziár, A. (2004). Life history pattern and feeding ecology of the introduced eastern mosquitofish, *Gambusia holbrooki*, in a thermal spa under temperate climate, of Lake Hévíz, Hungary. *Hydrobiologia* 522, 249–260. doi: 10.1023/B:HYDR.0000029978.46013.d1

Stock, B. C., Jackson, A. L., Ward, E. J., Parnell, A. C., Phillips, D. L., and Semmens, B. X. (2018). Analyzing mixing systems using a new generation of Bayesian tracer mixing models. *PeerJ* 6, e5096. doi: 10.7717/peerj.5096

Stoffels, R. J., and Humphries, P. (2003). Ontogenetic variation in the diurnal food and habitat associations of an endemic and an exotic fish in floodplain ponds: consequences for niche partitioning. *Environ. Biol. Fishes* 66, 293–305. doi: 10.1023/A:1023918420927

Tran, T. N. Q., Jackson, M. C., Sheath, D., Verreycken, H., and Britton, J. R. (2015). Patterns of trophic niche divergence between invasive and native fishes in wild communities are predictable from mesocosm studies. *J. Anim. Ecol.* 84, 1071–1080. doi: 10.1111/1365-2656.12360

Vander Zanden, M. J., Casselman, J. M., and Rasmussen, J. B. (1999). Food web consequences of species invasions in lakes. *Nature* 401, 464–467. doi: 10.1038/46762

Vizzini, S., and Mazzola, A. (2002). Stable carbon and nitrogen ratios in the sand smelt from a Mediterranean coastal area: feeding habits and effect of season and size. *J. Fish Biol.* 60, 1498–1510. doi: 10.1111/j.1095-8649.2002.tb02443.x

Vizzini, S., and Mazzola, A. (2005). Feeding ecology of the sand smelt *Atherina boyeri* (Risso 1810) (Osteichthyes, Atherinidae) in the western Mediterranean: evidence for spatial variability based on stable carbon and nitrogen isotopes. *Environ. Biol. Fishes* 72, 259–266. doi: 10.1007/s10641-004-2586-1

Vizzini, S., Savona, B., Thang, D. C., and Mazzola, A. (2005). Spatial variability of stable carbon and nitrogen isotope ratios in a Mediterranean coastal lagoon. *Hydrobiologia* 550, 73–82. doi: 10.1007/s10750-005-4364-2

Vizzini, S., Signa, G., and Mazzola, A. (2016). Guano-derived nutrient subsidies drive food web structure in coastal ponds. *PLoS ONE* 11, 1–15. doi: 10.1371/journal.pone.0151018

frontiers | Frontiers in Ecology and Evolution

TYPE Original Research
PUBLISHED 05 October 2022
DOI 10.3389/fevo.2022.942968

Check for updates

OPEN ACCESS

EDITED BY
Jason Newton,
University of Glasgow, United Kingdom

REVIEWED BY
W. Ryan James,
Florida International University, United States
Vincent Raoult,
The University of Newcastle, Australia

*CORRESPONDENCE
Alex S. J. Wyatt
wyatt@ust.hk

SPECIALTY SECTION
This article was submitted to Population, Community, and Ecosystem Dynamics, a section of the journal Frontiers in Ecology and Evolution

RECEIVED 13 May 2022
ACCEPTED 22 August 2022
PUBLISHED 05 October 2022

CITATION
Skinner C, Pei Y-D, Morimoto N, Miyajima T and Wyatt ASJ (2022) Stable isotopes elucidate body-size and seasonal fluctuations in the feeding strategies of planktivorous fishes across a semi-enclosed tropical embayment. *Front. Ecol. Evol.* 10:942968. doi: 10.3389/fevo.2022.942968

COPYRIGHT
© 2022 Skinner, Pei, Morimoto, Miyajima and Wyatt. This is an open-access article distributed under the terms of the Creative Commons Attribution License (CC BY). The use, distribution or reproduction in other forums is permitted, provided the original author(s) and the copyright owner(s) are credited and that the original publication in this journal is cited, in accordance with accepted academic practice. No use, distribution or reproduction is permitted which does not comply with these terms.

Stable isotopes elucidate body-size and seasonal fluctuations in the feeding strategies of planktivorous fishes across a semi-enclosed tropical embayment

Christina Skinner[1], Yu-De Pei[1], Naoko Morimoto[2], Toshihiro Miyajima[2] and Alex S. J. Wyatt[1,3]*

[1]Department of Ocean Science, The Hong Kong University of Science and Technology, Kowloon, Hong Kong SAR, China, [2]Department of Chemical Oceanography, Atmosphere and Ocean Research Institute, The University of Tokyo, Kashiwa, Japan, [3]Southern Marine Science and Engineering Guangdong Laboratory (Guangzhou), Guangzhou, China

Reef fish may switch feeding strategies due to fluctuations in resource availability or through ontogeny. A number of studies have explored these trophodynamics using carbon ($\delta^{13}C$) and nitrogen ($\delta^{15}N$) stable isotopes, but additional tracers such as sulfur isotopes ($\delta^{34}S$) show strong potential in systems, where $\delta^{13}C$ and $\delta^{15}N$ results are ambiguous. We tested the utility of adding $\delta^{34}S$ to conventional $\delta^{13}C$ and $\delta^{15}N$ analysis to detect seasonal and body size changes in resource use of two planktivorous damselfish, *Dascyllus reticulatus* and *Dascyllus trimaculatus* across the Puerto Galera embayment in the Philippines. We analyzed stable isotope ratios ($\delta^{13}C$, $\delta^{15}N$, and $\delta^{34}S$) in multiple fish tissues (liver, eye, and muscle) to represent different dietary time frames. We then compared fish tissue isotopes against particulate organic matter (POM) ($\delta^{13}C$ and $\delta^{15}N$) and POM suspension feeder (the tunicate *Polycarpa aurata*: $\delta^{13}C$, $\delta^{15}N$, and $\delta^{34}S$) across the same sites. There were size-based and seasonal differences in damselfish resource use, the latter of which was most pronounced in the fast-turnover liver. Small fish (<70 mm) demonstrated significant seasonality, appearing to switch their resource use between the rainy season and the dry season, while there was no seasonal variation in larger fish (>70 mm). This suggests that smaller fish across the embayment employ an opportunistic feeding strategy to take advantage of fluctuating resource availability, while larger fish exhibits more consistent resource use. Isotope ratios of tunicates and POM further confirmed strong seasonality in this system and a lack of a spatial isotopic gradient. $\delta^{15}N$ did not seem to contribute to consumer resource use patterns, while by contrast,

$\delta^{34}S$ fluctuated significantly between sampling periods and was crucial for demonstrating seasonality in resource use. We recommend including $\delta^{34}S$ when attempting to disentangle seasonal differences in resource use in aquatic food webs using stable isotopes.

KEYWORDS

damselfish, *Dascyllus trimaculatus*, *Dascyllus reticulatus*, multi-tissue analysis, sulfur isotope, carbon isotope, nitrogen isotope

Introduction

Coral reefs are exceptionally complex ecosystems with many internal and external resources available to the many consumers that they host (Hoegh-Guldberg and Dove, 2008). Due to the dynamic nature of these systems, resources fluctuate not only spatially, e.g., across environmental gradients of oceanic exposure (Wyatt et al., 2012b; Page et al., 2013; Zgliczynski et al., 2019), but also temporally, i.e., annually or across distinct seasons (Haas et al., 2010; Erler et al., 2019). Reef fish consumers may therefore alter their resource use according to what is available (Carreón-Palau et al., 2013; Fey et al., 2021), which affects the flow of energy across the entire coral reef food web. To date, seasonality in energy flows and consumer resource use on coral reefs has been poorly studied, with the majority of reef food web studies conducted over limited temporal windows (e.g., Thibodeau et al., 2013; Letourneur et al., 2017; Miller et al., 2019), despite the impact, this may have on the capacity to elucidate key trophodynamic processes (Skinner et al., in press).

In addition to temporal variation in consumer resource use from fluctuations in available material, organisms may change their resource use with ontogeny; as they grow larger they can access larger prey and/or take advantage of previously inaccessible resources (Layman et al., 2005; Cummings et al., 2010; Greenwood et al., 2010). Accessing different resources through ontogeny may provide populations with a degree of resilience to fluctuations in resource availability (Nakazawa, 2015), but there are also implications for the structure of the food web, i.e., as consumer resource use changes, so too does the energy transfer across subsequent trophic levels. Although the presence (or indeed absence) of body size-related changes in resource use is fairly well-documented in coral reef fish (Cocheret de la Morinière et al., 2003; Nakamura et al., 2008; O'Farrell et al., 2014; Plass-Johnson et al., 2015; Matley et al., 2017), interactions between body size and seasonality in resources are seldom considered. For example, do consumers from different size groups respond similarly to temporally fluctuating resources despite taxonomic, and apparent trophic grouping, similarities? Seasonality in basal resources and their use by higher trophic level consumers is highly evident in other equally dynamic systems such as embayments with seagrass beds (Morimoto et al., 2017) and temperate estuaries (Cobain et al., 2022), suggesting that more research into the intricacies of these dynamics on coral reefs is sorely needed.

Stable isotope analysis (SIA) is a useful tool for tracking energy flows and resource use across distinct trophic levels of a food web (Peterson and Fry, 1987; Boecklen et al., 2011). Rather than providing a snapshot view, such as those from traditional techniques, e.g., feeding observations and gut contents analyses, isotope ratios in consumer tissues represent material that has been ingested and assimilated over time, with different tissues representing different dietary time frames based on their rate of isotopic turnover (Tieszen et al., 1983). For example, muscle is a "slow" turnover tissue representing consumer diet over several months, while the liver is a "fast" turnover tissue, representing consumer diet over several weeks (Vander Zanden et al., 2015). While muscle is frequently used in SIA studies of coral reef systems, liver tissue is less often utilised (Skinner et al., in press; but see Roy et al., 2012; Davis et al., 2015; Matley et al., 2016). Studies are also beginning to perform SIA on fish eye lenses, as they have metabolically inert bands (laminae), which are successively deposited throughout their life span, allowing reconstruction of an individual's trophic history (Wallace et al., 2014; Bell-Tilcock et al., 2021). However, successfully dissecting and analyzing distinct bands of a fish's eye lens is time consuming, particularly for smaller species. Few studies have employed SIA of the whole eye (i.e., including the iris, cornea, and retina) despite it being a comparatively easier preparation. Although measuring stable isotope ratios across multiple consumer tissues can provide important information about the temporal dynamics of resource use, ~70% of coral reef food web SIA studies focus solely on a single tissue type (Skinner et al., in press). Furthermore, while studies regularly employ carbon ($\delta^{13}C$) and nitrogen ($\delta^{15}N$) stable isotopes to understand food web energy flows, sulfur ($\delta^{34}S$) is increasingly being used as a third tracer to disentangle sources in aquatic systems, as it can help determine the importance of benthic vs. pelagic inputs (Connolly et al., 2004; McCauley et al., 2014; Skinner et al., 2019b), and there is minimal fractionation across trophic levels

(Barnes and Jennings, 2007). As such, it may represent a highly useful tool for identifying seasonality in aquatic food webs.

To better understand seasonal fluctuations in reef food web dynamics, we set out to determine how the resource use of two damselfish (*Dascyllus reticulatus* and *Dascyllus trimaculatus*) varied seasonally and with body size across a semi-enclosed embayment in the Philippines, where primary production varies seasonally (San Diego-McGlone et al., 1995). These two species are well suited to investigate reef resource dynamics as follows: (1) they are known planktivores with a well-documented diet, and thought to play an important role in capturing available suspended material which then becomes available to higher trophic levels, (2) they are relatively site-attached so their isotope ratios represent the location at which they are caught, and (3) there are size-based behavioral differences in their habitat use as juveniles remain closely attached to small coral heads, while larger individuals exploit a large spatial area (Allen, 1991; Frédérich et al., 2009, 2016; Zikova et al., 2011; Wyatt et al., 2012a; Gajdzik et al., 2016). To further maximize the dietary information obtained from each individual, multiple tissue types assumed to have distinctly varying isotopic turnover rates were sampled (liver, whole eye, and muscle). Specifically, we asked: (1) does damselfish resource use vary seasonally and/or with body size? (2) Are patterns related to fluxes of available material and/or are they represented in the isotope ratios of other consumers of suspended material? and (3) How insightful is the addition of $\delta^{34}S$ as a tracer for exploring these food web dynamics?

Materials and methods

Study site

This study focused on five main sampling sites across the semi-enclosed embayment at Puerto Galera, Philippines (13.515°N, 120.96°E). Sites were chosen to represent the full range of hydrodynamic conditions across the embayment: they were located in two channels where water enters and exits the bay according to strong tidal currents, Manila Channel (MA) and Batangas Channel (BA), at an intermediary site (MB), and in the sheltered inner bay in the port of Muelle (MU) (**Figure 1**). An additional site outside the enclosed bay was established in Sabang (SA). The close proximity of the sites ensured that latitudinally driven differences in $\delta^{13}C$ values (e.g., Rau et al., 1982) would not confound the interpretation of the sample isotope values. Sampling was conducted during both the dry (monthly average rainfall March: ∼58 mm; March 2013: ∼19 mm) and the rainy seasons (monthly average rainfall September: ∼206 mm; September 2012: ∼305; September 2014: ∼219 mm) (World Weather Online, 2022). Water temperature in the dry season (March 2013) was 26.0 ± 0.3°C, while in the rainy season, it was 28.3 ± 0.6°C (September 2012) and 28.5 ± 0.5°C (September 2014). Available primary production (evidenced by levels of chlorophyll *a*) is higher during the dry season (March 2013: 0.39 ± 0.30 ppb; September 2012: 0.31 ± 0.18 ppb; Morimoto et al., unpublished data), while terrestrial run-off and levels of nitrate are higher during the rainy season (March 2013: 0.37 ± 0.30 μM; September 2012: 0.48 ± 0.51 μM; Morimoto et al., unpublished data; San Diego-McGlone et al., 1995).

Sample collection

Two species of planktivorous damselfish, the reticulate (*D. reticulatus*, n = 30) and the threespot dascyllus (*D. trimaculatus*, n = 25), were collected opportunistically at the five sites across the embayment by a SCUBA diver using either clove oil (smaller specimens) or a hand pole spear (larger specimens) in September 2012 (rainy season) and March 2013 (dry season). Additional *D. trimaculatus* (n = 4) were collected in October 2014 (rainy season). Both *D. reticulatus* and *D. trimaculatus* feed opportunistically on zooplankton, with smaller individuals predominantly occupying coral colonies, while larger individuals spend more time in the water column (Allen, 1991; Zikova et al., 2011; Frédérich et al., 2016; Gajdzik et al., 2016). To explore size-based changes in resource use, individuals were split into small (<70 mm) and large (>70 mm) size groups based on the size at maturity of other closely related *Dascyllus* species (*Dascyllus albisella*) (Booth, 1995).

To better characterize the available planktonic resources and energy pathways, particulate organic matter (POM) and a suspension feeding consumer (gold-mouth sea squirts, *Polycarpa aurata*, hereafter "tunicates") were also collected across the embayment. As POM baselines are inherently variable and difficult to characterize, tunicates may represent a time-integrated proxy for this pathway (Richoux and Froneman, 2009; Stowasser et al., 2012; Ménard et al., 2014). Tunicates were collected by the diver by hand (dry season n = 19; rainy season n = 29) to represent suspension feeders. Samples were stored and transported frozen (−20°C) until analysis. POM samples (dry season n = 15; rainy season n = 20) were collected (0–15 m) using a 10-L Van Dorn Sampler (Rigo) (**Supplementary Figures 1**, **2**). The collected water was immediately placed into acid-washed 10-L high-density polyethylene (HDPE) collapsible containers, which were filtered onto pre-combusted 47-mm GF/F filters (0.7 μm) within 6 h of collection prior to freezing (−20°C). The volume of water filtered through each GF/F was recorded based on the change in weight of the HDPE containers.

Voucher specimens of *D. reticulatus* (CECAM-AORI-AW003 and CECAM-AORI-AW007), *D. trimaculatus*

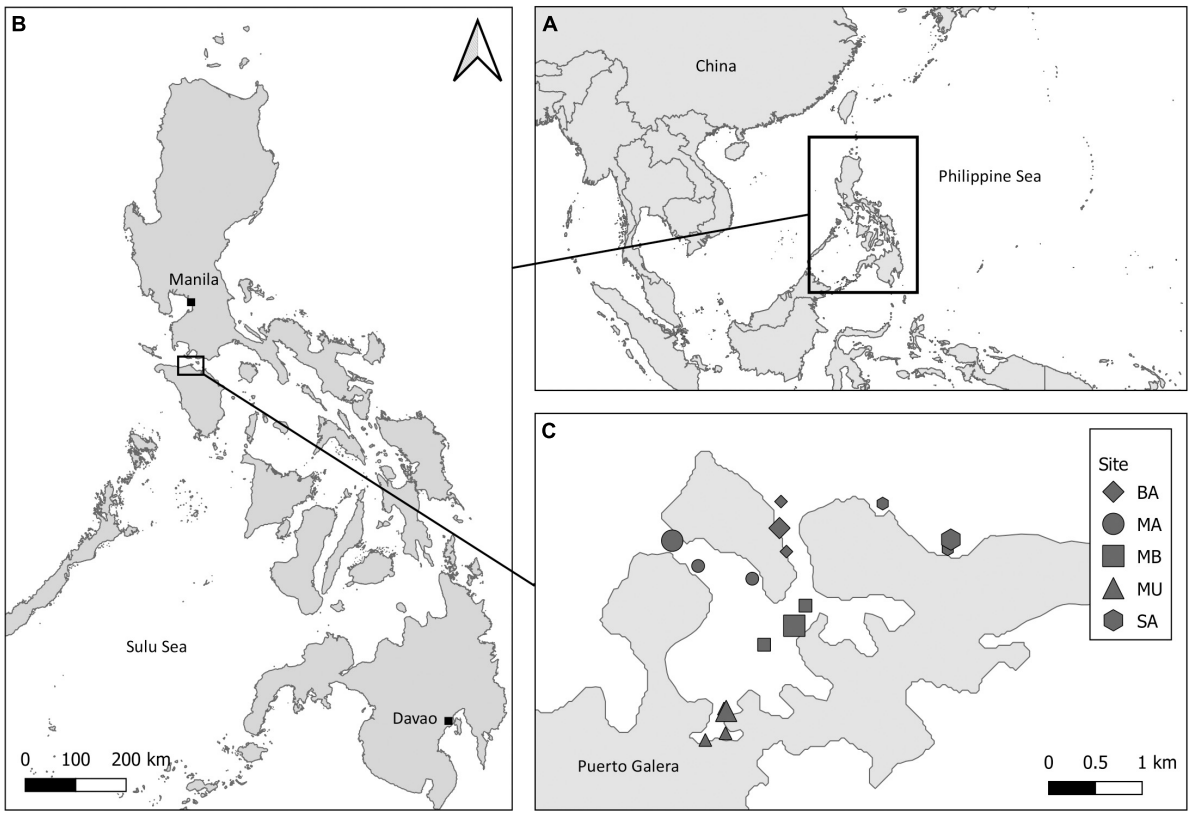

FIGURE 1
(A) Map of the world showing the location of **(B)** Philippines (12.8797° N, 121.7740° E) with **(C)** an inset showing the benthic sampling sites (large symbols: damselfish and tunicates) across the Puerto Galera embayment (13.515° N, 120.96° E). POM sampling locations are linked to nearby benthic sites (small black symbols and same shapes).

(CECAM-AORI-AW004), and *P. aurata* (CECAM-AORI-AW002 and CECAM-AORI-AW006) were deposited with the University of the Philippines' Marine Science Institute.

Sample processing and stable isotope analyses

Fish and tunicates were first thoroughly rinsed with deionized water to reduce the chances of contamination. Length and weight were measured for each *D. reticulatus* and *D. trimaculatus* before dissection of the liver, eye, and white muscle tissues. Total length (cm), the linear dimension between the tip of the snout and the end of the caudal fin, was measured using a Vernier caliper to the nearest millimeter. Weight (g) was measured with an analytical balance (PM400, Mettler Toledo, Columbus, OH, United States) to the nearest 0.1 g. The liver, eye, and white muscle tissues between the pectoral fin and caudal fin were carefully dissected from each specimen for SIA. For *P. aurata*, the incurrent and excurrent siphon tissues with the tunic attached were dissected as they were considered metabolically active (from constantly moving), and care was taken to avoid the inclusion of visceral organs, which may have different stable isotope signatures. All tissue samples were immediately transferred to individual 2 ml Eppendorf tubes after dissection, stored at −20°C, lyophilized (FreeZone 4.5 Liter Freeze Dryer, Labconco, United States) for 72 h, and ground to powder using a ball mill (Beads crusher μT-12, Taitec Ltd., Koshigaya, Saitama, Japan). Approximately ∼1.5 mg of ground samples of all tissue types were weighed into 5 × 9 mm tin capsules (Säntis Analytical, Teufen, Switzerland) on a microbalance (MC5, Sartorius, Göttingen, Germany). Where possible, if sufficient material was available, all samples were prepared in duplicate.

Particulate organic matter filters were freeze-dried and then fumigated with concentrated HCl for 48 h to remove inorganic carbonates. After fumigation, they were stored in a vacuum desiccator with several pellets of NaOH for ca. 1 week to remove excess acid. A half piece of each 47-mm filter sample was wrapped with a 10 × 9 mm silver capsule and a 10 × 9 mm tin capsule (Säntis Analytical, Teufen, Switzerland), and then pressed into a tablet using a hand-press tablet maker (internal diameter = 9 mm). The silver capsule was used to remove excess halogens that were normally contained in filter samples

and could poison catalysts in the Elemental Analyzer (EA). Combusted GF/F filters retain a small amount of carbon even after pre-combustion, so carbon content (calculated based on the filter C mass and the volume filtered, giving in $\mu g\ C\ L^{-1}$) and isotope ratios were blank-corrected based on analysis of a few unused filters that were acid-treated in a similar way as the sample filters.

Samples were analyzed for stable carbon, nitrogen, and sulfur in an EA IsoLink system (Thermo Fisher Scientific, Bremen, Germany) coupled with a Delta V Advantage isotope ratio mass spectrometer (IRMS) (Thermo Fisher Scientific, Bremen, Germany). Stable isotope ratios for $\delta^{15}N$, $\delta^{13}C$, and $\delta^{34}S$ are reported in delta notation (δ) which is: $[R_{Sample}/R_{Standard}-1]$, where R is the ratio of heavy-to-light isotopes and values are expressed in units of per mil (‰). Certified international reference materials were analyzed every six samples in all runs to correct the isotope values. Reference materials used for $\delta^{13}C$ and $\delta^{15}N$ were USGS40 (glutamic acid) and USGS-41A (glutamic acid enriched in ^{13}C and ^{15}N). Silver sulfide standards IAEA-S1 and IAEA-S2 were used for $\delta^{34}S$ correction. Internal reference material USGS-42 (Tibetan human hair powder) was placed in every ten samples for quality control and drift correction. Analytical precision across all reference materials was: $\delta^{13}C \leq 0.28$; $\delta^{15}N \leq 0.21$; and $\delta^{34}S \leq 0.84$. Two randomly spaced study-specific reference materials were also regularly analyzed to capture analytical variation: muscle tissue of *Salmo salar* and *Xiphias gladius* (analytical precision: $\delta^{13}C \leq 0.28$; $\delta^{15}N \leq 0.19$; and $\delta^{34}S \leq 1.2$; $n = 53$) (**Supplementary Table 1**).

Note that no $\delta^{34}S$ data are available for POM. While $\delta^{34}S$ analysis was not available for these samples, in addition, determination of $\delta^{34}S$ from POM (i.e., GF/F samples) can be technically difficult due to the contamination of seawater sulfate. The concentration of $SO4^{2-}$ in seawater is much higher (ca. 28 mM) than dissolved inorganic carbon (ca. 2 mM), and $SO4^{2-}$ is much more difficult than inorganic carbon to remove from samples without interference with organic carbon and total nitrogen analyses. As such, $\delta^{34}S$ could not have been determined accurately for POM, even if $\delta^{34}S$ analysis had been available. In addition, the $\delta^{34}S$ of phytoplankton is rarely measured directly, but often inferred from the $\delta^{34}S$ of organic-S in sinking particles or surface oxic sediment, or just assumed to be very similar to seawater sulfate (ca. +22‰) (cf. Trust and Fry, 1992).

Data analysis

Fish tissues with high lipid content can have biased $\delta^{13}C$ values due to the fractionation of carbon during lipid synthesis. If C:N ratios are >3.5, it is recommended that $\delta^{13}C$ values are corrected for lipid content (Sweeting et al., 2006; Post et al., 2007; Skinner et al., 2016). All fish tissues had a C:N ratio >3.5 (mean ± SD: liver 7.25 ± 2.66; eye 6.08 ± 1.65; and muscle 4.47 ± 1.17), so $\delta^{13}C$ values were mathematically corrected using a lipid normalization model following (Kiljunen et al., 2006), which changed $\delta^{13}C$ (mean ± SD) by 3.01 ± 1.35‰ (liver), 2.38 ± 0.93‰ (eye), and 1.4 ± 0.69‰ (muscle). This model is particularly appropriate for the correction of liver tissue as it accounts for non-linear relationships between $\delta^{13}C$ and C:N ratios as lipid content increases. High lipid levels in liver tissue may also influence $\delta^{34}S$ values: shark liver tissue $\delta^{34}S$ decreased by 4.6 ± 0.9‰ after chemical lipid extraction, but there was a minimal influence on muscle or fin tissue (Riverón et al., 2022). To account for the possible influence of high lipid levels on $\delta^{34}S$, damselfish liver $\delta^{34}S$ values were also corrected (−4.6‰). However, given the uncertainty in applying this correction factor to planktivorous reef fish, raw liver $\delta^{34}S$ values were used in all analyses in the main text, while lipid-corrected $\delta^{34}S$ analyses are reported in the **Supplementary material**. Lipid removal is not required for tunicate tissues as despite high C:N ratios (mean ± SD, 7.18 ± 1.09), they have low amounts of lipids (Hagen, 1988; Pakhomov et al., 2019). Similarly, unless nutrients are highly limited (leading to increased lipid storage and reduced growth; Mayzaud et al., 1989; Mock and Gradinger, 2000), pelagic POM lipid levels are low, and removal is not required (Søreide et al., 2006).

Since only the large (>70 mm) *D. trimaculatus* were collected in two separate rainy seasons (2012 and 2014), mixed-effects models were used to determine whether we could pool samples from each rainy season into one group. Using the R package *lme4* v 1.1-26 (Bates et al., 2015), a model was run for each isotope ($\delta^{13}C$, $\delta^{15}N$, or $\delta^{34}S$ as the response variable), with year, site, and their interaction as fixed effects, and tissue type (i.e., liver, eye, or muscle) as a random effect (random intercept). ANOVA determined whether the fixed effects were significant or not. While $\delta^{15}N$ varied significantly among sites overall, and $\delta^{34}S$ varied significantly between years overall, none of the isotopes varied significantly when considering the interaction between Year × Site, indicating no temporal differences at the site level. As such, for each site, large *D. trimaculatus* samples from 2012 to 2014 were pooled (**Supplementary Table 2**).

To explore changes in resource use across different size ranges, rather than separating samples by species, we grouped fish samples into small (<70 mm) and large (>70 mm) size groups. However, first, we used mixed-effects models (R package lme4 v. 1.1-26; Bates et al., 2015) to see whether there was a significant difference in isotope ratios between species within each size group. A model was run for each isotope ($\delta^{13}C$, $\delta^{15}N$, or $\delta^{34}S$ as the response variable), species as a fixed effect, and site, season, and tissue as random effects. There were no significant differences in $\delta^{13}C$, $\delta^{15}N$, or $\delta^{34}S$ between species for the small size group, so samples from both species were pooled into one "Small" group. For the large size group, there were no significant differences in $\delta^{13}C$ or $\delta^{34}S$ between species, but there was a marginally significant difference in $\delta^{15}N$ ($p = 0.04$). Upon inspection, the large group contained only one individual *D. reticulatus*, and its $\delta^{15}N$ values were within the ranges of those of the *D. trimaculatus*, so all large samples were considered

as one "Large" group (**Supplementary Table 3**). Consequently, for all remaining analyses, damselfish were considered as either small (<70 mm) or large (>70 mm) and sampled during the dry (March) or rainy (September) season.

Size and seasonal effects on isotope ratios in fish tissues

Length–weight and length–isotope relationships were initially explored for all fish across the embayment using regression analysis. Length–weight relationships were assessed using an exponential regression model with length (mm) as the response variable and log (weight) (g) as the predictor variable. To explore relationships between fish length (mm) and isotope ratios, and how this varied between seasons, a linear regression was used for each tissue, with the isotope ($\delta^{13}C$, $\delta^{15}N$, or $\delta^{34}S$) as the response variable and fish length (mm) and the interaction between fish length and season (dry/rainy) as predictor variables. ANOVA determined whether the fixed effects were significant or not. Where there was no significant effect of the interaction between fish length and season, the regression was rerun with only fish length (mm) as the predictor variable and all fish were pooled.

Different tissue types will vary in their natural isotopic discrimination making direct comparisons of seasonal effects among tissues problematic. To validate possible discrimination effects, we first adjusted tissues for tissue-dependent fractionation (Δ). In teleost fish, mean $\Delta^{13}C$ in the liver is 1.1‰ lower than in muscle, and mean $\Delta^{15}N$ is 0.9‰ lower (Canseco et al., 2022). For fish eye tissue, there is a 1:1 relationship with muscle $\delta^{13}C$, while $\delta^{15}N$ of eye tissue is ∼2‰ lower (Kanaya et al., 2019). However, isotopic differences between eye lens and muscle protein ($\Delta^{13}C$ and $\Delta^{15}N$) are <1‰, so likely obscured by analytical error (Quaeck-Davies et al., 2018). Finally, $\Delta^{34}S$ is minimal in teleost fish (Barnes and Jennings, 2007; Bell-Tilcock et al., 2021). As such, for all further analyses, we corrected liver tissue $\delta^{13}C$ and $\delta^{15}N$ by +1.1 and +0.9‰, respectively, but no correction factor was applied to eye $\delta^{13}C$ and $\delta^{15}N$, or to any $\delta^{34}S$ values.

To determine whether resource use varied between fish size groups and seasons across the three tissue types, we first examined each isotope individually (univariate), and then all three isotopes together (multivariate). For the univariate analyses, we ran mixed-effects models with a Bayesian framework in the R package *MCMCglmm* (Hadfield, 2010). By using a Bayesian framework, these models control for heterogeneity in variances and sample sizes and provide a mean estimate with 95% credible intervals for each parameter. For each tissue type (liver, eye, and muscle), we ran a separate model for each isotope ($\delta^{13}C$, $\delta^{15}N$, or $\delta^{34}S$). For $\delta^{13}C$, models were also run with raw (uncorrected) $\delta^{13}C$ values to assess the effect of the lipid correction on the results, while for liver $\delta^{34}S$, models were also run with the lipid-corrected values. Fixed effects were size (small/large), season (dry/rainy), and their interaction, while site was included as a random effect (random intercept). Models were run with Gaussian error distributions and informative priors (V = 1 as an inverse gamma distribution and a low degree of belief nu = 2 for more sampling space). For liver and eye, models were run with 4,000,000 iterations, a burn-in of 3,000,000, and a thinning interval of 300. Due to convergence issues, models were run with 6,000,000 iterations, a burn-in of 4,500,000, and a thin of 400, for muscle tissue. For each model, autocorrelation and convergence were assessed by checking the model trace plots and Geweke diagnostic to ensure less than 5% of the variables were outside the 95% CI.

To further explore fish resource use when considering all three isotopes, we used a principal component analysis (PCA) using the R package *FactoMineR* v.2.4 (Lê et al., 2008). This method visualizes patterns in the dataset with the PCA loadings providing a statistical estimate of the variables driving separation between the groups. Finally, to test the seasonal and tissue-specific differences in multivariate isotope ratios, we ran a Euclidean Permanova with 9,999 permutations for each fish size group using the R package vegan v2.5-7 (Oksanen et al., 2020). To explore how high lipid content in liver tissue might confound results when considering all three isotopes, we also ran the PCA and PERMANOVA using the lipid-corrected liver $\delta^{34}S$ values.

Suspension feeders and resource availability

For the tunicates ($\delta^{13}C$, $\delta^{15}N$, and $\delta^{34}S$) and POM ($\delta^{13}C$, $\delta^{15}N$) isotope ratios and the particulate organic carbon (POC) (μg/L) and particulate organic nitrogen (PON) (μg/L) sampled across the embayment in both seasons, a two-way ANOVA was carried out for each group to determine whether the isotope ratios or concentrations varied spatially or seasonally, with the isotope as the response variable, and season, site, and their interaction as factors. Tukey's honestly significant difference (HSD) test for multiple comparisons was used to identify significant differences between groups. The Shapiro–Wilk and Levene's tests were used to confirm that data conformed to normality and homoscedasticity of variances, respectively.

For all models, model normality and homogeneity assumptions were checked by plotting model residuals. All statistical analyses were conducted in R Statistical Software 4.1.0 (R Core Team, 2021) and RStudio v. 1.4.1717 (R Studio Team, 2020).

Results

A total of 33 small (<70 mm) and nine large (>70 mm) damselfish were sampled in the dry season (March 2013), and

nine small and nine large damselfish were sampled in the rainy season (September 2012 and 2014) across the embayment (Figure 2; Supplementary Tables 4, 5). Total ranges in isotope ratios across fish tissues were always narrower in the rainy season. In the dry season, fish $\delta^{13}C$ ranged across ~4.4‰ (−19.7 large liver to −15.3 small muscle), while in the rainy season, $\delta^{13}C$ ranged across ~4.1‰ (−19.4 large liver to −15.3 large muscle). For $\delta^{15}N$, dry season values ranged across ~4.5‰ (6.0 small liver to 10.4 large muscle), while in the rainy season, $\delta^{15}N$ ranged across ~4.1‰ (6.5 small eye to 10.6 large muscle). Finally, dry season $\delta^{34}S$ ranged across ~5.3‰ (19.5 small eye and large muscle to 24.75 small liver) but rainy season $\delta^{34}S$ ranged across ~4.9‰ (18.4 small muscle to 23.25 large liver) (Figure 2).

Size and seasonal effects on isotope ratios in fish tissues

The exponential relationship between fish length (mm) and body weight (g) was highly significant ($R^2 = 0.97$, $F_{1,52} = 1732$, $p \leq 0.001$; Figure 3A). For the isotope ratios, a significant positive relationship with fish length (mm) was found for eye $\delta^{13}C$ ($R^2 = 0.48$, $F_{1,56} = 52.2$, $p \leq 0.001$; Figure 3B) but a weak negative relationship with liver $\delta^{34}S$ ($R^2 = 0.11$, $F_{1,54} = 6.9$, $p = 0.01$; Figure 3D). In some cases, there was a significant interaction of fish length with season, so regression analyses were run for each season separately. For both eye and muscle $\delta^{15}N$, there were highly significant positive relationships with fish length in both the dry (eye: $R^2 = 0.70$, $F_{1,39} = 91.02$, $p \leq 0.001$; muscle: $R^2 = 0.38$, $F_{1,40} = 24.12$, $p \leq 0.001$) and the rainy season (eye: $R^2 = 0.81$, $F_{1,15} = 62.26$, $p \leq 0.001$; muscle: $R^2 = 0.74$, $F_{1,14} = 40.71$, $p \leq 0.001$) (Figure 3C). However, for muscle $\delta^{13}C$, relationships with fish length were significant in the dry ($R^2 = 0.71$, $F_{1,40} = 25.58$, $p \leq 0.001$) but not the rainy season ($R^2 = 0.01$, $F_{1,14} = 0.05$, $p = 0.825$) (Figure 3B). There were no significant relationships between fish length (mm) and muscle or eye $\delta^{34}S$, and liver $\delta^{13}C$ or $\delta^{15}N$ (Figure 3).

Differences in fish resource use between size groups and seasons were then determined using mixed-effects models within a Bayesian framework, which also provides a marginal and a conditional R^2 value (Table 1). Marginal R^2 (R^2_M) describes the proportion of model variance that is explained by the fixed effects (i.e., size, season, and their interaction), while conditional R^2 (R^2_C) describes the proportion of model variance that is explained by both the fixed and the random (i.e., including site) effects. For muscle tissue $\delta^{13}C$, there was a significant effect on size, and there was a significant interaction between size and season (mean ± SD, small dry: −17.57 ± 0.82 and rainy: −16.25 ± 0.20; large dry: −16.41 ± 0.48 and rainy: −16.24 ± 0.55), while for muscle $\delta^{15}N$, there was only a significant effect of size (mean ± SD, small: 9.64 ± 0.29; l: 10.07 ± 0.29). Marginal R^2 values confirmed that the fixed effects size and season described a good proportion of the variability in $\delta^{13}C$ ($R^2_M = 0.46$), but less so for $\delta^{15}N$ ($R^2_M = 0.26$; Table 1).

The patterns were similar in eye tissue. For eye $\delta^{13}C$, there was a significant effect of size, season, and a significant interaction between size and season (mean ± SD, small dry: −18.47 ± 0.76 and rainy: −16.87 ± 0.61; large dry: −17.16 ± 0.66 and rainy: −16.13 ± 0.46). For $\delta^{15}N$, there was only a significant effect of size (mean ± SD, small: 7.95 ± 0.40; large: 9.06 ± 0.36). Season and size described a high proportion of the variance in eye $\delta^{13}C$ ($R^2_M = 0.55$) and also $\delta^{15}N$ ($R^2_M = 0.51$). There were no significant effects on muscle or eye $\delta^{34}S$, and marginal R^2 values were low (R^2_M muscle = 0.02; eye = 0.00). The random effect of site did not describe the variance in muscle $\delta^{13}C$ ($R^2_C = 0.10$), $\delta^{15}N$ ($R^2_C = 0.12$), or $\delta^{34}S$ ($R^2_C = 0.06$), or in eye $\delta^{13}C$ ($R^2_C = 0.21$) or $\delta^{15}N$ ($R^2_C = 0.14$), however, it did for eye $\delta^{34}S$ ($R^2_C = 0.58$) (Table 1).

For liver tissue, patterns were different; there were no significant size or seasonal effects on $\delta^{13}C$ or $\delta^{15}N$, and marginal R^2 was low (R^2_M $\delta^{13}C = 0.06$; $\delta^{15}N = 0.11$). However, for $\delta^{34}S$, there were significant effects of size and a significant interaction between size and season (mean ± SD, small dry: 23.33 ± 1.28 and rainy: 21.27 ± 0.86; large dry: 22.21 ± 0.62 and rainy: 21.72 ± 1.39). These fixed effects described a higher proportion of the $\delta^{34}S$ variance ($R^2_M = 0.25$), while the random effect of site described a high proportion of variance across all three isotopes (R^2_C $\delta^{13}C = 0.59$; $\delta^{15}N = 0.24$; and $\delta^{34}S = 0.36$) (Table 1). Model results for lipid-corrected liver $\delta^{34}S$ values followed the same patterns (Supplementary Figure 1; Supplementary Table 6).

Models run on the raw (uncorrected) $\delta^{13}C$ values revealed mostly similar patterns for muscle and eye (Supplementary Table 7). For muscle, there was still a significant effect of size, and for eye, size and season were still significant. However, for both muscle and eye, the interaction between size and season was only marginally significant. For liver raw $\delta^{13}C$, unlike for the corrected values, there were significant effects of size and a significant interaction between size and season (Supplementary Table 6).

Patterns in resource use between seasons were visualized for each size group using a PCA generated from tri-isotope data ($\delta^{13}C$, $\delta^{15}N$, and $\delta^{34}S$). For small fish, seasons were separated largely along with PC1, which explained 58.1% of the variation in the data. This axis was strongly influenced by $\delta^{13}C$. Tissue differences were separated along with PC2 and influenced by $\delta^{15}N$ and $\delta^{34}S$. Both dry season liver and eye ellipses, and rainy season liver and eye ellipses overlapped, but there was no seasonal overlap of the same tissue type (Figure 4A). Differences between season ($F_{1,119} = 19.61$, $p < 0.001$), among tissues ($F_{2,119} = 45.75$, $p < 0.001$), and their interaction ($F_{2,119} = 4.51$, $p = 0.003$) were all significant (PERMANOVA, 9,999 permutations).

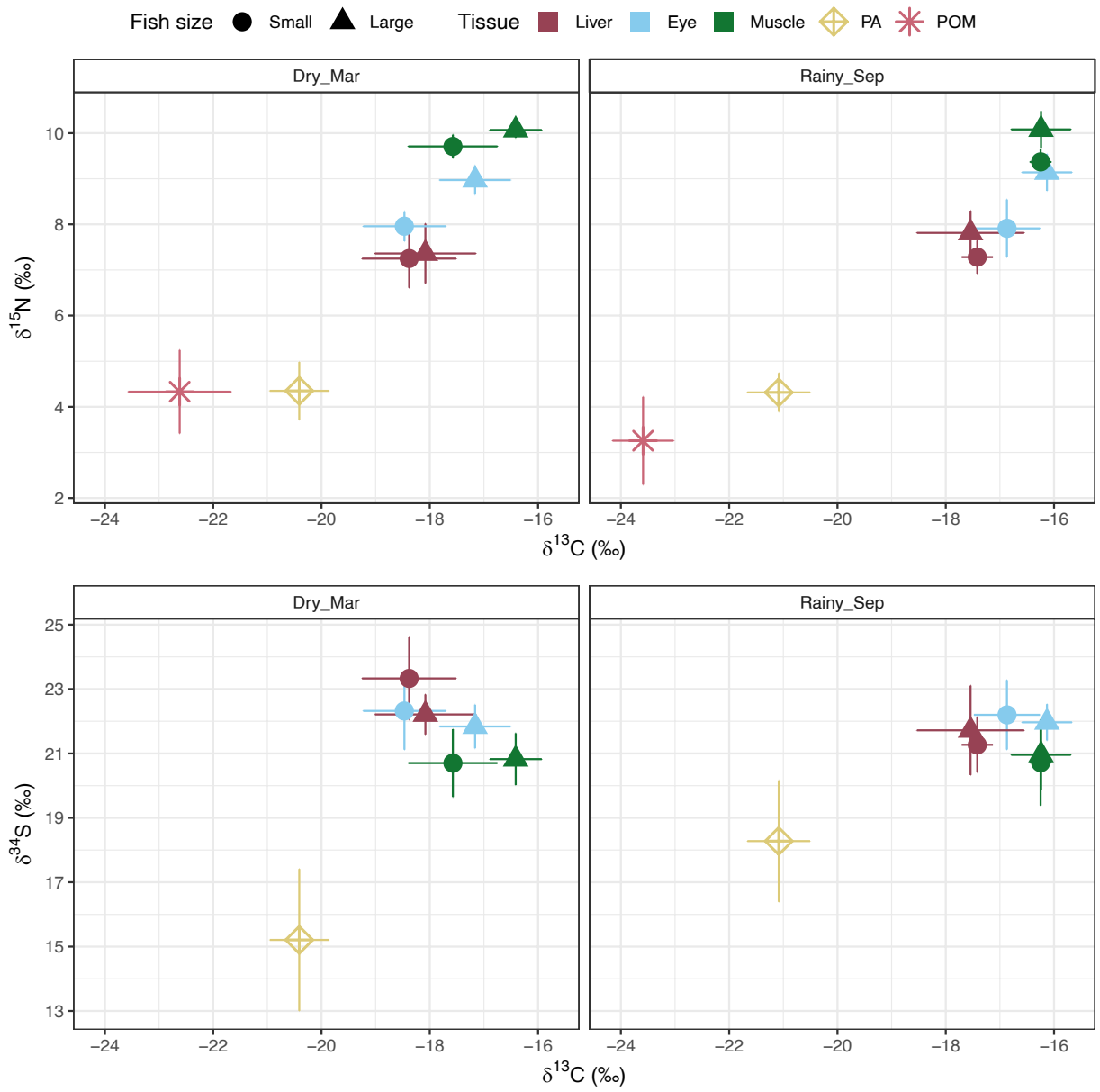

FIGURE 2
Isotope biplots of mean ± standard deviation $\delta^{13}C$ and $\delta^{15}N$ (top) and $\delta^{13}C$ and $\delta^{34}S$ (bottom panels) for all samples collected across the five sites in the dry season (March 2013) and the rainy season (September 2012 and 2014). $\delta^{13}C$ values are mathematically corrected for high lipid content (see section "Materials and methods"). PA = tunicate, *Polycarpa aurata*. POM, particulate organic matter. Damselfish are either small (<70 mm) or large (>70 mm). Note, no $\delta^{34}S$ data are reported for POM (see section "Materials and methods": Sample processing and stable isotope analyses).

For large fish, tissues were separated along PC2 (21.4% of the variation), predominantly influenced by $\delta^{34}S$ and $\delta^{15}N$, and differences were significant (PERMANOVA, 9,999 permutations, $F_{1,51} = 12.44$, $p < 0.001$). $\delta^{13}C$ was the primary variable leading to separation along PC1 (**Figure 4B**). In contrast to the small fish, large-fish ellipses from each season overlapped, with the exception of eye tissue, and, while there was a marginally significant overall difference between seasons (PERMANOVA, 9,999 permutations, $F_{1,51} = 3.43$, $p = 0.03$), the interaction between seasons and tissues was not significant ($F_{2,51} = 1.07$, $p = 0.37$).

The PCA using the lipid-corrected liver $\delta^{34}S$ values revealed a similar separation to the PCA using the raw $\delta^{34}S$ values (**Supplementary Figure 4**). However, unlike the raw values, the PERMANOVA using the corrected $\delta^{34}S$ values identified no significant differences among tissues for the large fish; for small

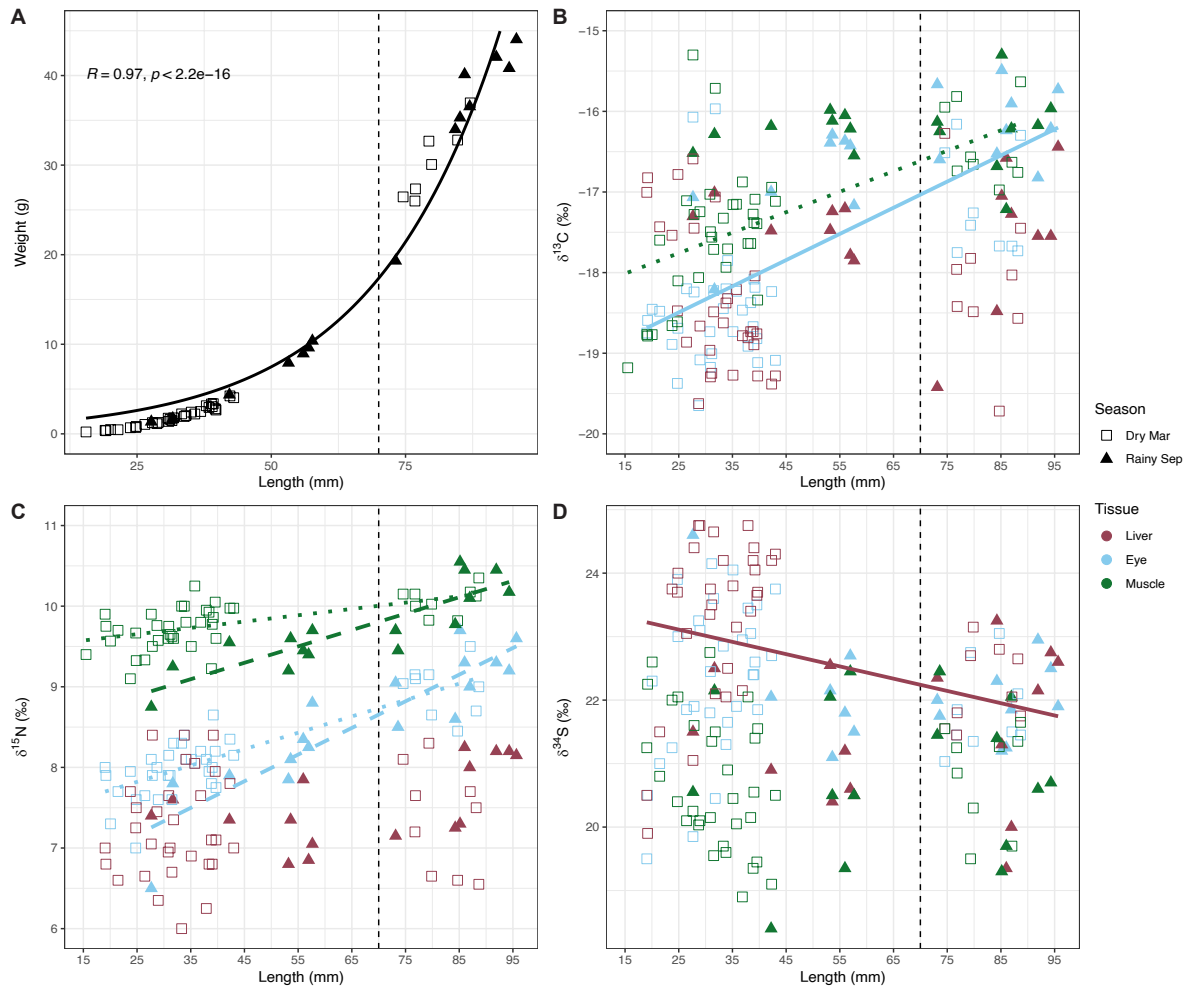

FIGURE 3
Relationships of fish **(A)** weight (g), **(B)** $\delta^{13}C$, **(C)** $\delta^{15}N$, and **(D)** $\delta^{34}S$ data plotted against length (mm). For the isotope ratios **(B–D)**, only significant relationships from the regression analysis models are plotted for each tissue. Solid lines represent fish across both seasons ($\delta^{15}N$), dotted lines represent fish in the dry season, and dashed lines represent fish in the rainy season ($\delta^{13}C$ and $\delta^{34}S$). $\delta^{13}C$ values are mathematically corrected for high lipid content (see section "Materials and methods").

fish, the interaction between season and tissue was no longer significant (Supplementary material).

Suspension feeders and resource availability

There was evidence of seasonality in tunicate $\delta^{13}C$ and $\delta^{34}S$ as season, and the interaction between season and site had a significant influence on both $\delta^{13}C$ (season: $F_{1,47} = 19.54$, $p < 0.001$; season × site: $F_{4,47} = 3.12$, $p = 0.03$) and $\delta^{34}S$ (season: $F_{1,47} = 49.82$, $p < 0.001$; season × site: $F_{4,47} = 9.56$, $p < 0.001$) isotope ratios (Supplementary Table 8; Figures 5A,C). While $\delta^{13}C$ was higher in the dry season (mean ± SD, −20.41 ± 0.54‰) than in the rainy (−21.08 ± 0.58‰), $\delta^{34}S$ was higher in the rainy season (18.28 ± 1.89‰) than the dry (15.21 ± 2.21‰). There were no spatial gradients in either $\delta^{13}C$ or $\delta^{34}S$ (Supplementary Table 8), but there were significant spatial differences in tunicate $\delta^{15}N$ ($F_{4,24} = 3.47$, $p = 0.02$); $\delta^{15}N$ was significantly higher at MU compared to MA and SA ($p = 0.02$, respectively). However, $\delta^{15}N$ did not vary seasonally (Supplementary Table 8); values were consistent across both dry (4.35 ± 0.63‰) and rainy (4.32 ± 0.42‰) seasons (Figure 5B).

Particulate organic matter $\delta^{13}C$ and $\delta^{15}N$ varied significantly between seasons ($F_{1,24} = 10.37$, $p = 0.02$ and $F_{1,24} = 9.98$, $p = 0.02$, respectively; Supplementary Table 8; Figures 5D,E), with higher mean $\delta^{13}C$ and $\delta^{15}N$ in the dry season ($\delta^{13}C$: −22.62 ± 0.95‰; $\delta^{15}N$: 4.33 ± 0.92‰) compared to the rainy season ($\delta^{13}C$: −23.59 ± 0.56‰; $\delta^{15}N$: 3.26 ± 0.96‰). There was

TABLE 1 Mixed-effects model parameter estimates exploring size and seasonal effects on fish $\delta^{13}C$, $\delta^{15}N$, and $\delta^{34}S$.

Predictors	$\delta^{13}C$		$\delta^{15}N$		$\delta^{34}S$	
Muscle (n = 3750)	**Estimate**	**95% CI**	**Estimate**	**95% CI**	**Estimate**	**95% CI**
Intercept	−16.44	**−17.00 to −15.89**	10.04	**9.77 to 10.33**	20.86	**20.00 to 21.74**
Small (<70 mm)	−1.12	**−1.65 to−0.58**	−0.34	**−0.58 to −0.07**	−0.16	−0.95 to 0.66
Rainy	0.18	−0.50 to 0.88	0.01	−0.32 to 0.30	0.16	−0.93 to 1.18
Small:Rainy	1.21	**0.34 to 2.11**	−0.32	−0.73 to 0.08	−0.24	−1.54 to 1.10
Random Effects						
Intercept Variance	0.17	0.00 to 0.47	0.05	0.00 to 0.16	0.27	0.00 to 1.01
Residual Variance	0.50	0.33 to 0.69	0.11	0.07 to 0.15	1.19	0.76 to 1.63
Marginal r^2	0.46	0.24 to 0.59	0.26	0.08 to 0.49	0.02	0.00 to 0.14
Conditional r^2	0.56	0.28 to 0.70	0.38	0.19 to 0.71	0.06	0.00 to 0.49
Eye (n = 3334)	**Estimate**	**95% CI**	**Estimate**	**95% CI**	**Estimate**	**95% CI**
Intercept	−17.14	**17.95 to −16.36**	8.95	**8.54 to 9.34**	21.83	**20.52 to 23.12**
Small (<70 mm)	−1.24	**−1.67 to −0.78**	−0.97	**−1.31 to −0.65**	0.40	−0.23 to 0.99
Rainy	0.86	**0.31 to 1.44**	0.08	−0.29 to 0.52	0.39	−0.36 to 1.17
Small:Rainy	0.70	**0.01 to 1.49**	−0.09	−0.62 to 0.43	−0.29	−1.25 to 0.71
Random Effects						
Intercept Variance	0.70	0.00 to 2.31	0.12	0.00 to 0.42	2.37	0.00 to 7.38
Residual Variance	0.36	0.22 to 0.50	0.18	0.12 to 0.25	0.66	0.41 to 0.92
Marginal r^2	0.55	0.20 to 0.71	0.51	0.21 to 0.68	0.00	0.00 to 0.10
Conditional r^2	0.76	0.62 to 0.93	0.65	0.45 to 0.82	0.58	0.31 to 0.97
Liver (n = 3334)	**Estimate**	**95% CI**	**Estimate**	**95% CI**	**Estimate**	**95% CI**
Intercept	−16.96	**−18.17 to −15.81**	8.40	**7.80 to 9.06**	22.31	**20.87 to 23.73**
Small (<70 mm)	−0.21	−0.64 to 0.32	−0.23	−0.66 to 0.22	0.9	**0.17 to 1.60**
Rainy	0.35	−0.24 to 0.97	0.34	−0.24 to 0.89	−0.29	−1.24 to 0.59
Small:Rainy	0.45	−0.39 to 1.23	−0.62	−1.39 to 0.09	−1.84	**−3.09 to −0.64**
Random Effects						
Intercept Variance	1.73	0.06 to 5.52	0.31	0.00 to 1.00	2.66	0.06 to 7.78
Residual Variance	0.36	0.23 to 0.51	0.34	0.21 to 0.48	0.88	0.53 to 1.22
Marginal r^2	0.06	0.00 to 0.22	0.11	0.01 to 0.27	0.27	0.02 to 0.42
Conditional r^2	0.65	0.45 to 0.99	0.35	0.07 to 0.80	0.63	0.44 to 0.945

$\delta^{13}C$ values have been mathematically corrected for high lipid content, and liver $\delta^{13}C$ and $\delta^{15}N$ have been corrected for tissue-dependent fractionation (see Section "Materials and methods"). Intercept values represent the average isotope value for a large (>70 mm) in the dry season. Estimates are means with 95% credible intervals (CI). Bold indicates non-overlapping CI. Marginal R^2 is the variance explained only by fixed effects, conditional R^2 is the variance explained by the entire model (fixed and random effects).

no significant effect of site, or of the interaction between season and site, on either $\delta^{13}C$ or $\delta^{15}N$ (**Supplementary Table 8**).

In contrast, while there was no seasonality in concentrations of POC and PON, there was a significant spatial gradient. For POC and PON, season, the interaction between seasons, and site, were non-significant (ANOVA, $p > 0.05$), while the effect of site was significant (POC: $F_{10,24} = 5.78$, $p = 0.02$; PON: $F_{10,24} = 8.08$, $p = 0.006$). Tukey's *post hoc* analyses revealed that this was driven exclusively by MU which had significantly higher POC (mean POC μg/L: MU 22.91, MB 9.11, BA 6.94, MA 6.23, SA 8.48) and PON (mean PON μg/L: MU 3.33, MB 1.22, BA 1.01, MA 0.81, SA 1.14) concentrations compared to the other sites.

Discussion

In the dynamic environment of coral reef ecosystems, resource availability may fluctuate markedly both spatially and temporally, with implications for associated food webs. Here, across a semi-enclosed tropical embayment in the Philippines, we did not see the expected spatial gradient in fish tissue isotopes (e.g., Wyatt et al., 2012b; Gajdzik et al., 2016; McMahon et al., 2016; Miller et al., 2019), despite the apparent hydrographic separation of sites with varying degrees of oceanic exposure. Instead, there appeared to be pronounced seasonal fluctuations in food web dynamics associated with the rainy and dry seasons, which was evident in the underlying resources (i.e., POM).

These fluctuations were reflected in resource use by suspension feeding primary consumers (i.e., tunicates) but only in some secondary consumers (i.e., small but not large damselfish), a pattern that only became pronounced through analysis of $\delta^{34}S$ as a third isotopic tracer.

Size and seasonal effects on isotope ratios in fish tissues

Small and large damselfish appeared to differ in their resource use, indicating that they might employ different feeding strategies with ontogeny. For example, there was a significant seasonal difference in the isotope ratios of small fish tissues, particularly muscle and eye $\delta^{13}C$, which were more enriched in the rainy season, and liver $\delta^{34}S$, which was lower in the rainy season. Taken together, these data are indicative of smaller fish benefitting from more benthic food chains during the rainy season. During the dry season, when phytoplankton production and chlorophyll *a* in the embayment are higher (San Diego-McGlone et al., 1995), there was evidence of greater reliance on oceanic food chains. In contrast, for the larger fish, isotope ratios of all tissues were similar between seasons, suggesting movement toward a seasonally consistent feeding strategy with age. The more enriched $\delta^{13}C$ and lower $\delta^{34}S$ of large fish tissues further indicated that they may preferentially target benthic invertebrates, possibly reflecting increased foraging movements away from coral heads (Nash et al., 2015). While size-based differences in *Dascyllus* feeding strategies have previously been recorded, they were not always comparable to those found here. In Madagascar, smaller individuals of *Dascyllus aruanus* fed on benthic prey, while larger individuals fed on more planktonic prey (Frédérich et al., 2010), perhaps reflecting the smaller adult size of *D. aruanus* (Kulbicki et al., 2005) and high site fidelity throughout their life span. *D. trimaculatus* larger adult body size might support increased local foraging area, explaining observations that they have some of the highest $\delta^{15}N$ values and the most variable $\delta^{13}C$ values across a range of sizes (Frédérich et al., 2009). Clearly, size-based differences in damselfish resource use and feeding strategies may not always be consistent between species and systems (Eurich et al., 2019) and may be impossible to detect without additional tracers such as $\delta^{34}S$ (see below). However, regardless of size, fish C:N ratios were consistently higher in the dry season across all tissues (**Supplementary Figure 3**), and this was particularly pronounced in liver tissue. Higher lipid levels are linked to better overall condition, suggesting that the food chains that the fish were accessing in the dry season were most beneficial to their growth. As the presence of lipids can influence stable isotope values, mathematical corrections were applied to the data to account for this. While the models run on the raw $\delta^{13}C$ values revealed similar patterns in muscle and eye tissue, for liver the outputs were very different: size and season had no effect on corrected liver $\delta^{13}C$, but for the raw values, size and size interacting with season were highly significant. This confirms that higher tissue lipid content can influence $\delta^{13}C$ values, so correcting the values is a more conservative approach that reduces the confounding influence that lipids may have on interpreting patterns.

Correcting for tissue-dependent fractionation allowed direct comparison of seasonal effects across the three tissue types without the confounding factor of varying isotopic discrimination. There was pronounced seasonality in all three tissues for small fish. While evidence of dietary shifts across seasons was expected in the faster turnover liver, there was also clear seasonal variation detected in both muscle and eye tissue. Muscle is a longer turnover tissue, reflecting a dietary time frame of several weeks to months in the body size range relevant here [mean turnover $\delta^{13}C$ at 28°C temperature (Iizuka et al., 2009)]: Small 39.5 days, Large 67.9 days; (Thomas and Crowther, 2015) but the dietary time frame of whole fish eye tissue is not well constrained. Here, the size and seasonal patterns of fish muscle and eye tissue $\delta^{13}C$ were comparable, and eye $\delta^{15}N$ was consistently lower than muscle $\delta^{15}N$. This correlates with one of the few studies to consider fish eye tissue (including retina), which found a significant positive correlation between fish muscle and eye $\delta^{13}C$ (with a regression relationship close to 1:1), and that eye $\delta^{15}N$ was consistently lower (~2‰) than muscle $\delta^{15}N$ (Kanaya et al., 2019). This suggests that whole eye tissue may represent a similar dietary time frame to that of muscle (i.e., weeks to months). However, evidence of seasonal variation in consumer resource use is less expected in longer turnover tissues. One explanation for the observed variation, is that fish samples were collected mid-season; rainy season samples were collected in September, but higher rainfall associated with the summer monsoon begins in June (Wang and LinHo, 2002). As such, given the calculated turnover rates for the sampled tissues (see above), the damselfish had already begun to assimilate resources available to them during the initial few months of the rainy season. Similarly, dry season samples were collected in March, but the dry season extends from November to May; fish likely already integrated dry season resources that were then reflected in their longer turnover tissues. Moreover, the calculated turnover rates for both size groups indicate that their tissues reflect the same season, further confirming the discrepancies between their foraging strategies. Careful consideration of tissue turnover times in the context of environmental dynamics is required, especially in the absence of analysis of "fast" turnover tissues with higher temporal resolution.

Surprisingly, while there were significant differences in small fish muscle and eye $\delta^{13}C$ between seasons, seasonal $\delta^{13}C$ differences in "fast" liver tissues were not significant. Similar to muscle and eye, liver $\delta^{13}C$ was more depleted in the dry compared to the rainy season, but there was a notable exception of the samples from the innermost site in the port of Muelle

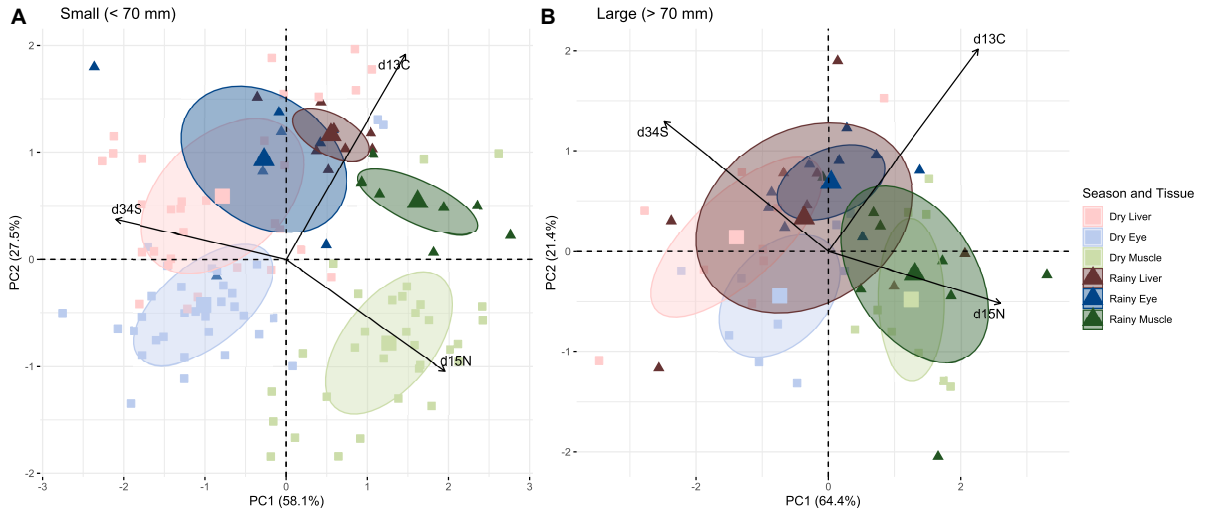

FIGURE 4
Principal component analysis (PCA) of **(A)** small (<70 mm) and **(B)** large (>70 mm) damselfish $\delta^{13}C$, $\delta^{15}N$, and $\delta^{34}S$ values from the liver, eye, and muscle tissues collected from five sites across the embayment in the dry season (March) and the rainy season (September). $\delta^{13}C$ values are mathematically corrected for high lipid content, and liver $\delta^{13}C$ and $\delta^{15}N$ are corrected for tissue-dependent fractionation (see section "Materials and methods"). Ellipses are 95% confidence ellipses with centroids. Variables are overlaid as vectors with arrows.

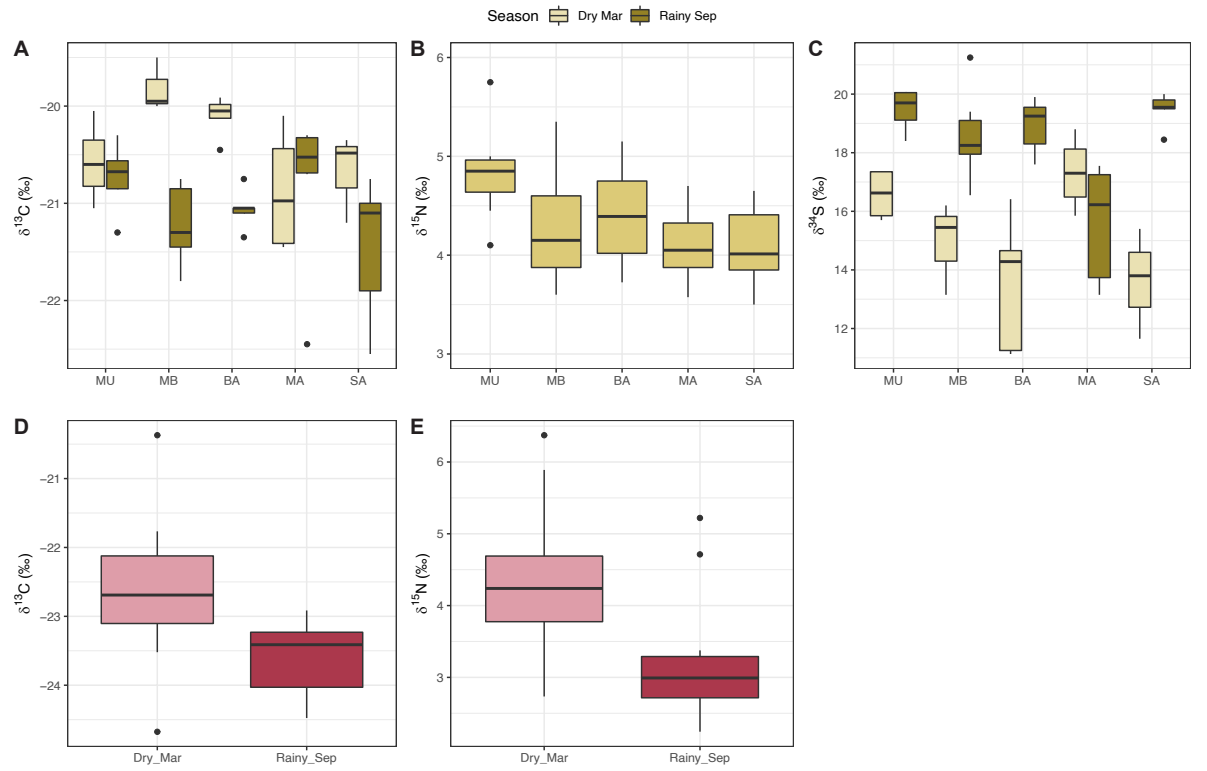

FIGURE 5
Stable isotope ratios of panels **(A–C)** tunicates (*Polycarpa aurata*) and panels **(D,E)** particulate organic matter (POM) sampled across Puerto Galera embayment. Data are pooled based on whether there were significant differences among groups or not. Tunicate $\delta^{15}N$ varied spatially, $\delta^{13}C$ and $\delta^{34}S$ seasonally and with an interaction between season and site; POM $\delta^{13}C$ and $\delta^{15}N$ varied only seasonally. Note, no $\delta^{34}S$ data are reported for POM.

(MU). At MU, dry season liver $\delta^{13}C$ values were comparable to those in the rainy season (more enriched). MU, being the most sheltered inshore site, has reduced water flow and is heavily influenced by surrounding terrestrial and anthropogenic inputs (Iizuka et al., 2009), evidenced by the higher concentrations of POC and PON. More consistent benthic foraging, i.e., enriched $\delta^{13}C$ values, at this site may have precluded a significant seasonal difference in liver $\delta^{13}C$ values from being observed. In contrast to $\delta^{13}C$, small fish liver $\delta^{34}S$ values were significantly lower in the rainy season (~21.3‰) than in the dry season (~23.5‰), indicative of a seasonal difference in the food web baseline. There was no corresponding seasonal shift in muscle or eye $\delta^{34}S$, which likely relates to the longer dietary time frames that these tissues represent. The lower $\delta^{34}S$ values in the fast turnover liver in the rainy season are suggestive of fluxes of terrestrial material entering the food web, likely from increased run-off (San Diego-McGlone et al., 1995). However, $\delta^{34}S$ takes longer than $\delta^{13}C$ or $\delta^{15}N$ to reach equilibrium in muscle tissue (Barnes and Jennings, 2007), and assuming that the turnover of eye tissue is similar, this may explain the absence of seasonal $\delta^{34}S$ variation in these two tissues. It is important to note also that high lipid content in liver tissues might have influenced the $\delta^{34}S$ values. While the patterns using the lipid-corrected $\delta^{34}S$ values were similar to those using the raw $\delta^{34}S$ values, seasonal effects were less pronounced. Unfortunately, the only current known $\delta^{34}S$ lipid correction factor derives from shark liver (Riverón et al., 2022), so it is not clear how appropriate this value is for planktivorous damselfish. Regardless, a better understanding of how lipid levels in tissues might influence $\delta^{34}S$ values is sorely needed. Finally, it is important to also consider sample sizes when interpreting this pattern. Here, opportunistic sampling led to an unbalanced sampling design; there were fewer small fish encountered during the rainy season than the dry season, and, notably, none were observed at MU or Sabang (SA). Though the patterns observed in this study strongly suggest that small fish vary in their resource use between seasons, future work would benefit from incorporating additional samples across the embayment to further explore these spatial and seasonal food web dynamics using the multi-tissue, multi-isotope approach.

Patterns in $\delta^{15}N$ values were as expected but not highly informative regarding changes in resource use. Many food web studies have a strong focus on $\delta^{15}N$ analysis (Skinner et al., in press), but this tracer may not always be the most informative for understanding resource use in coral reef food webs (Miyajima and Umezawa, 2010). Here, there were significant differences between small and large fish $\delta^{15}N$, and values increased with body size. Body size and $\delta^{15}N$ relationships are well studied in marine food webs but not always evident (Layman et al., 2005; Al-Habsi et al., 2008; Jennings et al., 2008; Zhu et al., 2019). Increasing $\delta^{15}N$ with body size suggested larger individuals exploited higher trophic position prey, possibly due to changes in their habitat use or fitness, or increased gape size (Munday, 2001; Newman et al., 2012). For fish from both size groups, there was evidence of tissue-specific discrimination that correlated well with previous studies; fish muscle was enriched in $\delta^{15}N$ compared to the liver (Pinnegar and Polunin, 1999; Chen et al., 2012) and eye (Kanaya et al., 2019), but applying corrections to account for tissue-dependent fractionation allowed direct comparisons of seasonal effects across tissues. There was no seasonality in the $\delta^{15}N$ values of any of the tissues of either size group, suggesting that they are consistently feeding on prey of a similar trophic position across seasons with no change in the underlying $\delta^{15}N$ baseline values. Although useful for determining consumer trophic position, $\delta^{15}N$ may not be as informative for detecting seasonal changes in consumer resource use.

Suspension feeders as indicators of resource availability

Tunicates were sampled across the embayment to better characterize the planktonic production pathway and how this might vary seasonally. While some patterns in the tunicate tissues clearly reflected those of the damselfish, others were less easy to reconcile. For example, similar to the small damselfish, there were no seasonal patterns in tunicate $\delta^{15}N$, but highly seasonal patterns in tunicate $\delta^{13}C$ and $\delta^{34}S$. However, the patterns in $\delta^{13}C$ and $\delta^{34}S$ were reversed; tunicate $\delta^{13}C$ was more enriched and $\delta^{34}S$ was lower in the dry season, indicative of reliance on nearshore production pathways. This is because there is a distinct spatial gradient in $\delta^{34}S$ values related to the biogeochemical cycling of sulfur; offshore marine sulfate values are close to 21‰, while in anaerobic and anoxic sediments in coastal environments, sulfate is reduced to hydrogen sulfide which has lower $\delta^{34}S$ values (Fry et al., 1982; Fry, 1986; Peterson, 1999). As such, lower tunicate $\delta^{34}S$ in the dry season (coupled with more enriched $\delta^{13}C$) indicate reliance on suspended material derived from benthic organic matter or sulfur-oxidizing bacteria (Peterson et al., 1986; Oakes and Connolly, 2004). In contrast, small damselfish tissues in the dry season indicated a response to the increased phytoplankton production and chlorophyll *a* concentrations that tend to prevail in this season (San Diego-McGlone et al., 1995). Tunicates, as suspension feeders, are often sampled to represent a time-integrated pelagic baseline, which is less variable than POM (Stowasser et al., 2012; Ménard et al., 2014); however, the dietary time frame that their tissues represent is not well known. Furthermore, recent evidence suggests that they may instead consume microbes, thus making it inappropriate to use them as representatives of the pelagic food chain (Pakhomov et al., 2019). Indeed, other suspension feeders, such as oysters, are known to preferentially select food particles (Newell and Jordan, 1983), suggesting that the tunicates may not be consuming all of the suspended POM. In addition, the damselfish occupy a higher trophic position than the tunicates, suggesting that

seasonal variations observed in the tunicates may have been different from those obscured in the damselfish, as these were diminished across trophic linkages. These caveats may explain the discrepancy between the damselfish and tunicate $\delta^{13}C$ and $\delta^{34}S$ patterns, further confirming that caution is needed when using tunicates as a "pelagic" baseline in reef food web studies. However, regardless of the food chain they represent, there was strong evidence of seasonality in their tissues consistent with the small damselfish, likely linked to fluctuations in resource availability between the rainy and dry seasons.

Particulate organic matter samples confirmed that suspended resources varied seasonally across the embayment. POM $\delta^{15}N$ was higher in the dry season, likely linked to pools of accumulated ammonia from anthropogenic waste (San Diego-McGlone et al., 1995). Similar to the tunicates, POM $\delta^{13}C$ was more enriched in the dry season, consistent with reduced terrestrial inputs (which have very depleted $\delta^{13}C$: −31 to −25‰; Mackensen and Schmiedl, 2019) due to lower rainfall. Differences in $\delta^{13}C$ values between seasons could relate to water temperature though, as isotopic fractionation of planktonic $\delta^{13}C$ decreases in warmer water, leading to more enriched values. Here, however, POM $\delta^{13}C$ values were more enriched in the dry season when water temperatures were lower. Furthermore, water temperatures varied by only 2°C between seasons, corresponding to a difference in fractionation of only 0.70‰ (0.35‰ per °C; Fontugne and Duplessy, 1981). This suggests that observed seasonal differences in $\delta^{13}C$ were not driven by differences in water temperature. Indeed, changes in phytoplankton $\delta^{13}C$ fractionation may also arise from differences in light conditions (intensity and duration) and nutrients (Brandenburg et al., 2022). These factors may be more relevant here than the temperature for explaining differences in $\delta^{13}C$ of POM (phytoplankton) between the rainy and dry seasons. It seems that the POM data reflect some aspects of the benthic food chain; the snapshot nature of POM sampling coupled with the dynamic environment of the embayment, i.e., variable flushing rates influencing residence times and accumulated nutrients (San Diego-McGlone et al., 1995; Iizuka et al., 2009), may influence oceanic contributions evident from POM $\delta^{13}C$. The lack of seasonal variation in POC and PON concentrations could suggest that the change in resources may be of a similar magnitude, leading to variations in POM isotope ratios but not in concentrations (Wyatt et al., 2013). Interestingly, despite distinct temporal differences, there was no significant spatial isotopic gradient in POM $\delta^{13}C$ or $\delta^{15}N$ and the spatial variation in POC and PON was driven solely by the most inshore site (MU). Although the mechanisms through which these food chains fluctuate and become available to primary and secondary consumers across the embayment remains unclear, it appears that this is predominantly a seasonally fluctuating system rather than a spatial one as previously assumed.

Incorporating $\delta^{34}S$ as a third isotope for exploring food web dynamics

Sulfur isotope ratios ($\delta^{34}S$) are increasingly being recommended as a useful third tracer for stable isotope food web studies (Connolly et al., 2004; Skinner et al., 2019a). Our data further support this; $\delta^{34}S$ was instrumental in identifying short-term resource use changes of small fish (as reflected in their liver tissues) but was also important for highlighting strong seasonal variation in the suspension-feeding tunicates. The lack of seasonal $\delta^{34}S$ variation in large fish argues against a simple seasonal change in the $\delta^{34}S$ baselines of this system, instead suggesting small fish and tunicates are utilizing different resources in each season. While larger fish may have a slower isotopic turnover, particularly in their muscle tissue, we would still expect to see changes in their liver $\delta^{34}S$ due to its faster turnover. Unfortunately, no POM $\delta^{34}S$ data are available to explore seasonal shifts in the underlying suspended resources that may be evident with sulfur. In this system, it seems that while $\delta^{13}C$ and $\delta^{34}S$ are key to understanding seasonal fluxes (Connolly et al., 2004; Briand et al., 2015), $\delta^{15}N$ may be less valuable, highlighting the utility of adding tracers like $\delta^{34}S$, especially in systems with minimal nitrogen isotope variation.

Conclusion

Investigations into seasonality in aquatic food webs are increasing (Wantzen et al., 2002; Cobain et al., 2022), but there is still limited understanding of how varying fluxes translate into variation in reef food webs (but see Briand et al., 2015), with the majority of coral reef stable isotope studies conducted during limited temporal windows and focusing on one or two tracers in a single tissue (Skinner et al., in press). Our data suggest that coral reef food web resources and consumer trophodynamics can vary substantially between seasons even over small spatial scales. Restricting sampling to a single period may therefore overlook important seasonal food web dynamics, which could alter our interpretation of production source pathways and consumer resource use. Furthermore, combining multiple isotopic tracers ($\delta^{13}C$, $\delta^{15}N$, and $\delta^{34}S$) with the analysis of separate tissue types (representing different dietary time frames, e.g., Wyatt et al., 2019) proved instrumental in identifying temporal changes in consumer dietary variation. Where lethal sampling is already occurring, we strongly recommend that researchers maximize the dietary information obtained from each individual by sampling a range of tissue types with different turnover times. In addition, given the ease at which $\delta^{34}S$ can now be measured along with $\delta^{13}C$ and $\delta^{15}N$, and the important food chain information it can convey (Connolly et al., 2004), we suggest that marine food web studies employ a tri-isotope approach by default. However, more research into the effect

of tissue lipid levels on $\delta^{34}S$ is sorely needed. As coral reefs are currently experiencing unprecedented worldwide declines (Hoegh-Guldberg et al., 2017; Hughes et al., 2017; Darling et al., 2019), improved quantification of food web dynamics across both fine and broad spatial and temporal scales is urgently needed.

Data availability statement

The raw data supporting the conclusions of this article will be made available by the authors, without undue reservation.

Ethics statement

This study was approved by Prior Informed Consent from the Municipality of Puerto Galera (PIC Certificate, Document No. 146, September 25, 2012) and a Gratuitous Permit from the Philippines Department of Agriculture (GP-No. 0073-14).

Author contributions

AW conceptualized the study and collected the samples with assistance from NM and TM. AW and CS formulated the statistical analyses and developed the methodology. Y-DP and CS processed the samples. CS analyzed the data and wrote the first draft of the manuscript. All authors contributed substantially to revisions.

Funding

Field collections were supported by the Coastal Ecosystem Conservation and Adaptive Management under Local and Global Environmental Impacts in the Philippines (CECAM) project supported by the "Science and Technology Research Partnership for Sustainable Development (SATREPS)" scheme jointly funded by the Japan Science and Technology Agency and the Japan International Cooperation Agency (JICA) to K. Nadaoka and M. D. Fortes. AW was supported during field work by a fellowship from the Japan Society for the Promotion of Science. Sample analysis was supported by funding from the Hong Kong Branch of the Southern Marine Science and Engineering Guangdong Laboratory (Guangzhou) (SMSEGL20SC01) to AW. Y-DP was supported by the Asian Future Leaders Scholarship Program, jointly contributed by The Hong Kong University of Science and Technology and Bai Xian Asia Institute.

Acknowledgments

We sincerely thank the Municipality of Puerto Galera, the JICA Philippines Office, including Y. Nagahama and Y. Geroleo, and the CECAM project coordinating office for logistical support in the field. R. M. Magturo of Sandbar Divers provided diving support. We also thank M. R. D. Cobain for helpful discussion regarding the analysis and the two reviewers for their helpful feedback which improved the manuscript.

Conflict of interest

The authors declare that the research was conducted in the absence of any commercial or financial relationships that could be construed as a potential conflict of interest.

Publisher's note

All claims expressed in this article are solely those of the authors and do not necessarily represent those of their affiliated organizations, or those of the publisher, the editors and the reviewers. Any product that may be evaluated in this article, or claim that may be made by its manufacturer, is not guaranteed or endorsed by the publisher.

Supplementary material

The Supplementary Material for this article can be found online at: https://www.frontiersin.org/articles/10.3389/fevo.2022.942968/full#supplementary-material

References

Al-Habsi, S., Sweeting, C., Polunin, N., and Graham, N. (2008). δ15N and δ13C elucidation of size-structured food webs in a Western Arabian Sea demersal trawl assemblage. *Marine Ecol. Prog. Series* 353, 55–63. doi: 10.3354/meps07167

Allen, G. R. (1991). *Damselfishes of the World*. Melle: Mergus.

Barnes, C., and Jennings, S. (2007). Effect of temperature, ration, body size and age on sulphur isotope fractionation in fish. *Rapid Commun. Mass Spectrom.* 21, 1461–1467. doi: 10.1002/rcm.2982

Bates, D., Maechler, M., Bolker, B., and Walker, S. (2015). Fitting Linear Mixed-Effects Models Using lme4. *J. Statist. Softw.* 67, 1–48.

Bell-Tilcock, M., Jeffres, C. A., Rypel, A. L., Sommer, T. R., Katz, J. V. E., Whitman, G., et al. (2021). Advancing diet reconstruction in fish eye lenses. *Meth. Ecol. Evol.* 12, 449–457. doi: 10.1111/2041-210X.13543

Boecklen, W. J., Yarnes, C. T., Cook, B. A., and James, A. C. (2011). On the Use of Stable Isotopes in Trophic Ecology. *Annu. Rev. Ecol. Evol. System.* 42, 411–440. doi: 10.1146/annurev-ecolsys-102209-144726

Booth, D. J. (1995). Juvenile Groups in a Coral-Reef Damselfish: Density-Dependent Effects on Individual Fitness and Population Demography. *Ecology* 76, 91–106. doi: 10.2307/1940634

Brandenburg, K. M., Rost, B., Van de Waal, D. B., Hoins, M., and Sluijs, A. (2022). Physiological control on carbon isotope fractionation in marine phytoplankton. *Biogeosciences* 19, 3305–3315. doi: 10.5194/bg-19-3305-2022

Briand, M. J., Bonnet, X., Goiran, C., Guillou, G., and Letourneur, Y. (2015). Major Sources of Organic Matter in a Complex Coral Reef Lagoon: Identification from Isotopic Signatures (δ13C and δ15N). *PLoS One* 10:e0131555. doi: 10.1371/journal.pone.0131555

Canseco, J. A., Niklitschek, E. J., and Harrod, C. (2022). Variability in δ13C and δ15N trophic discrimination factors for teleost fishes: A meta-analysis of temperature and dietary effects. *Rev. Fish Biol. Fish.* 32, 313–329. doi: 10.1007/s11160-021-09689-1

Carreón-Palau, L., Parrish, C. C., del Angel-Rodríguez, J. A., Pérez-España, H., and Aguiñiga-García, S. (2013). Revealing organic carbon sources fueling a coral reef food web in the Gulf of Mexico using stable isotopes and fatty acids. *Limnol. Oceanogr.* 58, 593–612. doi: 10.4319/lo.2013.58.2.0593

Chen, G., Zhou, H., Ji, D., and Gu, B. (2012). Stable isotope enrichment in muscle, liver, and whole fish tissues of brown-marbled groupers (Epinephelus fuscoguttatus). *Ecol. Process.* 1:7. doi: 10.1186/2192-1709-1-7

Cobain, M. R., McGill, R. A., and Trueman, C. N. (2022). Stable isotopes demonstrate seasonally stable benthic-pelagic coupling as newly fixed nutrients are rapidly transferred through food chains in an estuarine fish community. *J. Fish. Biol.* [Epub ahead of print]. doi: 10.1111/jfb.15005

Cocheret de la Morinière, E., Pollux, B. J. A., Nagelkerken, I., Hemminga, M. A., Huiskes, A. H. L., and Van der Velde, G. (2003). Ontogenetic dietary changes of coral reef fishes in the mangrove-seagrass-reef continuum: Stable isotopes and gut-content analysis. *Mar. Ecol. Prog. Series* 246, 279–289. doi: 10.3354/meps246279

Connolly, R. M., Guest, M. A., Melville, A. J., and Oakes, J. M. (2004). Sulfur stable isotopes separate producers in marine food-web analysis. *Oecologia* 138, 161–167. doi: 10.1007/s00442-003-1415-0

Cummings, D. O., Booth, D. J., Lee, R. W., Simpson, S. J., and Pile, A. J. (2010). Ontogenetic diet shifts in the reef fish Pseudanthias rubrizonatus from isolated populations on the North-West Shelf of Australia. *Mar. Ecol. Prog. Series* 419, 211–222. doi: 10.3354/meps08827

Darling, E. S., McClanahan, T. R., Maina, J., Gurney, G. G., Graham, N. A. J., and Januchowski-Hartley, F. (2019). Social–environmental drivers inform strategic management of coral reefs in the Anthropocene. *Nat. Ecol. Evol.* 3, 1341–1350. doi: 10.1038/s41559-019-0953-8

Davis, J. P., Pitt, K. A., Fry, B., and Connolly, R. M. (2015). Stable isotopes as tracers of residency for fish on inshore coral reefs. *Estuar. Coast. Shelf Sci.* 167, 368–376. doi: 10.1016/j.ecss.2015.10.013

Erler, D. V., Shepherd, B. O., Linsley, B. K., Nothdurft, L. D., Hua, Q., and Lough, J. M. (2019). Has Nitrogen Supply to Coral Reefs in the South Pacific Ocean Changed Over the Past 50 Thousand Years? *Paleoceanogr. Paleoclimatol.* 34, 567–579. doi: 10.1029/2019PA003587

Eurich, J. G., Matley, J. K., Baker, R., McCormick, M. I., and Jones, G. P. (2019). Stable isotope analysis reveals trophic diversity and partitioning in territorial damselfishes on a low-latitude coral reef. *Mar. Biol.* 166:17. doi: 10.1007/s00227-018-3463-3

Fey, P., Parravicini, V., Bănaru, D., Dierking, J., Galzin, R., Lebreton, B., et al. (2021). Multi-trophic markers illuminate the understanding of the functioning of a remote, low coral cover Marquesan coral reef food web. *Sci. Rep.* 11:20950. doi: 10.1038/s41598-021-00348-w

Fontugne, M. R., and Duplessy, J.-C. (1981). Organic carbon isotopic fractionation by marine plankton in the temperature range -1 to 31°C. *Oceanol. Acta* 4, 85–90.

Frédérich, B., Fabri, G., Lepoint, G., Vandewalle, P., and Parmentier, E. (2009). Trophic niches of thirteen damselfishes (Pomacentridae) at the Grand Récif of Toliara. *Madagascar. Ichthyol. Res.* 56, 10–17. doi: 10.1007/s10228-008-0053-2

Frédérich, B., Lehanse, O., Vandewalle, P., and Lepoint, G. (2010). Trophic Niche Width, Shift, and Specialization of Dascyllus aruanus in Toliara Lagoon, Madagascar. *Copeia* 2, 218–226. doi: 10.1643/CE-09-031

Frédérich, B., Olivier, D., Gajdzik, L., and Parmentier, É (2016). "Trophic Ecology of Damselfishes," in *Biology of Damselfishes*, eds B. Frédérich and E. Parmentier (Boca Raton, FL: CRC Press). doi: 10.1201/9781315373874

Fry, B. (1986). Stable Sulfur Isotopic Distributions and Sulfate Reduction in Lake Sediments of the Adirondack Mountains, New York. *Biogeochemistry* 2, 329–343. doi: 10.1007/BF02180324

Fry, B., Scalan, R. S., Winters, J. K., and Parker, P. L. (1982). Sulphur uptake by salt grasses, mangroves, and seagrasses in anaerobic sediments. *Geochim. Cosmochim. Acta* 46, 1121–1124. doi: 10.1016/0016-7037(82)90063-1

Gajdzik, L., Parmentier, E., Sturaro, N., and Frédérich, B. (2016). Trophic specializations of damselfishes are tightly associated with reef habitats and social behaviours. *Mar. Biol.* 163:249. doi: 10.1007/s00227-016-3020-x

Greenwood, N. D. W., Sweeting, C. J., and Polunin, N. V. C. (2010). Elucidating the trophodynamics of four coral reef fishes of the Solomon Islands using δ15N and δ13C. *Coral Reefs* 29, 785–792. doi: 10.1007/s00338-010-0626-1

Haas, A. F., Naumann, M. S., Struck, U., Mayr, C., el-Zibdah, M., and Wild, C. (2010). Organic matter release by coral reef associated benthic algae in the Northern Red Sea. *J. Exper. Mar. Biol. Ecol.* 389, 53–60. doi: 10.1016/j.jembe.2010.03.018

Hadfield, J. D. (2010). MCMC Methods for Multi-Response Generalized Linear Mixed Models: The MCMCglmm R Package. *J. Statist. Softw.* 33, 1–22. doi: 10.18637/jss.v033.i02

Hagen, W. (1988). On the significance of lipids in Antarctic zooplankton. *Ber Polarforsch* 49, 1–117.

Hoegh-Guldberg, O., and Dove, S. (2008). "Primary production, nutrient recycling and energy flow through coral reef ecosystems,". In *The Great Barrier Reef: Biology, Environment and Management* M. Kingsford, O. Hoegh-Guldberg, P. Hutchings (Clayton: CSIRO publishing)59–73.

Hoegh-Guldberg, O., Poloczanska, E. S., Skirving, W., and Dove, S. (2017). Coral Reef Ecosystems under Climate Change and Ocean Acidification. *Front. Mar. Sci.* 4:158. doi: 10.3389/fmars.2017.00158

Hughes, T. P., Kerry, J. T., Álvarez-Noriega, M., Álvarez-Romero, J. G., Anderson, K. D., and Baird, A. H. (2017). Global warming and recurrent mass bleaching of corals. *Nature* 543, 373–377. doi: 10.1038/nature21707

Iizuka, H., Tamura, H., Pokavanich, T., Rubio-Paringit, M. C. D., Nadaoka, K., and Fortes, M. D. (2009). Highly Skewed Tidal Circulation Pattern and Water Quality in Puerto Galera Bay. Mindoro Island, Philippines. *Coast. Eng. J.* 51, 341–361. doi: 10.1142/S0578563409002065

Jennings, S., Barnes, C., Sweeting, C. J., and Polunin, N. V. C. (2008). Application of nitrogen stable isotope analysis in size-based marine food web and macroecological research. *Rapid Commun. Mass Spectrom.* 22, 1673–1680. doi: 10.1002/rcm.3497

Kanaya, G., Solovyev, M. M., Shikano, S., Okano, J.-I., Ponomareva, N. M., and Yurlova, N. I. (2019). Application of stable isotopic analyses for fish host–parasite systems: An evaluation tool for parasite-mediated material flow in aquatic ecosystems. *Aqua. Ecol.* 53, 217–232. doi: 10.1007/s10452-019-09684-6

Kiljunen, M., Grey, J., Sinisalo, T., Harrod, C., Immonen, H., and Jones, R. I. (2006). A revised model for lipid-normalizing δ13C values from aquatic organisms, with implications for isotope mixing models. *J. Appl. Ecol.* 43, 1213–1222. doi: 10.1111/j.1365-2664.2006.01224.x

Kulbicki, M., Guillemot, N., and Amand, M. (2005). A general approach to length-weight relationships for New Caledonian lagoon fishes. *Cybium* 29, 235–252.

Layman, C. A., Winemiller, K. O., Arrington, D. A., and Jepsen, D. B. (2005). Body size and trophic position in a diverse tropical food web. *Ecology* 86, 2530–2535. doi: 10.1890/04-1098

Lê, S., Josse, J., and Husson, F. (2008). FactoMineR: An R Package for Multivariate Analysis. *J. Statist. Softw.* 25:18. doi: 10.18637/jss.v025.i01

Letourneur, Y., Briand, M. J., and Graham, N. A. J. (2017). Coral reef degradation alters the isotopic niche of reef fishes. *Mar. Biol.* 164:224. doi: 10.1007/s00227-017-3272-0

Mackensen, A., and Schmiedl, G. (2019). Stable carbon isotopes in paleoceanography: Atmosphere, oceans, and sediments. *Earth Sci. Rev.* 197:102893. doi: 10.1016/j.earscirev.2019.102893

Matley, J. K., Fisk, A. T., Tobin, A. J., Heupel, M. R., and Simpfendorfer, C. A. (2016). Diet-tissue discrimination factors and turnover of carbon and nitrogen stable isotopes in tissues of an adult predatory coral reef fish, Plectropomus leopardus. *Rapid Commun. Mass Spectrom.* 30, 29–44. doi: 10.1002/rcm.7406

Matley, J. K., Tobin, A. J., Simpfendorfer, C. A., Fisk, A. T., and Heupel, M. R. (2017). Trophic niche and spatio-temporal changes in the feeding ecology of two

sympatric species of coral trout (Plectropomus leopardus and P. laevis). *Mar. Ecol. Prog. Series* 563, 197–210. doi: 10.3354/meps11971

Mayzaud, P., Chanut, J. P., and Ackman, R. G. (1989). Seasonal changes of the biochemical composition of marine particulate matter with special reference to fatty acids and sterols. *Mar. Ecol. Prog. Series* 56, 189–204. doi: 10.3354/meps056189

McCauley, D. J., DeSalles, P. A., Young, H. S., Papastamatiou, Y. P., Caselle, J. E., Deakos, M. H., et al. (2014). Reliance of mobile species on sensitive habitats: A case study of manta rays (Manta alfredi) and lagoons. *Mar. Biol.* 161, 1987–1998. doi: 10.1007/s00227-014-2478-7

McMahon, K. W., Thorrold, S. R., Houghton, L. A., and Berumen, M. L. (2016). Tracing carbon flow through coral reef food webs using a compound-specific stable isotope approach. *Oecologia* 180, 809–821. doi: 10.1007/s00442-015-3475-3

Ménard, F., Benivary, H. D., Bodin, N., Coffineau, N., Le Loc'h, F., Mison, T., et al. (2014). Stable isotope patterns in micronekton from the Mozambique Channel. *Deep Sea Res. Part II* 100, 153–163. doi: 10.1016/j.dsr2.2013.10.023

Miller, S. D., Zgliczynski, B. J., Fox, M. D., Kaufman, L. S., Michener, R. H., Sandin, S. A., et al. (2019). Niche width expansion of coral reef fishes along a primary production gradient in the remote central Pacific. *Mar. Ecol. Prog. Series* 625, 127–143. doi: 10.3354/meps13023

Miyajima, T., and Umezawa, Y. (2010). "Stable isotope composition of nitrogen ($\delta^{15}N$) as a tool for investigating nitrogen cycling in coral reef ecosystems," in *Earth, Life, and Isotopes*, eds N. Ohkouchi, I. Tayasu, and K. Koba (kyoto: Kyoto University Press), 197–222.

Mock, T., and Gradinger, R. (2000). Changes in photosynthetic carbon allocation in algal assemblages of Arctic sea ice with decreasing nutrient concentrations and irradiance. *Mar. Ecol. Prog. Series* 202, 1–11. doi: 10.3354/meps202001

Morimoto, N., Umezawa, Y., San Diego-McGlone, M. L., Watanabe, A., Siringan, F. P., and Tanaka, Y. (2017). Spatial dietary shift in bivalves from embayment with river discharge and mariculture activities to outer seagrass beds in northwestern Philippines. *Mar. Biol.* 164:84. doi: 10.1007/s00227-016-3063-z

Munday, P. L. (2001). Fitness consequences of habitat use and competition among coral-dwelling fishes. *Oecologia* 128, 585–593. doi: 10.1007/s004420100690

Nakamura, Y., Horinouchi, M., Shibuno, T., Tanaka, Y., Miyajima, T., Koike, I., et al. (2008). Evidence of ontogenetic migration from mangroves to coral reefs by black-tail snapper Lutjanus fulvus: Stable isotope approach. *Mar. Ecol. Prog. Series* 355, 257–266. doi: 10.3354/meps07234

Nakazawa, T. (2015). Ontogenetic niche shifts matter in community ecology: A review and future perspectives. *Popul. Ecol.* 57, 347–354. doi: 10.1007/s10144-014-0448-z

Nash, K. L., Welsh, J. Q., Graham, N. A., and Bellwood, D. R. (2015). Home-range allometry in coral reef fishes: Comparison to other vertebrates, methodological issues and management implications. *Oecologia* 177, 73–83. doi: 10.1007/s00442-014-3152-y

Newell, R. I., and Jordan, S. J. (1983). Preferential ingestion of organic material by the American oyster Crassostrea virginica. *Mar. Ecol. Prog. Series.* 13, 47–53. doi: 10.3354/meps013047

Newman, S. P., Handy, R. D., and Gruber, S. H. (2012). Ontogenetic diet shifts and prey selection in nursery bound lemon sharks, Negaprion brevirostris, indicate a flexible foraging tactic. *Environ. Biol. Fishes* 95, 115–126. doi: 10.1007/s10641-011-9828-9

Oakes, J. M., and Connolly, R. M. (2004). Causes of sulfur isotope variability in the seagrass, Zostera capricorni. *J. Exper. Mar. Biol. Ecol.* 302, 153–164. doi: 10.1016/j.jembe.2003.10.011

O'Farrell, S., Bearhop, S., McGill, R. A. R., Dahlgren, C. P., Brumbaugh, D. R., and Mumby, P. J. (2014). Habitat and body size effects on the isotopic niche space of invasive lionfish and endangered Nassau grouper. *Ecosphere* 5, 1–11. doi: 10.1890/ES14-00126.1

Oksanen, J. F., Blanchet, G., Friendly, M., Kindt, R., Legendre, P., McGlinn, P., et al. (2020). *vegan: Community Ecology Package. R package version 2.5-7*.

Page, H. M., Brooks, A. J., Kulbicki, M., Galzin, R., Miller, R. J., Reed, D. C., et al. (2013). Stable Isotopes Reveal Trophic Relationships and Diet of Consumers in Temperate Kelp Forest and Coral Reef Ecosystems. *Oceanography* 26, 180–189. doi: 10.5670/oceanog.2013.61

Pakhomov, E. A., Henschke, N., Hunt, B. P. V., Stowasser, G., and Cherel, Y. (2019). Utility of salps as a baseline proxy for food web studies. *J. Plankton Res.* 41, 3–11. doi: 10.1093/plankt/fby051

Peterson, B. J. (1999). Stable isotopes as tracers of organic matter input and transfer in benthic food webs: A review. *Acta Oecol.* 20, 479–487. doi: 10.1016/S1146-609X(99)00120-4

Peterson, B. J., and Fry, B. (1987). Stable isotopes in ecosystem studies. *Annu. Rev. Ecol. System.* 18, 293–320. doi: 10.1146/annurev.es.18.110187.001453

Peterson, B. J., Howarth, R. W., and Garritt, R. H. (1986). Sulfur and Carbon Isotopes as Tracers of Salt-Marsh Organic Matter Flow. *Ecology* 67, 865–874. doi: 10.2307/1939809

Pinnegar, J. K., and Polunin, N. V. C. (1999). Differential fractionation of delta C-13 and delta N-15 among fish tissues: Implications for the study of trophic interactions. *Funct. Ecol.* 13, 225–231. doi: 10.1046/j.1365-2435.1999.00301.x

Plass-Johnson, J. G., McQuaid, C. D., and Hill, J. M. (2015). The effects of tissue type and body size on $\delta^{13}C$ and $\delta^{15}N$ values in parrotfish (Labridae) from Zanzibar, Tanzania. *J. Appl. Ichthyol.* 31, 633–637. doi: 10.1111/jai.12746

Post, D. M., Layman, C. A., Arrington, D. A., Takimoto, G., Quattrochi, J., and Montaña, C. G. (2007). Getting to the fat of the matter: Models, methods and assumptions for dealing with lipids in stable isotope analyses. *Oecologia* 152, 179–189. doi: 10.1007/s00442-006-0630-x

Quaeck-Davies, K., Bendall, V. A., MacKenzie, K. M., Hetherington, S., Newton, J., and Trueman, C. N. (2018). Teleost and elasmobranch eye lenses as a target for life-history stable isotope analyses. *PeerJ* 6:e4883. doi: 10.7717/peerj.4883

R Core Team (2021). *R: A language and environment for statistical computing*. Vienna: R Foundation for Statistical Computing.

R Studio Team (2020). *RStudio: Integrated Development for R*. Boston, MA: RStudio.

Rau, G. H., Sweeney, R. E., and Kaplan, I. R. (1982). Plankton 13C: 12C ratio changes with latitude: Differences between northern and southern oceans. *Deep Sea Res. Part A* 29, 1035–1039. doi: 10.1016/0198-0149(82)90026-7

Richoux, N. B., and Froneman, P. W. (2009). Plankton trophodynamics at the subtropical convergence, Southern Ocean. *J. Plankton Res.* 31, 1059–1073. doi: 10.1093/plankt/fbp054

Riverón, S., Raoult, V., Slip, D. J., and Harcourt, R. G. (2022). Lipid extraction has tissue-dependent effects on isotopic values (δ34S, δ13C, and δ15N) from different marine predators. *Rapid Commun. Mass Spectrom.* 36, e9346. doi: 10.1002/rcm.9346

Roy, A.-S., Frisch, A. J., Syms, C., Thorrold, S. R., and Jones, G. P. (2012). Retention of a transgenerational marker (137Barium) in tissues of adult female anemonefish and assessment of physiological stress. *Environ. Biol. Fishes* 96, 459–466. doi: 10.1007/s10641-012-0029-y

San Diego-McGlone, M. L., Villanoy, C. L., and Aliño, P. M. (1995). Nutrient mediated stress on the marine communities of a coastal lagoon (Puerto Galera, Philippines). *Mar. Pollut. Bull.* 31, 355–366. doi: 10.1016/0025-326X(95)00170-R

Skinner, C., Cobain, M. R. D., Zhu, Y., Wyatt, A. S., and Polunin, N. V. C. (in press). Progress and direction in the use of stable isotopes to understand complex coral reefecosystems: A review. *Oceanogr. Mar. Biol.* 60.

Skinner, C., Newman, S. P., Mill, A. C., Newton, J., and Polunin, N. V. C. (2019b). Prevalence of pelagic dependence among coral reef predators across an atoll seascape. *J. Anim. Ecol.* 88, 1564–1574. doi: 10.1111/1365-2656.13056

Skinner, C., Mill, A. C., Newman, S. P., Newton, J., Cobain, M. R. D., and Polunin, N. V. C. (2019a). Novel tri-isotope ellipsoid approach reveals dietary variation in sympatric predators. *Ecol. Evol.* 9, 13267–13277. doi: 10.1002/ece3.5779

Skinner, M. M., Martin, A. A., and Moore, B. C. (2016). Is lipid correction necessary in the stable isotope analysis of fish tissues? *Rapid Commun. Mass Spectrom.* 30, 881–889. doi: 10.1002/rcm.7480

Søreide, J. E., Tamelander, T., Hop, H., Hobson, K. A., and Johansen, I. (2006). Sample preparation effects on stable C and N isotope values: A comparison of methods in Arctic marine food web studies. *Mar. Ecol. Prog. Series* 328, 17–28. doi: 10.3354/meps328017

Stowasser, G., Atkinson, A., McGill, R. A. R., Phillips, R. A., Collins, M. A., and Pond, D. W. (2012). Food web dynamics in the Scotia Sea in summer: A stable isotope study. *Deep Sea Res. Part II* 59-60, 208–221. doi: 10.1016/j.dsr2.2011.08.004

Sweeting, C. J., Polunin, N. V., and Jennings, S. (2006). Effects of chemical lipid extraction and arithmetic lipid correction on stable isotope ratios of fish tissues. *Rapid Commun. Mass Spectrom.* 20, 595–601. doi: 10.1002/rcm.2347

Thibodeau, B., Miyajima, T., Tayasu, I., Wyatt, A. S. J., Watanabe, A., Morimoto, N., et al. (2013). Heterogeneous dissolved organic nitrogen supply over a coral reef: First evidence from nitrogen stable isotope ratios. *Coral Reefs* 32, 1103–1110. doi: 10.1007/s00338-013-1070-9

Thomas, S. M., and Crowther, T. W. (2015). Predicting rates of isotopic turnover across the animal kingdom: A synthesis of existing data. *J. Anim. Ecol.* 84, 861–870. doi: 10.1111/1365-2656.12326

Tieszen, L. L., Boutton, T. W., Tesdahl, K. G., and Slade, N. A. (1983). Fractionation and turnover of stable carbon isotopes in animal tissues: Implications for $\delta^{13}C$ analysis of diet. *Oecologia* 57, 32–37. doi: 10.1007/BF00379558

Trust, B. A., and Fry, B. (1992). Stable sulphur isotopes in plants: A review. *Plant Cell Environ.* 15, 1105–1110. doi: 10.1111/j.1365-3040.1992.tb01661.x

Vander Zanden, M. J., Clayton, M. K., Moody, E. K., Solomon, C. T., and Weidel, B. C. (2015). Stable isotope turnover and half-life in animal tissues: A literature synthesis. *PLoS One* 10:e0116182. doi: 10.1371/journal.pone.0116182

Wallace, A. A., Hollander, D. J., and Peebles, E. B. (2014). Stable Isotopes in Fish Eye Lenses as Potential Recorders of Trophic and Geographic History. *PLoS One* 9:e108935. doi: 10.1371/journal.pone.0108935

Wang, B., and LinHo. (2002). Rainy Season of the Asian–Pacific Summer Monsoon. *J. Climate* 15, 386–398. doi: 10.1175/1520-0442(2002)015<0386:RSOTAP>2.0.CO;2

Wantzen, K. M., de Arruda Machado, F., Voss, M., Boriss, H., and Junk, W. J. (2002). Seasonal isotopic shifts in fish of the Pantanal wetland, Brazil. *Aqua. Sci.* 64, 239–251. doi: 10.1007/PL00013196

World Weather Online (2022). *Puerto Galera Historical Weather*.Manchester: World Weather Online.

Wyatt, A. S. J., Falter, J. L., Lowe, R. J., Humphries, S., and Waite, A. M. (2012a). Oceanographic forcing of nutrient uptake and release over a fringing coral reef. *Limnol. Oceanogr.* 57, 401–419. doi: 10.4319/lo.2012.57.2.0401

Wyatt, A. S. J., Waite, A. M., and Humphries, S. (2012b). Stable isotope analysis reveals community-level variation in fish trophodynamics across a fringing coral reef. *Coral Reefs* 31, 1029–1044. doi: 10.1007/s00338-012-0923-y

Wyatt, A. S. J., Lowe, R. J., Humphries, S., and Waite, A. M. (2013). Particulate nutrient fluxes over a fringing coral reef: Source-sink dynamics inferred from carbon to nitrogen ratios and stable isotopes. *Limnol. Oceanogr.* 58, 409–427. doi: 10.4319/lo.2013.58.1.0409

Wyatt, A. S. J., Matsumoto, R., Chikaraishi, Y., Miyairi, Y., Yokoyama, Y., Sato, K., et al. (2019). Enhancing insights into foraging specialization in the world's largest fish using a multi-tissue, multi-isotope approach. *Ecol. Monogr.* 89:e01339. doi: 10.1002/ecm.1339

Zgliczynski, B. J., Williams, G. J., Hamilton, S. L., Cordner, E. G., Fox, M. D., Eynaud, Y., et al. (2019). Foraging consistency of coral reef fishes across environmental gradients in the central Pacific. *Oecologia* 191, 433–445. doi: 10.1007/s00442-019-04496-9

Zhu, Y., Newman, S. P., Reid, W. D. K., and Polunin, N. V. C. (2019). Fish stable isotope community structure of a Bahamian coral reef. *Mar. Biol.* 166:160. doi: 10.1007/s00227-019-3599-9

Zikova, A. V., Britaev, T. A., Ivanenko, V. N., and Mikheev, V. N. (2011). Planktonic and symbiotic organisms in nutrition of coralobiont fish. *J. Ichthyol.* 51, 769–775. doi: 10.1134/S0032945211060105

frontiers | Frontiers in Ecology and Evolution

TYPE Original Research
PUBLISHED 17 October 2022
DOI 10.3389/fevo.2022.986082

Check for updates

OPEN ACCESS

EDITED BY
Davide Valenti,
University of Palermo, Italy

REVIEWED BY
Paolo Lazzari,
Istituto Nazionale di Oceanografia e di Geofisica Sperimentale, Italy
Christian Briseño-Avena,
University of North Carolina Wilmington, United States

*CORRESPONDENCE
Boris Espinasse
boris.espinasse@laposte.net

SPECIALTY SECTION
This article was submitted to Population, Community, and Ecosystem Dynamics, a section of the journal Frontiers in Ecology and Evolution

RECEIVED 04 July 2022
ACCEPTED 08 September 2022
PUBLISHED 17 October 2022

CITATION
Espinasse B, Sturbois A, Basedow SL, Hélaouët P, Johns DG, Newton J and Trueman CN (2022) Temporal dynamics in zooplankton $\delta^{13}C$ and $\delta^{15}N$ isoscapes for the North Atlantic Ocean: Decadal cycles, seasonality, and implications for predator ecology.
Front. Ecol. Evol. 10:986082.
doi: 10.3389/fevo.2022.986082

COPYRIGHT
© 2022 Espinasse, Sturbois, Basedow, Hélaouët, Johns, Newton and Trueman. This is an open-access article distributed under the terms of the Creative Commons Attribution License (CC BY). The use, distribution or reproduction in other forums is permitted, provided the original author(s) and the copyright owner(s) are credited and that the original publication in this journal is cited, in accordance with accepted academic practice. No use, distribution or reproduction is permitted which does not comply with these terms.

Temporal dynamics in zooplankton $\delta^{13}C$ and $\delta^{15}N$ isoscapes for the North Atlantic Ocean: Decadal cycles, seasonality, and implications for predator ecology

Boris Espinasse[1]*, Anthony Sturbois[2,3], Sünnje L. Basedow[1], Pierre Hélaouët[4], David G. Johns[4], Jason Newton[5] and Clive N. Trueman[6]

[1]Department of Arctic and Marine Biology, UiT The Arctic University of Norway, Tromsø, Norway, [2]Laboratoire des Sciences de l'Environnement Marin (LEMAR), UMR 6539 CNRS/UBO/IRD/IFREMER, Plouzané, France, [3]Vivarmor Nature, Ploufragan, France, [4]The Marine Biological Association, Plymouth, United Kingdom, [5]National Environmental Isotope Facility (NEIF), Scottish Universities Environmental Research Centre (SUERC), East Kilbride, United Kingdom, [6]School of Ocean and Earth Science, University of Southampton, Southampton, United Kingdom

The limited amount of ecological data covering offshore parts of the ocean impedes our ability to understand and anticipate the impact of anthropogenic stressors on pelagic marine ecosystems. Isoscapes, i.e., spatial models of the distribution of stable isotope ratios, have been employed in the recent years to investigate spatio-temporal patterns in biogeochemical process and ecological responses. Development of isoscapes on the scale of ocean basins is hampered by access to suitable reference samples. Here we draw on archived material from long-running plankton survey initiatives, to build temporally explicit isoscape models for the North Atlantic Ocean (> 40°N). A total of 570 zooplankton samples were retrieved from Continuous Plankton Recorder archives and analysed for $\delta^{13}C$ and $\delta^{15}N$ values. Bayesian generalised additive models were developed to (1) model the relations between isotopic values and a set of predictors and (2) predict isotopic values for the whole of the study area. We produced yearly and seasonal isoscape models for the period 1998–2020. These are the first observation-based time-resolved C and N isoscapes developed at the scale of the North Atlantic Ocean. Drawing on the Stable Isotope Trajectory Analysis framework, we identify five isotopically distinct regions. We discuss the hydro-biogeochemical processes that likely explain theses modes, the differences in temporal dynamics (stability and cycles) and compare our results with previous bioregionalization efforts. Finally, we lay down the basis for using the isoscapes as a tool to define

predator distributions and their interactions with the trophic environment. The isoscapes developed in this study have the potential to update our knowledge of marine predator ecology and therefore our capacity to improve their conservation in the future.

KEYWORDS

feeding grounds, Bayesian spatial modelling, migration pathways, trophic baseline, ecoregion

Introduction

Oceans have been under continuous and increasing anthropogenic pressure over the last two centuries (Halpern et al., 2019). The diversity of the stressors, and their combined and interactive effects complicate the study of their impacts on marine ecosystems (Bundy et al., 2021; Heneghan et al., 2021). In addition, several gaps in our knowledge still hamper our ability to characterise how stressors affect different components of the ecosystem and to anticipate their evolution in the future. In particular, there is a need to distinguish between internal dynamic, natural variability intrinsic to the ecosystem, and stressor-induced variability that might result in irreversible shifts in ecosystem structure and functioning (Scheffer et al., 2001; Henson et al., 2017). Fundamental knowledge on spatial distribution of species and populations and their interactions is also commonly missing, particularly in remote, inaccessible regions such as ocean basins. To overcome these challenges, observational-based multidisciplinary datasets with resolutions matching spatio-temporal dynamics of ecological processes occurring in the oceans are needed. While monitoring programs are common in coastal areas, the offshore part of the oceans remains poorly monitored due to very large spatial scales, and the associated expense and logistical challenges of sampling the animals and their environment (Richardson and Poloczanska, 2008).

New approaches are being developed to fill observational gaps. Among them, natural biogeochemical tracers present the advantage of recording various parameters on *in situ* conditions experienced by animals, suitable for later retrospective analysis (McMahon et al., 2013a). Spatio-temporal variations of natural abundance stable isotope (SI) ratios of carbon and nitrogen (expressed as $\delta^{13}C$ and $\delta^{15}N$ values) have been widely used during the last decades to infer aspects of hydrological conditions (Kline, 1999), nutrient sources and limitations (Rau et al., 1991; Hobson et al., 1995), animal movement or trophic level (Jennings and Warr, 2003; Cherel and Hobson, 2007). Spatial modelling (mapping) of SI ratios at the base of the food web (with spatial models commonly termed "isoscapes"; West et al., 2010), allows consideration of underlying biogeochemical drivers responsible for producing spatial pattern in isotope ratios as well as providing a reference to interpret stable isotope compositions measured in tissues of mobile consumers (McMahon et al., 2013b; Trueman and St John Glew, 2019). Isoscapes can be produced using mechanistic (theoretical) or observation-based (statistical) approaches (Bowen, 2010). Mechanistic models have the advantage of producing isoscapes at global scale and potentially allow projection forward and backward in time (Tagliabue and Bopp, 2008; Schmittner and Somes, 2016), but their spatial resolution is limited by the data used to feed the model, the complexity of model structures required to represent biogeochemical reality and our incomplete understanding of the isotopic expression of biogeochemical processes (e.g., nitrate map). Observation-based isoscapes can be developed either by using simple interpolation methods (e.g., Schell et al., 1998) or can be modelled based on predictors to reinforce prediction power where observations are not available (St John Glew et al., 2019). Such isoscapes have already been produced in different places, including the North Pacific Ocean (Espinasse et al., 2020a), the North Sea (Mackenzie et al., 2014), the Arctic Ocean (Buchanan et al., 2021), and the Southern Ocean (St John Glew et al., 2021).

The North Atlantic Ocean is one of the most studied marine areas in the world, with some of the oldest monitoring programs still in activity (Hays et al., 2005). Major ecological concepts were established there, including the match-mismatch hypothesis (Cushing, 1990) with deep consequences on our understanding of cascading effects of climate change in marine ecosystems (Beaugrand et al., 2003; Chivers et al., 2017). Despite the intense study and detailed observation, only one interpolation model of SI variations in carbon and nitrogen across the North Atlantic is currently available (McMahon et al., 2013b), based on relatively sparsely distributed reference data. In this study, we use a long-term monitoring program to access samples of *Calanus*, a large copepod collected along transects across the North Atlantic Ocean. These copepods play a major role both by transferring carbon toward higher trophic levels, but also in the biological pump by contributing to the sequestration of carbon in the ocean bottom (Brun et al., 2019). We modelled yearly and seasonal isoscapes based on *Calanus* isotopic composition and environmental variables for 1998–2020. The objectives were (1) to identify ecoregions with similar isotopic regime, (2) to

describe the temporal dynamic (variability and trend) in carbon and nitrogen isoscapes, and (3) to lay the basis for future applications.

Materials and methods

Zooplankton sample collection

Zooplankton samples were retrieved from the archives of the Continuous Plankton Recorder (CPR) survey. The CPR survey consistent methodology started in 1958, and over a quarter of a million samples have been processed since then. Sample collection is made with an autonomous plankton sampler towed by ships of opportunity along their monthly commercial routes. The system does not need electrical power or human handling (other than putting the instrument in the water and retrieving it). It collects plankton in sub surface water (about 7–9 m depth) using a continuously moving band of filter silk. The silk is further divided into samples, each representing a ten nautical miles piece of transect (for a volume of about 3 m^3 of filtered water).

The extent of the study area was roughly designed by the occurrence of CPR samples and therefore covers the northern part of the North Atlantic Ocean from 40°N to 72°N and from 60°W to 16°E (**Figure 1**). We specifically target large herbivorous copepods, aiming to produce an isotopic baseline as consistent as possible by limiting inter-sample differences in trophic level. *Calanus finmarchicus* and *Calanus helgolandicus* are two congeneric calanoid copepod species with a similar life cycle which includes lipid storage and seasonal diapause in deep water (Wilson et al., 2015). The core distribution area of the two species is separated by the North Atlantic current, which flows across the North Atlantic Ocean from SW to NE. A total of 570 samples (CV and adult stages) were selected to cover the whole study area with both species being selected, although *C. finmarchicus* was predominantly used (n = 511).

The samples were selected from the CPR list, including several thousands of entries. The rationale behind the sample selection consisted of: presence of *C. finmarchicus* or *C. helgolandicus* in numbers required for SI analysis; availability of ocean colour data (subject to cloud coverage); distance of 50 km from the 200 m isobath; to represent most ecoregions defined in Beaugrand et al. (2019). The samples were selected within a 10-year time window 2009–2018, which is wide enough to smooth interannual variability, but still allow to have a significant number of samples for each year.

The main mechanisms driving changes in isotopic values of lower trophic level are not necessarily the same in coastal environments and in open ocean. Freshwater runoff, sediment resuspension and terrestrial inputs are some of the drivers that can dramatically affect isotopic values of organisms onto the shelf. Physical processes in coastal area tend to be highly variable in time, and complexify the modelling of relationship between parameters and observed isotopic composition. In the frame of this study, we focused on the offshore part of the ocean and therefore did not include a 50 km width band from the 200 m isobath.

We aimed to produce yearly as well as seasonal isoscapes. Seasonal time windows ideally maximise temporal variation among seasons while minimising temporal variance within seasons. Time windows for the seasonal isoscapes were defined based on sample availability and the state of the system (dynamic vs. stable). Relatively few samples are available from November to February, removing this time period as an option. The width of the time window needs to be large enough to provide sufficient samples to resolve a spatial model (we aim for 100 samples per time window). Also, tissues from individuals with different growth and metabolic rates reflect integration across varying timeframes so it is better to select a time window during which the ecosystem is relatively temporally consistent in terms of productivity, so that the isotopic values are stabilised. Taking these aspects in consideration (see **Supplementary Figure 1**), three seasonal time windows were defined: winter, mid-February to end of March (n = 90); summer, June (n = 300); and fall, mid-September to mid-October (n = 180).

Isotopic analysis

Isotopic ratios are expressed in the following standard notation $\delta X = R_{sample}/R_{standard} - 1$, where X is ^{13}C or ^{15}N and R is the $^{13}C/^{12}C$ or $^{15}N/^{14}N$. The $\delta^{13}C$ and $\delta^{15}N$ values are expressed in parts per thousand (‰) relative to external standards of Vienna Pee Dee Belemnite and atmospheric nitrogen, respectively. All samples were dried, encapsulated in tin foil and sent for SI analysis at the Scottish Universities Environmental Research Centre (SUERC) as part of National Environmental Isotope Facility (NEIF). Samples were loaded into an Elementar (Hanau, Germany) Pyrocube elemental analyser, which converted carbon and nitrogen in the samples to CO_2 and N_2 gases. $\delta^{13}C$ and $\delta^{15}N$ of evolved gases were measured on a Thermo-Fisher-Scientific (Bremen, Germany) Delta XP Plus isotope ratio mass spectrometer. The system was calibrated using laboratory standards and then independently checked for accuracy using USGS 40 glutamic acid reference material (Qi et al., 2003; Coplen et al., 2006). Measurement precision was assessed by running replicates of laboratory standards and resulted in a SD consistently < 0.1‰ and 0.2‰ for $\delta^{13}C$ and $\delta^{15}N$, respectively. A quality check was performed to discard samples having too low C or N mass, resulting in n = 506 for $\delta^{15}N$ and n = 567 for $\delta^{13}C$.

The sampling procedure of the CPR survey includes instantaneous conservation of the samples with 4% buffered formalin (Batten et al., 2003). Effects of formalin preservation on copepod isotopic composition have been shown to be negligible

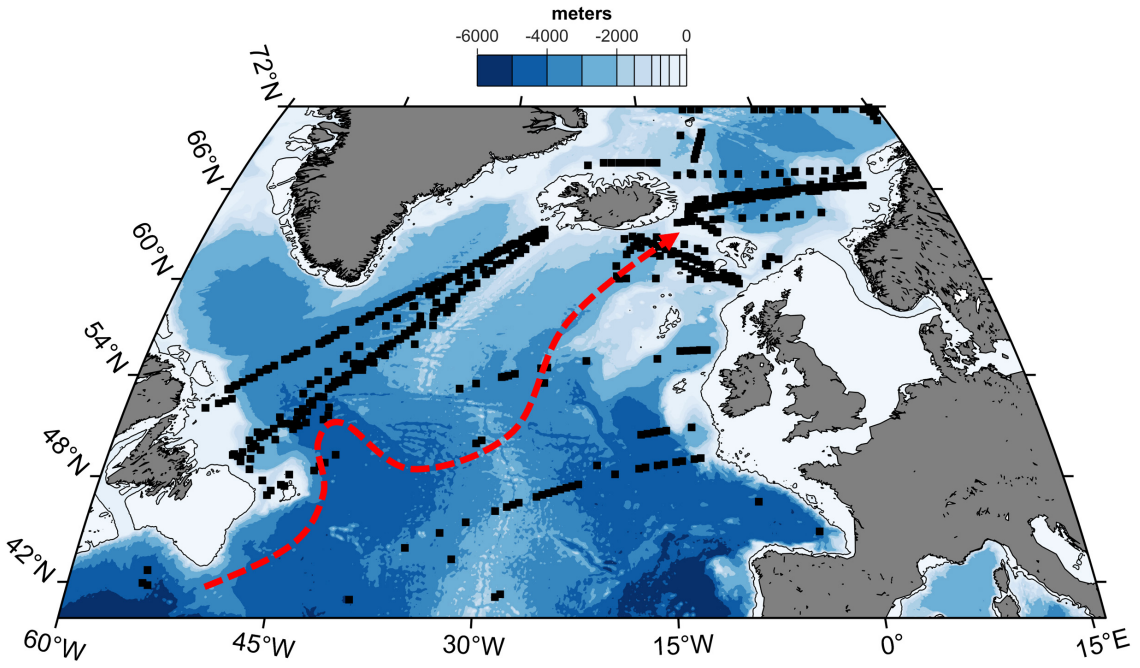

FIGURE 1
Location of zooplankton samples collected in the North Atlantic Ocean (> 40°N). The 200 m isobath is shown (thin black line). Dashed red line show approximate position of the main branch of the North Atlantic Current (from Drinkwater et al., 2020).

on $\delta^{15}N$ values and small on $\delta^{13}C$ values (Hetherington et al., 2019), with most of the effects occurring within the first weeks (Bicknell et al., 2011). In order to facilitate the comparison with other studies, we applied correction factors specifically developed for copepods sampling within the CPR survey (+0.68 and –0.33 for $\delta^{13}C$ and $\delta^{15}N$, respectively) (Bicknell et al., 2011).

Because *Calanus* store lipids and lipids are depleted in ^{13}C relative to proteins and carbohydrates, it is common to correct $\delta^{13}C$ values to remove effect of lipid content (Kiljunen et al., 2006; Post et al., 2007; Logan et al., 2008). High lipid content results in high carbon biomass and higher Carbon-to-Nitrogen (CN) ratios. Therefore, CN ratios are commonly used to establish correction model. However, CN ratios appeared to be very stable through samples (4.41 ± 0.43), close to expected values for chitinous copepod samples with little or no lipid content (El-Sabaawi et al., 2009; Espinasse et al., 2014). This might be due to the sampling procedure that tends to squeeze the copepods between the silks. We did not then correct $\delta^{13}C$ values for lipids.

Carbon dioxide originating from fossil fuel burning is also depleted in ^{13}C. With the increase of CO_2 concentration in the atmosphere driven by anthropogenic activities, $\delta^{13}C$ values follow a negative trend known as the Suess effect (Gruber et al., 1999). In the oceans, which capture a large part of CO_2, $\delta^{13}C$ values of autotroph organisms are impacted *via* two mechanisms. The Suess effect itself, which result in lowering $\delta^{13}C$ values for aqueous CO_2, and the increase in aqueous CO_2 concentration, which allows phytoplankton to use more ^{12}C, their preferential isotope. The combination of these two mechanisms results in an exponential decrease of $\delta^{13}C$ values at the base of the food webs, with the effect getting stronger in recent years (Espinasse et al., 2018). We correct our data using 2015 as a reference year. The correction factors were provided by the R-package SuessR (Clark et al., 2021).

Environmental variables

A range of variables were considered to produce parameters used to explain zooplankton SI variability. The main constraint was to obtain a consistent dataset covering the whole study area with good spatial resolution, and being available for a time period matching at least 2009–2018 (SI data). Observational data were prioritised. Available variables were: chlorophyll-a concentration (chla), net primary production (NPP), sea surface temperature (SST), wind speed (wind), mixed layer depth (MLD), and distance to the shelf (dist). Data were provided in various resolutions before being projected onto a 0.25° grid. All datasets were retrieved from the European Union Copernicus Marine Environmental Monitoring Service (CMEMS).[1] SST were extracted from the Operational Sea Surface Temperature and Ice Analysis (OSTIA) product, provided by the UK's Met

1 marine.copernicus.eu/

Office. OSTIA uses satellite data provided by the GHRSST project together with *in situ* observations to determine the sea surface temperature (Good et al., 2020). MLD was issued from the GLORYS12V1 product, which is a global ocean eddy-resolving reanalysis covering the satellite altimetry period 1993–2018. Wind data were provided by IFREMER, France. The product consists of L4 satellite-derived observations using scatterometer. Chla concentrations were collected from GlobColour.[2] GlobColour delivers a merged product that uses all satellite data available at the processing time (Maritorena et al., 2010). All Chla data used in this study has been developed, validated, and distributed by ACRI-ST, France. NPP was computed using the Eppley Vertically Generalized Production Model (Eppley-VGPM) calculation. The Eppley-VGPM calculation was adapted from the VGPM approach (Behrenfeld and Falkowski, 1997), in which the polynomial description of light-saturated photosynthetic efficiencies as a function of SST is replaced with the exponential relationship described by Morel (1991) and based on the curvature of the temperature-dependent growth function described by Eppley (1972). The script for the calculation was acquired from Oregon State University.[3] Chla and NPP products are dependent on atmospheric conditions, resulting in missing data for some areas due to persistent cloud coverage. The distance to the shelf (dist) was calculated as distance from the centre point of the grid cell to the 200 m isobath, based on ETOPO1 Global Relief Model. Each environmental covariate value was extracted at each sampling location.

Isotopic values of copepods sampled at a given time cannot systematically be explained by local, immediate environmental conditions (Rolff, 2000). Indeed, a change in environmental conditions might take a few days to be reflected into autotroph isotopic composition (driven by a wide range of factors including environmental conditions, phytoplankton composition, growth, and shape). As all heterotrophs, *Calanus* SI values are influenced by the isotopic baseline and the trophic structure linking the base of the food webs to the copepods. Therefore, isotopic composition of the autotrophs is not necessarily transferred directly into zooplankton. However, the presence of an intermediate trophic step between phytoplankton and herbivorous zooplankton, i.e., protozoan, was shown to not significantly affect zooplankton $\delta^{15}N$ values (Gutiérrez-Rodríguez et al., 2014). Furthermore, once the new conditions stabilise, it is the tissue turnover rate of copepods that will define when the final isotopic values are reached. It is estimated to take about 1–2 weeks for copepods (Graeve et al., 2005; Tiselius and Fransson, 2016). During this time, the animals are transported around with water masses and might experience different conditions complexifying the picture. We tested a range of integration windows for the environmental variables and concluded that 2 months produce the best models for explaining observed SI data.

Model development

Model development and metrics production were conducted using the software environment R v.4.1.3 (R Core Team, 2022). All maps were produced using the m_map package (Pawlowicz, 2019) running under Matlab 2020a. To produce isoscapes, we used the following sequence: (1) obtaining geo-referenced SI dataset, (2) extracting environmental variables at sampling locations and times, (3) carrying preliminary dataset checks, (4) selecting the best models using a frequentist approach, (5) implementing spatial component using Bayesian framework, and (6) predicting SI values for the whole study area using the modelled relationship and continuously observed environmental variables as predictors. The first two steps were introduced above.

We followed the protocol detailed by Zuur et al. (2010) for data exploration. Covariates were checked for outliers, normal distribution, and collinearity. It implied to log transform or cap some of the parameters (see **Supplementary Table 1** for details). The covariate NPP was removed in the process (variance-inflation factors, VIF > 5).

We developed several frequentist Generalized Additive models (GAMs) using the "mgcv" R-package (Wood et al., 2016; Wood, 2017). GAM are semi-parametric extensions of Generalized Linear Models, which allows the use of smoothers to fit covariates. The procedure for model selection includes trying several predictor combinations, defining the number of knots for the smoothers and comparing model efficiency (Akaike information criterion, AIC) (Akaike, 1974).

The Bayesian hierarchical spatial modelling framework, Integrated Nested Laplace Approximation (INLA) (Rue et al., 2009), was demonstrated to be a powerful spatial statistical package to produce isoscapes (St John Glew et al., 2019). Compared to the frequentist mixed modelling approach, the Bayesian framework enable uncertainty to be more easily interpretable, allow the inclusion of boundary effects and solve the spatial dependency term in an alternative and faster way. We used the guidelines in Lindgren and Rue (2015) to write and structure the code with the R-INLA package, and from Zuur et al. (2017) to adapt frequentist GAM smoothers to INLA. This allowed a better control on the number of knots which define the "wiggliness" of the smoothers (i.e., the amount of smoothing). In ecological studies, where datasets are often sparse and fragmented, it is recommended to apply greater amount of smoothing to dampen wiggliness as high-frequency variations in poorly constrained smooth terms can result in

2 https://www.globcolour.info/

3 science.oregonstate.edu/ocean.productivity

models which are too specific to the dataset and makes difficult to relate smoother shapes and ecological processes.

$$\text{Models were specified as : } Y_i = b + f_1(X_{1i}) + f_2(X_{2i}) \ldots + f_n(X_{ni}) + W_i$$

where Y_i is the isotope value ($\delta^{13}C$, $\delta^{15}N$) at location i; b is the intercept, f_n are smooth functions (thin plate regression splines in this case), and X_n are the covariates; W_i represents the smooth spatial effect, linking each observation with a spatial location. INLA uses the Stochastic Partial Differential Equations (SPDE) approach for the spatial effect (Lindgren et al., 2011). The SPDE approach enables the covariance matrix of the Gaussian field to be approximated as a Gaussian Markov Random Field using a Matérn covariance structure and Delaunay triangulation to create prediction locations in the form of a mesh (**Supplementary Figure 2**). The Matérn covariance function has two hyperparameters: the marginal standard deviation σ and κ (smoothness of the field, relates to the range r). As recommended by Fuglstad et al. (2019), we set priors for these two parameters such as $P(r < 100 \text{ km}) = 0.01$ and $P(\sigma > 2) = 0.01$.

All the models were validated by checking the homogeneity of variance and the normal distribution of residuals and by investigating any pattern in the plot of residuals against predictors (Zuur, 2012). The best fit models were used to predict $\delta^{13}C$ and $\delta^{15}N$ values across the whole North Atlantic Ocean spatial domain using environmental variables as predictors. Response variables were estimated at all mesh vertices which were then linearly interpolated within each triangle into a finer regular grid (0.25°) *via* Bayesian kriging. Mean and variance predictions were obtained for each grid cell. To ensure that predicted values fell within a sensible range, environmental variable surfaces were assessed to check that all values used for predictions fell within the range of values observed at zooplankton sampling locations (± 10%). Outlier grid cells were blanked from maps. Isoscapes were produced over the time period for which environmental variables were available, i.e., 1998–2020.

Several approaches can be used to model seasonal isoscapes using GAM: (1) splitting the dataset and developing independent models for each season, (2) using the global dataset and including season as a fixed effect,or (3) using the global dataset to develop a universal model and making predictions with seasonally explicit sets of predictors. Our dataset did not allow for the first option as not enough data were available for each season, especially for winter. The two other options gave similar results when comparing observation and modelled values at sampling locations (using frequentist models without spatial component) (**Supplementary Figure 3**). The third option was favoured over the second one because it resulted in simpler model structure.

Trajectory analysis and isoscape metrics

The stable isotope trajectory analysis (SITA) framework and its tools devoted to isoscape data sets were used to assess the long-term spatio-temporal dynamics of isoscape at year and seasonal scales (Sturbois et al., 2021b). The Space of analysis was defined by $\delta^{13}C$ and $\delta^{15}N$, and is called here after Ω^{δ}. In this study, SITA was used to evidence the broad spatial and temporal structure captured by the modelled isoscapes, aiming (1) to identify different eco-regions characterised by different SI compositions and temporal trends; (2) to represent the magnitude and the nature of changes at different temporal scales. Analysis has been performed with the R-package "ecotraj" (De Cáceres et al., 2019; Sturbois et al., 2021a). Modelled $\delta^{13}C$ and $\delta^{15}N$ values of a 1° × 1° spatial grid were subset from the original output model (0.25° × 0.25°). Mapping trajectory metrics requires that grid cells are synchronously resolved. Consequently, grid cells where values were missing for at least one date were excluded. Trajectory analyses of "year" isoscapes were thus performed on $\delta^{13}C$ and $\delta^{15}N$ values modelled for 1,125 grid cells from 1998 to 2020.

Length-based metrics were calculated to measure the magnitude of change. The segment length measures the shift in the $\delta^{13}C/\delta^{15}N$ 2D space (Euclidean distance, ‰) for a given sampling unit (here modelled grid cell) between two consecutive years. The trajectory path length is the sum of segment lengths for a given grid cell. This metric informs about the overall temporal change from 1998 to 2020. The net change is defined as the length between a pair of states, which includes a chosen baseline state, initial or reference state, in our case the first year of our time series, 1998. When calculated at the scale of an overall study period, this metric evaluates the difference between the initial and the final state, i.e., the overall net trajectory changes between 1998 and 2020. The greater the value of a length-based metric, the greater the distance between states is. These metrics are particularly relevant to analyse the magnitude and the variability of dynamics and to point gradual and abrupt changes.

Direction-based metrics were calculated to measure the nature of change. Angle α measures the trajectory segment directions with respect to the interpretation of the axes defining the $\delta^{13}C/\delta^{15}N$ 2D space. Angle α is measured considering the second axis of the 2D diagram as the North (0°). α allows comparing segment directions with respect to the influence of the variables used to interpret the two axes (e.g., α = 270° means a strict ^{13}C depletion). Dissimilarities between trajectories were calculated (Directed Segment Path Dissimilarity) (De Cáceres et al., 2019), and were used with the resulting symmetric matrix as input in a Hierarchical Cluster Analysis (Ward.D2 clustering Method), to identify groups of stations characterised by similar individual trajectories. Segment length, trajectory path length,

net change, angle α and $\delta^{13}C/\delta^{15}N$ values were summarised to illustrate the variability for each trajectory cluster.

Trajectory metrics were represented though trajectory maps, trajectory roses, and isoscape trajectory maps were computed for each of the 22 consecutive pairs of dates (1998–1999, 1999–2000,. . ., 2019–2020). Additionally, SITA was performed from 1998 to 2020 using angle α and segment lengths calculated for all pairs of dates (1998–1999,. . ., 2019–2020) as input for a trajectory heatmap. A similar analysis was performed at the finest temporal scale of the 69 successive isoscapes including all seasons*years from winter 1998 to fall 2020 for the 471 1° × 1° grid cells for which no isoscape value was missing at any dates for both isotopes. Net changes values were calculated and compared among trajectory clusters to look for isoscapes cycles and dynamics temporality.

Differences in $\delta^{13}C/\delta^{15}N$ values and length-based SITA metrics were tested with one-factor ANOVAs by permutation using the function "aovp" of the package "lmPerm." Direction-based metrics were tested using circular statistics (Landler et al., 2019). The Hermans–Rasson test was used to verify if there was unimodal bias in the distribution of angle α values for each cluster, i.e., if segment direction were evenly distributed (Package CircMLE) (Fitak and Johnsen, 2017). Watson–Williams two tests were performed to test the homogeneity (null hypothesis) of angle α values among trajectory clusters.

Results

Measured zooplankton stable isotope compositions ranged from −26.40 to −19.44‰ and from 1.49 to 9.81‰ for $\delta^{13}C$ and $\delta^{15}N$ values, respectively (**Supplementary Figure 4**). The covariates combination that resulted in the best fit models were:

$$\delta^{13}C \sim s(chla, k = 5) + s(sst, k = 5) + s(dist, k = 3) + wind$$

$$\delta^{15}N \sim chla + s(mld, k = 3) + s(sst, k = 5) + s(wind, k = 5) + dist$$

with s stands for smooth class, thin plate regression splines in this case, and k is the fixed number of knots for each smoother. The significance of the covariates is shown in **Table 1**. More details about the other models and the selection process are provided in **Supplementary Table 2**.

To investigate the overall spatial patterns emerging from yearly $\delta^{13}C$ and $\delta^{15}N$ isoscapes, we produced maps of average modelled isotopic values for 1998–2020 (**Figure 2**). North Atlantic zooplankton $\delta^{13}C$ isoscapes showed a clear SE to NW gradient with values decreasing northward. South of the North Atlantic current, $\delta^{13}C$ values were generally above −22.5‰ and up to about −20‰, while north of the current, $\delta^{13}C$ values ranged from −22.5 to −25‰. Isoscapes of $\delta^{15}N$ values showed several spots across the study area with high $\delta^{15}N$ values over 6‰, including the Gulf Stream area and the southeastern part of the study. Other high spots include an area north of Iceland and two spots near Norwegian and Irish coasts. Lowest $\delta^{15}N$ values were found along the east coast of Greenland with a minimum of about 2‰. The variance associated with the predictions was generally higher for $\delta^{15}N$ than $\delta^{13}C$. The spatial patterns were otherwise very similar, with higher value observed in area with low sampling coverage and/or environmental conditions at the edge of the initial distribution range.

Changes in spatial patterns of zooplankton isotopic composition were also investigated through seasons (**Figure 3** and **Supplementary Figure 5**). Similar to the yearly isoscapes, $\delta^{13}C$ values followed a NE to SW gradient, with values covering an identical range. However, the −22.5‰ isoline moves northward from winter to fall. On the other hand, $\delta^{15}N$ values increased across the North Atlantic through the seasons, with patches of high values extending significantly.

The isoscape trajectory maps highlight the areas characterised by different degrees of variability. To illustrate how the approach works, we chose as an example the variability in $\delta^{13}C/\delta^{15}N$ isoscapes modelled for 2014 and 2015 (**Figure 4**).

Trajectory analysis extended to the whole study period identified spatial patterns in the magnitude of yearly isoscape change (**Figure 5**). Two areas located respectively to the north of Iceland and from the Newfoundland basin extending NE were characterised by the highest trajectory path implying higher short-range spatio-temporal variability in SI compositions.

Results were synthesised in the trajectory heatmap (**Figure 6**), which pointed out that isoscape dynamics mainly involved direction ranges comprised between 0°and 45°, respectively (i.e., higher $\delta^{13}C$ and $\delta^{15}N$ values), and 180° and 225° (i.e., lower $\delta^{13}C$ and $\delta^{15}N$ values). These range of directions indicated that enrichment and depletion were more important for $\delta^{15}N$ values than for $\delta^{13}C$ values. These two contrasted patterns of both isotopes mainly occurred synchronously in the North Atlantic Ocean suggesting contrasting isoscape dynamics depending on areas. Sporadically, (e.g., 1998–99 and 2008–09), one main pattern characterised by important ^{15}N depletions and slight ^{13}C depletions was observed. An inverse dynamic (i.e., higher $\delta^{13}C$ and $\delta^{15}N$ values) was observed between 2005 and 2006. In some periods, a more homogenous distribution

TABLE 1 Description of the approximate significance of smooth terms for the two selected models (*F*-values and *p*-values).

Model	Intercept	SST	Wind	dist	chla	MLD
$\delta^{13}C$	−23.96	86.78***	11.26***	6.97**	4.48**	NA
$\delta^{15}N$	5.50	19.73***	25.10***	25.09***	4.87*	48.15***

SST, Sea surface temperature (°C), Wind, wind speed (m s^{-1}), dist, distance to nearest 200 m isobath (km), chla, chla concentrations (mg m^{-3}) and MLD, mixed layer depth (m). ***$p < 0.001$; **$p < 0.01$; *$p < 0.05$.

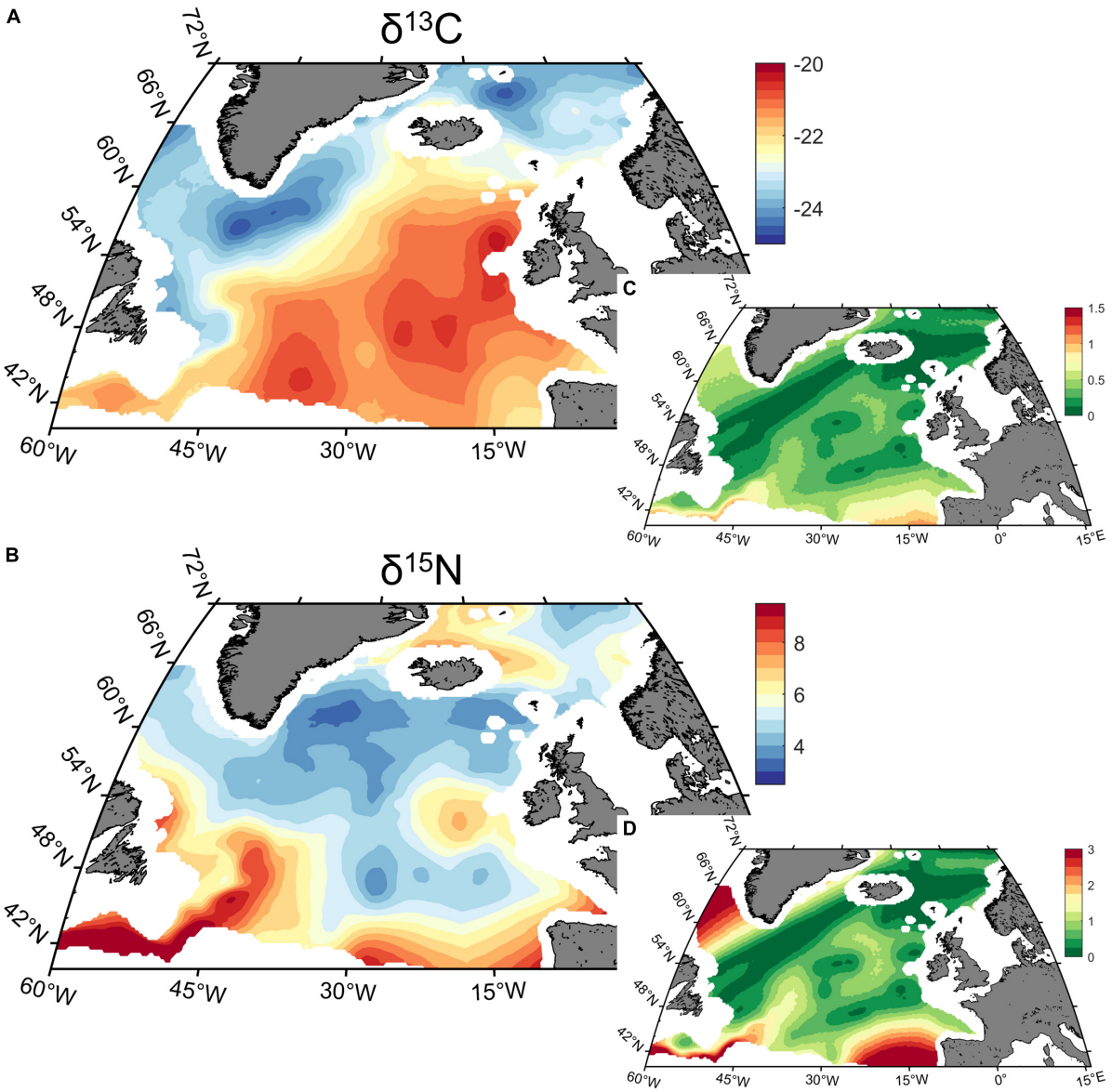

FIGURE 2
Average of **(A)** carbon ($\delta^{13}C$) and **(B)** nitrogen ($\delta^{15}N$) yearly isoscapes (‰) predicted for 1998–2020 in the North Atlantic Ocean, and **(C,D)** the associated variance of the posterior predicted distribution.

of the number of stations in the different direction ranges suggested no obvious pattern of isotope dynamics at the scale of the North Atlantic Ocean (e.g., periods 2010–2011 and 2019–2020).

Hierarchical cluster analysis identified five main trajectory clusters characterised by differences in $\delta^{13}C$ and $\delta^{15}N$ values and SITA metrics (Figure 7 and Supplementary Figure 6). Interestingly, the spatial representation of these clusters (hereafter isoregions) described different well-defined regions at the scale of North Atlantic Ocean (Figure 8). For instance, isoregion #1 exhibited among the highest $\delta^{13}C/\delta^{15}N$ values and distance-based trajectory metrics values (Figures 7, 9 and Table 2) and grid cells assigned to isoregion #1 were located in constrained areas close to the coast (Figure 8), contrasting with the lower $\delta^{15}N$ values and the broader distribution of isoregion #5. Similarly, the nature of changes varied among isoregions (i.e., trajectory segment directions, Figure 9). Results of the Herman and Rasson test confirmed that the trajectory segment directions were not evenly distributed in the 2D Ω^{δ} space ($p < 0.001$), implying particular enrichment and depletion patterns of both isotopes. Additionally, the Watson–William' two tests evidenced contrasts in the nature of change between isoregions (Figure 9 and Supplementary Table 3): (1) While isoregion #1 involved direction in the $\delta^{13}C/\delta^{15}N$ 2D space that

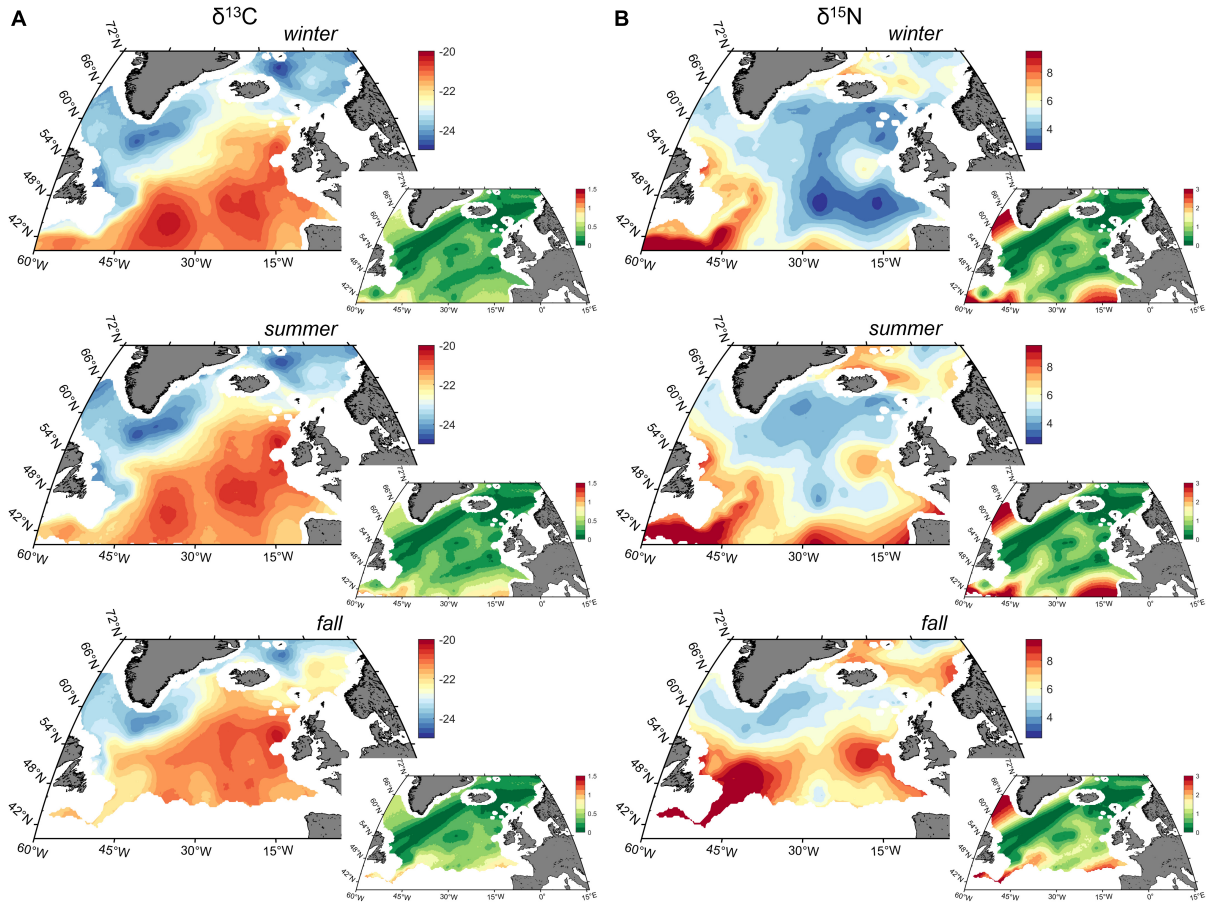

FIGURE 3
Average of **(A)** carbon ($\delta^{13}C$) and **(B)** nitrogen ($\delta^{15}N$) values winter, summer and fall isoscapes (‰) in the North Atlantic Ocean predicted for 1998–2020, and the associated variance of the posterior predicted distribution.

mainly characterised patterns of ^{15}N enrichment and depletion, such patterns were more balanced for both isotopes especially in isoregions #2, #3, and #4; (2) At finest scale, the distribution of less abundant direction occurring in an orthogonal way compared to the main directions patterns also varied among isoregions.

The net changes metric was used to assess temporal trend by comparing isoscape values to a reference, in our case the beginning of the time series, the 1998's isoscape. Potential year cycles were evidenced, especially for isoregions #4 and #5 also characterised by an increasing trend in net change values (Figure 10). At seasonal scales, cycles were evidenced when looking at the 69 successive isoscapes including all seasons*years from winter 1998 to fall 2020. All isoregions exhibited a cycle characterised by increasing net changes between summer and fall isoscapes followed by a winter reset (Figure 11A). Interestingly, some contrasts were observed in net changes values that characterised changes between winter 1998 and all other seasons. These values were higher for isoregions #1, #3, and #5, compared to isoregions #2 and #3, suggesting differences in the temporality of seasonal dynamics in the North Atlantic Ocean (Figure 11B).

Discussion

This study provides the first North Atlantic observation-based and time-resolved C and N isoscapes developed using environmental predictors. We modelled $\delta^{13}C$ and $\delta^{15}N$ isoscapes for three seasons over a time period of 23 years (1998–2020). This effort was made possible thanks to the CPR survey, which collects plankton samples routinely across the entire basin. In the first part of the discussion, we discuss the main drivers of spatio-temporal variation in zooplankton SI compositions in open ocean, firstly at the scale of the North Atlantic basin, then at regional scales. In the second part, we discuss methodological aspects and limitations associated with isoscapes development and use. Finally, we describe the potential of isoscapes in moving forward predator studies.

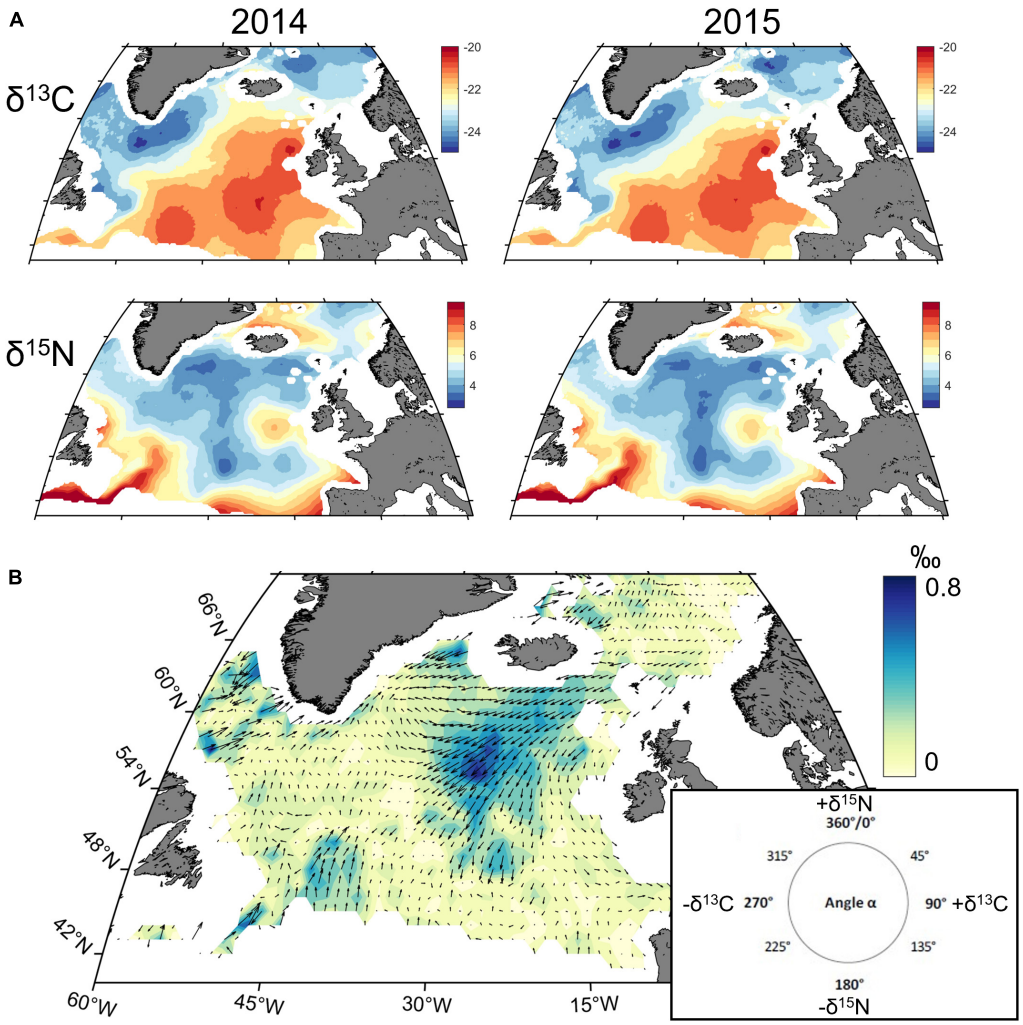

FIGURE 4
Shift in $\delta^{13}C/\delta^{15}N$ isoscapes in the North Atlantic Ocean between 2014 and 2015: **(A)** Isoscape for $\delta^{13}C/\delta^{15}N$ in 2014 and 2015; **(B)** Isoscape trajectory map synthetizing the shift for both isotopes between 2014 and 2015. Direction of arrows illustrates direction in the modelled 2D Ω^{δ} space according to increase and/or decrease in $\delta^{13}C$ and $\delta^{15}N$ values (0–90°: $+\delta^{13}C$ and $-\delta^{15}N$; 90–180°: $+\delta^{13}C$ and $\delta^{15}N$; 180–270°: $-\delta^{13}C$ and $-\delta^{15}N$; 270–360°: $-\delta^{13}C$ and $+\delta^{15}N$). Length of arrows and coloured background rasters illustrate modelled trajectory segment length (‰) at each 1° × 1° grid cell.

Potential drivers underpinning spatio-temporal variation in zooplankton isotope compositions

The yearly modelled $\delta^{13}C$ values showed two distinct areas, broadly separated by the North Atlantic Current (NAC). $\delta^{13}C$ values higher than c. –22.5‰ are likely to originate from the south-eastern region while lower values are associated with the NW area. In the open ocean, temperature is a primary covariate of $\delta^{13}C$ variability in phytoplankton. The extent of fractionation of carbon isotopes during photosynthetic fixation by phytoplankton depends on the concentration of CO_2 outside of the cell relative to the carbon demand of the cell (Popp et al., 1999; Hofmann et al., 2000; Laws et al., 2002). Increasing temperatures therefore reduce the extent of fractionation (and increase phytoplankton $\delta^{13}C$ values) through reductions in solubility of CO_2 coupled with increases in cell CO_2 demand associated with higher growth rates. The water temperature distribution in the North Atlantic Ocean is determined by the northward flow of warm water transported by the North Atlantic Current which delimits tropical to temperate and subpolar waters. SST was the most powerful covariate in the $\delta^{13}C$ model and, as expected, the isoscapes follow this spatial pattern. Other processes, such as influence of coastal waters or intense blooms (Deuser, 1970), also affect $\delta^{13}C$ values locally in the open ocean and might explain mesoscale features. Seasonal, temperature-associated isotope patterns identified in the INLA models include a trend of increasing $\delta^{13}C$ values potentially

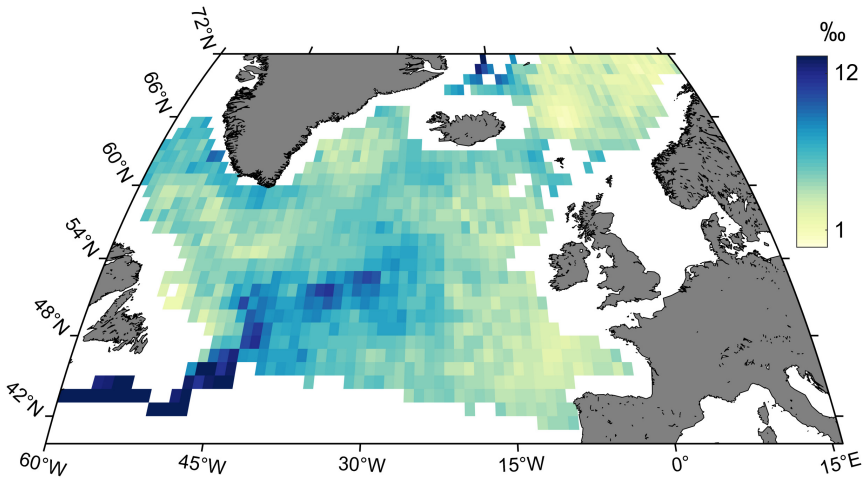

FIGURE 5
Trajectory map of trajectory path values (‰) for $\delta^{13}C/\delta^{15}N$ isoscapes in the North Atlantic Ocean from 1998 to 2020. Gradient of colours indicates the spatial trajectory path patterns for each 1° × 1° grid cell.

associated with water warming from winter through to fall periods. These trends are especially pronounced south of Iceland and in the Norwegian Sea.

The spatial distribution of $\delta^{15}N$ values in marine phytoplankton is strongly influenced by nitrate availability and associated variations in isotopically distinct sources of nitrogen taken up by phytoplankton. As with CO_2, phytoplankton preferentially use the light NO_3^- molecule (^{14}N vs. ^{15}N) resulting in $\delta^{15}N$ values varying conversely with nitrate concentrations (Rau et al., 1998; Rolff, 2000). In turn, nitrate concentrations are set by the balance between phytoplankton uptake and replenishment *via* exchanges with underneath water layer. Therefore, chla concentrations and mixed layer depth are important variables in defining $\delta^{15}N$ values. High $\delta^{15}N$ values occur in productive areas where conditions allow phytoplankton to develop and deplete nitrates (water stability in the surface layer). In addition to the southern part of the study area, i.e., the Gulf Stream area and the Iberian coast, three discrete regions of relatively high $\delta^{15}N$ values were identified, north of Iceland, the Norwegian Sea and offshore of the Irish coast.

Ecoregions

Interannual variations and temporal trends in SI values within a study area can be driven either by changes in the productivity/physical regime occurring in the core of the region or by intrusion of waters with distinct nutrient or plankton isotopic composition from adjacent regions. In this study, trajectory analysis implied that enrichment and depletion patterns of both modelled isotopes occurred simultaneously in the North Atlantic Ocean. This is in accordance with St John Glew et al. (2021) results at the scale of the Southern Ocean, but contrasted with Espinasse et al. (2020a) and (Sturbois et al., 2021a) who found that trajectories characterised by increases in $\delta^{13}C$ and $\delta^{15}N$ values alternated with decreases in both isotope values at the smallest scale of the Northeast Pacific. They showed that the level of intrusion of sub-tropical waters transporting zooplankton with higher isotopic values was the main driver of alternation between high and low SI values as represented by the SITA heatmap (Sturbois et al., 2021a). In this work, we show how large spatio-temporal scale isoscape modelling approaches can provide insight into local patterns and processes under the influence of environmental drivers, and the need to partition the study area in distinct isotopic regions.

Definitions of habitats, bioregions or ecoregions have been a useful tool to partition the ocean realm (Longhurst, 2010) and were recently updated for the North Atlantic Ocean (Beaugrand et al., 2019). The five isoregions defined in this study can be classified as follows: #1 and #3 potential coastal influence; #2 and #4 polar and sub-polar areas, respectively, part of the polar biome as defined by Longhurst (2010); #5 area south to the Gulf Stream/North Atlantic current, classified as Westerly Wind biome in Longhurst (2010). Isoregions #1 and #3 are distributed along continental shelves and are both likely to be influenced by coastal waters. Coastal/offshore water exchanges and associated plankton communities can be promoted by winds, eddies or freshwater runoff (Mackas and Coyle, 2005). Coastal waters usually transport zooplankton with specific isotopic values, which are generally higher than offshore, as these areas are often continuously productive (Kline, 2009; El-Sabaawi et al., 2013). The western distribution of the isoregion #1 corresponds roughly to the ecology unit *Gulf Stream Extension*, while its eastern part corresponds to *Pseudo-oceanic warm-temperate*, as defined by Beaugrand et al. (2019;

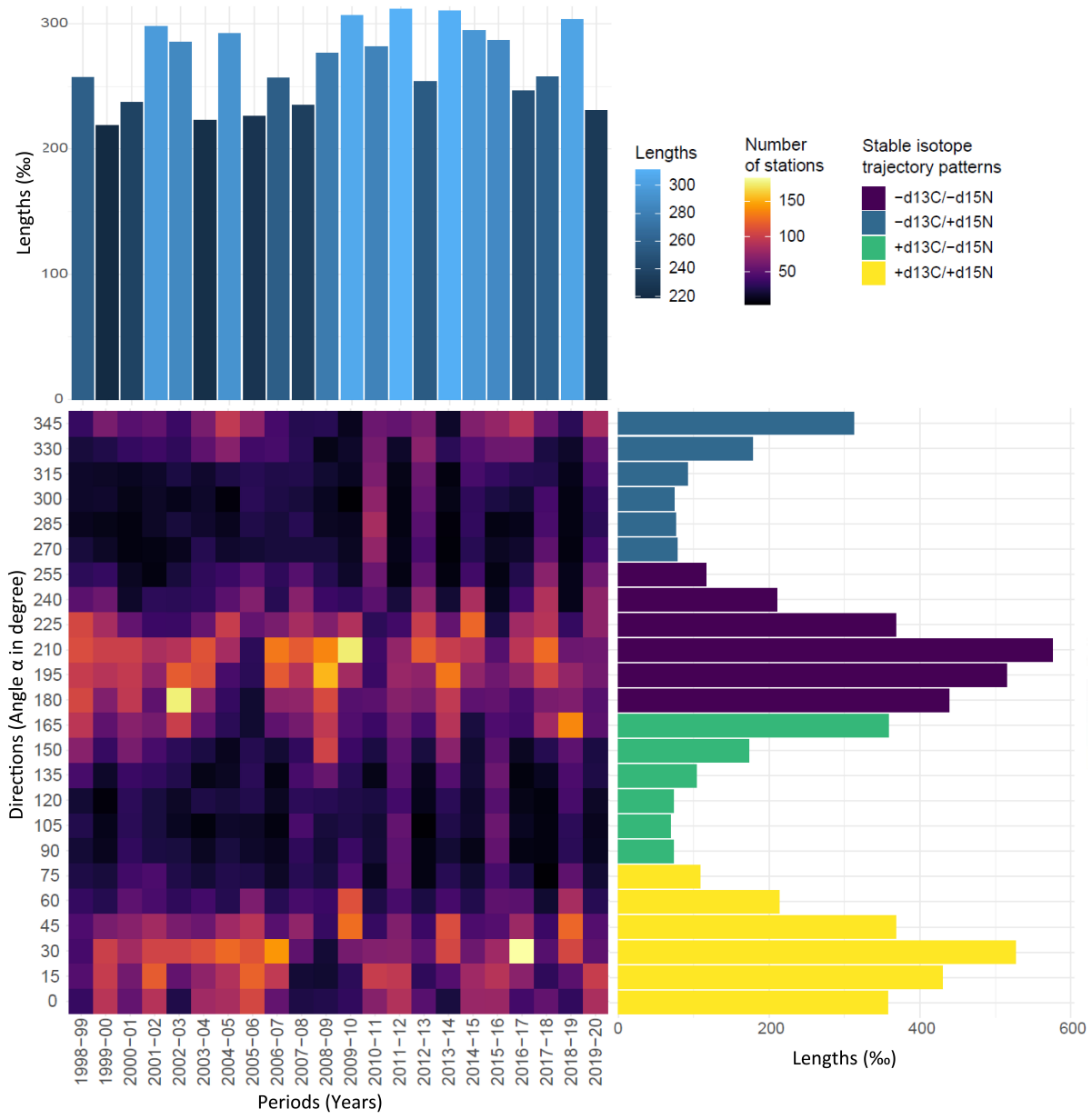

FIGURE 6
Trajectory heatmap. Heatmap panel: Angles α in the modelled 2D Ω^{δ} space exhibited by all stations within all pairs of dates (1998–1999,. . ., 2019–2020) are represented by range of direction (15° segments) according to period. Colour gradient from dark blue to yellow indicate the number of stations exhibited by a given range of direction within a given period. X barplot: Sum of segment lengths (‰) across stations and times, exhibiting the chosen range of direction. The blue gradient indicates the magnitude of the sum of segment lengths. Y barplot: Sum of segment lengths according to range of directions. Bars are coloured according to increase and/or decrease in δ^{13}C and δ^{15}N values.

see **Supplementary Figure 7**). They represent a mix of offshore and coastal waters and are influenced by subtropical climate. Isoregion #3 corresponds to the ecological unit *Polar Shelf Edge*, which is characterised by cold water, high chla concentrations and intermediate nitrate levels. Isoregions #2 and #4 corresponds to the ecological unit *Polar Oceanic* and *Sub-Polar Oceanic*, respectively. Both ecological units are characterised by cold waters and high nitrate concentrations. Isoregion #5 corresponds to ecological unit *Oceanic Warm Temperate* and *Diverse and Productive Oceanic Temperate*, characterised by warm waters and intermediate nitrate level. Overall, the temperature and nitrates concentrations between the isoregions/ecological units vary accordingly with the levels of δ^{13}C and δ^{15}N values, with expected similar trends between temperature and δ^{13}C and opposite trends between nitrates concentrations and δ^{15}N values.

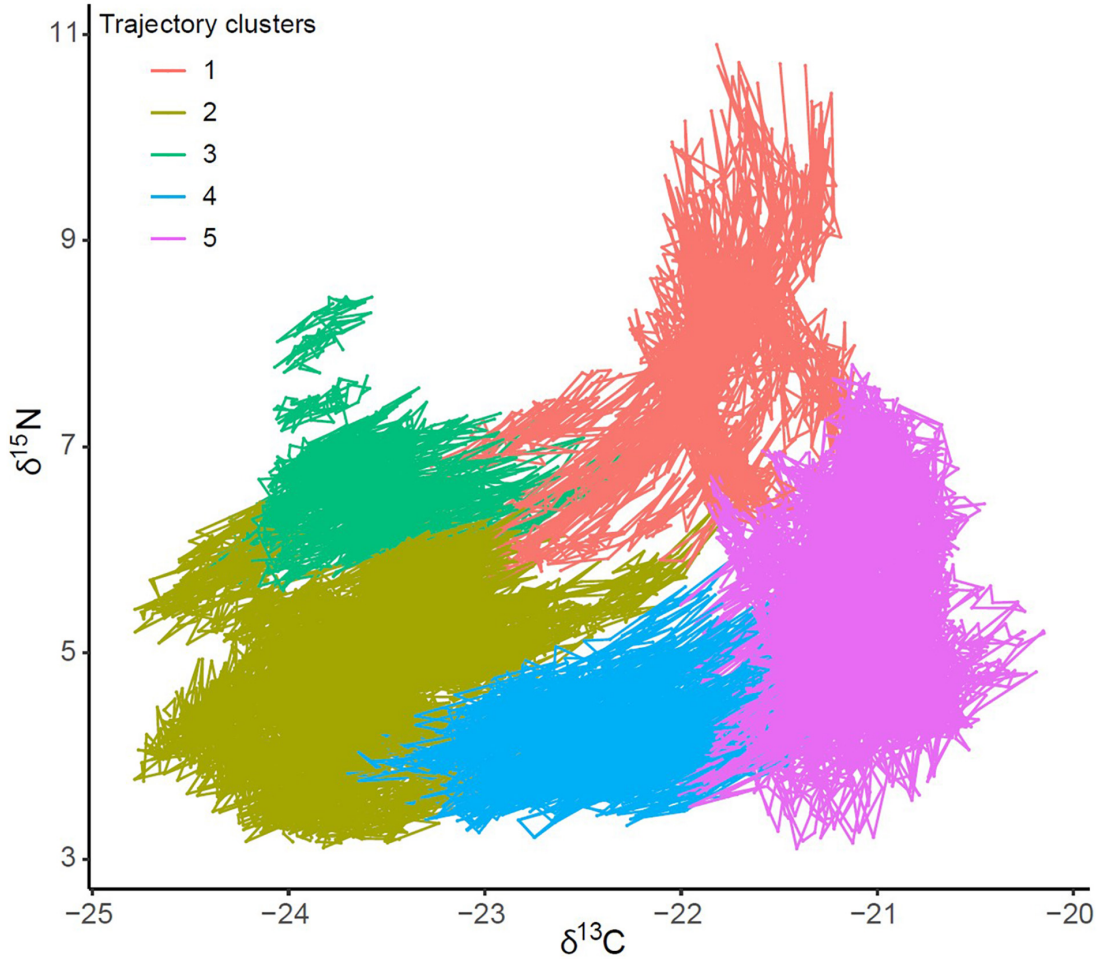

FIGURE 7
Trajectories of $\delta^{13}C$ and $\delta^{15}N$ predicted values (‰) at each grid cell for which values were predicted continuously for 1998–2020. Points are coloured according to the five clusters identified by the dissimilarities analyses between trajectories, and chronologically connected for consecutive grid cell values (1998–2020).

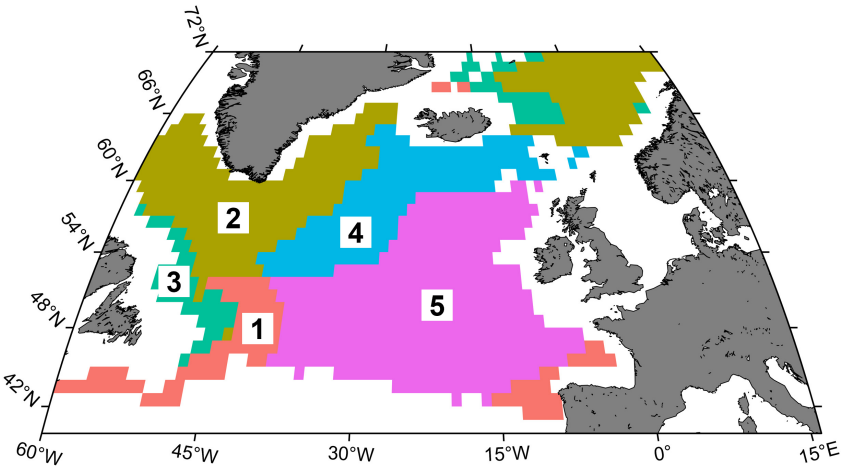

FIGURE 8
Distribution of the clusters/isoregions defined using all $\delta^{13}C$ and $\delta^{15}N$ predicted values for 1998–2020 in the North Atlantic Ocean.

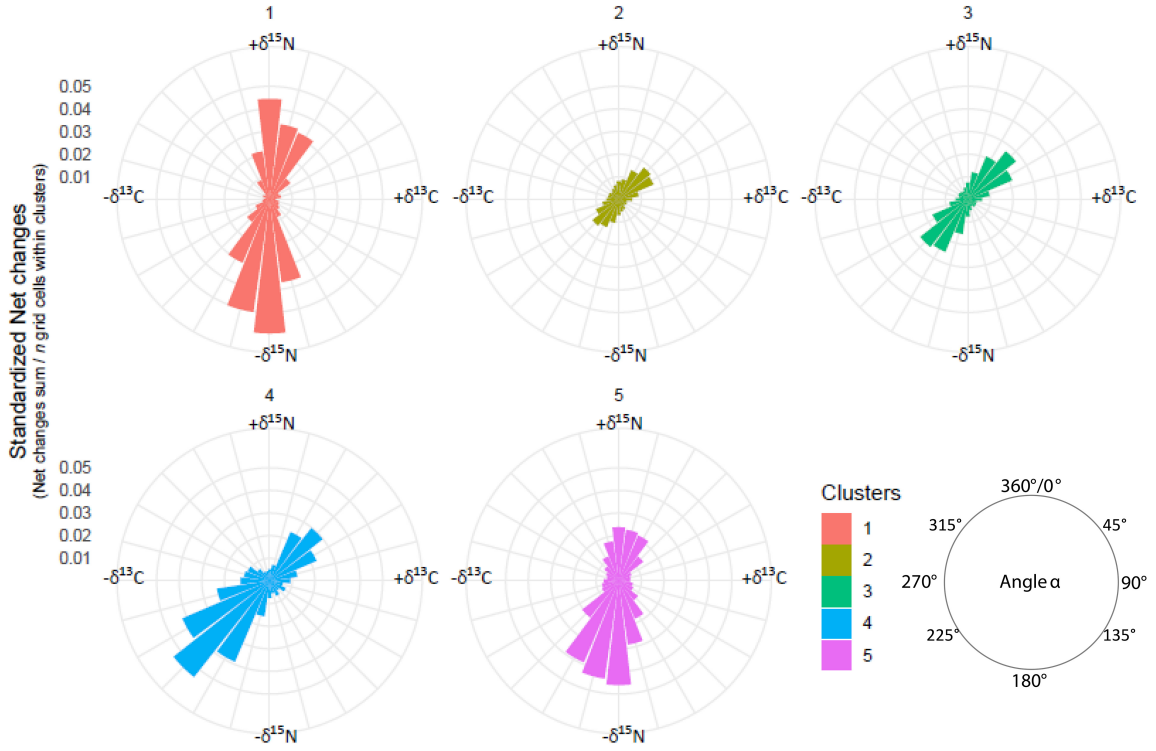

FIGURE 9
Trajectory direction (0–360°) in the modelled 2D Ω^{δ} space for the five isoregions according to increase and/or decrease in $\delta^{13}C$ and $\delta^{15}N$ values.

TABLE 2 Synthesis of $\delta^{13}C$ and $\delta^{15}N$ values (‰) and SITA length-based (‰) and direction-based (°) metrics for each trajectory clusters/isoregions with respective results of ANOVA permutation tests for stable isotope compositions and length-based metrics, and Herman–Rasson tests for direction-based metrics.

Cluster/isoregion	*n*	Stable isotope compositions		SITA metrics				HR test
		$\delta^{13}C$	$\delta^{15}N$	Trajectory path	Segment lengths	Net change	Angle α	
1	2162	−21.89 ± 0.39	5.28 ± 0.95	8.61 ± 3.81	0.39 ± 0.33	0.41 ± 0.33	360°/180°	***
2	9292	−23.61 ± 0.44	4.86 ± 0.68	4.40 ± 1.22	0.20 ± 0.14	0.21 ± 0.14	45°/225°	***
3	2208	−23.61 ± 0.33	6.47 ± 0.46	5.01 ± 2.19	0.23 ± 0.18	0.27 ± 0.22	45°/210–225°	***
4	4094	−22.38 ± 0.46	4.19 ± 0.38	5.54 ± 0.76	0.25 ± 0.15	0.39 ± 0.27	45°/225°	***
5	8119	−21.14 ± 0.28	5.34 ± 0.83	5.20 ± 1.45	0.24 ± 0.17	0.40 ± 0.27	360–15°/180–195°	***
Perm. ANOVA tests Pr(> F)		***	***	***	***	***	–	–

***$p < 0.001$.

Temporal trends

Interesting oscillating patterns in the intensity of changes were observed for some of the isoregions. The oscillations in the isoregions #4 and #5 showed a certain degree of synchronicity over the time period studied (**Figure 10**). The strength of the NAC is a natural candidate to explain these fluctuations. The NAC transports heat from the south to the eastern part of the North Atlantic and the recent weakening of the Atlantic meridional overturning circulation (AMOC) has led to negative temperature anomalies in the east part of the North Atlantic (Caesar et al., 2018). The fluctuations in net changes observed in these isoregions follow temperature anomalies recorded for these areas. These anomalies are driven by the balance between the relative proportion of water originating from sub tropical or sub polar areas (Desbruyères et al., 2021). It is interesting to note that $\delta^{13}C$ and $\delta^{15}N$ values vary together in isoregions #2 and #4, while there is a decoupling in the isoregion #5, for which mainly $\delta^{15}N$ values vary. Temperature changes in sub polar and polar waters (isoregions #2 and #4) are likely to influence both isotopic ratios, directly in the case of $\delta^{13}C$ and *via* an increase in stratification for $\delta^{15}N$. In isoregion #5, change in the North

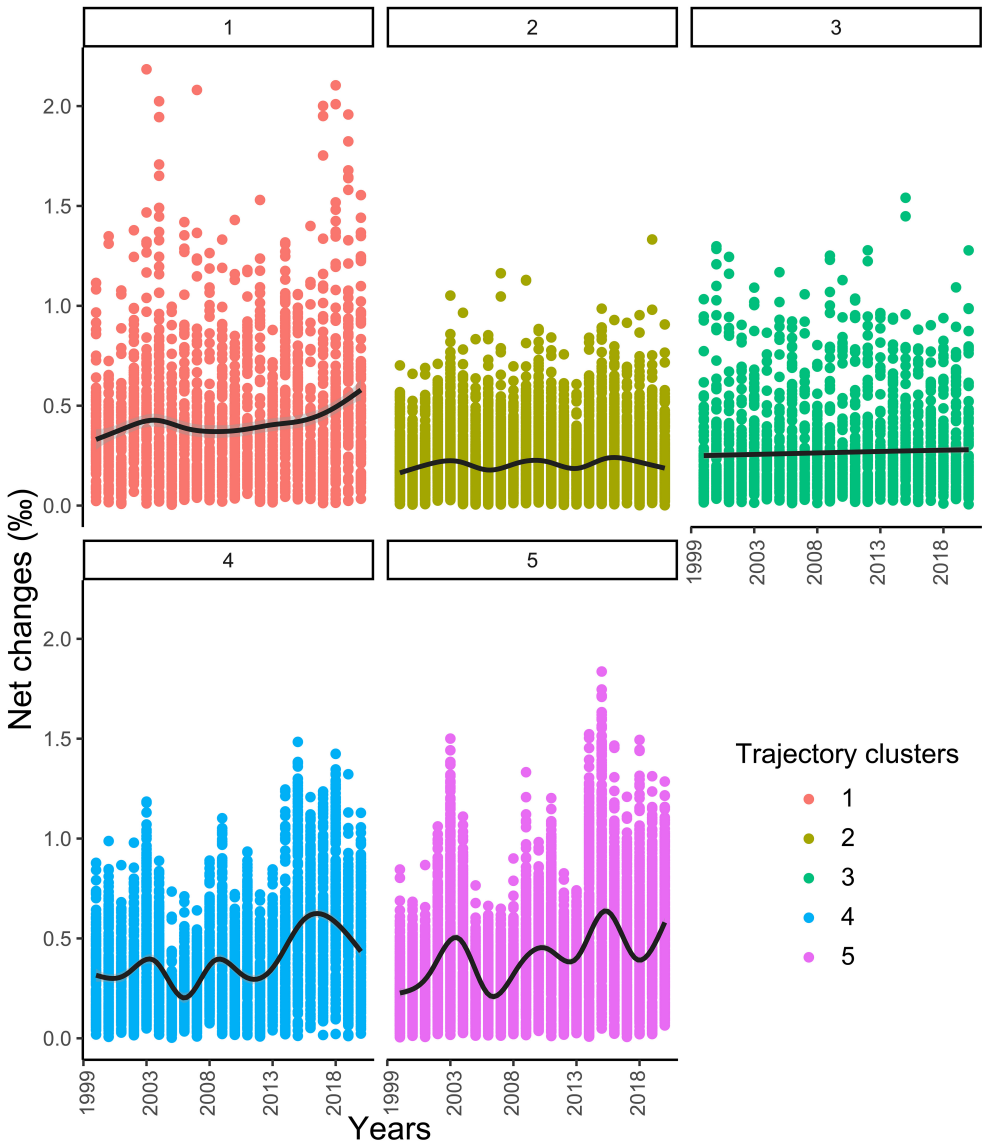

FIGURE 10
Temporal evolution of the isotopic net changes (‰) for the five isoregions over 1998–2020, taking 1998 as a year of reference. A smoothing line is shown (black thick line).

Atlantic Oscillation and associated wind regime might play a major role by affecting the MLD and indirectly the $\delta^{15}N$ values (Hurrell and Deser, 2009).

Model structure and isoscape limitations

Modelling isotopic values over large areas implies some constraints. Notably, the isoscapes should preferentially be based on consistent observational data, i.e., isotopic compositions of materials or organisms that belong to similar trophic level, and these individuals should be situated low enough in the food webs that most predators can be compared to them. Particulate organic matter (Kurle and Mcwhorter, 2017; Seyboth et al., 2018; St John Glew et al., 2021), jellyfish (Mackenzie et al., 2014; St John Glew et al., 2019), zooplankton composition or individuals (Brault et al., 2018; Espinasse et al., 2020b; Matsubayashi et al., 2020) have been used in previous studies to produce large spatial scale isoscapes. A balance needs to be found between the quality (spatiotemporal resolution, consistence in analysing, and sampling procedure among samples) and the quantity of data. In this study, the CPR survey provided us with excellent quality species specific samples with relatively high sample numbers providing reasonable, but not random, spatiotemporal coverage. Furthermore, the

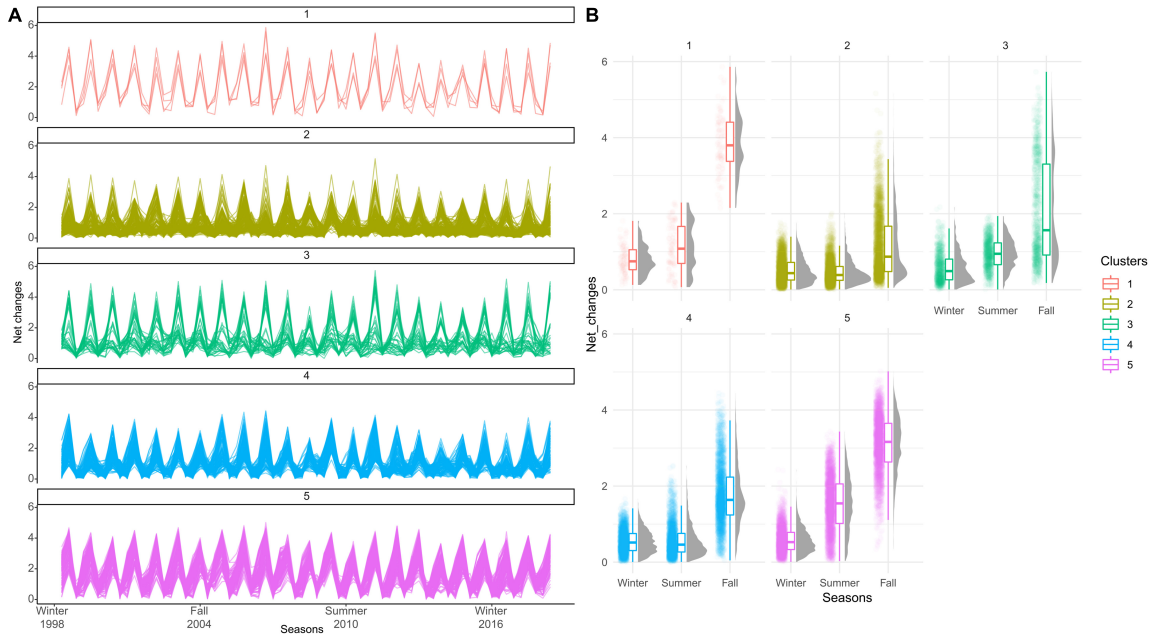

FIGURE 11
Seasonal isoscape cycles. **(A)** Temporal evolution of the isotopic net changes (‰) in the five isoregions for the 69 successive isoscapes including all seasons*years from winter 1998 to fall. **(B)** Box plots of net changes values (‰) exhibits by each trajectory cluster compared to winter 1998.

tissue turnover rates for copepods (ca 2 weeks) (Graeve et al., 2005; Tiselius and Fransson, 2016), acting as a smoothing buffer, help to match predictor and isotopic values and to create more stable isoscapes. Although the CPR survey samples copepods close to the surface, *Calanus* are known to undergo diel vertical migration (Dale and Kaartvedt, 2000), and can feed on prey distributed at different depths, integrating SI values along the water column. Particulate organic matter, despite its highly dynamic isotopic composition, represents a good alternative having the advantage of samples being generally available in greater number. Using SI data from higher trophic level animals such as small pelagic fish as a reference is also another option, but data are usually limited, and assumptions of true geolocation may be violated. Defining a "perfect" tissue to generate geo-referenced data supporting isoscape model development is challenging. However, a strong advantage of the Bayesian INLA framework used here to construct spatial models is that it allows the user to define and partition non-spatial sources of variance in isotope values, and to retrieve spatial uncertainties associated with source effects (St John Glew et al., 2019).

The variability in observed (measured) isotope data was expectedly greater than in modelled data. This implies that sources of variation were higher than the models capture. Some of the processes involved in setting and transferring the SI values along the trophic chain are difficult to translate into the model formulation (e.g., phytoplankton composition and cell geometry). However, the predictors selected during the model formation are sufficient to capture the main processes driving isotopic variations. It is relatively straight forward to model spatio-temporal variations in $\delta^{13}C$ values, as SST is a strong proxy for both CO_2 concentration and isotopic fractionation. SST data are available at high spatio-temporal resolution allowing effective prediction across unsampled regions. By contrast, nitrate concentrations, the main driver of variations in $\delta^{15}N$ values, are harder to resolve from remote sensed data. Chla concentrations derived from ocean colour data are an obvious alternative candidate, but complex phytoplankton dynamics and limits associated with measurements (surface layer only) weakens the relationship. Among the different hypotheses on mechanisms controlling phytoplankton dynamics (Behrenfeld and Boss, 2014; Lindemann and St. John, 2014) and bloom initiation (Mahadevan et al., 2012), the mix layer depth recurrently plays an important role. It might explain why MLD was found to be a more powerful predictor than chla to model $\delta^{15}N$ values (**Table 1**).

Overall the systematic and logically reasonable patterns observed in the modelled isoscapes make us confident of their consistency, however limited data are available to compare our isoscape values at regional scales. We compared our mean zooplankton modelled $\delta^{13}C$ values per isoregion (**Table 2**) with a review of previous observational data per Longhurst bioregion produced by Magozzi et al. (2017). Values were found to be consistent with –23.6 vs. –23.4‰ for the isoregion #2 vs. polar biome, –22.4 vs. –23.7‰ for the isoregion #2 vs. the subpolar

biome and –21.1 vs. –21.3‰ for the isoregion #5 vs. Westerly Wind biome.

Caution should be taken when using isoscapes values associated with high uncertainties values (i.e., high variances), particularly when drawing on isoscapes to infer aspects of predator ecology. Two main factors promote high uncertainties in predicted data, spatial segregation from observational data and extreme predictor values. A combination of both can lead to high uncertainties, as can be seen in the southeastern area of the δ^{15}N isoscapes (**Figures 3**, **4**). Accuracy in predicted data far away from observation will depend on distance to the nearest observation, mesh shape/resolution and correlation length distance. We aimed to find a compromise between isoscape resolution and data uncertainties as to keep the latter in reasonable range (ca 1.5‰ for δ^{13}C and 3‰ for δ^{15}N). Extreme predicator values are a problem toward the limits of the domain (e.g., warm water in the south border) and this problem is amplified within the more data-limited seasonal isoscapes. To reduce the uncertainties more observational should be added to the model, ideally coming from undersampled regions and/or during extreme events.

The models we developed could easily be updated in the future by integrating other datasets, still keeping a control on the accuracy of the predictions. Building a larger data base (see for example Verwega et al., 2021) would enable us to develop further the seasonal isoscape, in terms of coverage but also of model structures (e.g., to test specific seasonal model structure). Regarding seasonality, δ^{13}C and δ^{15}N values might vary asynchronously and will not necessarily share the same model structure. In this study, we modelled spatial variances using all-seasons data and produced seasonal isoscapes using seasonal predictors (environmental variables). Our approach assumes that the statistical relationship between the response variable and the predictors do not change over seasons. This is likely largely true for δ^{13}C values where temperature is a strong indirect driver, but it is less clear for δ^{15}N values. Developing fully seasonally specific models would be particularly interesting for δ^{15}N, where the value for one season can potentially be influenced by what happened previously during the year. There is a stronger seasonal pattern in δ^{15}N values, as in contrast to δ^{13}C values the limiting molecule (CO_2 vs. nitrates), is only replenished over winter. Fall isotopic composition of copepods will therefore be influenced by the strength of the fall bloom but also potentially of the spring bloom.

Implications for predator movements and trophic interactions

Spatio-temporal patterns in isoscapes have strong implications for the study of food web and animal movements in space and time (Graham et al., 2010; McMahon et al., 2013b; Trueman and St John Glew, 2019). Our study has direct applications for the interpretation consumer stable isotope values in the North Atlantic Ocean where isoregions exhibited contrasting spatio-temporal patterns in modelled isoscapes. The yearly and seasonal dynamics in stable isotope values inferred offers the possibility to investigate predator dynamics at different temporal scales depending on their life cycles. Stable isotope compositions can be measured in a wide range of tissues with different characteristics in terms of turnover rates and growth structures. For example, considering marine mammals, incrementally grown tissues such as seal whiskers, fish eye lenses, baleen plates or seal teeth allow for the description of seasonal, annual or multi-annual resolution (Kernaléguen et al., 2012; Borrell et al., 2013; Trueman et al., 2019; De La Vega et al., 2022). Among other top predators, the practical potential for drawing valuable inferences from tissue isotopes informed from ocean-basin isoscapes is particularly high for species which spend a large part of their life cycle in open ocean but migrate occasionally to coastal areas where they are accessible for sampling (e.g., central point breeding seabirds, and marine mammals, or fish with coastally or freshwater directed spawning such as salmon; e.g., Mackenzie et al., 2011; Trueman et al., 2012; Cherel et al., 2016). Quantifying likely scales of temporal variance in baseline stable isotope values is especially important, particularly where tissues sampled reflect a discrete time period, or where studies draw on time series or compile data across multiple sampling years or seasons. Variation in consumer tissue isotope values is caused by spatio-temporal variation in the isotopic composition of the dietary baseline, differences in diet organisms (including trophic level) and physiological differences in the extent of isotopic spacing between tissue and diet. The potentially confounding effect of these processes can be mitigated by analysing stable isotope compositions of individual amino acids. Essential (source) amino acids are considered to reflect the isotopic composition of primary production conserved through food webs (e.g., Chikaraishi et al., 2009). The isoscapes presented here describe expected spatio-temporal variations in baseline isotope compositions as expressed in bulk protein, and absolute differences among regions are likely to be more pronounced in amino acids such as phenylalanine. Drawing on individual amino acid data may therefore improve accuracy of spatial assignment (Matsubayashi et al., 2020). Such helpful information should be coupled with a strong knowledge of consumers ecology and isotopic integration time (Possamai et al., 2021), other biogeochemical tracers in complementary tissues (Vander Zanden et al., 2016) and, when possible, telemetry data in order to disentangle dynamics in SI compositions due to migrations or changes in feeding strategy (Cherel et al., 2016). Knowledge in spatial niche arrangement of top predators at large scale is necessary to develop conservation measures such as Marine Protected Areas (Reisinger et al., 2022). The isoscapes presented here are provided in the hope that they may help to improve our understanding of poorly

documented parts of migratory marine species' life cycles, many of which have seen their population decline dramatically over the last decades (e.g., Dias et al., 2019).

Data availability statement

Observational stable isotope data as well as the isoscapes and variance predictions produced in the present study are available at https://github.com/borisespinasse/ISOSCAPE_NA. Further queries should be directed to the corresponding author.

Author contributions

BE, SB, and CT conceived the project. PH and DJ provided the access to new materials (zooplankton). JN analysed the samples for stable isotope values. BE developed the spatial Bayesian models to produce the isoscapes. BE and AS carried out the data analysis and wrote the manuscript. All authors provided the editorial advice, and read and approved the final manuscript.

Funding

The CPR Survey would not be possible without the support of the shipping industry, nor the dedication of the past and present team. Current funding includes the UK Natural Environment Research Council, Grant/Award Numbers: NE/R002738/1 and NE/M007855/1; EMFF; Climate Linked Atlantic Sector Science, Grant/Award Number: NE/R015953/1, DEFRA UK ME-5308, NSF USA OCE-1657887, DFO CA F5955-150026/001/HAL, NERC UK NC-R8/H12/100, Horizon 2020: 862428 Mission Atlantic and AtlantECO 862923, IMR Norway and the French Ministry of Environment, Energy, and the Sea (MEEM). Stable isotope measurements were funded by a National Environmental Isotope Facility grant-in-kind (no. 2323) to CT and BE. BE was funded from the European Union's Horizon 2020 MSCA program under Grant agreement no. 894296 – Project ISOMOD.

Conflict of interest

The authors declare that the research was conducted in the absence of any commercial or financial relationships that could be construed as a potential conflict of interest.

Publisher's note

All claims expressed in this article are solely those of the authors and do not necessarily represent those of their affiliated organizations, or those of the publisher, the editors and the reviewers. Any product that may be evaluated in this article, or claim that may be made by its manufacturer, is not guaranteed or endorsed by the publisher.

Supplementary material

The Supplementary Material for this article can be found online at: https://www.frontiersin.org/articles/10.3389/fevo.2022.986082/full#supplementary-material

References

Akaike, H. (1974). A new look at the statistical model identification. *IEEE Trans. Autom. Control* 19, 716–723. doi: 10.1109/TAC.1974.1100705

Batten, S. D., Clark, R., Flinkman, J., Hays, G., John, E., John, A. W. G., et al. (2003). CPR sampling: The technical background, materials and methods, consistency and comparability. *Prog. Oceanogr.* 58, 193–215. doi: 10.1016/j.pocean.2003.08.004

Beaugrand, G., Brander, K. M., Alistair Lindley, J., Souissi, S., and Reid, P. C. (2003). Plankton effect on cod recruitment in the North Sea. *Nature* 426, 661–664. doi: 10.1038/nature02164

Beaugrand, G., Edwards, M., and Hélaouët, P. (2019). An ecological partition of the Atlantic Ocean and its adjacent seas. *Prog. Oceanogr.* 173, 86–102. doi: 10.1016/j.pocean.2019.02.014

Behrenfeld, M. J., and Boss, E. S. (2014). Resurrecting the ecological underpinnings of ocean plankton blooms. *Annu. Rev. Mar. Sci.* 6, 167–194. doi: 10.1146/annurev-marine-052913-021325

Behrenfeld, M. J., and Falkowski, P. G. (1997). Photosynthetic rates derived from satellite-based chlorophyll concentration. *Limnol. Oceanogr.* 42, 1–20. doi: 10.4319/lo.1997.42.1.0001

Bicknell, A. W. J., Campbell, M., Knight, M. E., Bilton, D. T., Newton, J., and Votier, S. C. (2011). Effects of formalin preservation on stable carbon and nitrogen isotope signatures in calanoid copepods: Implications for the use of continuous plankton recorder survey samples in stable isotope analyses. *Rapid Commun. Mass Spectrom.* 25, 1794–1800. doi: 10.1002/rcm.5049

Borrell, A., Velásquez Vacca, A., Pinela, A. M., Kinze, C., Lockyer, C. H., Vighi, M., et al. (2013). Stable isotopes provide insight into population structure and segregation in eastern North Atlantic sperm whales. *PLoS One* 8:e82398. doi: 10.1371/journal.pone.0082398

Bowen, G. J. (2010). Isoscapes: Spatial pattern in isotopic biogeochemistry. *Annu. Rev. Earth Planet. Sci.* 38, 161–187. doi: 10.1146/annurev-earth-040809-152429

Brault, E. K., Koch, P. L., Mcmahon, K. W., Broach, K. H., Rosenfield, A. P., Sauthoff, W., et al. (2018). Carbon and nitrogen zooplankton isoscapes in West Antarctica reflect oceanographic transitions. *Mar. Ecol. Prog. Ser.* 593, 29–45. doi: 10.3354/meps12524

Brun, P., Stamieszkin, K., Visser, A. W., Licandro, P., Payne, M. R., and Kiørboe, T. (2019). Climate change has altered zooplankton-fuelled carbon export in the North Atlantic. *Nat. Ecol. Evol.* 3, 416–423. doi: 10.1038/s41559-018-0780-3

Buchanan, P. J., Tagliabue, A., De La Vega, C., and Mahaffey, C. (2021). Oceanographic and biogeochemical drivers cause divergent trends in the nitrogen isoscape in a changing Arctic Ocean. *Ambio* 51, 383–397. doi: 10.1007/s13280-021-01635-6

Bundy, A., Renaud, P. E., Coll, M., Koenigstein, S., Niiranen, S., Pennino, M. G., et al. (2021). Editorial: Managing for the future: Challenges and approaches for

disentangling the relative roles of environmental change and fishing in marine ecosystems. *Front. Mar. Sci.* 8:753459. doi: 10.3389/fmars.2021.753459

Caesar, L., Rahmstorf, S., Robinson, A., Feulner, G., and Saba, V. (2018). Observed fingerprint of a weakening Atlantic Ocean overturning circulation. *Nature* 556, 191–196. doi: 10.1038/s41586-018-0006-5

Cherel, Y., and Hobson, K. A. (2007). Geographical variation in carbon stable isotope signatures of marine predators: A tool to investigate their foraging areas in the Southern Ocean. *Mar. Ecol. Prog. Ser.* 329, 281–287. doi: 10.3354/meps329281

Cherel, Y., Quillfeldt, P., Delord, K., and Weimerskirch, H. (2016). Combination of at-sea activity, geolocation and feather stable isotopes documents where and when seabirds molt. *Front. Ecol. Evol.* 4:3. doi: 10.3389/fevo.2016.00003

Chikaraishi, Y., Ogawa, N. O., Kashiyama, Y., Takano, Y., Suga, H., Tomitani, A., et al. (2009). Determination of aquatic food-web structure based on compound-specific nitrogen isotopic composition of amino acids. *Limnol. Oceanogr. Methods* 7, 740–750. doi: 10.4319/lom.2009.7.740

Chivers, W. J., Walne, A. W., and Hays, G. C. (2017). Mismatch between marine plankton range movements and the velocity of climate change. *Nat. Commun.* 8:14434. doi: 10.1038/ncomms14434

Clark, C. T., Cape, M. R., Shapley, M. D., Mueter, F. J., Finney, B. P., and Misarti, N. (2021). SuessR: Regional corrections for the effects of anthropogenic CO_2 on δ13C data from marine organisms. *Methods Ecol. Evol.* 12, 1508–1520. doi: 10.1111/2041-210X.13622

Coplen, T. B., Brand, W. A., Gehre, M., Gröning, M., Meijer, H. A. J., Toman, B., et al. (2006). New guidelines for δ13C measurements. *Anal. Chem.* 78, 2439–2441. doi: 10.1021/ac052027c

Cushing, D. H. (1990). "Plankton production and year-class strength in fish populations: An update of the match/mismatch hypothesis," in *Advances in marine biology*, Vol. 26, eds J. H. S. Blaxter and A. J. Southward (Cambridge, MA: Academic Press), 249–293. doi: 10.1016/S0065-2881(08)60202-3

Dale, T., and Kaartvedt, S. (2000). Diel patterns in stage-specific vertical migration of *Calanus finmarchicus* in habitats with midnight sun. *ICES J. Mar. Sci.* 57, 1800–1818. doi: 10.1006/jmsc.2000.0961

De Cáceres, M., Coll, L., Legendre, P., Allen, R. B., Wiser, S. K., Fortin, M.-J., et al. (2019). Trajectory analysis in community ecology. *Ecol. Monogr.* 89:e01350. doi: 10.1002/ecm.1350

De La Vega, C., Buchanan, P. J., Tagliabue, A., Hopkins, J. E., Jeffreys, R. M., Frie, A. K., et al. (2022). Multi-decadal environmental change in the Barents Sea recorded by seal teeth. *Glob. Change Biol.* 28, 3054–3065. doi: 10.1111/gcb.16138

Desbruyères, D., Chafik, L., and Maze, G. (2021). A shift in the ocean circulation has warmed the subpolar North Atlantic Ocean since 2016. *Commun. Earth Environ.* 2:48. doi: 10.1038/s43247-021-00120-y

Deuser, W. G. (1970). Isotopic evidence for diminishing supply of available carbon during diatom bloom in the Black Sea. *Nature* 225, 1069–1071. doi: 10.1038/2251069a0

Dias, M. P., Martin, R., Pearmain, E. J., Burfield, I. J., Small, C., Phillips, R. A., et al. (2019). Threats to seabirds: A global assessment. *Biol. Conserv.* 237, 525–537. doi: 10.1016/j.biocon.2019.06.033

Drinkwater, K. F., Sundby, S., and Wiebe, P. H. (2020). Exploring the hydrography of the boreal/arctic domains of North Atlantic seas: results from the 2013 BASIN survey. *Deep Sea Res. Part II: Top. Stud. Oceanograp.* 180:104880. doi: 10.1016/j.dsr2.2020.104880

El-Sabaawi, R., Dower, J., Kainz, M., and Mazumder, A. (2009). Characterizing dietary variability and trophic positions of coastal calanoid copepods: Insight from stable isotopes and fatty acids. *Mar. Biol.* 156, 225–237. doi: 10.1007/s00227-008-1073-1

El-Sabaawi, R., Trudel, M., and Mazumder, A. (2013). Zooplankton stable isotopes as integrators of bottom-up variability in coastal margins: A case study from the Strait of Georgia and adjacent coastal regions. *Prog. Oceanogr.* 115, 76–89. doi: 10.1016/j.pocean.2013.05.010

Eppley, R. W. (1972). Temperature and phytoplankton growth in the sea. *Fish. Bull.* 70, 1063–1085.

Espinasse, B., Harmelin-Vivien, M., Tiano, M., Guilloux, L., and Carlotti, F. (2014). Patterns of variations in C and N stable isotope ratios in size-fractionated zooplankton in the Gulf of Lion, NW Mediterranean Sea. *J. Plankton Res.* 36, 1204–1215. doi: 10.1093/plankt/fbu043

Espinasse, B., Hunt, B. P. V., Doson Coll, Y., and Pakhomov, E. A. (2018). Investigating high seas foraging conditions for salmon in the North Pacific: Insights from a 100-year scale archive for Rivers Inlet sockeye salmon. *Can. J. Fish. Aquat. Sci.* 76, 918–927. doi: 10.1139/cjfas-2018-0010

Espinasse, B., Hunt, B. P. V., Batten, S. D., and Pakhomov, E. A. (2020a). Defining isoscapes in the Northeast Pacific as an index of ocean productivity. *Glob. Ecol. Biogeogr.* 29, 246–261. doi: 10.1111/geb.13022

Espinasse, B., Hunt, B. P. V., Finney, B. P., Fryer, J. K., Bugaev, A. V., and Pakhomov, E. A. (2020b). Using stable isotopes to infer stock-specific high-seas distribution of maturing sockeye salmon in the North Pacific. *Ecol. Evol.* 10, 13555–13570. doi: 10.1002/ece3.7022

Fitak, R. R., and Johnsen, S. (2017). Bringing the analysis of animal orientation data full circle: Model-based approaches with maximum likelihood. *J. Exp. Biol.* 220, 3878–3882. doi: 10.1242/jeb.167056

Fuglstad, G.-A., Simpson, D., Lindgren, F., and Rue, H. (2019). Constructing priors that penalize the complexity of Gaussian random fields. *J. Am. Stat. Assoc.* 114, 445–452. doi: 10.1080/01621459.2017.1415907

Good, S., Fiedler, E., Mao, C., Martin, M. J., Maycock, A., Reid, R., et al. (2020). The current configuration of the OSTIA system for operational production of foundation sea surface temperature and ice concentration analyses. *Remote Sens.* 12:720. doi: 10.3390/rs12040720

Graeve, M., Albers, C., and Kattner, G. (2005). Assimilation and biosynthesis of lipids in Arctic *Calanus* species based on feeding experiments with a 13C labelled diatom. *J. Exp. Mar. Biol. Ecol.* 317, 109–125. doi: 10.1016/j.jembe.2004.11.016

Graham, B. S., Koch, P. L., Newsome, S. D., McMahon, K. W., and Aurioles, D. (2010). "Using isoscapes to trace the movements and foraging behavior of top predators in oceanic ecosystems," in *Isoscapes: Understanding movement, pattern, and process on Earth through isotope mapping*, eds J. B. West, G. J. Bowen, T. E. Dawson, and K. P. Tu (Dordrecht: Springer Netherlands), 299–318. doi: 10.1007/978-90-481-3354-3_14

Gruber, N., Keeling, C. D., Bacastow, R. B., Guenther, P. R., Lueker, T. J., Wahlen, M., et al. (1999). Spatiotemporal patterns of carbon-13 in the global surface oceans and the oceanic Suess effect. *Glob. Biogeochem. Cycles* 13, 307–335. doi: 10.1029/1999GB900019

Gutiérrez-Rodríguez, A., Décima, M., Popp, B. N., and Landry, M. R. (2014). Isotopic invisibility of protozoan trophic steps in marine food webs. *Limnol. Oceanogr.* 59, 1590–1598. doi: 10.4319/lo.2014.59.5.1590

Halpern, B. S., Frazier, M., Afflerbach, J., Lowndes, J. S., Micheli, F., O'Hara, C., et al. (2019). Recent pace of change in human impact on the world's ocean. *Sci. Rep.* 9:11609. doi: 10.1038/s41598-019-47201-9

Hays, G. C., Richardson, A. J., and Robinson, C. (2005). Climate change and marine plankton. *Trends Ecol. Evol.* 20, 337–344. doi: 10.1016/j.tree.2005.03.004

Heneghan, R. F., Galbraith, E., Blanchard, J. L., Harrison, C., Barrier, N., Bulman, C., et al. (2021). Disentangling diverse responses to climate change among global marine ecosystem models. *Prog. Oceanogr.* 198:102659. doi: 10.1016/j.pocean.2021.102659

Henson, S. A., Beaulieu, C., Ilyina, T., John, J. G., Long, M., Séférian, R., et al. (2017). Rapid emergence of climate change in environmental drivers of marine ecosystems. *Nat. Commun.* 8:14682. doi: 10.1038/ncomms14682

Hetherington, E. D., Kurle, C. M., Ohman, M. D., and Popp, B. N. (2019). Effects of chemical preservation on bulk and amino acid isotope ratios of zooplankton, fish, and squid tissues. *Rapid Commun. Mass Spectrom.* 33, 935–945. doi: 10.1002/rcm.8408

Hobson, K. A., Ambrose, W. G. Jr., and Renaud, P. E. (1995). Sources of primary production, benthic-pelagic coupling, and trophic relationships within the Northeast Water Polynya: Insights from ÃŽÂ´13C and ÃŽÂ´15N analysis. *Mar. Ecol. Prog. Ser.* 128, 1–10. doi: 10.3354/meps128001

Hofmann, M., Wolf-Gladrow, D. A., Takahashi, T., Sutherland, S. C., Six, K. D., and Maier-Reimer, E. (2000). Stable carbon isotope distribution of particulate organic matter in the ocean: A model study. *Mar. Chem.* 72, 131–150. doi: 10.1016/S0304-4203(00)00078-5

Hurrell, J. W., and Deser, C. (2009). North Atlantic climate variability: The role of the North Atlantic oscillation. *J. Mar. Syst.* 78, 28–41. doi: 10.1016/j.jmarsys.2008.11.026

Jennings, S., and Warr, K. J. (2003). Environmental correlates of large-scale spatial variation in the δ15N of marine animals. *Mar. Biol.* 142, 1131–1140. doi: 10.1007/s00227-003-1020-0

Kernaléguen, L., Cazelles, B., Arnould, J. P. Y., Richard, P., Guinet, C., and Cherel, Y. (2012). Long-term species, sexual and individual variations in foraging strategies of fur seals revealed by stable isotopes in whiskers. *PLoS One* 7:e32916. doi: 10.1371/journal.pone.0032916

Kiljunen, M., Grey, J., Sinisalo, T., Harrod, C., Immonen, H., and Jones, R. I. (2006). A revised model for lipid-normalizing δ13C values from aquatic organisms, with implications for isotope mixing models. *J. Appl. Ecol.* 43, 1213–1222. doi: 10.1111/j.1365-2664.2006.01224.x

Kline, T. C. Jr. (1999). Temporal and spatial variability of 13C/12C and 15N/14N in pelagic biota of Prince William Sound, Alaska. *Can. J. Fish. Aquat. Sci.* 56, 94–117. doi: 10.1139/f99-212

Kline, T. C. Jr. (2009). Characterization of carbon and nitrogen stable isotope gradients in the northern Gulf of Alaska using terminal feed stage copepodite-V *Neocalanus cristatus*. *Deep Sea Res. II Top. Stud. Oceanogr.* 56, 2537–2552. doi: 10.1016/j.dsr2.2009.03.004

Kurle, C. M., and Mcwhorter, J. K. (2017). Spatial and temporal variability within marine isoscapes: Implications for interpreting stable isotope data from marine systems. *Mar. Ecol. Prog. Ser.* 568, 31–45. doi: 10.3354/meps12045

Landler, L., Ruxton, G. D., and Malkemper, E. P. (2019). The Hermans–Rasson test as a powerful alternative to the Rayleigh test for circular statistics in biology. *BMC Ecol.* 19:30. doi: 10.1186/s12898-019-0246-8

Laws, E. A., Popp, B. N., Cassar, N., and Tanimoto, J. (2002). 13C discrimination patterns in oceanic phytoplankton: Likely influence of CO_2 concentrating mechanisms, and implications for palaeoreconstructions. *Funct. Plant Biol.* 29, 323–333. doi: 10.1071/PP01183

Lindemann, C., and St. John, M. A. (2014). A seasonal diary of phytoplankton in the North Atlantic. *Front. Mar. Sci.* 1:37. doi: 10.3389/fmars.2014.00037

Lindgren, F., and Rue, H. (2015). Bayesian spatial modelling with R-INLA. *J. Stat. Softw.* 63, 1–25. doi: 10.18637/jss.v063.i19

Lindgren, F., Rue, H., and Lindström, J. (2011). An explicit link between Gaussian fields and Gaussian Markov random fields: The stochastic partial differential equation approach. *J. R. Stat. Soc. Ser. B Stat. Methodol.* 73, 423–498. doi: 10.1111/j.1467-9868.2011.00777.x

Logan, J. M., Jardine, T. D., Miller, T. J., Bunn, S. E., Cunjak, R. A., and Lutcavage, M. E. (2008). Lipid corrections in carbon and nitrogen stable isotope analyses: Comparison of chemical extraction and modelling methods. *J. Anim. Ecol.* 77, 838–846. doi: 10.1111/j.1365-2656.2008.01394.x

Longhurst, A. R. (2010). *Ecological geography of the sea*. Amsterdam: Elsevier.

Mackas, D. L., and Coyle, K. O. (2005). Shelf–offshore exchange processes, and their effects on mesozooplankton biomass and community composition patterns in the northeast Pacific. *Deep Sea Res. II Top. Stud. Oceanogr.* 52, 707–725. doi: 10.1016/j.dsr2.2004.12.020

Mackenzie, K. M., Longmore, C., Preece, C., Lucas, C. H., and Trueman, C. N. (2014). Testing the long-term stability of marine isoscapes in shelf seas using jellyfish tissues. *Biogeochemistry* 121, 441–454. doi: 10.1007/s10533-014-0011-1

Mackenzie, K. M., Palmer, M. R., Moore, A., Ibbotson, A. T., Beaumont, W. R. C., Poulter, D. J. S., et al. (2011). Locations of marine animals revealed by carbon isotopes. *Sci. Rep.* 1:21. doi: 10.1038/srep00021

Magozzi, S., Yool, A., Zanden, H. B. V., Wunder, M. B., and Trueman, C. N. (2017). Using ocean models to predict spatial and temporal variation in marine carbon isotopes. *Ecosphere* 8:e01763. doi: 10.1002/ecs2.1763

Mahadevan, A., D'Asaro, E., Lee, C., and Perry Mary, J. (2012). Eddy-driven stratification initiates North Atlantic spring phytoplankton blooms. *Science* 337, 54–58. doi: 10.1126/science.1218740

Maritorena, S., D'Andon, O. H. F., Mangin, A., and Siegel, D. A. (2010). Merged satellite ocean color data products using a bio-optical model: Characteristics, benefits and issues. *Remote Sens. Environ.* 114, 1791–1804. doi: 10.1016/j.rse.2010.04.002

Matsubayashi, J., Osada, Y., Tadokoro, K., Abe, Y., Yamaguchi, A., Shirai, K., et al. (2020). Tracking long-distance migration of marine fishes using compound-specific stable isotope analysis of amino acids. *Ecol. Lett.* 23, 881–890. doi: 10.1111/ele.13496

McMahon, K. W., Hamady, L. L., and Thorrold, S. R. (2013a). "Ocean ecogeochemistry: A review," in *Oceanography and marine biology*, eds R. N. Hughes, D. J. Hughes, and I. P. Smith (Boca Raton, FL: CRC PRESS), 327–373.

McMahon, K. W., Hamady, L. L., and Thorrold, S. R. (2013b). A review of ecogeochemistry approaches to estimating movements of marine animals. *Limnol. Oceanogr.* 58, 697–714. doi: 10.4319/lo.2013.58.2.0697

Morel, A. (1991). Light and marine photosynthesis: A spectral model with geochemical and climatological implications. *Prog. Oceanogr.* 26, 263–306. doi: 10.1016/0079-6611(91)90004-6

Pawlowicz, R. (2019). *M_Map: A Mapping Package for MATLAB. 1.4k ed*, Vancouver.

Popp, B. N., Trull, T., Kenig, F., Wakeham, S. G., Rust, T. M., Tilbrook, B., et al. (1999). Controls on the carbon isotopic composition of southern ocean phytoplankton. *Glob. Biogeochem. Cycles* 13, 827–843. doi: 10.1029/1999GB900041

Possamai, B., Hoeinghaus, D. J., and Garcia, A. M. (2021). Shifting baselines: Integrating ecological and isotopic time lags improves trophic position estimates in aquatic consumers. *Mar. Ecol. Prog. Ser.* 666, 19–30. doi: 10.3354/meps13682

Post, D. M., Layman, C. A., Arrington, D. A., Takimoto, G., Quattrochi, J., and Montaña, C. G. (2007). Getting to the fat of the matter: Models, methods and assumptions for dealing with lipids in stable isotope analyses. *Oecologia* 152, 179–189. doi: 10.1007/s00442-006-0630-x

Qi, H., Coplen, T. B., Geilmann, H., Brand, W. A., and Böhlke, J. K. (2003). Two new organic reference materials for δ13C and δ15N measurements and a new value for the δ13C of NBS 22 oil. *Rapid Commun. Mass Spectrom.* 17, 2483–2487. doi: 10.1002/rcm.1219

R Core Team (2022). *R: A language and environment for statistical computing*. Vienna: R Foundation for Statistical Computing.

Rau, G., Sullivan, C., and Gordon, L. I. (1991). δ13C and δ15N variations in Weddell Sea particulate organic matter. *Mar. Chem.* 35, 355–369. doi: 10.1016/S0304-4203(09)90028-7

Rau, G. H., Low, C., Pennington, J. T., Buck, K. R., and Chavez, F. P. (1998). Suspended particulate nitrogen δ15N versus nitrate utilization: Observations in Monterey Bay, CA. *Deep Sea Res. II Top. Stud. Oceanogr.* 45, 1603–1616. doi: 10.1016/S0967-0645(98)80008-8

Reisinger, R. R., Brooks, C. M., Raymond, B., Freer, J. J., Cotté, C., Xavier, J. C., et al. (2022). Predator-derived bioregions in the Southern Ocean: Characteristics, drivers and representation in marine protected areas. *Biol. Conserv.* 272:109630. doi: 10.1016/j.biocon.2022.109630

Richardson, A. J., and Poloczanska, E. S. (2008). Under-resourced, under threat. *Science* 320:1294. doi: 10.1126/science.1156129

Rolff, C. (2000). Seasonal variation in delta^{13}C and delta^{15}N of size-fractionated plankton at a coastal station in the northern Baltic proper. *Mar. Ecol. Prog. Ser.* 203, 47–65. doi: 10.3354/meps203047

Rue, H., Martino, S., and Chopin, N. (2009). Approximate Bayesian inference for latent Gaussian models by using integrated nested Laplace approximations. *J. R. Stat. Soc. Ser. B Stat. Methodol.* 71, 319–392. doi: 10.1111/j.1467-9868.2008.00700.x

Scheffer, M., Carpenter, S., Foley, J. A., Folke, C., and Walker, B. (2001). Catastrophic shifts in ecosystems. *Nature* 413, 591–596. doi: 10.1038/35098000

Schell, D. M., Barnett, B. A., and Vinette, K. A. (1998). Carbon and nitrogen isotope ratios in zooplankton of the Bering, Chukchi and Beaufort seas. *Mar. Ecol. Prog. Ser.* 162, 11–23. doi: 10.3354/meps162011

Schmittner, A., and Somes, C. J. (2016). Complementary constraints from carbon (13C) and nitrogen (15N) isotopes on the glacial ocean's soft-tissue biological pump. *Paleoceanography* 31, 669–693. doi: 10.1002/2015PA002905

Seyboth, E., Botta, S., Mendes, C. R. B., Negrete, J., Dalla Rosa, L., and Secchi, E. R. (2018). Isotopic evidence of the effect of warming on the northern Antarctic Peninsula ecosystem. *Deep Sea Res. II Top. Stud. Oceanogr.* 149, 218–228. doi: 10.1016/j.dsr2.2017.12.020

St John Glew, K., Espinasse, B., Hunt, B. P. V., Pakhomov, E. A., Bury, S. J., Pinkerton, M., et al. (2021). Isoscape models of the Southern Ocean: Predicting spatial and temporal variability in carbon and nitrogen isotope compositions of particulate organic matter. *Glob. Biogeochem. Cycles* 35:e2020GB006901. doi: 10.1029/2020GB006901

St. John Glew, K., Graham, L. J., Mcgill, R. A. R., and Trueman, C. N. (2019). Spatial models of carbon, nitrogen and sulphur stable isotope distributions (isoscapes) across a shelf sea: An INLA approach. *Methods Ecol. Evol.* 10, 518–531. doi: 10.1111/2041-210X.13138

Sturbois, A., De Cáceres, M., Sánchez-Pinillos, M., Schaal, G., Gauthier, O., Mao, P. L., et al. (2021b). Extending community trajectory analysis: New metrics and representation. *Ecol. Model.* 440:109400. doi: 10.1016/j.ecolmodel.2020.109400

Sturbois, A., Cucherousset, J., De Cáceres, M., Desroy, N., Riera, P., Carpentier, A., et al. (2021a). Stable isotope trajectory analysis (SITA): A new approach to quantify and visualize dynamics in stable isotope studies. *Ecol. Monogr.* 92:e1501. doi: 10.1002/ecm.1501

Tagliabue, A., and Bopp, L. (2008). Towards understanding global variability in ocean carbon-13. *Glob. Biogeochem. Cycles* 22, 1–13. doi: 10.1029/2007GB003037

Tiselius, P., and Fransson, K. (2016). Daily changes in δ15N and δ13C stable isotopes in copepods: Equilibrium dynamics and variations of trophic level in the field. *J. Plankton Res.* 38, 751–761. doi: 10.1093/plankt/fbv048

Trueman, C. N., Jackson, A. L., Chadwick, K. S., Coombs, E. J., Feyrer, L. J., Magozzi, S., et al. (2019). Combining simulation modeling and stable isotope analyses to reconstruct the last known movements of one of Nature's giants. *PeerJ* 7:e7912. doi: 10.7717/peerj.7912

Trueman, C. N., Mackenzie, K. M., and Palmer, M. R. (2012). Identifying migrations in marine fishes through stable-isotope analysis. *J. Fish Biol.* 81, 826–847. doi: 10.1111/j.1095-8649.2012.03361.x

Trueman, C. N., and St John Glew, K. (2019). "Chapter 6–Isotopic tracking of marine animal movement," in *Tracking animal migration with stable isotopes*, 2nd

Edn, eds K. A. Hobson and L. I. Wassenaar (Cambridge, MA: Academic Press), 137–172. doi: 10.1016/B978-0-12-814723-8.00006-4

Vander Zanden, H. B., Soto, D. X., Bowen, G. J., and Hobson, K. A. (2016). Expanding the isotopic toolbox: Applications of hydrogen and oxygen stable isotope ratios to food web studies. *Front. Ecol. Evol.* 4:20. doi: 10.3389/fevo.2016.00020

Verwega, M. T., Somes, C. J., Schartau, M., Tuerena, R. E., Lorrain, A., Oschlies, A., et al. (2021). Description of a global marine particulate organic carbon-13 isotope data set. *Earth Syst. Sci. Data Discuss.* 2021, 1–27.

West, J., Bowen, G. J., Dawson, T. E., and Tu, K. (2010). *Isoscapes: Understanding movement, pattern, and process on Earth through isotope mapping*. Dordrecht: Springer. doi: 10.1007/978-90-481-3354-3

Wilson, R. J., Speirs, D. C., and Heath, M. R. (2015). On the surprising lack of differences between two congeneric calanoid copepod species, *Calanus finmarchicus* and *C. helgolandicus*. *Prog. Oceanogr.* 134, 413–431. doi: 10.1016/j.pocean.2014.12.008

Wood, S. N. (2017). *Generalized additive models: An introduction with R*. Boca Raton, FL: CRC. doi: 10.1201/9781315370279

Wood, S. N., Pya, N., and Säfken, B. (2016). Smoothing parameter and model selection for general smooth models. *J. Am. Stat. Assoc.* 111, 1548–1563. doi: 10.1080/01621459.2016.1180986

Zuur, A. F. (2012). *A beginner's guide to generalized additive models with R*. Newburgh, NY: Highland Statistics Limited.

Zuur, A. F., Ieno, E. N., and Elphick, C. S. (2010). A protocol for data exploration to avoid common statistical problems. *Methods Ecol. Evol.* 1, 3–14. doi: 10.1111/j.2041-210X.2009.00001.x

Zuur, A. F., Ieno, E. N., and Saveliev, A. A. (2017). *Beginner's guide to spatial, temporal, and spatial-temporal ecological data analysis with R-INLA: Using GLM and GLMM*. Newburgh: Highland Statistics Limited.

frontiers | Frontiers in Ecology and Evolution

TYPE Original Research
PUBLISHED 18 October 2022
DOI 10.3389/fevo.2022.951047

Check for updates

OPEN ACCESS

EDITED BY
Jason Newton,
University of Glasgow, United Kingdom

REVIEWED BY
Bobby Nakamoto,
University of New Brunswick
Fredericton, Canada
Sturbois Anthony,
UMR 6539 Laboratoire des Sciences
de L'Environnement Marin (LEMAR),
France

*CORRESPONDENCE
Philip M. Riekenberg
phrieken@gmail.com

SPECIALTY SECTION
This article was submitted to
Population, Community,
and Ecosystem Dynamics,
a section of the journal
Frontiers in Ecology and Evolution

RECEIVED 23 May 2022
ACCEPTED 07 September 2022
PUBLISHED 18 October 2022

CITATION
Riekenberg PM, van der Heide T,
Holthuijsen SJ, van der Veer HW and
van der Meer MTJ (2022)
Compound-specific stable isotope
analysis of amino acid nitrogen reveals
detrital support of microphytobenthos
in the Dutch Wadden Sea benthic food
web.
Front. Ecol. Evol. 10:951047.
doi: 10.3389/fevo.2022.951047

COPYRIGHT
© 2022 Riekenberg, van der Heide,
Holthuijsen, van der Veer and van der
Meer. This is an open-access article
distributed under the terms of the
Creative Commons Attribution License
(CC BY). The use, distribution or
reproduction in other forums is
permitted, provided the original
author(s) and the copyright owner(s)
are credited and that the original
publication in this journal is cited, in
accordance with accepted academic
practice. No use, distribution or
reproduction is permitted which does
not comply with these terms.

Compound-specific stable isotope analysis of amino acid nitrogen reveals detrital support of microphytobenthos in the Dutch Wadden Sea benthic food web

Philip M. Riekenberg[1]*, Tjisse van der Heide[2,3], Sander J. Holthuijsen[2], Henk W. van der Veer[2] and Marcel T. J. van der Meer[1]

[1]Department of Marine Microbiology and Biogeochemistry, Royal Netherlands Institute for Sea Research (NIOZ), Den Burg, Netherlands, [2]Department of Coastal Systems, Royal Netherlands Institute for Sea Research (NIOZ), Den Burg, Netherlands, [3]Conservation Ecology Group, Groningen Institute for Evolutionary Life Sciences, University of Groningen, Groningen, Netherlands

The Wadden Sea is the world's largest intertidal ecosystem and provides vital food resources for a large number of migratory bird and fish species during seasonal stopovers. Previous work using bulk stable isotope analysis of carbon found that microphytobenthos (MPB) was the dominant resource fueling the food web with particulate organic matter making up the remainder. However, this work was unable to account for the trophic structure of the food web or the considerable increase in δ^{15}N values of bulk tissue throughout the benthic food web occurring in the Eastern regions of the Dutch Wadden Sea. Here, we combine compound-specific and bulk analytical stable isotope techniques to further resolve the trophic structure and resource use throughout the benthic food web in the Wadden Sea. Analysis of δ^{15}N for trophic and source amino acids allowed for better identification of trophic relationships due to the integration of underlying variation in the nitrogen resources supporting the food web. Baseline-integrated trophic position estimates using glutamic acid (Glu) and phenylalanine (Phe) allow for disentanglement of baseline variations in underlying δ^{15}N sources supporting the ecosystem and trophic shifts resulting from changes in ecological relationships. Through this application, we further confirmed the dominant ecosystem support by MPB-derived resources, although to a lesser extent than previously estimated. In addition to phytoplankton-derived particulate, organic matter and MPB supported from nutrients from the overlying water column there appears to be an additional resource supporting the benthic community. From the stable isotope mixing models, a subset of species appears to focus on MPB supported off recycled (porewater) N and/or detrital organic matter mainly driven by increased phenylalanine δ^{15}N values. This additional

resource within MPB may play a role in subsidizing the exceptional benthic productivity observed within the Wadden Sea ecosystem and reflect division in MPB support along green (herbivory) and brown (recycled/detrital) food web pathways.

KEYWORDS

trophic discrimination, intertidal, diatoms, microbial loop, permeable sands

Introduction

Tracing the sources and fate of primary productivity as it supports an ecosystem or food web is challenging in coastal ecosystems, and stable isotope techniques have been useful tools that have allowed for further insight into these processes (Fry, 1984; Middelburg et al., 2000; Evrard et al., 2010). As shallow intertidal ecosystems are important sites for both primary production and the interception and reworking of carbon and nitrogen prior to export to shallow seas (Bauer et al., 2013a,b; Chua et al., 2022), it is important to resolve the relative incorporation of these elements into the wider food web. The world's largest intertidal ecosystem (Compton et al., 2013), the Wadden Sea, stretches from Netherlands to Denmark behind a barrier island chain with connection to the North Sea (Postma, 1996). This intertidal ecosystem has been designated as a culturally significant UNESCO World Heritage site due to considerable biodiversity within the system as benthic productivity supports an estimated 10–12 million migratory birds across each year (Reise et al., 2010). The Wadden Sea has a long history of multiple direct impacts from human activity (Eriksson et al., 2010; Wolff, 2013) that includes land reclamation, partial damming and hydraulic changes, eutrophication, overfishing, and extensive dredging for shellfish. These impacts have resulted in a shift from a benthos dominated by seagrass, extensive bivalve reefs, and supporting apex predators toward one dominated by polychaetes, with minimal fringing bivalve reefs, and largely devoid of apex predators (Philippart et al., 2007). Despite historical and recent anthropogenic impacts, the Wadden Sea remains a very productive intertidal ecosystem and direct support of macrozoobenthos by phytoplankton has been identified as a controlling factor of benthic biomass in the Wadden Sea (Beukema et al., 2002). However, changes in higher trophic level species have coincided with shifts in the benthic community as inferred from bird species shifting from primary bivalve carnivores toward polychaete carnivores (Van Roomen et al., 2005; Eriksson et al., 2010) and the drivers of these shifts remain unclear.

Analysis of the stable isotope composition of carbon ($\delta^{13}C$) and nitrogen ($\delta^{15}N$) in animal tissues is routinely used to identify underlying resource use and trophic relationships within ecosystems (Minagawa and Wada, 1984; Fry, 1988). Through the application of trophic discrimination factors (TDFs) for carbon and nitrogen ($\Delta^{13}C$ and $\Delta^{15}N$) stepwise isotopic increases that occur between a consumer's diet and their tissues during metabolism can be accounted for (Post, 2002; McCutchan et al., 2003), allowing for the identification of the animal's trophic level. Accounting for isotopic changes across trophic levels allows for the application of both simple and complex stable isotope mixing models (SIMMs) to be used to resolve the relative use of food resources by consumers within a food web (Fernandes et al., 2014; Stock et al., 2018). Approaches for characterizing resource use using SIMMs have typically been based on either bottom-up or top-down approaches to examine consumer resource use. Bottom-up approaches combine measured dietary resources and clearly defined TDFs to estimate resource use within ecosystems [McCormack et al. (2019) and references within, Cresson et al. (2020) and Kahma et al. (2020)] while top-down approaches rely on identification of unique consumer values within an ecosystem to identify cryptic or under-sampled resources without which the mixing envelope for all consumers in that ecosystem cannot be adequately resolved [Supplementary material 6 and references within Chi et al. (2021) and Then et al. (2021)]. For the Dutch part of the Wadden Sea, Christianen et al. (2017) identified that the majority of the biomass is supported by both pelagic phytoplankton and microphytobenthos (MPB). Their study used a two-source mixing model with a single isotopic tracer ($\delta^{13}C$) and clearly identified benthic productivity from MPB as an important resource supporting the benthic community. However, they may have overestimated the amount of support due to compression of the MPB end member through the use of an animal proxy instead of directly measured resources (Post, 2002).

Thus far, it has not been possible to assess the trophic structure within the Dutch Wadden Sea benthic community due to the large variability in $\delta^{15}N$ values observed in multiple benthic species. Christianen et al. (2015) found clear trends of increased $\delta^{15}N$ values for filter feeders (*Mytilus edulis*) in the eastern Dutch Wadden Sea indicating the potential for either a more positive $\delta^{15}N$ baseline value or altered trophic structure. Potential causes for locally increased $\delta^{15}N$ values could be (1) unaccounted for source of N to the ecosystem (e.g., terrestrial input), (2) altered trophic structure resulting in regionally increased $\delta^{15}N$ values in benthic consumers

(Durante et al., 2022), or (3) altered nitrogen cycling, e.g., increased denitrification resulting in increased $\delta^{15}N$ values in residual pool of N supporting remineralization (Vokhshoori and McCarthy, 2014). Terrestrial inputs have been found to be limited within the Dutch Wadden Sea (Christianen et al., 2017). Intertidal areas within the German Wadden Sea have been identified as having high rates of denitrification associated with tidal pumping and long exposure times within intertidal sediments (Marchant et al., 2016, 2017, 2018). Increased porewater processing of nitrogen may coincide with the unique distribution of sandy sediments and pore sizes due to the parallel flow of tidal waters through the Wadden Sea basin. These physical attributes result in reverse grading of sediments with coarser grains toward the basin edges and finer sediment centrally deposited along with longer exposure times in the East than in West (Otto et al., 1990; Compton et al., 2013). This combination of unique physical and biogeochemical settings may contribute to increased underlying $\delta^{15}N$ values but identifying any use of denitrification-affected N porewater resources by MPB and the food web has remained largely intractable solely using traditional bulk isotope techniques.

Microphytobenthos thrive in unvegetated sandy sediments where they can contribute significantly to the primary production supporting an ecosystem (Miller et al., 1996) as benthic diatoms fix carbon and take up nitrogen from the overlying water column and porewaters (Cook et al., 2007; Oakes et al., 2012; Riekenberg et al., 2020a). Much of the fixed carbon is excreted as extracellular polymeric substances (EPS), which are sticky, sugar-rich substrates that help to stabilize sediment and facilitate diatom motility throughout sand (Goto et al., 1999; Stal, 2010), but also serve as a labile carbon source for heterotrophic bacteria (Taylor et al., 2013). Diatom motility in sandy sediments is an adaptation to the physiochemical variations that occur within intertidal settings. Diel vertical migration of diatoms coincides with tidal cycles and available sunlight to support favorable conditions for photosynthesis at the surface (Barnett et al., 2020) and to maximize nutrient availability for cell growth and division in the subsurface (Saburova and Polikarpov, 2003). Due to the diel vertical migration of several centimeters and a strong coupling between diatoms and heterotrophic bacteria, MPB actively straddle the boundary between water column and sediment porewaters to maximize resource availability.

Food webs are often described as either green or brown depending on whether consumers are supported by herbivory of primary producers or supported by detrital reworking through the microbial loop (Middelburg, 2014; Potapov et al., 2019). MPB-supported food webs blur the line between green (MPB_{green}) and brown (MPB_{brown}) designations as MPB-derived material that can be used by consumers comes in several forms: (1) newly fixed organic matter from water column nutrients (MPB_{green} throughout), (2) MPB-derived organic matter formed from recycled detrital material by heterotrophs through oxic or anoxic pathways in sediment porewaters, or (3) detrital MPB-derived material such as reworked EPS that is still labile within the sediment (MPB_{brown} throughout). Microbial subsidies to MPB of both C and N from heterotrophic bacterial reworking of organic matter in porewaters blur the line between primary production and detrital resource use. Consumers such as deposit feeders have access to MPB biomass (living or dead) and EPS made using a mixture of resources derived directly from the water column or from heterotrophic processing within porewaters (e.g., denitrification affected N pools). This biogeochemical complexity can make identification of carbon and nitrogen food web support from MPB difficult to identify using bulk isotope techniques.

Application of compound-specific stable isotope analysis techniques (e.g., analysis of individual amino acid $\delta^{15}N$ values) could allow for identification of the trophic structure of the benthic community in the Wadden Sea without requiring measurement of all primary producers and all N sources within the ecosystem. This is because amino acid $\delta^{15}N$ values provide additional information for each sample analyzed in comparison with traditional bulk analysis due to the different fractionations that occur during metabolic reworking of trophic and source amino acids (O'Connell, 2017). Trophic amino acids such as glutamic acid (Glu) fractionate considerably between diet and the consumer resulting in a TDF ranging from 3–3.8‰ in marine mammals and sharks (Whiteman et al., 2018; Ruiz-Cooley et al., 2021) to as high as 11‰ in teleost fish fed a diet of low protein quality (McMahon et al., 2015b). $\delta^{15}N$ values for source amino acids such as phenylalanine (Phe) are relatively preserved as they are processed throughout food webs due to a low and consistent TDF of ∼0–0.5‰ (Chikaraishi et al., 2009; McMahon et al., 2015a). Integration of source amino acid values into trophic level estimates removes the effects from baseline N variations across an ecosystem using a single chemical analytical method (Vokhshoori et al., 2019; Xing et al., 2020) instead of requiring multiple comparisons and adjustments using resource or primary consumer measurements.

In this study, we apply natural abundance stable isotope analysis of amino acid nitrogen to resolve the trophic structure for 28 species from within the Dutch part of the Wadden Sea benthic ecosystem, which was previously not possible using solely bulk isotope values. Through the application of this amino acid–based method, it should be possible to further investigate the widespread nature of the driver causing increased variability in $\delta^{15}N$ across the ecosystem, which we have postulated as potentially being either caused by (1) changed food web complexity, (2) widespread variability in underlying biogeochemical processes (denitrification), or (3) unique sources such as freshwater inflow or groundwater influx coming from terrestrial sources.

Materials and methods

Study site

The Wadden Sea is a large intertidal ecosystem formed behind a chain of 12 sand barrier islands that stretch from the Netherlands to Denmark (Christianen et al., 2017). It is an highly productive estuarine ecosystem formed of sedimentary tidal flats that receive direct and indirect terrestrial inputs from the Ems, Weser, Elbe, IJssel, Muse, and Rhine rivers (Eriksson et al., 2010). Extensive long-term sampling of the benthic community has occurred in the Dutch Wadden Sea with spatial coverage extending from the Marsdiep (52° 58′ 12′ N, 4° 44′ 24″ E) to the Ems River mouth at the border of Germany (53° 19′ 48″ N, 7° 1′ 12″ E; **Figure 1** and **Supplementary Figure 1**).

Sampling

Sampling for macrozoobenthic species occurred between June and October of 2011–2014 as part of a yearly spatially extensive long-term monitoring campaign within the Dutch Wadden Sea (SIBES, Synoptic Intertidal BEnthic Survey). The SIBES program performs core sampling of the intertidal mudflats either by foot or with the use of a rigid hulled inflatable boat, with the aim of comprehensive identification and collection of benthic species in a gridded pattern (500 m separation) throughout the Dutch Wadden Sea that are spatially randomly sampled across the sampling season to minimize the possibility of temporal effects between the years with additional random sample points that result in ∼4,500 samples per year (Bijleveld et al., 2012; Compton et al., 2013). Samples were sieved using 1-mm mesh size and all retained animals were stored frozen after collection. Identification and dissection was done either aboard the ship or in the laboratory. In addition, samples of the filter feeding community (e.g., *Mytilus edulis* and *Balanus crenatus*) were obtained from buoys in the main tidal channels in 2014 to constrain regional N variability throughout the Dutch Wadden Sea. Encrusting communities were scraped from the sides of free-standing anchored buoys and were collected, dissected, and frozen on board (Christianen et al., 2015). Fish were collected from long-term monitoring efforts from the NIOZ Fyke. For all sampling campaigns, samples of muscle tissue (fish, crustaceans, and bivalves), soft tissue (invertebrates), or whole animals (smaller specimens) were freeze-dried, homogenized, and placed in sample vials prior to bulk tissue or amino acid stable isotope analysis. Species were selected for bulk stable isotope analysis based on their contribution to total biomass within the Dutch Wadden Sea ecosystem (Christianen et al., 2017), with 35 species contributing 99% of the total benthic biomass for the system. From these samples, 28 species (25 consumers, three macroalgae) were selected for amino acid isotope analysis based on tissue availability (>3 mg), spatial representation across the Dutch Wadden Sea, and adequate replication (>5 individuals) within the data set. Also samples for particulate organic matter (POM) were collected and filtered through combusted GFF filters (Whatman). MPB were filtered onto GFF filters after migration into combusted sand through a 100-μm mesh (Eaton and Moss, 1966). This method will preferentially select for motile (epipelic) diatoms vs. sessile (episammic) diatoms. Additional sampling details for the SIBES campaigns can be found in Bijleveld et al. (2012), Compton et al. (2013), and Christianen et al. (2017).

Isotope analyses

For bulk stable isotope analysis of $\delta^{13}C$ and $\delta^{15}N$ values, 0.4–2 mg of freeze-dried, homogenized, and non-lipid extracted animal tissue was loaded into tin capsules. Because the presence of inorganic carbonates can greatly influence $\delta^{13}C$ values (Androuin et al., 2019; Sturbois et al., 2022), samples were initially analyzed without acidification for $\delta^{15}N$ and $\delta^{13}C$ values and then re-analyzed after acidification for a $\delta^{13}C$ value of the organic matter in tissue if (1) the animal has a shell, (2) if the animal is in contact with sediment, or (3) if C/N ratios were higher than eight. Acidification was performed through an initial addition of two drops of 2N hydrochloric acid, gentle shaking to mix, allowing time for bubbling to evolve (15 min), and then adding two more drops and gently shaking until the addition of acid does not cause bubbling. After a final addition of a few drops of acid, sample vials were then shaken overnight, repeatedly rinsed with double distilled water to a pH of five, and then freeze-dried to completely remove any remaining acid prior to analysis. Samples were analyzed with a Flash 2000 elemental analyzer coupled to a Delta V Advantage isotope ratio mass spectrometer (Thermo Scientific, Bremen, Germany). Stable isotope ratios are expressed using the δ notation in units per mil:

$$\delta(\%) = ((R_{sample}/R_{standard}) - 1) \times 1000, \text{ where}$$

$$R = {}^{13}C/{}^{12}C \text{ or } {}^{15}N/{}^{14}N \quad (1)$$

respectively, reported relative to Vienna Pee Dee belemnite and atmospheric N_2. Certified laboratory standards of acetanilide, urea, and casein with known $\delta^{13}C$ and $\delta^{15}N$ values and known %TOC and %TN values calibrated against NBS-22 and IAEA-N1 were used for calibration with each sample run. Average precision for standards and replicate samples was ± 0.1‰ for $\delta^{13}C$ and 0.2‰ for $\delta^{15}N$.

For analysis of $\delta^{15}N$ values in individual amino acids, 2–5 mg of tissue was hydrolyzed and derivatized to

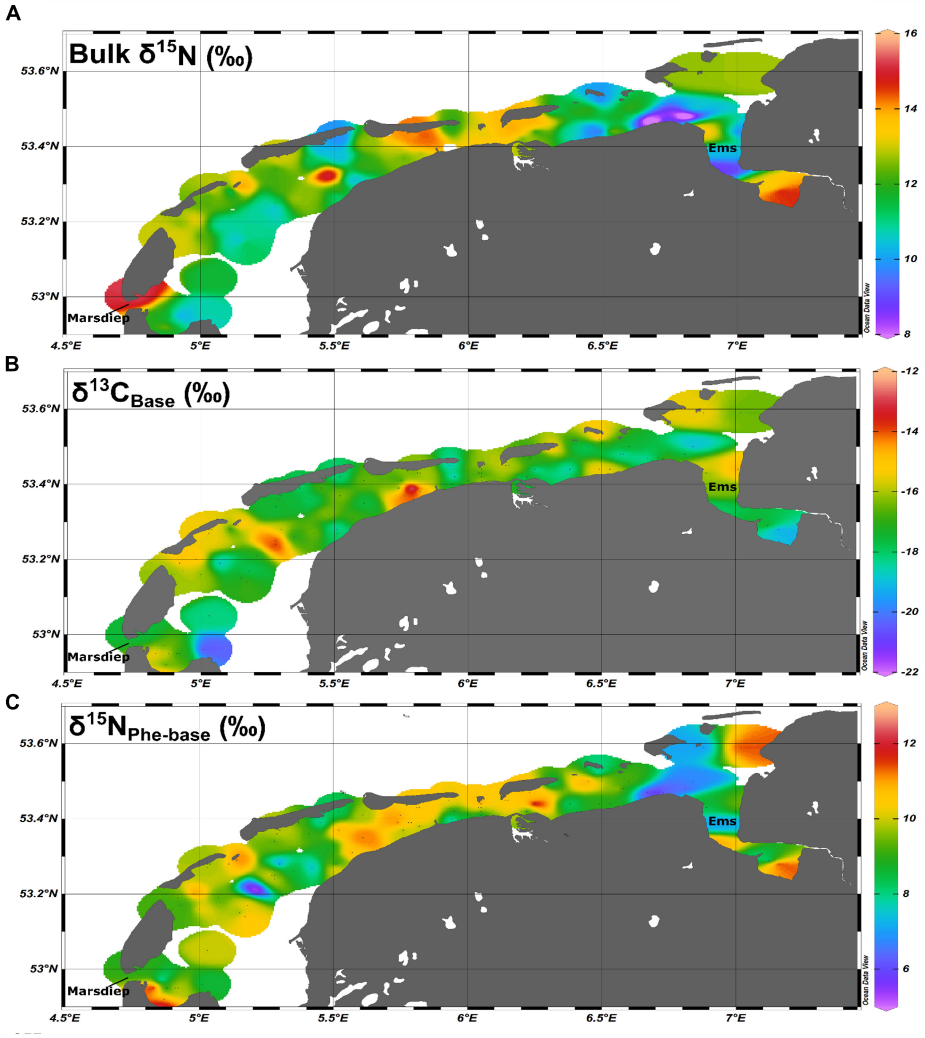

FIGURE 1
Spatial coverage for **(A)** regionally adjusted bulk $\delta^{15}N$ values, **(B)** $\delta^{13}C_{Base}$ values, and **(C)** $\delta^{15}N_{Phe-base}$ values for the Dutch Wadden Sea.

N-pivaloyl/isopropyl (NPiP) derivatives. Analysis occurred using two different gas chromatography combustion isotope ratio mass spectrometers with similar ramp schedules, flow rates, and combustion temperatures measured at the NIOZ Royal Netherlands Institute for Sea Research between 2012 and 2019. ∼90% of the samples were analyzed in duplicate with a Trace 1310 gas chromatograph coupled to a Delta V advantage isotope ratio mass spectrometer through an IsoLink II using a modified version of the amino acid preparation and analysis method used by Chikaraishi et al. (2007) that is described in further detail in Riekenberg et al. (2020b). From this analysis, we report 12 amino acid $\delta^{15}N$ values including alanine, aspartic acid, Glu, glycine, isoleucine, leucine, lysine, methionine, Phe, serine, threonine, tyrosine, and valine with a precision for samples and standards of $<\pm0.5$‰. Due to the conditions during hydrolysis, the terminal amines contained in glutamine and aspartamine are cleaved thereby converting to glutamine to glutamic acid and aspartamine to aspartic acid; so Glu represents a pool of combined material in this work. The remaining 10% of the samples were analyzed in duplicate on an Agilent 6890 gas chromatograph coupled to a Delta V advantage isotope ratio mass spectrometer through a combustion III interface using the method presented in Svensson et al. (2016) reporting five amino acids (alanine, glycine, norleucine, Glu, and Phe) with an average precision for standards and samples of ±1‰. We, therefore, present only Glu and Phe for the 338 amino acid analyses presented here due to the reduced precision and reduced number of reported amino acids present in 10% of the data set.

Trophic-level calculations

Trophic levels were estimated using single trophic and source amino acids (Glu and Phe, respectively) with the equation presented in Chikaraishi et al. (2009) modified with an ecosystem-specific TDF and β following Bradley et al. (2015) to account for the range of TDFs present from primary producers to tertiary consumers within the benthic community.

$$\text{Trophic level} = (\delta^{15}N_{Glu} - \delta^{15}N_{Phe} - \beta)/\text{TDF} + 1 \quad (2)$$

where TDF, the stepwise increase in $\delta^{15}N$ value between a consumer and their diet, is 4.9‰ and β, the difference between Glu and Phe in the ecosystem's primary producers, is 4.3‰. These values are obtained from the slope and intercept of the linear relationship between the difference between $\delta^{15}N$ values for Glu and Phe and trophic position as determined by stomach content and ecological observation. This relationship was then adjusted to place primary producers at the intercept of 0 using a re-arranged version of Equation 2 as further described in Bradley et al. (2015):

$$\Delta_{Glu-Phe} = (TP_{SCA} - 1)^{*}TDF + \beta \quad (3)$$

where $\Delta_{Glu\text{-}Phe}$ is the measured isotopic difference between Glu and Phe for each species and TP_{SCA} is the trophic level as indicated by stomach content analysis or ecological determination of direct feeding and was determined for each species using FishBase for fish species (Froese and Pauly, 2000), literature determinations for invertebrates (Christianen et al., 2015, 2017; Borst et al., 2018), and estimation through interpolation of centroid placement for the remaining species relative to ecosystem trends (**Table 1**).

Adjustment to account for the small trophic increase in $\delta^{15}N$ values of the source AA phenylalanine to establish baseline $\delta^{15}N$ values for individual species was calculated as:

$$\delta^{15}N_{Phe-Base} = \delta^{15}N_{Phe} - (0.2^{*}(\text{trophic level} - 2)) \quad (4)$$

which accounts for the small increase observed in the $\delta^{15}N_{Phe}$ (‰) value that is associated with consumer fractionation of diet during metabolism of Phe (0–0.4‰) (Chikaraishi et al., 2009; McMahon and McCarthy, 2016) and trophic level is the trophic level estimate for each individual species. Correction for the trophic increase in bulk $\delta^{13}C$ values was calculated as:

$$\delta^{13}C_{Base} = \delta^{13}C_{Bulk} - (0.5^{*}(\text{trophic level} - 2)) \quad (5)$$

where 0.5 is the increase observed in bulk $\delta^{13}C$ values between diet and consumer. This value falls between the TDF values observed for bulk $\delta^{13}C$ for whole tissue from consumers (0.3 ± 0.1‰) and consumer muscle tissues (1.3 ± 0.3‰) (McCutchan et al., 2003). Due to the wide range of animals included in this analysis ranging from invertebrate primary consumers to teleost tertiary consumers, we have found it appropriate to use a single intermediate TDF value for bulk $\delta^{13}C$ for all consumers across the trophic structure.

Data analysis

Statistical analyses were performed in R (v 4.0.3) using RStudio (v 1.3.1056), OriginLab 2020b, or in Ocean Data View (5.6.0) (Schlitzer, 2022). Mixing models were performed using Food Reconstruction Using Isotope Transferred Signals (FRUITS v 2.1) and the MixSIAR package in R (Stock et al., 2018). We first used FRUITS to model the species means against measured values for end members (**Tables 1**, **2**) for two sources (POM and MPB global averages) using $\delta^{13}C_{Base}$ values only and then three sources (POM, MPB_{green}, and MPB_{brown}) using $\delta^{13}C_{Base}$ and $\delta^{15}N_{Phe\text{-}Base}$ values with SD values set to 0.2‰ for $\delta^{13}C$ and 0.5‰ for $\delta^{15}N$ reflecting global measurement errors. Both MPB_{green} and MPB_{brown} end members from minimum and maximum bulk $\delta^{15}N$ values for MPB and POM are the average measured during the sampling campaigns. Models in FRUITS were run using 50,000 updates, a burn-in of 10,000 and a minimum uncertainty of 0.001. We then proceeded to modeling individuals within species groupings in MixSIAR using end member values for $\delta^{15}N_{Phe}$ that allowed for the resolution of individuals within the mixing envelope between end members (**Table 2b**) with minimal exclusion of consumer data points (4% excluded, $n = 302$ remaining). For individual models using three source end members, values for N were expanded for both MPB-derived end members with $\delta^{15}N$ values of 5.0‰ for MPB_{green} and 13.0‰ for MPB_{brown} taken from values observed for $\delta^{15}N_{Phe-Base}$ for individuals from *Peringia ulvae* (Cone mudsnail) and *Littorina littorea* (Periwinkle). Models in MixSIAR were run using the "long" setting, where three Markov chain Monte–Carlo algorithms with a length of 300,000 run with a burn-in of 200,000. Results are presented from the species averages along with correlation indices comparing the two modeling approaches. Additional details about model fit are provided in the **Supplementary material**.

Results

Bulk $\delta^{13}C$ and $\delta^{15}N$ values and standard errors (SE) for the 28 species included in this study are listed in **Table 1** and bulk $\delta^{13}C$ and $\delta^{15}N$ values and standard errors (SE) for resources identified as supporting the ecosystem are listed in **Table 2a**. We confirmed that bulk $\delta^{15}N$ values were increased for samples taken from the Ems-Dollard region (eastern Dutch Wadden Sea) in comparison with other regions in the Dutch Wadden Sea and have now adjusted for this regionally observed increase in

TABLE 1 $\delta^{15}N$ values for bulk material, glutamic acid, and phenylalanine along with $\delta^{13}C$ values, trophic position from stomach content and trophic position calculated from amino acids (AAs) for the subset of 25 consumers and three macroalgae species examined in this study sampled from the Dutch Wadden Sea benthic food web during SIBES and Waddensleutels campaigns spanning from 2011 to 2014 and in the NIOZ Fyke during routine monitoring.

Species name	Common name	*n*	$\delta^{15}N$ (‰)	SE	$\delta^{13}C$ (‰)	SE	Trophic position stomach content	Trophic position from AAs	SE	Glutamic acid $\delta^{15}N$ (‰)	SE	Phenyalanine $\delta^{15}N$ (‰)	SE	Glu-phe $\delta^{15}N$ (‰)	SE
Arenicola marina	Lugworm	14	12.8	0.4	−16.0	0.5	1.9	2.1	0.1	21.0	0.7	11.2	0.5	9.8	0.4
Balanus crenatus	Acorn barnacle	13	12.5	0.2	−17.4	0.4	1.9	2.4	0.2	20.7	1.0	9.3	0.4	10.9	0.8
Carcinus maenas	Green crab	18	14.0	0.3	−15.8	0.2	3	3.2	0.1	24.2	0.7	8.9	0.3	14.5	0.6
Cerastoderma edule	Common cockle	21	11.0	0.4	−18.8	0.1	1.8	2.2	0.1	20.1	0.6	9.8	0.5	10.0	0.5
Chrysaora hysoscella	Compass jellyfish	8	13.4	0.3	−19.2	0.5	3.4	3.5	0.1	26.7	0.3	10.4	0.6	15.8	0.5
Clupea harengus	Herring	10	14.6	0.2	−18.0	0.3	3.4	3.4	0.0	23.6	0.7	7.4	0.7	15.3	0.2
Crangon crangon	Shrimp	17	13.6	0.3	−14.9	0.3	3.2	3.5	0.1	26.2	0.4	9.7	0.4	15.7	0.5
Magallan gigas	Pacific oyster	13	12.3	0.3	−17.9	0.2	1.8	2.2	0.1	20.0	0.6	9.6	0.3	10.2	0.6
Crepidula fornicata	Slipper limpet	8	10.5	0.3	−17.4	0.1	2	1.7	0.1	17.1	0.3	9.0	0.5	7.9	0.3
Dicentrarchus labrax	European bass	10	15.9	0.5	−15.9	0.5	3.5	4.0	0.2	27.8	0.6	8.3	0.3	17.9	0.7
Ensis directus	Razor clam	9	9.9	0.4	−17.8	0.3	2	1.2	0.1	14.0	0.3	8.3	0.4	5.5	0.3
Pomatoschistus sp.	Goby	8	14.6	0.3	−14.9	0.5	3.2	3.6	0.1	24.7	0.4	8.8	0.3	15.9	0.4
Hediste diversicolor	Ragworm	17	12.3	0.4	−16.5	0.3	2.6	2.6	0.1	20.1	0.7	7.8	0.3	11.6	0.6
Hydrobia ulvae	Cone mudsnail	10	9.2	0.3	−15.1	0.8	2	1.4	0.1	15.3	0.5	8.2	0.7	6.7	0.5
Lanice conchilega	Sand mason worm	11	11.1	0.5	−18.1	0.3	1.8	2.2	0.1	19.3	0.7	9.1	0.5	9.9	0.6
Liocarcinus holsatus	Flying crab	7	13.7	0.4	−18.1	0.5	3	3.3	0.1	26.5	0.4	11.7	0.6	14.8	0.3
Littorina littorea	Periwinkle	17	11.5	0.3	−14.5	0.4	2.3	2.3	0.1	20.7	0.4	9.8	0.2	10.6	0.4
Macoma balthica	Baltic clam	20	11.9	0.3	−16.2	0.2	1.8	1.7	0.1	18.5	0.6	10.1	0.4	7.8	0.5
Mytilus edulis	Blue mussel	30	11.1	0.3	−18.6	0.2	2	1.7	0.1	17.2	0.3	8.7	0.3	8.1	0.3
Osmerus eperlanus	European smelt	8	16.4	0.4	−17.2	1.0	3.5	3.8	0.1	27.0	0.5	9.4	0.4	17.1	0.3
Platichthys flesus	European flounder	8	15.1	0.5	−14.5	0.4	3.5	3.4	0.1	25.7	0.7	9.9	0.3	15.3	0.4
Pleuronectes platessa	European plaice	10	13.4	0.3	−15.6	0.3	3.2	3.2	0.1	22.7	0.5	7.4	0.5	14.2	0.4
Rhizostoma pulmo	Barrel jellyfish	7	13.0	0.3	−20.5	0.9	3	2.9	0.2	23.5	0.6	10.1	0.3	13.1	0.7
Solea solea	Flatfish	11	14.8	0.2	−16.8	0.3	3.2	3.0	0.1	25.5	0.6	11.4	0.5	13.6	0.6
Zoarces viviparus	Eelpout	8	15.9	0.2	−15.0	0.2	3.5	3.8	0.1	27.6	0.5	10.4	0.3	16.8	0.4
Ceramium rubrum	Red horn weed	8	11.6	0.3	−18.4	0.9	1.5	1.7	0.1	14.5	0.7	6.6	0.8	7.7	0.3
Fucus vesiculosus	Bladderwrack	8	8.0	0.9	−15.3	0.6	1	0.3	0.1	12.1	0.8	10.3	0.8	1.8	0.3
Ulva sp.	Sea lettuce	8	11.1	0.7	−13.5	0.6	1	0.8	0.1	15.7	0.6	11.5	0.4	4.1	0.4

10.3389/fevo.2022.951047

TABLE 2 Bulk $\delta^{15}N$ and $\delta^{13}C$ values for the end member values supporting the Dutch Wadden Sea benthic food web used for two and three source mixing models on species means.

End members	*n*	$\delta^{15}N$ (‰)	SE	$\delta^{13}C$ (‰)	SE
Particulate organic matter	101	8.6	0.1	−21.2	0.1
Microphybenthos average	95	9.2	0.2	−13.4	0.2
Microphybenthos green	20	7.3	0.2	−14.2	0.3
Microphybenthos brown	25	11.3	0.3	−13.4	0.2

End members	$\delta^{15}N$ (‰)	SE	$\delta^{13}C$ (‰)	SE
Particulate organic matter	8.6	0.1	−21.2	0.1
Microphybenthos average	9.2	0.2	−13.4	0.2
Microphybenthos green	5.0		−14.2	0.3
Microphybenthos brown	13.0		−13.4	0.2

bulk $\delta^{15}N$ values for filter feeders [−2.3‰; One-way ANOVA, $F_{(2,43)} = 6.8$, $p = 0.003$; Supplementary Table 1]. Adjustment of $\delta^{15}N$ values was identified as necessary in both *M. edulis* (blue mussel) and *B. crenatus* (acorn barnacle) from samples pooled into regional categories within the Wadden Sea (West < 5.5°E, East > 5.5°E, and Ems-Dollard associated with the mouth of the river Ems). Despite application of a regional adjustment, ranges for bulk $\delta^{13}C$ and $\delta^{15}N$ values remained large for consumers (Figures 1A,B) as well as for POM and MPB sampled from across the Dutch Wadden Sea (POM −15.4 to −21.7‰; 13.7 to 5.7‰ and MPB −10.4‰ to −16.2‰; 13.6 to 6.5‰).

Increased $\delta^{15}N_{Phe}$ values were observed for filter feeders sampled from Ems-Dollard in comparison with the rest of the Dutch Wadden Sea and values were adjusted in a similar manner as the bulk $\delta^{15}N$ values [−2.1‰; One-way ANOVA, $F_{(2,43)} = 5.7$, $p = 0.006$; Supplementary Table 1]. Values for $\delta^{15}N_{Phe}$ ranged from 6.6‰ observed for *Ceramium vigatum* (Red horn weed) to 11.7‰ for *Liocarcinus holsatus* (Flying crab) and mean values for species correspondingly increased with larger Glu-Phe differences reflecting the minor trophic increases expected for source amino acids (Table 1). $\delta^{15}N_{Glu}$ values ranged from 12.1‰ for *Fucus vesiculosus* (Bladderwrack) to 27.8‰ for *Dicentrarchus labrax* (European bass) and were higher than $\delta^{15}N_{Phe}$ values as expected for the larger fractionation associated with trophic amino acids. $\delta^{15}N$ values for Glu and Phe were correlated across trophic levels (Pearson's correlation coefficient; Figure 2; TL 1 $R^2 = 0.26$ $n = 24$, $p < 0.01$; TL 2 $R^2 = 0.37$ $n = 166$, $p < 0.001$; TL 3 $R^2 = 0.39$ $n = 96$, $p < 0.002$; TL 4 $R^2 = 0.14$ $n = 34$, $p = 0.03$), but the relationships were weaker for both TL 1 and TL 4 when compared to TL 2 and TL 3. The relationship between $\Delta_{Glu-Phe}$ $\delta^{15}N$ values and TP_{SCA} −1 had a strong correlation (Figure 3; $n = 337$, $R^2 = 0.7$, $p < 0.001$) with a slope of 4.9 ± 0.3‰ and an intercept of 4.3 ± 0.2‰ that reflect TDF and β, respectively, for the Dutch Wadden Sea benthic food web. These values for TDF and β are different than the canonical values of 7.6 and 3.4‰ found by Chikaraishi et al. (2009) and resulted in a slope of 0.99 for TL vs. TP_{SCA} while using the canonical TDF and β resulted in a slope of 0.64 (both $R^2 = 0.72$).

Calculated trophic levels for primary producers ranged from 0.3 for *Fucus vesiculosus* (Bladderwrack) to 1.7 for *C. rubrum* (Figure 4). Primary consumers ranged from 1.2 for *Ensis leii* (Razor clam) to 2.3 for *Littorina littorea* (Periwinkle), secondary consumers from 2.6 for *Hediste diversicolor* (Ragworm) to 3.5 for *Crangon crangon* (shrimp) and tertiary consumers from 3.6 for *Pomatoschistus* sp. (Goby sp.) to 4 for *D. labrax* (European bass, Figure 4). No amino acid measurements were possible for POM or MPB as part of this study as the sample weights remaining after the initial bulk analysis between 2012 and 2015 were below detection limits for this analysis. Consumer $\delta^{13}C$ values fell between the measured values for POM and MPB (−21.2 and −13.4‰). We therefore used the trophic level estimates calculated using system-specific TDF and β to account for fractionation while estimating values for $\delta^{13}C_{Base}$ and $\delta^{15}N_{Phe-base}$.

We then used $\delta^{13}C_{Base}$ values from POM and MPB (Table 2) and each consumer to calculate dietary contributions for species averages (Figure 5A) and for all individuals within each species. Dietary contributions from these two source mixing models are presented in Supplementary Table 2A and indicated use of POM (>0.5) for 11 of the 25 consumer species examined with the highest contribution being observed for *Rhizostoma pulmo* (Barrel jellyfish, 0.86 ± 0.09 and 0.76 ± 0.04). To further investigate the use of MPB within the ecosystem, we used $\delta^{13}C_{Base}$ and $\delta^{15}N_{Phe-Base}$ values from POM, MPB_{green}, a proxy of freshly fixed MPB-derived material, and MPB_{brown}, a proxy of MPB-derived material using reworked N and OM associated with heterotrophic reworking of detrital OM and denitrification occurring across the tidal cycle (Table 2b), to calculate dietary contributions from species average values (Figure 5B). Similar to the two source models, dietary contribution

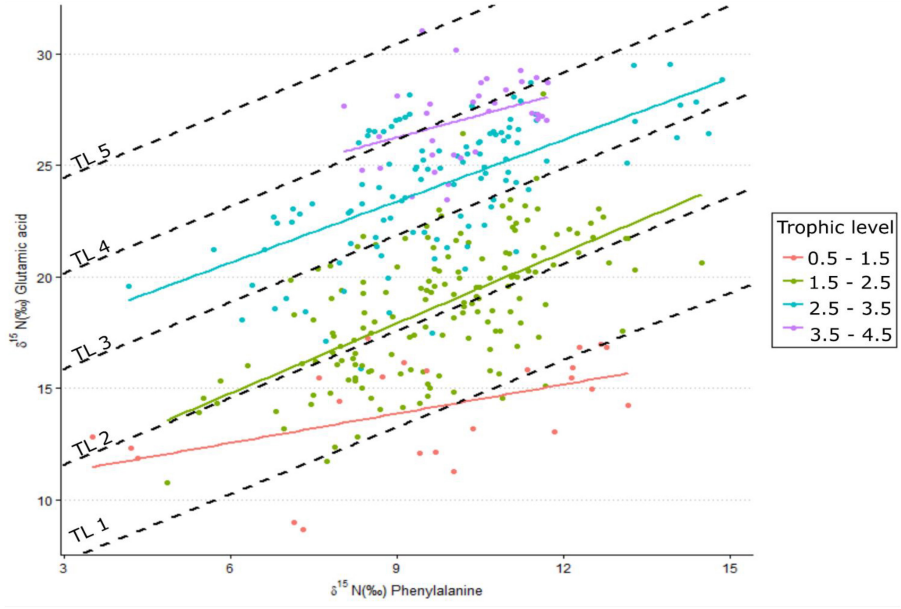

FIGURE 2
δ^{15}N values for the amino acids glutamic acid and phenylalanine measured for species across different trophic levels. Dashed lines are expected linear relationships for trophic levels 1–5 using a trophic discrimination factor of 4.9% and a β of 4.3%, while colored linear regressions are trophic-level relationships by grouping trophic levels across species (n = 24–166).

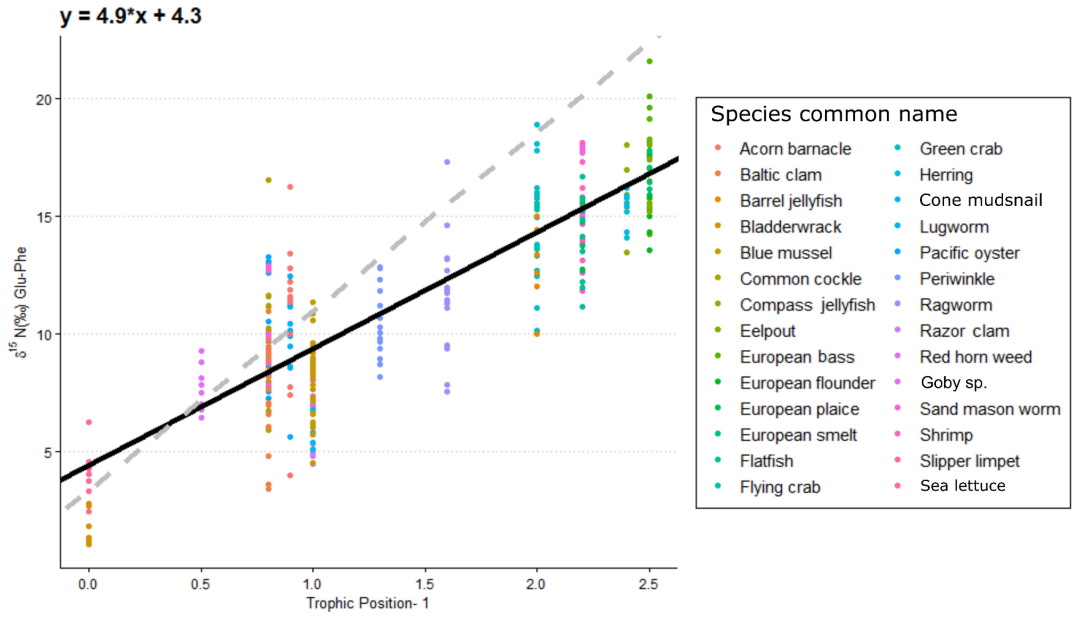

FIGURE 3
The per mil difference in δ^{15}N value between glutamic acid and phenylalanine in relation to trophic levels for individual species minus one level to account for primary producers. The black line is the fitted linear regression across all species (r^2 = 0.7, n = 337) with the equation presented at the top left of figure. The dashed gray line is the linear trophic level relationship using a slope of 7.6% and a β of 3.4% as presented in Chikaraishi et al. (2009).

from POM was considerable (>0.5) for 11 of the 25 consumer species with *R. pulmo* (Barrel jellyfish) having the highest contribution (0.78 ± 0.1). For the two MPB end members, dietary contribution of MPB_{green} was considerable for six species with *Pleuronectes platessa* (European plaice) having the highest contribution (0.75 ± 0.1) and dietary

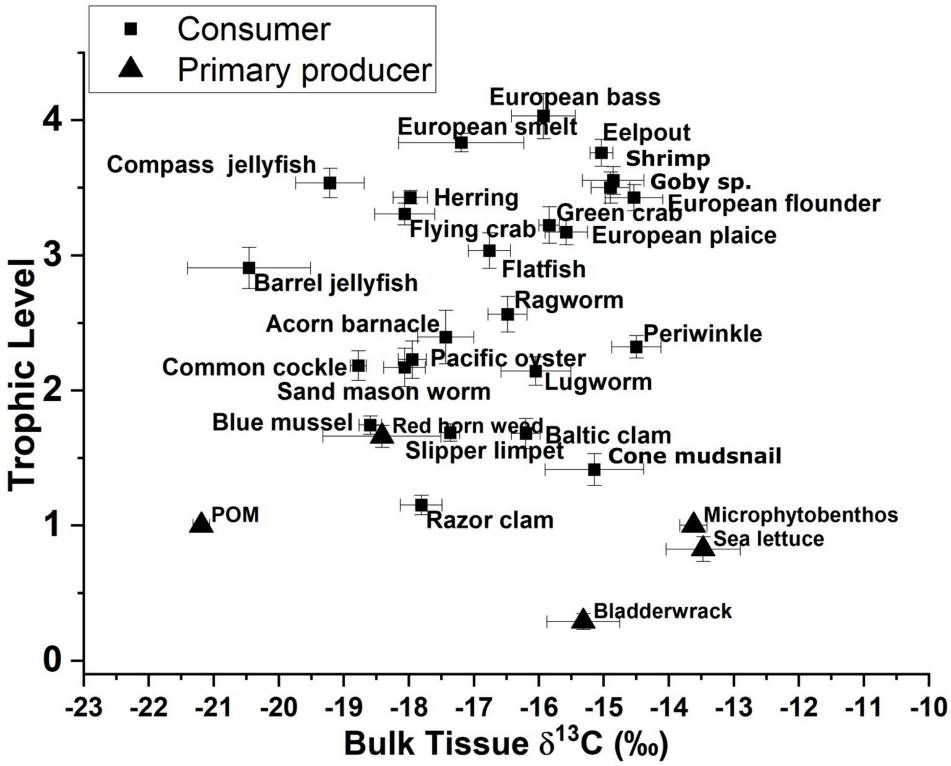

FIGURE 4
Trophic-level estimates from amino acid $\delta^{15}N$ values for glutamic acid and phenylalanine vs. bulk $\delta^{13}C$ values for both consumers and primary producers.

contribution from MPB_{brown} was considerable for five species with *Zoarces viviparus* (Eelpout) having the highest contribution (0.57 ± 0.13). Dietary contributions from POM were > 0.5 for 10 species with *Chrysaora hysoscella* (Compass jellyfish) having the highest contribution (0.78 ± 0.04), while contributions for MPB_{green} were lower with no species > 0.5, but with four species having a contribution of >0.4 with *H. diversicolor* (Ragworm) having the highest contribution (0.47 ± 0.05), and contributions for MPB_{brown} being > 0.5 for six species with *Arenicola marina* (Lugworm) having the highest contribution (0.67 ± 0.05). Both two-source and three-source mixing models indicated good agreement between the use of POM with a correlation between the models using species averages and individual values of 0.88 and 0.89, respectively (R^2, Figure 5C).

Discussion

In the Dutch Wadden Sea, we found that using amino acid $\delta^{15}N$ values allowed for more detailed and reliable identification of the trophic structure of the benthic food web than possible in previous work using solely bulk isotope methodologies. This improvement allowed for the identification of a subset of species that rely on microbially reworked materials supported through active tidal pumping. Across all four simple and complex SIMMs, mean consumer reliance on MPB was 0.55–0.6, but fell short of the 0.7 previously assessed (Christianen et al., 2017). This smaller contribution from MPB is likely due to the combined use of $\delta^{13}C$ and $\delta^{15}N$ values to assess resource contributions instead of using consumer integrators as a proxy for MPB resource values (Post, 2002). Additionally, analysis of individual amino acid $\delta^{15}N$ values allowed for trophic adjustment of $\delta^{13}C$ and $\delta^{15}N$ values to account for trophic discrimination for the 25 benthic consumer species prior to analysis with SIMMs. Through the application of source amino acids, we were able to construct a trophic structure within the Dutch Wadden Sea despite the considerable underlying variability present in bulk $\delta^{15}N$ values across the area (Figure 1A). This variability was potentially caused by widespread biogeochemical processing in porewaters unique to regions of intense tidal flushing within intertidal sands (e.g., denitrification). Analysis of trophic and source amino acid $\delta^{15}N$ values allowed for the development and application of a system-specific TDF and β to determine the trophic structure of the Wadden Sea benthic food web that was previously impossible using solely bulk isotopic techniques.

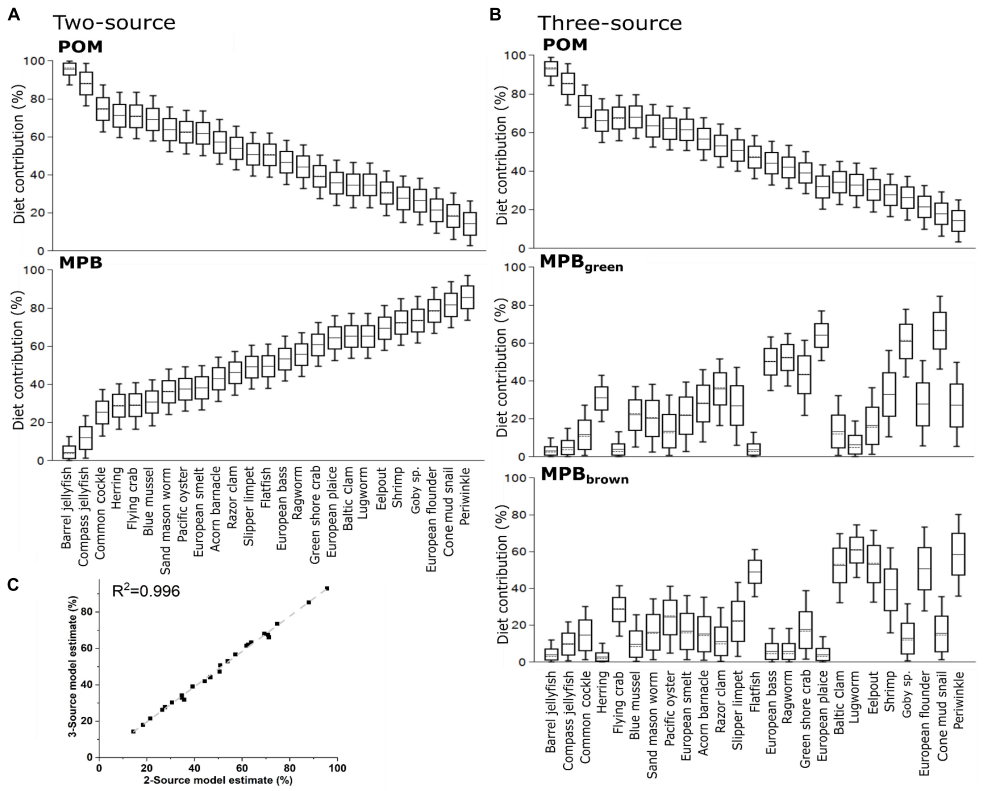

FIGURE 5
Estimated dietary contributions from primary producers using **(A)** a two source mixing model using only $\delta^{13}C$ and mean values for each species and **(B)** a three source mixing model using both $\delta^{13}C$ and $\delta^{15}N_{Phe-Base}$ and mean values for each species and **(C)** the correlations between two and three source mixing models when applied to means values and individuals for each species. Trophic structure has been accounted for in both models using trophic-level estimates from amino acid analysis of $\delta^{15}N$.

A bulk isotope approach and its complications

We confirm that MPB is a major source of productivity that widely supports the food web in the Dutch Wadden Sea (Christianen et al., 2017). The majority of consumers examined here (21 out of 25 consumer species) have $\delta^{13}C$ values higher than −18‰, indicating reliance on a resource with a higher value than POM (−21.2 ± 0.2‰; n = 101). MPB (−13.4 ± 0.2‰; n = 95) is a widely available resource across the Dutch Wadden Sea (**Figure 1B**) with variable $\delta^{13}C$ values indicating the use of both dissolved inorganic carbon (DIC) from the overlying water column and remineralized organic matter from porewater DIC. Due to the sandy nature of the sediment and extensive tidal pumping that occurs in the basin, benthic-associated MPB, primarily pennate diatoms (Scholz and Liebezeit, 2012) are widely available to consumers during diel inundation and exposure. Other potential candidate resources available to consumers include sediment organic matter, terrestrial input, macroalgae, or seagrasses, but are unlikely to play a significant role in supporting production. Sediment organic matter (−21.8 ± 0.3‰; n = 117) and terrestrial inputs [−27‰ (Middelburg and Herman, 2007) and −23‰ (Jung et al., 2019)] have lower $\delta^{13}C$ values than POM and therefore cannot contribute to explain the higher values widely observed across consumers in the Dutch Wadden Sea. Green macroalgae such as *Ulva* sp. (Sea lettuce; −13.5 ± 0.6‰, n = 8) have a higher value that could meaningfully contribute but are spatially limited due to their need for hard anchoring points such as exposed rocks within the larger landscape of mud and sand. This limited distribution constrains the amount of contribution from this resource as blooms of *Ulva* or so-called green tides (Charlier et al., 2008) did not occur in the period between 2011 and 2014 in the Dutch Wadden Sea. This makes *Ulva* sp. an unlikely resource to support more than half of the food web. Similarly, seagrasses have previously occurred extensively in the Wadden Sea, but due to their current extremely limited spatial ranges in the German and Danish Wadden Sea (Folmer et al., 2016) are unlikely to be a large source of productivity supporting consumers in the Dutch Wadden Sea.

Further examination of MPB as a resource reveals substantial variability in $\delta^{15}N$ values ranging from 7.3 to 11.3‰

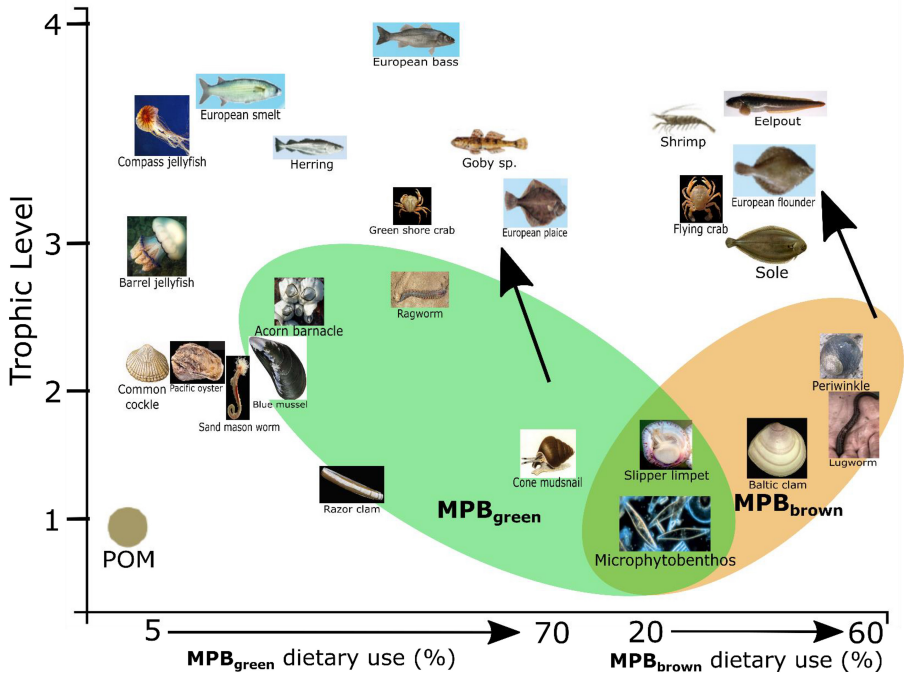

FIGURE 6
Conceptual diagram indicating increased use of microphytobenthos-derived matter from either reworked material (MPB_{Brown}) or newly produced material (MPB_{green}) as use of particulate organic matter (POM) decreases. Photograph credits: Henk Heesen, Ales Kladnik, Francesca Crippa, Hans Hillewaert, Matthisas Buschmann, Sytske Dijksen, and Gordon Taylor.

when grouping the minimum and maximum measurements taken from across the study site (**Table 2a**; MPB_{green} and MPB_{brown}). This variability could potentially reflect the input from an unaccounted resource or a biogeochemical process that is occurring across the basin. Although freshwater input from terrestrial sources has a $\delta^{15}N$ of 10–14‰ (Jung et al., 2019), the limited inputs to the Wadden Sea and $\delta^{13}C$ value of −23‰ indicate at best a regionally confined contribution to the ecosystem. Another possible unaccounted source includes submarine groundwater discharge, which due to the relatively porous nature of the sandy sediment in the Wadden Sea basin could contribute reworked N with higher $\delta^{15}N$ values to the benthos. Previous work has identified freshwater groundwater discharge as a minor input (Santos et al., 2015) that is unlikely to have a basin wide impact. However, this work did confirm considerable porewater exchange resulting in efflux of waters with higher total dissolved nitrogen and lower dissolved oxygen saturation as tidal exchange flushes previously isolated porewaters that have accumulated products from remineralization. Porewater exchange across the sediment surface during tidal flushing resulted in porewater total dissolved nitrogen that decreased with depth that is expected with efflux into the overlying water column. Tidal pumping through permeable sands (Marchant et al., 2018) is a potentially region-wide process providing nutrients that have undergone considerable denitrification that may provide substrate pools in porewaters with increased $\delta^{15}N$ values that then support MPB production within the Wadden Sea. Increased $\delta^{15}N$ values are most apparent in the Ems-Dollard region and required adjustment for both bulk $\delta^{15}N$ and $\delta^{15}N_{Phe-Base}$ values (**Supplementary Table 1**). Despite this adjustment within the wider data set, there remains considerable variability in $\delta^{15}N$ values (**Figure 1A**) across the basin that has made identifying a trophic structure using bulk $\delta^{15}N$ values alone difficult without a method to integrate underlying shifts in baseline $\delta^{15}N$ values across the Dutch Wadden Sea.

Trophic discrimination factor and ecosystem baseline using amino acids

The TDF value from analysis of the difference between Glu and Phe throughout the food web is lower in this study than the most often applied canonical value (4.9‰ compared to 7.6‰) (Chikaraishi et al., 2009); as has been previously observed in multiple studies (McMahon and McCarthy, 2016; Hebert et al., 2016; Lemons et al., 2020; Nuche-Pascual et al., 2021). The lower TDF value reflects an ecosystem-wide application to species ranging from macroalgae to teleosts, and represents a compromise between the use of a single canonical TDF (Chikaraishi et al., 2009; Kato et al., 2021; Vokhshoori et al., 2021), application of multiple species-specific TDFs as

determined by feeding studies (28×, 1 per species) or feeding group-dependent strategies based on the relative diet vs. tissue quality comparisons (McMahon et al., 2015b; McMahon and McCarthy, 2016; Bode et al., 2021; Le-Alvarado et al., 2021). Using wild caught animals across an entire ecosystem to derive a system-wide TDF, we relied on measured variations in the difference between Glu and Phe between individuals in each species sampling to estimate the TDF value that was then applied to estimate the trophic structure within the ecosystem. To this end, we combined trophic position estimates of teleosts from FishBase (Froese and Pauly, 2000), literature values for trophic position of invertebrate species (Christianen et al., 2015) and measured $\delta^{15}N_{Glu-Phe}$ values for primary producers to ensure representation across the food web and found a TDF that is broadly comparable to one developed using solely marine teleosts (5.7‰). Application of a system-specific TDF was possible here due to the relatively large number of replicates for each species examined across the food web. Developing the TDF was necessary due to the presence of a large number of species for which no controlled feeding studies have been performed where the stable isotope composition of amino acids have been analyzed (e.g., a wide range of benthic invertebrates).

Application of $\delta^{15}N$ values from amino acids allows for the integration of underlying variability in N sources when characterizing the trophic relationships within the benthic community. The large range observed for $\delta^{15}N_{Phe-Base}$ (**Figure 1C**) in consumers further confirms that use of N with a high $\delta^{15}N$ value is not regionally confined and occurs across the basin. In contrast, variability in the $\delta^{13}C_{Base}$ values is more regionally confined, likely indicating the widespread use of MPB-derived carbon that is more consistently available across the basin and therefore less variable. These contrasting patterns and wide range of $\delta^{15}N$ values observed across the MPB sampling support splitting of the MPB end member into two distinct resources: (1) MPB_{green} which reflects newly fixed organic matter from MPB supported by dissolved inorganic C (DIC) and N substrates from the overlying water column and (2) MPB_{brown} which reflects newly fixed organic matter from MPB supported from bacterially reworked C and N substrates provided from porewater associated materials (**Table 2a**). Furthermore, $\delta^{15}N_{Phe-Base}$ values for a subset of the measured individuals of *Peringia ulvae* (Cone mudsnail; 5.6 ± 0.2‰; $n = 3$ vs. 8.2 ± 0.7‰; $n = 10$) indicated the individual specialization on a specific resource in a species previously used as an end member proxy for MPB (Christianen et al., 2017) while *Littorina littorea* (Periwinkle; 9.8 ± 0.2‰; $n = 17$; **Table 1**) had a substantially higher $\delta^{15}N_{Phe-Base}$ value despite similar use of MPB between these two species indicated by the two source mixing model (**Figure 5A**; 71 and 82%, respectively). A 5‰ difference between source amino acid $\delta^{15}N$ values between two primary consumers using similar amounts of MPB-derived carbon further confirms the substantial variation in MPB-$\delta^{15}N$ values due to availability of porewaters that have been impacted by denitrification. This difference warranted further examination using three-source mixing models with two distinct MPB sources after adjustment for trophic position indicated using the ecosystem-dependent TDF from amino acid $\delta^{15}N$ values.

Identifying detrital contributions from microphytobenthos into the wider food web

Food webs are often split into herbivory (green) and detrital (brown) pathways depending on whether newly fixed productivity or detrital reworking are the predominate basal resource supporting them (Odum, 1969; Middelburg, 2014). These are often not clear-cut distinctions, but rather a spectrum of resource use split between multiple sources depending on the diet of each individual species. Application of the three source mixing models (**Figure 5B**) reveals separation between species groups that use the MPB_{green} and the MPB_{brown} resources. Species using MPB_{green} include *Carcinus maenas* (Green crab), *Pomatoschistus* sp. (Goby sp.), *P. platessa* (European plaice), and *P. ulvae* (Cone mudsnail), indicating reliance on newly fixed MPB-derived organic matter supported from the overlying water column (DIC and available N). Species using MPB_{brown} include *M. baltica* (Baltic clam), *A. marina* (Lugworm), *L. littorea* (Periwinkle), *C. crangon* (Shrimp), *Z. vivparus* (Eelpout), *Platicthys flesus* (European flounder), and *Solea solea* (Sole) indicating reliance on MPB-derived organic matter supported-off of microbially reworked N substrates that are readily available due to tidal pumping (**Figure 6**). The separation observed between these two groups of species appears to be along the boundaries of green vs. brown food webs (Evans-White and Halvorson, 2017; Cordone et al., 2020), where green food webs are directly supported by newly fixed OM from primary producers and brown food webs have detrital and microbial support through the breakdown, processing, and reuse of organic matter through an efficient microbial loop (Azam et al., 1983; Fenchel, 2008). The re-entry and reuse of detrital products (MPB_{brown}) in this system appear to be mediated by MPB and may reflect either (1) support of live MPB using reworked nutrients and porewater DIC or (2) the direct use of reworked dead MPB-derived organic matter by deposit feeders. MPB samples in this study required migration across a permeable filter pressed against the sand so both MPB_{green} and MPB_{brown} end members reflect live-sampled MPB.

The large variability for both bulk $\delta^{13}C$ and $\delta^{15}N$ values found in the MPB end members points to the need for further investigation into how MPB are supported across the tidal cycle as well as better characterization for all primary producers using compound-specific techniques (PLFAs, AA-C, and AA-N) within the Wadden Sea. Partitioning support from MPB throughout the food web into green and brown pathways highlights that each individual resource in this shallow system

(POM, MPB) likely has multiple forms due to the shallow nature of the basin as green and brown food webs interact and exchange materials (Krumins et al., 2013). The various forms of organic matter reflect the stages of processing that have occurred: (1) direct initial use of phytoplankton (green POM), (2) deposition and partial reworking of phytoplankton that are resuspended and used (brown POM/SOM), (3) direct uptake of water column N and DIC (MPB_{green}), (4) use of reworked nutrients and porewater DIC (MPB_{brown}), or (5) direct use of detrital MPB biomass (MPB_{brown}). Environmental bulk isotope samples can often have quite variable values, but this variance likely represents inputs from a variety of resource pools and the combined application of other compound-specific techniques may be able to contribute to teasing apart individual contributions from these pools.

Due to the diversification of MPB resources, there is support of two distinct food web pathways in the Dutch Wadden Sea for MPB-derived resources as indicated by the three source mixing models (**Figures 5B**, **6**): newly fixed production from the overlying water column (MPB_{green}) and use of microbially reworked substrates from porewaters (MPB_{brown}). This resource diversification likely contributes to the outstanding productivity that has been observed within the Wadden Sea. Specialization on the two different MPB types allows for further feeding niche differentiation beyond the classic model of deposit and surface/particulate feeders through identification of MPB specialist consumers that predominantly rely on either newly fixed or reworked MPB-derived organic matter. This specialization likely reduces competition between feeding types in a highly productive ecosystem and reflects efficient use of not only newly fixed organic matter but also efficient use of reworked OM as either direct uptake or through nutrient and DIC support of MPB through tidal pumping.

Conclusion

Compound-specific analysis of amino acid nitrogen allowed for further identification and adjustment for underlying baseline shifts in $\delta^{15}N$ values within the Dutch Wadden Sea that were not possible using solely bulk stable isotope methods. The resulting regional adjustments allowed for the development and application of a system-specific TDF that could then successfully be applied to estimate the trophic level of 28 species within the food web. Further application of SIMMs confirmed the dominant support of the food web by MPB (2-source models) and identified biogeochemical pathways supporting MPB along separate green and brown pathways (3-source models). This subsidy of nutrients derived from microbial processing in permeable sands may account for some of the exceptional productivity supporting the Wadden Sea fishery and seabird populations. Separate support of MPB between newly fixed and reworked organic matter showcases that diatom connectivity with underlying porewaters needs to be further considered in food web studies examining the considerable productivity that occurs within intertidal ecosystems.

Data availability statement

The original contributions presented in this study are included in the article/**Supplementary material**, further inquiries can be directed to the corresponding author. The data is available at data.4tu.nl, the amino acid data is available at doi: 10.4121/21207470, and bulk carbon and nitrogen data are available at doi: 10.4121/21213113.

Ethics statement

This study used animals previously obtained as part of the SIBES and NIOZ Fyke projects in 2011 to 2014, so no further ethical approval was needed for samples associated with this study.

Author contributions

PR, SH, HV, and MM contributed to conception and design of the study. SH, HV, and TH contributed to sample design and collection of the samples through the SIBES and Waddensleutels projects that support this study. PR and SH organized the databases. PR performed the statistical analysis and wrote the first draft of the manuscript. All authors contributed to manuscript revision and read and approved the submitted version.

Funding

This study was carried out as part of the project "Waddensleutels" funded by "Waddenfonds" (WF203930). SIBES-monitoring was financially supported by NAM, NWO-ALW (ZKO program), and Royal NIOZ. This study also had support from the UU-NIOZ project "Using Isotopic Indicators" (NZ4543.13).

Acknowledgments

For sampling the food web, we thank the crew of RV Navicula and the volunteers, staff, and students in the field. We also thank Kevin Donkers, Ronald van Bommel, Jort Ossebaar, Monique Verweij, Anchelique Mets, Elisabeth Svensson, and Thomas Leerink (NIOZ) for technical assistance in both bulk and compound-specific stable isotope analyses.

Conflict of interest

The authors declare that the research was conducted in the absence of any commercial or financial relationships that could be construed as a potential conflict of interest.

Publisher's note

All claims expressed in this article are solely those of the authors and do not necessarily represent those of their affiliated organizations, or those of the publisher, the editors and the reviewers. Any product that may be evaluated in this article, or claim that may be made by its manufacturer, is not guaranteed or endorsed by the publisher.

Supplementary material

The Supplementary Material for this article can be found online at: https://www.frontiersin.org/articles/10.3389/fevo.2022.951047/full#supplementary-material

References

Androuin, T., Dubois, S. F., Decottignies, P., Pelleter, E., and Carlier, A. (2019). The dark side of soft tissues: Unexpected inorganic carbonate in the invasive slipper limpet Crepidula fornicata and its implications for stable isotope interpretations. *Rapid Commun. Mass Spectrom.* 33, 107–115.

Azam, F., Fenchel, T., Field, J. G., Gray, J. S., Meyer-Reil, L.-A., and Thingstad, F. (1983). The ecological role of water-column microbes in the sea. *Mar. Ecol. Progr. Ser.* 10, 257–263. doi: 10.3354/meps010257

Barnett, A., Méléder, V., Dupuy, C., and Lavaud, J. (2020). The vertical migratory rhythm of intertidal microphytobenthos in sediment depends on the light photoperiod, intensity, and spectrum: Evidence for a positive effect of blue wavelengths. *Front. Mar. Sci.* 7:212. doi: 10.3389/fmars.2020.00212

Bauer, J. E., Cai, W. J., and Raymond, P. A. (2013a). The changing carbon cycle of the coastal ocean. *Nature* 504, 61–70. doi: 10.1038/nature12857

Bauer, J. E., Cai, W.-J., Raymond, P. A., Bianchi, T. S., Hopkinson, C. S., and Regnier, P. A. G. (2013b). The changing carbon cycle of the coastal ocean. *Nature* 504, 61–70. doi: 10.1038/nature12857

Beukema, J. J., Cadée, G. C., and Dekker, R. (2002). Zoobenthic biomass limited by phytoplankton abundance: Evidence from parallel changes in two long-term data series in the Wadden Sea. *J. Sea Res.* 48, 111–125.

Bijleveld, A. I., van Gils, J. A., van der Meer, J., Dekinga, A., Kraan, C., van der Veer, H. W., et al. (2012). Designing a benthic monitoring programme with multiple conflicting objectives. *Methods Ecol. Evol.* 3, 526–536. doi: 10.1111/j.2041-210X.2012.00192.x

Bode, A., Olivar, M. P., and Hernández-León, S. (2021). Trophic indices for micronektonic fishes reveal their dependence on the microbial system in the north atlantic. *Sci. Rep.* 11:8488. doi: 10.1038/s41598-021-87767-x

Borst, A. C. W., Verberk, W. C. E. P., Angelini, C., Schotanus, J., Wolters, J.-W., Christianen, M. J. A., et al. (2018). Foundation species enhance food web complexity through non-trophic facilitation. *PLoS One* 13:e0199152. doi: 10.1371/journal.pone.0199152

Bradley, C. J., Wallsgrove, N. J., Choy, C. A., Drazen, J. C., Hetherington, E. D., Hoen, D. K., et al. (2015). Trophic position estimates of marine teleosts using amino acid compound specific isotopic analysis. *Limnol. Oceanogr. Methods* 13, 476–493. doi: 10.1002/lom3.10041

Charlier, R. H., Morand, P., and Finkl, C. W. (2008). How Brittany and Florida coasts cope with green tides. *Int. J. Environ. Stud.* 65, 191–208. doi: 10.1080/00207230701791448

Chi, X., Dierking, J., Hoving, H.-J., Lüskow, F., Denda, A., Christiansen, B., et al. (2021). Tackling the jelly web: Trophic ecology of gelatinous zooplankton in oceanic food webs of the eastern tropical Atlantic assessed by stable isotope analysis. *Limnol. Oceanogr.* 66, 289–305. doi: 10.1002/lno.11605

Chikaraishi, Y., Kashiyama, Y., Ogawa, N. O., Kitazato, H., and Ohkouchi, N. (2007). Metabolic control of nitrogen isotope composition of amino acids in macroalgae and gastropods: Implications for aquatic food web studies. *Mar. Ecol. Progr. Ser.* 342, 85–90. doi: 10.3354/meps342085

Chikaraishi, Y., Ogawa, N. O., Kashiyama, Y., Takano, Y., Suga, H., Tomitani, A., et al. (2009). Determination of aquatic food-web structure based on compound-specific nitrogen isotopic composition of amino acids. *Limnol. Oceanogr. Methods* 7, 740–750. doi: 10.4319/lom.2009.7.740

Christianen, M. J. A., Holthuijsen, S. J., van der Zee, E. M., van der Eijk, A., Govers, L. L., van der Heide, T., et al. (2015). . *Ecotopen- en Kansrijkdomkaart van de Nederlandse Waddenzee. Rapportnummer 2015.04.01, Waddenfondsproject Waddensleutels.*

Christianen, M. J. A., Middelburg, J. J., Holthuijsen, S. J., Jouta, J., Compton, T. J., van der Heide, T., et al. (2017). Benthic primary producers are key to sustain the Wadden Sea food web: Stable carbon isotope analysis at landscape scale. *Ecology* 98, 1498–1512. doi: 10.1002/ecy.1837

Chua, E. J., Huettel, M., Fennel, K., and Fulweiler, R. W. (2022). A case for addressing the unresolved role of permeable shelf sediments in ocean denitrification. *Limnol. Oceanogr. Lett.* 7, 11–25. doi: 10.1002/lol2.10218

Compton, T. J., Holthuijsen, S., Koolhaas, A., Dekinga, A., ten Horn, J., Smith, J., et al. (2013). Distinctly variable mudscapes: Distribution gradients of intertidal macrofauna across the dutch wadden sea. *J. Sea Res.* 82, 103–116. doi: 10.1016/j.seares.2013.02.002

Cook, P. L. M., Veuger, B., Boer, S., and Middelburg, J. J. (2007). Effect of nutrient availability on carbon and nitrogen and flows through benthic algae and bacteria in near-shore sandy sediment. *Aquatic Microb. Ecol.* 49, 165–180. doi: 10.3354/ame01142

Cordone, G., Salinas, V., Marina, T. I., Doyle, S. R., Pasotti, F., Saravia, L. A., et al. (2020). Green vs brown food web: Effects of habitat type on multidimensional stability proxies for a highly-resolved antarctic food web. *Food Webs* 25:e00166. doi: 10.1016/j.fooweb.2020.e00166

Cresson, P., Chouvelon, T., Bustamante, P., Bănaru, D., Baudrier, J., Le Loc'h, F., et al. (2020). Primary production and depth drive different trophic structure and functioning of fish assemblages in French marine ecosystems. *Progr. Oceanogr.* 186:102343. doi: 10.1016/j.pocean.2020.102343

Durante, L., Wing, S., Ingram, T., Sabadel, A., and Shima, J. (2022). Changes in trophic structure of an exploited fish community at the centennial scale are linked to fisheries and climate forces. *Sci. Rep.* 12, 1–12. doi: 10.1038/s41598-022-08391-x

Eaton, J. W., and Moss, B. (1966). The estimation of numbers and pigment content in epipelic algal populations. *Limnol. Oceanogr.* 11, 584–595. doi: 10.4319/lo.1966.11.4.0584

Eriksson, B. K., van der Heide, T., van de Koppel, J., Piersma, T., van der Veer, H. W., and Olff, H. (2010). Major changes in the ecology of the wadden sea: Human impacts, ecosystem engineering and sediment dynamics. *Ecosystems* 13, 752–764. doi: 10.1007/s10021-010-9352-3

Evans-White, M. A., and Halvorson, H. M. (2017). Comparing the ecological stoichiometry in green and brown food webs – a review and meta-analysis of freshwater food webs. *Front. Microbiol.* 8:1184. doi: 10.3389/fmicb.2017.01184

Evrard, V., Soetaert, K., Heip, C. H., Huettel, M., Xenopoulos, M. A., and Middelburg, J. J. (2010). Carbon and nitrogen flows through the benthic food web of a photic subtidal sandy sediment. *Mar. Ecol. Progr. Ser.* 416, 1–16. doi: 10.3354/meps08770

Fenchel, T. (2008). The microbial loop–25 years later. *J. Exp. Mar. Biol. Ecol.* 366, 99–103. doi: 10.1016/j.jembe.2008.07.013

Fernandes, R., Millard, A. R., Brabec, M., Nadeau, M.-J., and Grootes, P. (2014). Food reconstruction using isotopic transferred signals (fruits): A bayesian model for diet reconstruction. *PLoS One* 9:e87436. doi: 10.1371/journal.pone.0087436

Folmer, E. O., van Beusekom, J. E. E., Dolch, T., Gräwe, U., van Katwijk, M. M., Kolbe, K., et al. (2016). Consensus forecasting of intertidal seagrass habitat in the Wadden Sea. *J. Appl. Ecol.* 53, 1800–1813. doi: 10.1111/1365-2664.12681

Froese, R., and Pauly, D. (2000). *Fishbase 2000: Concepts designs and data sources. Fishbase 2000: Concepts Designs and Data Sources*. Penang: WorldFish.

Fry, B. (1984). $^{13}C/^{12}C$ ratios and the trophic importance of algae in Florida Syringodium filiforme seagrass meadows. *Mar. Biol.* 79, 11–19. doi: 10.1007/BF00404980

Fry, B. (1988). Food web structure on georges bank from stable C, N, and S isotopic compositions. *Limnol. Oceanogr.* 33, 1182–1190. doi: 10.4319/lo.1988.33.5.1182

Goto, N., Kawamura, T., Mitamura, O., and Terai, H. (1999). Importance of extracellular organic carbon production in the total primary production by tidal-flat diatoms in comparison to phytoplankton. *Mar. Ecol. Progr. Ser.* 190, 289–295. doi: 10.3354/meps190289

Hebert, C. E., Popp, B. N., Fernie, K. J., Ka'apu-Lyons, C., Rattner, B. A., and Wallsgrove, N. (2016). Amino acid specific stable nitrogen isotope values in avian tissues: Insights from captive american kestrels and wild herring gulls. *Environ. Sci. Technol.* 50, 12928–12937. doi: 10.1021/acs.est.6b04407

Jung, A. S., van der Veer, H. W., van der Meer, M. T. J., and Philippart, C. J. M. (2019). Seasonal variation in the diet of estuarine bivalves. *PLoS One* 14:e0217003. doi: 10.1371/journal.pone.0217003

Kahma, T. I., Karlson, A. M., Sun, X., Mörth, C. M., Humborg, C., Norkko, A., et al. (2020). Macroalgae fuels coastal soft-sediment macrofauna: A triple-isotope approach across spatial scales. *Mar. Environ. Res.* 162:105163. doi: 10.1016/j.marenvres.2020.105163

Kato, Y., Togashi, H., Kurita, Y., Osada, Y., Amano, Y., Yoshimizu, C., et al. (2021). Segmental isotope analysis of the vertebral centrum reveals the spatiotemporal population structure of adult japanese flounder *Paralichthys olivaceus* in sendai bay, japan. *Mar. Biol.* 168:57. doi: 10.1007/s00227-021-03868-1

Krumins, J. A., van Oevelen, D., Bezemer, T. M., De Deyn, G. B., Hol, W. G., Van Donk, E., et al. (2013). Soil and freshwater and marine sediment food webs: Their structure and function. *Bioscience* 63, 35–42. doi: 10.1525/bio.2013.63.1.8

Le-Alvarado, M., Romo-Curiel, A. E., Sosa-Nishizaki, O., Hernández-Sánchez, O., Barbero, L., and Herzka, S. Z. (2021). Yellowfin tuna (*Thunnus albacares*) foraging habitat and trophic position in the gulf of mexico based on intrinsic isotope tracers. *PLoS One* 16:e0246082. doi: 10.1371/journal.pone.0246082

Lemons, G. E., Lewison, R. L., Seminoff, J. A., Coppenrath, C. M., and Popp, B. N. (2020). Nitrogen isotope fractionation of amino acids from a controlled study on the green turtle (*Chelonia mydas*): Expanding beyond glx/phe for trophic position. *Mar. Biol.* 167, 1–13. doi: 10.1007/s00227-020-03745-3

Marchant, H. K., Ahmerkamp, S., Lavik, G., Tegetmeyer, H. E., Graf, J., Klatt, J. M., et al. (2017). Denitrifying community in coastal sediments performs aerobic and anaerobic respiration simultaneously. *ISME J.* 11, 1799–1812. doi: 10.1038/ismej.2017.51

Marchant, H. K., Holtappels, M., Lavik, G., Ahmerkamp, S., Winter, C., and Kuypers, M. M. M. (2016). Coupled nitrification–denitrification leads to extensive N loss in subtidal permeable sediments. *Limnol. Oceanogr.* 61, 1033–1048. doi: 10.1002/lno.10271

Marchant, H. K., Tegetmeyer, H. E., Ahmerkamp, S., Holtappels, M., Lavik, G., Graf, J., et al. (2018). Metabolic specialization of denitrifiers in permeable sediments controls N^2O emissions. *Environ. Microbiol.* 20, 4486–4502. doi: 10.1111/1462-2920.14385

McCormack, S. A., Trebilco, R., Melbourne-Thomas, J., Blanchard, J., Fulton, E., and Constable, A. (2019). Using stable isotope data to advance marine food web modelling. *Rev. Fish Biol. Fish.* 29, 277–296. doi: 10.1007/s11160-019-09552-4

McCutchan, J. H., Lewis, W. M. Jr., Kendall, C., and McGrath, C. C. (2003). Variation in trophic shift for stable isotope ratios of carbon, nitrogen, and sulfur. *Oikos* 102, 378–390. doi: 10.1034/j.1600-0706.2003.12098.x

McMahon, K. W., and McCarthy, M. D. (2016). Embracing variability in amino acid $\delta^{15}N$ fractionation: Mechanisms, implications, and applications for trophic ecology. *Ecosphere* 7:e01511. doi: 10.1002/ecs2.1511

McMahon, K. W., Polito, M. J., Abel, S., McCarthy, M. D., and Thorrold, S. R. (2015a). Carbon and nitrogen isotope fractionation of amino acids in an avian marine predator, the gentoo penguin (pygoscelis papua). *Ecol. Evol.* 5, 1278–1290. doi: 10.1002/ece3.1437

McMahon, K. W., Thorrold, S. R., Elsdon, T. S., and McCarthy, M. D. (2015b). Trophic discrimination of nitrogen stable isotopes in amino acids varies with diet quality in a marine fish. *Limnol. Oceanogr.* 60, 1076–1087. doi: 10.1002/lno.10081

Middelburg, J. J. (2014). Stable isotopes dissect aquatic food webs from the top to the bottom. *Biogeosciences* 11, 2357–2371. doi: 10.5194/bg-11-2357-2014

Middelburg, J. J., and Herman, P. M. J. (2007). Organic matter processing in tidal estuaries. *Mar. Chem.* 106, 127–147. doi: 10.1016/j.marchem.2006.02.007

Middelburg, J. J., Barranguet, C., Boschker, H. T., Herman, P. M., Moens, T., and Heip, C. H. (2000). The fate of intertidal microphytobenthos carbon: An *in situ* ^{13}C-labeling study. *Limnol. Oceanogr.* 45, 1224–1234. doi: 10.4319/lo.2000.45.6.1224

Miller, D. C., Geider, R. J., and MacIntyre, H. L. (1996). Microphytobenthos: The ecological role of the "secret garden" of unvegetated, shallow-water marine habitats. Ii. Role in sediment stability and shallow-water food webs. *Estuaries* 19, 202–212. doi: 10.2307/1352225

Minagawa, M., and Wada, E. (1984). Stepwise enrichment of ^{15}N along food chains: Further evidence and the relation between $\delta^{15}N$ and animal age. *Geochim. Cosmochim. Acta* 48, 1135–1140. doi: 10.1016/0016-7037(84)90204-7

Nuche-Pascual, M. T., Ruiz-Cooley, R. I., and Herzka, S. Z. (2021). A meta-analysis of amino acid $\delta^{15}N$ trophic enrichment factors in fishes relative to nutritional and ecological drivers. *Ecosphere* 12:e03570. doi: 10.1002/ecs2.3570

O'Connell, T. C. (2017). 'Trophic' and 'source' amino acids in trophic estimation: A likely metabolic explanation. *Oecologia* 184, 317–326. doi: 10.1007/s00442-017-3881-9

Oakes, J. M., Eyre, B. D., and Middelburg, J. J. (2012). Transformation and fate of microphytobentos carbon in subtropical shallow subtidal sands: A ^{13}C-labeling study. *Limnol. Oceanogr.* 57, 1846–1856. doi: 10.4319/lo.2012.57.6.1846

Odum, E. P. (1969). The strategy of ecosystem development: An understanding of ecological succession provides a basis for resolving man's conflict with nature. *Science* 164, 262–270. doi: 10.1126/science.164.3877.262

Otto, L., Zimmerman, J., Furnes, G., Mork, M., Saetre, R., and Becker, G. (1990). Review of the physical oceanography of the north sea. *Netherlands J. Sea Res.* 26, 161–238. doi: 10.1016/0077-7579(90)90091-T

Philippart, C. J., Beukema, J. J., Cadée, G. C., Dekker, R., Goedhart, P. W., van Iperen, J. M., et al. (2007). Impacts of nutrient reduction on coastal communities. *Ecosystems* 10, 96–119. doi: 10.1007/s10021-006-9006-7

Post, D. M. (2002). Using stable isotopes to estimate trophic position: Models, methods, and assumptions. *Ecology* 83, 703–718. doi: 10.1890/0012-9658(2002)083[0703:USITET]2.0.CO;2

Postma, H. (1996). "Sea-level rise and the stability of barrier islands, with special reference to the wadden sea," in *Sea-Level Rise and Coastal Subsidence*, eds J.D. Milliman and B.U. Haq (Berlin: Springer). doi: 10.1007/978-94-015-8719-8_15

Potapov, A. M., Brose, U., Scheu, S., and Tiunov, A. V. (2019). Trophic position of consumers and size structure of food webs across aquatic and terrestrial ecosystems. *Am. Nat.* 194, 823–839. doi: 10.1086/705811

Reise, K., Baptist, M., Burbridge, P., Dankers, N., Fischer, L., Flemming, B., et al. (2010). "The wadden sea-a universally outstanding tidal wetland," in *The Wadden Sea 2010 Common Wadden Sea Secretariat (cwss)*, eds H. Marencic and J. de vlas (Wilhelmshaven: Trilateral Monitoring and Assessment Group).

Riekenberg, P. M., Oakes, J. M., and Eyre, B. D. (2020a). A shift in the pool of retained microphytobenthos nitrogen under enhanced nutrient availability. *Water Res.* 187:116438. doi: 10.1016/j.watres.2020.116438

Riekenberg, P. M., van der Meer, M., and Schouten, S. (2020b). Practical considerations for improved reliability and precision during determination of $\delta^{15}N$ values in amino acids using a single combined oxidation-reduction reactor. *Rapid Commun. Mass Spectr.* 34:e8797. doi: 10.1002/rcm.8797

Ruiz-Cooley, R. I., Gerrodette, T., Chivers, S. J., and Danil, K. (2021). Cooperative feeding in common dolphins as suggested by ontogenetic patterns in $\delta^{15}N$ bulk and amino acids. *J. Anim. Ecol.* 90, 1583–1595. doi: 10.1111/1365-2656.13478

Saburova, M. A., and Polikarpov, I. G. (2003). Diatom activity within soft sediments: Behavioural and physiological processes. *Mar. Ecol. Progr. Ser.* 251, 115–126. doi: 10.3354/meps251115

Santos, I. R., Beck, M., Brumsack, H.-J., Maher, D. T., Dittmar, T., Waska, H., et al. (2015). Porewater exchange as a driver of carbon dynamics across a terrestrial-marine transect: Insights from coupled ^{222}Rn and pCO^2 observations in the german wadden sea. *Mar. Chem.* 171, 10–20. doi: 10.1016/j.marchem.2015.02.005

Schlitzer, R. (2022). *Ocean Data View*. Available online at: https://odv.Awi.De (accessed November 15, 2021).

Scholz, B., and Liebezeit, G. (2012). Microphytobenthic dynamics in a wadden sea intertidal flat – part i: Seasonal and spatial variation of diatom communities

in relation to macronutrient supply. *Eur. J. Phycol.* 47, 105–119. doi: 10.1080/09670262.2012.663793

Stal, L. J. (2010). Microphytobenthos as a biogeomorphological force in intertidal sediment stabilization. *Ecol. Eng.* 36, 236–245. doi: 10.1016/j.ecoleng.2008.12.032

Stock, B. C., Jackson, A. L., Ward, E. J., Parnell, A. C., Phillips, D. L., and Semmens, B. X. (2018). Analyzing mixing systems using a new generation of bayesian tracer mixing models. *PeerJ* 6:e5096. doi: 10.7717/peerj.5096

Sturbois, A., Riera, P., Desroy, N., Brébant, T., Carpentier, A., Ponsero, A., et al. (2022). Spatio-temporal patterns in stable isotope composition of a benthic intertidal food web reveal limited influence from salt marsh vegetation and green tide. *Mar. Environ. Res.* 175:105572.

Svensson, E., Schouten, S., Hopmans, E. C., Middelburg, J. J., and Sinninghe Damsté, J. S. (2016). Factors controlling the stable nitrogen isotopic composition (δ^{15}N) of lipids in marine animals. *PLoS One* 11:e0146321. doi: 10.1371/journal.pone.0146321

Taylor, J. D., McKew, B. A., Kuhl, A., McGenity, T. J., and Underwood, G. J. C. (2013). Microphytobenthic extracellular polymeric substances (EPS) in intertidal sediments fuel both generalist and specialist EPS-degrading bacteria. *Limnol. Oceanogr.* 58, 1463–1480. doi: 10.4319/lo.2013.58.4.1463

Then, A. Y., Adame, M. F., Fry, B., Chong, V. C., Riekenberg, P. M. R., Mohammad Zakaria, R., et al. (2021). Stable isotopes clearly track mangrove inputs and food web changes along a reforestation gradient. *Ecosystems* 24, 939–954. doi: 10.1007/s10021-020-00561-0

Van Roomen, M., Van Turnhout, C., Van Winden, E., Koks, B., Goedhart, P., Leopold, M., et al. (2005). Trends in benthivorous waterbirds in the dutch wadden sea 1975–2002: Large differences between shellfish-eaters and worm-eaters. *Limosa* 78, 21–38.

Vokhshoori, N. L., and McCarthy, M. D. (2014). Compound-specific δ15N amino acid measurements in littoral mussels in the California upwelling ecosystem: A new approach to generating baseline δ^{15}N Isoscapes for coastal ecosystems. *PLoS One* 9:e98087. doi: 10.1371/journal.pone.0098087

Vokhshoori, N. L., McCarthy, M. D., Close, H. G., Demopoulos, A. W. J., and Prouty, N. G. (2021). New geochemical tools for investigating resource and energy functions at deep-sea cold seeps using amino acid δ^{15}N in chemosymbiotic mussels (bathymodiolus childressi). *Geobiology* 19, 601–617. doi: 10.1111/gbi.12458

Vokhshoori, N. L., McCarthy, M. D., Collins, P. W., Etnier, M. A., Rick, T., Eda, M., et al. (2019). Broader foraging range of ancient short-tailed albatross populations into california coastal waters based on bulk tissue and amino acid isotope analysis. *Mar. Ecol. Progr. Ser.* 610, 1–13.

doi: 10.3354/meps12839

Whiteman, J. P., Kim, S. L., McMahon, K. W., Koch, P. L., and Newsome, S. D. (2018). Amino acid isotope discrimination factors for a carnivore: Physiological insights from leopard sharks and their diet. *Oecologia* 188, 977–989. doi: 10.1007/s00442-018-4276-2

Wolff, W. J. (2013). Ecology of the wadden sea: Research in the past and challenges for the future. *J. Sea Res.* 82, 3–9. doi: 10.1016/j.seares.2013.03.006

Xing, D., Choi, B., Takizawa, Y., Fan, R., Sugaya, S., Tsuchiya, M., et al. (2020). Trophic hierarchy of coastal marine fish communities viewed *via* compound-specific isotope analysis of amino acids. *Mar. Ecol. Progr. Ser.* 652, 137–144. doi: 10.3354/meps13475

frontiers | Frontiers in Ecology and Evolution

TYPE Original Research
PUBLISHED 24 November 2022
DOI 10.3389/fevo.2022.958032

Check for updates

OPEN ACCESS

EDITED BY
Rona A. R. McGill,
University of Glasgow, United Kingdom

REVIEWED BY
Vincent Balter,
Centre National de la Recherche Scientifique (CNRS), France
Joshua Robinson,
Boston University, United States
Laszlo Kocsis,
Université de Lausanne, Switzerland

*CORRESPONDENCE
Tina Lüdecke
tina.luedecke@mpic.de
Jennifer N. Leichliter
jennifer.leichliter@mpic.de

†These authors have contributed equally to this work and share first authorship

‡These authors share senior authorship

SPECIALTY SECTION
This article was submitted to Population, Community, and Ecosystem Dynamics, a section of the journal Frontiers in Ecology and Evolution

RECEIVED 31 May 2022
ACCEPTED 27 October 2022
PUBLISHED 24 November 2022

CITATION
Lüdecke T, Leichliter JN, Aldeias V, Bamford MK, Biro D, Braun DR, Capelli C, Cybulski JD, Duprey NN, Ferreira da Silva MJ, Foreman AD, Habermann JM, Haug GH, Martínez FI, Mathe J, Mulch A, Sigman DM, Vonhof H, Bobe R, Carvalho S and Martínez-García A (2022) Carbon, nitrogen, and oxygen stable isotopes in modern tooth enamel: A case study from Gorongosa National Park, central Mozambique. *Front. Ecol. Evol.* 10:958032. doi: 10.3389/fevo.2022.958032

Carbon, nitrogen, and oxygen stable isotopes in modern tooth enamel: A case study from Gorongosa National Park, central Mozambique

Tina Lüdecke[1,2,3,4*†], Jennifer N. Leichliter[1,2,5*†], Vera Aldeias[6], Marion K. Bamford[7], Dora Biro[8,9], David R. Braun[3,10,11], Cristian Capelli[8,12], Jonathan D. Cybulski[1,13,14], Nicolas N. Duprey[1], Maria J. Ferreira da Silva[15,16,17], Alan D. Foreman[1], Jörg M. Habermann[18], Gerald H. Haug[3,19], Felipe I. Martínez[20], Jacinto Mathe[3,21], Andreas Mulch[4,22], Daniel M. Sigman[23], Hubert Vonhof[24], René Bobe[3,6,21], Susana Carvalho[3,6,21,25‡] and Alfredo Martínez-García[1‡]

[1]Organic Isotope Geochemistry Group, Max Planck Institute for Chemistry, Mainz, Germany, [2]Emmy Noether Group for Hominin Meat Consumption, Max Planck Institute for Chemistry, Mainz, Germany, [3]Primate Models for Behavioural Evolution, Institute of Human Sciences, University of Oxford, Oxford, United Kingdom, [4]Senckenberg Biodiversity and Climate Research Centre, Frankfurt, Germany, [5]Institute of Geosciences, Johannes Gutenberg University, Mainz, Germany, [6]Interdisciplinary Center for Archaeology and Evolution of Human Behaviour, Universidade do Algarve, Faro, Portugal, [7]Evolutionary Studies Institute, University of the Witwatersrand, Johannesburg, South Africa, [8]Department of Zoology, University of Oxford, Oxford, United Kingdom, [9]Department of Brain and Cognitive Sciences, University of Rochester, Rochester, NY, United States, [10]Technological Primates Group, Max Planck Institute for Evolutionary Anthropology, Leipzig, Germany, [11]Center for the Advanced Study of Human Paleobiology, George Washington University, Washington, DC, United States, [12]Department of Chemistry, Life Sciences and Environmental Sustainability, University of Parma, Parma, Italy, [13]Smithsonian Tropical Research Institute, Balboa, Panama, [14]Graduate School of Oceanography, University of Rhode Island, Narragansett, RI, United States, [15]Centro de Investigação em Biodiversidade e Recursos Genéticos, InBIO Laboratório Associado, Universidade do Porto, Vairão, Portugal, [16]BIOPOLIS Program in Genomics, Biodiversity and Land Planning, Centro de Investigação em Biodiversidade e Recursos Genéticos, Vairão, Portugal, [17]Organisms and Environment Division, School of Biosciences, Cardiff University, Cardiff, United Kingdom, [18]GeoZentrum Nordbayern, Friedrich-Alexander-Universität Erlangen-Nürnberg, Erlangen, Germany, [19]Department of Climate Geochemistry, Max Planck Institute for Chemistry, Mainz, Germany, [20]Escuela de Antropología, Facultad de Ciencias Sociales, Pontificia Universidad Católica de Chile, Santiago, Chile, [21]Gorongosa National Park, Sofala, Mozambique, [22]Institute of Geosciences, Goethe University Frankfurt, Frankfurt, Germany, [23]Department of Geosciences, Princeton University, Princeton, NJ, United States, [24]Inorganic Gas Isotope Geochemistry Group, Max Planck Institute for Chemistry, Mainz, Germany, [25]Centre for Functional Ecology, University of Coimbra, Coimbra, Portugal

The analyses of the stable isotope ratios of carbon ($\delta^{13}C$), nitrogen ($\delta^{15}N$), and oxygen ($\delta^{18}O$) in animal tissues are powerful tools for reconstructing the feeding behavior of individual animals and characterizing trophic interactions in food webs. Of these biomaterials, tooth enamel is the hardest, most mineralized vertebrate tissue and therefore least likely to be affected by chemical alteration (i.e., its isotopic composition can be preserved over millions of years), making it an important and widely available archive

for biologists and paleontologists. Here, we present the first combined measurements of $\delta^{13}C$, $\delta^{15}N$, and $\delta^{18}O$ in enamel from the teeth of modern fauna (herbivores, carnivores, and omnivores) from the well-studied ecosystem of Gorongosa National Park (GNP) in central Mozambique. We use two novel methods to produce high-precision stable isotope enamel data: (i) the *"oxidation-denitrification method,"* which permits the measurement of mineral-bound organic nitrogen in tooth enamel ($\delta^{15}N_{enamel}$), which until now, has not been possible due to enamel's low organic content, and (ii) the *"cold trap method,"* which greatly reduces the sample size required for traditional measurements of inorganic $\delta^{13}C_{enamel}$ and $\delta^{18}O_{enamel}$ (from $\geq$0.5 to $\leq$0.1 mg), permitting analysis of small or valuable teeth and high-resolution serial sampling of enamel. The stable isotope results for GNP fauna reveal important ecological information about the trophic level, dietary niche, and resource consumption. $\delta^{15}N_{enamel}$ values clearly differentiate trophic level (i.e., carnivore $\delta^{15}N_{enamel}$ values are 4.0‰ higher, on average, than herbivores), $\delta^{13}C_{enamel}$ values distinguish C_3 and/or C_4 biomass consumption, and $\delta^{18}O_{enamel}$ values reflect local meteoric water ($\delta^{18}O_{water}$) in the park. Analysis of combined carbon, nitrogen, and oxygen stable isotope data permits geochemical separation of grazers, browsers, omnivores, and carnivores according to their isotopic niche, while mixed-feeding herbivores cannot be clearly distinguished from other dietary groups. These results confirm that combined C, N, and O isotope analyses of a single aliquot of tooth enamel can be used to reconstruct diet and trophic niches. Given its resistance to chemical alteration, the analysis of these three isotopes in tooth enamel has a high potential to open new avenues of research in (paleo)ecology and paleontology.

KEYWORDS

diet, ecology, trophic level reconstruction, food webs, vertebrate, savanna

Introduction

In modern ecosystems, stable isotope geochemistry can complement traditional ecological approaches (e.g., field observations and behavioral studies) and help researchers to better understand the dietary niche and habitat use of animals in the wild. The stable carbon ($\delta^{13}C$), nitrogen ($\delta^{15}N$), and oxygen ($\delta^{18}O$) isotope compositions of body tissues can provide information about an individual's metabolism and feeding behavior, trophic interactions, and even record aspects of the (paleo)environment such as aridity, seasonality, and vegetation composition (e.g., DeNiro and Epstein, 1981; Ambrose, 1986; Cerling et al., 1997; Bocherens and Drucker, 2003; Kingston and Harrison, 2007; Segalen et al., 2007; Bocherens, 2009; Lüdecke et al., 2016, 2018).

In modern fauna, isotopic measurements are routinely conducted on a variety of biological materials such as collagen (from bone or dentin), soft tissues (e.g., muscle), and body fluids (e.g., blood and urea). Paleontologists have long sought a reliably preserved tissue (i.e., without diagenetic alteration) in which to measure isotope ratios of all three elements—carbon, nitrogen, and oxygen—in deep time contexts. Tooth enamel, as the densest and most mineralized vertebrate tissue, has great potential in this respect (Leichliter et al., 2022). Hydroxyapatite content is about 95% wt. in mature enamel (Sakae et al., 1997; Passey and Cerling, 2002; Lacruz et al., 2017; Gil-Bona and Bidlack, 2020), which makes it more resistant to diagenetic alteration during fossilization than more porous and poorly mineralized tissues such as bone or dentin (mineralization ca. 70% wt.; Goldberg et al., 2011).

As such, the inorganic mineral phase of tooth enamel has long been the focus of carbon ($\delta^{13}C_{enamel}$) and oxygen ($\delta^{18}O_{enamel}$) stable isotope analyses for the reconstruction of the diet of extinct and extant species (Ambrose and Norr, 1993).

Typically, 500–1,000 μg of tooth enamel, which contains less than 5% structural carbonate, is needed for precise $\delta^{13}C_{enamel}$ and $\delta^{18}O_{enamel}$ analysis with traditional continuous-flow isotope ratio mass spectrometry. The "*cold trap method*" presented in

this study permits high-precision $\delta^{13}C_{enamel}$ and $\delta^{18}O_{enamel}$ analysis of as little as 50 μg tooth enamel. The method employs a cryofocusing step during which the sample gas is collected in a liquid N_2 trap (Vonhof et al., 2020a,b). This results in >80% reduction in the sample size typically required for conventional analyses (refer to e.g., Merceron et al., 2021; Jaouen et al., 2022).

Recently, Leichliter et al. (2021) showed that $\delta^{15}N_{enamel}$ records the nitrogen isotopic composition of an animal's diet under controlled conditions in a feeding experiment with rodents. The significant advantage of measuring $\delta^{15}N$ in tooth enamel ($\delta^{15}N_{enamel}$) instead of (bone/dentin) collagen is that enamel is more resistant to digenesis (Lee-Thorp and Van der Merwe, 1987; Wang and Cerling, 1994; Koch et al., 1997; Koch, 2007). The dense mineralization of enamel thus has a high potential to protect inorganic components from isotopic alteration during fossilization (Leichliter et al., 2022). In fact, the tooth enamel biomineral matrix appears to act as a closed system during oxidative attack, dissolution, and thermal alteration, leaving the $\delta^{15}N_{enamel}$ value of a fossil unchanged (Martinez-Garcia et al., 2022), demonstrating the potential utility of $\delta^{15}N_{enamel}$ as a new trophic proxy in paleoecological studies. However, high-precision analysis of $\delta^{15}N_{enamel}$ in tooth enamel-bound nitrogen has been hampered by its low nitrogen content (about 0.5–2.5 g N/100 g in mature mammalian enamel; Teruel et al., 2015). To fill this gap in our isotopic toolbox, we recently developed a method to determine the nitrogen isotopic composition of the organic matter preserved in tooth enamel (Leichliter et al., 2021). This method, adapted from studies of marine microfossils (i.e., diatoms and foraminifera; Sigman et al., 2001; Robinson et al., 2004; Ren et al., 2009) and macrofossils (Wang et al., 2014, 2015, 2017; Lueders-Dumont et al., 2018; Kast et al., 2022), involves the oxidation of nitrogen in enamel-bound organic matter to nitrate, followed by bacterial conversion of nitrate to N_2O. This "*oxidation-denitrification method*" requires 5 nmol of N (i.e., 5 mg of enamel; Leichliter et al., 2021), which reflects ca. 1% of the material needed for conventional combustion measurements and ca. half the material used for nano-elemental analyzer measurements (e.g., Polissar et al., 2009; Fulton et al., 2018). Importantly, the "*oxidation-denitrification method*" drastically improves analytical precision from ∼1.0‰ 1σ standard deviation for nano-EA measurements at 8 nmol of N (Fulton et al., 2018) to <0.2‰ at 5 nmol of N. This precision is more than sufficient to resolve the 3–5‰ trophic level enrichment in $\delta^{15}N$ observed in large-scale ecological studies (Schoeninger and DeNiro, 1984; Bocherens and Drucker, 2003; Caut et al., 2009).

Here, we present the first combined $\delta^{13}C_{enamel}$, $\delta^{15}N_{enamel}$, and $\delta^{18}O_{enamel}$ isotope data measured in the same aliquot of tooth enamel. We analyzed the tooth enamel of modern mammalian fauna (17 taxa; bovids, equids, suids, elephants, hippos, primates, felids) and one reptile (crocodiles) from Gorongosa National Park (GNP), a well-studied ecosystem in central Mozambique (refer to e.g., Wilson, 2014; Correia et al., 2017; Atkins et al., 2019; Martinez et al., 2019; Pansu et al., 2019; Stalmans et al., 2019; Bobe et al., 2020; Guyton et al., 2020). In addition, we analyzed $\delta^{18}O_{water}$ of (permanent and ephemeral) lakes, ponds, streams, floodplains, rain-, and groundwater to evaluate isotope patterns of available drinking water, which are the main determinants of $\delta^{18}O_{enamel}$ in large mammals (Kohn and Cerling, 2002). With this dataset, we test two novel methods, as well as gain new insight into wild animal foraging behavior and the food web dynamics of GNP.

Tooth enamel as dietary proxy material

Dental material chronologically records the diet of an individual during a distinct time period in their life. During enamel maturation, the organic matrix is removed and replaced with inorganic minerals over a period of weeks, months, or years, depending on taxon, rate of wear, and tooth size (Ungar, 2010). Once mature enamel has fully mineralized, it has no regenerative capacity, and thus preserves an animal's isotopic composition during the time of tooth formation. This differentiates enamel from other tissues (e.g., soft tissues, but also bone or dentin) that undergo continuous remodeling (e.g., Balasse et al., 1999; Kohn and Cerling, 2002; Passey and Cerling, 2002; Zazzo et al., 2005; Abou Neel et al., 2016; Yang et al., 2020). Tooth enamel is, therefore, one of the only archives in the vertebrate body that records dietary information from early life stages (i.e., infant to young-adult) and that is also preserved in the fossil record. To reconstruct the adult diet and avoid the isotopic effect of breast milk consumption (Fuller et al., 2006; Tsutaya and Yoneda, 2015; Dailey-Chwalibóg et al., 2020; Chinique de Armas et al., 2022), we targeted the latest-forming permanent tooth (i.e., usually M3) in each specimen (for details refer to **Supplementary Data Sheet 1** and **Supplementary Table 1**).

For this study, we sampled bulk enamel, meaning that the resulting isotope data are time-averaged and record several months or even years depending on tooth mineralization rate (which can vary between taxa), as well as sampling strategy.

Isotope ratios for tooth enamel are reported using per mil (‰) notation relative to VPDB (Vienna Pee Dee Belemnite) for carbon, AIR for nitrogen, or VSMOW (Vienna Standard Mean Ocean Water) for oxygen, where ^{a}X is the heavier and ^{b}X is the lighter isotope ($^{13}C/^{12}C$, $^{15}N/^{14}N$, or $^{18}O/^{16}O$) for $\delta^{13}C_{enamel}$, $\delta^{15}N_{enamel}$, $\delta^{18}O_{enamel}$, and $\delta^{18}O_{water}$, respectively:

$$\delta^{a/b}X = \frac{(^{a}X/^{b}X)_{sample}}{(^{a}X/^{b}X)_{standard}} - 1$$

$\delta^{18}O_{enamel}$ values were converted from VPDB into VSMOW after Coplen (1988).

Nitrogen isotopes in tooth enamel

All living organisms require nitrogen as a major nutrient, which animals acquire from the food they consume (Ambrose and Norr, 1993). Due to isotopic fractionation during metabolism and subsequent excretion of waste, a consumer's $^{15}N/^{14}N$ ratio is elevated compared to their diet. As a result, animals typically have $\delta^{15}N$ tissue values that are ca. 3–5‰ higher than the foods they consume (**Figure 1**; Schoeninger and DeNiro, 1984; Bocherens and Drucker, 2003; Fox-Dobbs et al., 2007; Krajcarz et al., 2018; Leichliter et al., 2021).

The living part of any terrestrial food web starts with plants (which in turn use energy from the sun). Most plants obtain nitrogen from the soil, and soil $\delta^{15}N$ systematically decreases with increasing mean annual precipitation and decreasing mean annual temperature (Evans, 2001; Robinson, 2001; Amundson et al., 2003). Soil $\delta^{15}N$ has an effect on the $\delta^{15}N$ values of plants (Codron et al., 2005) which in turn determines the $\delta^{15}N$ tissue values of primary and secondary consumers. Thus, climate influences the nitrogen isotope composition of animals living in a given ecosystem, which can vary across space and time (Ambrose, 1986, 1991; Ambrose and DeNiro, 1986). To avoid the confounding effects of regional baseline variability in nitrogen, we focus on the vertebrate community living in GNP. Our aim is to characterize the $\delta^{15}N_{enamel}$ values of herbivores (i.e., grazers, mixed-feeders, and browsers), omnivores, and carnivores living within this single and well-constrained ecosystem (**Figure 2**).

In addition to climate and habitat-driven baseline variation, digestive physiology and water dependence have also been proposed to affect the $\delta^{15}N$ of animals' tissues (Sealy et al., 1987; Ambrose, 1991; Hartman, 2010). For instance, studies suggest that the $\delta^{15}N$ values of ruminant herbivores differ from non-ruminants as the result of the incorporation of ^{15}N-enriched microbes community in their hindgut (Steinhour et al., 1982; Sutoh et al., 1987). Additionally, herbivore species with physiological adaptations for water conservation, such as the excretion of concentrated urine, are proposed to have higher $\delta^{15}N$ values than water-dependent animals (Ambrose, 1991 and references therein). However, the effects of digestive physiology and water dependence are still poorly understood and not well-tested (Ambrose, 1991; Cantalapiedra-Hijar et al., 2015). In this study, herbivorous ruminants and non-ruminants, as well as obligate drinkers and non-obligate drinkers were analyzed to evaluate these hypotheses.

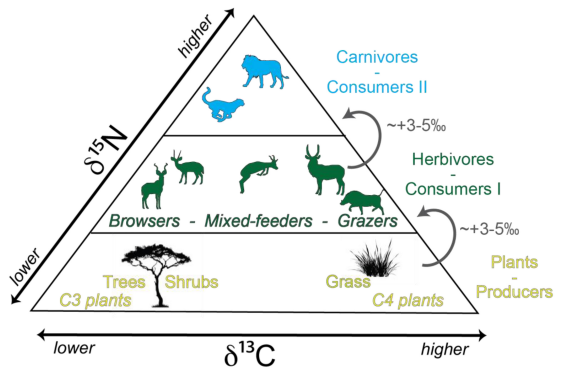

FIGURE 1
Simplified summary of variations in $\delta^{13}C$ and $\delta^{15}N$ values in an African terrestrial food web. Modified after Bocherens (2009).

Carbon isotopes in tooth enamel

In contrast to $\delta^{15}N$, $\delta^{13}C$ of animal tissues increases only slightly with each step in the food chain (ca. 1‰ per trophic level; DeNiro and Epstein, 1981; Schoeniger and DeNiro, 1984; Bocherens and Drucker, 2003; O'Connell et al., 2012). In Africa, this signal is usually overprinted by the larger $\delta^{13}C$ differences between plants using different photosynthetic pathways; therefore, $\delta^{13}C_{enamel}$ cannot be reliably used for trophic-level reconstructions. However, $\delta^{13}C_{enamel}$ is a robust and well-established tool for reconstructing the plant-based diet of an animal (**Figure 1**; e.g., Cerling et al., 2015).

Dicots (trees, bushes, and herbs) use the C_3 photosynthetic pathway, whereas most tropical grasses and sedges use the C_4 photosynthetic pathway (e.g., Pearcy and Ehleringer, 1984). C_4 photosynthesis is advantageous in warm and seasonally dry, open environments with high light intensity, whereas the C_3 pathway is typically prevalent under low water stress and high-pCO_2 conditions (Kohn, 2010). Another pathway (Crassulacean Acid Metabolism; Wolf, 1960; Lüttge, 2004) is used by very arid-adapted plants like succulents, but these are rare at GNP and do not contribute significantly to the diet of the studied animals.

As a result of differential discrimination against $^{13}CO_2$ during photosynthesis, C_3 and C_4 types can be distinguished based on their $\delta^{13}C$ values (**Figure 1**). The $\delta^{13}C$ values of African C_4 plants range from –19‰ to –9‰, while those of C_3 plants lie between –29‰ and –25‰, resulting in bimodal and non-overlapping $\delta^{13}C$ values (Smith and Epstein, 1971; Pearcy and Ehleringer, 1984; Cerling et al., 2003; Kohn, 2010). Plant $\delta^{13}C$ values are reflected in the tissues of the animals that consume them, such that C_4 grazing (>70% C_4 grass consumption), mixed-feeding (>30% C_4 grass and >30% C_3 browse), and browsing (>70% C_3 browse) taxa can be differentiated (Cerling et al., 2003). Isotopic fractionation from diet to tooth takes place during enamel biomineralization. Large herbivore $\delta^{13}C_{enamel}$ values are enriched by ~14.5 to 12.0 ± 1.0‰ compared to the plants that they consume, depending on their digestive strategies (Cerling and Harris, 1999; Tejada-Lara et al., 2018, Cerling et al., 2021). Generally, browsers have $\delta^{13}C_{enamel}$ values lower than –8‰, grazers have values above –2‰, and values in between are typical for mixed-feeders (Cerling and Harris, 1999; Uno et al., 2018). Carnivore $\delta^{13}C_{enamel}$ values are determined by the isotopic composition of their prey, with negligible isotopic fractionation (Bocherens and Drucker, 2003).

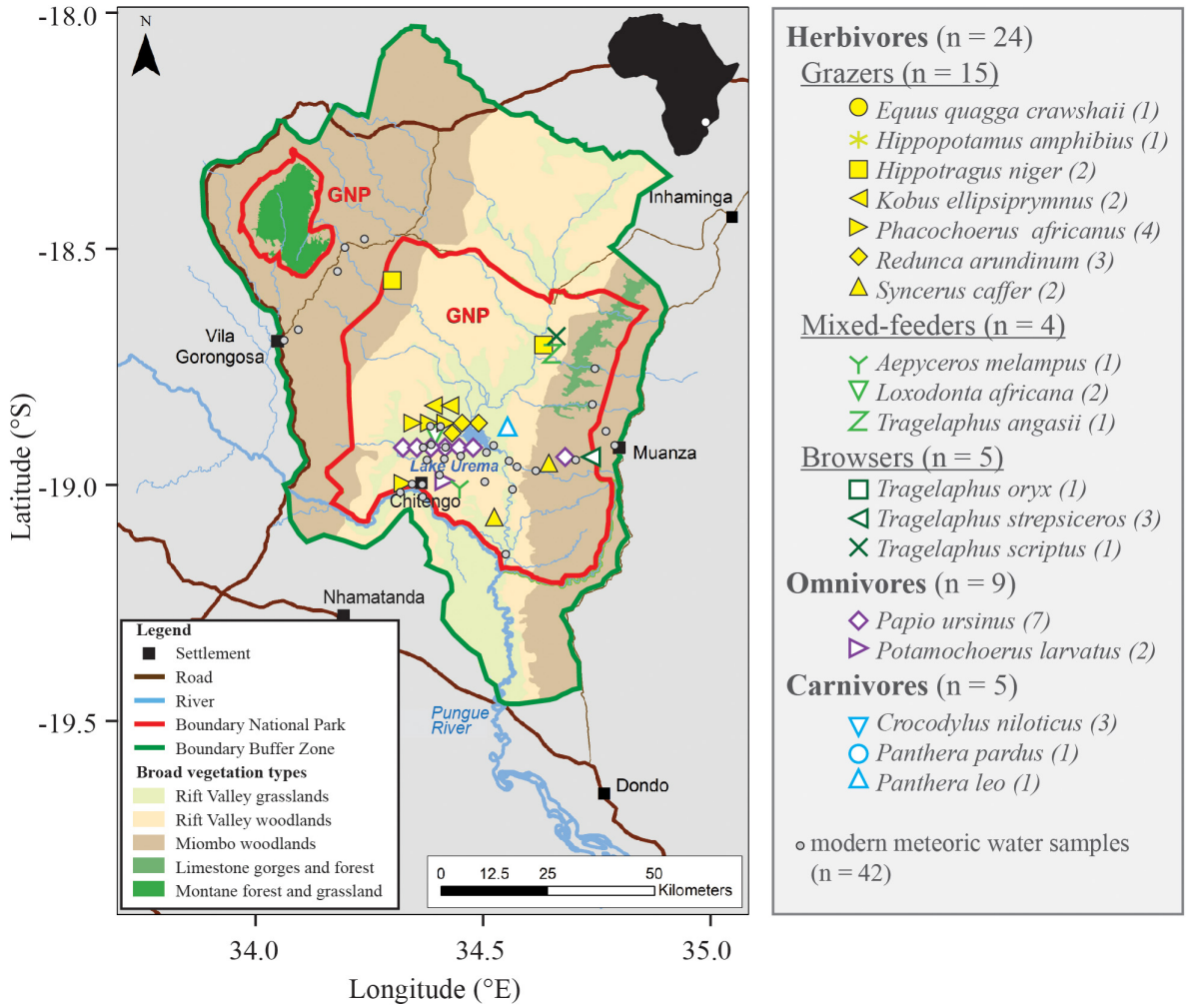

FIGURE 2
Map of Gorongosa National Park (red outline) and the Buffer Zone (green outline) indicating main vegetation types (modified after Stalmans and Beilfuss, 2008) with faunal and meteoric water collection sites. GPS coordinates for fauna specimens and water samples can be found in **Supplementary Tables 1**, **2**. Note that the exact location of nine faunal specimens is not known, because they were collected before the start of the PPPG, but all specimens are from inside the park or Buffer Zone. A black line drawing of Africa shows the position of GNP (white circle).

Stable oxygen isotopes in tooth enamel and drinking water

The oxygen isotope composition of tooth enamel can be measured in either structural carbonate (CO_3) or phosphate (PO_4). Here, we report measurements on structural carbonate. For mammals, the $\delta^{18}O$ values of both components can be converted with the equation $\delta^{18}O_{PO4} \approx 0.98 * \delta^{18}O_{CO3} - 8.5$ after Iacumin et al. (1996). While reptiles may have a slightly different PO_4 to CO_3 relationship than mammals due to physiological effects (Stanton and Carlson, 2004), this has not been adequately studied to establish a separate equation for this group.

The oxygen isotope composition of tooth enamel is directly linked to the $\delta^{18}O$ values of body water which itself is a complex function of (micro)habitat, climate, diet, drinking behavior, and physiology (e.g., Bryant and Froelich, 1995; Kohn, 1996; Pederzani and Britton, 2019). The body's main oxygen sources are drinking water, food, and atmospheric O_2.

In sub-Saharan Africa, meteoric water (i.e., available drinking water) is often strongly influenced by the composition of the source water and evaporation processes (for details regarding GNP meteoric water, refer to the following section and Steinbruch, 2010; Steinbruch and Weise, 2014). To interpret variability in $\delta^{18}O_{enamel}$ in the GNP fauna, we measured $\delta^{18}O$ of potential drinking water (i.e., permanent and ephemeral lakes and streams, rain, and groundwater, in the park and surrounding areas).

In warm-blooded mammals with an internally regulated body temperature (ca. 37°C for most mammals larger than 1 kg), biogenic hydroxyapatite is precipitated at a constant

temperature, and thus the oxygen isotopic signature of ingested food and water is recorded without temperature-dependent fractionation. For large herbivores, digested water is assumed to be equivalent to surficial water (Bryant and Froelich, 1995). There is an offset between $\delta^{18}O$ of body water and the $\delta^{18}O$ of the bioapatite (Bryant et al., 1996; Iacumin et al., 1996) according to the generalized equation for mammalian taxa of $\delta^{18}O_{water} \approx (\delta^{18}O_{enamel(PO4)} - 23)/0.9$ (Kohn and Cerling, 2002); taxon-specific variations (refer to e.g., Ayliffe et al., 1992), relative humidity, and water temperature can, however, change this correlation (Kohn, 1996). The oxygen isotope compositions of *Crocodylus* correlate with those of ambient water according to the equation $\delta^{18}O_{enamel(PO4)} \approx (\delta^{18}O_{water} + 19.13)/0.82$ (Amiot et al., 2007).

In additional consideration, African mammals can be divided into obligate and non-obligate drinkers. $\delta^{18}O_{enamel}$ of large-bodied (>100 kg), obligate drinkers have been shown to primarily reflect the $\delta^{18}O_{water}$ values of consumed water, and hence their $\delta^{18}O_{enamel}$ is closely related to the isotopic composition of their ambient environment (Bryant and Froelich, 1995; Kohn, 1996; Hoppe, 2006). However, non-obligate drinking animals, such as drought-adapted herbivores, obtain large proportions (or even all) of their water from the plant foods they consume (e.g., Nicholson, 1985). This behavior can lead to an increase in $\delta^{18}O_{enamel}$ values because leaf water is sensitive to evaporation, resulting in high $\delta^{18}O$ values in this part of the plant (Levin et al., 2006).

Additionally, plant $\delta^{18}O$ composition can vary as the result of differences in feeding behavior (e.g., $\delta^{18}O_{enamel}$ values typically decrease with increasing fraction of C_3 diet, because C_3 plants have lower $\delta^{18}O$ values than coexisting C_4 plants) (Bocherens et al., 1996).

At GNP, both obligate drinkers, which mostly include grazers and omnivores (e.g., hippos, equids, elephants, primates, suids), as well as non-obligate drinkers, mainly browsers and mixed-feeders (e.g., eland, bushbuck, kudu, nyala, and sable, refer to Cain et al., 2012), were sampled (refer to **Table 1**).

Materials and methods

Gorongosa National Park

Gorongosa National Park is located in the Sofala Province in central Mozambique (**Figure 2**) in the Urema Rift, the southernmost part of the East African Rift System. The unfenced park encompasses a 3,688 km^2 mosaic of diverse habitats and is surrounded by an inhabited "Buffer Zone" consisting mostly of agricultural lands (**Figure 2**). The valley floor is ca. 40 km wide and flanked to the east and west by hilly terrain rising to 400 m (Stalmans and Beilfuss, 2008; Stalmans et al., 2019). The region's climate is influenced by the migration of the Intertropical Convergence Zone and is dominated by hot wet summers and cooler dry winters with a mean annual rainfall of 700–900 mm. Over 80% of the annual rainfall occurs between November and March and is derived from the Indian Ocean, although some rainfall can also occur in the dry months as a result of the inflow of sub-polar mist cold air and continental compression (Steinbruch and Weise, 2014; Stalmans et al., 2019; Ma et al., 2021).

A central feature of the park is Lake Urema, which is on average only 2 m deep (Böhme, 2005) and is drained through a floodplain and the Urema River into the Pungwe River (**Figure 2**). The lake is fed by several ephemeral rivers that flow only in the wet season. In the dry season, the lake water infiltrates aquifer systems at the transition of the escarpments of the Urema Graben (Steinbruch, 2010; Arvidsson et al., 2011). The Lake Urema floodplain extends for >300 km^2 and floods annually (Steinbruch and Merkel, 2008), becoming uninhabitable for most terrestrial animals during the wet season. Stalmans and Beilfuss (2008) identified and mapped five major habitat types within GNP (**Figure 2**). From west to east, these are (i) Midlands miombo woodland (*Brachystegia* and *Julbernardia* sp.) on the western rim of the Rift Valley (331 km^2); (ii) Alluvial Fan *Acacia*, *Combretum,* and palm savannas (1,265 km^2); (iii) floodplain grasslands (759 km^2) around Lake Urema; (iv) Colluvial Fan savannas (326 km^2) within the Rift Valley; and (v) Cheringoma Plateau miombo woodlands and forested limestone gorges on the eastern rim of the Rift Valley (938 km^2).

These landscapes have an overall proportional tree cover of 0.39 (Daskin et al., 2016) and support a large diversity of herbivores, including grazers, browsers, and mixed-feeders (Tinley, 1977; Stalmans and Beilfuss, 2008; Daskin et al., 2016; Stalmans et al., 2019; Gaynor et al., 2021). However, while Gorongosa was once renowned for its large mammal population (Tinley, 1977), the ecosystem experienced severe perturbation during 15 years of civil war (1977–1992), from which it is still recovering today. Most apex predators were extirpated from the park during this time, including leopards, African wild dogs, and spotted hyenas. Of these taxa, leopards have recently re-colonized the Buffer Zone by migrating from surrounding areas, and five additional adult leopards as well as two founding packs of wild dogs have been re-introduced from different regions in South Africa (Bouley et al., 2021). Lions and crocodiles are the only apex predators that persisted throughout the periods of war and recovery; however, the lions' abundance was greatly reduced (Pringle, 2017; Bouley et al., 2018). Herbivore populations were similarly decimated. Before the war, elephants, hippos, buffalo, zebra, and wildebeest dominated the herbivore fauna but today are outnumbered by waterbuck and other small to mid-size antelopes (Stalmans et al., 2019).

The Gorongosa Restoration Project, established in 2006, is focused on long-term biodiversity conservation, sustainable development of the neighboring Buffer Zone, training farmers in new practices to improve crop yields, and improving the health and education of communities in the greater Gorongosa

TABLE 1 List of all 38 analyzed specimens including diet, common and Latin name, catalog ID, and stable nitrogen, carbon, and oxygen values in % and nitrogen content. Mean values for each dietary group are shown in bold.

Diet	Common name	Taxon	Catalog ID	$\delta^{15}N_{enamel}$ (% vs. AIR)	$\delta^{13}C_{enamel}$ (% vs. VPDB)	$\delta^{18}O_{enamel}$ (% vs. VSMOW)	N content (nmol/mg)
Grazing	Buffalo	*Syncerus caffer*	PPG2017-B-19	4.3 ± 0.3 (3)	1.5 ± 0.1 (2)	30.4 ± 0.3 (2)	7.9 ± 2.0 (3)
	Buffalo	*Syncerus caffer*	PPG2017-B-41	7.6 ± 0.0 (2)	−2.1 ± 0.3 (2)	28.9 ± 0.2 (2)	3.4 ± 0.3 (2)
	Hippo	*Hippopotamus amphibius*	PPG2016-B-07	7.6 ± 0.4 (2)	−4.0 ± 0.1 (2)	26.2 ± 0.0 (2)	3.7 ± 0.0 (2)
	Reedbuck	*Redunca arundinum*	PPG2016-B-27	3.6 ± 0.6 (2)	0.5 ± 0.0 (2)	31.4 ± 0.3 (2)	6.8 ± 1.0 (2)
	Reedbuck	*Redunca arundinum*	PPG2017-B-17	4.7 ± 0.3 (2)	0.6 ± 0.2 (3)	31.4 ± 0.2 (3)	6.1 ± 0.7 (2)
	Reedbuck	*Redunca arundinum*	PPG2017-B-59	4.7 ± 0.3 (2)	0.3 ± 0.0 (2)	33.1 ± 0.2 (2)	5.7 ± 0.1 (2)
	Sable	*Hippotragus niger*	PPG-B-01	4.8 ± 0.1 (2)	1.2 ± 0.0 (2)	31.3 ± 0.0 (2)	5.9 ± 0.9 (2)
	Sable	*Hippotragus niger*	PPG2017-B-47	5.9 ± 0.0 (2)	1.8 ± 0.1 (2)	32.7 ± 0.2 (2)	3.6 ± 0.1 (2)
	Warthog	*Phacochoerus africanus*	PPG2017-B-30	6.3 ± 0.4 (2)	−1.9 ± 0.4 (2)	29.3 ± 0.3 (2)	3.8 ± 0.8 (2)
	Warthog	*Phacochoerus africanus*	PPG2017-B-04	5.9 (1)	−3.8 ± 0.3 (2)	28.7 ± 0.3 (2)	4.7 (1)
	Warthog	*Phacochoerus africanus*	PPG2016-B-25	5.5 ± 0.1 (2)	−2.7 ± 0.1 (2)	30.1 ± 0.3 (2)	4.7 ± 1.7 (2)
	Warthog	*Phacochoerus africanus*	PPG2017-B-29	5.1 ± 0.2 (2)	−1.3 ± 0.6 (2)	31.8 ± 0.6 (2)	4.9 ± 0.4 (2)
	Waterbuck	*Kobus ellipsiprymnus*	PPG2016-B-15	7.5 ± 0.3 (2)	0.6 ± 0.1 (2)	32.7 ± 0.2 (2)	4.8 ± 0.0 (2)
	Waterbuck	*Kobus ellipsiprymnus*	PPG2016-B-24	7.9 ± 0.1 (2)	−4.3 ± 0.0 (3)	31.1 ± 0.5 (3)	4.9 ± 0.3 (2)
	Zebra	*Equus quagga crawshaii*	PPG-B-02	6.9 (1)	−3.3 ± 0.0 (2)	29.1 ± 0.5 (2)	2.2 (1)
Grazers mean values (n = 15)				***5.9 ± 1.4***	***−1.1 ± 2.2***	***30.5 ± 1.9***	***4.9 ± 1.5***
Mixed-feeding	Elephant	*Loxodonta africana*	PPG-B-08	7.3 ± 0.2 (2)	−10.7 ± 0.1 (2)	28.9 ± 0.1 (2)	6.0 ± 0.6 (2)
	Elephant	*Loxodonta africana*	PPG-B-03	8.1 ± 0.2 (2)	−10.5 ± 0.1 (2)	29.8 ± 0.3 (2)	5.8 ± 1.5 (2)
	Impala	*Aepyceros melampus*	PPG2017-B-28	7.0 ± 0.4 (3)	−3.6 ± 0.0 (2)	29.8 ± 0.3 (2)	4.8 ± 0.8 (3)
	Nyala	*Tragelaphus angasii*	PPG2017-B-45	4.5 ± 0.2 (2)	−14.8 ± 0.1 (4)	31.4 ± 0.1 (4)	4.8 ± 0.2 (2)
Mixed-feeders mean values (n = 4)				***6.7 ± 1.6***	***−9.9 ± 4.7***	***30.0 ± 1.1***	***5.4 ± 0.6***
Browsing	Bushbuck	*Tragelaphus scriptus*	PPG2017-B-44	7.2 ± 0.1 (2)	−11.8 ± 0.0 (2)	31.9 ± 0.0 (2)	6.7 ± 2.0 (2)
	Eland	*Tragelaphus oryx*	PPG2017-B-31	4.5 ± 0.0 (2)	−14.7 ± 0.1 (2)	31.2 ± 0.2 (2)	4.9 ± 0.1 (2)
	Greater Kudu	*Tragelaphus strepsiceros*	PPG-B-04	6.1 ± 0.1 (2)	−15.1 ± 0.2 (2)	31.2 ± 0.4 (2)	4.4 ± 0.5 (2)
	Greater Kudu	*Tragelaphus strepsiceros*	PPG-B-05	5.9 ± 0.2 (2)	−14.4 ± 0.2 (2)	30.5 ± 0.2 (2)	4.0 ± 0.2 (2)
	Greater Kudu	*Tragelaphus strepsiceros*	PPG2017-B-58	3.8 ± 0.0 (2)	−15.8 ± 0.1 (2)	29.9 ± 0.3 (2)	3.8 ± 0.4 (2)
Browsers mean values (n = 5)				***5.5 ± 1.5***	***14.3 ± 1.5***	***31.0 ± 0.8***	***4.8 ± 1.2***
All herbivores mean values (n = 24)				***5.9 ± 1.4***	***−5.4 ± 6.2***	***30.5 ± 1.2***	***4.9 ± 1.3***
Omnivorous	Bushpig	*Potamochoerus larvatus*	PPG2017-B-32	4.5 ± 0.2 (2)	−13.7 ± 0.0 (2)	26.0 ± 0.2 (2)	8.3 ± 1.2 (3)
	Bushpig	*Potamochoerus larvatus*	PPG2017-B-25	6.2 ± 0.6 (3)	−9.5 ± 0.0 (2)	28.4 ± 0.0 (2)	3.6 ± 0.2 (2)
	Baboon	*Papio ursinus*	PPG2016-B-05	4.6 ± 0.4 (3)	−12.78 ± 0.0 (2)	30.5 ± 0.2 (2)	3.5 ± 0.4 (2)
	Baboon	*Papio ursinus*	PPG2018-B-28	2.2 ± 0.2 (2)	−13.1 ± 0.2 (3)	28.4 ± 0.3 (3)	4.9 ± 0.7 (2)
	Baboon	*Papio ursinus*	PPG2017-B-34	5.5 ± 0.5 (2)	−8.2 ± 0.3 (2)	28.9 ± 0.3 (2)	4.6 ± 0.3 (2)
	Baboon	*Papio ursinus*	PPG2016-B-10	3.9 ± 0.2 (2)	−7.9 ± 0.0 (2)	28.5 ± 0.2 (2)	4.8 ± 1.1 (2)
	Baboon	*Papio ursinus*	PPG2016-B-16	6.3 ± 0.3 (2)	−8.4 ± 0.2 (3)	29.2 ± 0.1 (3)	3.9 ± 0.3 (2)
	Baboon	*Papio ursinus*	PPG2016-B-20	5.9 ± 0.4 (2)	−11.7 ± 0.3 (3)	29.0 ± 0.4 (3)	2.0 ± 0.1 (2)
	Baboon	*Papio ursinus*	PPG2017-B-28	6.6 ± 0.2 (2)	−9.9 ± 0.1 (3)	28.5 ± 0.3 (3)	2.5 ± 0.2 (3)
Omnivores mean values (n = 9)				***5.1 ± 1.4***	***−10.6 ± 2.3***	***28.6 ± 1.2***	***4.2 ± 1.8***
Carnivorous	Leopard	*Panthera pardus*	PPG2019-B-09	7.2 ± 0.3 (2)	−11.0 ± 0.0 (2)	28.1 ± 0.3 (2)	4.0 ± 0.2 (2)
	Lion	*Panthera leo*	PPG2018-B-02	12.3 ± 0.2 (2)	−8.1 ± 0.3 (3)	29.9 ± 0.5 (3)	4.0 ± 0.4 (2)
	Crocodile	*Crocodylus niloticus*	PPG2016-B-39	10.9 ± 0.4 (2)	−6.4 ± 0.2 (2)	27.1 ± 0.2 (2)	9.7 ± 1.0 (2)
	Crocodile	*Crocodylus niloticus*	PPG2016-B-38	9.3 ± 0.3 (3)	−6.9 ± 0.1 (2)	27.2 ± 0.5 (2)	8.4 ± 1.5 (3)
	Crocodile	*Crocodylus niloticus*	PPG-B-06	10.0 ± 0.1 (2)	−3.1 ± 0.3 (2)	29.0 ± 0.0 (2)	10.6 ± 1.2 (2)
Carnivores mean values (n = 5)				***9.9 ± 1.9***	***−7.1 ± 2.9***	***28.3 ± 1.2***	***7.4 ± 3.1***

The number of analyses, typically duplicate, is given in brackets.

region. Due to these efforts, the GNP ecosystem is slowly recovering and offers a unique setting in which to study the adaptation of mammals to dynamic and complex environments. Today, numerous projects are underway in GNP. These studies use a combination of methods including motion-triggered cameras (Gaynor et al., 2018, 2021; Easter et al., 2019), biologgers (often including Global Positioning System units, triaxial accelerometers, and sometimes video recorders; e.g., Branco et al., 2019a,b; Becker et al., 2021; Bouley et al., 2021), aerial counts (Cumming et al., 1994; Dutton and Carvalho, 2002; Dunham, 2004; Stalmans, 2012; Stalmans et al., 2019), animal follows (Hammond et al., 2022), molecular studies (Martinez et al., 2019; Santander et al., 2022), and other field observation tools (e.g., Muschinski et al., 2019) to gain insights in the park's ecology. The $\delta^{13}C_{enamel}$, $\delta^{15}N_{enamel}$, and $\delta^{18}O_{enamel}$ datasets of Gorongosa's fauna presented here—the first stable isotopes result for any terrestrial fauna in Mozambique—will help us to better understand dietary patterns of the large-bodied animals which roam GNP today.

Material and sampling protocol

Tooth enamel

Since 2016, remains of modern fauna have been collected from different regions of the park and the surrounding Buffer Zone (**Figure 2** and **Supplementary Table 1**) by members of the Paleo-Primate Project Gorongosa (PPPG). We selected as many different vertebrate taxa as possible and analyzed the tooth enamel of 38 adult individuals (17 mammalian taxa and one reptile; refer to **Table 1**) for organic $\delta^{15}N_{enamel}$ as well as inorganic $\delta^{13}C_{enamel}$ and $\delta^{18}O_{enamel}$. These include 15 grazers, four mixed-feeders, five browsers, nine omnivores, and five carnivores. The bone weathering stage was 0–1, suggesting that all animals died within the last few years prior to field collection (after Behrensmeyer, 1978).

During sampling, the topmost ca. 0.2 mm of enamel was discarded to avoid contamination by any adherent sediment. Tooth enamel powder was sampled using a Dremel handheld drill with a diamond ball head drill tip (0.9 mm diameter) at low to medium speed (1,000–2,000 RMP). For herbivore specimens, which generally have thick enamel, the sampling depth was 0.5–1 mm. For carnivores and some omnivores which have only a thin layer of enamel, great care was taken to avoid the underlying dentin, and sampling was conducted to a shallower depth, over a larger area of the tooth. Bulk enamel samples were usually taken longitudinally, between the cusp and the cervix, integrating at least 3 months of the dietary signal. We collected 10–50 mg of enamel for carbon, nitrogen, and oxygen isotope analyses, which were measured in duplicate or triplicate whenever possible.

Meteoric water

Water samples from the lake (n = 15), river (n = 18), rain (n = 4), and groundwater (n = 5) sources were collected from GNP and the surrounding Buffer Zone between 2016 and 2019 (**Figure 2** and **Supplementary Table 2**) in both dry seasons (May to October; n = 32; mostly permanent lakes and rivers, groundwater) and wet season (November to April; n = 10; rainwater, ephemeral and permanent lakes/water holes, floodplain). These water sources represent potential drinking water for the Gorongosa fauna.

At each sampling site, 30 ml of unfiltered water was collected with as little air volume as possible in high-density polyethylene bottles. Rainwater was captured directly from the runoff of an aluminum roof at Camp Chitengo (**Figure 2**). Groundwater was sampled from water pumps which were run for at least 3 min prior to sampling. Samples were stored at room temperature and in the dark until returned to the laboratory for refrigeration and subsequent analysis.

Analyses

Nitrogen isotope analysis of tooth enamel using a novel "*oxidation-denitrification method*"

We use the "*oxidation-denitrification method*" to measure the $\delta^{15}N_{enamel}$ of mineral-bound nitrogen in tooth enamel at the Max Planck Institute for Chemistry (MPIC). The "*oxidation-denitrification method*" was first used for marine-dissolved organic nitrogen (Knapp et al., 2005) and marine microfossil-bound nitrogen (Robinson et al., 2004; Ren et al., 2009). The protocol used here for enamel-bound nitrogen follows Leichliter et al. (2021). It includes reductive-oxidative cleaning of enamel powder followed by oxidation of enamel-bound organic matter to nitrate using a basic solution of potassium peroxydisulfate in a specially designed clean room. Nitrate is subsequently converted to N_2O using the bacteria *Pseudomonas chlororaphis*, grown, cultured, and harvested at the MPIC following the methods outlined by Sigman et al. (2001) and Weigand et al. (2016). The isotopic composition of the N_2O is extracted, purified, and analyzed by an automated purge-trap, gas chromatography-isotope ratio mass spectrometry, in this case by a custom-built system online to a Thermo Scientific MAT253-Plus isotope ratio mass spectrometer (Weigand et al., 2016). Coupled with the denitrification step for N_2O production, this system results in high-precision measurements ($1\sigma < 0.1‰$) of nitrogen isotopes of nitrate down to 5 nmol N (Weigand et al., 2016).

We cleaned and measured each sample (5–7 mg of enamel powder) in duplicate or triplicate (exceptions are PPG-B-02 and PPG2017-B-04 due to limited sample amounts) in different batches, resulting in 78 individual measurements in five different batches.

Individual nitrate isotopic analyses are referenced to injections of N_2O and standardized using international nitrate reference materials IAEA-NO3 and USGS34. Additionally,

sample data were corrected for the contribution of the blank using the nitrogen content and $\delta^{15}N$ values of oxidation blanks after Leichliter et al. (2021). Blank N content was between 0.3 and 0.4 nmol/ml, resulting in an average blank contribution of 3% or less. Inter-batch precision ($\pm 1\sigma$) in $\delta^{15}N$ for international standards is <0.2‰ for USGS65 (glycine; n = 7); <0.3‰ for USGS 40 (L-glutamic acid; n = 16); and <0.4‰ for USGS41 (L-glutamic acid; n = 11; **Supplementary Table 3**). For in-house standards (refer to Leichliter et al., 2021), this precision is <0.4‰ for coral standard PO-1 (*Porites* sp.; n = 18) and LO-1 (*Lophelia pertusa*; n = 17) and <0.5‰ for tooth enamel standards AG-Lox (modern *Loxodonta africana*; n = 18) and Noto-1 (Late-Pleistocene *Notochoerus scotti*; n = 17), across all analytical batches (**Supplementary Table 4**).

Stable carbon and oxygen isotope analyses of tooth enamel

High-precision stable carbon and oxygen isotope analysis of small sample amounts (~50–100 μg of untreated enamel) was performed using the "*cold trap method*" (Vonhof et al., 2020a) at the laboratories of the Climate Geochemistry Department at MPIC in Mainz, Germany. We used a Thermo Delta-V mass spectrometer in continuous flow configuration, directly interfaced with a GasBench II gas preparation unit with an integrated pneumatically operated cold trap system. In automated mode, digestion of enamel occurs in 12 ml He-flushed exetainer vials with >99% H_3PO_4 at 70°C for 90 min. Then, the CO_2 sample is carried with ultrapure He to the cold trap where it is cryogenically focused for 6–7 min by cooling the trap with liquid N_2. After lifting the trap out of the liquid N_2, the carrier gas with the sample CO_2 passes through a standard Poraplot-Q Gas Chromatography (GC) column where the entire CO_2 sample is delivered to the mass spectrometer for carbon and oxygen isotope analyses in a single peak, preceded by five reference gas peaks. Calculation of isotope values follows Vonhof et al., 2020a,b with the international standards IAEA-603, NBS18, and/or NBS120c in addition to two internal house standards: a carbonate standard (VICS) and tooth enamel standard AG-Lox, the latter was also used as a standard for $\delta^{15}N_{enamel}$ for reference (**Supplementary Table 5**). Overall analytical uncertainties are better than 0.09‰ for $\delta^{13}C_{enamel}$ and 0.14‰ for $\delta^{18}O_{enamel}$ (1σ standard deviation of AG-Lox within batches). Carbonate contents were derived from standard vs. sample total peak area ratios (7.5% structural carbonate content for AG-Lox; after Vonhof et al., 2020b).

Oxygen isotope analyses of meteoric waters

Oxygen isotope ratios were measured on 1 ml aliquots using an LGR 24d liquid water isotope analyzer at the Goethe University-Senckenberg BiK-F Joint Stable Isotope Facility, Frankfurt, Germany (Schemmel et al., 2013). The $\delta^{18}O_{water}$ values are calibrated and reported against VSMOW, with an analytical precision of <0.2‰ (2σ).

Statistical analyses

Statistical analyses of elemental content and univariate isotope values were performed using Paleontological Statistics (PAST4) version 4 (Hammer et al., 2001). Statistical significance between isotopic groups was determined using one-way ANOVA with a Tukey–Kramer HSD *post hoc* test if not stated otherwise with a level of significance of p = 0.050. Pearson correlation coefficient (r) is given for correlations.

Statistical analyses of multivariate isotope comparisons were performed in R (version 4.2.0; R Core Team, 2022). Isotopic niches were analyzed using the Stable Isotopes Bayesian Ellipses (SIBER) package (version 2.1.6; Jackson et al., 2011) and the Turner et al. (2010) statistical code. Data normality was first checked using the Shapiro–Wilk test for both individual groups by element using the *nor.test* function from the *onewaytests* package (Dag et al., 2018), and with a multivariate Shapiro–Wilk test for the entire dataset using the *mshapiro_test* function from the *rstatix* package (Kassambra, 2021). Data normality was assumed if $p > 0.050$ for all tests. The isotopic niches of the four different *a priori* dietary groups with $n \geq 5$ were determined by fitting their distribution of $\delta^{13}C_{enamel}$, $\delta^{15}N_{enamel}$, and $\delta^{18}O_{enamel}$ isotope values with estimated standard ellipse areas corrected for sample size (SEA_C; Jackson et al., 2011). The SEA_C contains 40% of the variation of a group and was chosen over SEA as it limits calculation biases due to small and unbalanced sample sizes and is appropriate when the analyzed groups contain fewer than 30 individuals (Syväranta et al., 2013; Pinzone et al., 2019). However, the mixed feeding group was not included in the multivariate analyses because of its sample size (n = 4) which does not meet the minimum sampling requirements for SEA_C as recommended by Jackson et al. (2011). Its mean value, standard deviation, and convex hull were still calculated and plotted for visual comparisons.

Geometric overlap between ellipses was calculated and compared between analyzed groups, both in total overlap (in $‰^2$) and in proportional overlap (Jackson et al., 2011; refer to **Supplementary Tables 6–8**). Niche standard ellipse areas for each group were further explored using Bayesian modeling (SEA_B) and 50, 75, and 95% credible intervals were calculated and compared across groups. Finally, to determine whether the location of each group's niche differed in isotopic space, the Euclidean distance between the centroids of each group was calculated and compared in pairs. A residual permutation procedure and Hotelling T^2 test were used to evaluate significance, with $p < 0.050$ indicating that the two compared niches occupy significantly different areas in isotopic space (Turner et al., 2010).

Results

We report $\delta^{15}N_{enamel}$, $\delta^{13}C_{enamel}$, $\delta^{18}O_{enamel}$, and N content data from 35 mammals and three reptiles sampled

in GNP, and the results are given in Table 1. For calculated $\delta^{18}O_{drinking-water}$, carbonate contents, tooth position, sex, GPS coordinates, and collection date and locality (habitat), refer to Supplementary Table 1. Additionally, we report $\delta^{18}O_{water}$ data from 42 meteoric water samples, results with water type (rain, river, lake, and groundwater), GPS coordinates, elevation, and collection date are given in Supplementary Table 2.

Nitrogen isotope values

$\delta^{15}N_{enamel}$ values of all 38 specimens range from 2.2 to 12.3‰, with mean $\delta^{15}N_{enamel}$ values of 5.9 ± 1.4‰ (n = 24) for herbivores, 5.1 ± 1.4‰ (n = 9) for omnivores, and 9.9 ± 1.9‰ (n = 5) for carnivores (Figure 3A). Carnivore nitrogen isotope ratios differ significantly from herbivores and omnivores ($p < 0.001$), while the $\delta^{15}N_{enamel}$ values of omnivores (bushpigs and baboons) do not differ significantly from herbivores ($p = 0.324$). Grazers (6.9 ± 1.4‰, n = 15), mixed-feeders (6.7 ± 1.6‰, n = 4), and browsers (5.5 ± 1.3‰, n = 5) show no significant difference in their $\delta^{15}N_{enamel}$ values ($p = 0.428$). Herbivore taxa do not display significantly different $\delta^{15}N_{enamel}$ values when grouped according to digestive physiology ($p = 0.104$) or water dependency ($p = 0.128$; Figure 4A).

Nitrogen content in tooth enamel

The nitrogen content of clean tooth enamel ranges from 2.0 to 10.6 nmol/mg with an average of 5.1 ± 1.9 nmol/mg (Figure 5 and Table 1). No significant correlation is observed between $\delta^{15}N_{enamel}$ and nitrogen content ($r = 0.285$; $p = 0.083$; Figure 5A). Carnivores have slightly higher N contents compared to the other dietary groups ($p = 0.008$). However, this difference is entirely driven by the high nitrogen content of crocodile enamel, and crocodiles were the only reptiles sampled (Figure 5B). No other differences in the N content of tooth enamel were observed between dietary groups.

Carbon isotope values

The complete range of C_3 to C_4 $\delta^{13}C$ values is represented in the Gorongosa fauna. $\delta^{13}C_{enamel}$ values range from −15.7 to 1.8‰, with mean $\delta^{13}C_{enamel}$ values for herbivores of −5.4 ± 6.2‰ (n = 24), −10.6 ± 21.4‰ (n = 9) for omnivores, and −7.1 ± 2.9‰ (n = 5) for carnivores. $\delta^{13}C_{enamel}$ values for grazing herbivores (mean = −1.1 ± 2.2‰; n = 15), mixed-feeders (−9.9 ± 4.7‰, n = 4), and browsers (−14.3 ± 1.5‰; n = 5) are significantly different ($p < 0.001$). Herbivores do not display significant differences in $\delta^{13}C_{enamel}$ values when grouped according to digestive physiology [ruminant (n = 16) vs. non-ruminant (n = 8); $p = 0.761$]. Herbivorous obligate drinkers (n = 16) have higher $\delta^{13}C_{enamel}$ values compared to non-obligate drinkers (n = 8; $p = 0.002$; Figure 4B).

The structural carbonate component of enamel powder ranges from 3 to 9% (Supplementary Table 1) with a mean of 6 ± 1%. Herbivores have slightly higher carbonate content than omnivores ($p < 0.001$), while the other dietary groups do not differ ($p > 0.050$).

Oxygen isotope values

The $\delta^{18}O_{enamel}$ values for the Gorongosa fauna range from 26.0 to 33.1‰ with mean values of 30.5 ± 1.6‰ (n = 24) for herbivores, 28.6 ± 1.2‰ (n = 9) for omnivores, and 28.3 ± 1.2‰ for carnivores (n = 5). Herbivores differ statistically from other dietary groups ($p < 0.008$), while carnivores and omnivores are similar ($p = 0.907$). Ruminant $\delta^{18}O_{enamel}$ values are significantly higher than those of non-ruminants ($p < 0.001$). $\delta^{18}O_{enamel}$ values for herbivorous non-obligate drinkers are not significantly different than those of obligate drinkers ($p = 0.108$; Figure 4C).

The $\delta^{18}O_{water}$ values of drinking water range from −6.2 to 13.1‰ with a mean value of −0.8 ± 5.3‰ (n = 42; Figure 6 and Supplementary Table 2). Groundwaters have the lowest $\delta^{18}O_{water}$ values with an average of −5.2 ± 0.6‰ (n = 5), followed by waters sampled from rivers (−3.4 ± 1.8‰; n = 18), rainfall (−2.5 ± 1.3‰; n = 4), and lakes (4.1 ± 6.1‰; n = 15); this difference is statistically significant only when comparing lake water to samples from other reservoirs ($p < 0.020$). Lake $\delta^{18}O_{water}$ values sampled in the wet season (−4.9 to −1.5‰; mean = −3.2 ± 1.4‰, n = 5) are significantly ($p < 0.001$) lower than dry season data (2.9–13.1‰; mean = 7.8 ± 3.4‰; n = 10), and there is no overlap in these two datasets.

Isotope niche analyses

Isotopic niche overlap, niche area, and distinction of niche space differed depending on the pairing of isotope values analyzed (Figure 7 and Supplementary Tables 6–8). We could not reject the null hypotheses for all Shapiro–Wilks tests indicating data were normal for both the individual feeding group by element (all groups $p > 0.050$) as well as the entire multivariate dataset ($p = 0.212$).

For $\delta^{13}C_{enamel}$ vs. $\delta^{15}N_{enamel}$, there is no SEA_C overlap present (Figure 7A), and the Bayesian modes of niche size ranged from 4.0 to 13.1‰^{2} with no statistical differences based on 95% credible intervals (Figure 7B). All dietary groups were statistically distinct in isotopic space ($p < 0.035$).

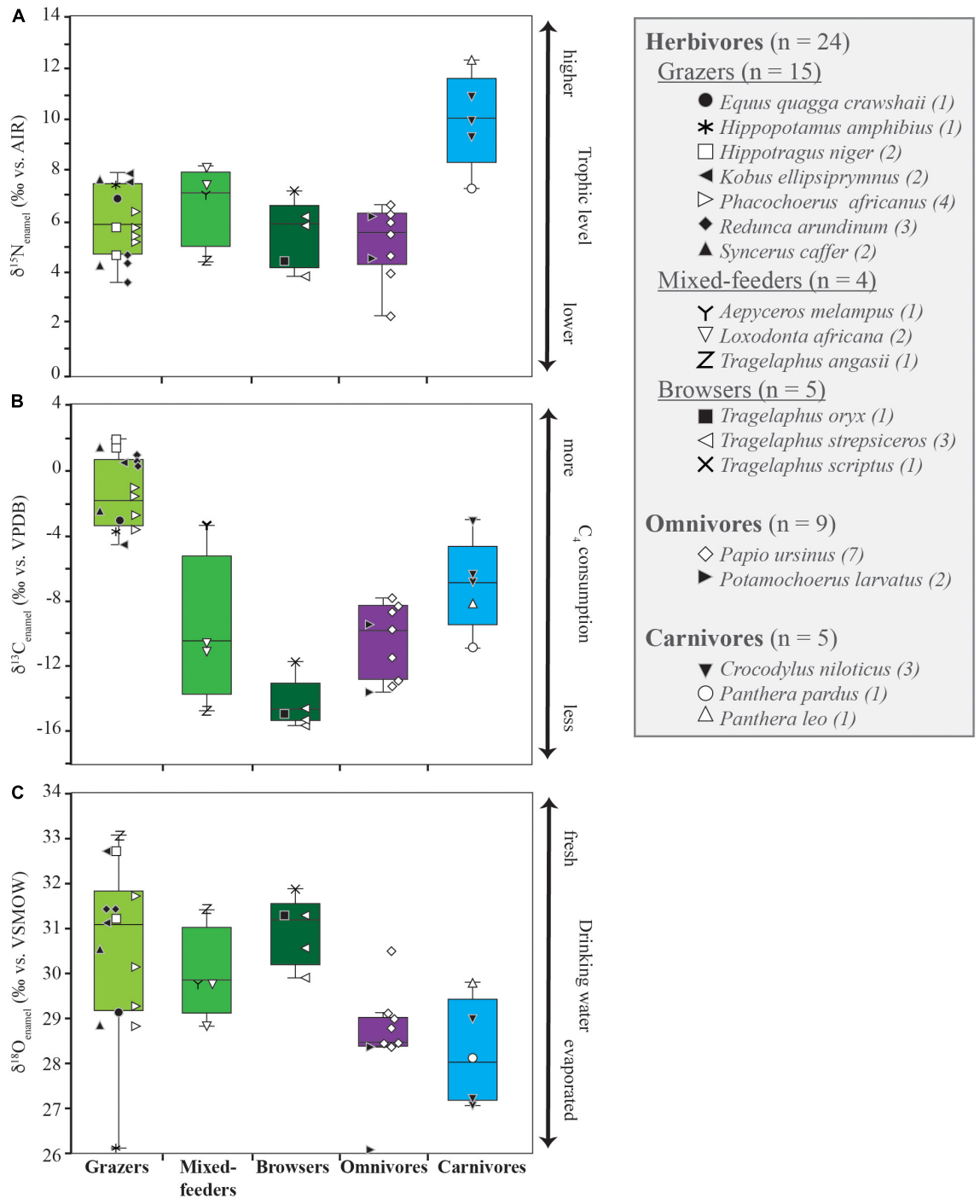

FIGURE 3
$\delta^{15}N_{enamel}$ **(A)**, $\delta^{13}C_{enamel}$ **(B)**, and $\delta^{18}O_{enamel}$ **(C)** values for Gorongosa fauna by diet. Boxplots show the interquartile range (note outliers in omnivore $\delta^{18}O_{enamel}$ dataset), with the median indicated by the solid line. Symbols correspond to individual specimens.

For $\delta^{18}O_{enamel}$ vs $\delta^{15}N_{enamel}$, SEA_C overlap ranged from 0 to 78%, and the Bayesian modes of niche size ranged from 2.2 to 7.2‰^{2} with no statistical differences based on 95% credible intervals (Figure 7C). Isotopic niches were indistinct between grazers and browsers (p = 0.790) and were nearly indistinct between browsers and omnivores (p = 0.048). All other dietary groups were statistically distinct in isotopic space when compared to one another ($p < 0.010$).

For $\delta^{13}C_{enamel}$ vs. $\delta^{18}O_{enamel}$, SEA_C overlap ranged from 0 to 30% (Figure 7E), and the Bayesian modes of niche size

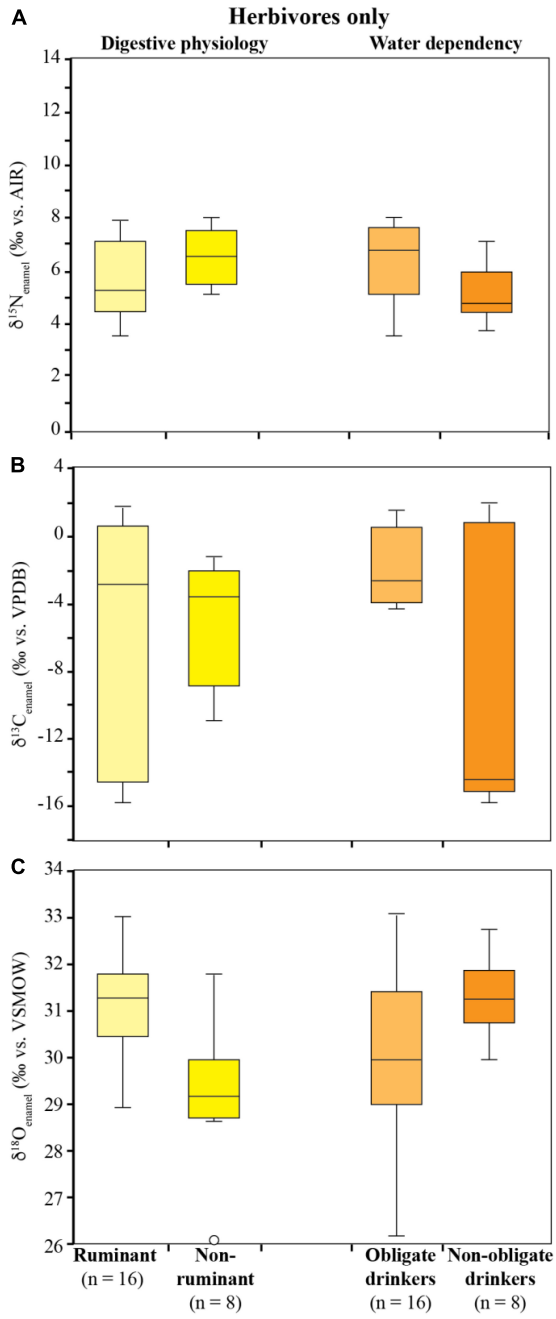

FIGURE 4
$\delta^{15}N_{enamel}$ **(A)**, $\delta^{13}C_{enamel}$ **(B)**, and $\delta^{18}O_{enamel}$ **(C)** values for Gorongosa herbivores grouped by digestive physiology and water dependency. Boxplots show the interquartile range, with the median indicated by solid lines and outliers by open circles. Water dependency after Hamilton (1986), Bothma (2005), Wilson and Mittermeier (2009), and Hempson et al. (2015); see **Supplementary Table 1**.

ranged from 2.4 to 9.1‰[2] with no statistical differences based on 95% credible intervals (**Figure 7F**). All dietary groups were statistically distinct in $\delta^{13}C_{enamel}$ vs $\delta^{18}O_{enamel}$ space when compared to one another ($p < 0.020$).

Sample sizes for some groups analyzed could affect calculated niche values. Small sample sizes (i.e., ∼5) have been shown to underrepresent ellipse area (Jackson et al., 2011) and increase niche size uncertainty (Syväranta et al., 2013), although SEA_C aims to minimize this (Jackson et al., 2011). Increased replication could possibly change the niche overlap, shape, and areas of dietary groups. However, SEA_B accounts for this variability in its credible intervals, and the Turner et al. (2010) analysis of centroid position remains statistically valid.

Discussion

We use stable isotope values in the tooth enamel of modern fauna living in and around GNP to (a) understand food web dynamics and dietary behavior in this well-constrained faunal community, (b) provide the first test of the suitability of using $\delta^{15}N_{enamel}$ data in a natural ecosystem to reconstruct trophic level, (c) apply a new method for measuring $\delta^{13}C_{enamel}$ and $\delta^{18}O_{enamel}$ of ≤100 μg of tooth enamel, and (d) investigate isotopic niche overlap, size, and separation within and between groups by analyzing the three isotope systems ($\delta^{13}C_{enamel}$, $\delta^{15}N_{enamel}$, and $\delta^{18}O_{enamel}$).

Reconstructing trophic levels using $\delta^{15}N_{enamel}$

Gorongosa carnivores have an average of 4.0‰ higher $\delta^{15}N_{enamel}$ values and occupy distinct isotopic niche space compared to herbivores (**Figures 3**, **7**). This trophic enrichment agrees well with a documented 3–5‰ increase in $\delta^{15}N$ between diet and consumer reported by numerous large-scale ecological studies using other biological tissues (e.g., Schoeninger and DeNiro, 1984; Bocherens and Drucker, 2003; Caut et al., 2009). These results clearly show that $\delta^{15}N_{enamel}$ values obtained with the "*oxidation-denitrification method*" reflect expected patterns in natural settings and have great potential for reconstructing (paleo)food webs.

Herbivore $\delta^{15}N_{enamel}$

In our dataset, herbivore $\delta^{15}N_{enamel}$ values vary by 4.3‰, with values ranging from 3.8 to 8.1‰ (**Figure 3A**). Similar variability has been reported for herbivores in studies using bone collagen and is believed to be related to differences in feeding strategies (e.g., grazing vs. browsing), digestive physiology (e.g., ruminant vs. non-ruminant), the nutritional value of the consumed plant material (e.g., low vs. high protein content), foraging habitat (e.g., savanna vs. forest) (Ambrose, 1991; Robbins et al., 2005), and location (Leichliter et al., 2022). However, we do not observe any significant differences in $\delta^{15}N_{enamel}$ between herbivores grouped according to grazing,

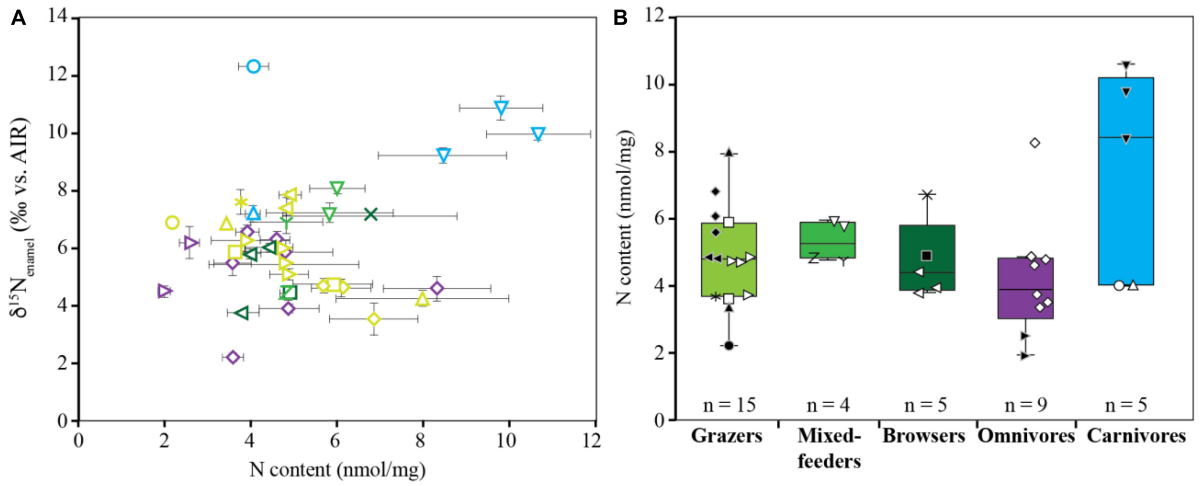

FIGURE 5
Biplot of $\delta^{15}N_{enamel}$ values vs. N content of modern tooth enamel from GNP fauna **(A)** and N content grouped according to diet **(B)**. For taxon-specific symbols, refer to **Figures 2**, **3**.

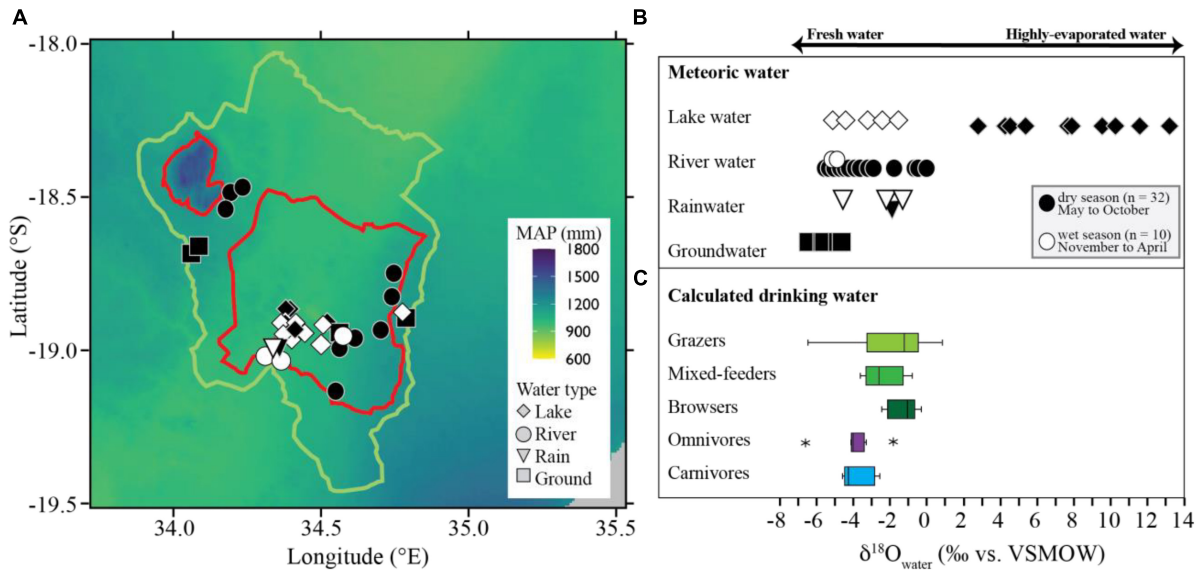

FIGURE 6
Map of mean annual precipitation (MAP) for Gorongosa National Park (red line), Buffer Zone (green line), and the surrounding region indicating the locations of water sampling sites included in this study **(A)**. Mean annual precipitation data were generated using WorldClim version 2.1 bioclimatic variables (1970–2000) at a resolution of ~1 km^2 (Fick and Hijmans, 2017). $\delta^{18}O_{water}$ values of meteoric water sampled in and around GNP during the dry (open symbols) and wet (closed symbols) seasons from 2016 to 2019 **(B)**. Colored boxplots show the range of possible drinking water for each dietary group when bioapatite $\delta^{18}O_{enamel}$ to is converted to $\delta^{18}O_{water}$ (after Kohn and Cerling, 2002); stars indicate outliers **(C)**.

browsing, or mixed-feeding (**Figure 3A**), ruminant vs. non-ruminant, or water dependency (**Figure 4A**).

These results suggest that local variation in plant $\delta^{15}N$ values (likely associated with variation in soil $\delta^{15}N$) appears to be the principal mechanism influencing herbivore $\delta^{15}N$ values. The observed 4.3‰ variation in $\delta^{15}N_{enamel}$ within the herbivore trophic level agrees well with the reported 4‰ baseline variation in $\delta^{15}N$ of savanna plants from different microhabitats of Kruger National Park in South Africa (Codron et al., 2005). This dry savanna biome lies ca. 650 km southwest of GNP and is similar in size to GNP and its Buffer Zone. In Kruger, some deciduous trees (e.g., *Cassia abbreviate*) and tussock-forming grasses (e.g., *Heteropogon contortus* and *Themeda triandra*) have low $\delta^{15}N$ values (≤1.5‰), while other trees (e.g., *Ficus*

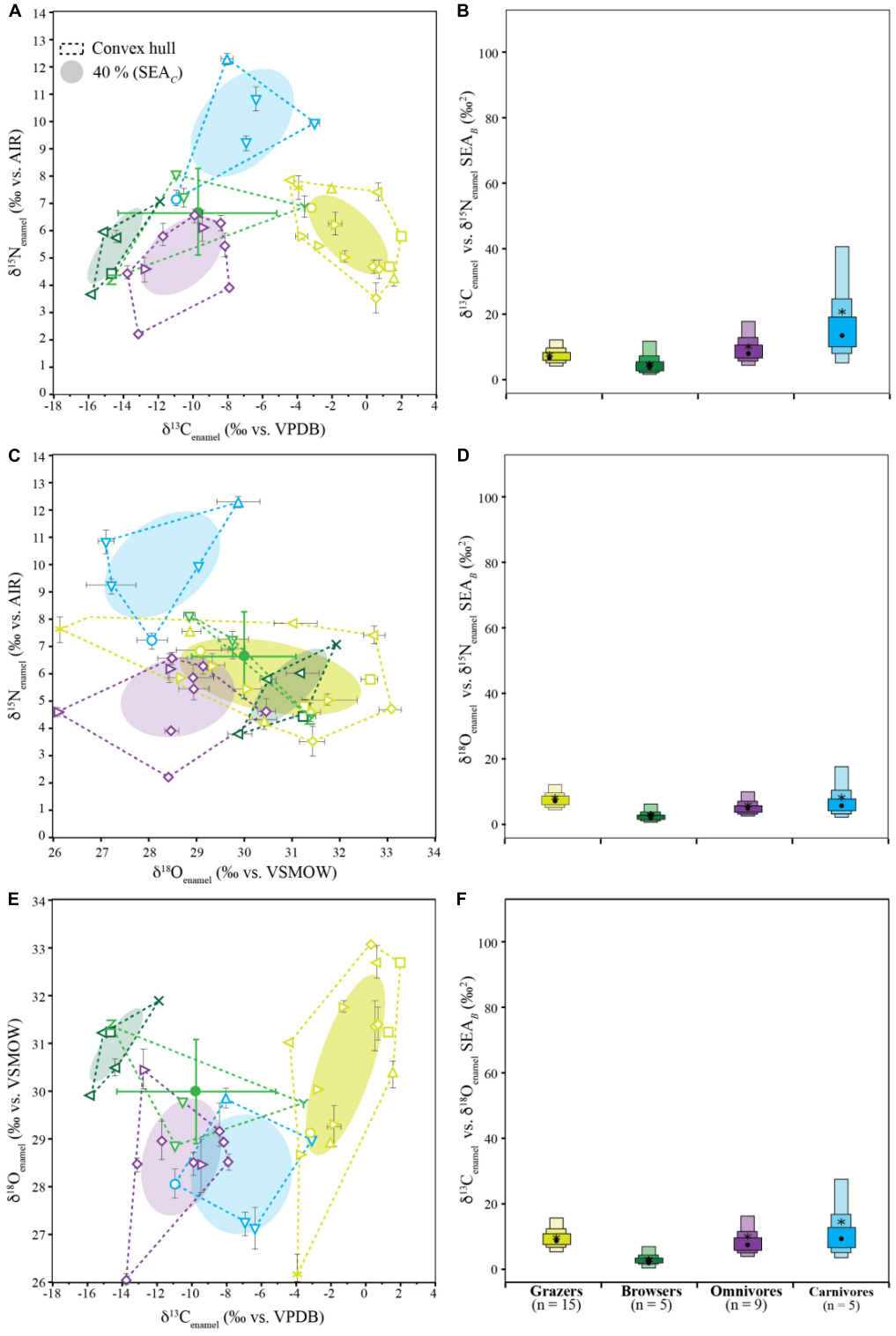

FIGURE 7
Biplots **(A,C,E)** and calculated SEA_B boxplots **(B,D,F)** for $\delta^{13}C_{enamel}$ vs. $\delta^{15}N_{enamel}$ **(A,B)**, $\delta^{18}O_{enamel}$ vs. $\delta^{15}N_{enamel}$ **(C,D)**, and $\delta^{13}C_{enamel}$ vs. $\delta^{18}O_{enamel}$ **(E,F)**. Biplots show raw isotope values with 1σ standard deviation, convex hulls encompass the full variation in the data, and ellipses indicate 40% estimated SEA_C for Gorongosa fauna grouped by diet (light green: grazers; bright green: mixed-feeders; dark green: browsers; purple: omnivores; blue: carnivores; for taxon-specific symbols refer to **Figure 2**). Boxplots show the variability of SEA_B, with 50, 75, and 95% credible intervals represented by light, medium, and dark colored boxes, respectively. Black dots are the SEA_B mode and stars are the calculated SEA_C, which correspond to biplot ellipses. Box plots and SEA_C of mixed-feeders are not shown due to their small sample size (n = 4) instead, their mean values and 1σ standard deviation are given (green cycle with error bar).

sycomorus, Grewia sp., and *Ziziphus mucronate*) and grasses (e.g., *Dactyloctenium australe*) have much higher $\delta^{15}N$ values (>5.0‰). All these plant taxa are present in GNP and, therefore, available as a food resource for the studied herbivores. Different ungulate individuals occupy different habitats within GNP (e.g., floodplain vs. savanna), where they are observed to eat radically different diets (Becker et al., 2021), and therefore possibly consume plants with varying nitrogen isotope values.

Therefore, the large variety of herbivore $\delta^{15}N_{enamel}$ is expected and probably reflects variations in plant $\delta^{15}N$ values in GNP with its diverse microhabitats, soil types, plant taxa, and water availability, even if faunal migration ranges are relatively small (Stalmans and Beilfuss, 2008).

Omnivore $\delta^{15}N_{enamel}$

The $\delta^{15}N_{enamel}$ values for omnivores are significantly different from those of carnivores, but not herbivores (**Figure 3A** and **Table 1**). Our omnivore dataset includes seven baboons (*Papio ursinus* with genetic variants of *P. cynocephalus*, Santander et al., 2022) and two bushpigs (*Potamochoerus larvatus*); the two taxa are indistinguishable in their $\delta^{15}N_{enamel}$ values.

Plant material consumed by baboons mainly consists of specific plant parts such as fruits, drupes, tubers, and other underground materials, depending on the habitat and foraging season (Nowak, 1999). The baboons sampled for this study have $\delta^{15}N_{enamel}$ values between 2.2 and 6.6‰, a large range of variation in $\delta^{15}N_{enamel}$ despite the fact that six of the seven specimens were collected within a small geographic area (0.6 km^2) of open C_4 grasslands with some isolated acacia trees and could possibly have even belonged to the same troop (**Figure 2** and **Supplementary Table 2**). This large intra-taxon variation indicates a diverse and flexible diet and possibly distinct individual dietary preferences.

Baboons and bushpigs are omnivorous generalists, their diet often consisting of up to 30% of animal resources (e.g., insects, small mammals, small reptiles, eggs, and nestlings). GNP baboons have been observed to consume mussels and snails, as well as to hunt small mammals (e.g., warthog, reedbuck or bushbuck infants, and ducklings) on rare occasions, usually during the birthing season (L. Lewis-Bevan, *personal communication*). However, only adults (usually dominant males) have been directly observed consuming meat, although high-ranking adult females occasionally consume scraps discarded by the males. Young, low-ranking troop members, however, whose teeth are still mineralizing, rarely have access to these protein-rich resources before vultures claim leftovers. The teeth sampled for this study would have formed during this juvenile period, which likely explains the low $\delta^{15}N_{enamel}$ values observed for the GNP baboons. Moreover, while occasional meat consumption should increase omnivore $\delta^{15}N_{enamel}$ values, available data on bone collagen and fecal samples show that chacma baboons tend to have low $\delta^{15}N$ values compared to sympatric herbivores (Ambrose and DeNiro, 1986; Codron et al., 2006). This pattern is possibly related to the consumption of N_2-fixing plants, underground storage organs, fruits, roots, and termites, all of which have relatively low $\delta^{15}N$ values (Codron et al., 2005, 2007).

Despite the fact that the two sampled bushpigs (*Potamochoerus larvatus*) were found over 120 km apart, they have similar $\delta^{15}N_{enamel}$ values, which are comparable to those of the baboons (**Figure 3A**). While baboons are not observed to scavenge, bushpigs do eat carrion, and their opportunistic diet includes roots, crops, bulbs, insects, and fallen fruit (e.g., discarded by baboons; Ghiglieri et al., 2008).

Carnivore $\delta^{15}N_{enamel}$

Carnivore $\delta^{15}N_{enamel}$ values are significantly higher than the values of the other dietary groups ($p < 0.001$; **Figure 3A**). Compared to their potential prey the GNP carnivores had, on average 4.0‰ higher $\delta^{15}N_{enamel}$ values. This trophic enrichment falls well within the expected range of 3–5‰ between trophic levels (**Figure 1**). While our carnivore dataset is small, niche separation between carnivore taxa is observed. The lion (*Panthera leo*) has the highest $\delta^{15}N_{enamel}$ value (12.3‰) recorded in the GNP dataset, indicating that it fed on prey with high $\delta^{15}N_{enamel}$ values. In contrast, the only other felid, a single leopard (*Panthera pardus*), has the lowest $\delta^{15}N_{enamel}$ value of all the carnivores and is the only individual that overlaps with herbivores (but not omnivores). Its $\delta^{15}N_{enamel}$ value of 7.2‰ is several permil lower than the other analyzed carnivores. $\delta^{15}N_{enamel}$ values lower than coexisting carnivores have also been reported from two leopards from Angola (Leichliter et al., 2022). This is probably the result of different habitat use and prey preference, which is also apparent in the leopard's more negative $\delta^{13}C_{enamel}$ values compared to the GNP lion and crocodiles (refer to $\delta^{13}C_{enamel}$ section; **Figure 3B**). Accordingly, our bulk $\delta^{15}N_{enamel}$ data possibly reflect a time in the animal's life where it fed on prey with low $\delta^{15}N$ tissue values.

Only one apex predator, the Nile crocodile (*Crocodylus niloticus*), sustains a stable population in GNP (Stalmans et al., 2014). In this study, only fully grown *C. niloticus* were sampled, as physiological and ontogenetic factors such as body size can influence their $\delta^{15}N$ values (Villamarin et al., 2018). GNP crocodiles are reported to be highly generalized predators, feeding on carnivorous and herbivorous fish species (i.e., Siluriformes) as well as mammalian prey (Wilson, 2014). However, crocodilians which consume a large variety of prey from tropical coastal floodplains derive the majority of their nutrition from the consumption of (occasional) terrestrial prey (Adame et al., 2018). Thus, while the aquatic prey consumed by GNP crocodiles may influence the $\delta^{15}N$ values of the crocodiles to some degree (these resources derive from the aquatic food chain with a possibly different N isotope baseline), the nitrogen isotope values of the crocodilians should reflect mostly their terrestrial prey. The GNP crocodilian's $\delta^{15}N_{enamel}$ values fall well

between those of the two felids, suggesting that both groups share isotopic niche space.

We analyzed all carnivore specimens available from GNP at the time of this study. The lion died naturally within the park's boundaries (**Figure 1**) and the leopard was poached within the Buffer Zone (the body was later confiscated by park rangers, exact coordinates were not reported). Planned analyses will incorporate additional GNP predators as well as aquatic resources for their isotopic composition once they become available, to fully understand the observed patterns. However, even our small dataset shows promising results from an ecological perspective, and more importantly, shows expected $\delta^{15}N$ patterns in enamel.

Nitrogen contents in tooth enamel

Nitrogen contents of mammalian tooth enamel from GNP fauna have a relatively small range (2.0–8.3 nmol/mg) and do not show any correlation with $\delta^{15}N_{enamel}$. Moreover, N contents are remarkably similar across different individuals and dietary groups (p = 0.357) and are in good agreement with those previously reported for rodents in a controlled feeding experiment (Leichliter et al., 2021) and other mammals from different sites across Africa (Leichliter et al., 2022). These findings suggest that mammalian tooth enamel N content is relatively consistent regardless of feeding strategy.

Interestingly, the nitrogen content of crocodile tooth enamel is, on average, nearly 5 nmol/mg higher than any of the mammalian taxa [9.6 ± 1.1 nmol/mg for crocodiles (n = 3) vs. 4.7 ± 1.4 nmol/mg for mammalians (n = 35); **Figure 5** and **Table 1**]. While the structure of reptilian enamel is reported to be generally similar to mammalian enamel (Dauphin and Williams, 2008), we were unable to find any information regarding the N content of reptilian tooth enamel. Our results suggest that reptilian tooth enamel contains more nitrogen than mammalian tooth enamel, possibly as the result of differences in their respective physiology or mineralization mechanisms. We considered the possibility that the higher N content of the reptilian specimens was caused by contamination with dentin during sampling. Measurements of dentin N content of in-house standard AG-Lox (n = 3) indicate that the nitrogen content is substantially lower in dentin than in enamel after the reductive-oxidative cleaning (**Supplementary Table 9**). This is not surprising because dentin has a lower proportion of mineral-bound organic material that can survive the cleaning treatment. Therefore, possible contamination with dentin cannot be the cause of the elevated N contents of the analyzed crocodile enamel.

Overall, the fact that mammalian tooth enamel N content is relatively consistent and is not correlated with $\delta^{15}N_{enamel}$ suggests that N content could be used in paleodietary studies as a diagnostic tool to asses potential signs of diagenetic alteration or contamination by exogenous organic N, as it has been suggested for invertebrate organisms, such as foraminifera and corals (Ren et al., 2009; Straub et al., 2013; Martinez-Garcia et al., 2014; Ren et al., 2017; Wang et al., 2017; Kast et al., 2019, Auderset et al., 2022).

Reconstructing plant-based diet using $\delta^{13}C_{enamel}$

Our $\delta^{13}C_{enamel}$ data reflects the niche partitioning that is present between taxa feeding on different plants, and animals consuming prey with different feeding strategies (**Figures 3B**, **7**).

Herbivore $\delta^{13}C_{enamel}$

Herbivore $\delta^{13}C_{enamel}$ data from GNP indicate a wide range of foraging strategies, including mixed-feeders, browsers, and grazers (**Figure 3B**), reflecting the wide range of ecosystems present in the park (**Figure 2**).

Within the GNP herbivores, browsers have $\delta^{13}C_{enamel}$ values of –11.8‰ to –15.8‰, reflecting diets consisting almost exclusively of C_3 plants (≥93%; calculated after Cerling et al., 2011). Most grazers, in contrast, have $\delta^{13}C_{enamel}$ values > –2‰ which reflect at least 70% of C_4 consumption. Three individuals are hypergrazers with >95% C_4 grass consumption (one buffalo and two sable antelopes). However, five individuals (two warthogs and one zebra, waterbuck, and hippo) that are typically considered to be grazing species have somewhat low $\delta^{13}C_{enamel}$ value (–2.7‰ to –4.3‰), reflecting up to 45% of C_3 intake (refer to **Figure 3B**). This unusually high C_3 consumption may be the result of grazing on C_3 grasses (*Oryza longistaminata*), which grow in the floodplain grasslands near Lake Urema, or feeding on forbs and other C_3 understory vegetation. For example, hippos are reported to feed on *Oryza* (Noirard et al., 2008), and we observed warthogs in GNP digging up the underground rhizomes of *Oryza* and sedges.

Mixed-feeders usually have a diet of >30% C_4 grass and >30% C_3 browse, resulting in $\delta^{13}C_{enamel}$ values between –2‰ and –8‰. In the GNP dataset, only the impala (*Aepyceros melampus*) has a mixed-feeder $\delta^{13}C_{enamel}$ value (**Figure 3B**). Impalas are known to exhibit dietary flexibility and rely on browse in some areas and graze in others, sometimes on a seasonal basis which can result in a large range of $\delta^{13}C_{enamel}$ values (Monro, 1980; Sponheimer et al., 2003). The single impala specimen from GNP has a $\delta^{13}C_{enamel}$ value of –3.6‰ corresponding to ca. 37% C_3 consumption. In contrast, the analyzed nyala (*Tragelaphus angasii*) and the two elephants (*Loxodonta africana*) primarily browsed (≥85% C_3 biomass). African elephants are also mixed-feeding generalists, but with a diet that consists largely of C_3 browse (Codron et al., 2012), agreeing well with our data. Gorongosa elephants have been regularly observed raiding nutritious crops (e.g., fruits, maize,

and tubers) in the Buffer Zone when the quality and abundance of natural forages are low within the park (Branco et al., 2019b). The majority of these crops are C_3 plants (e.g., banana, tomato, papaya, peas, sweet potato, pumpkin, and sorghum; Sage and Zhu, 2011); only maize and sugar cane are C_4. Hence, crop raiding probably contributed to the low $\delta^{13}C_{enamel}$ values observed for the elephants.

Herbivore $\delta^{13}C_{enamel}$ values do not differ when grouped by digestive physiology (**Figure 4B**), as ruminants include bovids with diverse feeding behaviors (grazers, mixed-feeders, and browsers) and have a large range in $\delta^{13}C_{enamel}$ values which overlap with the non-ruminants. In our dataset, the non-ruminants are mostly grazers with high $\delta^{13}C_{enamel}$ values, but also include elephants that ate C_3 plants. Obligate drinkers have statistically higher $\delta^{13}C_{enamel}$ values compared to non-obligate drinkers, likely reflecting the higher water content of browse compared to graze (i.e., mostly C_4 grasses) which must be supplemented with drinking water.

Overall, $\delta^{13}C_{enamel}$ data reflects the diversity of GNP habitats, providing niches for herbivores with different feeding behaviors, ranging from hyperbrowsers to hypergrazers.

Omnivore $\delta^{13}C_{enamel}$

Omnivore $\delta^{13}C_{enamel}$ values (−13.7 to −8.2‰) indicate a predominantly C_3 diet for Gorongosa baboons and bushpigs (**Figure 3B**). Grasses and other C_4-based foods comprise less than a third of the bulk diet of all sampled individuals, and three individuals (two primates and one suid) consumed an exclusively C_3 diet (**Figure 3C** and **Supplementary Table 1**). One of the bushpigs, which are typically forest-dwelling, was collected in a C_4-dominated grassland (*Digitaria swaziensis;* **Supplementary Table 1**), yet its low $\delta^{13}C_{enamel}$ value (−13.7‰) reflects pure browsing, suggesting that dietary preference rather than the locally dominant vegetation drove the feeding behavior in this individual. Overall, our findings are consistent with previously published $\delta^{13}C$ data for baboons and bushpigs which also indicate a diet consisting largely of C_3 foods (e.g., Ambrose and DeNiro, 1986; Thackeray et al., 1996; Codron et al., 2006; Venter and Kalule-Sabiti, 2016 and references therein).

Carnivore $\delta^{13}C_{enamel}$

Few studies have investigated the $\delta^{13}C$ (or $\delta^{18}O$) ecology of carnivores in Africa (Codron et al., 2007, 2016, 2018; Voigt et al., 2018; Hopley et al., 2022), which makes interpretation of the GNP dataset challenging. The GNP carnivores have $\delta^{13}C_{enamel}$ values which fall between those of herbivores and omnivores, indicating that grazers, browsers, mixed-feeders, and/or omnivores were all potentially consumed (**Figure 3B**). The three crocodiles have the highest $\delta^{13}C_{enamel}$ values (between −6.9‰ and −3.1‰), which could be the result of the consumption of aquatic resources, or grazers and mixed-feeders, while the single leopard individual's low $\delta^{13}C_{enamel}$ value (−11.0‰) indicates that it was feeding almost exclusively on browsing taxa. The lion's higher $\delta^{13}C_{enamel}$ (−8.1‰) indicates that this individual preyed on more grazers compared to the leopard. According to field observations (Bouley et al., 2018), waterbuck ($\delta^{13}C_{enamel}$ = −4.3 to 0.6‰) make up ca. 60% of the prey biomass consumed by Gorongosa's lions. The lion's intermediate $\delta^{13}C_{enamel}$ value indicates that it must have also consumed some prey with lower $\delta^{13}C$ values such as browsers (e.g., kudu, eland, and bushbuck) or mixed-feeders with a C_3-dominated diet (e.g., nyala). The specimen for this study was collected in the tall-grass margins that border the savanna woodlands, which is a preferred hunting habitat for lions as it provides access to abundant grazing, browsing, and mixed-feeding prey. The lion's $\delta^{13}C_{enamel}$ is nearly 3‰ higher than that of the leopard, indicating that it focused more on grazing prey while the leopard consumed more browsers. A similar difference in $\delta^{13}C_{enamel}$ between leopard and lion is observed in a modern felid dataset from Turkana Basin (Kenya; Hopley et al., 2022).

Reconstructing drinking behavior using $\delta^{18}O_{enamel}$ and $\delta^{18}O_{water}$

$\delta^{18}O_{water}$ of meteoric water sampled between 2016 and 2019 within GNP agree well with data reported from meteoric water stations of the Global Network of Isotopes (GNI) in Precipitation (sampled in Chitengo in 2010 to 2011; IAEA/WISER, 2020a) and GNI in Rivers (Pungwe River in 2009; IAEA/WISER, 2020b). Moreover, data fall on the Local Meteoric Water Line (LMWL) and Local Evaporation Line (LEL) established with $\delta^{18}O_{water}$ and deuterium ($\delta^{2}H_{water}$) data of samples from springs, boreholes, river, and Lake Urema taken in the Urema catchment in the period 2006–2010 (Steinbruch and Weise, 2014). Note that the $\delta^{2}H_{water}$ values are reported in **Supplementary Table 2** but are not discussed in this study.

$\delta^{18}O_{water}$ of available drinking water reported in this study has a range of >20‰ (**Figure 6**), and varies much more than the $\delta^{18}O_{enamel}$ values measured for the fauna (i.e., ∼7‰, **Figure 3C**). After converting bioapatite $\delta^{18}O_{enamel}$ to $\delta^{18}O_{water}$ (using equations by Kohn and Cerling, 2002), the measured range of 26.0 to 33.1‰ in $\delta^{18}O_{enamel}$ translates into the intake of water with $\delta^{18}O_{water}$ values between −6.6‰ and 1.0‰, which falls, with the exception of a hippo and a baboon specimen, in low to medium range of measured meteoric waters (−6.2 to 13.1‰; **Figure 6**). This indicates that the animals in this study consumed primarily fresh water that was only moderately influenced by evaporative enrichment. Time-averaging of temporal signals during the progressive mineralization of tooth enamel could dampen the variation in $\delta^{18}O_{water}$ ingested by a single individual through time (i.e., information about seasonal variability of the drinking water is lost).

Meteoric water $\delta^{18}O_{water}$

Potentially available drinking water for animals living in GNP overlaps greatly in their $\delta^{18}O_{water}$ values and falls generally between −6.2 and 0.8‰, with the exception of dry season lake waters, which range from 2.9‰ up to 13.1‰ (**Figure 6**). Therefore, dry season lake water displays significantly higher $\delta^{18}O_{water}$ values, compared to all other types of water ($p < 0.001$; there is no overlap with other $\delta^{18}O_{water}$ datasets; **Figure 6**). During the dry season, standing water in lakes or ponds is most strongly influenced by evaporation (Clark and Fritz, 1997; Kendall and McDonnell, 1998). $\delta^{18}O_{water}$ of rainwater sampled during the wet season and rain samples were taken from the end of the dry season overlap. This agrees well with previously published isotope data from Gorongosa meteoric waters, which indicate that wet season rainfall was formed over the Indian Ocean without undergoing major fractionation, while dry season rainfall comes partly from the same source, and also indicates locally evaporated or recycled waters from the floodplains of the Urema Graben (Steinbruch and Weise, 2014).

Herbivore $\delta^{18}O_{enamel}$

With a mean of 30.6 ± 1.6‰ (n = 24) herbivores have the highest $\delta^{18}O_{enamel}$ values compared to other dietary groups (**Figure 3C**), but no differences are observed for browsing, mixed-feeding, or grazing taxa, indicating similar drinking behaviors, from a mix of sources, among these groups. Ranging from 26.2 to 33.1‰, $\delta^{18}O_{enamel}$ values of grazers have the largest spread of any dietary group. In herbivores, ruminants have significantly higher $\delta^{18}O_{enamel}$ values compared to non-ruminants, but obligate drinkers do not have significantly different $\delta^{18}O_{enamel}$ values compared to non-obligate drinkers (**Figure 4C**). This indicates that animals had regular access to fresh water that has experienced only limited evaporation, or to leaf water and/or parts of plants that are not affected much by evaporation (e.g., stems, roots, bark, and fruits) in mesic environments.

No significant correlation was observed between $\delta^{13}C_{enamel}$ and $\delta^{18}O_{enamel}$ for most groups; however, a strong and significant positive relationship exists between $\delta^{13}C_{enamel}$ and $\delta^{18}O_{enamel}$ in grazers and obligate drinkers (r = 0.700; p = 0.004 for grazers; r = 0.493; p = 0.052 for obligate drinkers), indicating increased intake of ^{18}O-depleted water (e.g., from Lake Urema or waterholes) associated with greater C_4 plant consumption (e.g., grasses from the floodplain) for these groups.

Omnivore $\delta^{18}O_{enamel}$

Omnivore $\delta^{18}O_{enamel}$ values are significantly lower than those of herbivores but overlap with those of carnivores. The two bushpigs show slightly lower $\delta^{18}O_{enamel}$ values compared to the seven baboons. As obligate drinkers, both $\delta^{18}O_{enamel}$ values in both taxa reflect the oxygen isotope composition of local meteoric waters as expected (Moritz et al., 2012; Steinbruch and Weise, 2014). Their relatively low $\delta^{18}O_{enamel}$ values point toward a regular recharge of their body water by drinking from meteoric sources which are only moderately influenced by evaporation (Fricke and O'Neil, 1996; Levin et al., 2006; Blumenthal et al., 2017), limited intake of evaporated plant tissues or animal fats (refer to nitrogen section; Crowley, 2012; Nelson, 2013; Carter and Bradbury, 2016), and little sweating or panting (thermoregulatory processes which induce evaporative fractionation; Kohn et al., 1996; Sponheimer and Lee-Thorp, 1999).

Carnivore $\delta^{18}O_{enamel}$

Studies about the water requirements of African savanna carnivores are rare and observations of drinking behavior in Gorongosa's felids are anecdotal; thus, oxygen stable isotope data can provide valuable additional information regarding water intake in predators.

Most African felids have low water needs and receive their moisture from the metabolic water of their prey (Bothma and Walker, 2013), but drink water from waterholes when it is available (Wilson and Mittermeier, 2009; Hayward and Hayward, 2012). Through this intake of prey body fluids and standing water, $\delta^{18}O_{enamel}$ data of lions and leopards from eastern Africa are strongly influenced by local meteoric $\delta^{18}O_{water}$, similar to what has been documented for herbivores (Kohn, 1996; Hopley et al., 2022). Gorongosa carnivores have, on average, ca. 2‰ lower $\delta^{18}O_{enamel}$ values compared to their prey (**Figure 3C**), and therefore relatively low calculated $\delta^{18}O_{drinking-water}$. This suggests that the GNP carnivores had access to freshwater and drank regularly. While the lion's $\delta^{18}O_{enamel}$ value overlaps with those of the herbivores, the leopard's does not, possibly indicating that the leopard consumed more fresh river water rather than evaporated lake water.

A rough linear correlation is reported between the oxygen isotopic ratios of crocodiles' phosphate tooth enamel and ambient water which is influenced by mean air temperature, diet, and physiology (Amiot et al., 2007). GNP crocodile carbonate $\delta^{18}O_{enamel}$ values are generally low, indicating that the sampled individuals lived in relatively fresh water that was rarely influenced by evaporation.

Isotopic niches and inferred ecology from paired $\delta^{13}C_{enamel}$, $\delta^{15}N_{enamel}$, and $\delta^{18}O_{enamel}$ data

Traditionally, paired carbon and nitrogen isotope values are analyzed in ecological studies to reconstruct isotopic niches and infer some trophic information (Newsome et al., 2007). Until recently, this type of reconstruction using tooth enamel has not been possible due to the methodological limitations of measuring $\delta^{15}N_{enamel}$ (Leichliter et al., 2021). This study is the first to combine nitrogen, carbon, and oxygen stable

isotope values obtained from diagenetically robust tooth enamel, permitting ecological interpretations based on the combination of these three isotopes. We compare the different pairs of isotope values ($\delta^{13}C_{enamel}$-$\delta^{15}N_{enamel}$, $\delta^{15}N_{enamel}$-$\delta^{18}O_{enamel}$, and $\delta^{13}C_{enamel}$-$\delta^{18}O_{enamel}$; **Figure 7**) to investigate niche overlap, size, and separation within and between dietary groups of modern fauna from GNP. Isotopic niches calculated in this way can be used to infer information about trophic ecology and resources used by determined groups (Layman et al., 2007; Newsome et al., 2007; Layman and Allgeier, 2012). Given the small sample size of the mixed-feeder (n = 4; not included in niche analysis), browser (n = 5), and carnivore (n = 5) groups, we consider our statistical conclusions to be preliminary but promising. Our isotopic niche results are best interpreted as (1) relative but not absolute values for niche overlap; (2) SEA_B is variable and increased sample size would likely decrease the uncertainty around the estimates and lead to a more robust analysis resolving potential size differences, but generalities are valid; and (3) unique locations in isotopic space are statistically accurate, and small changes to niche size from additional sampling would likely not move centroids enough to effect centroid distance. Additional Bayesian analyses are becoming increasingly popular in ecological studies and could also be included in future multi-isotope tooth enamel studies if sample sizes are increased. For example, 3-dimensional isotopic analysis using SIBER has proven useful for determining isotopic niches of complex trophic systems such as coral reef atolls (Cybulski et al., 2022), and other analyses such as nicheROVER allow for incorporation of additional dimensions of isotopes or other continuous ecological indicators (Swanson et al., 2015). Even with uncertainties, isotopic investigations coupled with Bayesian statistics have significant implications for future (paleo)ecological reconstructions.

In the GNP fauna, the niches of different dietary groups are completely distinct in $\delta^{13}C_{enamel}$-$\delta^{15}N_{enamel}$ space (**Figure 7A**), with no SEA_C overlap between any dietary groups (**Supplementary Table 6**). Thus, animals with these diets can be classified into distinct isotopic niches based on their carbon and nitrogen isotope values in our dataset. Although we cannot quantify the niche of the mixed-feeders due to limited sampling, we can explore potential overlap with other groups. For example, even with only four samples, mixed-feeders convex-hull overlaps with the omnivores niche in $\delta^{13}C_{enamel}$-$\delta^{15}N_{enamel}$ space. This overlap would be expected, as it occurs around typical $\delta^{13}C_{enamel}$ values for C_3 dominated diets (Cerling et al., 2003), on which GNP omnivores and some of the analyzed mixed-feeders (nyala and elephants) rely (**Figure 3B** and **Supplementary Table 1**). We would expect that even with additional sampling, isotopic niche overlap between these two groups would remain.

$\delta^{18}O$ data are not frequently used in ecological studies; however, some research has shown that $\delta^{18}O$ can complement the information provided by carbon and nitrogen (e.g., Crowley et al., 2015; Roberts, 2017). Gorongosa grazers exhibit a wide range of $\delta^{18}O_{enamel}$ values and share $\delta^{15}N_{enamel}$-$\delta^{18}O_{enamel}$ niche space with browsers (**Figures 7B,E**). Omnivores tend to have lower $\delta^{18}O_{enamel}$ values and only overlap slightly with grazers in $\delta^{15}N_{enamel}$-$\delta^{18}O_{enamel}$ niche space. Due to the trophic enrichment in $\delta^{15}N_{enamel}$ and relatively low $\delta^{18}O_{enamel}$ values, carnivores do not overlap with any other group in $\delta^{15}N_{enamel}$-$\delta^{18}O_{enamel}$ space. This shows that animals with a plant-dominated diet (i.e., herbivores and omnivores) cannot be distinguished in $\delta^{15}N_{enamel}$-$\delta^{18}O_{enamel}$ alone. In contrast, carnivores with their specialized diet occupy a distinct isotopic space and can be clearly distinguished from other groups, even though terrestrial mammalian and aquatic reptilian carnivores were combined in this group. While $\delta^{15}N_{enamel}$ vs. $\delta^{18}O_{enamel}$ comparisons can potentially reveal isotope niche distinction between some dietary groups, niche separation is mostly driven by trophic elevation in $\delta^{15}N_{enamel}$ in this dataset.

In $\delta^{13}C_{enamel}$–$\delta^{18}O_{enamel}$ space (**Figure 7C**), the SEA_C of the grazers and browsers are well separated, while omnivores and carnivores overlap by 20–30%. The convex hull of the four sampled mixed-feeders overlaps with all isotopic niches except the grazers, indicating that further sampling may lead to significant niche overlaps. In the $\delta^{13}C_{enamel}$ vs. $\delta^{18}O_{enamel}$ biplot, most of the dietary information is derived from carbon. The small trophic enrichment of 1% sometimes observed in $\delta^{13}C$ of tissues (DeNiro and Epstein, 1981; Schoeniger and DeNiro, 1984; Bocherens and Drucker, 2003; O'Connell et al., 2012) is obscured by differences in $\delta^{13}C$ between consumed C_3 and C_4 plants (or prey that consumed those plants; Cerling and Harris, 1999; Hopley et al., 2022), while $\delta^{18}O_{enamel}$ cannot serve as a trophic proxy (but can reveal information about drinking behavior and source waters instead). This shows that there is a minimal ecologically expected organization of isotopic niches without the information gained from $\delta^{15}N_{enamel}$ data.

In conclusion, analysis of combined carbon, nitrogen, and oxygen stable isotope values leads to the isotopic separation of grazers, browsers, omnivores, and carnivores dietary groups, with significant niche overlap of mixed-feeding herbivores with all groups expected upon further sampling. Niche separation is clearest in $\delta^{13}C_{enamel}$-$\delta^{15}N_{enamel}$ space with no overlap between any of the dietary groups. This illustrates the high potential of $\delta^{15}N_{enamel}$ combined with $\delta^{13}C_{enamel}$ and $\delta^{18}O_{enamel}$ measured from a single aliquot of tooth enamel for reconstructing isotopic niches and inferring dietary and trophic information. Carnivores—arguably the most isotopically distinguishable group—provide a useful example of the benefits of this type of combined isotopic approach. Typical and recent studies of trophic behavior using stable isotope data from teeth and/or bone have been limited to $\delta^{13}C$ and $\delta^{18}O$ (e.g., Domingo et al., 2020), though zinc (Bourgon et al., 2020, 2021; McCormack et al., 2021; Jaouen et al., 2022) and calcium (Martin et al., 2015, 2020, 2022) are also used for trophic studies. If we consider only $\delta^{13}C_{enamel}$ vs. $\delta^{18}O_{enamel}$, carnivores would not

occupy a distinct isotopic niche space since they would overlap with omnivores (20%) and with the mixed-feeders convex hull. Ecologically, however, carnivores occupy a distinct dietary niche, as they consume animal resources almost exclusively. In contrast, GNP omnivores (baboons and bushpigs) consume meat only occasionally while mixed-feeders rely exclusively on plant biomass. Thus, carnivores should not overlap with either group unless there is wide variation in baseline $\delta^{15}N$ (refer e.g., Schmidt and Stewart, 2003; Codron et al., 2005). The addition of $\delta^{15}N_{enamel}$ to both $\delta^{13}C_{enamel}$ and $\delta^{18}O_{enamel}$ analysis clearly shows that carnivores do occupy a statistically significant isotopic niche space, with no SEA_C overlap with any other groups' niche.

Conclusion

We present the first stable carbon, nitrogen, and oxygen isotope data from tooth enamel for fauna from GNP. We validate two novel geochemical methods and draw conclusions about the dietary patterns of animals living within this well-constrained and well-studied African ecosystem. While field observations are extremely useful for understanding the dietary ecology of modern fauna, they are very labor intensive, requiring following an individual (or a group of animals) for days or months, or the deployment and evaluation of hours of camera trap footage. Moreover, such studies often only record a snapshot in time (e.g., one single feeding event) rather than capturing long-term behavior. In contrast, our bulk stable isotope data of herbivores (including grazers, mixed-feeders, and browsers), omnivores, and carnivores, reflect $\delta^{13}C$, $\delta^{15}N$, and $\delta^{18}O$ of consumed food and water averaged over the course of tooth enamel mineralization.

Our results generally exhibit robust isotopic patterns and therefore support ecological information about the trophic level, dietary niche, and resource consumption. We show that $\delta^{15}N_{enamel}$ analyzed with the *"oxidation-denitrification method"* records the trophic position of an individual within its local food web. This is evidenced by a trophic enrichment of 4.0‰ between herbivores and carnivores in the GNP dataset. This method applies not only to a wide range of sample-limited ecosystems but also has potential applications in paleoecology. $\delta^{13}C_{enamel}$ analysis using the "*cold trap method*," tailored to measure small sample sizes (down to 50 μg tooth enamel), distinguishes C_3 and/or C_4 biomass consumption, while $\delta^{18}O_{enamel}$ values reflect drinking water.

This first tri-isotope approach conducted on the tooth enamel of fauna from a single, well-constrained ecosystem indicates that combined C, N, and O isotope data analyses permit the separation of grazers, browsers, omnivores, and carnivores according to their isotopic niche, while preliminary analysis of mixed-feeding herbivores indicate that they cannot be clearly distinguished from other groups. This illustrates the high potential of our multi-isotope approach for paleontological applications using diagenetically robust tooth enamel. We plan to apply this novel multi-isotope approach to recently discovered vertebrate fossils from GNP, which represent the only Miocene fossil locality in the southern East African Rift (Habermann et al., 2019; Bobe et al., 2021). Thus, the datasets presented here will serve as an excellent comparison for the interpretation of fossil stable isotope data.

Data availability statement

The original contributions presented in this study are included in the article/**Supplementary material**, further inquiries can be directed to the corresponding authors.

Ethics statement

Ethical review and approval was not required for the animal study because samples were taken from specimens collected after natural death and curated by the faunal bone collection of Gorongosa National Park.

Author contributions

TL and JL: conceptualization and analysis. TL, JL, AF, ND, HV, DS, and AM-G: methodology. RB and SC: Paleo-Primate Project Gorongosa direction. TL, VA, MB, DB, DRB, CC, MF, JH, FM, JM, RB, and SC: fieldwork. JM and RB: curating of PPPG collection. TL, JL, and JC: statistical analysis. TL, JL, and AM-G: writing—original draft. All authors contributed to the article and approved the submitted version.

Funding

This study was funded by the Deutsche Forschungsgemeinschaft (DFG) grant LU 2199/1-1 and Emmy Noether Fellowship LU 2199/2-1 to TL, the Max Planck Society to GH, HV, and AM-G, and the National Geographic Society grants NGS-51478R to TL and JH, NGS-57285R to SC, and NGS-51140R-18 to RB. MF worked under an FCT-funded associate researcher contract (CEECIND/01937/2017), AM-G received funding from DFG grant MA 8270/1-1, and ND from the Paul Crutzen Nobel Prize fellowship of the Max Planck Society. The Paleo-Primate-Project Gorongosa was funded by the Gorongosa Restoration Project, the Leverhulme Trust (Philip Leverhulme Prize 114 to SC); the John Fell Fund, Oxford, and the St Hugh's College, University of Oxford.

Acknowledgments

We are grateful to the Gorongosa Restoration Project and especially Greg Carr for their vital support of the Paleo-Primate Project Gorongosa. Research and export permits were granted by the Direcção Nacional do Património Cultural, Mozambique, with the support of professors H. Madiquida and S. Macamo of Eduardo Mondlane University. We thank the dedicated staff from Gorongosa National Park, the *fiscais*, our students, and colleagues across many institutions who have been very enthusiastic about this project. Special thanks to P. Hammond, L. Lewis-Bevan (University of Oxford), and R. A. Farassi (Universidade Eduardo Mondlane) for first-hand observational data on Gorongosa baboons, and E. W. Negash (George Washington University) for helpful comments on the manuscript. We thank J. Delinger and M. Stalmans for their vital support and assistance with data collection throughout the years. We also thank F. Rubach, S. Brömme, M. Schmitt, B. Hinnenberg (Max Planck Institute for Chemistry, Germany), and U. Treffert (Senckenberg Biodiversity and Climate Research Centre, Frankfurt, Germany) for technical support, and I. Conti-Jerpe (UC Berkley) for the SIBER advice. This manuscript was greatly improved by the thoughtful comments of VB, JR, LK, and the editor.

Conflict of interest

The authors declare that the research was conducted in the absence of any commercial or financial relationships that could be construed as a potential conflict of interest.

Publisher's note

All claims expressed in this article are solely those of the authors and do not necessarily represent those of their affiliated organizations, or those of the publisher, the editors and the reviewers. Any product that may be evaluated in this article, or claim that may be made by its manufacturer, is not guaranteed or endorsed by the publisher.

Supplementary material

The Supplementary Material for this article can be found online at: https://www.frontiersin.org/articles/10.3389/fevo.2022.958032/full#supplementary-material

References

Abou Neel, E. A., Aljabo, A., Strange, A., Ibrahim, S., Coathup, M., Young, A. M., et al. (2016). Demineralization-remineralization dynamics in teeth and bone. *Int. J. Nanomed.* 11, 4743–4763. doi: 10.2147/IJN.S107624

Adame, F., Jardine, T., Fry, B., Valdez, D., Lindner, G., Nadji, J., et al. (2018). Estuarine crocodiles in a tropical coastal floodplain obtain nutrition from terrestrial prey. *PLoS One* 13:e0197159. doi: 10.1371/journal.pone.0197159

Ambrose, S. H. (1986). Stable carbon and nitrogen isotope analysis of human and animal diet in Africa. *J. Hum. Evol.* 15, 707–731. doi: 10.1016/S0047-2484(86)80006-9

Ambrose, S. H. (1991). Effects of diet, climate and physiology on nitrogen isotope abundances in terrestrial foodwebs. *J. Archaeol. Sci.* 18, 293–317. doi: 10.1016/0305-4403(91)90067-Y

Ambrose, S. H., and DeNiro, M. J. (1986). The isotopic ecology of East-African mammals. *Oecologia* 69, 395–406. doi: 10.1007/bf00377062

Ambrose, S. H., and Norr, L. (1993). "Experimental Evidence for the Relationship of the Carbon Isotope Ratios of Whole Diet and Dietary Protein to Those of Bone Collagen and Carbonate," in *Prehistoric Human Bone: Archaeology at the Molecular Level*, eds J. B. Lambert and G. Grupe (Berlin: Springer Berlin Heidelberg), 1–37.

Amiot, R., Lécuyer, C., Escarguel, G., Billon-Bruyat, J. P., Buffetaut, E., Langlois, C., et al. (2007). Oxygen isotope fractionation between crocodilian phosphate and water. *Palaeogeogr. Palaeoclimatol. Palaeoecol.* 243, 412–420. doi: 10.1016/j.palaeo.2006.08.013

Amundson, R., Austin, A. T., Schuur, E. A. G., Yoo, K., Matzek, V., Kendall, C., et al. (2003). Global patterns of the isotopic composition of soil and plant nitrogen. *Glob. Biogeochem. Cycles* 17:31. doi: 10.1029/2002gb001903

Arvidsson, K., Stenberg, L., Chirindja, F., Dahlin, T., Owen, R., and Steinbruch, F. (2011). A hydrogeological study of the Nhandugue River, Mozambique – A major groundwater recharge zone. *Phys. Chem. Earth* 36, 789–797. doi: 10.1016/j.pce.2011.07.036

Atkins, J. L., Long, R. A., Pansu, J., Daskin, J. H., Potter, A. B., Stalmans, M. E., et al. (2019). Cascading impacts of large-carnivore extirpation in an African ecosystem. *Science* 364, 173–177. doi: 10.1126/science.aau3561

Auderset, A., Moretti, S., Taphorn, B., Ebner, P. R., Kast, E., Wang, X. T., et al. (2022). Enhanced ocean oxygenation during Cenozoic warm periods. *Nature* 609, 77–82. doi: 10.1038/s41586-022-05017-0

Ayliffe, L. K., Lister, A. M., and Chivas, A. R. (1992). The preservation of glacial-interglacial climatic signatures in the oxygen isotopes of elephant skeletal phosphate. *Palaeogeogr. Palaeoclimatol. Palaeoecol.* 99, 179–191.

Balasse, M., Bocherens, H., and Mariotti, A. (1999). Intra-bone variability of collagen and apatite isotopic composition used as evidence of a change of diet. *J. Archaeol. Sci.* 26, 593–598.

Becker, J. A., Hutchinson, M., Potter, A., Park, S., Guyton, J., Abernathy, K., et al. (2021). Ecological and behavioral mechanisms of density-dependent habitat expansion in a recovering African ungulate population. *Ecol. Monogr.* 91:e01476. doi: 10.1002/ECM.1476

Behrensmeyer, A. K. (1978). Taphonomic and Ecologic Information from Bone Weathering. *Paleobiology* 4, 150–162.

Blumenthal, S. A., Levin, N. E., Brown, F. H., Brugal, J. P., Chritz, K. L., Harris, J. M., et al. (2017). Aridity and hominin environments. *Proc. Natl. Acad. Sci. U. S. A.* 114, 7331–7336. doi: 10.1073/pnas.1700597114

Bobe, R., Aldeias, V., Alemseged, Z., Archer, W., Aumaître, G., Bamford, M. K., et al. (2021). The first Miocene fossils from coastal woodlands in the southern East African Rift. *Biorxiv* [Preprint]. doi: 10.1101/2021.12.16.472914

Bobe, R., Martínez, F. I., and Carvalho, S. (2020). Primate adaptations and evolution in the Southern African Rift Valley. *Evol. Anthropol.* 29, 94–101. doi: 10.1002/evan.21826

Bocherens, H. (2009). "Neanderthal Dietary Habits: Review of the Isotopic Evidence," in *The Evolution of Hominin Diets: Integrating Approaches to the Study of Palaeolithic Subsistence*, eds J. J. Hublin and M. P. Richards (Dordrecht: Springer Netherlands), 241–250.

Bocherens, H., and Drucker, D. (2003). Trophic level isotopic enrichment of carbon and nitrogen in bone collagen: Case studies from recent and ancient terrestrial ecosystems. *Int. J. Osteoarchaeol.* 13, 46–53.

Bocherens, H., Koch, P. L., Mariotti, A., Geraads, D., and Jaeger, J. J. (1996). Isotopic biogeochemistry (^{13}C, ^{18}O) of mammalian enamel from African Pleistocene hominid sites. *Palaios* 11, 306–318. doi: 10.2307/3515241

Böhme, B. (2005). Geo ecology of the Lake Urema / Central Mozambique. *Freiberg Online Geosci.* 14:2005. doi: 10.23689/fidgeo-881

Bothma, J. (2005). Water-use by southern Kalahari leopards. *S. Afr. J. Wildl. Res.* 35, 131–137. doi: 10.10520/EJC117220

Bothma, J., and Walker, C. (2013). *Larger Carnivores of the African Savannas*. Heidelberg: Springer.

Bouley, P., Paulo, A., Angela, M., Du Plessis, C., and Marneweck, D. G. (2021). The successful reintroduction of African wild dogs (*Lycaon pictus*) to Gorongosa National Park, Mozambique. *PLoS One* 16:e0249860. doi: 10.1371/journal.pone.0249860

Bouley, P., Poulos, M., Branco, R., and Carter, N. H. (2018). Post-war recovery of the African lion in response to large-scale ecosystem restoration. *Biol. Conserv.* 227, 233–242. doi: 10.1016/j.biocon.2018.08.024

Bourgon, N., Jaouen, K., Bacon, A. M., Dufour, E., McCormack, J., Tran, N. H., et al. (2021). Trophic ecology of a Late Pleistocene early modern human from tropical Southeast Asia inferred from zinc isotopes. *J. Hum. Evol.* 161:103075. doi: 10.1016/j.jhevol.2021.103075

Bourgon, N., Jaouen, K., Bacon, A. M., Jochum, K. P., Dufour, E., Duringer, P., et al. (2020). Zinc isotopes in Late Pleistocene fossil teeth from a Southeast Asian cave setting preserve paleodietary information. *Proc. Natl. Acad. Sci. U. S. A.* 117, 4675–4681. doi: 10.1073/pnas.1911744117

Branco, P., Merkle, J., Pringle, R., King, L., Tindall, T., Stalmans, M., et al. (2019a). An experimental test of community-based strategies for mitigating human-wildlife conflict around protected areas. *Conserv. Lett.* 13:e12679. doi: 10.1111/conl.12679

Branco, P., Merkle, J., Pringle, R., Pansu, J., Potter, A., Reynolds, A., et al. (2019b). Determinants of elephant foraging behaviour in a coupled human-natural system: Is brown the new green?. *J. Anim. Ecol.* 88, 780–792. doi: 10.1111/1365-2656.12971

Bryant, D. J., and Froelich, P. N. (1995). A model of oxygen isotope fractionation in body water of large mammals. *Geochim. Cosmochim. Acta* 59, 4523–4537. doi: 10.1016/0016-7037(95)00250-4

Bryant, D. J., Koch, P. L., Froelich, P. N., Showers, W. J., and Genna, B. J. (1996). Oxygen isotope partitioning between phosphate and carbonate in mammalian apatite. *Geochim. Cosmochim. Acta* 60, 5145–5148. doi: 10.1016/S0016-7037(96)00308-0

Cain, J. III, Owen-Smith, N., and Macandza, V. (2012). The costs of drinking: Comparative water dependency of sable antelope and zebra. *J. Zool.* 286, 58–67. doi: 10.1111/j.1469-7998.2011.00848.x

Cantalapiedra-Hijar, G., Ortigues-Marty, I., Sepchat, B., Agabriel, J., Huneau, J. F., and Fouillet, H. (2015). Diet–animal fractionation of nitrogen stable isotopes reflects the efficiency of nitrogen assimilation in ruminants. *Br. J. Nutr.* 113, 1158–1169. doi: 10.1017/S0007114514004449

Carter, M. L., and Bradbury, M. W. (2016). Oxygen isotope ratios in primate bone carbonate reflect amount of leaves and vertical stratification in the diet. *Am. J. Primatol.* 78, 1086–1097. doi: 10.1002/ajp.22432

Caut, S., Angulo, E., and Courchamp, F. (2009). Variation in discrimination factors ($\Delta^{15}N$ and $\Delta^{13}C$): The effect of diet isotopic values and applications for diet reconstruction. *J. Appl. Ecol.* 46, 443–453. doi: 10.1111/j.1365-2664.2009.01620.x

Cerling, E., Harris, J. M., and Passey, B. H. (2003). Diets of East African bovidae based on stable isotope analysis. *J. Mammal.* 84, 456–470. doi: 10.2307/1383890

Cerling, T., Andanje, S., Blumenthal, S., Brown, F., Chritz, K., Harris, J., et al. (2015). Dietary changes of large herbivores in the Turkana Basin, Kenya from 4 to 1 Ma. *Proc. Natl. Acad. Sci. U. S. A.* 112:201513075. doi: 10.1073/pnas.1513075112

Cerling, T. E., Bernasconi, S. M., Hofstetter, L. S., Jaggi, M., Wyss, F., Rudolf von Rohr, C., et al. (2021). CH_4/CO_2 ratios and carbon isotope enrichment between diet and breath in herbivorous mammals. *Front. Ecol. Evol.* 9:638568. doi: 10.3389/fevo.2021.638568

Cerling, T. E., and Harris, J. M. (1999). Carbon isotope fractionation between diet and bioapatite in ungulate mammals and implications for ecological and paleoecological studies. *Oecologia* 120, 347–363. doi: 10.1007/s004420050868

Cerling, T. E., Harris, J. M., Ambrose, S. H., Leakey, M. G., and Solounias, N. (1997). Dietary and environmental reconstruction with stable isotope analyses of herbivore tooth enamel from the Miocene locality of Fort Ternan, Kenya. *J. Hum. Evol.* 33, 635–650. doi: 10.1006/jhev.1997.0151

Cerling, T. E., Wynn, J. G., Andanje, S. A., Bird, M. I., Korir, D. K., Levin, N. E., et al. (2011). Woody cover and hominin environments in the past 6 million years. *Nature* 476, 51–56. doi: 10.1038/nature10306

Chinique de Armas, Y., Mavridou, A. M., Garcell Domínguez, J., Hanson, K., and Laffoon, J. (2022). Tracking breastfeeding and weaning practices in ancient populations by combining carbon, nitrogen and oxygen stable isotopes from multiple non-adult tissues. *PLoS One* 17:e0262435. doi: 10.1371/journal.pone.0262435

Clark, I. D., and Fritz, P. (1997). *Environmental isotopes in hydrogeology*. Boca Raton: CRC press.

Codron, D., Codron, J., Lee-Thorp, J. A., Sponheimer, M., de Ruiter, D., and Brink, J. S. (2007). Stable isotope characterization of mammalian predator–prey relationships in a South African savanna. *Eur. J. Wildl. Res.* 53, 161–170. doi: 10.1007/s10344-006-0075-x

Codron, D., Codron, J., Sponheimer, M., and Clauss, M. (2016). Within-population isotopic niche variability in savanna mammals: Disparity between carnivores and herbivores. *Front. Ecol. Evol.* 4:15. doi: 10.3389/fevo.2016.00015

Codron, D., Lee-Thorp, J. A., Sponheimer, M., de Ruiter, D., and Codron, J. (2006). Inter- and intrahabitat dietary variability of chacma baboons (*Papio ursinus*) in South African savannas based on fecal $\delta^{13}C$, $\delta^{15}N$, and %N. *Am. J. Phys. Anthropol.* 129, 204–214. doi: 10.1002/ajpa.20253

Codron, D., Radloff, F. G., Codron, J., Kerley, G. I., and Tambling, C. J. (2018). Meso-carnivore niche expansion in response to an apex predator's reintroduction–a stable isotope approach. *Afr. J. Wildl. Res.* 48, 1–16. doi: 10.3957/056.048.013004

Codron, J., Codron, D., Lee-Thorp, J. A., Sponheimer, M., Bond, W. J., de Ruiter, D., et al. (2005). Taxonomic, anatomical, and spatio-temporal variations in the stable carbon and nitrogen isotopic compositions of plants from an African savanna. *J. Archaeol. Sci.* 32, 1757–1772. doi: 10.1016/j.jas.2005.06.006

Codron, J., Codron, D., Sponheimer, M., Kirkman, K., Duffy, K. J., Raubenheimer, E. J., et al. (2012). Stable isotope series from elephant ivory reveal lifetime histories of a true dietary generalist. *Proc. R. Soc. B Biol. Sci.* 279, 2433–2441. doi: 10.1098/rspb.2011.2472

Coplen, T. B. (1988). Normalization of oxygen and hydrogen isotope data. *Chem. Geol.* 72, 293–297. doi: 10.1016/0168-9622(88)90042-5

Correia, M., Timóteo, S., Rodríguez-Echeverría, S., Mazars-Simon, A., and Heleno, R. (2017). Refaunation and the reinstatement of the seed-dispersal function in Gorongosa National Park. *Conserv. Biol.* 31, 76–85. doi: 10.1111/cobi.12782

Crowley, B. (2012). Stable Isotope Techniques and Applications for Primatologists. *Int. J. Primatol.* 33, 673–701. doi: 10.1007/s10764-012-9582-7

Crowley, B. E., Melin, A. D., Yeakel, J. D., and Dominy, N. J. (2015). Do oxygen isotope values in collagen reflect the ecology and physiology of neotropical mammals?. *Front. Ecol. Evol.* 3:127. doi: 10.3389/fevo.2015.00127

Cumming, D., Mackie, C., Magane, S., and Taylor, R. (1994). *Aerial census of large herbivores in the Gorongosa National Park and the Marromeu Area of the Zambezi Delta in Mozambique: June 1994*. Harare, ZW: IUCN ROSA.

Cybulski, J. D., Skinner, C., Wan, Z., Wong, C. K. M., Toonen, R. J., Gaither, M. R., et al. (2022). Improving stable isotope assessments of inter- and intra-species variation in coral reef fish trophic strategies. *Ecol. Evol.* 12:e9221. doi: 10.1002/ece3.9221

Dag, O., Dolgun, A., and Konar, N. M. (2018). onewaytests: An R Package for One-Way Tests in Independent Groups Designs. *R J.* 10, 175–199.

Dailey-Chwalibóg, T., Huneau, J. F., Mathé, V., Kolsteren, P., Mariotti, F., Mostak, M. R., et al. (2020). Weaning and stunting affect nitrogen and carbon stable isotope natural abundances in the hair of young children. *Sci. Rep.* 10:2522. doi: 10.1038/s41598-020-59402-8

Daskin, J. H., Stalmans, M., and Pringle, R. M. (2016). Ecological legacies of civil war: 35-year increase in savanna tree cover following wholesale large-mammal declines. *J. Ecol.* 104, 79–89. doi: 10.1111/1365-2745.12483

Dauphin, Y., and Williams, C. (2008). Chemical composition of enamel and dentine in modern reptile teeth. *Mineral. Mag.* 72, 247–250. doi: 10.1180/minmag.2008.072.1.247

DeNiro, M. J., and Epstein, S. (1981). Influence of diet on the distribution of nitrogen isotopes in animals. *Geochim. Cosmochim. Acta* 45, 341–351. doi: 10.1016/0016-7037(81)90244-1

Domingo, L., Tomassini, R. L., Montalvo, C. I., Sanz-Pérez, D., and Alberdi, M. T. (2020). The Great American Biotic Interchange revisited: A new perspective from the stable isotope record of Argentine Pampas fossil mammals. *Sci. Rep.* 10:1608. doi: 10.1038/s41598-020-58575-6

Dunham, K. M. (2004). *Aerial Survey of Large Herbivores in Gorongosa National Park, Mozambique: 2004*. Cambridge MA: The Gregory C. Carr Foundation.

Dutton, P., and Carvalho, F. (2002). Final Report for the GERFFA Project on the Status of Fauna in the Sofala Province 1990–2001, with Reference to Previous Data. Unpublished consultancy report. Maputo, Mozambique.

Easter, T., Bouley, P., and Carter, N. (2019). Opportunities for biodiversity conservation outside of Gorongosa National Park, Mozambique: A multispecies approach. *Biol. Conserv.* 232, 217–227. doi: 10.1016/j.biocon.2019.02.007

Evans, R. D. (2001). Physiological mechanisms influencing plant nitrogen isotope composition. *Trends Plant Sci.* 6, 121–126. doi: 10.1016/S1360-1385(01)01889-1

Fick, S. E., and Hijmans, R. J. (2017). WorldClim 2: New 1-km spatial resolution climate surfaces for global land areas. *Int. J. Climatol.* 37, 4302–4315. doi: 10.1002/joc.5086

Fox-Dobbs, K., Bump, J. K., Peterson, R. O., Fox, D. L., and Koch, P. (2007). Carnivore-specific stable isotope variables and variation in the foraging ecology of modern and ancient wolf populations: Case studies from Isle Royale, Minnesota, and La Brea. *Can. J. Zool.* 85, 458–471. doi: 10.1139/Z07-018

Fricke, H. C., and O'Neil, J. R. (1996). Inter- and intra-tooth variation in the oxygen isotope composition of mammalian tooth enamel phosphate: Implications for palaeoclimatological and palaeobiological research. *Palaeogeogr. Palaeoclimatol. Palaeoecol.* 126, 91–99. doi: 10.1016/S0031-0182(96)00072-7

Fuller, B. T., Fuller, J. L., Harris, D. A., and Hedges, R. E. M. (2006). Detection of breastfeeding and weaning in modern human infants with carbon and nitrogen stable isotope ratios. *Am. J. Phys. Anthropol.* 129, 279–293. doi: 10.1002/ajpa.20249

Fulton, J., Arthur, M., Thomas, R., and Freeman, K. (2018). Pigment carbon and nitrogen isotopic signatures in euxinic basins. *Geobiology* 16, 429–445. doi: 10.1111/gbi.12285

Gaynor, K., Branco, P., Long, R., Gonçalves, D., Granli, P., and Poole, J. (2018). Effects of human settlement and roads on diel activity patterns of elephants (*Loxodonta africana*). *Afr. J. Ecol.* 56, 872–881. doi: 10.1111/aje.12552

Gaynor, K. M., Daskin, J. H., Rich, L. N., and Brashares, J. S. (2021). Postwar wildlife recovery in an African savanna: Evaluating patterns and drivers of species occupancy and richness. *Anim. Conserv.* 24, 510–511. doi: 10.1111/acv.12661

Ghiglieri, M., Butynski, T., Struhsaker, T., Leland, L., Wallis, S., and Waser, P. (2008). Bush pig (*Potamochoerus porcus*) polychromatism and ecology in Kibale Forest, Uganda. *Afr. J. Ecol.* 20, 231–236. doi: 10.1111/j.1365-2028.1982.tb00298.x

Gil-Bona, A., and Bidlack, F. B. (2020). Tooth enamel and its dynamic protein matrix. *Int. J. Mol. Sci.* 21:4458. doi: 10.3390/ijms21124458

Goldberg, M., Kulkarni, A. B., Young, M., and Boskey, A. (2011). Dentin: Structure, composition and mineralization. *Front. Biosci.* 3:711–735. doi: 10.2741/e281

Guyton, J. A., Pansu, J., Hutchinson, M. C., Kartzinel, T. R., Potter, A. B., Coverdale, T. C., et al. (2020). Trophic rewilding revives biotic resistance to shrub invasion. *Nat. Ecol. Evol.* 4, 712–724. doi: 10.1038/s41559-019-1068-y

Habermann, J. M., Alberti, M., Aldeias, V., Alemseged, Z., Archer, W., Bamford, M., et al. (2019). Gorongosa by the sea: First Miocene fossil sites from the Urema Rift, central Mozambique, and their coastal paleoenvironmental and paleoecological contexts. *Palaeogeogr. Palaeoclimatol. Palaeoecol.* 514, 723–738. doi: 10.1016/j.palaeo.2018.09.032

Hamilton, W. J. III (1986). Namib desert chacma baboon (*Papio ursinus*) use of food and water resources during a food shortage. *Madoqua* 1986, 397–407. doi: 10.10520/AJA10115498_477

Hammer, Ø., Harper, D. A., and Ryan, P. D. (2001). PAST: Paleontological statistics software package for education and data analysis. *Palaeontol. Electron.* 4, 1–9.

Hammond, P., Lewis-Bevan, L., Biro, D., and Carvalho, S. (2022). Risk perception and terrestriality in primates: A quasi-experiment through habituation of chacma baboons (*Papio ursinus*) in Gorongosa National Park, Mozambique. *Am. J. Biol. Anthropol.* 179, 48–59. doi: 10.1002/ajpa.24567

Hartman, G. (2010). Are elevated $\delta^{15}N$ values in herbivores in hot and arid environments caused by diet or animal physiology?. *Funct. Ecol.* 25, 122–131. doi: 10.1111/j.1365-2435.2010.01782.x

Hayward, M. W., and Hayward, M. D. (2012). Waterhole use by African Fauna. *S. Afr. J. Wildl. Res.* 42, 117–127.

Hempson, G. P., Archibald, S., and Bond, W. J. (2015). A continent-wide assessment of the form and intensity of large mammal herbivory in Africa. *Science* 350, 1056–1061. doi: 10.1126/science.aac7978

Hopley, P. J., Cerling, T. E., Crété, L., Werdelin, L., Mwebi, O., Manthi, F. K., et al. (2022). Stable isotope analysis of carnivores from the Turkana Basin, Kenya: Evidence for temporally-mixed fossil assemblages. *Quat. Int.* doi: 10.1016/j.quaint.2022.04.004

Hoppe, K. A. (2006). Correlation between the oxygen isotope ratio of North American bison teeth and local waters: Implication for paleoclimatic reconstructions. *Earth Planet. Sci. Lett.* 244, 408–417. doi: 10.1016/j.epsl.2006.01.062

Iacumin, P., Bocherens, H., Mariotti, A., and Longinelli, A. (1996). Oxygen isotope analyses of co-existing carbonate and phosphate in biogenic apatite: A way to monitor diagenetic alteration of bone phosphate?. *Earth Planet. Sci. Lett.* 142, 1–6. doi: 10.1016/0012-821X(96)00093-3

IAEA/WISER (2020a). *Global Network of Isotopes in Precipitation*. Available online at: https://www.iaea.org/services/networks/gnip (accessed on Mar 11, 2022).

IAEA/WISER (2020b). *Global Network of Isotopes in Rivers*. Available online at: https://www.iaea.org/services/networks/gnir (accessed on Mar 11, 2022).

Jackson, A., Inger, R., Parnell, A., and Bearhop, S. (2011). Comparing isotopic niche width among and within communities: SIBER – Stable Isotope Bayesian Ellipses in R. *J. Anim. Ecol.* 80, 595–602. doi: 10.1111/j.1365-2656.2011.01806.x

Jaouen, K., Villalba-Mouco, V., Smith, G. M., Trost, M., Leichliter, J., Lüdecke, T., et al. (2022). A Neandertal dietary conundrum: New insights provided by tooth enamel Zn isotopes from Gabasa, Spain. *Proc. Natl. Acad. Sci. U. S. A.* 119:e2109315119. doi: 10.1073/pnas.2109315119

Kassambra, A. (2021). *rstatix: Pipe-friendly framework for basic statistical tests. R package version 0.7.0.* Available online at: https://CRAN.R-project.org/package=rstatix (accessed September 29, 2022).

Kast, E. R., Griffiths, M. L., Kim, S. L., Rao, Z. C., Shimada, K., Becker, M. A., et al. (2022). Cenozoic megatooth sharks occupied extremely high trophic positions. *Sci. Adv.* 8:eabl6529. doi: 10.1126/sciadv.abl6529

Kast, E. R., Stolper, D. A., Auderset, A., Higgins, J. A., Ren, H., Wang, X. T., et al. (2019). Nitrogen isotope evidence for expanded ocean suboxia in the early Cenozoic. *Science* 364, 386–389. doi: 10.1126/science.aau5784

Kendall, C., and McDonnell, J. J. (1998). *Isotope tracers in catchment hydrology*. Amsterdam: Elsevier.

Kingston, J. D., and Harrison, T. (2007). Isotopic dietary reconstructions of Pliocene herbivores at Laetoli: Implications for early hominin paleoecology. *Palaeogeogr. Palaeoclimatol. Palaeoecol.* 243, 272–306. doi: 10.1016/j.palaeo.2006.08.002

Knapp, A., Sigman, D., and Lipschultz, F. (2005). N isotopic composition of dissolved organic nitrogen and nitrate at the Bermuda Atlantic time-series study site . *Glob. Biogeochem. Cycles* 19. doi: 10.1029/2004GB002320

Koch, P. L. (2007). "Isotopic Study of the Biology of Modern and Fossil Vertebrates," in *Stable Isotopes in Ecology and Environmental Science*, eds R. Michener and K. Lajtha (Hoboken, NJ: Wiley), 99–154.

Koch, P. L., Tuross, N., and Fogel, M. L. (1997). The effects of sample treatment and diagenesis on the isotopic integrity of carbonate in biogenic hydroxylapatite. *J. Archaeol. Sci.* 24, 417–429. doi: 10.1006/jasc.1996.0126

Kohn, M. J. (1996). Predicting animal δ18O: Accounting for diet and physiological adaptation. *Geochim. Cosmochim. Acta* 60, 4811–4829. doi: 10.1016/S0016-7037(96)00240-2

Kohn, M. J. (2010). Carbon isotope compositions of terrestrial C3 plants as indicators of (paleo)ecology and (paleo)climate. *Proc. Natl. Acad. Sci. U. S. A.* 107:19691. doi: 10.1073/pnas.1004933107

Kohn, M. J., and Cerling, T. E. (2002). "Stable Isotope Compositions of Biological Apatite," in *Phosphates. Geochemical, Geobiological, and Materials Importance*, eds M. J. Kohn, J. Rakovan, and J. M. Hughes (Washington, DC: Mineralogical Society of America), 455–488.

Kohn, M. J., Schoeninger, M. J., and Valley, J. W. (1996). Herbivore tooth oxygen isotope compositions: Effects of diet and physiology. *Geochim. Cosmochim. Acta* 60, 3889–3896. doi: 10.1016/0016-7037(96)00248-7

Krajcarz, M. T., Krajcarz, M., and Bocherens, H. (2018). Collagen-to-collagen prey-predator isotopic enrichment ($\Delta^{13}C$, $\Delta^{15}N$) in terrestrial mammals - a case study of a subfossil red fox den. *Palaeogeogr. Palaeoclimatol. Palaeoecol.* 490, 563–570. doi: 10.1016/j.palaeo.2017.11.044

Lacruz, R. S., Habelitz, S., Wright, J. T., and Paine, M. L. (2017). Dental enamel formation and implications for oral health and disease. *Physiol. Rev.* 97, 939–993. doi: 10.1152/physrev.00030.2016

Layman, C., and Allgeier, J. (2012). Characterizing trophic ecology of generalist consumers: A case study of the invasive lionfish in The Bahamas. *Mar. Ecol. Progress Ser.* 448, 131–141. doi: 10.3354/meps09511

Layman, C. A., Arrington, D. A., Montaña, C. G., and Post, D. M. (2007). Can stable isotope ratios provide for community-wide measures of trophic structure?. *Ecology* 88, 42–48. doi: 10.1890/0012-9658200788[42:csirpf]2.0.co;2

Lee-Thorp, J., and Van der Merwe, N. J. (1987). Carbon isotope analysis of fossil bone apatite. *S. Afr. J. Sci.* 83, 712–715.

Leichliter, J. N., Lüdecke, T., Foreman, A., Bourgon, N., Vonhof, H., Souksavatdy, V., et al. (2022). Nitrogen isotopic composition of tooth enamel organic matter records trophic position in modern and fossil ecosystems. *Res. Square* [Preprint]. doi: 10.21203/rs.3.rs-1942250/v1

Leichliter, J. N., Lüdecke, T., Foreman, A. D., Duprey, N. N., Winkler, D. E., Kast, E. R., et al. (2021). Nitrogen isotopes in tooth enamel record diet and trophic level enrichment: Results from a controlled feeding experiment. *Chem. Geol.* 563:120047. doi: 10.1016/j.chemgeo.2020.120047

Levin, N. E., Cerling, T. E., Passey, B. H., Harris, J. M., and Ehleringer, J. R. (2006). A stable isotope aridity index for terrestrial environments. *Proc. Natl. Acad. Sci. U. S. A.* 103, 11201–11205. doi: 10.1073/pnas.0604719103

Lüdecke, T., Kullmer, O., Wacker, U., Sandrock, O., Fiebig, J., Schrenk, F., et al. (2018). Dietary versatility of Early Pleistocene hominins. *Proc. Natl. Acad. Sci. U. S. A.*115, 13330–13335. doi: 10.1073/pnas.1809439115

Lüdecke, T., Mulch, A., Kullmer, O., Sandrock, O., Thiemeyer, H., Fiebig, J., et al. (2016). Stable isotope dietary reconstructions of herbivore enamel reveal heterogeneous wooded savanna ecosystems in the Plio-Pleistocene Malawi Rift. *Palaeogeogr. Palaeoclimatol. Palaeoecol.* 459, 170–181. doi: 10.1016/j.palaeo.2016.07.010

Lueders-Dumont, J. A., Wang, X. T., Jensen, O. P., Sigman, D. M., and Ward, B. B. (2018). Nitrogen isotopic analysis of carbonate-bound organic matter in modern and fossil fish otoliths. *Geochim. Cosmochim. Acta* 224, 200–222. doi: 10.1016/j.gca.2018.01.001

Lüttge, U. (2004). Ecophysiology of Crassulacean Acid Metabolism (CAM). *Ann. Bot.* 93, 629–652. doi: 10.1093/aob/mch087

Ma, Y., Weldeab, S., Schneider, R. R., Andersen, N., Garbe-Schönberg, D., and Friedrich, T. (2021). Strong Southern African Monsoon and weak Mozambique Channel throughflow during Heinrich events: Implication for Agulhas leakage. *Earth Planet. Sci. Lett.* 574:117148. doi: 10.1016/j.epsl.2021.117148

Martin, J. E., Hassler, A., Montagnac, G., Therrien, F., and Balter, V. (2022). The stability of dinosaur communities before the K-Pg boundary: A perspective from southern Alberta using calcium isotopes as a dietary proxy. *GSA Bull.* 134, 2548–2560. doi: 10.1130/b36222.1

Martin, J. E., Tacail, T., Adnet, S., Girard, C., and Balter, V. (2015). Calcium isotopes reveal the trophic position of extant and fossil elasmobranchs. *Chem. Geol.* 415, 118–125. doi: 10.1016/j.chemgeo.2015.09.011

Martin, J. E., Tacail, T., Braga, J., Cerling, T. E., and Balter, V. (2020). Calcium isotopic ecology of Turkana Basin hominins. *Nat. Commun.* 11:3587. doi: 10.1038/s41467-020-17427-7

Martinez, F. I., Capelli, C., Ferreira da Silva, M. J., Aldeias, V., Alemseged, Z., Archer, W., et al. (2019). A missing piece of the Papio puzzle: Gorongosa baboon phenostructure and intrageneric relationships. *J. Hum. Evol.* 130, 1–20. doi: 10.1016/j.jhevol.2019.01.007

Martinez-Garcia, A., Jung, J., Ai, X. E., Sigman, D. M., Auderset, A., Duprey, N. N., et al. (2022). Laboratory Assessment of the Impact of Chemical Oxidation, Mineral Dissolution, and Heating on the Nitrogen Isotopic Composition of Fossil-bound Organic Matter. *Geochem. Geophys. Geosyst.* 23:e2022GC010396. doi: 10.1029/2022GC010396

Martinez-Garcia, A., Sigman, D. M., Ren, H., Anderson, R. F., Straub, M., Hoderll, D. A., et al. (2014). Iron Fertilization of the Subantartic Ocean During the Last Ice Age. *Science* 343, 1347–1350.

McCormack, J., Szpak, P., Bourgon, N., Richards, M., Hyland, C., Méjean, P., et al. (2021). Zinc isotopes from archaeological bones provide reliable trophic level information for marine mammals. *Commun. Biol.* 4:683. doi: 10.1038/s42003-021-02212-z

Merceron, G., Berlioz, E., Vonhof, H., Green, D., Garel, M., and Tütken, T. (2021). Tooth tales told by dental diet proxies: An alpine community of sympatric ruminants as a model to decipher the ecology of fossil fauna. *Palaeogeogr. Palaeoclimatol. Palaeoecol.* 562:110077. doi: 10.1016/j.palaeo.2020.110077

Monro, R. H. (1980). Observations on the Feeding Ecology of Impala. *S. Afr. J. Zool.* 15, 107–110. doi: 10.1080/02541858.1980.11447695

Moritz, G. L., Fourie, N., Yeakel, J. D., Phillips-Conroy, J. E., Jolly, C. J., Koch, P. L., et al. (2012). Baboons, Water, and the Ecology of Oxygen Stable Isotopes in an Arid Hybrid Zone. *Physiol. Biochem. Zool.* 85, 421–430. doi: 10.1086/667533

Muschinski, J., Biro, D., Lewis-Bevan, L., and Carvalho, S. (2019). Could it be culture? An inter-troop comparison of baboon behaviour in Gorongosa National Park, Mozambique. *Neuroscience* 91, 350–351.

Nelson, S. (2013). Chimpanzee fauna isotopes provide new interpretations of fossil ape and hominin ecologies. *Proc. Biol. Sci. R. Soc.* 280:20132324. doi: 10.1098/rspb.2013.2324

Newsome, S., Rio, C., Bearhop, S., and Phillips, D. (2007). A niche for isotopic ecology. *Front. Ecol. Environ.* 5:429–436. doi: 10.1890/060150.1

Nicholson, M. J. (1985). The water requirements of livestock in Africa. *Outl. Agric.* 14, 156–164. doi: 10.1177/003072708501400401

Noirard, C., Le Berre, M., Ramousse, R., and Lena, J. P. (2008). Seasonal variation of thermoregulatory behaviour in the *Hippopotamus* (*Hippopotamus amphibius*). *J. Ethol.* 26, 191–193. doi: 10.1007/s10164-007-0052-1

Nowak, R. M. (1999). *Walker's mammals of the world*. Baltimore, MD: Johns Hopkins University Press.

O'Connell, T. C., Kneale, C. J., Tasevska, N., and Kuhnle, G. G. C. (2012). The diet-body offset in human nitrogen isotopic values: A controlled dietary study. *Am. J. Phys. Anthropol.* 149, 426–434. doi: 10.1002/ajpa.22140

Pansu, J., Guyton, J. A., Potter, A. B., Atkins, J. L., Daskin, J. H., Wursten, B., et al. (2019). Trophic ecology of large herbivores in a reassembling African ecosystem. *J. Ecol.* 107, 1355–1376. doi: 10.1111/1365-2745.13113

Passey, B. H., and Cerling, T. E. (2002). Tooth enamel mineralization in ungulates: Implications for recovering a primary isotopic time-series. *Geochim. Cosmochim. Acta* 66, 3225–3234. doi: 10.1016/S0016-7037(02)00933-X

Pearcy, R. W., and Ehleringer, J. (1984). Comparative ecophysiology of C3 and C4 plants. *Plant Cell Environ.* 7, 1–13. doi: 10.1111/j.1365-3040.1984.tb01194.x

Pederzani, S., and Britton, K. (2019). Oxygen isotopes in bioarchaeology: Principles and applications, challenges and opportunities. *Earth Sci. Rev.* 188, 77–107. doi: 10.1016/j.earscirev.2018.11.005

Pinzone, M., Damseaux, F., Michel, L. N., and Das, K. (2019). Stable isotope ratios of carbon, nitrogen and sulphur and mercury concentrations as descriptors of trophic ecology and contamination sources of Mediterranean whales. *Chemosphere* 237:124448. doi: 10.1016/j.chemosphere.2019.124448

Polissar, P. J., Fulton, J. M., Junium, C. K., Turich, C. C., and Freeman, K. H. (2009). Measurement of 13C and 15N Isotopic Composition on Nanomolar Quantities of C and N. *Anal. Chem.* 81, 755–763. doi: 10.1021/ac801370c

Pringle, R. M. (2017). Upgrading protected areas to conserve wild biodiversity. *Nature* 546, 91–99. doi: 10.1038/nature22902

R Core Team (2022). *R: A language and environment for statistical computing*. Vienna: R Foundation for Statistical Computing.

Ren, H., Sigman, D. M., Martínez-García, A., Anderson, R. F., Chen, M. T., and Ravelo, A. C. (2017). Impact of glacial/interglacial sea level change on the ocean nitrogen cycle. *Proc. Natl. Acad. Sci. U. S. A.* 114, E6759–E6766. doi: 10.1073/pnas.1701315114

Ren, H., Sigman, D. M., Meckler, A. N., Plessen, B., Robinson, R. S., Rosenthal, Y., et al. (2009). Foraminiferal Isotope Evidence of Reduced Nitrogen Fixation in the Ice Age Atlantic Ocean. *Science* 323, 244–248. doi: 10.1126/science.1165787

Robbins, C. T., Felicetti, L. A., and Sponheimer, M. (2005). The effect of dietary protein quality on nitrogen isotope discrimination in mammals and birds. *Oecologia* 144, 534–540. doi: 10.1007/s00442-005-0021-8

Roberts, P. (2017). Stable carbon, oxygen, and nitrogen, isotope analysis of plants from a South Asian tropical forest: Implications for primatology. *Am. J. Primatol.* 79. doi: 10.1002/ajp.22656

Robinson, D. (2001). δ15N as an integrator of the nitrogen cycle. *Trends Ecol. Evol.* 16, 153–162. doi: 10.1016/S0169-5347(00)02098-X

Robinson, R. S., Brunelle, B. G., and Sigman, D. M. (2004). Revisiting nutrient utilization in the glacial Antarctic: Evidence from a new method for diatom-bound N isotopic analysis. *Paleoceanography* 19:A3001. doi: 10.1029/2003pa000996

Sage, R. F., and Zhu, X.-G. (2011). Exploiting the engine of C_4 photosynthesis. *J. Exp. Bot.* 62, 2989–3000. doi: 10.1093/jxb/err179

Sakae, T., Suzuki, K., and Kozawa, Y. (1997). "A short review of studies on chemical and physical properties of enamel crystallites," in *Tooth Enamel Microstructure: Proceedings of the enamel microstructure workshop*, (Boca Raton, FL: CRC Press).

Santander, C., Molinaro, L., Mutti, G., Martínez, F. I., Mathe, J., Ferreira da Silva, M. J., et al. (2022). Genomic variation in baboons from central Mozambique unveils complex evolutionary relationships with other Papio species. *BMC Ecol. Evol.* 22:44. doi: 10.1186/s12862-022-01999-7

Schemmel, F., Mikes, T., Rojay, B., and Mulch, A. (2013). The impact of topography on isotopes in precipitation across the Central Anatolian Plateau (Turkey). *Am. J. Sci.* 313, 61–80. doi: 10.2475/02.2013.01

Schmidt, S., and Stewart, G. R. (2003). $\delta^{15}N$ values of tropical savanna and monsoon forest species reflect root specialisations and soil nitrogen status. *Oecologia* 134, 569–577. doi: 10.1007/s00442-002-1150-y

Schoeniger, M. J., and DeNiro, M. J. (1984). $^{15}N/^{14}N$ ratios of bone collagen reflect marine and terrestrial components of prehistoric diets. *Geochim. Cosmochim. Acta* 48, 625–639. doi: 10.1126/science.6344217

Schoeninger, M. J., and DeNiro, M. J. (1984). Nitrogen and carbon isotopic composition of bone collagen from marine and terrestrial animals. *Geochim. Cosmochim. Acta* 48, 625–639. doi: 10.1016/0016-7037(84)90091-7

Sealy, J. C., van der Merwe, N. J., Thorp, J. A. L., and Lanham, J. L. (1987). Nitrogen isotopic ecology in southern Africa: Implications for environmental and dietary tracing. *Geochim. Cosmochim. Acta* 51, 2707–2717. doi: 10.1016/0016-7037(87)90151-7

Segalen, L., Lee-Thorp, J. A., and Cerling, T. (2007). Timing of C_4 grass expansion across sub-Saharan Africa. *J. Hum. Evol.* 53, 549–559. doi: 10.1016/j.jhevol.2006.12.010

Sigman, D. M., Casciotti, K. L., Andreani, M., Barford, C., Galanter, M., and Böhlke, J. K. (2001). A bacterial method for the nitrogen isotopic analysis of nitrate in seawater and freshwater. *Anal. Chem.* 73, 4145–4153.

Smith, B. N., and Epstein, S. (1971). Two categories of c/c ratios for higher plants. *Plant Physiol.* 47, 380–384. doi: 10.1104/pp.47.3.380

Sponheimer, M., Grant, R., Ruiter, D., Lee-Thorp, J., Codron, D., and Codron, J. (2003). Diets of impala from Kruger National Park: Evidence from stable carbon isotopes. *Koedoe* 46, 101–106. doi: 10.4102/koedoe.v46i1.43

Sponheimer, M., and Lee-Thorp, J. A. (1999). Oxygen Isotopes in Enamel Carbonate and their Ecological Significance. *J. Archaeol. Sci.* 26, 723–728. doi: 10.1006/jasc.1998.0388

Stalmans, M. (2012). *Monitoring the recovery of wildlife in the Parque Nacional da Gorongosa through aerial surveys. A preliminary analysis.* Sofala: Parque Nacional da Gorongosa.

Stalmans, M., and Beilfuss, R. (2008). *Landscapes of the gorongosa national park.* Available online at: https://www.researchgate.net/publication/314878798_Landscapes_of_the_Gorongosa_National_Park

Stalmans, M., Peel, M., and Massad, T. (2014). *Aerial Wildlife Count of the Parque Nacional Da Gorongosa, Mozambique, October 2014.* Sofala: Parque Nacional da Gorongosa.

Stalmans, M. E., Massad, T. J., Peel, M. J. S., Tarnita, C. E., and Pringle, R. M. (2019). War-induced collapse and asymmetric recovery of large-mammal populations in Gorongosa National Park, Mozambique. *PLoS One* 14:e0212864. doi: 10.1371/journal.pone.0212864

Stanton, K., and Carlson, S. (2004). Microscale $\delta^{18}O$ and $\delta^{13}C$ isotopic analysis of an ontogenetic series of the hadrosaurid dinosaur Edmontosaurus: Implications for physiology and ecology. *Palaeogeogr. Palaeoclimatol. Palaeoecol.* 206, 257–287. doi: 10.1016/j.palaeo.2004.01.007

Steinbruch, F. (2010). Geology and geomorphology of the Urema Graben with emphasis on the evolution of Lake Urema. *J. Afr. Earth Sci.* 58, 272–284. doi: 10.1016/j.jafrearsci.2010.03.007

Steinbruch, F., and Merkel, B. (2008). Characterization of a Pleistocene thermal spring in Mozambique. *Hydrogeol. J.* 16, 1655–1668. doi: 10.1007/s10040-008-0343-9

Steinbruch, F., and Weise, S. (2014). Analysis of Water Stable Isotopes fingerprinting to inform conservation management : Lake Urema Wetland System, Mozambique. *Phys. Chem. Earth* 72–75, 13–23. doi: 10.1016/j.pce.2014.09.007

Steinhour, W. D., Stokes, M. R., Clark, J. H., Rogers, J. A., Davis, C. L., and Nelson, D. R. (1982). Estimation of the proportion of non-ammonia-nitrogen reaching the lower gut of the ruminant derived from bacterial and protozoal nitrogen. *Br. J. Nutr.* 48, 417–431. doi: 10.1079/BJN19820124

Straub, M., Sigman, D. M., Ren, H., Martínez-García, A., Meckler, A. N., Hain, M. P., et al. (2013). Changes in North Atlantic nitrogen fixation controlled by ocean circulation. *Nature* 501, 200–203. doi: 10.1038/nature12397

Sutoh, M., Koyama, T., and Yoneyama, T. (1987). Variations of natural 15N abundances in the tissues and digesta of domestic animals. *Radioisotopes* 36, 74–77. doi: 10.3769/radioisotopes.36.2_74

Swanson, H. K., Lysy, M., Power, M., Stasko, A. D., Johnson, J. D., and Reist, J. D. (2015). A new probabilistic method for quantifying n-dimensional ecological niches and niche overlap. *Ecology* 96, 318–324. doi: 10.1890/14-0235.1

Syväranta, J., Lensu, A., Marjomäki, T. J., Oksanen, S., and Jones, R. I. (2013). An Empirical Evaluation of the Utility of Convex Hull and Standard Ellipse Areas for Assessing Population Niche Widths from Stable Isotope Data. *PLoS One* 8:e56094. doi: 10.1371/journal.pone.0056094

Tejada-Lara, J. V., MacFadden, B. J., Bermudez, L., Rojas, G., Salas-Gismondi, R., and Flynn, J. J. (2018). Body mass predicts isotope enrichment in herbivorous mammals. *Proc. R. Soc. B Biol. Sci.* 285:20181020. doi: 10.1098/rspb.2018.1020

Teruel, J. D. D., Alcolea, A., Hernández, A., and Ruiz, A. J. O. (2015). Comparison of chemical composition of enamel and dentine in human, bovine, porcine and ovine teeth. *Arch. Oral Biol.* 60, 768–775. doi: 10.1016/j.archoralbio.2015.01.014

Thackeray, J. F., Henzi, S. P., and Brain, C. (1996). Stable carbon and nitrogen isotope analysis of bone collagen in *Papio cynocephalus ursinus*: Comparison with ungulates and *Homo sapiens* from southern and East African environments. *S. Afr. J. Sci.* 92, 209–213.

Tinley, K. L. (1977). *Framework of the Gorongosa ecosystem*. Pretoria: University of Pretoria.

Tsutaya, T., and Yoneda, M. (2015). Reconstruction of breastfeeding and weaning practices using stable isotope and trace element analyses: A review. *Am. J. Phys. Anthropol.* 156, 2–21. doi: 10.1002/ajpa.22657

Turner, T. F., Collyer, M. L., and Krabbenhoft, T. J. (2010). A general hypothesis-testing framework for stable isotope ratios in ecological studies. *Ecology* 91, 2227–2233. doi: 10.1890/09-1454.1

Ungar, P. S. (2010). *Mammal Teeth: Origin, Evolution, and Diversity*. Baltimore, MD: Johns Hopkins University Press.

Uno, K. T., Rivals, F., Bibi, F., Pante, M., Njau, J., and de la Torre, I. (2018). Large mammal diets and paleoecology across the Oldowan–Acheulean transition at Olduvai Gorge, Tanzania from stable isotope and tooth wear analyses. *J. Hum. Evol.* 120, 76–91. doi: 10.1016/j.jhevol.2018.01.002

Venter, J., and Kalule-Sabiti, M. (2016). Diet Composition of the Large Herbivores in Mkambati Nature Reserve, Eastern Cape, South Africa. *Afr. J. Wildl. Res.* 46, 49–56. doi: 10.3957/056.046.0049

Villamarin, F., Jardine, T. D., Bun, S. E., Marioni, B., and Magnusson, W. E. (2018). Body size is more important than diet in determining stable-isotope estimates of trophic position in crocodilians. *Sci. Rep.* 8:2020. doi: 10.1038/s41598-018-19918-6

Voigt, C. C., Krofel, M., Menges, V., Wachter, B., and Melzheimer, J. (2018). Sex-specific dietary specialization in a terrestrial apex predator, the leopard, revealed by stable isotope analysis. *J. Zool.* 306, 1–7. doi: 10.1111/jzo.12566

Vonhof, H., De Graaf, S., Spero, H., Schiebel, R., Verdegaal, S., Metcalfe, B., et al. (2020a). High-precision stable isotope analysis of <5 μg $CaCO_3$ samples by continuous-flow mass spectrometry. *Rapid Commun. Mass Spectrom.* 34:e8878. doi: 10.1002/rcm.8878

Vonhof, H., Tütken, T., Leichiter, J. N., Lüdecke, T., and Haug, G. H. (2020b). "High-precision stable isotope analysis of structural carbonate in $<$ 100 μg tooth enamel samples by continuous-flow mass spectrometry," in *The Society of Vertebrate Paleontology 80th Annual Meeting*. Available online at: https://vertpaleo.org/wp-content/uploads/2021/03/SVP_2020_Program-Abstracts-Volume-FINAL-for-Publishing-1.27.2021.pdf

Wang, X. T., Prokopenko, M. G., Sigman, D. M., Adkins, J. F., Robinson, L. F., Ren, H., et al. (2014). Isotopic composition of carbonate-bound organic nitrogen

in deep-sea scleractinian corals: A new window into past biogeochemical change. *Earth Planet. Sci. Lett.* 400, 243–250.

Wang, X. T., Sigman, D. M., Cohen, A. L., Sinclair, D. J., Sherrell, R. M., Weigand, M. A., et al. (2015). Isotopic composition of skeleton-bound organic nitrogen in reef-building symbiotic corals: A new method and proxy evaluation at Bermuda. *Geochim. Cosmochim. Acta* 148, 179–190.

Wang, X. T., Sigman, D. M., Prokopenko, M. G., Adkins, J. F., Robinson, L. F., Hines, S. K., et al. (2017). Deep-sea coral evidence for lower Southern Ocean surface nitrate concentrations during the last ice age. *Proc. Natl. Acad. Sci. U. S. A.* 114, 3352–3347. doi: 10.1073/pnas.1615718114

Wang, Y., and Cerling, T. E. (1994). A model of fossil tooth and bone diagenesis: Implications for paleodiet reconstruction from stable isotopes. *Palaeogeogr. Palaeoclimatol. Palaeoecol.* 107, 281–289. doi: 10.1016/0031-0182(94)90100-7

Weigand, M. A., Foriel, J., Barnett, B., Oleynik, S., and Sigman, D. M. (2016). Updates to instrumentation and protocols for isotopic analysis of nitrate by the denitrifier method. *Rapid Commun. Mass Spectrom.* 30, 1365–1383.

Wilson, D. E., and Mittermeier, R. A. (2009). *Handbook of the Mammals of the World*. Barcelona: Lynx Wsicions.

Wilson, E. O. (2014). *A window on eternity: A biologist's walk through Gorongosa National Park*. New York, NY: Simon and Schuster.

Wolf, J. (1960). "Der diurnale Säurerhythmus," in *Plant Respiration Inclusive Fermentations and Acid Metabolism/Pflanzenatmung Einschliesslich Gärungen und Säurestoffwechsel. Encyclopedia of Plant Physiology / Handbuch der Pflanzenphysiologie*, ed. J. Wolf (Berlin: Springer), 1930–2010.

Yang, D., Uno, K. T., Souron, A., McGrath, K., Pubert, É., and Cerling, T. E. (2020). Intra-tooth stable isotope profiles in warthog canines and third molars: Implications for paleoenvironmental reconstructions. *Chem. Geol.* 554:119799. doi: 10.1016/j.chemgeo.2020.119799

Zazzo, A., Balasse, M., and Patterson, W. P. (2005). High-resolution δ13C intratooth profiles in bovine enamel: Implications for mineralization pattern and isotopic attenuation. *Geochim. Cosmochim. Acta* 69, 3631–3642. doi: 10.1016/j.gca.2005.02.031

COPYRIGHT

© 2022 Lüdecke, Leichliter, Aldeias, Bamford, Biro, Braun, Capelli, Cybulski, Duprey, Ferreira da Silva, Foreman, Habermann, Haug, Martínez, Mathe, Mulch, Sigman, Vonhof, Bobe, Carvalho and Martínez-García. This is an open-access article distributed under the terms of the Creative Commons Attribution License (CC BY). The use, distribution or reproduction in other forums is permitted, provided the original author(s) and the copyright owner(s) are credited and that the original publication in this journal is cited, in accordance with accepted academic practice. No use, distribution or reproduction is permitted which does not comply with these terms.

frontiers | Frontiers in Ecology and Evolution

TYPE Original Research
PUBLISHED 19 December 2022
DOI 10.3389/fevo.2022.1059155

Check for updates

OPEN ACCESS

EDITED BY
Jason Newton,
University of Glasgow,
United Kingdom

REVIEWED BY
Daniel Ernesto Naya,
Universidad de la República,
Uruguay
Leandro Bergamino,
Universidad de la República,
Uruguay

*CORRESPONDENCE
Jenilee Gobin
jenileegobin@trentu.ca

SPECIALTY SECTION
This article was submitted to Population, Community, and Ecosystem Dynamics, a section of the journal Frontiers in Ecology and Evolution

RECEIVED 30 September 2022
ACCEPTED 29 November 2022
PUBLISHED 19 December 2022

CITATION
Gobin J, Szumski CM, Roth JD and Murray DL (2022) Patterns of dietary niche breadth and overlap are maintained for two closely related carnivores across broad geographic scales.
Front. Ecol. Evol. 10:1059155.
doi: 10.3389/fevo.2022.1059155

COPYRIGHT
© 2022 Gobin, Szumski, Roth and Murray. This is an open-access article distributed under the terms of the Creative Commons Attribution License (CC BY). The use, distribution or reproduction in other forums is permitted, provided the original author(s) and the copyright owner(s) are credited and that the original publication in this journal is cited, in accordance with accepted academic practice. No use, distribution or reproduction is permitted which does not comply with these terms.

Patterns of dietary niche breadth and overlap are maintained for two closely related carnivores across broad geographic scales

Jenilee Gobin[1]*, Christa M. Szumski[2], James D. Roth[2] and Dennis L. Murray[1,2]

[1]Biology Department, Trent University, Peterborough, ON, Canada, [2]Department of Biological Sciences, University of Manitoba, Winnipeg, MB, Canada

Ecological studies investigating niche breadth and overlap often have limited spatial and temporal scale, preventing generalizations across varying environments and communities. For example, it is not clear whether species having restricted diets maintain such patterns relative to closely related species and across their geographic range of co-occurrence. We used stable isotope analysis of hair and fur samples collected from four regions of sympatry for Canada lynx (*Lynx canadensis*) and bobcat (*Lynx rufus*) spanning southern Canada and the northern United States, to test the prediction that the more generalist species (bobcat) exhibits a wider dietary niche than the more specialist species (Canada lynx) and that this pattern is consistent across different regions. We further predicted that Canada lynx diet would consistently exhibit greater overlap with that of bobcat compared to overlap of bobcat diet with Canada lynx. We found that Canada lynx had a narrower dietary niche than bobcat, with a high probability of overlap (85–95%) with bobcat, whereas the bobcat dietary niche had up to a 50% probability of overlap with Canada lynx. These patterns of dietary niche breadth and overlap were consistent across geographic regions despite some regional variation in diet breadth and position, for both species. Such consistent patterns could reflect a lack of plasticity in species dietary niches. Given the increasingly recognized importance of understanding dietary niche breadth and overlap across large spatial scales, further research is needed to investigate the mechanisms by which broad-scale patterns are maintained across species and systems.

KEYWORDS

***Lynx canadensis*, *Lynx rufus*, specialist-generalist paradigm, niche breadth, niche overlap, broad-scale patterns**

Introduction

Variation in dietary niche breadth has been associated with various aspects of species distributions, including range size and expansion (Lanszki et al., 2022), heterogeneity of spatial distributions (Alberdi et al., 2020) and environments occupied (Walsh and Tucker, 2020; Fargallo et al., 2022), and responses to landscape change (Kellner et al., 2019). This

diversity of outcomes highlights that many factors likely contribute to shaping dietary niche breadth. It also emphasizes the relevance of broad-scale patterns in dietary niche breadth to understanding community and ecosystem dynamics, predicting species responses to global change, and addressing biodiversity declines. Given the various factors that can influence dietary niche breadth and overlap, regional variation could affect broad-scale patterns of niche breadth within a species and overlap between species. However, these uncertainties have rarely been investigated across broad spatial scales, especially among species that occupy large geographic ranges and occur at low densities across the landscape.

Niche breadth is influenced by the availability of preferred resources, which may be impacted by community interactions, and proclivity to exploit alternate resources (Mac Arthur and Levins, 1964; Rosenzweig, 1991; McGill et al., 2006). Foraging theory predicts that, owing to their higher proficiency to acquire preferred resources, species with restricted food preferences will have narrow dietary niches that overlap with those of sympatric species having more generalized feeding patterns (Stephens and Krebs, 1986). Alternatively, species with broad food preferences and that consume alternate food types when preferred resources are scarce will be reflected by wider dietary niches (Stephens and Krebs, 1986). However, local conditions or circumstances such as the frequency with which resources, environments, or communities fluctuate spatially and/or temporally can alter foraging strategies (Mac Arthur and Levins, 1964; Devictor et al., 2010). Individual specialization further contributes to the population-level diet breadth and variation observed across different spatial and temporal scales (Bolnick et al., 2003; Devictor et al., 2010; Costa-Pereira et al., 2019). Given the challenges of collecting data on trophic interactions across large scales in the field, the prediction that patterns of dietary niche position, breadth, and overlap are maintained across geographic ranges has rarely been tested. It follows that stable isotope analysis offers a novel and informative means for assessing this prediction and potentially overcoming challenges associated with conducting expansive research.

We assessed the dietary niche of two closely related carnivores, known to consume similar prey, across multiple regions spanning a broad geographic scale. Canada lynx (*Lynx canadensis*) and bobcat (*Lynx rufus*) are typically classified as "specialist" and "generalist" consumers, respectively (Anderson and Lovallo, 2003), although these classifications are recognized as being over-simplifications when considered across temporal or spatial scales (e.g., see Roth et al., 2007; Burstahler et al., 2016). Canada lynx primarily occupy the North American boreal forest, Rocky Mountains, and northeast United States, whereas bobcat occur in southern Canada, throughout the contiguous United States and extend into Mexico (Anderson and Lovallo, 2003). The two species thus occur in sympatry only across the Canada-United States border and in the Rocky Mountains (Peers et al., 2013). Increased abundance of bobcats as well as their recent range expansion (Lavoie et al., 2009; Roberts and Crimmins, 2010), and reductions in lynx abundance and range retraction (Koen et al., 2014b; Marrotte and Bowman, 2021) could also be related to dietary niche variation for one or both species. We evaluated dietary niche position, breadth and overlap for Canada lynx and bobcat using stable isotope analysis of hair and fur samples collected from multiple regions spanning their sympatric range. We predicted that: (1) dietary niche position of both species would vary regionally (e.g., due to regional differences in prey availability and/or isotopic signatures); (2) Canada lynx dietary niche would consistently be narrower than that of bobcat; and (3) dietary niche of Canada lynx would be more similar to that of bobcat (i.e., have a higher probability of overlap) than vice versa.

Materials and methods

Sample collection and isotopic analysis

Canada lynx and bobcat hair and fur samples were collected between 2009 and 2012 from the North American Fur Auctions (Toronto, ON) and Fur Harvester Auction Inc. (North Bay, ON). We analyzed samples available for areas of sympatry between Canada lynx and bobcat in four regions: (1) southeastern British Columbia (Canada lynx, $n = 28$; bobcat, $n = 54$), (2) west of Lake Superior in Ontario and Minnesota (Canada lynx, $n = 63$; bobcat, $n = 19$), (3) the interlake region of Sault Ste. Marie, Ontario and Michigan (Canada lynx, $n = 18$; bobcat, $n = 8$), and (4) southern Québec along the St. Lawrence river (Canada lynx, $n = 32$; bobcat, $n = 23$), hereafter referred to as British Columbia, western Ontario, central Ontario, and Québec, respectively. Geolocations for harvested pelts represent the centroid of the trapline or management unit from which each animal was harvested (Row et al., 2014; Figure 1). Note that despite these regions of sympatry, there is limited evidence that the two species hybridize (Koen et al., 2014a).

We measured stable isotope ratios ($\delta^{13}C$ and $\delta^{15}N$) of fur samples to assess niche position, breadth and overlap for the two species. Canada lynx and bobcat share similar hair growth patterns, moulting once in the spring (April–May) and once in the autumn (October–November; Quinn and Parker, 1987; Anderson and Lovallo, 2003). Canada lynx and bobcat fur samples were taken from the hind leg of pelts from winter-harvested animals and therefore, stable isotope measurements reflect the autumn diet for both species. All fur samples were washed with soap and water, rinsed thoroughly, and then oven-dried at 60°C for 48 h. Samples were homogenized into a fine powder using a ball mill, wrapped in tin capsules, and sent to the Chemical Tracers Laboratory, Windsor, ON, Canada for $\delta^{13}C$ and $\delta^{15}N$ measurement using a continuous-flow isotope ratio mass spectrometer.

Data analysis

Based on previous studies that found little annual variation in the diets of Canada lynx in the southern part of their range (Szumski et al., in review), we assumed limited temporal variation in Canada lynx and bobcat diets during the 4 years of our study

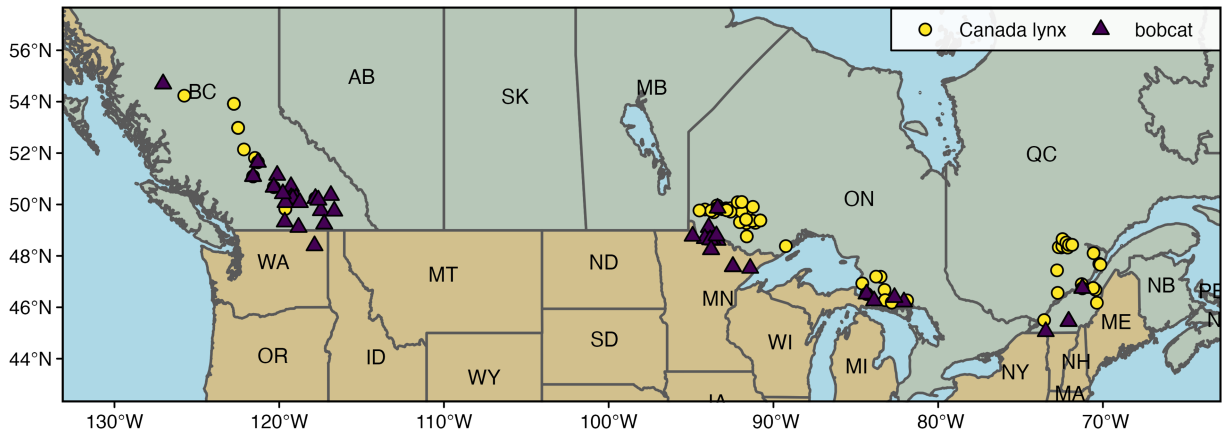

FIGURE 1
Map of Canada lynx and bobcat sampling locations in North America.

and therefore pooled observations within each region across years. Note that isotopic signatures did not differ qualitatively according to year in which samples were taken for region (Supplementary Figure 1). To further confirm our assumption, we fit a multivariate generalized linear mixed effects model using the MCMCglmm package in R (Hadfield, 2010) with species and region as fixed effects and random intercepts for year. The random year effect was almost zero (posterior mean = 0.0017, lower 95% CI = 1.6e-17, upper 95% CI = 0.0026) and explained <1% of the total variation in $\delta^{13}C$ and $\delta^{15}N$ ratios, confirming the negligible effect of year.

We compared niche breadth and overlap of lynx and bobcat within each region using the R packages "SIBER" (Jackson et al., 2011) and "nicheROVER" (Lysy et al., 2015; Swanson et al., 2015). The isotopic niche region is defined by each niche axis ($\delta^{13}C$ and $\delta^{15}N$) and treated as a trait probability density function that can be compared against other groups (Carmona et al., 2016). Uncertainty is incorporated into niche region estimates using a Bayesian framework, whereby the 95% highest density interval for each niche axis is used as a continuous distribution from which to sample iteratively. We estimated niche regions based on the mean and variance of $\delta^{13}C$ and $\delta^{15}N$ for each species using an uninformative, normal Inverse Wishart prior ($\alpha = 95\%$). We ran two chains of 10,000 iterations, burning the first 1,000 draws and thinning every 10 draws.

The breadth of resource use along both diet axes ($\delta^{13}C$ and $\delta^{15}N$) can be summarized by standard ellipse area (*SEA*) in SIBER, and further broken down into each niche axis for analysis of niche position and overlap in nicheROVER. Posterior distributions represent the full range of feasible parameter values, given observed data and prior probabilities (which we kept vague to minimize the influence on the posterior). Thus, probabilistic difference in niche position and variance between species is inferred from overlap of posterior distributions. As probability density functions integrate to 1, density of posterior solutions is directly proportional to relative proportion of that trait value in the population (Carmona et al., 2016) and thus may be used as a proxy for exploitation proficiency of the population (Devictor et al., 2010). Niche overlap is then calculated as the probability that the isotopic ratio of a random individual from one species would occur within the 95% highest density niche region of the competitor species.

Multivariate normality is assumed for both SIBER and nicheROVER, which we verified graphically using qq-plots of Mahalanobis distances (Legendre and Legendre, 2012) for each species and region. Three bobcat samples were identified as statistical outliers that were excluded from analysis: one from British Columbia with very low $\delta^{15}N$ (−0.32‰), one from British Columbia with very high $\delta^{13}C$ (−17.5‰), and one from Québec that was enriched in both ^{13}C and ^{15}N ($\delta^{13}C = -18.5$‰, $\delta^{15}N = 9.14$‰). Given that these stable isotope ratios are nonetheless consistent with the scope of values reported for North American mammals (Roth et al., 2007), we repeated the analysis with these outliers included and found that the results (Supplementary Figures 2–5) remained consistent with those presented here.

Results

As expected, niche position of each species varied regionally (Figures 2, 3). Mean $\delta^{13}C$ of Canada lynx varied by up to 0.66‰ across regions, and less than that of bobcat, which varied by up to 1.90‰. Alternatively, mean $\delta^{15}N$ of bobcat varied by up to 1.09‰, and less than that of Canada lynx, which varied by up to 1.83‰. The relative niche position of Canada lynx and bobcat also differed along one niche axis ($\delta^{13}C$ or $\delta^{15}N$) across all study regions (Figures 2, 3). In all regions except British Columbia, the mean $\delta^{15}N$ for bobcat was 0.7–0.9‰ higher than that for lynx, but mean $\delta^{13}C$ values were similar for both species. In British Columbia, mean $\delta^{13}C$ for bobcat was 1.7‰ higher than that for lynx and mean $\delta^{15}N$ was similar for both species. Variance in $\delta^{13}C$ and $\delta^{15}N$

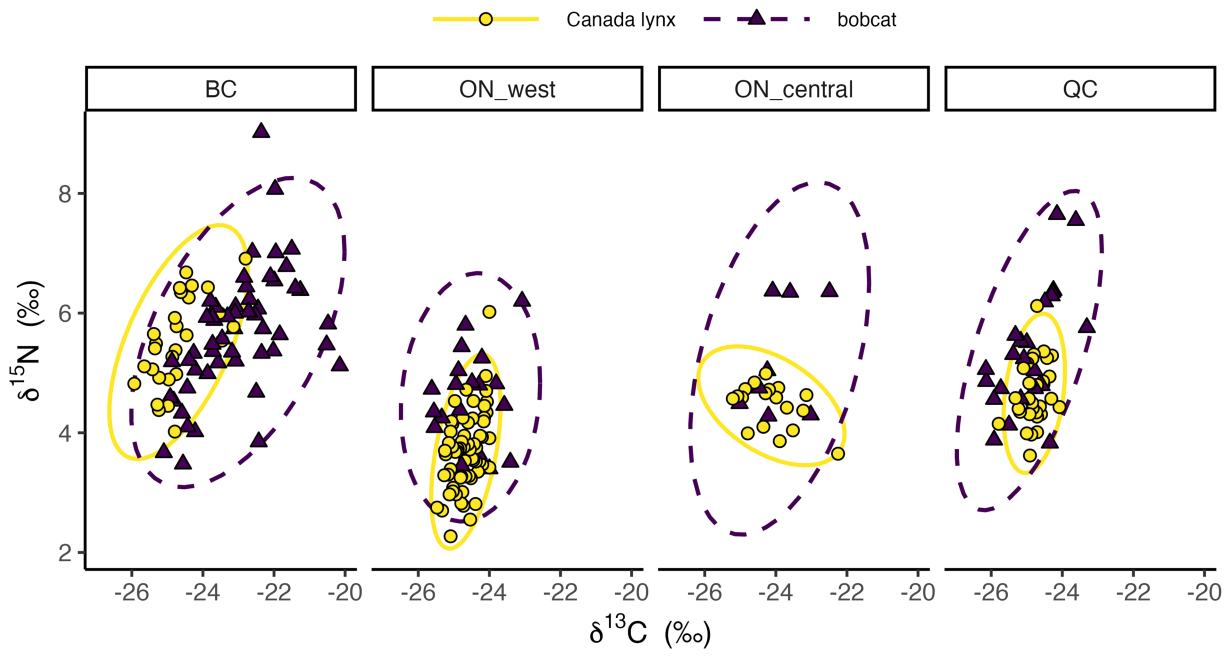

FIGURE 2
Stable isotope ratios of Canada lynx and bobcat in each study region: British Columbia (BC), western Ontario (ON_west), central Ontario (ON_central), and Québec (QC). Ellipses depict 95% confidence levels.

were generally higher for bobcat than lynx, reflecting the presumed broader range of prey consumed by bobcat, except for $\delta^{13}C$ in central Ontario and $\delta^{15}N$ in western Ontario, where estimates for both species were similar. Covariances of $\delta^{13}C$ and $\delta^{15}N$ were generally positive, except for lynx in central Ontario that was negative, suggesting that isotopic ratios of $\delta^{13}C$ and $\delta^{15}N$ tend to vary together.

Stable isotope ratios revealed greater variation in bobcat diet, reflecting consumption of a greater diversity of prey compared to Canada lynx. This observation was consistent across all four regions, supporting the prediction that the dietary niche of lynx would consistently be narrower than that of bobcat (Figures 2, 4). Mean estimates of isotopic niche breadth (measured as the standard ellipse area) for bobcat ranged between 1.8–3.3‰^{2} and were consistently higher than that of Canada lynx (0.5–1.5‰^{2}) by a factor of 2.3 (British Columbia) to 3.8 (Québec; Figure 4).

Our findings further support the prediction that dietary niche of Canada lynx would exhibit a higher probability of overlap with that of bobcat than vice versa (Figure 5). The probabilities of a lynx's isotopic ratios occurring within the dietary niche region of bobcat were consistently skewed toward 100% (mean estimates ranging between 85% and 95% across study regions), indicating the likelihood of complete niche overlap of lynx with sympatric bobcat populations. In contrast, the probability of an individual bobcat's diet overlapping with dietary niche of the sympatric lynx population was considerably lower in all regions (mean estimates of 35–50%; Figure 5). Credible intervals for estimates of mean diet overlap between species were broader for central and western Ontario, likely due to smaller sample sizes ($n = 19$ bobcat in western Ontario; $n = 8$ bobcat and $n = 18$ Canada lynx in central Ontario). Nonetheless, the remarkable consistency in these species' dietary niche breadth and overlap across regions suggests that general patterns of diet breadth and differentiation operate at large spatial scales.

Discussion

Our results revealed consistent patterns in dietary niche breadth and overlap of two sympatric carnivores, across a broad spatial scale. The dietary niche of Canada lynx was narrower and had a high probability of overlapping with the niche region of bobcat, whose dietary niche was broader and had a lower probability of overlapping with that of Canada lynx, across all four regions. Consistency in these patterns occurred despite regional variation in the niche position and breadth of each carnivore, providing compelling evidence that patterns in niche breadth and overlap are maintained across broad geographic scales.

Previous investigations into broad geographic patterns in dietary niches and their drivers have mainly focused on interspecific variation (e.g., Papacostas and Freestone, 2016; Gainsbury and Meiri, 2017; Granot and Belmaker, 2019), whereas studies investigating intraspecific variation have largely focused on individual specialization and niche characteristics in the context of environmental variation occurring at more localized scales within a single region or population (e.g., Woo et al., 2008; Abbas et al., 2011; Navarro-López and Fargallo, 2015). Therefore, the current study is unique in that we investigate intraspecific

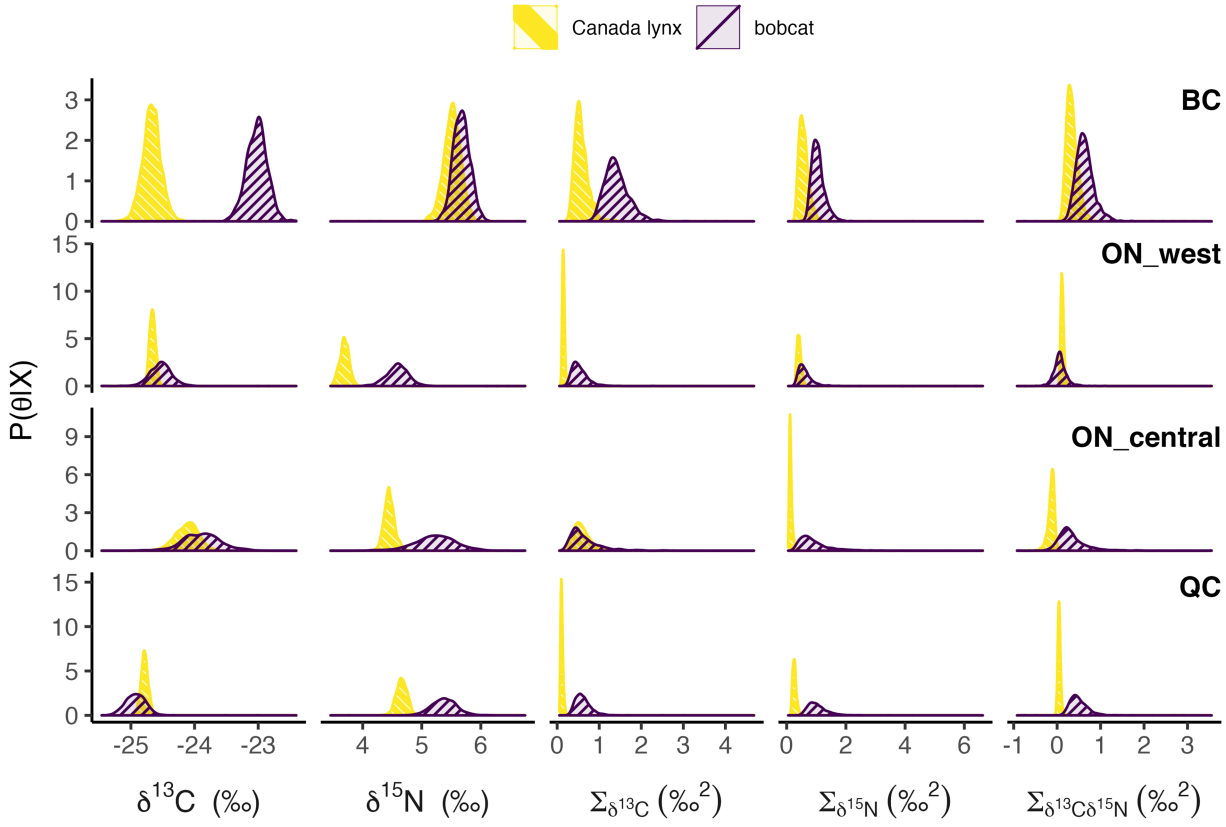

FIGURE 3
Posterior distributions of mean and variance/covariance (Σ) of $\delta^{13}C$ and $\delta^{15}N$ stable isotope ratios for Canada lynx and bobcat in each study region: British Columbia (BC), western Ontario (ON_west), central Ontario (ON_central), and Québec (QC).

variation in niche position and breadth across a broad spatial scale, and show that despite regional variation, interspecific patterns in niche breadth and overlap appear to be maintained for two closely related species. As predicted by the ecological theory, the niche region of the species with more restricted feeding (Canada lynx) consistently exhibited a narrower dietary niche with a high probability of overlap with the more generalist consumer (bobcat), whereas the broader niche region of bobcat exhibited much lower probability of overlap with Canada lynx. Although we did not infer the specific drivers of this consistency, observed patterns could arise from interspecific variation in dietary preferences or competitive interactions. Previous studies examining spatial and temporal variation in niche breadth of Canada lynx found that it appears to vary with the dynamics of its primary prey (snowshoe hare) both over time (Burstahler et al., 2016) and spatially along a latitudinal gradient (Roth et al., 2007; Szumski et al., in review), suggesting that prey availability might be key in determining feeding strategy. If this is the case for both bobcat and Canada lynx, we might expect regional variation in niche breadth to be positively correlated for the two species. While we observed this trend overall (Supplementary Figure 6), we lack sufficient data to formally test this prediction. Yurkowski et al. (2016) is one of the few other examples of studies having characterized dietary niches across a broad spatial scale. That study detected lower population-level niche breadth of both ringed seals and beluga whales at higher latitudes, presumably due to lower prey diversity in the high Arctic (Yurkowski et al., 2016). They further revealed dietary generalization in beluga whales and individual specialization in ringed seal that was higher in populations with wider niche breadth (Yurkowski et al., 2016), implying that latitudinal variation in population-level niche breadth is driven by different foraging strategies at the individual level for each species. The above findings highlight the need for further research investigating intraspecific variation in niche breadth over broad geographic scales, its role in population-level and interspecific patterns, and the underlying driving mechanisms. Such efforts will be especially important to better understand the implications of observed broad-scale changes in species distributions and biodiversity loss.

Many factors could influence spatial variation in niche breadth. Niche breadth is predicted to vary with prey diversity and availability (Yurkowski et al., 2016; Carvalho and Davoren, 2020). Likewise, predator densities can also influence feeding strategies *via* intraspecific interactions (Svanbäck and Bolnick, 2007). Environments that are either extreme or stable could promote dietary restriction due to lower ecological opportunity or local adaptation of

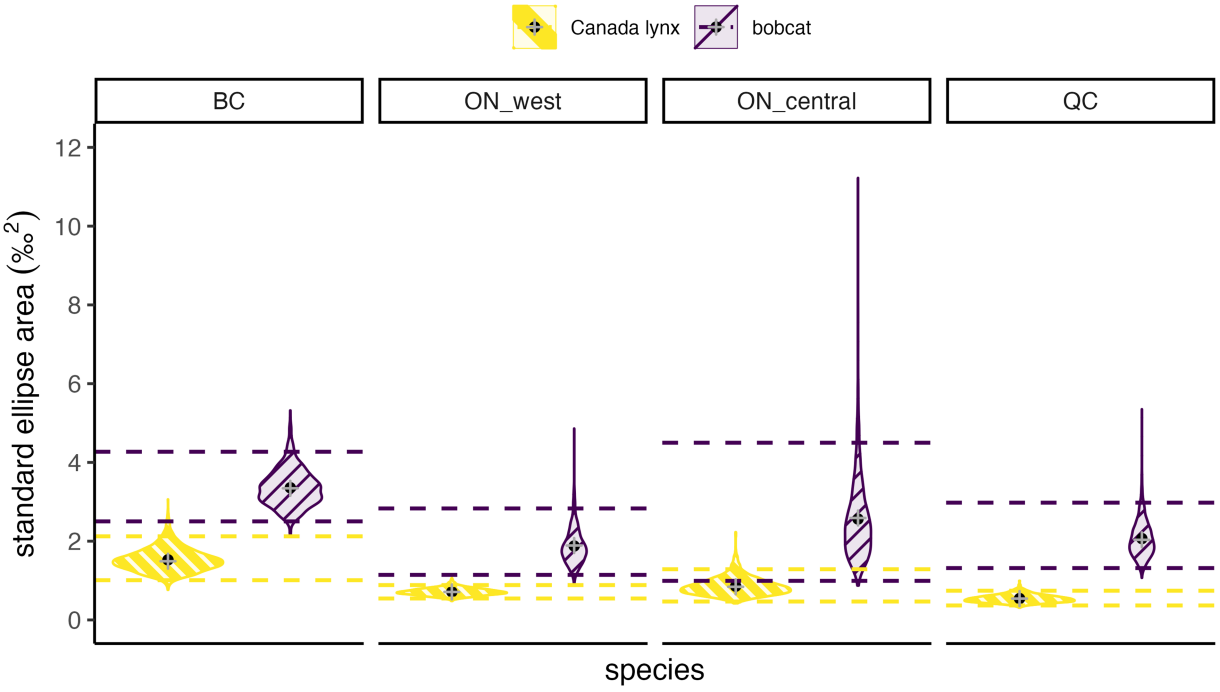

FIGURE 4
Posterior distributions of dietary niche breadth estimates measured as standard ellipse area for lynx and bobcat in each study region: British Columbia (BC), western Ontario (ON_west), central Ontario (ON_central), and Québec (QC). Black points show the mean, gray plus signs show the sample-corrected standard ellipse area, and dashed lines show 95% credible intervals of the posterior distribution.

narrow ecological niches (Jocque et al., 2010; Bonetti and Wiens, 2014; Rivas-Salvador et al., 2019). Ecological specialization is also widely predicted to arise in environments with greater species richness owing to more opportunity for community-level interactions (Kartzinel et al., 2015; Granot and Belmaker, 2019). Mechanisms underlying patterns in niche breadth and overlap we observed could be important for understanding range expansion and retraction of bobcat and Canada lynx, respectively (Koen et al., 2014; Marrotte and Bowman, 2021). A recent study suggested that trophic niches based on resource use (i.e., Eltonian niche) may be more relevant to the distribution of species at fine spatial scales, while habitat niches based on climate or environmental conditions (i.e., Grinnellian niche) may be more important across large geographic scales (Stevens, 2022). However, due to challenges associated with collecting necessary field data, few studies have characterized trophic niches across broad spatial scales thus limiting their incorporation into species distribution models (Austin, 2002; Araújo and Guisan, 2006). Peers et al. (2013) investigated the Grinnellian niche of Canada lynx and bobcat, concluding that bobcat may displace Canada lynx when both species overlap. However, they also found that bobcat habitat niche breadth expanded in regions of sympatry with lynx (Peers et al., 2013), suggesting that the former species might also be displaced by Canada lynx. We do not know whether these habitat and space use dynamics translate to our observations of Canada lynx and bobcat dietary breadth and overlap. It is notable that Grinnellian and Eltonian niches are not independent of each other, as co-occurring species have access to similar resources. However, the mechanisms influencing breadth of one type of niche does not imply that the same mechanisms act on the other. Further investigation into spatial variation in niche breadth and the relative importance of environmental conditions and resource use in species distributions will therefore be valuable, especially for those species undergoing range shifts, expansions, and contractions, like Canada lynx and bobcat. Stable isotope analysis of fur or other samples provides an efficient and robust method for addressing these questions, compared to more traditional approaches involving intensive field research.

When trying to assess dietary niches using stable isotopes, spatial and temporal variation in isotopic ratios of both consumers and their food sources therefore need be considered, as isotopic signatures are expected to vary with carbon sources, assimilation, as well as community trophic structure (Farquhar et al., 1989; Layman et al., 2012). Other studies have measured isotope ratio variation across regions for both snowshoe hare and red squirrel (*Tamiasciurus hudsonicus*), the primary prey for lynx (Roth et al., 2007; Merkle et al., 2017) and bobcat (Newbury and Hodges, 2018) in our study regions. Red squirrels (and other rodents) are typically enriched in both $\delta^{13}C$ and $\delta^{15}N$ compared to snowshoe hares (Roth et al., 2007; Merkle et al., 2017; Szumski et al., submitted). The mean values of $\delta^{13}C$ and $\delta^{15}N$ of Canada lynx in our study are consistent with values reflecting high consumption of snowshoe hares, whereas mean $\delta^{13}C$ or $\delta^{15}N$ of bobcat were consistently elevated. Our findings are also consistent with previous studies showing general patterns of prey consumption for both species (e.g., O'Donoghue et al., 2001; Witczuk et al., 2015; Ivan and Shenk, 2016; Newbury and Hodges,

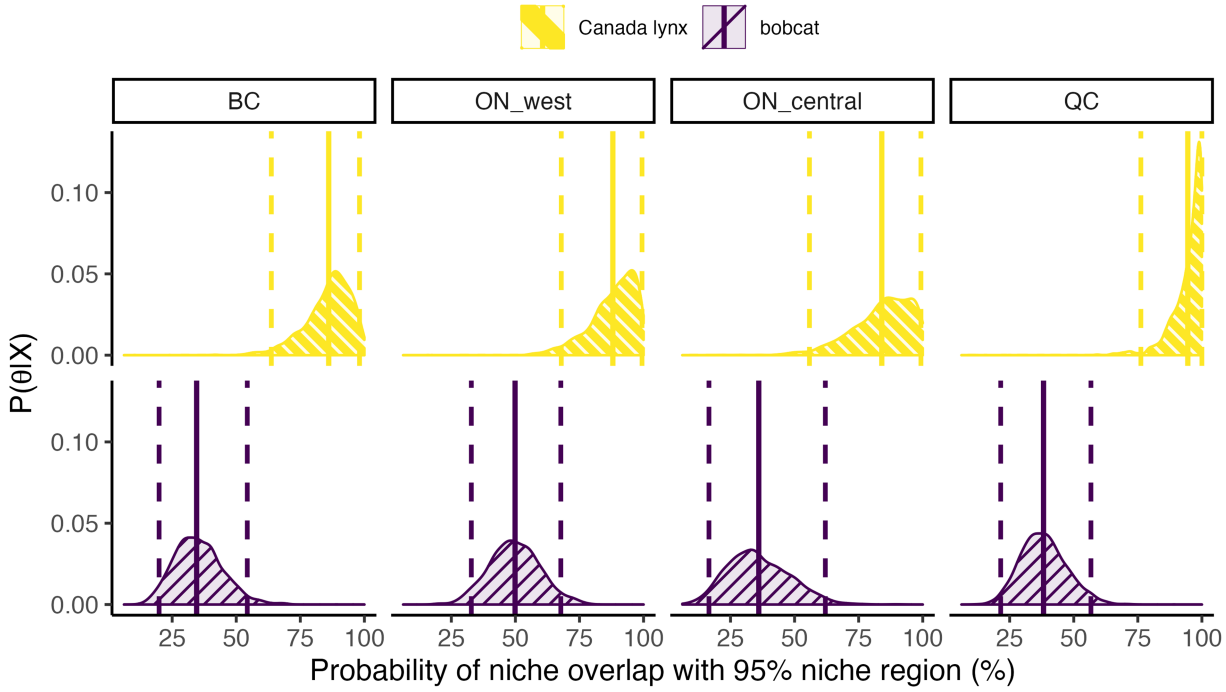

FIGURE 5
Posterior distributions of the probability that an individual of one species falls within the 95% niche region of the competitor species in each study region: British Columbia (BC), western Ontario (ON_west), central Ontario (ON_central), and Québec (QC). Vertical lines show the mean (solid) and 95% credible intervals (dashed) of the posterior distribution.

2018). Consequently, it is likely that Canada lynx in our study consumed a greater proportion of snowshoe hares, whereas the broader dietary niche of bobcat reflects a greater reliance on different prey types such as red squirrels and other rodents.

Although dietary niches may be related to isotopic niches, they are not the same. Variation in isotopic niches arises not only from changes in diet but also from variation in isotopic baselines and diet-tissue discrimination factors (Wolf et al., 2009; Hette-Tronquart, 2019). For example, food availability was shown to influence individual isotopic signatures through differences in diet-consumer isotope fractionation associated with variation in growth rates (Gorokhova, 2018). Various stress factors (e.g., malnutrition, parasitism, exposure to toxic substances) were also found to influence isotopic signatures, which could also be misinterpreted as variation in dietary niches (Karlson et al., 2018). Isotope ratios like those used in our study reflect a mean value of an individual's diet and, consequently, measures of dietary niches (i.e., position, breadth, and overlap) reflect between-individual variation rather than within-individual variation (Bearhop et al., 2004; Jackson et al., 2011). Within-individual variation in dietary niches can be measured by sampling various tissues from the same individual that vary in the time with which dietary signatures are integrated (Bearhop et al., 2004) or by performing stable isotope analysis on serially sectioned tissues (Rogers et al., 2020). Demographic factors such as age/size structure and sex ratios are also expected to influence intra- and interpopulation variation in isotopic signatures (Bolnick et al., 2003; Burstahler et al., 2016). In one lynx population, age classes responded differently to changes in hare density, with diet breadth of yearlings increasing at low hare densities, while adults and dependent juveniles maintained a constant diet through the initial decline in hare density (Burstahler et al., 2016). Although these data were not available in the current study, future studies investigating mechanisms underlying patterns in niche breadth and overlap would therefore benefit from ancillary data collected at the level of individuals (e.g., age, sex, health status) and stable isotope analyses that permit estimation of both between- and within-individual variation to assess the role of individual specialization across broad geographic scales.

To conclude, we recognize that organisms can adjust foraging strategies in response to a range of ecological conditions and constraints (e.g., Díaz-Ruiz et al., 2013, Manenti et al., 2013, Karanth et al., 2017). Despite this, Canada lynx and bobcat exhibit a remarkably consistent pattern of niche breadth and overlap across regions spanning a broad spatial scale, for which the underlying mechanisms remain unknown. However, this finding provides evidence that could suggest a lack of plasticity in species' diet features, implying that many community-level trophic interactions and ecosystem dynamics may be shaped largely by evolutionary processes that operate at the scale of the species rather than the population. Connecting mechanisms driving niche breadth and overlap at fine scales to those resulting in maintenance of consistent patterns across broad spatial scales will be important for furthering our understanding of factors influencing distribution of species and biodiversity loss, as well as incorporating trophic interactions into

models aimed at predicting responses to climate change, range shifts, species invasions, habitat loss and fragmentation, and other sources of environmental variation.

Data availability statement

The datasets presented in this study can be found in online repositories. The names of the repository/repositories and accession number(s) can be found at: https://github.com/JenileeGobin/lynx-bobcat-diet.

Author contributions

CS, JR, and DM conceived the study. CS processed samples and sent them for analysis, performed preliminary data analysis, and wrote an initial draft of the manuscript. JG conducted the data analyses presented in the current manuscript and supplementary materials, generated figures, and wrote the final draft of the manuscript with input from CS, JR, and DM. All authors contributed to the article and approved the submitted version.

Funding

Funding was provided by a Strategic NSERC grant awarded to DM and co-authors.

Acknowledgments

We would like to thank the North American Fur Auctions Inc. who made this work possible.

Conflict of interest

The authors declare that the research was conducted in the absence of any commercial or financial relationships that could be construed as a potential conflict of interest.

Publisher's note

All claims expressed in this article are solely those of the authors and do not necessarily represent those of their affiliated organizations, or those of the publisher, the editors and the reviewers. Any product that may be evaluated in this article, or claim that may be made by its manufacturer, is not guaranteed or endorsed by the publisher.

Supplementary material

The Supplementary material for this article can be found online at: https://www.frontiersin.org/articles/10.3389/fevo.2022.1059155/full#supplementary-material

References

Abbas, F., Morellet, N., Hewison, A. J. M., Merlet, J., Cargnelutti, B., Lourtet, B., et al. (2011). Landscape fragmentation generates spatial variation of diet composition and quality in a generalist herbivore. *Oecologia* 167, 401–411. doi: 10.1007/s00442-011-1994-0

Alberdi, A., Razgour, O., Aizpurua, O., Novella-Fernandez, R., Aihartza, J., Budinski, I., et al. (2020). DNA metabarcoding and spatial modelling link diet diversification with distribution homogeneity in European bats. *Nat. Commun.* 11, 1154–1162. doi: 10.1038/s41467-020-14961-2

Anderson, E. M., and Lovallo, M. J. (2003). "Bobcat and lynx," in *Wild mammals of North America*. eds. G. A. Feldhamer and B. Thompson (Baltimore, MD: Johns Hopkins University Press), 758–786.

Araújo, M. B., and Guisan, A. (2006). Five (or so) challenges for species distribution modelling. *J. Biogeogr.* 33, 1677–1688. doi: 10.1111/j.1365-2699.2006.01584.x

Austin, M. P. (2002). Spatial prediction of species distribution: an interface between ecological theory and statistical modelling. *Ecol. Model.* 157, 101–118. doi: 10.1016/S0304-3800(02)00205-3

Bearhop, S., Adams, C. E., Waldron, S., Fuller, R. A., and Macleod, H. (2004). Determining trophic niche width: a novel approach using stable isotope analysis. *J. Anim. Ecol.* 73, 1007–1012. doi: 10.1111/j.0021-8790.2004.00861.x

Bolnick, D. I., Svanbäck, R., Fordyce, J. A., Yang, L. H., Davis, J. M., Hulsey, C. D., et al. (2003). The ecology of individuals: incidence and implications of individual specialization. *Am. Nat.* 161, 1–28. doi: 10.1086/343878

Bonetti, M. F., and Wiens, J. J. (2014). Evolution of climatic niche specialization: a phylogenetic analysis in amphibians. *Proc. R. Soc. B* 281:20133229. doi: 10.1098/rspb.2013.3229

Burstahler, C. M., Roth, J. D., Gau, R. J., and Murray, D. L. (2016). Demographic differences in diet breadth of Canada lynx during a fluctuation in prey availability. *Ecol. Evol.* 6, 6366–6375. doi: 10.1002/ece3.2115

Carmona, C. P., de Bello, F., Mason, N. W. H., and Leps, J. (2016). Traits without borders: integrating functional diversity across scales. *Trends Ecol. Evol.* 31, 382–394. doi: 10.1016/j.tree.2016.02.003

Carvalho, P. C., and Davoren, G. K. (2020). Niche dynamics of sympatric non-breeding shearwaters under varying prey availability. *IBIS* 162, 701–712. doi: 10.1111/ibi.12783

Costa-Pereira, R., Araújo, M. S., Souza, F. L., and Ingram, T. (2019). Competition and resource breadth shape niche variation and overlap in multiple trophic dimensions. *Proc. R. Soc. B* 286:20190369. doi: 10.1098/rspb.2019.0369

Devictor, V., Clavel, J., Julliard, R., Lavergne, S., Mouillot, D., Thuiller, W., et al. (2010). Defining and measuring ecological specialization. *J. Appl. Ecol.* 47, 15–25. doi: 10.1111/j.1365-2664.2009.01744.x

Díaz-Ruiz, F., Delibes-Mateos, M., García-Moreno, J. L., López-Martín, J. M., Ferreira, C., and Ferreras, P. (2013). Biogeographical patterns in the diet of an opportunistic predator: the red fox Vulpes vulpesin the Iberian Peninsula. *Mammal Rev.* 43, 59–70. doi: 10.1111/j.1365-2907.2011.00206.x

Fargallo, J. A., Navarro-López, J., Cantalapiedra, J. L., Pelegrin, J. S., and Fernández, M. H. (2022). Trophic niche breadth of Falconidae species predicts biomic specialization but not range size. *Biology* 11, 522–537. doi: 10.3390/biology11040522

Farquhar, G. D., Ehleringer, J. R., and Hubick, K. T. (1989). Carbon isotope discrimination and photosynthesis. *Annu. Rev. Plant Physiol. Plant Mol. Biol.* 40, 503–537. doi: 10.1146/annurev.pp.40.060189.002443

Gainsbury, A., and Meiri, S. (2017). The latitudinal diversity gradient and interspecific competition: no global relationship between lizard dietary niche breadth and species richness. *Glob. Ecol. Biogeogr.* 26, 536–572. doi: 10.1111/geb.12560

Gorokhova, E. (2018). Individual growth as a non-dietary determinant of the isotopic niche metrics. *Methods Ecol. Evol.* 9, 269–277. doi: 10.1111/2041-210X.12887

Granot, I., and Belmaker, J. (2019). Niche breadth and species richness: correlation strength, scale and mechanisms. *Glob. Ecol. Biogeogr.* 29, 159–170. doi: 10.1111/geb.13011

Hadfield, J. D. (2010). MCMC methods for multiresponse generalised linear mixed models: the MCMCglmm R package. *J. Stat. Softw.* 33, 1–22. doi: 10.18637/jss.v033.i02

Hette-Tronquart, N. (2019). Isotopic niche is not equal to trophic niche. *Ecol. Lett.* 22, 1987–1989. doi: 10.1111/ele.13218

Ivan, J. S., and Shenk, T. M. (2016). Winter diet and hunting success of Canada lynx in Colorado. *J. Wildl. Manag.* 80, 1049–1058. doi: 10.1002/jwmg.21101

Jackson, A. L., Inger, R., Parnell, A. C., and Bearhop, S. (2011). Comparing isotopic niche widths among and within communities: SIBER-Stable Isotope Bayesian Ellipses in R. *J. Anim. Ecol.* 80, 595–602. doi: 10.1111/j.1365-2656.2011.01806.x

Jocque, M., Field, R., Brendonck, L., and De Meester, L. (2010). Climatic control of dispersal-ecological specialization trade-offs: a metacommunity process at the heart of the latitudinal diversity gradient? *Glob. Ecol. Biogeogr.* 19, 244–252. doi: 10.1111/j.1466-8238.2009.00510.x

Karanth, K. U., Srivathsa, A., Vasudev, D., Puri, M., Parameshwaran, R., and Kumar, S. (2017). Spatio-temporal interactions facilitate large carnivore sympatry across a resource gradient. *Proc. R. Soc. B* 284:20161860. doi: 10.1098/rspb.2016.1860

Karlson, A. M., Reutgard, M., Garbaras, A., and Gorokhova, E. (2018). Isotopic niche reflects stress-induced variability in physiological status. *R. Soc. Open Sci.* 5:171398. doi: 10.1098/rsos.171398

Kartzinel, T. R., Chen, P. A., Coverdale, T. C., Erickson, D. L., Kress, W. J., Kuzmina, M. L., et al. (2015). DNA metabarcoding illuminates dietary niche partitioning by African large herbivores. *Proc. Natl. Acad. Sci.* 112, 8019–8024. doi: 10.1073/pnas.1503283112

Kellner, K. F., Duchamp, J. E., and Swihart, R. K. (2019). Niche breadth and vertebrate sensitivity to habitat modification: signals from multiple taxa across replicated landscapes. *Biodivers. Conserv.* 28, 2647–2667. doi: 10.1007/s10531-019-01785-w

Koen, E. L., Bowman, J., Lalor, J. L., and Wilson, P. J. (2014a). Continental-scale assessment of the hybrid zone between bobcat and Canada lynx. *Biol. Conserv.* 178, 107–115. doi: 10.1016/j.biocon.2014.07.016

Koen, E. L., Bowman, J., Murray, D. L., and Wilson, P. J. (2014b). Climate change reduces genetic diversity of Canada lynx at the trailing edge range. *Ecography* 37, 754–762. doi: 10.1111/j.1600-0587.2013.00629.x

Lanszki, J., Hayward, M. W., Ranc, N., and Zalewski, A. (2022). Dietary flexibility promotes range expansion: the case of golden jackals in Eurasia. *J. Biogeogr.* 49, 993–1005. doi: 10.1111/jbi.14372

Lavoie, M., Collin, P.-Y., Lemieux, F., Jolicoeur, H., Canac-Marquis, P., and Larivière, S. (2009). Understanding fluctuations in bobcat harvest at the northern limit of their range. *J. Wildl. Manag.* 73, 870–875. doi: 10.2193/2008-275

Layman, C. A., Araujo, M. S., Boucek, R., Hammerschlag-Peyer, C. M., Harrison, E., Jud, Z. R., et al. (2012). Applying stable isotopes to examine food-web structure: an overview of analytical tools. *Biol. Rev.* 87, 545–562. doi: 10.1111/j.1469-185X.2011.00208.x

Legendre, P., and Legendre, L. (2012). "Tests of normality and multinormality," in *Numerical Ecology*. eds: P. Legendre and L. Legendre (Oxford: Elsevier B.V), 187–194.

Lysy, M., Stasko, A. D., and Swanson, H. K.. (2015). R package 'niche ROVER': (Niche) (R)egion and Niche (Over)lap Metrics for Multidimensional Ecological Niches, v 1.0.

Mac Arthur, R. H., and Levins, R. (1964). Competition, habitat selection, and character displacement in a patchy environment. *Proc. Natl. Acad. Sci. U. S. A.* 51, 1207–1210. doi: 10.1073/pnas.51.6.1207

Manenti, R., Denoël, M., and Ficetola, G. F. (2013). Foraging plasticity favours adaptation to new habitats in fire salamanders. *Anim. Behav.* 86, 375–382. doi: 10.1016/j.anbehav.2013.05.028

Marrotte, R. R., and Bowman, J. (2021). Seven decades of southern range dynamics of Canada lynx. *Ecol. Evol.* 11, 4644–4655. doi: 10.1002/ece3.7364

McGill, B. J., Enquist, B. J., Weiher, E., and Westoby, M. (2006). Rebuilding community ecology from functional traits. *Trends Ecol. Evol.* 21, 178–185. doi: 10.1016/j.tree.2006.02.002

Merkle, J. A., Polfus, J. L., Debridge, J. J., and Heinemeyer, K. S. (2017). Dietary niche partitioning among black bears, grizzly bears, and wolves in a multiprey ecosystem. *Can. J. Zool.* 95, 663–671. doi: 10.1139/cjz-2016-0258

Navarro-López, J., and Fargallo, J. A. (2015). Trophic niche in a raptor species: the relationship between diet diversity, habitat diversity and territory quality. *PLoS One* 10:e0128855. doi: 10.1371/journal.pone.0128855

Newbury, R. K., and Hodges, K. E. (2018). Regional differences in winter diets of bobcats in their northern range. *Ecol. Evol.* 8, 11100–11110. doi: 10.1002/ece3.4576

O'Donoghue, M., Boutin, S., Murray, D. L., Krebs, C. J., Hofer, E. J., Breittenmoser, U., et al. (2001). *Coyotes and Lynx in Ecosystem Dynamics of the Boreal Forest: The Kluane Project*. eds. C. J. Krebs, S. Boutin and R. Boonstra (New York: Oxford University Press), 275–323.

Papacostas, K. J., and Freestone, A. L. (2016). Latitudinal gradient in niche breadth of brachyuran crabs. *Glob. Ecol. Biogeogr.* 25, 207–217. doi: 10.1111/geb.12400

Peers, M. J. L., Thornton, D. H., and Murray, D. L. (2013). Evidence for large-scale effects of competition: niche displacement in Canada lynx and bobcat. *Proc. R. Soc. B Biol. Sci.* 280:20132495. doi: 10.1098/rspb.2013.2495

Quinn, N. W. S., and Parker, G. (1987). "Lynx," in *Wild furbearer management and conservation in North America*. eds. M. Novak, J. A. Baker, M. E. Obbard and B. Malloch (Peterborough, ON: Ontario Fur Managers Federation), 682–694.

Rivas-Salvador, J., Hořák, D., and Reif, J. (2019). Spatial patterns in habitat specialization of European bird communities. *Ecol. Indic.* 105, 57–69. doi: 10.1016/j.ecolind.2019.05.063

Roberts, N. M., and Crimmins, S. M. (2010). Bobcat population status and management in North America: evidence of large-scale population increase. *J. Fish Wildl. Manag.* 1, 169–174. doi: 10.3996/122009-JFWM-026

Rogers, M. C., Hilderbrand, G. V., Gustine, D. D., Joly, K., Leacock, W. B., Mangipane, B. A., et al. (2020). Splitting hairs: dietary niche breadth modelling using stable isotope analysis of sequentially grown tissue. *Isot. Environ. Health Stud.* 56, 358–369. doi: 10.1080/10256016.2020.1787404

Rosenzweig, M. L. (1991). Habitat selection and population interactions: The search for mechanism. *Am. Nat.* 137:S5-S28. doi: 10.1086/285137

Roth, J. D., Marshall, J. D., Murray, D. L., Nickerson, D. M., and Steury, T. D. (2007). Geographical gradients in diet affect population dynamics of Canada lynx. *Ecology* 88, 2736–2743. doi: 10.1890/07-0147.1

Row, J. R., Wilson, P. J., Gomez, C., Koen, E. L., Bowman, J., Thornton, J., et al. (2014). The subtle role of climate change on population genetic structure in Canada lynx. *Glob. Chang. Biol.* 20, 2076–2086. doi: 10.1111/gcb.12526

Stephens, D.W., and Krebs, J. R.. (1986). *Foraging Theory*. New Jersey: Princeton University Press.

Stevens, R. D. (2022). Reflections of Grinnellian and Eltonian niches on the distribution of phyllostomid bats in the Atlantic Forest. *J. Biogeogr.* 49, 94–103. doi: 10.1111/jbi.14284

Svanbäck, R., and Bolnick, D. I. (2007). Intraspecific competition drives increased resourxe use diversity. Within a natural population. *Proc. R. Soc. B* 274, 839–844. doi: 10.1098/rspb.2006.0198

Swanson, H. K., Lysy, M., Power, M., Stasko, A. D., Johnson, J. D., and Reist, J. D. (2015). A new probabilistic method for quantifying n-dimensional ecological niches and niche overlap. *Ecology* 96, 318–324. doi: 10.1890/14-0235.1

Walsh, L. L., and Tucker, P. K. (2020). Isotopic niche breadth of a generalist mesopredator increases with habitat heterogeneity across its range. *Ecosphere* 11:e03314. doi: 10.1002/ecs2.3314

Witczuk, J., Pagacz, S., Gliwicz, J., and Mills, S. (2015). Niche overlap between sympatric coyotes and bobcats in highland zones of Olympic Mountains, Washington. *J. Zool.* 297, 176–183. doi: 10.1111/jzo.12270

Wolf, N., Carleton, S. A., and Martinez del Rio, C. (2009). Ten years of experimental animal isotopic ecology. *Funct. Ecol.* 23, 17–26. doi: 10.1111/j.1365-2435.2009.01529.x

Woo, K. J., Elliot, K. H., Davidson, M., Gaston, A. J., and Davoren, G. K. (2008). Individual specialization in diet by a generalist marine predator reflects specialization in foraging behaviour. *J. Anim. Ecol.* 77, 1082–1091. doi: 10.1111/j.1365-2656.2008.01429.x

Yurkowski, D. J., Ferguson, S., Choy, E. S., Loseto, L. L., Brown, T. M., Muir, D. C. G., et al. (2016). Latitudinal variation in ecological opportunity and intraspecific competition indicates differences in niche variability and diet specialization of Arctic marine predators. *Ecol. Evol.* 6, 1666–1678. doi: 10.1002/ece3.1980

frontiers | Frontiers in Ecology and Evolution

TYPE Original Research
PUBLISHED 21 December 2022
DOI 10.3389/fevo.2022.953042

Check for updates

OPEN ACCESS

EDITED BY
Jason Newton,
University of Glasgow,
United Kingdom

REVIEWED BY
Derek Hamilton,
University of Glasgow,
United Kingdom
Piotr Chibowski,
University of Warsaw,
Poland

*CORRESPONDENCE
Eric J. Guiry
ejg26@leicester.ac.uk

SPECIALTY SECTION
This article was submitted to Population, Community, and Ecosystem Dynamics, a section of the journal Frontiers in Ecology and Evolution

RECEIVED 25 May 2022
ACCEPTED 23 November 2022
PUBLISHED 21 December 2022

CITATION
Guiry EJ, Orchard TJ, Needs-Howarth S and Szpak P (2022) Freshwater wetland–driven variation in sulfur isotope compositions: Implications for human paleodiet and ecological research.
Front. Ecol. Evol. 10:953042.
doi: 10.3389/fevo.2022.953042

COPYRIGHT
© 2022 Guiry, Orchard, Needs-Howarth and Szpak. This is an open-access article distributed under the terms of the Creative Commons Attribution License (CC BY). The use, distribution or reproduction in other forums is permitted, provided the original author(s) and the copyright owner(s) are credited and that the original publication in this journal is cited, in accordance with accepted academic practice. No use, distribution or reproduction is permitted which does not comply with these terms.

Freshwater wetland–driven variation in sulfur isotope compositions: Implications for human paleodiet and ecological research

Eric J. Guiry[1,2]*, Trevor J. Orchard[3], Suzanne Needs-Howarth[4,5] and Paul Szpak[2]

[1]School of Archaeology and Ancient History, University of Leicester, Leicester, MA, United Kingdom, [2]Department of Anthropology, Trent University, Peterborough, ON, Canada, [3]Department of Anthropology, University of Toronto Mississauga, Mississauga, ON, Canada, [4]Perca Zooarchaeological Research, Toronto, ON, Canada, [5]The Archaeology Centre, University of Toronto, Toronto, ON, Canada

Sulfur isotope (δ^{34}S) analyses are an important archaeological and ecological tool for understanding human and animal migration and diet, but δ^{34}S can be difficult to interpret, particularly in archaeological human-mobility studies, when measured isotope compositions are strongly ^{34}S-depleted relative to regional baselines. Sulfides, which accumulate under anoxic conditions and have distinctively low δ^{34}S, are potentially key for understanding this but are often overlooked in studies of vertebrate δ^{34}S. We analyze an ecologically wide range of archaeological taxa to build an interpretive framework for understanding the impact of sulfide-influenced δ^{34}S on vertebrate consumers. Results provide the first demonstration that δ^{34}S of higher-level consumers can be heavily impacted by freshwater wetland resource use. This source of δ^{34}S variation is significant because it is linked to a globally distributed habitat and occurs at the bottom of the δ^{34}S spectrum, which, for archaeologists, is primarily used for assessing human mobility. Our findings have significant implications for rethinking traditional interpretive frameworks of human mobility and diet, and for exploring the historical ecology of past freshwater wetland ecosystems. Given the tremendous importance of wetlands' ecosystem services today, such insights on the structure and human dynamics of past wetlands could be valuable for guiding restoration work.

KEYWORDS

wetlands, sulfur isotopes, historical ecology, migration, archaeology

Introduction

Stable sulfur isotopes (δ^{34}S) are used widely in archaeological and ecological research (Krouse, 1989; Canfield, 2001) and their importance continues to grow, particularly in the context of understanding patterns in past human and animal migration and diet (Nehlich, 2015). With recent improvements in instrumentation, allowing smaller sample sizes and

more efficient simultaneous measurement of $\delta^{34}S$ alongside other isotopic compositions (e.g., Sayle et al., 2019), generation of these data is likely to see even faster growth moving forward. However, it is still common, particularly in the archaeological literature, for interpretation of some published $\delta^{34}S$ values to remain preliminary or tentative, especially when lower values do not appear to fit with regional expectations based on local faunal baseline isotopic compositions. In the early days of applying stable carbon ($\delta^{13}C$) and nitrogen ($\delta^{15}N$) isotope data to archaeological contexts, a very simple interpretive framework was employed: more or fewer C_4 plants, lower or higher trophic position, and more or fewer marine resources (Schwarcz and Schoeninger, 1991). It is now apparent that a much wider range of biogeochemical processes can influence the $\delta^{13}C$ and $\delta^{15}N$ compositions throughout the biosphere, often in systematic ways, facilitating a wider interpretive context for archaeological and ecological plant, animal, and human remains. A similar widening of our isotopic interpretive framework for $\delta^{34}S$ is currently underway.

In archaeological and ecological work, $\delta^{34}S$ is typically used as a marker for mobility or diet (Nehlich, 2015; Hobson, 2019). Because $\delta^{34}S$ compositions are not thought to undergo significant fractionation between diet and consumer (Peterson and Howarth, 1987; Fry, 1988; Krajcarz et al., 2019), they can be considered as an indicator for provenance. The premise for this is that the $\delta^{34}S$ compositions of the bedrock and overlying geology and hydrology (Thode, 1991) are passed on to primary producers and up to higher-level consumers (Krouse, 1989; Canfield, 2001). This means that, across wider landscapes encompassing regions with varying underlying baseline $\delta^{34}S$, the origin of consumers can be assessed (Vika, 2009). In this context, region-specific differences between underlying geological baselines and baselines associated with adjacent riverine environments have also been used to assess the importance of freshwater resource use (Privat et al., 2007). A second major use of $\delta^{34}S$ relies on the distinctive and homogenous isotopic composition of $\delta^{34}S$ of seawater sulfates (+20‰; Rees et al., 1978), which can differ from the (often lower) $\delta^{34}S$ characterizing baselines and food webs in adjacent terrestrial environments (Fry, 1988; Dance et al., 2018). This means that sulfate contributions from sea spray, with a marine $\delta^{34}S$ composition, can have a large impact on the $\delta^{34}S$ values of consumers in coastal areas (Zazzo et al., 2011), even masking local terrestrial sulfate contributions entirely (Guiry and Szpak, 2020). For this reason, consumer $\delta^{34}S$ is sometimes used to assess residence in coastal areas (Richards et al., 2001). This distinction between $\delta^{34}S$ in marine and non-marine ecosystems has also provided a basis for assessing the presence of marine contributions to diet, with consumers of marine foods at inland locations potentially also taking on higher $\delta^{34}S$ values (e.g., Craig et al., 2006). A third interpretation of $\delta^{34}S$ includes use as a marker for estuarine resources. It is sometimes suggested that marine consumers in estuarine areas could have lower $\delta^{34}S$ due to the influence of freshwater sulfate contributions that may have a lower baseline $\delta^{34}S$ (e.g., Nehlich et al., 2013). However, studies of consumers across modern estuarine gradients show that this will not always be the case (Fry and Chumchal, 2011) on the basis of simple mass balance, since it takes a very small amount of (sulfate-rich) seawater added to freshwater (typically an order of magnitude poorer in sulfate; Marschner, 2011) to mask a freshwater $\delta^{34}S$ signal.

More recently, there has been a growing awareness among archaeologists (e.g., Szpak and Buckley, 2020; Rand et al., 2021; Guiry et al., 2021a; Lamb and Madgwick, 2022) of the potential for sulfides, which have a very low $\delta^{34}S$, to influence the isotopic composition of consumer tissues, a relationship that has been noted ecologically for decades in select marine-influenced environments (Carlson and Forrest, 1982; Fry et al., 1982). Following their earlier ecological counterparts (Peterson and Howarth, 1987; Mizota et al., 1999; Oakes and Connolly, 2004; Chasar et al., 2005), recent archaeological studies have shown, for instance, that in marine-influenced settings, such as saltmarshes (Guiry et al., 2021a), seagrass beds (Guiry et al., 2021c), and benthic microalgal-subsidized areas (Szpak and Buckley, 2020), coastal and marine archaeological consumers and their broader food webs can have $\delta^{34}S$ values that are strongly impacted by sulfur with a sulfide-influenced $\delta^{34}S$ value. Although this relationship between low $\delta^{34}S$ and sulfide-rich environments is established in investigations of marine and coastal settings, it remains comparatively unexplored in higher-level consumers at inland-terrestrial and freshwater environments (though see Cornwell et al., 1995).

Here we explore the question of whether sulfur with sulfide-influenced $\delta^{34}S$ could play an important role in determining the $\delta^{34}S$ of terrestrial and aquatic consumers of resources from freshwater wetland areas. While recent work has shown that this is certainly the case for higher-level consumers (mammalian livestock) in at least some areas where primary production is dominated by coastal saltmarsh plants in the genus *Spartina* (Guiry et al., 2021a), it is possible that these and other plants in saltmarsh areas have an unusual tolerance for, or the ability to draw directly on, sulfur from otherwise highly toxic sulfides. Guiry et al. (2021a) suggest that this relationship showing ^{34}S-depleted isotopic compositions in terrestrial consumers of coastal wetland environments may also provide a marker for the broader use of, or proximity to, freshwater wetlands, and call for more research to establish this relationship. For its part, while the ecological literature has explored variation in $\delta^{34}S$ of coastal terrestrial plants in a variety of contexts (e.g., Stribling et al., 1998), little experimental work has been done in freshwater wetlands, although one early paper by Cornwell et al. (1995) does clearly suggest that lower $\delta^{34}S$ could also be characteristic of primary producers in some freshwater wetland areas.

We investigate $\delta^{34}S$ of an ecologically wide range of taxa to assess the extent to which $\delta^{34}S$ co-varies with use of terrestrial (land-based), lacustrian (lake-based), and wetland (slower-moving marsh- and small water body–based) environments. Using archaeological animals from southern Ontario, Canada, with differing, known ecologies, that are further constrained and verified through analyses of $\delta^{13}C$ and $\delta^{15}N$ compositions, we build

an interpretive framework for investigating the impact of wetland use on consumer δ^{34}S. By exploring the impact of wetland resource use on the isotopic compositions of non-human vertebrates, we aim to provide a better understanding of implications for δ^{34}S interpretations of both human and animal mobility and diet in contemporary, historical, and ancient contexts. Our data show that the use of resources from wetlands can have a very large impact on the δ^{34}S of higher-level consumers across a food web and indicates that archaeological and ecological interpretations in areas of the world where freshwater wetlands are present should consider wetland resource use as a potential source of variation in δ^{34}S when assessing mobility and diet. In showing that δ^{34}S compositions can be driven by wetland-oriented dietary choices, and are therefore not always an accurate provenance tracer, this study has global implications for the way archaeological δ^{34}S are interpreted. While this may be a source of interpretive uncertainty for some research questions, it opens new and potentially highly valuable avenues for others.

Context and hypotheses

Sulfur in wetlands

Sulfides can form under waterlogged, anoxic conditions as the metabolic end product of dissimulatory sulfate reducers, including both bacteria and archaea, which oxidize organic compounds using sulfate as an electron acceptor (Postgate, 1959). The redox and other conditions present in wetland sediment profiles, with slow water movement and limited oxygen, can lead to the accumulation of sulfides (Bagarinao, 1992; Marschner, 2011). These processes strongly discriminate against ^{34}S, with fractionations of −40‰ to −45‰ observed in natural and culture experiments (Kaplan and Rittenberg, 1964; Kemp and Thode, 1968; Chambers et al., 1975; Habicht and Canfield, 1997). However, a large portion of these sulfides can be re-oxidized *via* a suite of chemical and biological pathways (Jørgensen, 1982), making isotopically light sulfate available to primary producers. Furthermore, stronger depletions (up to −70‰) observed in analyses of natural sediments suggest these microbially mediated processes can cycle sulfur in ways that create even more ^{34}S-depleted isotopic compositions in waterlogged sediments (Canfield and Teske, 1996; Habicht and Canfield, 2001). While the processes responsible for driving the sulfur cycle in waterlogged sediments, and thus the fractionation of ^{34}S, are clearly tremendously complex and still under investigation (Findlay and Kamyshny, 2017; Jørgensen et al., 2019), it is widely acknowledged that they often drive δ^{34}S downwards.

It is also well documented that sulfides are both directly toxic to most plants (Lamers et al., 2013) and, by lowering soil redox potential, can lead indirectly to root oxygen deficiency stress (Koch et al., 1990). While some plants have demonstrated tolerance of sulfides (Carlson and Forrest, 1982; Fry et al., 1982), none are fully immune to higher concentrations (Koch and Mendelssohn, 1989). The means by which sulfur with sulfide-derived δ^{34}S enters the food web remains unclear. It is possible, for instance, that plants growing in anoxic soil conditions have symbiotic relationships with sulfur-oxidising bacteria, or are themselves chemolithotrophic, allowing them to incorporate sulfide-derived sulfur and grow in areas with low soil sulfate concentrations (Morris et al., 1996). Alternatively, plants and other primary producers could incorporate sulfates that have been created from re-oxidized sulfides. In either case, aquatic and wetland primary producers would take on sulfide-influenced δ^{34}S values.

Research design and hypotheses

We analyzed bone collagen, which, owing to its slower turnover, has isotopic compositions integrating a long-term, multi-year-averaged perspective on foods consumed (Hobson and Clark, 1992; Hyland et al., 2021) (although we note that turnover rates vary within and between bones and across biological ages). Species were selected to represent different ecological groups (i.e., predominantly terrestrial, lacustrian, or wetland inhabiting), with the aim of constructing an interpretive framework that includes taxa with both more constrained and more flexible habitat preferences. Mustelids, represented by American marten (*Martes americana,* $n = 3$), fisher (*Martes pennanti,* $n = 2$), and American mink (*Neovison vison,* $n = 3$), are terrestrial carnivores that prey largely on smaller animals (Baker and Hill, 2003). Previously published δ^{13}C and δ^{15}N values for these samples (Guiry et al., 2021b) allowed for selection of specimens with diets typical of terrestrial predators in the region. Our terrestrial baseline also includes samples from American red squirrels (*Tamiasciurus hudsonicus,* $n = 3$), Eastern gray squirrels (*Sciurus carolinensis,* $n = 4$), turkeys (*Meleagris gallopavo,* $n = 2$), and ruffed grouse (*Bonasa umbellus,* $n = 3$). Lake Ontario's[1] now-extinct population of Atlantic salmon [*Salmo salar,* $n = 16$; data from Guiry et al. (2016a)] was made up of large lacustrian piscivores with a narrowly constrained pelagic niche[2] (Guiry, 2019; Guiry et al., 2020b). Both of these groups will have had diets that were minimally influenced by wetland-derived nutrients and therefore represent baselines for δ^{34}S in the two main non-wetland biomes in the region—terrestrial (with δ^{34}S influenced by local geology and hydrology) and lacustrian (with δ^{34}S influenced mainly by

1 While there are several large lakes in the study region, the most important major water body for this study is Lake Ontario (Figure 1), in part because Niagara Falls created a natural barrier preventing key species, including Atlantic salmon and American eel, from inhabiting upstream lakes.

2 The term "pelagic" can refer to both marine and freshwater environments. Samples come from Lake Ontario's now-extinct endemic complex of Atlantic salmon populations, which were potamodromous. In other words, these fish lived their entire lives in Lake Ontario and its tributaries and did not travel to the ocean as part of their life cycle.

upstream Great Lakes, but also by local watershed inputs), respectively. At the other end of the spectrum, American beavers (*Castor canadensis, n* = 14) and a variety of turtles (snapping, *Chelydra serpentina, n* = 2; painted, *Chrysemys picta, n* = 10; Blanding's, *Emydoidea blandingii, n* = 3; map, *Graptemys geographica, n* = 1), which are primarily wetland denizens (Mac Culloch, 2002), will have had diets with a stronger influence from wetland δ^{34}S.

Together, these groups with constrained habitat preferences provide anchor points for interpreting patterns along a continuum from wetland to non-wetland (i.e., terrestrial and lacustrian) ecosystems. Natural experiments such as this come with some inherent uncertainties and we acknowledge that individuals in our wetland baseline group could have diets and habitat preferences that are not as narrowly focused as the categories into which they have been placed. Beavers, for instance consume both aquatic and terrestrial (tree bark) plant foods (Baker and Hill, 2003), while turtles may also use lacustrian environments. Although we have selected terrestrial fauna based on previous isotope work (Guiry et al., 2021b), which allowed us to target individuals that had terrestrially oriented diets, we are also aware that some of these taxa, such as the fishers and American minks, are capable of foraging in aquatic or wetland habitats. However, for the present study we expect that, while variation in individual behavior may create more isotopic variation, emergent patterns will still provide a basis for establishing general directions of isotopic shifts associated with wetland-influenced diets.

Other taxa represent a range of more flexible ecologies and we hypothesise that they will show a wider spectrum of wetland to non-wetland δ^{34}S. Muskrats (*Ondatra zibethicus, n* = 9) are capable wetland specialists, but are also well adapted for use of faster-moving lacustrian and riverine environments (Baker and Hill, 2003). We also include fish taxa with a large degree of behavioral and habitat-preference flexibility. American eels (*Anguilla rostrata, n* = 36), for instance, live for decades in Lake Ontario and its tributary watersheds before returning to the sea to reproduce and can specialize in both lacustrian and upstream wetland areas (COSEWIC, 2012). They are particularly well known for their ability to climb over obstacles and work their way inland to access habitats in slower-moving wetland areas (Allen, 2010; Jellyman and Arai, 2016). It is also worth pointing out that given that the vast majority of their growth (and life span) occurs after migration into freshwater, we do not expect a marine isotopic signal for the earliest phases of their catadromous life cycle to be retained in adult tissues (Guiry, 2019). Lastly, lake sturgeon (*Acipenser fulvescens, n* = 21) are benthic feeders and while they do travel and forage up smaller tributaries (meaning they have potential to show some wetland-influenced δ^{34}S values), based on the sampled specimens' larger, adult size, we might expect the majority to show a closer affinity with the broader lacustrian δ^{34}S baseline (COSEWIC, 2014).

While, ideally, we would also have a detailed contemporary isoscape for the study region to further refine our interpretations, differences observed between species with similar ecologies in the archaeological past and their modern counterparts (Colborne et al., 2016; Guiry et al., 2016a) suggest that there may have been a δ^{34}S baseline shift due to modern atmospheric sulfur contributions (Zhao et al., 2003). While further work would be needed to resolve this, for the present study we believe that together, these baseline- (ecologically constrained terrestrial, lacustrian and wetland endpoints) and hypotheses-driven (ecologically flexible) sample selections create a strong interpretive framework for assessing the impact of wetlands resource use on consumer δ^{34}S.

Materials and methods

Samples (n = 132) come from 39 sites in southern Ontario, Canada (Figure 1 and Table 1), and date to between 500 CE and 1900 CE, although the vast majority (83%) date to between 1250 and 1650 CE (Supplementary Table S1). Bone samples were selected based on minimum number of individual estimates per archaeological context in order to minimise the possibility of sampling the same individual more than once. Bone collagen extractions followed well established methods (Longin, 1971). Samples were cut into small chunks, demineralized in 0.5 M hydrochloric acid (HCl), and then rinsed to neutrality in Type 1 water. For fish, prior to demineralization, samples were soaked in a bath of 2: 1 chloroform methanol to remove potential residual lipids (Guiry et al., 2016b). Following demineralization, samples were soaked in 0.1 M sodium hydroxide in an ultrasonic bath (solution refreshed every 15 min until solution remained clear) to remove base soluble contaminants. Samples were then neutralized in Type 1 water and refluxed in 10^{-3} HCl (pH 3) at 70°C for 36 h. Samples were centrifuged and the solubilized fraction was transferred into a fresh tube, frozen, and lyophilized.

Stable carbon and nitrogen isotope and elemental compositions were measured on 0.5 mg subsamples of collagen using a Vario MICRO cube elemental analyzer (EA) coupled to an Isoprime isotope ratio mass spectrometer (IRMS; Elementar, Hanover, Germany) or an EA 300 (Eurovector, Pavia, Italy) coupled to a Horizon IRMS (Nu Instruments, Wrexham, United Kingdom). Stable sulfur isotope and elemental compositions were measured separately on 8.0 mg (for mammals and reptiles) or 6.0 mg (for fish) subsamples of collagen along with a combustion enhancer (10 mg of V_2O_5) using an ANCA EA coupled to a Europa SL/20–20 IRMS (Europa, Crewe, United Kingdom). Replicate analyses were performed on *ca.* 30 and 10% of samples for δ^{13}C/δ^{15}N and δ^{34}S, respectively. Isotopic compositions were calibrated relative to VPDB and AIR for δ^{13}C and δ^{15}N and to VCDT for δ^{34}S (Supplementary Table S2). We monitored precision and accuracy with internal collagen standards (Supplementary Table S2). Long-term observed averages (check standards) or known (calibration standards) values for all reference materials are reported in Supplementary Table S3. Averages and standard deviations for calibration standards (Supplementary Table S4), check standards

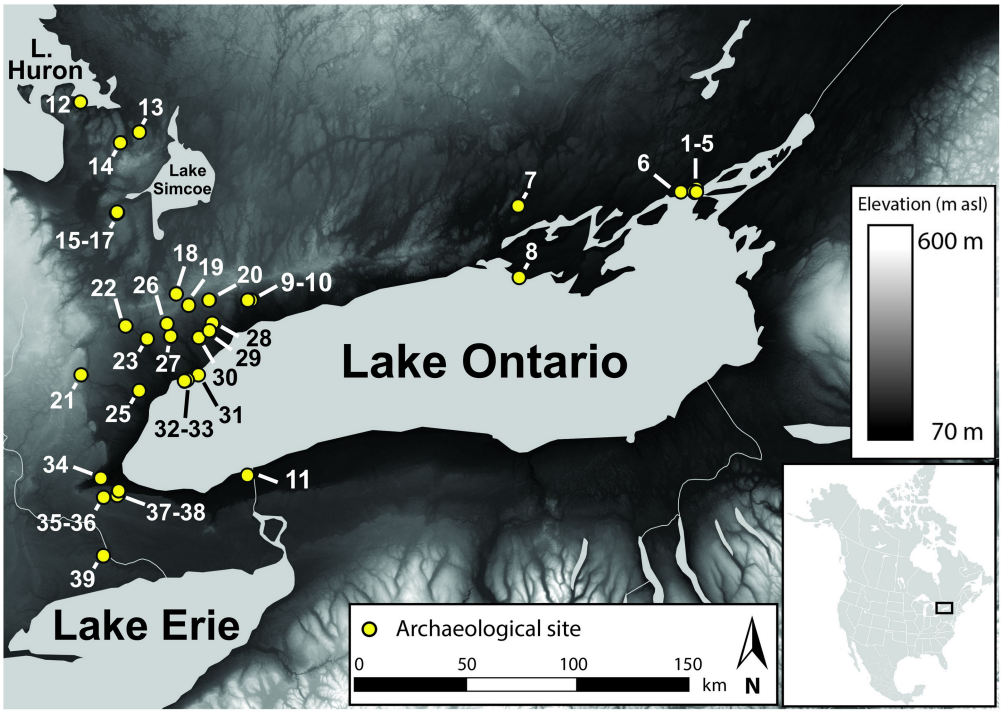

FIGURE 1
Map showing sites and study region. Numbers correspond to site contextual details listed in Supplementary Tables S1; S6.

(Supplementary Table S5), and sample replicates (Supplementary Table S6) for all analytical sessions are also available in the Supplementary material. For $\delta^{13}C$, $\delta^{15}N$, and $\delta^{34}S$, systematic errors [$\mu_{(bias)}$] were ± 0.11‰, ±0.12‰, and ± 0.23‰, respectively; random errors [$\mu R_{(w)}$] were ± 0.12‰, ±0.14‰, and ± 0.12‰, respectively; and standard uncertainty was ±0.16‰, ±0.19‰, and ± 0.26‰, respectively (Szpak et al., 2017). Collagen quality control (QC) was assessed using conservative C: N (Guiry and Szpak, 2021), %C (>13%), and %N (>4.8%) criteria (Ambrose, 1990). Statistical comparisons were performed in PAST version 3.22 (Hammer et al., 2001). Pearson's r tests were used to test the significance of correlations between $\delta^{13}C$ and $\delta^{34}S$.

Results and discussion

All samples passed collagen QC criteria. Stable sulfur isotope compositions show a very large range spanning 17.0‰ (−5.0 to +12.0‰; Figures 2A,B; data summarized in Table 1, full results in Supplementary Table S6). Data from baseline species map closely onto our ecological expectations based on their terrestrial, lacustrian, or wetland habitat preferences. There is a slight difference between our terrestrial (mustelids, squirrels, and ground-dwelling birds; $n = 20$, mean $\delta^{34}S = +6.9 \pm 1.8$‰, range = +3.6 to +11.8‰) and lacustrian (Atlantic salmon; $n = 17$, mean $\delta^{34}S = +8.8 \pm 1.6$‰, range = +5.8 to +11.4‰) taxa, suggesting that $\delta^{34}S$ baselines from these environments, while potentially variable, may rely on isotopically different sources.

Limited geological and hydrological isotopic baseline data are available for the study region (some examples exist from adjacent regions to the north; e.g., Hesslein et al., 1988). The isotopic variability in our data could, for instance, reflect broad-scale differences in the geologies (OGS, 1991; Henry et al., 2008) that underlie local terrestrial and aquatic vs. upstream aquatic habitats. The uppermost geology across much of the study region is composed of marine-derived sedimentary bedrock of various ages and compositions, which typically has relatively high $\delta^{34}S$ values (Bottrell and Newton, 2006). In contrast, the deeper bedrock underlying this, which becomes exposed immediately to the north of the study region and is an important bedrock system for some of the upstream Great Lakes (Huron and Superior), is the Canadian Shield. The Canadian Shield is a large region of Precambrian igneous and metamorphic rock, a rock type that, although variable, typically has $\delta^{34}S$ values that are lower than those found in marine environments (for review see, Thode, 1991). This latter source is, however, unlikely to be a major contributor of sulfate to biota due to the low sulfur content of silicious igneous rocks, which often means that ecosystems in these regions rely mainly on atmospheric deposition for their sulfur budget (for review see, Mitchell et al., 1998). Nonetheless, in this context, to the extent that the sulfur budget of lacustrian habitats of Lake Ontario might be subsidized by sulfate contributions from upstream watersheds, we might expect to find higher $\delta^{34}S$ values in terrestrial fauna living atop bedrock composed of ancient marine sediments compared with lacustrian counterparts, for which baselines could reflect greater

TABLE 1 Summary statistics for archaeological faunal bone collagen isotopic compositions.

Taxon	Ecology	Sample *n*=	Site *n*=	δ^{34}S (‰)		δ^{13}C (‰)		δ^{15}N (‰)	
				Range	Mean ± 1σ	Range	Mean ± 1σ	Range	Mean ± 1σ
Lake sturgeon	Flexible	21	17	8.1	+9.3 ± 2.0	9.1	−18.4 ± 2.3	2.5	+10.1 ± 0.8
American eel	Flexible	36	19	13.0	+8.5 ± 3.8	11.6	−19.6 ± 2.8	5.5	+9.2 ± 1.0
Muskrat	Flexible	9	6	10.3	+3.6 ± 3.7	6.8	−21.6 ± 2.2	7.8	+4.7 ± 2.5
Atlantic salmon	Lacustrian	16	5	5.6	+8.8 ± 1.6	1.2	−19.9 ± 0.3	4.0	+10.8 ± 1.2
American beaver	Wetland	14	6	13.1	+0.5 ± 4.1	4.7	−23.0 ± 1.3	4.8	+4.1 ± 1.3
Turtles (all)	Wetland	16	7	10.0	+4.4 ± 2.4	7.1	−24.8 ± 2.3	6.5	+7.0 ± 1.8
Snapping turtle	Wetland	2	2	2.2	+4.5 ± 1.6	0.9	−26.7 ± 0.6	0.5	+8.4 ± 0.4
Painted turtle	Wetland	10	5	8.5	+5.0 ± 2.5	5.9	−24.6 ± 2.0	3.0	+6.3 ± 0.9
Blanding's turtle	Wetland	3	3	3.0	+2.0 ± 1.7	6.0	−25.4 ± 3.2	6.2	+7.3 ± 3.1
Map turtle	Wetland	1	1		+5.1		−21.1		+10.5
Furbearers (all)	Terrestrial	8	2	2.7	+6.4 ± 1.1	5.6	−18.7 ± 1.5	3.7	+9.0 ± 1.0
American marten	Terrestrial	3	2	2.5	+6.9 ± 1.3	0.5	−19.0 ± 0.3	0.7	+8.8 ± 0.4
Fisher	Terrestrial	2	1	0.6	+5.7 ± 0.4	5.6	−18.2 ± 4.0	3.7	+9.2 ± 2.6
American mink	Terrestrial	3	1	2.4	+6.4 ± 1.2	0.1	−18.7 ± 0.1	0.4	+9.0 ± 0.2
Squirrels (all)	Terrestrial	7	6	8.2	+7.6 ± 2.6	0.9	−19.2 ± 0.3	1.6	+5.4 ± 0.6
Eastern gray squirrel	Terrestrial	4	4	3.6	+7.5 ± 1.6	0.6	−19.1 ± 0.3	1.2	+5.6 ± 0.6
Red squirrel	Terrestrial	3	3	8.2	+7.8 ± 4.1	0.5	−19.4 ± 0.2	1.4	+5.2 ± 0.7
Ground birds (all)	Terrestrial	5	3	2.1	+6.4 ± 0.9	2.9	−21.8 ± 1.1	1.2	+5.9 ± 0.5
Turkey	Terrestrial	2	2	1.3	+7.2 ± 0.9	0.4	−20.7 ± 0.3	0.1	+6.4 ± 0.1
Ruffed grouse	Terrestrial	3	3	0.8	+6.0 ± 0.4	1.3	−22.6 ± 0.7	0.5	+5.5 ± 0.2

contributions from older, non-marine geologies and/or atmosphere-dominated sources. Although the average difference we see between our terrestrial and lacustrian groups is small (<2.0‰), we observe the opposite pattern. We note, however that this basic interpretive scenario (marine vs. non-marine origins of uppermost bedrock) is highly simplified and that surface geology may be influenced by a wide range of other factors, such as the presence of glacially re-deposited, non-marine sediments and local variation in the presence of other bedrock types. It is also possible that Lake Ontario's lacustrian and terrestrial sulfur isotope baselines are simply dominated by sulfate sources endemic to the watershed (i.e., a combination of glacial re-deposition, marine-derived bedrock, atmospheric deposition, and smaller contributions from other local bedrock types). Regardless of what geological or hydrological processes are responsible for the differences we observed between our lacustrian and terrestrial fauna, we consider them to be valid, if approximate, baselines for establishing a backdrop against which to compare and contrast wetland-derived δ^{34}S variation. We also note that, although sample sizes are too small (averaging 3.3 samples per each of our 39 sites) to assess covariance between site location and δ^{34}S values for our terrestrial and lacustrian baseline groups, we see no obvious patterns between geographical locations and isotopic variation across the study region (Figure 1; Supplementary Table S6).

In comparison to these terrestrial and lacustrian baselines, our wetland taxa (beavers $n = 14$, mean $\delta^{34}S = +0.5 \pm 4.1$‰, range = −5.0 to +8.3‰; turtles; $n = 16$, mean $\delta^{34}S = +4.4 \pm 2.4$‰, range = +0.1 to +10.1‰) both indicate a lower baseline δ^{34}S for wetland denizens. Variation among turtles includes individuals with δ^{34}S that overlap with the lacustrian and terrestrial baseline taxa, suggesting that some may have lived in larger water bodies and/or made use of terrestrial resources. Beavers show the lowest values, with the widest range (spanning 13.1‰). This matches closely with their diet range which includes both roots from wetland plants [these structures have been observed to have δ^{34}S values that are more sulfide-influenced than plant tissues that are not in contact with sediments; Frederiksen et al., 2006)] and bark from trees in adjacent terrestrial habitat. This supports the use of these groups as δ^{34}S baselines for assessing the influence of wetland (i.e., sulfide-cycled) sulfur on the δ^{34}S of more behaviorally flexible taxa.

In that context, the wide spectrum of δ^{34}S values from eels ($n = 36$, mean $\delta^{34}S = +8.5 \pm 3.8$‰) which spans 17‰ and matches well with their known ecology, including both high (+12.0‰) and low (−1.0‰) δ^{34}S values that closely follow our wetland and lacustrian baselines. Muskrats also show a wide, but on average lower, range of δ^{34}S values ($n = 9$, mean $\delta^{34}S = +3.6 \pm 3.7$‰, range = −0.8 to +9.5‰) consistent with their flexible ecology feeding along a lacustrian–wetland spectrum. In contrast, but as expected, the bulk of lake sturgeon samples produced δ^{34}S values falling at the lacustrian end of the spectrum ($n = 21$, mean $\delta^{34}S = +9.3 \pm 2.0$‰, range = +3.2 to +11.3‰), with only one individual producing a value significantly lower than our lacustrian baseline, suggesting significant use of wetland-influenced areas.

Considering δ^{15}N helps to further contextualize the ecology of these taxa. Each species' δ^{15}N (Figures 2B,C) is broadly consistent with its respective trophic position (DeNiro and Epstein, 1981),

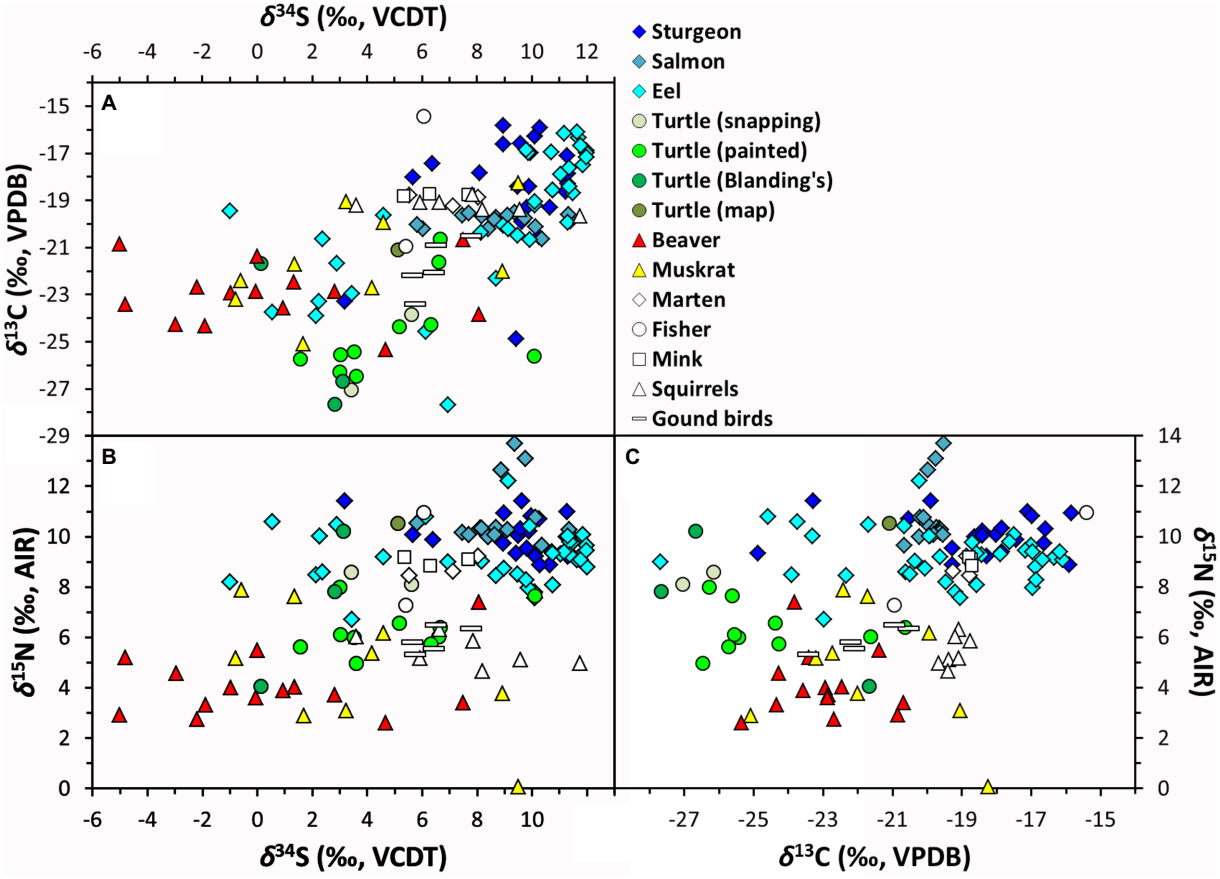

FIGURE 2
(A–C) Stable isotope compositions of archaeological fauna.

with more herbivorous aquatic (beavers, $n = 14$, $+4.1 \pm 1.3$‰; muskrats $n = 9$, $+4.7 \pm 2.5$‰) and terrestrial (squirrels $n = 6$, $+7.0 \pm 1.8$‰; ground birds $n = 5 + 5.9 \pm 0.5$‰) animals having lower values than apex predators (Atlantic salmon, $n = 16$, $+10.8 \pm 1.2$‰; mustelids $n = 8$, $+9.0 \pm 1.0$‰) in their respective habitat types. Atlantic salmon and one eel with higher δ^{15}N (> 12‰) provide an exception to this observation, but these samples come from historical contexts after 1850 CE, postdating a large-scale, early nineteenth-century isotopic shift in Lake Ontario's nitrogen cycle that followed major forestry activities in the watershed (Guiry et al., 2020a). Consistency among the δ^{34}S values of these historical Atlantic salmon with higher δ^{15}N and earlier salmon with lower δ^{15}N suggests that Lake Ontario's broader sulfur cycle did not undergo a similar isotopic shift at this time. These individuals aside, the overall consistency between δ^{15}N and expected trophic positions across our dataset suggests that, with respect to nitrogen cycling and sources, these samples are from a well-integrated wider biome with a consistent δ^{15}N baseline.

Stable carbon isotope compositions (Table 1 and Figures 2A,C) show patterns that complement and reinforce our interpretations of those observed in δ^{34}S. Freshwater ecosystems such as Lake Ontario can have extremely variable δ^{13}C (Schelske and Hodell, 1991; Hodell and Schelske, 1998), owing to complex and multifaceted processes that govern the cycling, sourcing, and partitioning of dissolved inorganic carbon (DIC) pools across varied intra- and inter-annual temporal scales and physical and biological conditions (Guiry, 2019). In this context, variation at the higher end of our observed δ^{13}C spectrum, which characterizes samples from lacustrian taxa such as Atlantic salmon ($n = 16$, -19.9 ± 0.3‰) and lake sturgeon ($n = 21$, -18.4 ± 2.3‰), are consistent with their expected foraging behavior in more pelagic and littoral areas, respectively (France, 1995; Guiry, 2019). In contrast, the extremely low δ^{13}C and high degree of variation among turtles ($n = 16$, -24.8 ± 2.3‰) suggests a wetland DIC budget more heavily influenced by CO_2 sourced from the breakdown of allochthonous terrestrial detritus [typically ^{13}C-depleted relative to atmospheric sources used by their terrestrial and, to some extent, lacustrian counterparts (Finlay and Kendall, 2007)]. Together these data show that, for this study region, while lacustrian food webs have higher δ^{13}C values, wetlands have distinctively low δ^{13}C, as might be expected in contexts where water movement is slow and CO_2 released from breakdown of allochthonous organic matter can contribute to a larger fraction of the DIC budget. In that context, we note that low δ^{13}C values are also apparent among eels (as low as -27.7‰, with 22% of individuals falling below the range for lacustrian taxa) which have the most ecological flexibility of our taxa, enabling them to thrive

anywhere along a wetland-to-lacustrian continuum. A strong positive correlation between $\delta^{13}C$ and $\delta^{34}S$ for eels ($n = 36$, Pearson's $r = 0.674$, $p = <0.000$) indicates that factors driving $\delta^{34}S$ downward occur in areas where $\delta^{13}C$ is more impacted by wetland isotopic compositions (i.e., influenced by ^{13}C-depleted carbon from allochthonous terrestrial detritus). What is more, while this correlation does not appear within other taxa (as expected given their less flexible ecologies, although see below for more detail; Supplementary Table S7), it is observed to a similar degree across the entire dataset (i.e., from all species; Figures 2A, $n = 132$, Pearson's $r = 0.608$, $p = <0.000$), indicating that the relationship operates at a much broader level than species-specific behavior. In other words, the known ecologies of these taxa, coupled with the observed isotopic patterns (in $\delta^{34}S$ and the correlation between $\delta^{13}C$ and $\delta^{34}S$) matching expectations based on these ecologies, strongly supports our interpretation that the primary driver of variation in $\delta^{34}S$ toward the lower end of the spectrum is an influence from ^{34}S-depleted sulfides in wetlands.

Results include another noteworthy species-specific pattern. The $\delta^{13}C$ and $\delta^{34}S$ correlation between wetland use and the most ecologically flexible taxa (i.e., eels) does not appear in beavers. In particular, although beavers are wetland specialists, with diets that include wetland plants as well as terrestrial trees, we do not see $\delta^{13}C$ co-vary with $\delta^{34}S$. Instead we see $\delta^{13}C$ values ($n = 14$, -23.0 ± 1.3‰) that appear to consistently suggest that the primary production upon which beavers relied drew CO_2 from atmospheric (terrestrial; i.e., higher $\delta^{13}C$) sources[3] rather than from sources where CO_2 came from the breakdown of allochthonous organic matter (i.e., lower $\delta^{13}C$). Dietary ecology, however, offers a clear explanation for this difference (Baker and Hill, 2003). Of the aquatic plants consumed by beavers, the favorites are lily pads (*Nymphaea* spp., *Nuphar* spp.) and other emergent aquatic vegetation (Jenkins, 1981; Novak, 1987), which, unlike other, fully aquatic primary producers (e.g., algae, macrophytes), draw a significant portion of their CO_2 directly from the atmosphere. This means that, although specialists in wetlands habitats, beavers are not necessarily expected to share low $\delta^{13}C$ values with other wetland denizens. For instance, in contrast to beavers, eels and turtles (carnivores and omnivores) consume a wider range of prey for which the basal primary production occurs in the water column (i.e., integrating isotopic compositions influenced by CO_2 from the breakdown of allochthonous materials). It therefore makes sense that beavers, while still showing a wetland diet spectrum, sit somewhat apart from other taxa. This also explains why a relationship between $\delta^{13}C$ and $\delta^{34}S$ for muskrats is weaker (and not statistically significant, Supplementary Table S7). While muskrats are omnivorous, their dominant food sources are plants, with overall diets that can be more similar isotopically to beavers that focus on emergent aquatic vegetation.

Broader implications and conclusion

Our data indicate that wetland fauna can have $\delta^{34}S$ values that incorporate an isotopic signal from sulfides. This means that higher-level consumers using resources from these environments, including humans, can have $\delta^{34}S$ values that do not reflect prevailing local baselines. While this phenomenon has been documented archaeologically before for various marine and coastal settings (Szpak and Buckley, 2020; Guiry et al., 2021a,c), its observation among vertebrates in freshwater wetlands is new and is something that could have a significant, and largely overlooked, impact on interpretations of $\delta^{34}S$ data from archaeological and ecological contexts.

To date, the vast majority of archaeological studies examining past diet and mobility have done so based on the premise that $\delta^{34}S$ compositions in consumers primarily reflect underlying geology and hydrology, with the added caveat that these values could be influenced near the top end of a typical $\delta^{34}S$ range by marine sulfates (through either sea spray or direct consumption of marine primary producers and animals; Nehlich, 2015). This study shows that the use of wetland resources could influence consumer $\delta^{34}S$ towards the bottom end of a typical $\delta^{34}S$ interpretive range. In other words, where interpretations involve data from humans or animals that could have lived near and used wetland resources, $\delta^{34}S$ values could be influenced. This finding has important, global implications for the utility of $\delta^{34}S$ as a tool for reconstructing past human mobility and migration. The existence of a source of $\delta^{34}S$ variation that is not linked to location (i.e., not derived from geology or hydrology), means that human $\delta^{34}S$ compositions, even at inland areas (i.e., far from sea spray influences and where marine foods were not available), could be driven at least partly by wetland-oriented dietary choices and would, therefore, not provide a faithful provenance tracer. Because wetlands are globally distributed and provide a resource-rich area attracting human habitation, this finding could have implications for interpretation of $\delta^{34}S$ data on a broad scale. While this could make interpretation of potentially affected data more complicated, it should also help to clarify interpretations of lower $\delta^{34}S$, which are sometimes left with tentative interpretations (e.g., Pearson et al., 2016; Rand et al., 2020; Le Roy et al., 2022), by linking them with potential consumption of local wetland resources, rather than mobility to distant or unknown areas with very low $\delta^{34}S$ baselines.

It is also worth considering these data for what they can tell us about variation in wetland $\delta^{34}S$ as well as our ability to identify it archaeologically. It is apparent from the wide $\delta^{34}S$ ranges among species, even within our baseline groups, that $\delta^{34}S$ associated with ecotonal areas that include wetlands can be highly variable. It is only when we combine a wide range of ecologically diverse taxa,

3 Note that mustelids and squirrels, although also terrestrial, are expected to have higher $\delta^{13}C$. For squirrels, this is based on their consumption of tree mast that, being composed of non-photosynthetic tissues, is relatively ^{13}C enriched (Guiry et al., 2021b) in the context of local C_3 plant foods. For mustelids, this is based on their consumption of taxa that focus on tree mast, such as squirrels.

constrained by other isotopic data, that a cohesive pattern emerges. The high degree of variation may simply reflect the fact that these kinds of natural experiments, particularly ones using archaeological materials that integrate longer time spans, are prone to incorporating data influenced by a wider range of biogeochemical processes. It is nonetheless the case that, for mobile, higher-trophic-level vertebrate consumers, especially in archaeological studies, in which our aim is to interpret cultural behaviors from both human and animal data, these kinds of issues with broader spatial and temporal scales will often necessarily be present. This heightened variability means that we can expect that interpreting smaller numbers of (or isolated) $\delta^{34}S$ data from bone collagen (typically the only material available to archaeologists) may be challenging or impossible and suggests that larger numbers of samples may be needed to observe clear patterns. Additional research with plants and bone collagen from contemporary samples from known species and carefully selected locations may allow this relationship to be characterized in finer detail and perhaps offer new insights to help further constrain interpretations of wetland-related $\delta^{34}S$ variation in the archaeological past.

A further point, of broader relevance, is that these data also speak to the value of including a wider variety of taxa in archaeological and ecological faunal isotopic baselines. If, for instance, we had instead examined only one or two of these species, the overall pattern we have observed might have been less clear. In other words, it is only by incorporating data from a broader suite of species across ecosystems that we gain a fuller understanding of the primary axes of isotopic variation relevant for interpreting human and animal behaviors. While the key roles that faunal baselines, particularly from animals of major economic importance, can play in isotopic research have long been recognized (Katzenberg, 1989), in this context, our results provide a clear example for the value of sampling more widely, and including species that are traditionally overlooked or seen as having less interpretive value. In order to make space for this kind of open exploration, and generation of more substantial datasets, curators may need to remain open to larger, broad-scale sampling programs. In this way we can gain a more detailed picture of the wider environmental framework in which humans and animals lived. At the same time, we acknowledge that budgetary constraints and limitations on what taxa have been preserved in relevant archaeological assemblages may mean that some archaeological projects will necessarily be limited to smaller-scale, less taxonomically diverse sampling programs.

Lastly, but perhaps most importantly, while our finding of a potentially globally significant source of variation at the bottom end of the $\delta^{34}S$ spectrum adds a source of interpretive uncertainty for some research questions, it opens the way for others. Wetlands were and are areas of tremendous cultural and ecological importance (Bernick, 2011). At the same time that wetlands continue to disappear due to human impacts (Davidson, 2014), we are learning more about the ecosystem services they provide and their value for mitigating or reversing major environmental issues, such as biodiversity loss, pollution/eutrophication, and climate change (Zedler and Kercher, 2005). In this context, having a broad-scale marker for human interactions with and use of wetlands in the past could help shed light and temporal depth on how wetlands have responded to human land management pressures through time. Moreover, such a marker for changes in the importance of wetlands for the ecology of archaeological fauna (whether wild or domestic) could provide an important source of information about the long-term ecological structure of wetlands in general, and in particular those which have long since disappeared due to human impacts. This can further inform archaeological interpretation of the importance of wetland resources for ancestors, thereby helping contemporary Indigenous peoples to reclaim part of their heritage (General and Warrick, 2012; Lesage, 2016). These findings also open the way for a range of historical-ecological research programs that could use $\delta^{34}S$ of archaeological animal remains to contribute directly to our understanding of the ecology of endangered or recovering wetland species. In turn, information from these and other lines of study have potential to help shape future conservation strategy and policy.

Data availability statement

The original contributions presented in the study are included in the article/Supplementary material, and further inquiries can be directed to the corresponding author.

Author contributions

EG designed research. SN-H, TO, and EG contributed samples and background knowledge for analysis. EG performed isotopic analyses and interpreted results. EG wrote the manuscript with assistance from PS, SN-H, and TO. All authors contributed to the article and approved the submitted version.

Funding

This work was supported by Department of Anthropology, University of British Columbia; Social Sciences and Humanities Research Council of Canada (SSHRC) Insight Development Grant. The award number for the listed Insight Development Grant is "430-2017-01120".

Acknowledgments

We thank representatives of descendant First Nations (Louis Lesage, Huron-Wendat Nation, and Henry Lickers, Mohawks of Akwesasne) for permission for this analysis. For a full list of persons and organizations we wish to thank, see the Supplementary material.

Conflict of interest

The authors declare that the research was conducted in the absence of any commercial or financial relationships that could be construed as a potential conflict of interest.

Publisher's note

All claims expressed in this article are solely those of the authors and do not necessarily represent those of their affiliated organizations, or those of the publisher, the editors and the reviewers. Any product that may be evaluated in this article, or claim that may be made by its manufacturer, is not guaranteed or endorsed by the publisher.

Supplementary material

The Supplementary material for this article can be found online at: https://www.frontiersin.org/articles/10.3389/fevo.2022.953042/full#supplementary-material

References

Allen, W. A. (2010). Archaeology comes to the rescue of species at risk. *Arch Notes*, 15, 5–14.

Ambrose, S. H. (1990). Preparation and characterization of bone and tooth collagen for isotopic analysis. *J. Archaeol. Sci.* 17, 431–451. doi: 10.1016/0305-4403(90)90007-R

Bagarinao, T. (1992). Sulfide as an environmental factor and toxicant: tolerance and adaptations in aquatic organisms. *Aquat. Toxicol.* 24, 21–62. doi: 10.1016/0166-445X(92)90015-F

Baker, B., and Hill, E. (2003). "Beaver (*Castor canadensis*)" in *Wild mammals of North America: Biology, management, and conservation*. eds. G. A. Feldhamer, B. C. Thompson and J. A. Chapman (Baltimore, MD: Johns Hopkins University Press), 288–310.

Bernick, K. (2011). *Hidden dimensions: The cultural significance of wetland archaeology*. Vancouver: University of British Columbia Press.

Bottrell, S. H., and Newton, R. J. (2006). Reconstruction of changes in global sulfur cycling from marine sulfate isotopes. *Earth Sci. Rev.* 75, 59–83. doi: 10.1016/j.earscirev.2005.10.004

Canfield, D. (2001). Biogeochemistry of sulfur isotopes. *Rev. Mineral. Geochem.* 43, 607–636. doi: 10.2138/gsrmg.43.1.607

Canfield, D. E., and Teske, A. (1996). Late Proterozoic rise in atmospheric oxygen concentration inferred from phylogenetic and Sulfur-isotope studies. *Nature* 382, 127–132. doi: 10.1038/382127a0

Carlson, P. R., and Forrest, J. (1982). Uptake of dissolved sulfide by *Spartina alterniflora*: evidence from natural sulfur isotope abundance ratios. *Science* 216, 633–635. doi: 10.1126/science.216.4546.633

Chambers, L. A., Trudinger, P. A., Smith, J. W., and Burns, M. S. (1975). Fractionation of sulfur isotopes by continuous cultures of *Desulfovibrio desulfuricans*. *Can. J. Microbiol.* 21, 1602–1607. doi: 10.1139/m75-234

Chasar, L. C., Chanton, J. P., Koenig, C. C., and Coleman, F. C. (2005). Evaluating the effect of environmental disturbance on the trophic structure of Florida bay, United States: Multiple stable isotope analyses of contemporary and historical specimens. *Limnol. Oceanogr.* 50, 1059–1072. doi: 10.4319/lo.2005.50.4.1059

Colborne, S. F., Rush, S. A., Paterson, G., Johnson, T. B., Lantry, B. F., and Fisk, A. T. (2016). Estimates of lake trout (*Salvelinus namaycush*) diet in Lake Ontario using two and three isotope mixing models. *J. Great Lakes Res.* 42, 695–702. doi: 10.1016/j.jglr.2016.03.010

Cornwell, J. C., Stevenson, J. C., and Neill, C. (1995). Biogeochemical origin of δ^{34}S isotopic signatures in a prairie marsh. *Can. J. Fish. Aquat. Sci.* 52, 1816–1820. doi: 10.1139/f95-174

COSEWIC. (2012). *COSEWIC assessment and status report on the American eel Anguilla rostrata in Canada*. Ottawa, Canada: Committee on the Status of Endangered Wildlife. ed. E. Taylor.

COSEWIC. (2017). *COSEWIC assessment and update status report on the lake sturgeon Acipenser fulvescens in Canada*. Ottawa, Canada: Committee on the Status of Endangered Wildlife. ed. N. Mandrak.

Craig, O., Ross, R., Andersen, S. H., Milner, N., and Bailey, G. (2006). Focus: Sulfur isotope variation in archaeological marine fauna from northern Europe. *J. Archaeol. Sci.* 33, 1642–1646. doi: 10.1016/j.jas.2006.05.006

Dance, K. M., Rooker, J. R., Shipley, J. B., Dance, M. A., and Wells, R. J. D. (2018). Feeding ecology of fishes associated with artificial reefs in the Northwest Gulf of Mexico. *PLoS One* 13:e0203873. doi: 10.1371/journal.pone.0203873

Davidson, N. C. (2014). How much wetland has the world lost? Long-term and recent trends in global wetland area. *Mar. Freshw. Res.* 65, 934–941. doi: 10.1071/MF14173

DeNiro, M. J., and Epstein, S. (1981). Influence of diet on the distribution of nitrogen isotopes in animals. *Geochim. Cosmochim. Acta* 45, 341–351. doi: 10.1016/0016-7037(81)90244-1

Findlay, A. J., and Kamyshny, A. (2017). Turnover rates of intermediate sulfur species (Sx2-, S0, S2O32-, S4O62-, SO32-) in anoxic freshwater and sediments. *Front. Microbiol.* 8:2551. doi: 10.3389/fmicb.2017.02551

Finlay, J. C., and Kendall, C. (2007). Stable isotope tracing of temporal and spatial variability in organic matter sources to freshwater ecosystems. *Stable Isotop. Ecol. Environ. Sci.* 2, 283–333. doi: 10.1002/9780470691854.ch10

France, R. (1995). Carbon-13 enrichment in benthic compared to planktonic algae: foodweb implications. *Mar. Ecol. Prog. Ser.* 124, 307–312. doi: 10.3354/meps124307

Frederiksen, M. S., Holmer, M., Borum, J., and Kennedy, H. (2006). Temporal and spatial variation of sulfide invasion in eelgrass (*Zostera marina*) as reflected by its sulfur isotopic composition. *Limnol. Oceanogr.* 51, 2308–2318. doi: 10.4319/lo.2006.51.5.2308

Fry, B. (1988). Food web structure on Georges Bank from stable C, N, and S isotopic compositions. *Limnol. Oceanogr.* 33, 1182–1190. doi: 10.4319/lo.1988.33.5.1182

Fry, B., and Chumchal, M. M. (2011). Sulfur stable isotope indicators of residency in estuarine fish. *Limnol. Oceanogr.* 56, 1563–1576. doi: 10.4319/lo.2011.56.5.1563

Fry, B., Scalan, R. S., Winters, J. K., and Parker, P. L. (1982). Sulfur uptake by salt grasses, mangroves, and seagrasses in anaerobic sediments. *Geochim. Cosmochim. Acta* 46, 1121–1124. doi: 10.1016/0016-7037(82)90063-1

General, P., and Warrick, G. (2012). The Grand River sturgeon fishery. *Ontario Archaeol.* 92, 27–37.

Guiry, E. (2019). Complexities of stable carbon and nitrogen isotope biogeochemistry in ancient freshwater ecosystems: implications for the study of past subsistence and environmental change. *Front. Ecol. Evol.* 7. 1–24 doi: 10.3389/fevo.2019.00313

Guiry, E. J., Buckley, M., Orchard, T. J., Hawkins, A. L., Needs-Howarth, S., Holm, E., et al. (2020a). Deforestation caused abrupt shift in Great Lakes nitrogen cycle. *Limnol. Oceanogr.* 65, 1921–1935. doi: 10.1002/lno.11428

Guiry, E. J., Kennedy, J. R., O'Connell, M. T., Gray, D. R., Grant, C., and Szpak, P. (2021c). Early evidence for historical overfishing in the Gulf of Mexico. Science. *Advances* 7:2525. doi: 10.1126/sciadv.abh2525

Guiry, E. J., Needs-Howarth, S., Friedland, K. D., Hawkins, A. L., Szpak, P., Macdonald, R., et al. (2016a). Lake Ontario salmon (*Salmo salar*) were not migratory: a long-standing historical debate solved through stable isotope analysis. *Sci. Rep.* 6:36249. doi: 10.1038/srep36249

Guiry, E., Noël, S., and Fowler, J. (2021a). Archaeological herbivore δ13C and δ34S provide a marker for saltmarsh use and new insights into the process of 15N-enrichment in coastal plants. *J. Archaeol. Sci.* 125:105295. doi: 10.1016/j.jas.2020.105295

Guiry, E., Orchard, T. J., Needs-Howarth, S., and Szpak, P. (2021b). Isotopic evidence for garden hunting and resource depression in the late woodland of northeastern North America. *Am. Antiq.* 86, 90–110. doi: 10.1017/aaq.2020.86

Guiry, E. J., Royle, T. C. A., Orchard, T. J., Needs-Howarth, S., Yang, D. Y., and Szpak, P. (2020b). Evidence for freshwater residency among Lake Ontario Atlantic salmon (*Salmo salar*) spawning in New York. *J. Great Lakes Res.* 46, 1036–1043. doi: 10.1016/j.jglr.2020.05.009

Guiry, E., and Szpak, P. (2020). Seaweed-eating sheep show that δ^{34}S evidence for marine diets can be fully masked by sea spray effects. *Rapid Commun. Mass Spectrom.* 34:e 8868. doi: 10.1002/rcm.8868

Guiry, E. J., and Szpak, P. (2021). Improved quality control criteria for stable carbon and nitrogen isotope measurements of ancient bone collagen. *J. Archaeol. Sci.* 132:105416. doi: 10.1016/j.jas.2021.105416

Guiry, E. J., Szpak, P., and Richards, M. P. (2016b). Effects of lipid extraction and ultrafiltration on stable carbon and nitrogen isotopic compositions of fish bone collagen. *Rapid Commun. Mass Spectrom.* 30, 1591–1600. doi: 10.1002/rcm.7590

Habicht, K. S., and Canfield, D. E. (1997). Sulfur isotope fractionation during bacterial sulfate reduction in organic-rich sediments. *Geochim. Cosmochim. Acta* 61, 5351–5361. doi: 10.1016/S0016-7037(97)00311-6

Habicht, K. S., and Canfield, D. E. (2001). Isotope fractionation by sulfate-reducing natural populations and the isotopic composition of sulfide in marine sediments. *Geology* 29, 555–558. doi: 10.1130/0091-7613(2001)029<0555:IFBSRN>2.0.CO;2

Hammer, Ø., Harper, D. A., and Ryan, P. D. (2001). PAST: paleontological statistics software package for education and data analysis. *Palaeontol. Electron.* 4:9

Henry, AP, Barnett, PJ, and Cowan, WR. (2008). *Quaternary geology of Ontario, southern sheet, Ontario geological survey, M 2556*. Sudbury, Ontario: Ministry of Energy, Northern Development and Mines.

Hesslein, R., Capel, M., and Fox, D. (1988). Sulfur isotopes in sulfate in the inputs and outputs of a Canadian shield watershed. *Biogeochemistry* 5, 263–273. doi: 10.1007/BF02180067

Hobson, K. A. (2019). "Application of isotopic methods to tracking animal movements," in *Tracking animal migration with stable isotopes*. eds. K. A. Hobson and L. I. Wassenaar. *Second* ed (New York: Academic Press), 85–115. doi: 10.1016/B978-0-12-814723-8.00004-0

Hobson, K. A., and Clark, R. G. (1992). Assessing avian diets using stable isotopes I: turnover of ^{13}C in tissues. *Condor* 94, 181–188. doi: 10.2307/1368807

Hodell, D. A., and Schelske, C. L. (1998). Production, sedimentation, and isotopic composition of organic matter in Lake Ontario. *Limnol. Oceanogr.* 43, 200–214. doi: 10.4319/lo.1998.43.2.0200

Hyland, C., Scott, M. B., Routledge, J., and Szpak, P. (2021). Stable carbon and nitrogen isotope variability of bone collagen to determine the number of isotopically distinct specimens. *J. Archaeol. Method Theory* 29, 666–686. doi: 10.1007/s10816-021-09533-7

Jellyman, D. J., and Arai, T. (2016). "Juvenile eels: upstream migration and habitat use," in *Biology and ecology of anguillid eels*. ed. T. Arai (Boco Ratton, FL: CRC Press), 171–191.

Jenkins, S. (1981). "Problems, progress, and prospects in studies of food selection by beavers," in *Proceedings of the worldwide furbearer conference*. eds. A. Chapman and D. Pursley (Worldwide Furbearer Conference: Baltimore, MD), 559–579.

Jørgensen, B. B. (1982). Mineralization of organic matter in the sea bed—the role of sulfate reduction. *Nature* 296, 643–645. doi: 10.1038/296643a0

Jørgensen, B. B., Findlay, A. J., and Pellerin, A. (2019). The biogeochemical sulfur cycle of marine sediments. *Front. Microbiol.* 10:849. doi: 10.3389/fmicb.2019.00849

Kaplan, I., and Rittenberg, S. (1964). Microbiological fractionation of Sulfur isotopes. *Microbiology* 34, 195–212.

Katzenberg, M. A. (1989). Stable isotope analysis of archaeological faunal remains from southern Ontario. *J. Archaeol. Sci.* 16, 319–329. doi: 10.1016/0305-4403(89)90008-3

Kemp, A., and Thode, H. (1968). The mechanism of the bacterial reduction of sulfate and of sulfite from isotope fractionation studies. *Geochim. Cosmochim. Acta* 32, 71–91. doi: 10.1016/0016-7037(68)90088-4

Koch, M., and Mendelssohn, I. (1989). Sulfide as a soil phytotoxin: differential responses in two marsh species. *J. Ecol.* 77, 565–578. doi: 10.2307/2260770

Koch, M. S., Mendelssohn, I. A., and McKee, K. L. (1990). Mechanism for the hydrogen sulfide-induced growth limitation in wetland macrophytes. *Limnol. Oceanogr.* 35, 399–408. doi: 10.4319/lo.1990.35.2.0399

Krajcarz, M. T., Krajcarz, M., Drucker, D. G., and Bocherens, H. (2019). Prey-to-fox isotopic enrichment of ^{34}S in bone collagen: implications for paleoecological studies. *Rapid Commun. Mass Spectrom.* 33, 1311–1317. doi: 10.1002/rcm.8471

Krouse, H. (1989). "Sulfur isotope studies of the pedosphere and biosphere" in *Stable isotopes in ecological research*. eds. W. Rundel, J. Ehleringer and K. Nagy (New York: Springer), 424–444. doi: 10.1007/978-1-4612-3498-2_24

Lamb, A., and Madgwick, R. (2022). "Wet feet—using Sulfur isotope analysis to identify wetland dwellers," in *United Kingdom archaeological science conference* (Aberdeen)

Lamers, L. P., Govers, L. L., Janssen, I. C., Geurts, J. J., Van der Welle, M. E., Van Katwijk, M. M., et al. (2013). Sulfide as a soil phytotoxin—a review. *Front. Plant Sci.* 4:268. doi: 10.3389/fpls.2013.00268

Le Roy, M., Magniez, P., and Goude, G. (2022). Stable-isotope analysis of collective burial sites in southern France at late Neolithic/early bronze age transition. *Int. J. Osteoarchaeol.* 32, 396–407. doi: 10.1002/oa.3074

Lesage, C-L. (2016). Écologie historique et connaissances écologiques traditionnelles huronnes-wendat relatives à douze espèces animales et végétale dans le Wendake Sud: Report prepared by Bureau du Nionwentsïo, Nation huronne-wendat, in collaboration with Environment and Climate Change Canada/Environnement et Changement climatique Canada.

Longin, R. (1971). New method of collagen extraction for radiocarbon dating. *Nature* 230, 241–242. doi: 10.1038/230241a0

Mac Culloch, RD.(2002). *The ROM field guide to amphibians and reptiles of Ontario*. Ontario: McClelland & Stewart Limited.

Marschner, H. (2011). *Marschner's mineral nutrition of higher plants*. New York: Academic press.

Mitchell, M. J., Roy Krouse, H., Mayer, B., Stam, A. C., and Zhang, Y. (1998). "Chapter 15- use of stable isotopes in evaluating sulfur biogeochemistry of Forest ecosystems," in *Isotope tracers in catchment hydrology*. eds. C. Kendall and J. J. McDonnell (Amsterdam: Elsevier), 489–518. doi: 10.1016/B978-0-444-81546-0.50022-7

Mizota, C., Shimoyama, S., and Yamanaka, T. (1999). An isotopic characterization of sulfur uptake by benthic animals from Tsuyazaki inlet, northern Kyushu, Japan. *Benthos Res.* 54, 81–85. doi: 10.5179/benthos1996.54.2_81

Morris, J. T., Haley, C., and Krest, R. (1996). Effects of Sulfide on Growth and Dimethylsulfoniopropionate (DMSP) Concentration in Spartina Alterniflora. In: Kiene RP, Visscher PT, Keller MD, Kirst GO, editors. Biological and Environmental Chemistry of DMSP and Related Sulfonium Compounds. Boston, MA: Springer, US. 87–95.

Nehlich, O. (2015). The application of Sulfur isotope analyses in archaeological research: a review. *Earth Sci. Rev.* 142, 1–17. doi: 10.1016/j.earscirev.2014.12.002

Nehlich, O., Barrett, J. H., and Richards, M. P. (2013). Spatial variability in Sulfur isotope values of archaeological and modern cod (Gadus morhua). *Rapid Commun. Mass Spectrom.* 27, 2255–2262. doi: 10.1002/rcm.6682

Novak, M. (1987). "Beaver" in *Wild furbearer management and conservation in North America*. eds. M. Novak, J. A. Baker, M. E. Obbard and B. Malloch (Toronto: Ontario Trappers Association and Ontario Ministry of Natural Resources), 283–312.

Oakes, J. M., and Connolly, R. M. (2004). Causes of sulfur isotope variability in the seagrass, Zostera capricorni. *J. Exp. Mar. Biol. Ecol.* 302, 153–164. doi: 10.1016/j.jembe.2003.10.011

OGS. (1991). *Bedrock geology of Ontario, southern sheet, Ontario geological survey, map 2544*. Sudbury, Ontario: Ministry of Energy, Northern Development and Mines.

Pearson, M. P., Chamberlain, A., Jay, M., Richards, M., Sheridan, A., Curtis, N., et al. (2016). Beaker people in Britain: migration, mobility and diet. *Antiquity* 90, 620–637. doi: 10.15184/aqy.2016.72

Peterson, B. J., and Howarth, R. W. (1987). Sulfur, carbon, and nitrogen isotopes used to trace organic matter flow in the salt-marsh estuaries of Sapelo Island, Georgia. *Limnol. Oceanogr.* 32, 1195–1213. doi: 10.4319/lo.1987.32.6.1195

Postgate, J. (1959). Sulfate reduction by bacteria. *Ann. Rev. Microbiol.* 13, 505–520. doi: 10.1146/annurev.mi.13.100159.002445

Privat, K. L., O'Connell, T. C., and Hedges, R. E. (2007). The distinction between freshwater- and terrestrial-based diets: methodological concerns and archaeological applications of Sulfur stable isotope analysis. *J. Archaeol. Sci.* 34, 1197–1204. doi: 10.1016/j.jas.2006.10.008

Rand, A. J., Freiwald, C., and Grimes, V. (2021). A multi-isotopic (δ13C, δ15N, and δ34S) faunal baseline for Maya subsistence and migration studies. *J. Archaeol. Sci. Rep.* 37:102977. doi: 10.1016/j.jasrep.2021.102977

Rand, A. J., Matute, V., Grimes, V., Freiwald, C., Źrałka, J., and Koszkul, W. (2020). Prehispanic Maya diet and mobility at Nakum, Guatemala: a multi-isotopic approach. *J. Archaeol. Sci. Rep.* 32:102374. doi: 10.1016/j.jasrep.2020.102374

Rees, C. E., Jenkins, W. J., and Monster, J. (1978). The Sulfur isotopic composition of ocean water sulfate. *Geochim. Cosmochim. Acta* 42, 377–381. doi: 10.1016/0016-7037(78)90268-5

Richards, M., Fuller, B., and Hedges, R. (2001). Sulfur isotopic variation in ancient bone collagen from Europe: implications for human palaeodiet, residence mobility, and modern pollutant studies. *Earth Planet. Sci. Lett.* 191, 185–190. doi: 10.1016/S0012-821X(01)00427-7

Sayle, K. L., Brodie, C. R., Cook, G. T., and Hamilton, W. D. (2019). Sequential measurement of δ15N, δ13C and δ34S values in archaeological bone collagen at the Scottish universities environmental research Centre (SUERC): a new analytical frontier. *Rapid Commun. Mass Spectrom.* 33, 1258–1266. doi: 10.1002/rcm.8462

Schelske, C. L., and Hodell, D. A. (1991). Recent changes in productivity and climate of Lake Ontario detected by isotopic analysis of sediments. *Limnol. Oceanogr.* 36, 961–975. doi: 10.4319/lo.1991.36.5.0961

Schwarcz, H. P., and Schoeninger, M. J. (1991). Stable isotope analyses in human nutritional ecology. *Am. J. Phys. Anthropol.* 34, 283–321. doi: 10.1002/ajpa.1330340613

Stribling, J. M., Cornwell, J. C., and Currin, C. (1998). Variability of stable sulfur isotopic ratios in Spartina alterniflora. *Mar. Ecol. Prog. Ser.* 166, 73–81. doi: 10.3354/meps166073

Szpak, P., and Buckley, M. (2020). Sulfur isotopes (δ34S) in Arctic marine mammals: indicators of benthic vs. pelagic foraging. *Mar. Ecol. Prog. Ser.* 653, 205–216. doi: 10.3354/meps13493

Szpak, P., Metcalfe, J. Z., and Macdonald, R. A. (2017). Best practices for calibrating and reporting stable isotope measurements in archaeology. *J. Archaeol. Sci. Rep.* 13, 609–616. doi: 10.1016/j.jasrep.2017.05.007

Thode, H. (1991). "Sulfur isotopes in nature and the environment: an overview" in *Stable isotopes: Natural and anthropogenic Sulfur in the environment*. eds. H. Krouse and V. Grinenko (Chichester, United Kingdom: Wiley), 1–26.

Vika, E. (2009). Strangers in the grave? Investigating local provenance in a Greek bronze age mass burial using δ34S analysis. *J. Archaeol. Sci.* 36, 2024–2028. doi: 10.1016/j.jas.2009.05.022

Zazzo, A., Monahan, F., Moloney, A., Green, S., and Schmidt, O. (2011). Sulfur isotopes in animal hair track distance to sea. *Rapid Commun. Mass Spectrom.* 25, 2371–2378. doi: 10.1002/rcm.5131

Zedler, J. B., and Kercher, S. (2005). Wetland resources: status, trends, ecosystem services, and restorability. *Annu. Rev. Environ. Resour.* 30, 39–74. doi: 10.1146/annurev.energy.30.050504.144248

Zhao, F. J., Knights, J. S., Hu, Z. Y., and McGrath, S. P. (2003). Stable sulfur isotope ratio indicates long-term changes in sulfur deposition in the Broadbalk experiment since 1845. *J. Environ. Qual.* 32, 33–39. doi: 10.2134/jeq2003.3300

frontiers | Frontiers in Ecology and Evolution

TYPE Original Research
PUBLISHED 12 January 2023
DOI 10.3389/fevo.2022.1061636

Check for updates

OPEN ACCESS

EDITED BY
Rona A. R. McGill,
University of Glasgow, United Kingdom

REVIEWED BY
Zachary Feiner,
Wisconsin Department of Natural Resources, United States
Michael Rennie,
Lakehead University,
Canada

*CORRESPONDENCE
Ariana Chiapella
✉ ariana.chiapella@uvm.edu

SPECIALTY SECTION
This article was submitted to Population, Community, and Ecosystem Dynamics, a section of the journal Frontiers in Ecology and Evolution

RECEIVED 04 October 2022
ACCEPTED 13 December 2022
PUBLISHED 12 January 2023

CITATION
Chiapella A, Possamai B, Marsden JE, Kainz MJ and Stockwell JD (2023) Contrasting energy pathways suggest differing susceptibility of pelagic fishes to an invasive ecosystem engineer in a large lake system.
Front. Ecol. Evol. 10:1061636.
doi: 10.3389/fevo.2022.1061636

COPYRIGHT
© 2023 Chiapella, Possamai, Marsden, Kainz and Stockwell. This is an open-access article distributed under the terms of the Creative Commons Attribution License (CC BY). The use, distribution or reproduction in other forums is permitted, provided the original author(s) and the copyright owner(s) are credited and that the original publication in this journal is cited, in accordance with accepted academic practice. No use, distribution or reproduction is permitted which does not comply with these terms.

Contrasting energy pathways suggest differing susceptibility of pelagic fishes to an invasive ecosystem engineer in a large lake system

Ariana Chiapella[1]*, Bianca Possamai[1], J. Ellen Marsden[1], Martin J. Kainz[2] and Jason D. Stockwell[1]

[1]Rubenstein Ecosystem Science Laboratory, University of Vermont, Burlington, VT, United States, [2]WasserCluster Lunz, Lunz am See, Austria

Species invasions can lead to ecological regime shifts by altering food web structure and changing nutrient cycling. Stable isotopes are a powerful tool to understand the potential and realized impacts of invasive species on food webs, especially when used in tandem with other dietary tracers. An invasion by one of the most notorious freshwater invaders in North America, the quagga mussel (*Dreissena bugensis*), is imminent in Lake Champlain, United States. An invasion by this filter feeder has the potential to drastically alter energy pathways and destabilize pelagic fisheries *via* bottom-up impacts. However, the extent and magnitude of these impacts depend on the current food web structure of the mid-trophic pelagic food web, which was previously not well described. We used Bayesian stable isotope mixing models informed by stomach content analysis to identify which energy pathways are currently most important to mid-trophic level fishes. We determined that in the Main Lake basin, the spring phytoplankton bloom and deep chlorophyll layer – the resources most vulnerable to quagga mussels – provide a disproportionate amount of support to the pelagic food web *via* zooplankton and the migrating macroinvertebrate *Mysis*. The food web in the Northeast Arm of Lake Champlain is supported by epilimnetic phytoplankton, which is more protected from the filtration effects of quagga mussels than the deep chlorophyll layer. However, the Northeast Arm will likely not provide a high-quality foraging refuge to coldwater pelagic fish due to unfavorable oxythermal conditions. The mid-trophic food web of Lake Champlain—and consequently piscivores who rely on these prey—may be vulnerable to the impending quagga mussel invasion if migratory *Mysis* are not able to shift their diet to benthic resources.

KEYWORDS

dreissenid mussels, MixSIAR, alewife, rainbow smelt, *Mysis*, food webs

1. Introduction

Understanding food web structure and energy flow is critical for successful management and conservation of ecosystems threatened by anthropogenic change (Vander Zanden et al., 2006; Naman et al., 2022). For example, species invasions often lead to ecological regime shifts and have major impacts on ecosystem services (e.g., Charles and Dukes, 2007; Pejchar and Mooney, 2009); therefore, understanding the effects of invaders may be one of the most important ways managers can anticipate and effectively respond to ecosystem change. We must first understand the relative importance of top-down or bottom-up processes and the basal resources most critical for at-risk native species to evaluate the potential impact of an introduced species. Understanding the factors that favor invasion, how similar systems responded to the same invasive species, and the biogeochemical and ecological configuration of the at-risk system are necessary for anticipating the socio-ecological consequences of an invasion (David et al., 2017; Flood et al., 2020).

The invasive zebra [*Dreissena polymorpha* (Pallas, 1771)] and quagga (*D. bugensis* Andrusov, 1897) mussels are major drivers of ecological change in fresh waters of North America. The mechanisms and impacts of their invasions have been extensively documented (e.g., Limburg et al., 2010; Karatayev et al., 2015; Strayer et al., 2019). Dreissenid mussels are ecosystem engineers (Sousa et al., 2009) and are one the most successful freshwater invaders in the northern hemisphere (e.g., Higgins and Vander Zanden, 2010; Nalepa and Schloesser, 2014). They have high fecundity (Keller et al., 2007) and filtration capacity (Higgins and Vander Zanden, 2010), and can create extensive, dense colonies that are highly effective at suspension feeding. As a result, dreissenids sequester nutrients and phytoplankton from the water column to the benthos, resulting in system oligotrophication (Higgins and Vander Zanden, 2010). By sequestering nutrients and phytoplankton during annual turnover events, dreissenids incrementally reduce pelagic productivity over time, which has led to the disappearance of spring phytoplankton blooms, reduction of the deep chlorophyll layer (DCL), and increased benthic algal blooms in many lakes (e.g., Cecala et al., 2008; Higgins and Vander Zanden, 2010; Pothoven and Fahnenstiel, 2013). In the Laurentian Great Lakes, reductions in pelagic primary production are associated with declines of important invertebrate prey species, such as zooplankton, *Mysis*, and *Diporeia* spp. (Nalepa et al., 2009; Higgins and Vander Zanden, 2010; Johannsson et al., 2011); consequently, growth and biomass of mid-trophic level fishes often decline after mussels become established (Pothoven and Madenjian, 2008; Eppehimer et al., 2019). The extent of these impacts depends on whether one or both species of mussel has invaded a system.

Zebra mussels typically precede quagga mussels and spread to new systems quickly, but high densities are usually confined to littoral zones (Karatayev et al., 2015; Knight et al., 2018). Quagga mussels, despite spreading more slowly to new systems, reach greater densities than zebra mussels because they have higher growth and filtration rates, colonize deeper profundal areas, and outcompete and rapidly displace zebra mussels in shallow areas (Mills et al., 1999; Karatayev et al., 2015; Metz et al., 2018). Thus, quagga mussels often have more extensive ecosystem impacts than zebra mussels (Karatayev et al., 2015). Because the impacts of dreissenids are fairly predictable, management agencies may have time to adjust policies (e.g., adjust stocking rates or game fish catch limits) in response to an early invasion to partially offset predicted food web impacts.

Lake Champlain, United States/Canada, has only been invaded by zebra mussels, and therefore the opportunity exists to inform management actions that could help counteract the food web impacts of an imminent quagga mussel invasion. Zebra mussels were first discovered in the lake in 1993 but have been primarily limited to depths shallower than 25 m (Marsden et al., 2013; Knight et al., 2018). Quagga mussels have not yet invaded, despite their presence in the nearby St. Lawrence and Hudson Rivers (Figure 1; Riccardi et al., 1996; Strayer et al., 2020). An invasion is looming, given the connectivity of these systems to Lake Champlain (Figure 1). Hull inspections of vessels entering Lake Champlain from the Great Lakes are rare, but inspection of a vessel entering the lake from the Richelieu River (Figure 1) in 2016 found 30% of a sample of dreissenids on the hull were adult quagga mussels (Marsden, *unpublished data*). While the impacts of zebra mussels on Lake Champlain's food web and water quality have been limited (e.g., Smeltzer et al., 2012; Knight et al., 2018), quagga mussels could colonize all depths of Lake Champlain, to the maximum depth of 122 m (Mills et al., 1996) and outcompete existing zebra mussel colonies (Ginn et al., 2018). Thus, quagga mussels are likely to have a greater impact on the Lake Champlain system than the established zebra mussel population. Although profundal quagga mussel colonies may have limited epilimnetic effects in large lakes with stratification (e.g., Karatayev et al., 2015), filtration during spring turnover could substantially reduce the spring phytoplankton bloom, which maybe an important source of food for pelagic primary consumers (e.g., Pothoven and Vanderploeg, 2022). Further, any production in the hypolimnion is vulnerable to filtration by quagga mussels. In lakes with a deep chlorophyll layer, quagga mussels can substantially reduce hypolimnetic production (e.g., Fahnenstiel et al., 2010; Malkin et al., 2012; Pothoven and Fahnenstiel, 2013). Consequently, quagga mussels could propagate bottom-up impacts in Lake Champlain by reducing the pelagic resources that support the pelagic fish community, exacerbating growing top-down pressure from a recovering lake trout (*Salvelinus namaycush*) population (Marsden et al., 2018; Wilkins and Marsden, 2021), resulting in a "trophic squeeze."

Lake Champlain's salmonid populations were re-introduced by stocking in the early 1970s; however, natural recruitment of lake trout did not begin until 2012, and Atlantic salmon recruitment is severely limited by dams. The most important prey for adult lake trout and Atlantic salmon (*Salmo salar*) in Lake Champlain are pelagic alewife (*Alosa pseudoharengus*) and rainbow smelt (*Osmerus mordax*), and the benthic slimy sculpin

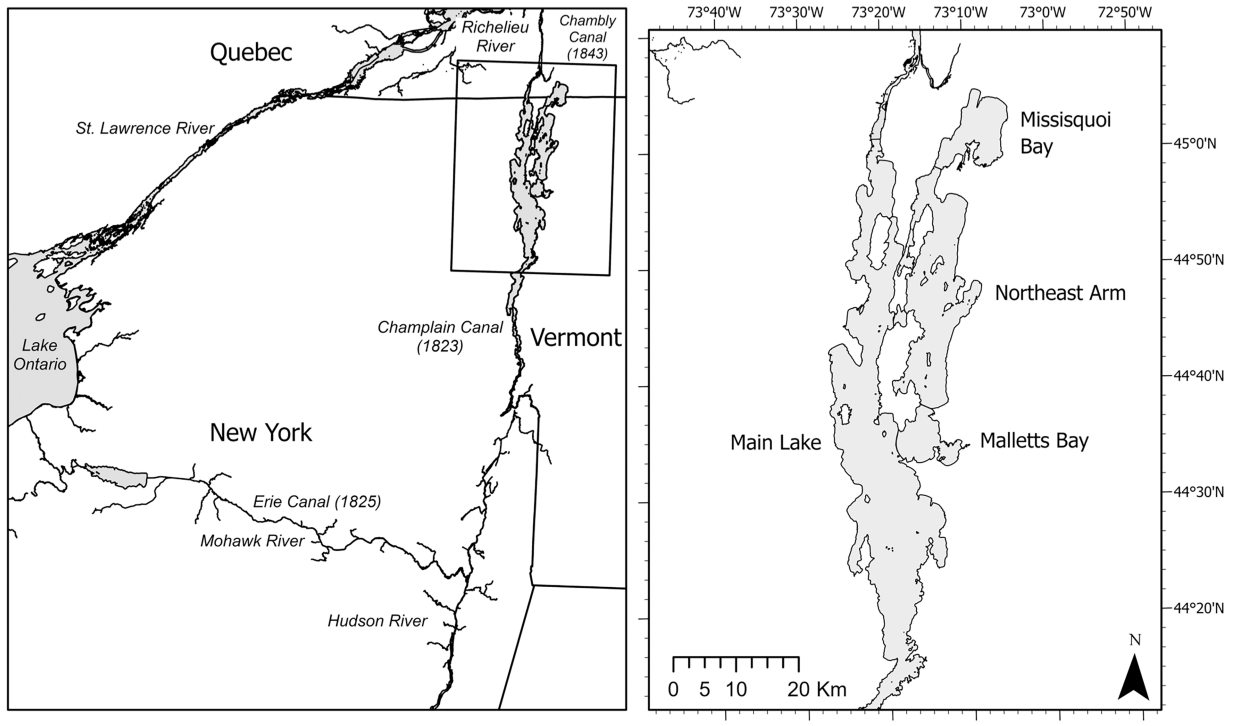

FIGURE 1
Map of Lake Champlain and its basins, showing connectivity of Lake Champlain and adjacent waterways. The Hudson River connects to Lake Champlain *via* the Champlain Canal in the south, and the lake flows north *via* the Richelieu River into the St. Lawrence River. Quagga mussels are established in Lake Ontario, the Hudson River, and the St. Lawrence River.

(*Cottus cognatus*; Kirn and LaBar, 1996; Simonin et al., 2018; Marsden et al., 2022). A wild population of lake trout is becoming established, and wild age-0 lake trout rely on the macroinvertebrate *Mysis* as a primary prey (Marsden et al., 2022). Stocking numbers have been reduced because an increased abundance of predators due to natural recruitment may add predation pressure to prey fishes (Marsden et al., 2018; Wilkins and Marsden, 2021). Rainbow smelt and alewife feed on a combination of crustacean zooplankton and *Mysis,* and rainbow smelt are also cannibalistic (Labar, 1993). However, the relative importance of each prey group is unknown, especially *Mysis*, which represents an important link between benthic and pelagic habitats (Stockwell et al., 2020). The impact of quagga mussels on *Mysis*, and consequently on lake trout recruitment, will depend on the relative contributions of benthic and pelagic resources to *Mysis* diets.

The role of *Mysis* in the Lake Champlain food web is of particular importance because they are omnivorous and exhibit diel vertical migration (Euclide et al., 2017; O'Malley et al., 2018). The daily movement between benthic and pelagic habitat allows *Mysis* to feed on both detritus and planktonic resources (O'Malley and Stockwell, 2019), and exposes them to predation by both benthic (e.g., slimy sculpin, age-0 lake trout) and pelagic fishes (e.g., Gamble et al., 2011a, 2011b). We do not know the relative contribution of detritus, epilimnetic phytoplankton, and hypolimnetic phytoplankton (directly or *via* zooplankton and benthic invertebrates) to *Mysis* production or the contribution of *Mysis* to the mid-trophic level fish community in Lake Champlain, and thus we do not know how dependent the mid-trophic level fish community is on pelagic versus benthic energy pathways and thus its consequent vulnerability to quagga mussels.

We hypothesized that alewife and rainbow smelt primarily rely on pelagic energy pathways, specifically the spring phytoplankton bloom and DCL. As such, a reduction in hypolimnetic pelagic resources by quagga mussels would lead to declines in key zooplankton prey and consequent declines in pelagic planktivorous fish populations. Subsequently, pelagic piscivore populations may face a bottom-up-induced prey decline, which would reduce both the ecological integrity and recreational fishing opportunities in Lake Champlain. In contrast, because slimy sculpins rely on benthic energy pathways we hypothesize that they will be un-impacted or positively impacted by quagga mussels, therefore sculpin could partially offset the impacts on piscivores who forage in both benthic and pelagic habitats. We conducted bi-weekly sampling of the lower and middle food web of Lake Champlain's two largest basins over 7 months, then used Bayesian isotope mixing models (MixSIAR; Stock et al., 2018) to identify the importance of benthic versus pelagic resources for Lake Champlain's mid-trophic level fish community. We then used the model results to estimate the susceptibility of the same fish community to a quagga mussel invasion due to concurrent top-down and bottom-up pressures.

2. Materials and methods

2.1. Sample sites

Lake Champlain is a large, freshwater lake situated among northwestern Vermont, northeastern New York, United States, and southern Quebec, Canada. Water flows northward into the Richelieu River, and then into the St. Lawrence River (Figure 1). The Chambly Canal allows boat traffic, a potential invasion vector, to bypass rapids in the Richelieu River, while the Champlain Canal creates a pathway for invasive species by connecting the southern end of the lake to the Hudson River and Erie Canal (Marsden and Hauser, 2009). Causeways and islands separate the 193-km-long lake into four major basins (Figure 1), each with contrasting morphometry and trophic conditions. The Main Lake is the largest (up to 19 km wide) and deepest basin (maximum 122 m) and is mesotrophic. The Northeast Arm is the second largest basin by area, with a maximum depth of 49 m, and is eutrophic. Cyanobacteria blooms are common in both basins in summer, but more severe and expansive in the Northeast Arm. Openings in the causeways that separate the basins are shallow (1–7 m) and narrow (<100 m), so passage of cold-water species between basins is presumed to be restricted to the non-stratified season. Slimy sculpin, rainbow smelt, and lake whitefish populations in the Main Lake and Northeast Arm are not genetically isolated (Euclide et al., 2018, 2019, 2020), and lake trout are found in the the Northeast Arm in winter but not during the stratified seasons, indicating that transfer of fishes and nutrients does occur between basins. Water flow is mostly from the Northeast Arm into the Main Lake, which may account for the slow colonization of zebra mussels into the Northeast Arm (Marsden and Langdon, 2012).

We sampled a 40-m and a 100-m deep site in the Main Lake and a 40-m deep site in the Northeast Arm (Figure 1). At each site, we sampled the lower food web (invertebrates, phytoplankton, sediment) biweekly and the full food web (fish, *Mysis*, and lower food web) monthly from May to November, 2019. On all sampling dates we recorded mean Secchi depth (m) and measured water-column profiles using a CastAway temperature-depth probe (SonTek©, San Diego, CA, United States) or Seabird CTD (Sea-Bird Scientific).

2.2. Sample collection

We collected three replicate samples of phytoplankton, zooplankton, benthic invertebrate, and sediment (proxy for detritus) every 2 weeks at each site. Integrated photic zone water samples for phytoplankton were collected by lowering a 25-m garden hose (2-cm diameter) with weight on the end to a depth of 2.5× the Secchi depth and emptying the filled hose into a bucket. The sample was mixed, then poured into a 4-L opaque Nalgene bottle. Zooplankton were collected from the whole water column using a 150-µm Bongo net, then concentrated into a 250-ml sample jar. Benthic invertebrates were sampled using a 152 × 152 mm Ponar grab. All samples were kept in a cooler on ice until returning to the lab.

At each 40-m site, we conducted daytime bottom trawls, and at the 100-m site we conducted daytime and nighttime midwater trawls to target alewife, smelt, and sculpin. Trawl depths varied ±10 m. Bottom trawls were not conducted at the 100-m site due to gear limitations. Fish were measured (total length; TL, in mm) on board and separated by size class; 20 of each size class of each species was collected at each site. Alewife were split into small (<100 mm), medium (100–200 mm), and large (>200 mm) size classes; rainbow smelt into small (<100 mm), medium (100–150 mm), and large (>150 mm) classes; and sculpin into small (<60 mm) and large (>60 mm) classes. All fish were promptly frozen onboard before transferring to a −20°C freezer at the laboratory.

2.3. Laboratory processing and analysis

Water samples were refrigerated and then filtered within 24 h of collection onto 1.2-µm glass fiber filters for stable isotope analysis. Zooplankton samples were filtered through a 350-µm sieve to remove filamentous algae, then left to settle for 30–60 min to separate from remaining phytoplankton. The top clear layer was poured off and inspected and picked for any remaining debris or large phytoplankton, then the concentrated sample was added to a scintillation vial in preparation for drying and stable isotope analysis. Benthic invertebrate samples were sieved to remove large debris, then picked for all conspicuous taxa, grouped by major taxonomic group (chironomids, oligochaetes, amphipods, gastropods), then rinsed with deionized water. Each *Mysis* replicate was sorted into juvenile (TL < 10 mm; from the tip of the rostrum to the tip of the telson) and adult (TL > 10 mm) size classes and counted; 10–20 individuals of each size class were then rinsed in deionized water and grouped into scintillation vials in preparation for drying and stable isotope analysis. Fish were measured for total length (mm) and wet weight (g), then dissected. Dorsal muscle tissue plugs were taken for isotope analysis, and stomachs were removed, weighed, then preserved in 90% ethanol. Fish, invertebrate, phytoplankton, and sediment samples were then prepared for bulk isotope analysis by drying at 40°C for 24–48 h, depending on density and water content, then homogenized (with the exception of filtered samples) with a mortar and pestle or a glass rod in a scintillation vial. Homogenized samples were then subsampled, phytoplankton were scraped from filters, weighed (µm), and packed in tin capsules for bulk stable isotope analysis. All isotope samples were analyzed for $\delta^{13}C$ and $\delta^{15}N$ at the UC Davis Stable Isotope Facility using a PDZ Europa ANCA-GSL elemental analyzer interfaced to a PDZ Europa 20–20 isotope ratio mass spectrometer (Sercon Ltd., Cheshire, United Kingdom) with reference material Vienna PeeDee Belemnite and air for carbon and nitrogen, respectively (SD was 0.2‰ for ^{13}C and 0.3‰ for ^{15}N). Internal duplicates ($n = 22$) indicated samples were well-homogenized (paired t-test; $p = 0.35$ for $\delta^{13}C$ and $p = 0.82$ for $\delta^{15}N$).

2.4. Stomach analysis

Fish stomach contents were identified by microscope and prey were coarsely grouped as amphipods, oligochaetes, zooplankton, detritus, terrestrial insects, *Mysis*, fish, or eggs. Each item was assigned a percent of total composition by weight. For the first 20 stomachs of each fish species, each prey group was weighed separately to determine percent composition; percent composition of each taxon was subsequently estimated by eye for the remaining stomachs. We evaluated this protocol by comparing the precise measurements of percent composition to those estimated by eye; estimates were within 10% error of true percent composition by weight. Estimates were also within 5% error among individual technicians.

2.5. Trophic discrimination factors

We calculated $\delta^{15}N$ and $\delta^{13}C$ trophic discrimination factors (TDFs, $\Delta^{y}X$) for fish using our isotope and diet data because the isotope mixing space better aligned with consumer isotope data relative to data calculated with literature TDFs (e.g., Caut et al., 2009; Bastos et al., 2017). For each size class of each fish species, we calculated the mean dietary contributions of each prey type (p_{prey}) using our stomach data. We then used (p_{prey}) to weigh the relative importance of each prey's nitrogen and carbon isotope values when calculating the difference in $\delta^{15}N$ and $\delta^{13}C$ between the consumer and the prey (the TDF) using the following equation:

$$\Delta^{y}X = mean\,\delta^{y}X_{consumer} - \Sigma\left(p_{prey} \times \delta^{y}X_{prey}\right)$$

For size classes that consumed primarily one prey source (e.g., small alewife were exclusively zooplanktivorous), we calculated the TDF as the difference between consumer and prey isotope values. All fish $\delta^{13}C$ data were lipid-corrected with the following equation: $\Delta^{13}C = -3.32 + 0.99 \times C{:}N$ (Post et al., 2007). Literature TDF values were used for zooplankton and *Mysis* (Brauns et al., 2018). Final TDF values used in the models are listed in Table 1.

TABLE 1 Trophic enrichment factors (TEF) used in the Bayesian mixing models for each consumer in the different life stages (juveniles × adult) and sites of Lake Champlain.

Consumer	Site	$\delta^{13}C$	±SD	$\delta^{15}N$	±SD
Alewife (juvenile)	Main Lake	2.30	0.81	2.00	1.25
Alewife (adult)	Main Lake	2.30	0.81	2.00	1.25
Alewife (juvenile)	Northeast Arm	2.30	0.81	2.00	1.25
Alewife (adult)	Northeast Arm	2.30	0.81	2.00	1.25
Smelt (juvenile)	Main Lake	2.20	0.98	3.12	1.18
Smelt (adult)	Main Lake	1.60	0.94	1.75	0.65
Smelt (juvenile)	Northeast Arm	0.60	0.37	4.90	0.76
Smelt (adult)	Northeast Arm	0.20	0.18	1.30	0.52
Sculpin (juvenile)	Main Lake	1.90	0.93	3.70	0.88
Sculpin (adult)	Main Lake	1.90	0.93	3.70	0.88
Sculpin (juvenile)	Northeast Arm	0.00	0.98	4.30	0.66
Sculpin (adult)	Northeast Arm	0.00	0.98	4.30	0.66
Mysis diluviana	Main Lake	0.60	0.40	4.00	0.40
Zooplankton	Main Lake	0.60	0.40	4.00	0.40
Zooplankton	Northeast Arm	0.60	0.40	4.00	0.40

2.6. Estimating pelagic × benthic contributions to fish and invertebrates

To evaluate the relative contributions of pelagic and benthic resources to mid-trophic level fishes, we used Bayesian mixing models (MixSIAR; Stock et al., 2018). For each fish species at each site, two models were run: a prey-based model, and a primary producer-based model (using average $\delta^{13}C$ and $\delta^{15}N$ of the respective sources). For *Mysis* and zooplankton, only the primary producer model was employed. The invertebrate samples were divided into Early Season (May–July) and Late Season (August–October) because zooplankton isotopic turnover is a few weeks (Emery et al., 2015) – zooplankton tissues reflect consumption from 1 to 2 weeks before collection. Isotopic turnover for juvenile fish, however, is from 1 to 3 months (Oliveira et al., 2017; Hernández-Urcera et al., 2022), and this time lag between consumption and consumer isotopic assimilation must be considered in the models for more reliable results (Vander Zanden and Rasmussen, 2001; Hussey et al., 2014; Lanari et al., 2021; Possamai et al., 2021).

Due to the possible ontogenetic shifts in the diet of the fish species and *Mysis*, these consumers were categorized into size classes based on their total length (*Mysis*: TL < 10 mm small, and TL > 10 mm large; Fish: see section 2.2). Diets of medium and large size classes of rainbow and alewife were similar, therefore we combined medium and large fish (hereafter referred to as "large" fish) within each species in the models to increase the sample size. Size class was included as a fixed factor in the model. The sources included in the prey-based model were selected based on the stomach contents of each fish species/size class, and the seasonal averages of $\delta^{13}C$ and $\delta^{15}N$ values of the prey species were used. We used the seasonal averages of $\delta^{13}C$ and $\delta^{15}N$ of

small rainbow smelt as the values for prey fish, as these were the only fish species identified in stomachs. *Mysis* had a low abundance in the Northeast Arm, therefore models for this species were only run in the Main Lake. In the producer models, sources were selected based on their presence/absence at the site. Source $\delta^{13}C$ and $\delta^{15}N$ values for epilimnetic phytoplankton and detritus were seasonal averages. The $\delta^{13}C$ and $\delta^{15}N$ values for the spring bloom were an average of all Main Lake samples collected during spring turnover (April and May), and we assumed the isotopic composition of the bloom in the Northeast Arm was similar. The isotopic values for the DCL were taken from the literature (Francis et al., 2011); this source was only included in the Main Lake models, as the Northeast Arm is too productive to develop a DCL.

Trophic discrimination factors (TDF) used for each fish species/site were calculated based on the stomach content analysis and $\delta^{13}C$ and $\delta^{15}N$ values of prey species. For all Bayesian models, no informative priors were used, because (i) no prior information is available for producers' contributions to these consumers in this system, and (ii) although we had stomach content information for these species to include in the prey-based models, informative priors can bias models with a small number of samples (Brown et al., 2018). Moreover, our models represent a season with rapid isotopic turnover of producers, but isotopic assimilation into tissues is relatively slow, therefore diet information may differ from the modeled diet based on the stable isotopes. The mixing models were fitted using the Markov Chain Monte Carlo (MCMC) method, running 100,000 simulations for each model and discarding the first 50,000 simulations used for burn-in. If the model did not reach good diagnostics (Gelman-Rubin Diagnostic <1.05, and Geweke Diagnostic ±1.96), we ran the model again using 300,000 simulations with 200,000 burn-ins. Results were reported as the median (50%) and 95% Bayesian credibility intervals of the estimated contributions. Bayesian analyses were performed using JAGS 4.3.1 (Denwood, 2016), and the models were performed by MixSIAR package (Stock and Semmens, 2016) in R 4.2.0 (R Core Team, 2022).

3. Results

Diet data and mixing models indicated that mid-trophic fish in Lake Champlain generally rely on pelagic pathways, *via* zooplankton and *Mysis* as their primary food resources, with some variation between basins. In the Main Lake, zooplankton and *Mysis* dominated the stomach contents of pelagic fish, while *Mysis* and benthic invertebrates were more prevalent in the stomachs of benthic fish (Figure 2). In the Northeast Arm, *Mysis* abundance is low; amphipods and zooplankton were the primary prey sources for pelagic fish, and amphipods and other benthic invertebrates (oligochaetes and chironomids) dominated benthic fish stomachs. The prey-based MixSIAR models largely aligned with the stomach content analysis, and the producer-based models revealed that seasonal resources are very important in sustaining the Lake Champlain food web.

3.1. Alewife

Alewife consumed primarily zooplankton across all life stages and at both sites (Figure 2A). *Mysis* (Main Lake) and amphipods (Northeast Arm) occasionally dominated (>60%) stomach contents of large alewife, depending on the time of year (early season for *Mysis* and late season for Amphipoda; Figure 2A; Supplementary Table 1). The prey-based mixing models indicated that small and large alewife at both sites acquired the majority of their energy from zooplankton; zooplankton diet contributions were greater than 80% in the Main Lake, and greater than 60% in the Northeast Arm (Figure 3A; Supplementary Table 1). The primary producer-based models suggested that phytoplankton (55% contribution) and the spring bloom (44% contribution) were similarly important for sustaining alewife during the summer and autumn in the Main Lake, for both size groups of alewife. However, in the Northeast Arm, spring bloom had lower importance (<35%); epilimnetic phytoplankton production was the major contributor of carbon to small (72%) and large (66%) alewife (Figure 3B; Supplementary Table 2).

3.2. Rainbow smelt

Rainbow smelt diets exhibited an ontogenetic shift where small individuals primarily preyed on zooplankton and *Mysis* at both sites, while large individuals had higher consumption of *Mysis* and juvenile rainbow smelt (Figure 2B). Prey-based MixSIAR models also showed ontogenetic shifts in rainbow smelt diet, with higher contributions of zooplankton to the small individuals (57%), and *Mysis* (50%) and fish (43%) to the large smelt in the Main Lake (Figure 3C; Supplementary Table 1). Northeast Arm prey-based models did not resolve well because large rainbow smelt did not fit within the isotope mixing space (Supplementary Figure 1A), whereas stomach data indicated a diet of almost exclusively juvenile smelt; issues of sample size and tissue turnover relative to timing of movement to the Northeast Arm may explain this discrepancy. Small rainbow smelt from the Northeast Arm had a large contribution of amphipods (43%) in the diet (Figure 3C), but this result did not align with stomach content data, which indicated a diet of almost exclusively zooplankton (Figure 2B). Producer-based models showed inverted patterns for small and large rainbow smelt in the Main Lake. Benthic energy (detritus) was the largest contributor to diets of small individuals (57%), followed by the pelagic spring phytoplankton bloom (>38%). This pattern was the opposite for large individuals, with detritus the smallest contributor (30%) and the spring bloom the largest (62%; Figure 3D; Supplementary Table 2). For small rainbow smelt in the Northeast

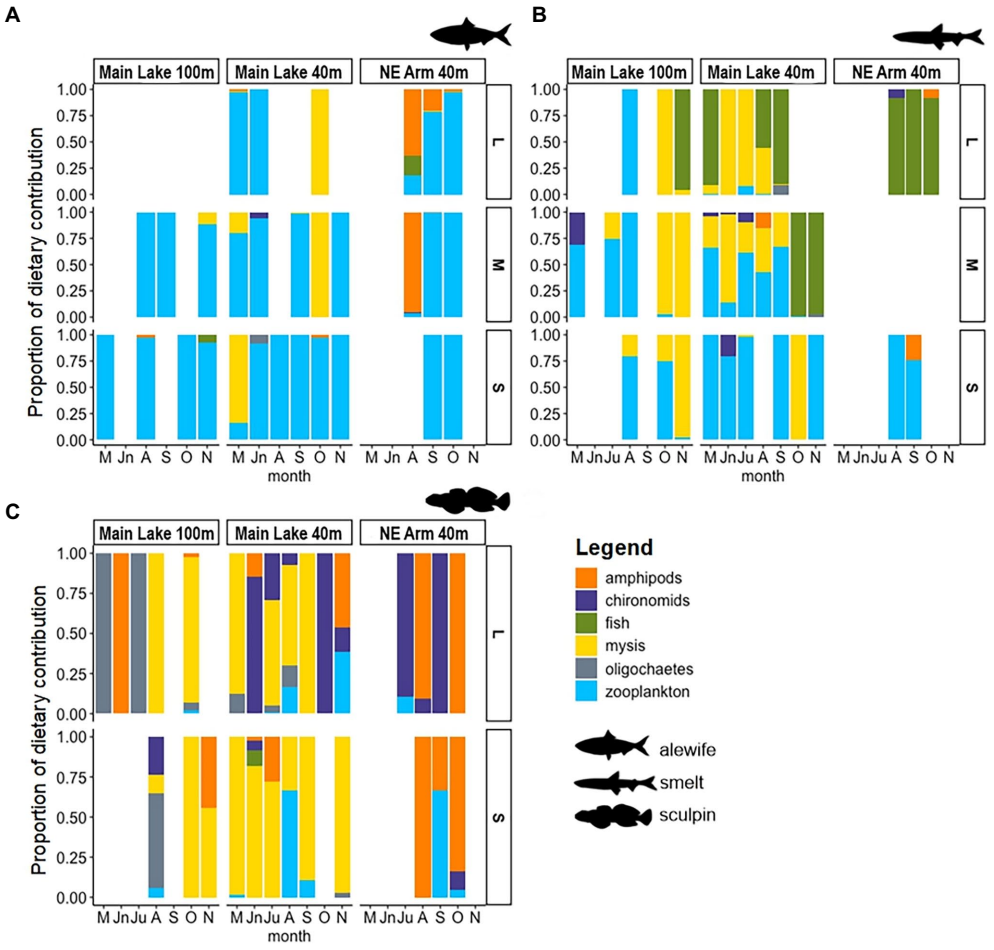

FIGURE 2
Stomach content composition of three different sizes (small, medium, and large) of **(A)** alewife (n=124), **(B)** rainbow smelt (n=137), and **(C)** slimy sculpin (n=152) for three sites in Lake Champlain: Main Lake at 100-m depth, Main Lake at 40-m depth, and Northeast Arm at 40-m depth. Sampling period months start in May (M) and end November (N) 2019. 'Fish' in the figure legend corresponds to juvenile rainbow smelt.

Arm, the producer-based model showed contributions >90% from epilimnetic phytoplankton (Figure 3D), more aligned to the stomach contents results than the prey-based model. Primary-producer based models for large rainbow smelt in the Northeast Arm were not well resolved (Supplementary Figure 1B).

3.3. Slimy sculpin

In the Main Lake, the diets of small slimy sculpins comprised mainly *Mysis*, while large individuals also preyed on benthic invertebrates such as chironomids and amphipods (Figure 2C). The slimy sculpins captured in the Northeast Arm showed the same pattern for both small and large individuals, with the diet comprised entirely of amphipods and other benthic invertebrates (Figure 2C). The prey-based MixSIAR model showed a similar diet for both small and large slimy sculpin in Main Lake, with *Mysis* composing more than 90% of the diet (Figure 3E; Supplementary Table 1). For the Northeast Arm, the model could not distinguish well between amphipods and benthic invertebrate contributions (Supplementary Figure 2), given both prey groups likely rely on benthic basal resources (Figure 3E). The combined contributions of amphipods and benthic invertebrates were > 70% for both small and large slimy sculpin. In the producer-based MixSIAR models, the spring bloom showed a great contribution to slimy sculpin in both small (55%) and large (52%) body sizes in the Main Lake, followed by high contributions of detritus (41 and 43% for small and large, respectively; Figure 3F; Supplementary Table 2). In the Northeast Arm, pelagic resources were the main contributor to slimy sculpin diets, with an estimated contribution >80% for both small and large individuals (Figure 3F; Supplementary Table 2).

3.4. *Mysis diluviana*

Mysis were abundant in the Main Lake but rare in the Northeast Arm. Models showed some isotopic differences between small and large individuals and across the open water season.

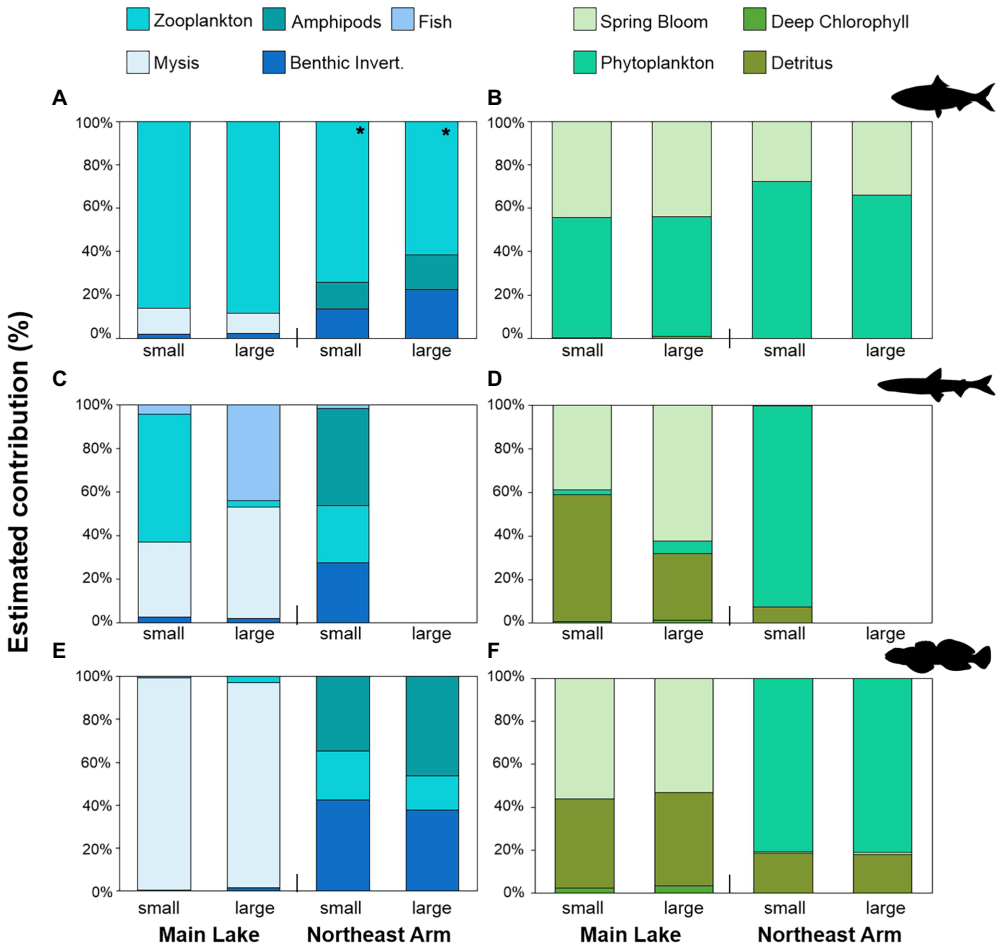

FIGURE 3
Relative contributions (%) of each carbon source to the fish species estimated by MixSIAR models. Contributions were estimated for small and large individuals from two sites in Lake Champlain (Main Lake and Northeast Arm). **(A)** Prey contributions to alewife, **(B)** producer contributions to alewife, **(C)** prey contributions to rainbow smelt, **(D)** producer contributions to rainbow smelt, **(E)** prey contributions to slimy sculpin, and **(F)** producer contributions to slimy sculpin. *Mysis*, *Mysis diluviana*; Benthic Invert., benthic invertebrates including bivalves, insect larvae, gastropods, and oligochaetes. Spring bloom refers to a spring phytoplankton bloom that occurred during spring turnover in May 2019. Phytoplankton refers to epilimnetic phytoplankton. * Prey-based models for alewife in the Northeast Arm included the contribution of zooplankton from the Main Lake.

During the early season (May–June), our model suggested small *Mysis* preyed primarily on zooplankton (67%), while zooplankton (40%) and detritus (30%) contributed almost equally to the large individuals (Figure 4A; Supplementary Table 3). The spring bloom was not identified as an important resource for *Mysis* foraging, with contributions of just 15%. However, the model to estimate large *Mysis* diets in early season was not well resolved among sources (Supplementary Figure 3C). In the late season, an ontogenic pattern was observed, with benthic resources serving as the major contributor to small *Mysis* (>55%), while pelagic sources were the major contributor to large *Mysis* (68%; Figure 4A; Supplementary Table 3).

3.5. Zooplankton

The MixSIAR models indicated that, during the early season, spring blooms compose more than 60% of the energy sources for zooplankton in Main Lake, with the remainder from epilimnetic phytoplankton (19%) and the DCL (10%) (Figure 4B; Supplementary Table 3). In the Northeast Arm, the model could not distinguish well between contributions from detritus versus phytoplankton (Supplementary Figure 4), but estimated 57% from detritus and 33% from epilimnetic phytoplankton (Figure 4B; Supplementary Table 3). During the late season, the DCL is an important resource for the zooplankton in the Main Lake (90%), while in the Northeast Arm the main contributors to zooplankton diets are phytoplankton (55%), and detritus (44%; Figure 4B; Supplementary Table 3).

4. Discussion

Carbon and nitrogen stable isotopes are commonly used to define trophic connections in aquatic systems through carbon flow, organic contamination, and ecosystem functioning (Ishikawa

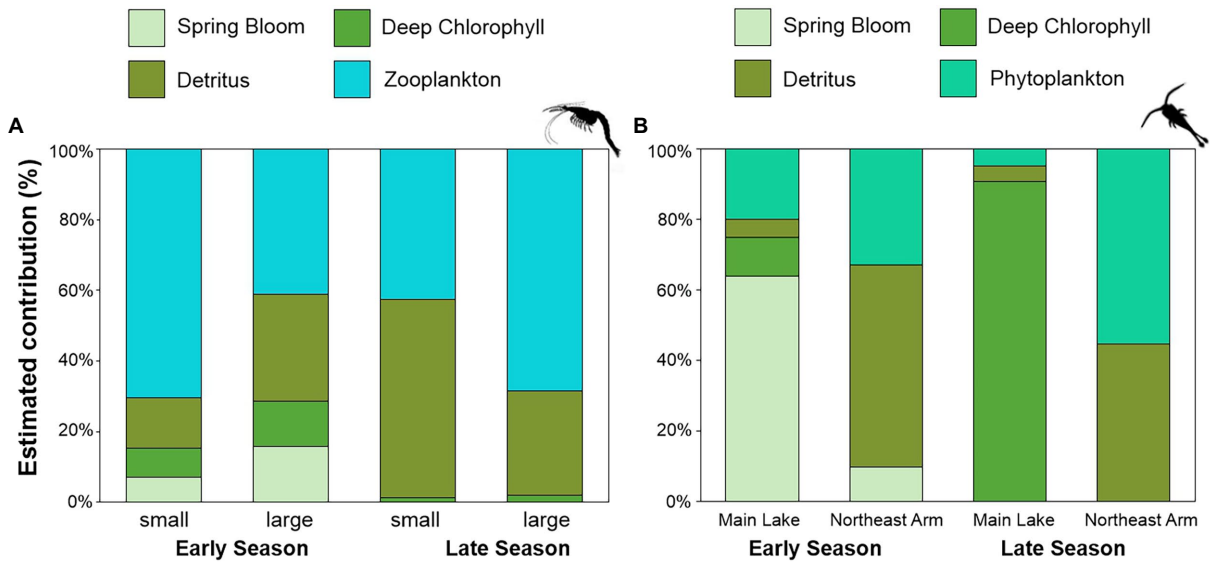

FIGURE 4
Relative contributions (%) of each prey source to consumers estimated by MixSIAR models. **(A)** Contributions to *Mysis* estimated for small and large individuals in Main Lake, Lake Champlain during the early (May–July) and late (August–November) seasons. **(B)** Contributions to zooplankton estimated in both sites (Main Lake and Northeast Arm) during early and late seasons. Spring bloom refers to a spring phytoplankton bloom that occurred during spring turnover in May 2019. Phytoplankton refers to epilimnetic phytoplankton.

et al., 2017; Dias et al., 2018; Possamai et al., 2020). We used stable isotopes to predict the potential effects of an imminent biological invasion on the aquatic food chain and species interaction. Moreover, by combining stable isotope methodology with stomach content data, we were able to calculate specific trophic discrimination factors to better resolve our mixing models. Our field and modeling results suggest a quagga mussel invasion in Lake Champlain could have a large impact on the pelagic food web, but this effect would likely be stronger in the Main Lake than in the isolated Northeast Arm. The current Main Lake lower food web is heavily supported by the spring phytoplankton bloom early in the open-water season, then support shifts to the DCL later in the summer. Both sources of primary production are important for zooplankton; together they contribute >70% of the energy for zooplankton vs. <20% from epilimnetic phytoplanktonic production. Zooplankton is a primary prey of rainbow smelt and *Mysis*, and the predominant prey for alewife (Figure 5A). If quagga mussels reduce the biomass of the spring phytoplankton bloom and DCL as observed in the Great Lakes (e.g., Vanderploeg et al., 2010; Pothoven and Fahnenstiel, 2013), these energy pathways will likely weaken (Figure 5B) and zooplankton biomass will decline, presumably to the detriment of their predators (e.g., Pothoven and Madenjian, 2008; Nalepa et al., 2009; Higgins and Vander Zanden, 2010; Eppehimer et al., 2019).

Although the mixing models did not detect a DCL contribution to fish, the DCL likely contributes to these consumers late in the year, but did not appear in our models due to tissue turnover time. Isotopic turnover for fish can be about 1–4 months longer than zooplankton (Emery et al., 2015; Oliveira et al., 2017), and potentially up to 6 months longer for cold water fish species (Skinner et al., 2017). Consequently, if the DCL is important to fish species, it would be detected during the winter. Unfortunately, we do not have samples during winter time to corroborate this hypothesis, but given our model results indicate the DCL is important for the lower food web, we can infer that it is also likely important for zooplanktivorous fishes.

Mysis is also an important component of the Lake Champlain food web, supporting both pelagic and benthic fish populations. The impact on *Mysis* of losing spring bloom and DCL production is still uncertain, as their dietary plasticity may allow them to shift to a predominantly benthic diet. Our models agree with existing literature (Hrycik et al., 2015) and indicate zooplankton have high importance for both juvenile and adult *Mysis* in Lake Champlain. In addition to zooplankton, *Mysis* were also strongly supported by the detrital pathway (detritus and macroinvertebrates), especially when the spring bloom was absent. Benthic habitats are often an underestimated resource for *Mysis* (Stockwell et al., 2020) and quagga mussels do not seem to negatively impact benthic invertebrate biomass (Ward and Ricciardi, 2007; Ozersky et al., 2011). In fact, increased production of detritus and the production of pseudofeces by quagga mussels may present a novel dietary resource for *Mysis*. If so, pelagic fish that rely on *Mysis* (e.g., rainbow smelt) may have their energetic pathway shifted from pelagic to benthic, without large dietary shifts or losses to population biomass. However, preliminary fatty acid and deuterium fatty acid data indicate pelagic prey are an important source of essential fatty acids for *Mysis* (Supplementary Figures 5, 6). For instance, an essential dietary fatty acid (Docosahexaenoic acid, DHA) was not present in high enough concentrations in sediment for compound-specific isotopic analysis, which indicates this fatty acid is not readily available for benthic consumers. Further, *Mysis* fatty acid

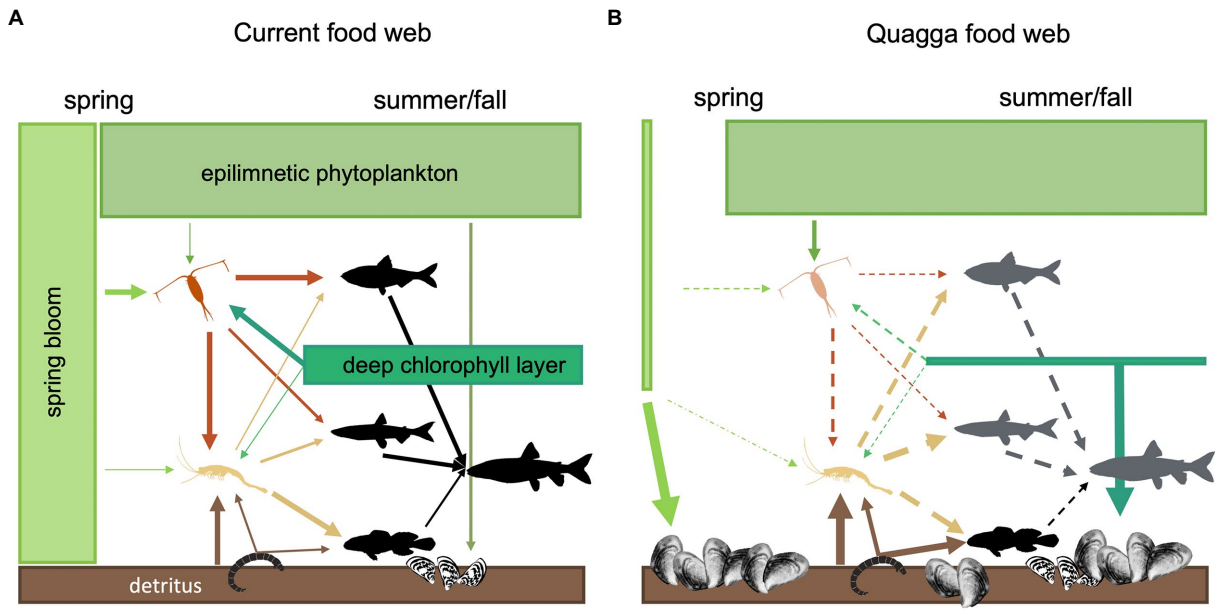

FIGURE 5
Conceptual figure of **(A)** current energy pathways and **(B)** our assessment of how quagga mussels may impact energy flow once established in the Main Lake of Lake Champlain. The orange copepod represents zooplankton populations, the yellow *Mysis* represents *Mysis* populations, the fish (from top to bottom) represent alewife, rainbow smelt, lake trout, and slimy sculpin populations. Size of the boxes represents biomass of the basal resource pool. Line thickness indicates relative strength of each energy pathway before and after invasion. Dotted lines indicate a weak or uncertain pathway. Faded color in the quagga food web **(B)** indicates uncertain population sustainability. If a quagga invasion weakens the most important pelagic energy sources (the spring bloom and deep chlorophyll layer) to the pelagic food web in the Main Lake **(B)**, and stocking of predator populations continues at current rates, mid-trophic level fish may experience a "trophic squeeze."

deuterium values aligned with zooplankton more than benthic invertebrates, indicating essential nutrients likely come from pelagic resources (Supplementary Figure 6). Therefore, if *Mysis* shift to a predominantly benthic diet after quagga mussels establish, their quality as a prey resource may decline, consequently impacting slimy sculpin and rainbow smelt. For example, the physiological condition of *Mysis* in Lake Huron may have declined due to either invasion-induced competition and/or dreissenid-related loss of diatoms and zooplankton (Mida Hinderer et al., 2012). Additionally, the projected loss of zooplankton biomass may increase predation pressure on *Mysis* by zooplanktivorous pelagic fish (e.g., alewife, rainbow smelt), and therefore negatively impact *Mysis* population size; however, this may be mitigated by top-down pressures from lake trout on *Mysis* predators, as wild lake trout recruitment is increasing in Lake Champlain (Marsden et al., 2018; Wilkins and Marsden, 2021). Despite the uncertainty around food quality, the ability of *Mysis* to make use of benthic energy sources may make them a key player in maintaining some amount of stability in the mid-trophic level food web in the Main Lake. This dietary plasticity of consumers is argued to contribute to the capacity of lakes to adapt to stressors such as invasive species (McMeans et al., 2016). However, *Mysis* population densities already experienced an apparent rapid decline in the mid-1990s (Ball et al., 2015), and so the ability of *Myisis* to adapt to the arrival of quagga mussels is uncertain.

In contrast with the Main Lake, the mid-trophic level fish community in the Northeast Arm may not be as susceptible to a quagga mussel invasion. The basin is eutrophic and epilimnetic production is too high to allow the formation of a DCL in the hypolimnion. Our models suggested epilimnetic production was the most important basal energy resource for zooplankton in this basin. Consequently, pelagic fish – and even slimy sculpin – were primarily supported by epilimnetic phytoplankton *via* zooplankton. The epilimnion is often more protected from filtration by dreissenids than the hypolimnion (Fahnenstiel et al., 2010) and given the Northeast Arm is eutrophic during summer stratification, dreissenid-induced decreases in epilimnetic production would be more incremental and unlikely to decrease enough to compromise the availability of this basal resource. Further, the volume of epilimnetic production is much greater than the volume of production in the DCL, such that more time would be needed to see meaningful decreases in epilimnetic production relative to the DCL. Lastly, quagga mussels colonize deep waters prior to littoral areas, and thus access the DCL before epilimnetic production. Therefore, we do not expect the food web in the Northeast Arm to be as severely impacted by a quagga invasion. The spring bloom was minimally important for zooplankton in this basin; however, we used the isotope values for the bloom in the Main Lake in our Northeast Arm models, as sampling in the Northeast Arm did not start until after spring turnover. Therefore, if the isotopic composition of the spring

bloom in the Northeast Arm differs from the Main Lake (for example, due to differences in phytoplankton community composition or CO_2 availability; Vuorio et al., 2006), we may not have accurately represented this potential resource. Future studies should explore biomass and relative importance of hypolimnetic and epilimnetic phytoplankton in the Northeast Arm food web to better assess the potential impact of quagga mussels in this basin.

The impacts of quagga mussel invasion on productivity could potentially lead to greater spatial segregation among basins of mid-trophic level fish populations in Lake Champlain. Rainbow smelt are more confined to the Main Lake (Bruel et al., 2021) while alewife may fare better in the warmer Northeast Arm. Although the Northeast Arm may be more resistant to the impacts of quagga mussels than the Main Lake on important basal resource pools, it may not provide a high-quality alternative foraging habitat for rainbow smelt relative to the Main Lake because of differences in water quality and resource availability. Water temperature and productivity is higher, dissolved oxygen is lower, and depth is shallower in the Northeast Arm than in the Main Lake, and rainbow smelt abundance in the Northeast Arm is generally declining (Bruel et al., 2021). Additionally, as lake temperatures warm due to climate change (O'Reilly et al., 2015; Woolway et al., 2020), the low availability of appropriate oxythermal habitat for pelagic coldwater species such as rainbow smelt in the Northeast Arm will continue to decrease. Alewife, which have a higher thermal tolerance than rainbow smelt (Simonin et al., 2012), may fare better in the Northeast Arm, where zooplankton populations may be less at-risk to the impacts of an invasion. However, when alewife first invaded Lake Champlain, they became the dominant pelagic species, overlapping with the rainbow smelt niche (Marsden and Langdon, 2012; Simonin et al., 2012, 2018). Alewife could pose a competitive risk to rainbow smelt if they can adapt to the food web changes introduced by quagga mussels. Therefore, populations of both species may necessarily become more spatially segregated between the Main Lake and Northeast Arm. Further, the potential lower availability of food for rainbow smelt in the Main Lake combined with the higher competitive ability of alewife could pose a risk to rainbow smelt stocks after quagga mussels become established in Lake Champlain.

Another mid-trophic fish, the slimy sculpin, may provide some relief to piscivores if pelagic mid-trophic species decline. The primary carbon source for slimy sculpin is provided by the benthic pathway (*via* detrital epilimnetic carbon) and is unlikely to be impacted by a quagga mussel invasion (Ward and Ricciardi, 2007; Ozersky et al., 2011). Slimy sculpin is a dominant prey of juvenile lake trout in the Great Lakes (Elrod, and O'Gorman, R., 1991; Owens and Bergstedt, 1994; Madenjian et al., 2005). Therefore, regardless of the losses in the rainbow smelt population, lake trout may switch to slimy sculpin as their primary prey in Lake Champlain, assuming the recent re-emergence of wild recruitment (Marsden et al., 2018) is unrelated to the increased prey availability introduced by the alewife invasion (which is unlikely; Lesser et al., in review).

Although our models provided robust results for the majority of the species and basins, isotope values of detritus and phytoplankton cannot be readily resolved, which means the majority of detritus is likely derived from epilimnetic phytoplankton – suggesting other phytoplankton (the spring bloom and DCL) is more likely to be consumed before contributing to the detrital pool. The importance of non-epilimnetic phytoplankton in the Main Lake models supports this possibility; they are available for less time, so any signal they contribute to detritus could become diluted by epilimnetic phytoplankton. Resolving the differences in detrital and epilimnetic energy pathways is less important for understanding the potential impacts of a quagga invasion on zooplankton and mid-trophic level fishes than resolving differences among pelagic resource pools, given quagga mussels will primarily impact the spring bloom and DCL (Vanderploeg et al., 2010; Pothoven and Fahnenstiel, 2013). However, we do need to resolve the importance of benthic and pelagic/epilimnetic pathways to determine the potential impact of quagga mussels on *Mysis,* whose diet includes both detritus and benthic invertebrates. The preliminary data on hydrogen stable isotopes of fatty acids provided more precise insight by indicating where certain essential nutrients (DHA, EPA) were derived, but the sample size was exploratory. Finally, the contributions of littoral production to the pelagic food web are unknown, but likely important. Dreissenids shunt production away from offshore areas to littoral zones; therefore, organisms that move laterally between habitats could potentially access littoral energy subsidies if sufficient food is no longer present in offshore pelagic zones. To fully resolve benthic, epilimnetic, and littoral energy sources in Lake Champlain, we need a three-isotope mixing model; sulfur would likely be a useful third isotope to use in future studies (e.g., Croisetière et al., 2009).

An inverse pattern in $\delta^{15}N$ of epilimnetic phytoplankton and detritus was observed from May to November. Early in the season, phytoplankton was less enriched in $\delta^{15}N$ relative to detritus, and gradually increased by +2‰ across the sampling period (Supplementary Figure 4). Detritus exhibited the opposite pattern – more enriched at the beginning of the season and depleted by −2‰ over the course of the sampling period. The time sequence of phytoplankton production, senescence, and sinking, and the inverse pattern in $\delta^{15}N$ of epilimnetic phytoplankton and detritus from spring to autumn supports the hypothesis that detritus in Lake Champlain primarily comprises epilimnetic phytoplankton. Moreover, this pattern in phytoplankton $\delta^{15}N$ suggests that after the early season pool of nutrients is depleted, nitrogen remineralization in the water column commences and phytoplankton $\delta^{15}N$ becomes enriched (Möbius, 2013). This hypothesis explains the lack of resolution between epilimnetic phytoplankton and detritus in the mixing models. We used the $\delta^{15}N$ and $\delta^{13}C$ averages of all seasons in the models, which removed the monthly differences of the isotopic values. In the future, sampling phytoplankton and detritus 2 months before the initial fish sampling will help resolve differences in isotopic turnover between producers and consumers (Vander Zanden and Rasmussen, 2001; Lanari et al., 2021; Possamai et al., 2021) and provide the opportunity to apply the MixSIAR models using early and late season averages to better resolve pathways (as we did with *Mysis* and zooplankton models).

5. Conclusion

We used carbon and nitrogen stable isotopes and diet data to address how a biological invasion may disrupt ecosystem processes and linkages. By recognizing important trophic links in the ecosystem and retrieving the impacts of invasions in similar systems, we can predict the potential effects of a biological invasion in the system of our interest. Describing Lake Champlain's food web structure and quantifying energy flow is important to elucidate the relative importance of bottom-up and top-down processes and the risk a quagga mussel invasion poses to the forage food web. While the impacts of quagga mussels on a system will be context-dependent, the ability of quagga mussels to sequester nutrients and productivity and consequently reduce the biomass of the spring bloom and DCL does not lead to a positive outlook for the Main Lake food web. To add complexity, a number of other species are expected to invade in the near future, adding further uncertainty to the stability of the food web. For example, another potential invader, round goby (*Neogobius melanostomus*; George et al., 2021), can forage on quagga mussels (Walsh et al., 2007), but their ability to sufficiently control quagga populations to mitigate the impacts on planktonic basal resources will depend on the timing and success of each invasion. Future work is needed to (1) better elucidate the relative importance of pelagic and benthic energy pathways with a third isotope, (2) determine whether *Mysis* will be able to shift and survive on a more benthic diet, and (3) determine whether lateral resource movement from the littoral zone could subsidize the pelagic food web after a quagga mussel invasion. However, our models provide fairly strong evidence that the mid-trophic food web in the Main Lake of Lake Champlain is at risk if quagga mussels invade, due to a combination of bottom-up and top-down pressures. The importance of the Main Lake as forage habitat relative to the Northeast Arm during the open-water season means some of the most important basal energy resources could be lost after invasion. This research can inform managers about which courses of action (e.g., reduce lake trout stocking) may best reduce the socio-ecological impacts of an invasion. Moreover, we demonstrate how simple stable isotope techniques can provide insights into the consequences of biological invasion, and thus replicated in other systems to address similar problems and predict how invasive species affect bottom-up and top-down effects.

Data availability statement

The raw data supporting the conclusions of this article will be made available by the authors, without undue reservation.

Ethics statement

This work was conducted with a Vermont state collectors permit using best practices as outlined in the "Guidelines for the Use of Fishes in Research" by the American Fisheries Society (https://fisheries.org/docs/wp/Guidelines-for-Use-of-Fishes.pdf). Vertebrates used in this research were dead when acquired and did not require an Institutional Animal Care and Use Committee protocol.

Author contributions

AC contributed to the data collection, managed laboratory processing and data, conducted the data analyses, and led manuscript development. BP contributed to data analysis and manuscript writing. MK analyzed samples for fatty acid and deuterium, and contributed to writing. JM and JS conceived the research, managed data collection, and contributed to manuscript writing. All authors made significant intellectual contributions to the manuscript.

Funding

This work was supported by funds made available for Lake Champlain Research by Senator Patrick Leahy through the Great Lakes Fishery Commission (Award Number 2018_MAR_95003).

Acknowledgments

We thank the captain and crew of the R/V *Melosira*, technicians Russell Dauksis, Cecilia Vichi, Katharina Winter, and Samuel Karl-Kaemmer, and undergraduate students Bethany Smith, Madeline Lerz, Danielle Berger, Amelia Koval, Grace Hemmelgarn, and Posy Labombard for their assistance in the field and lab. Members of the Stockwell and Marsden Laboratories provided valuable field and lab assistance, and feedback on the manuscript. Ben Marcy-Quay provided the map in Figure 1.

Conflict of interest

The authors declare that the research was conducted in the absence of any commercial or financial relationships that could be construed as a potential conflict of interest.

Publisher's note

All claims expressed in this article are solely those of the authors and do not necessarily represent those of their affiliated organizations, or those of the publisher, the editors and the reviewers. Any product that may be evaluated in this article, or claim that may be made by its manufacturer, is not guaranteed or endorsed by the publisher.

Supplementary material

The Supplementary material for this article can be found online at: https://www.frontiersin.org/articles/10.3389/fevo.2022.1061636/full#supplementary-material

References

Ball, S. C., Mihuc, T. B., Myers, L. W., and Stockwell, J. D. (2015). Ten-fold decline in *Mysis diluviana* in Lake Champlain between 1975 and 2012. *J. Great Lakes Res.* 41, 502–509. doi: 10.1016/j.jglr.2015.03.002

Bastos, R. F., Corrêa, F., Winemiller, K. O., and Garcia, A. M. (2017). Are you what you eat? Effects of trophic discrimination factors on estimates of food assimilation and trophic position with a new estimation method. *Ecol. Indic.* 75, 234–241. doi: 10.1016/j.ecolind.2016.12.007

Brauns, M., Boëchat, I. G., de Carvalho, A. P. C., Graeber, D., Gücker, B., Mehner, T., et al. (2018). Consumer-resource stoichiometry as a predictor of trophic discrimination (Δ13C, Δ15N) in aquatic invertebrates. *Freshw. Biol.* 63, 1240–1249. doi: 10.1111/fwb.13129

Brown, C. J., Brett, M. T., Adame, M. F., Stewart-Koster, B., and Bunn, S. E. (2018). Quantifying learning in biotracer studies. *Oecologia* 187, 597–608. doi: 10.1007/s00442-018-4138-y

Bruel, R., Marsden, J. E., Pientka, B., Staats, N., Mihuc, T., and Stockwell, J. D. (2021). Rainbow smelt population responses to species invasions and change in environmental condition. *J. Great Lakes Res.* 47, 1171–1181. doi: 10.1016/j.jglr.2021.04.008

Caut, S., Angula, E., and Courchamp, F. (2009). Variation in discrimination factors (Δ15N and Δ13C): the effect of diet isotopic values and applications for diet reconstruction. *J. Appl. Ecol.* 46, 443–453. doi: 10.1111/j.1365-2664.2009.01620.x

Cecala, R. K., Mayer, C. M., Schulz, K. L., and Mills, E. L. (2008). Increased benthic algal primary production in response to the invasive zebra mussel (*Dreissena polymorpha*) in a productive ecosystem, Oneida Lake, New York. *J. Integr. Plant. Biol.* 50, 1452–1466. doi: 10.1111/j.1744-7909.2008.00755.x

Charles, H., and Dukes, J. S. (2007). "Impacts of invasive species on ecosystem services" in *Biological Invasions*. ed. W. Nentwig (Berlin, Heidelberg, Germany: Springer)

Croisetière, L., Hare, L., Tessier, A., and Cabana, G. (2009). Sulphur stable isotopes can distinguish trophic dependence on sediments and plankton in boreal lakes. *Freshw. Biol.* 54, 1006–1015. doi: 10.1111/j.1365-2427.2008.02147.x

David, P., Thebault, E., Anneville, O., Duyck, P. F., Chapuis, E., and Loeuille, N. (2017). Impacts of invasive species on food webs: a review of empirical data. *Adv. Ecol. Res.* 56, 1–60. doi: 10.1016/bs.aecr.2016.10.001

Denwood, M. J. (2016). Runjags: an R package providing interface utilities, model templates, parallel computing methods and additional distributions for MCMC models in JAGS. *J. Stat. Softw.* 71, 1–25. doi: 10.18637/jss.v071.i09

Dias, P. S., Cipro, C. V., Colabuonan, F. I., Taniguchi, S., and Montone, R. C. (2018). Persistent organic pollutants and stable isotopes in seabirds of the Rocas Atoll, equatorial Atlantic, Brazil. *Mar. Ornithol.* 46, 139–148.

Elrod, J. H., and O'Gorman, R. (1991). Diet of juvenile lake trout in southern Lake Ontario in relation to abundance and size of prey fishes, 1979–1987. *Trans. Am. Fish. Soc.* 120, 290–302. doi: 10.1577/1548-8659(1991)120<0290:DOJLTI>2.3.CO;2

Emery, K. A., Wilkinson, G. M., Ballard, F. G., and Pace, M. L. (2015). Use of allochthonous resources by zooplankton in reservoirs. *Hydrobiologia* 758, 257–269. doi: 10.1007/s10750-015-2338-6

Eppehimer, D. E., Bunnell, D. B., Armenio, P. M., Warner, D. M., Eaton, L. A., Wells, D. J., et al. (2019). Densities, diets, and growth rates of larval alewife and bloater in a changing Lake Michigan ecosystem. *Trans. Am. Fish. Soc.* 148, 755–770. doi: 10.1002/tafs.10171

Euclide, P. T., Flores, N., Wargo, M., Kilpatrick, C. W., and Marsden, J. E. (2018). Lack of genetic population structure of slimy sculpin in a large, fragmented lake. *Ecol. Freshw. Fish* 27, 699–709. doi: 10.1111/eff.12385

Euclide, P. T., Hansson, S., and Stockwell, J. D. (2017). Partial diel vertical migration in an omnivorous macroinvertebrate, *Mysis diluviana*. *Hydrobiologia* 787, 387–396. doi: 10.1007/s10750-016-2982-5

Euclide, P., Marsden, J. E., and Kilpatrick, W. C. (2019). Genetic structure of lake whitefish (*Coregonus clupeaformis*) in Lake Champlain, Vermont, 100 years after commercial fishery closure. *J. Great Lakes Res.* 45, 1310–1319. doi: 10.1016/j.jglr.2019.09.010

Euclide, P., Pientka, B., and Marsden, J. E. (2020). Genetic versus demographic stock structure of rainbow smelt in a large fragmented lake. *J. Great Lakes Res.* 46, 622–632. doi: 10.1016/j.jglr.2020.02.009

Fahnenstiel, G., Pothoven, S., Vanderploeg, H., Klarer, D., Nalepa, T., and Scavia, D. (2010). Recent changes in primary production and phytoplankton in the offshore region of southeastern Lake Michigan. *J. Great Lakes Res.* 36, 20–29. doi: 10.1016/j.jglr.2010.03.009

Flood, P. J., Duran, A., Barton, M., Mercado-Molina, A. E., and Trexler, J. C. (2020). Invasion impacts on functions and services of aquatic ecosystems. *Hydrobiologia* 847, 1571–1586. doi: 10.1007/s10750-020-04211-3

Francis, T. B., Schindler, D. E., Holtgrieve, G. W., Larson, E. R., Scheuerell, M. D., Semmens, B. X., et al. (2011). Habitat structure determines resource use by zooplankton in temperate lakes. *Ecol. Lett.* 14, 364–372. doi: 10.1111/j.1461-0248.2011.01597.x

Gamble, A. E., Hrabik, T. R., Stockwell, J. D., and Yule, D. L. (2011a). Trophic connections in Lake Superior part I: the offshore fish community. *J. Great Lakes Res.* 37, 541–549. doi: 10.1016/j.jglr.2011.06.003

Gamble, A. E., Hrabik, T. R., Stockwell, J. D., and Yule, D. L. (2011b). Trophic connections in Lake Superior part II: the nearshore fish community. *J. Great Lakes Res.* 37, 550–560. doi: 10.1016/j.jglr.2011.06.008

George, S. D., Baldigo, B. P., Rees, C. B., Bartron, M. L., and Winterhalter, D. (2021). Eastward expansion of round goby in New York: assessment of detection methods and current range. *Trans. Am. Fish. Soc.* 150, 258–273. doi: 10.1002/tafs.10290

Ginn, B. K., Bolton, R., Coulombe, D., Fleischaker, T., and Yerex, G. (2018). Quantifying a shift in benthic dominance from zebra (*Dreissena polymorpha*) to quagga (*Dreissena rostriformis bugensis*) mussels in a large, inland lake. *J. Great Lakes Res.* 44, 271–282. doi: 10.1016/j.jglr.2017.12.003

Hernández-Urcera, J., Carneiro, M. D. D., and Planas, M. (2022). Turnover rates and diet–tissue discrimination factors of nitrogen and carbon stable isotopes in seahorse *Hippocampus reidi* juveniles following a laboratory diet shift. *Animals* 12:1232. doi: 10.3390/ani12101232

Higgins, S. N., and Vander Zanden, M. J. (2010). What a difference a species makes: a meta–analysis of dreissenid mussel impacts on freshwater ecosystems. *Ecol. Monogr.* 80, 179–196. doi: 10.1890/09-1249.1

Hrycik, A. R., Simonin, P. W., Rudstam, L. G., Parrish, D. L., Pientka, B., and Mihuc, T. B. (2015). *Mysis* zooplanktivory in Lake Champlain: a bioenergetics analysis. *J. Great Lakes Res.* 41, 492–501. doi: 10.1016/j.jglr.2015.03.011

Hussey, N. E., MacNeil, M. A., McMeans, B. C., Olin, J. A., Dudley, S. F., Cliff, G., et al. (2014). Rescaling the trophic structure of marine food webs. *Ecol. Lett.* 17, 239–250. doi: 10.1111/ele.12226

Ishikawa, N. F., Chikaraishi, Y., Ohkouchi, N., Murakami, A. R., Tayasu, I., Togashi, H., et al. (2017). Integrated trophic position decreases in more diverse communities of stream food webs. *Sci. Rep.* 7:2130. doi: 10.1038/s41598-017-02155-8

Johannsson, O. E., Bowen, K. L., Holeck, K. T., and Walsh, M. G. (2011). *Mysis diluviana* population and cohort dynamics in Lake Ontario before and after the establishment of *Dreissena* spp., *Cercopagis pengoi,* and *Bythotrephes longimanus*. *Can. J. Fish. Aquat. Sci.* 68, 795–811. doi: 10.1139/f2011-028

Karatayev, A. Y., Burlakova, L. E., and Padilla, D. K. (2015). Zebra versus quagga mussels: a review of their spread, population dynamics, and ecosystem impacts. *Hydrobiologia* 746, 97–112. doi: 10.1007/s10750-014-1901-x

Keller, R. P., Drake, J. M., and Lodge, D. M. (2007). Fecundity as a basis for risk assessment of nonindigenous freshwater molluscs. *Cons. Biol.* 21, 191–200. doi: 10.1111/j.1523-1739.2006.00563.x

Kirn, R. A., and Labar, G. W. (1996). Growth and survival of rainbow smelt, and their role as prey for stocked salmonids in Lake Champlain. *Trans. Am. Fish. Soc.* 125, 87–96. doi: 10.1577/1548-8659(1996)125<0087:GASORS>2.3.CO;2

Knight, J. C., O'Malley, B. P., and Stockwell, J. D. (2018). Lake Champlain offshore benthic invertebrate community before and after zebra mussel invasion. *J. Great Lakes Res.* 44, 283–288. doi: 10.1016/j.jglr.2018.01.004

Labar, G. W. (1993). Use of bioenergetics models to predict the effect of increased lake trout predation on rainbow smelt following sea lamprey control. *Trans. Am. Fish. Soc.* 122, 942–950. doi: 10.1577/1548-8659(1993)122<0942:UOBMTP>2.3.CO;2

Lanari, M., Possamai, B., Garcia, A. M., and Copertino, M. (2021). Seasonal and *El Niño* southern oscillation-driven variations in isotopic and elemental patterns among estuarine primary producers: implications for ecological studies. *Hydrobiologia* 848, 593–611. doi: 10.1007/s10750-020-04462-0

Limburg, K. E., Luzadis, V. A., Ramsey, M., Schulz, K. L., and Mayer, C. M. (2010). The good, the bad, and the algae: perceiving ecosystem services and disservices generated by zebra and quagga mussels. *J. Great Lakes Res.* 36, 86–92. doi: 10.1016/j.jglr.2009.11.007

Madenjian, C. P., Hondorp, D. W., Desorcie, T. J., and Holuszko, J. D. (2005). Sculpin community dynamics in Lake Michigan. *J. Great Lakes Res.* 31, 267–276. doi: 10.1016/S0380-1330(05)70258-6

Malkin, S. Y., Silsbe, G. M., Smith, R. E. H., and Howell, T. (2012). A deep chlorophyll maximum nourishes benthic filter feeders in the coastal zone of a large clear lake. *Limnol. Oceanogr.* 57, 735–748. doi: 10.4319/lo.2012.57.3.0735

Marsden, J. E., and Hauser, M. (2009). Exotic species in Lake Champlain. *J. Great Lakes Res.* 35, 250–265. doi: 10.1016/j.jglr.2009.01.006

Marsden, J. E., Kozel, C. L., and Chipman, B. D. (2018). Recruitment of lake trout in Lake Champlain. *J. Great Lakes Res.* 44, 166–173. doi: 10.1016/j.jglr.2017.11.006

Marsden, J. E., and Langdon, R. W. (2012). The history and future of Lake Champlain's fishes and fisheries. *J. Great Lakes Res.* 38, 19–34. doi: 10.1016/j.jglr.2011.09.007

Marsden, J. E., Schumacher, M. N., Wilkins, P. D., Marcy-Quay, B., Alger, B., Rokosz, K., et al. (2022). Diet differences between wild and stocked age-0 to age-3 lake trout indicate influence of early rearing environments. *J. Great Lakes Res.* 48, 782–789. doi: 10.1016/j.jglr.2022.02.004

Marsden, J. E., Stangel, P., and Shambaugh, A. D. (2013). "Influence of environmental factors on zebra mussel population expansion in Lake Champlain" in *Quagga and Zebra Mussels: Biology, Impacts, and Control*. eds. T. F. Nalepa and D. W. Schloesser (Boca Raton, FL: CRC Press), 1994–2010.

McMeans, B. C., McCann, K. S., Tunney, T. D., Fisk, A. T., Muir, A. M., Lester, N., et al. (2016). The adaptive capacity of lake food webs: from individuals to ecosystems. *Ecol. Monogr.* 86, 4–19. doi: 10.1890/15-0288.1

Metz, O., Temmen, A., von Oheimb, K. C. M., Albrecht, C., Schubert, P., and Wilke, T. (2018). Invader vs. invader: intra- and interspecific competition mechanisms in zebra and quagga mussels. *Aquat. Invasions* 13, 472–480. doi: 10.3391/ai.2018.13.4.05

Mida Hinderer, J. L., Jude, D. J., Schaeffer, J. S., Marner, D. M., and Scavia, D. (2012). Lipids and fatty acids of *Mysis diluviana* in lakes Michigan and Huron, 2008. *J. Great Lakes Res.* 38, 93–97. doi: 10.1016/j.jglr.2011.07.001

Mills, E. L., Chrisman, J. R., Baldwin, B., Owens, R. W., O'Gorman, R., Howell, T., et al. (1999). Changes in the dreissenid community in the lower Great Lakes with emphasis on southern Lake Ontario. *J. Great Lakes Res.* 25, 187–197. doi: 10.1016/S0380-1330(99)70727-6

Mills, E. L., Rosenberg, G., Spidle, A. P., Ludyanksu, M., Pligin, Y., and May, B. (1996). A review of the biology and ecology of the quagga mussel (*Dreissena bugensis*), a second species of freshwater dreissenid introduced to North America. *Am. Zool.* 36, 271–286. doi: 10.1093/icb/36.3.271

Möbius, J. (2013). Isotope fractionation during nitrogen remineralization (ammonification): implications for nitrogen isotope biogeochemistry. *Geochim. Cosmochim. Acta* 105, 422–432. doi: 10.1016/j.gca.2012.11.048

Nalepa, T. F., Fanslow, D. L., and Lang, G. (2009). Transformation of the offshore benthic community in Lake Michigan: recent shift from the native amphipod *Diporeia* spp. to the invasive mussel *Dreissena rostriformis bugensis*. *Freshw. Biol.* 54, 466–479. doi: 10.1111/j.1365-2427.2008.02123.x

Nalepa, T. F., and Schloesser, D. W. (Eds.) (2014). *Quagga and Zebra Mussels: Biology, Impacts, and Control*. CRC Press, Boca Raton, FL.

Naman, S. M., White, S. M., Bellmore, J. R., McHugh, P. A., Kaylor, M. J., Baxter, C. V., et al. (2022). Food web perspectives and methods for riverine fish conservation. *WIREs Water* 9:e1590. doi: 10.1002/wat2.1590

O'Malley, B. P., Dillon, R. A., Paddock, R. W., Hansson, S., and Stockwell, J. D. (2018). An underwater video system to assess abundance and behavior of epibenthic *Mysis*. *Limnol. Oceanogr. Methods* 16, 868–880. doi: 10.1002/lom3.10289

Oliveira, M. C. L. M., Mont Alverne, R., Sampaio, L. A., Tesser, M. B., Ramos, L. R. V., and Garcia, A. M. (2017). Elemental turnover rates and trophic discrimination in juvenile Lebranche mullet *Mugil liza* under experimental conditions. *J. Fish Biol.* 91, 1241–1249. doi: 10.1111/jfb.13408

O'Malley, B. P., and Stockwell, J. D. (2019). Diel feeding behavior in a partially migrant *Mysis* population: a benthic-pelagic comparison. *Food Webs* 20:e00117. doi: 10.1016/j.fooweb.2019.e00117

O'Reilly, C. M., Sharma, S., Gray, D. K., Hampton, S. E., Read, J. S., Rowley, R. J., et al. (2015). Rapid and highly variable warming of lake surface waters around the globe. *Geophys. Res. Lett.* 42, 10–773. doi: 10.1002/2015GL066235

Owens, R. W., and Bergstedt, R. A. (1994). Response of slimy sculpins to predation by juvenile lake trout in southern Lake Ontario. *Trans. Am. Fish. Soc.* 123, 28–36. doi: 10.1577/1548-8659(1994)123<0028:ROSSTP>2.3.CO;2

Ozersky, T., Barton, D. R., and Evans, D. O. (2011). Fourteen years of dreissenid presence in the rocky littoral zone of a large lake: effects on macroinvertebrate abundance and diversity. *J. N. Am. Benth. Soc.* 30, 913–922. doi: 10.1899/10-122.1

Pejchar, L., and Mooney, H. A. (2009). Invasive species, ecosystem services and human well-being. *Trends in Ecol. Evol.* 24, 497–504. doi: 10.1016/j.tree.2009.03.016

Possamai, B., Hoeinghaus, D. J., and Garcia, A. M. (2021). Shifting baselines: integrating ecological and isotopic time lags improves trophic position estimates in aquatic consumers. *Mar. Ecol. Prog. Ser.* 666, 19–30. doi: 10.3354/meps13682

Possamai, B., Hoeinghaus, D. J., Odebrecht, C., Abreu, P. C., Moraes, L. E., Santos, A. C., et al. (2020). Freshwater inflow variability affects the relative importance of allochthonous sources for estuarine fishes. *Estuar. Coasts* 43, 880–893. doi: 10.1007/s12237-019-00693-0

Post, D. M., Layman, C. A., Arrington, D. A., Takimoto, G., Quattrochi, J., and Montana, C. G. (2007). Getting to the fat of the matter: models, methods and assumptions for dealing with lipids in stable isotope analyses. *Oecologia* 152, 179–189. doi: 10.1007/s00442-006-0630-x

Pothoven, S. A., and Fahnenstiel, G. L. (2013). Recent change in summer chlorophyll a dynamics of southeastern Lake Michigan. *J. Great Lakes Res.* 39, 287–294. doi: 10.1016/j.jglr.2013.02.005

Pothoven, S. A., and Madenjian, C. P. (2008). Changes in consumption by alewives and lake whitefish after dreissenid mussel invasions in lakes Michigan and Huron. *N. Am. J. Fish Manag.* 28, 308–320. doi: 10.1577/M07-022.1

Pothoven, S. J., and Vanderploeg, H. A. (2022). Variable changes in zooplankton phenology associated with the disappearance of the spring phytoplankton bloom in Lake Michigan. *Freshw. Biol.* 67, 365–377. doi: 10.1111/fwb.13846

R Core Team (2022). *R: A Language and Environment for Statistical Computing*. Vienna, Austria: R Foundation for Statistical Computing.

Riccardi, A., Whoriskey, F. G., and Rasmussen, J. B. (1996). Impact of the *Dreissena* invasion on native unionid bivalves in the upper St. Lawrence River. *Can. J. Fish. Aquat. Sci.* 53, 1434–1444. doi: 10.1139/f96-068

Simonin, P. W., Parrish, D. L., Rudstam, L. G., Sullivan, P. J., and Pientka, B. (2012). Native rainbow smelt and nonnative alewife distribution related to temperature and light gradients in Lake Champlain. *J. Great Lakes Res.* 38, 115–122. doi: 10.1016/j.jglr.2011.06.002

Simonin, P. W., Rudstam, L. G., Parrish, D. L., Pientka, B., and Sullivan, P. J. (2018). Piscivore diet shifts and trophic level change after alewife establishment in Lake Champlain. *Trans. Am. Fish. Soc.* 147, 939–947. doi: 10.1002/tafs.10080

Skinner, M. M., Cross,- B. K., and Moore, B. C. (2017). Estimating *in situ* isotopic turnover in rainbow trout (*Oncorhynchus mykiss*) muscle and liver tissue. *J. Freshw. Ecol.* 32, 209–217. doi: 10.1080/02705060.2016.1259127

Smeltzer, E., Shambaugh, A. D., and Stangel, P. (2012). Environmental change in Lake Champlain revealed by long-term monitoring. *J. Great Lakes Res.* 38, 6–18. doi: 10.1016/j.jglr.2012.01.002

Sousa, R., Guiterrez, J. L., and Aldridge, D. C. (2009). Non-indigenous invasive bivalves as ecosystem engineers. *Biol. Invasions* 11, 2367–2385. doi: 10.1007/s10530-009-9422-7

Stock, B. C., Jackson, A. L., Ward, E. J., Parnell, A. C., Phillips, D. L., and Semmens, B. X. (2018). Analyzing mixing systems using a new generation of Bayesian tracer mixing models. *PeerJ* 6:e5096. doi: 10.7717/peerj.5096

Stock, B. C., and Semmens, B. X. (2016). Unifying error structures in commonly used biotracer mixing models. *Ecology* 97, 2562–2569. doi: 10.1002/ecy.1517

Stockwell, J. D., O'Malley, B. P., Hanson, S., Chapina, R. J., Rudstam, L. G., and Weidel, B. C. (2020). Benthic habitat is an integral part of freshwater *Mysis* ecology. *Freshw. Biol.* 65, 1997–2009. doi: 10.1111/fwb.13594

Strayer, D. L., Adamovich, B. V., Adrian, R., Aldridge, D. C., Balohg, C., Burlakova, L. E., et al. (2019). Long-term population dynamics of dreissenid mussels (*Dreissena polymorpha* and *D. rostriformis*): a cross-system analysis. *Ecosphere* 10:e02701. doi: 10.1002/ecs2.2701

Strayer, D. L., Fischer, D. T., Hamilton, S. K., Malcolm, H. M., Pace, M. L., and Solomon, C. T. (2020). Long-term variability and density dependence in Hudson River *Dreissena* populations. *Freshw. Biol.* 65, 474–489. doi: 10.1111/fwb.13444

Vander Zanden, M. J., Olden, J. D., and Gratton, C. (2006). "Food-web approaches in restoration ecology" in *Foundations of Restoration Ecology*. eds. M. A. Palmer, J. B. Zedler and D. A. Falk (Washington, DC: Island Press), 165–189.

Vander Zanden, M. J., and Rasmussen, J. B. (2001). Variation in $\delta^{15}N$ and $\delta^{13}C$ trophic fractionation: implications for aquatic food web studies. *Limnol. Oceanogr.* 46, 2061–2066. doi: 10.4319/lo.2001.46.8.2061

Vanderploeg, H. A., Liebig, J. R., Nalepa, T. F., Fahnenstiel, G., and Pothoven, S. A. (2010). *Dreissena* and the disappearance of the spring phytoplankton bloom in Lake Michigan. *J. Great Lakes Res.* 36, 50–59. doi: 10.1016/j.jglr.2010.04.005

Vuorio, K., Meili, M., and Sarvala, J. (2006). Taxon-specific variation in the stable isotopic signatures (δ13C and δ15N) of lake phytoplankton. *Freshw. Biol.* 51, 807–822. doi: 10.1111/j.1365-2427.2006.01529.x

Walsh, M. G., Dittman, D. E., and O'Gorman, R. (2007). Occurrence and food habits of the round goby in the profundal zone of southwestern Lake Ontario. *J. Great Lakes Res.* 33, 83–92. doi: 10.3394/0380-1330(2007)33[83:OAFHOT]2.0.CO;2

Ward, J. M., and Ricciardi, A. (2007). Impacts of *Dreissena* invasions on benthic macroinvertebrate communities: a meta-analysis. *Diversity and Distrib.* 13, 155–165. doi: 10.1111/j.1472-4642.2007.00336.x

Wilkins, P. D., and Marsden, J. E. (2021). Spatial and seasonal comparisons of growth of wild and stocked juvenile lake trout in Lake Champlain. *J. Great Lakes Res.* 47, 204–212. doi: 10.1016/j.jglr.2020.11.007

Woolway, R. I., Kraemer, B. M., Lenters, J. D., Merchant, C. J., O'Reilly, C. M., and Sharma, S. (2020). Global lake responses to climate change. *Nat. Rev. Earth Environ.* 1, 388–403. doi: 10.1038/s43017-020-0067-5

Frontiers in
Ecology and Evolution

Ecological and evolutionary research into our natural and anthropogenic world

This multidisciplinary journal covers the spectrum of ecological and evolutionary inquiry. It provides insights into our natural and anthropogenic world, and how it can best be managed.

Discover the latest Research Topics

See more →

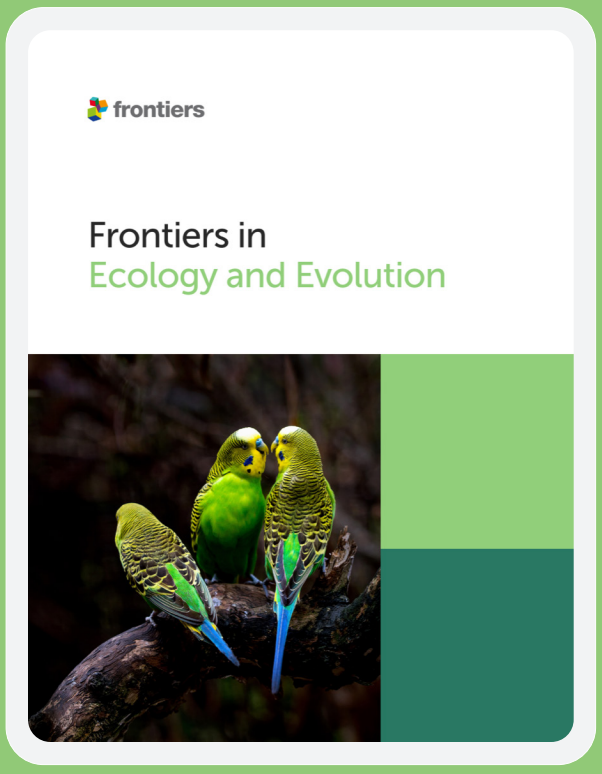

Frontiers

Avenue du Tribunal-Fédéral 34
1005 Lausanne, Switzerland
frontiersin.org

Contact us

+41 (0)21 510 17 00
frontiersin.org/about/contact